seit 1558

Friedrich-Schiller-Universität Jena

Chemisch-Geowissenschaftlichen Fakultät

Functional PLA based (co)polymers *via* ROP and RAFT polymerization

Dissertation

(kumulativ)

zur Erlangung des akademischen Grades

doctor rerum naturalium (Dr. rer. nat.)

vorgelegt dem Rat der Chemisch-Geowissenschaftlichen Fakultät der

Friedrich-Schiller-Universität Jena

von M.Sc. Ilknur Yildirim

geboren am 19. August 1989 in Istanbul (Türkei)

Gutachter:

1. .....
2. .....
3. (.....)

Tag der öffentlichen Verteidigung: ……

Ananeme

Table of Contents

Documentation of authorship

This section contains a list of the individual contributions to the publications reprinted in this thesis.

P1	Ilknur Yildirim,[1] Christine Weber,[2] Ulrich S. Schubert,[3] Old meets new: Combination of PLA and RDRP to obtain sophisticated macromolecular architectures, *Prog. Polym. Sci.* **2017**, http://dx.doi.org/10.1016/j.progpolymsci.2017.07.010.		
Author	**1**	**2**	**3**
Conceptual development	×	×	
Preparation of the manuscript	×	×	
Correction of the manuscript		×	×
Supervision of I. Yildirim		×	×
Proposed publication equivalent	0.5		

P2	Julia Kötteritzsch,[1] Stefan Bode,[2] Ilknur Yildirim,[3] Christine Weber,[4] Martin D. Hager,[5] Ulrich S. Schubert,[6] Reversible oligomerization of 3-aryl-2-cyanothioacrylamides *via* [2_s + 4_s] cycloaddition to substituted 3,4-dihydro-*2H*-thiopyrans, *Des. Monomers Polym*. **2015**, *18*, 627–640.					
Author	**1**	**2**	**3**	**4**	**5**	**6**
Conceptual development	×			×	×	
Synthesis & characterization of monomers	×	×				
Synthesis and analysis of oligomer	×					
Polylactide synthesis & characterization	×		×			
Preparation of the manuscript	×	×				
Correction of the manuscript	×	×	×	×	×	×
Supervision of J. Kötteritzsch					×	×
Supervision of I. Yildirim				×		×
Proposed publication equivalent			0.25			

P3	Ilknur Yildirim,[1] Sarah Crotty,[2] Claas H. Loh,[3] Grit Festag,[4] Christine Weber,[5] Pier-Francesco Caponi,[6] Michael Gottschaldt,[7] Matthias Westerhausen,[8] Ulrich S. Schubert,[9] End-functionalized polylactides using a calcium-based precatalyst: Synthesis and insights by mass spectrometry, *J. Polym. Sci., Part A: Polym. Chem.* **2016**, *54*, 437–448.								
Author	**1**	**2**	**3**	**4**	**5**	**6**	**7**	**8**	**9**
Conceptual development					×		×	×	
Polymer synthesis & characterization	×								
Mass spectrometry analyses		×							
Catalyst/co-initiator synthesis			×						
SEC measurements				×					
Preparation of the manuscript	×								
Correction of the manuscript		×	×	×	×	×	×	×	×
Supervision of I. Yildirim					×	×			×
Proposed publication equivalent	1.0								

P4	Ilknur Yildirim,[1, #] Turgay Yildirim,[2, #] Diana Kalden,[3] Grit Festag,[4] Nicole Fritz,[5] Christine Weber,[6] Stephanie Schubert,[7] Matthias Westerhausen,[8] Ulrich S. Schubert,[9] Retinol initiated poly(lactide)s: Stability upon polymerization and nanoparticle preparation, *Polym. Chem.* **2017**, *8*, 4378–4387. [#]Authors contributed equally.								
Author	**1**	**2**	**3**	**4**	**5**	**6**	**7**	**8**	**9**
Conceptual development	×	×				×	×		
Polymer synthesis & characterization	×	×							
Catalyst/co-initiator synthesis			×						
Nanoparticle preparation & characterization		×							
Stability investigation	×								
SEC measurements				×					
Mass spectrometry analyses					×				
Preparation of the manuscript	×	×							
Correction of the manuscript			×	×	×	×	×	×	×
Supervision of I. Yildirim						×			×
Proposed publication equivalent	1.0								

P5	Ilknur Yildirim,[1] Pelin Sungur,[2] Anna C. Crecelius-Vitz,[3] Turgay Yildirim,[4] Diana Kalden,[5] Stephanie Hoeppener,[6] Matthias Westerhausen,[7] Christine Weber,[8] Ulrich S. Schubert,[9] One-pot synthesis of PLA-*b*-PHEA *via* sequential ROP and RAFT polymerizations, *Polym. Chem.* **2017**, DOI: 10.1039/C7PY01176H.

Author	**1**	**2**	**3**	**4**	**5**	**6**	**7**	**8**	**9**
Conceptual development	×							×	
Polymer synthesis & characterization	×								
Mass spectrometry analyses			×						
Cryo-TEM analyses		×				×			
DLS measurements				×					
Catalyst/co-initiator synthesis					×				
Preparation of the manuscript	×								
Correction of the manuscript		×	×	×	×	×	×	×	×
Supervision of I. Yildirim								×	×
Proposed publication equivalent	1.0								

P6	Ilknur Yildirim,[1] Tanja Bus,[2] Martin Sahn,[3] Turgay Yildirim,[4] Diana Kalden,[5] Stephanie Hoeppener,[6] Anja Traeger,[7] Matthias Westerhausen,[8] Christine Weber,[9] Ulrich S. Schubert,[10] Fluorescent amphiphilic heterografted comb polymers comprising biocompatible PLA and PEtOx side chains, *Polym. Chem.* **2016**, *7*, 6064–6074.

Author	**1**	**2**	**3**	**4**	**5**	**6**	**7**	**8**	**9**	**10**
Conceptual development	×								×	
Polymer synthesis & characterization	×									
Biological investigations		×								
POx macromonomer preparation			×							
DLS measurements				×						
Catalyst/co-initiator synthesis					×					
Cryo-TEM analysis						×				
Preparation of the manuscript	×									
Correction of the manuscript		×	×	×	×	×	×	×	×	×
Supervision of I. Yildirim									×	×
Proposed publication equivalent	1.0									

Erklärung zu den Eigenanteilen des Promovenden/der Promovendin sowie der weiteren Doktoranden/Doktorandinnen als Koautoren an den Publikationen und Zweitpublikationsrechten bei einer kumulativen Dissertation

Für alle in dieser kumulativen Dissertation verwendeten Manuskripte liegen die notwendigen Genehmigungen der Verlage („Reprint permissions") für die Zweitpublikation vor.

Die Co-Autoren der in dieser kumulativen Dissertation verwendeten Manuskripte sind sowohl über die Nutzung, als auch über die oben angegebenen Eigenanteile informiert und stimmen dem zu.

Die Anteile der Co-Autoren an den Publikationen sind in diesem Kapitel aufgeführt (Documentation of authorship).

Ich bin mit der Abfassung der Dissertation als publikationsbasiert, d.h. kumulativ, einverstanden und bestätige die vorstehenden Angaben. Eine entsprechend begründete Befürwortung mit Angabe des wissenschaftlichen Anteils des Doktoranden/der Dokorandin an den verwendeten Publikationen werde ich parallel an den Rat der Falkultät der Chemisch-Geowissenschaftlichen Fakultät richten.

Ilknur Yildirim	Datum	Ort	Unterschrift
Prof. Dr. Ulrich S. Schubert	Datum	Ort	Unterschrift

1. Introduction

Polylactide (PLA) is a polyester which is derived from lactic acid and is the "polymer of choice" for many biomedical applications since it possesses the most demanded features such as biodegradability and biocompatibility.[1] Thanks to the presence of ester bonds PLA degrades by hydrolysis or enzymatic reaction in physiological conditions to form its constituent α-hydroxy acids which are subsequently eliminated through normal cellular activity.[2] Since its approval by the US Food and Drug Administration (FDA) for absorbable sutures in 1970s, PLA based co(polymers) have been used for tissue engineering scaffolds, bone fixation implants, drug delivery vehicles, absorbable/implantable devices and coatings.[3] PLA also represents a sustainable alternative to polymers derived from petrochemical resources, since it is a biomass-derived polymer (**Figure 1.1**) and possesses mechanical properties comparable to commodity polymers such as polyethylene (PE), polypropylene (PP), polystyrene (PS) and poly(ethylene terephthalate) (PET).[3]

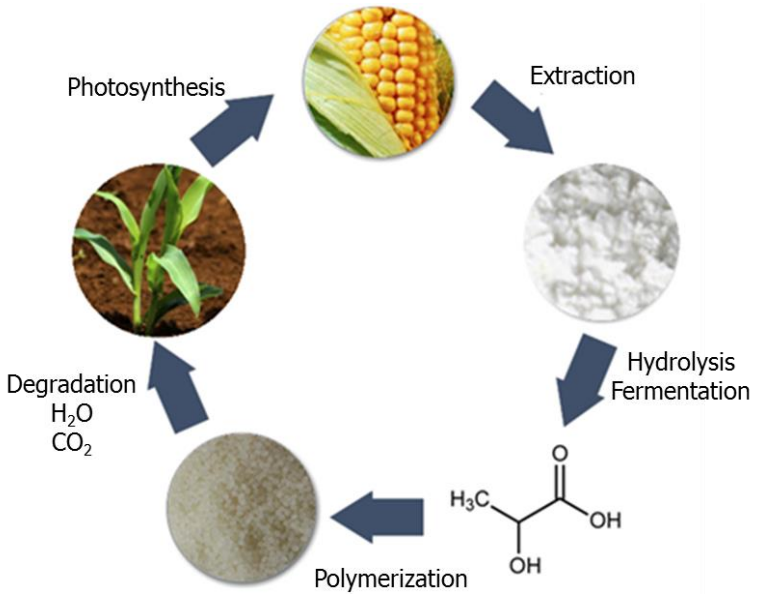

Figure 1.1. The life cycle of PLA in nature.

The industrial production process of PLA starts from the fermentation of corn glucose into L-lactic acid.[4] The condensation of L-lactic acid into oligomers, and the subsequent catalytic depolymerization under reduced pressure yields lactide monomer. Subsequently, the resulting lactide is polymerized *via* ring opening polymerization (ROP) using stannous octoate ($Sn(Oct)_2$) as catalyst in bulk. Although $Sn(Oct)_2$ enables to produce high molar mass PLA both in bulk and in solution, there is an increasing concern about its toxicity and poor control over the ROP

process *i.e.* broad dispersities and low end group fidelity.[5] As a consequence, there has been an increasing effort on the development alternative (co)catalyst/initiator systems (**Figure 1.2**) including several organocatalytic and enzyme based approaches yielding PLA without absence of toxic catalyst residues.[5] Simultaneously, several metal-alkoxide based initiators based on lithium,[6] aluminum,[7] magnesium,[8] calcium,[9] yttrium, zinc[8] and lanthanides[10] have been investigated for the controlled ROP of lactide. However, to the best of our knowledge none of these promising metal-alkoxide initiator systems have been exploited to its full potential yet in terms of polymer chemistry.

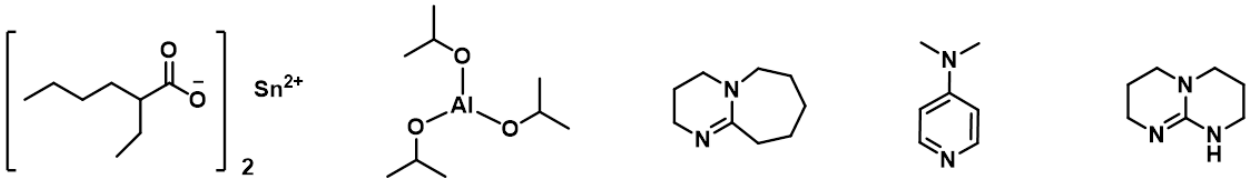

Figure 1.2. Schematic representation of the commonly utilized catalysts for the ROP of lactide; 4-(*N*,*N*-dimethylamino)pyridine (DMAP), 1,8-diazabicyclo[5.4.0]undec-7-ene (DBU), 1,5,7-triazabicyclo[4.4.0]dec-5-ene (TBD).

Although, the above mentioned great features, PLA suffers from brittleness (poor toughness), slow degradation rates (depending on the crystallinity and the molar mass), hydrophobicity and lack of reactive side chain functionality, which limits its use in certain applications.[11] Therefore, lactide is usually copolymerized with glycolic acid resulting in amorphous PLGA[12] or the ROP of lactide is initiated with poly(ethylene glycol) PEG yielding amphiphilic PEG-*b*-PLA block copolymers.[13] Although these approaches represent innovatory developments in PLA research, they do not enable the introduction of reactive/functional groups which would be very beneficial for specialized biomedical applications. For this purpose, post-polymerization modifications can be applied. However, it should be kept in mind that the PLA can be degraded under both acidic and alkaline reaction conditions. At this point, combination of ROP of lactide with reversible-deactivation radical polymerization (RDRP) techniques represents an elegant way to prepare functional PLA based copolymers with a variety of architectures such as linear, graft, and star-shaped, since PLA remains intact in the presence of radical species if the reaction conditions are carefully adjusted.

The focus of this thesis is to develop facile approaches to a variety of end functional PLAs and to utilize the combination of ROP and reversible addition-fragmentation chain transfer (RAFT)

polymerization techniques to access amphiphilic PLA based block and comb type copolymers. First of all, the second chapter provides an overview about the state of the art strategies for the combination of ROP of lactide with RDRP techniques that can be followed to prepare PLA based copolymers with sophisticated macromolecular architectures. As such synthetic strategies rely on end-functionalized PLA, the preparation of chain end-functional PLAs is in focus in the third chapter by utilizing different ROP catalysts, *i.e.* $Sn(Oct)_2$ and a calcium based complex together with a number of functional alcohols. Moreover, the use of mass spectrometry techniques such as electrospray ionization (ESI) and matrix-assisted laser desorption/ionization (MALDI) time-of-flight mass spectrometry (ToF-MS) is discussed in order to gain in-depth information about the end group fidelity of the synthesized PLAs and the ROP mechanism in the presence of calcium alkoxide formation. Considering the fact that the potential biological applications of the synthesized PLAs is of high importance, the fourth chapter will focus on the use of bioactive compounds as ROP initiators such as retinol and cholesterol. In addition, the stability of the retinol-PLA conjugates upon polymerization and nanoparticle preparation is enclosed in order to give insights into the challenges and the limitations of the choice of the "initiating alcohol". Utilizing such end-functional PLA homopolymers, the development of one pot approaches for the synthesis of block copolymers by sequential ROP and RAFT polymerization processes by utilizing a heterofunctional inifer is in the focus of **Chapter 5**. A detailed characterization of the block copolymers both in bulk and solution will be enclosed, too. Going one step further, the synthesis of fluorescent heterografted comb type copolymers presented in **Chapter 6** relies on the modification of both PLA end groups, as α,ω-end functional macromonomers are the fundamental building blocks required for this purpose. The self-assembly and the detailed cytotoxicity/cellular uptake behavior of the fluorescent heterografted comb polymers will be discussed as well.

2. Combination of ROP of lactide with RDRP techniques

Parts of this chapter will be published **P1**) Ilknur Yildirim, Christine Weber, Ulrich S. Schubert, Old meets new: Combination of PLA and RDRP to obtain sophisticated macromolecular architectures, *Prog. Polym. Sci.* **2017**, http://dx.doi.org/10.1016/j.progpolymsci.2017.07.010.

Based on the robustness of radical chemistry, reversible-deactivation radical polymerization (RDRP) methods enable the preparation of polymers under mild experimental conditions with well-defined properties *i.e.* pre-determined molar masses, end groups and architecture.[14] Atom transfer radical polymerization (ATRP), reversible addition-fragmentation chain transfer (RAFT) polymerization and nitroxide-mediated polymerization (NMP) are among the most commonly utilized RDRP techniques. The combination of ring opening polymerization (ROP) with RDRP techniques has been extensively applied to prepare polylactide (PLA) based copolymers with various sophisticated macromolecular structures such as linear, star-shaped and branched polymers.[15, 16] As outlined in **Figure 2.1**, linear and star-shaped block copolymers of PLA are accessible by the use of dual initiators and end functionalization methods, respectively. More complicated synthetic pathways such as macromonomer, grafting from and grafting onto approaches are usually employed in order to prepare comb and graft copolymers.

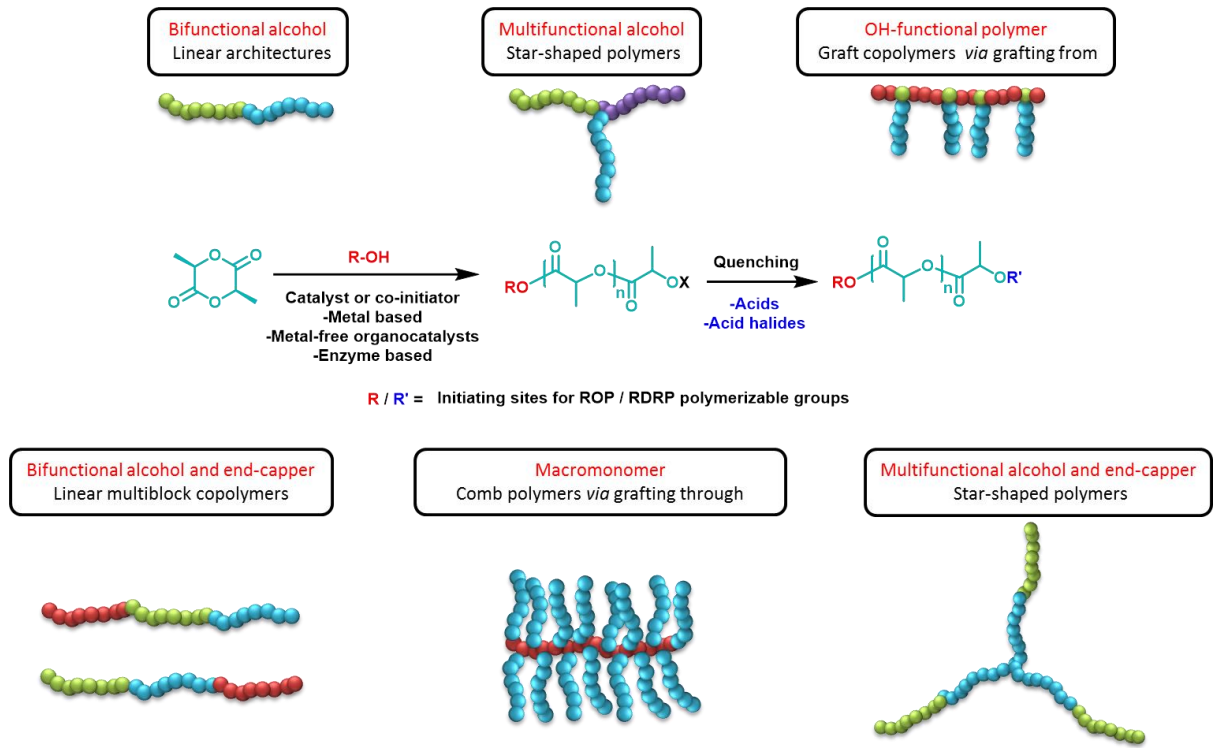

Figure 2.1. Schematic representation for access to various copolymer architectures by exploitation of functional moieties at the α- and ω-chain ends of PLA.

Dual initiators are also known as heterofunctional initiators, since they enable to combine mechanistically different polymerization processes without the need of intermediate transformation and protection steps (**Figure 2.2**).[17, 18] For the combination of ROP and RDRP methods, the dual initiator has to bear a hydroxyl functionality in order to serve as an initiating site for the ROP of lactide. The second functionality of the dual initiator can be an alkyl halide or alkoxyamine as typical initiation sites for ATRP and NMP, respectively. The RAFT polymerization is initiated by an external radical source (*vide infra*). Therefore, the heterofunctional thiocarbonylthio compounds act actually as initiator-transfer agent (inifer) rather than a dual initiator.[19]

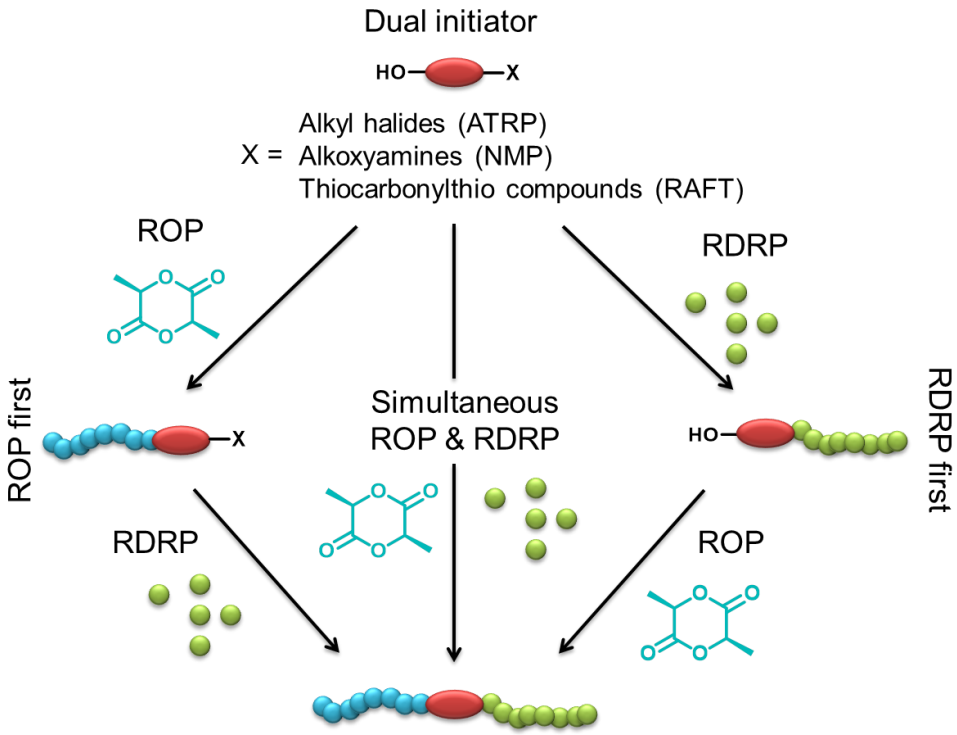

Figure 2.2. Schematic representation of synthetic approaches for combination of ROP and RDRPs using dual initiators.

The sequence of the synthetic pathways followed for the preparation of PLA based copolymers by using dual initiators can vary, although the final polymers reveal the same molecular structure. For instance, in the "RDRP first method", the radical polymerization is performed in the first step, which yields a macro ROP initiator thanks to the terminal hydroxyl group.[20, 21] However, it has to be taken into account that the functional moieties present in the macro ROP initiator has to be tolerated during the subsequent ROP step. Therefore, due to sensitivity of the ROP mechanism of lactide, the diversity of the vinylic monomers used is limited for the "RDRP first" approaches.

In contrast, in the "ROP first method", the ROP of lactide is performed in the first step yielding a PLA based macroinitiator[22] or macro chain transfer agent (CTA)[23] that will be used for the following RDRP method (**Figure 2.2**). In particular to enable the synthesis of PLA-containing copolymers with functional moieties that would not be tolerated by the ROP of lactide, the "ROP first technique" represents a reasonable alternative method. In comparison to the "RDRP first method", a greater variety of vinylic monomers can be applied by utilizing the "ROP first method", since the risk of interference with the ROP conditions is not present anymore. Hence, benefiting from functional end groups and dual initiators with further tailor-made functionalities broadens the range of possible applications of the obtained block copolymers. However, special care has to be taken that the functional vinylic monomers applied in the second polymerization step do not induce a degradation of the PLA block that is already present. Finally, both polymerizations can be performed in one pot in a sequential polymerization approach,[24] and even proceed simultaneously.[25] For this purpose, the compatibility of the reagents *i.e.* the catalysts, initiators, monomers required for both polymerization types with each other is required. As soon as these requirements can be fulfilled, this technique enables a convenient and experimentally elegant way of combining two mechanistically distinct polymerization techniques.

Herein, the exploitation of these approaches, especially by combination of ROP with RAFT polymerization technique will be in focus, since the next chapters includes the utilization of this effective and versatile RDRP method. The RAFT polymerization is compatible with various polar and non-polar monomers and tolerates many functional moieties. It is initiated by a common radical initiator, while an additional CTA provides control over the polymerization in terms of kinetics, end groups and molar mass.[26] For this reason, as discussed above, hydroxyl-functional CTAs do not represent dual initiators but would rather be named as inifers, since they bear a transfer agent for RAFT polymerization and an initiating function for ROP.[19] As discussed above, in order to employ an inifer for the "ROP first" approach, the CTA should not undergo or induce undesired side reactions during the ROP process. Indeed, many CTAs remain intact with various catalysts that have been applied during the ROP *i.e.* tin(II),[27] 1,8-diazabicyclo[5.4.0]undec-7-ene (DBU),[28, 29] or the thiourea/(-)-sparteine co-catalyst system,[30, 31] yielding suitable macro CTAs based on PLA. Representative hydroxyl-functional CTAs are shown in **Figure 2.3**, which enables the synthesis of PLA bas copolymers with various architectures.

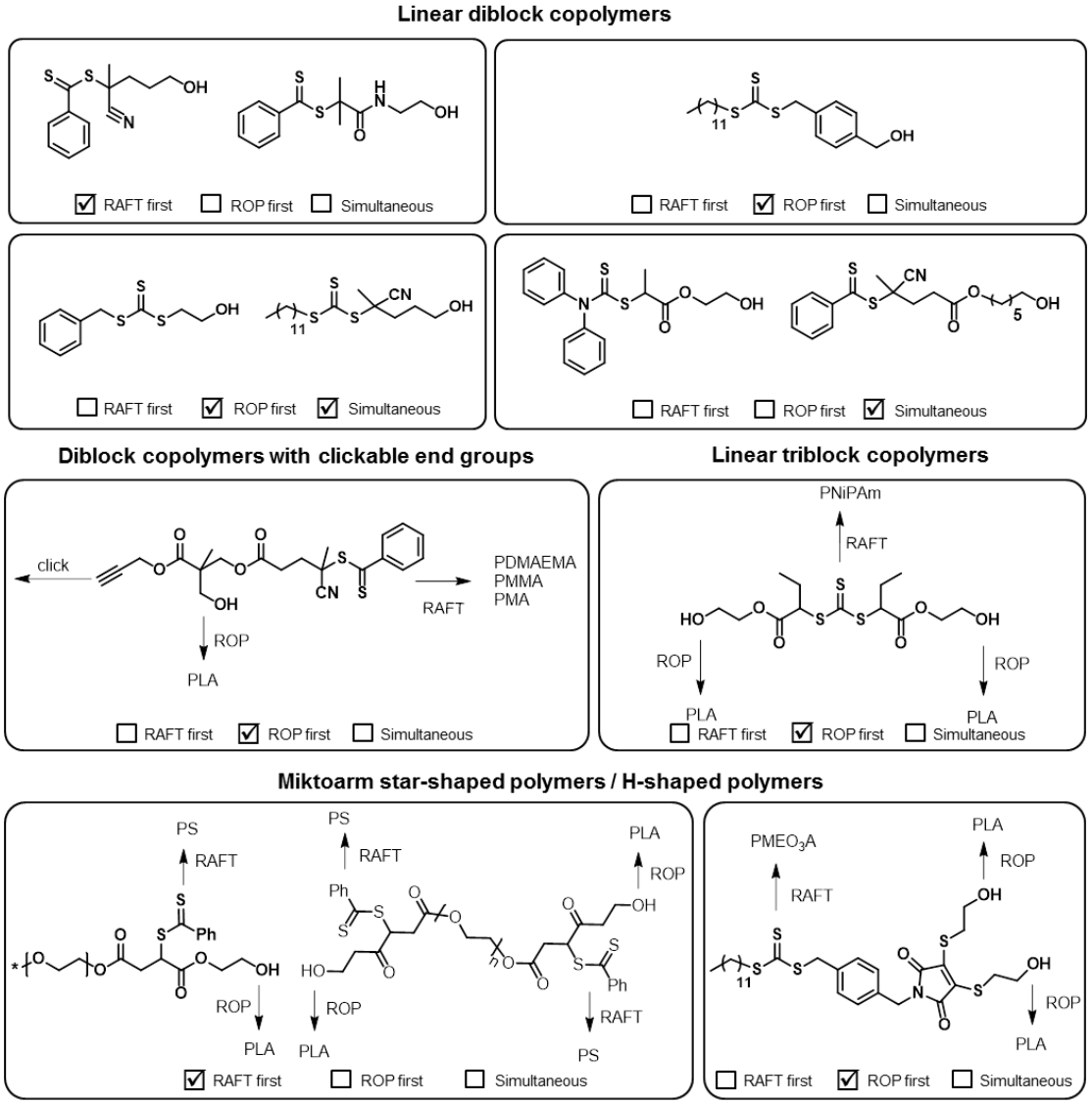

Figure 2.3. Representative hydroxy-functional CTAs used as inifers for the combination of RAFT polymerization and ROP of lactide.

Apart from using dual initiators, PLA can be transformed into a macro-CTA by end-functionalization techniques to be further used in a RAFT process (**Figure 2.4**). For instance, the ROP of lactide is usually quenched by a protic source to yield PLA with a hydroxyl moiety at the ω-chain end. The hydroxyl group can be transformed into another initiating site by post-polymerization modification process.[32, 33] This could be done by coupling the hydroxyl end groups with activated carboxylic acid derivatives which can be either prepared separately or formed *in situ*. Alternatively, the living PLA chain ends can be directly quenched with suitable electrophilic reagents that already contain the CTA *i.e.* using an acyl chloride functional CTA.[34, 35]

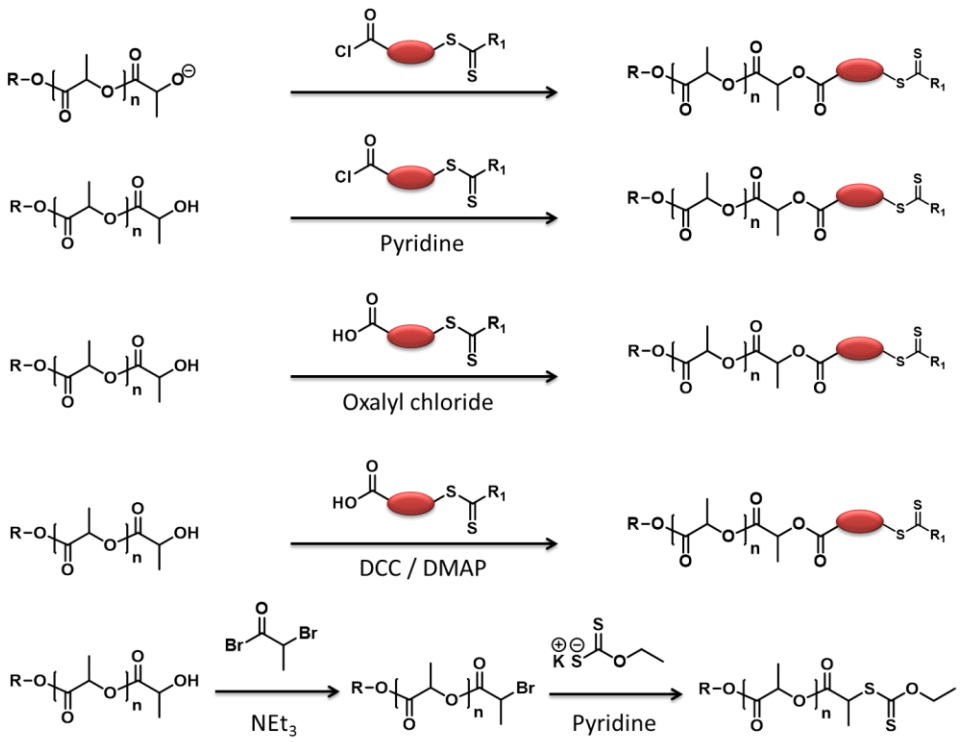

Figure 2.4. Schematic representation of the synthetic approaches for ω-end functionalization of PLA with a CTA; *N,N'*-dicyclohexylcarbodiimide (DCC), 4-(*N*,*N*-dimethylamino)pyridine (DMAP). R_1 represents either the homolytic leaving group (R) or the activating/stabilizing group (Z).

Linear and star-shaped block copolymers of PLA are accessible by utilizing heterofunctional inifers and mechanism transformation approaches (**Figure 2.5**). However, the synthesis of comb and graft copolymers requires appropriate synthetic strategies such as macromonomer (grafting through) and grafting from methods. To the best of our knowledge the grafting onto method has not been reported so far to attach PLA side chains to a polymer backbone prepared by any RDRP technique. However, this method comes into play for the additional attachment of other building blocks to the polymeric architectures.

PLA based macromonomers are obtained by attachment of a polymerizable moiety at either α- or ω-end (**Scheme 2.1**). For instance, a hydroxyl functional monomer such as 2-hydroxethyl (meth)acrylate HE(M)A can be used as an initiator for the ROP of lactide.[36, 37] In analogy to the methods described above for the preparation of PLA based macro-CTA, the ω- chain end of PLA can be functionalized with a polymerizable group by the post polymerization modification of PLA. This could be done by utilizing methacrylic anhydride[38] or methacryloyl chloride together with trimethylamine as an auxiliary base.[39, 40] The latter approach also enables the preparation of α, ω- end functional macromonomers.[40]

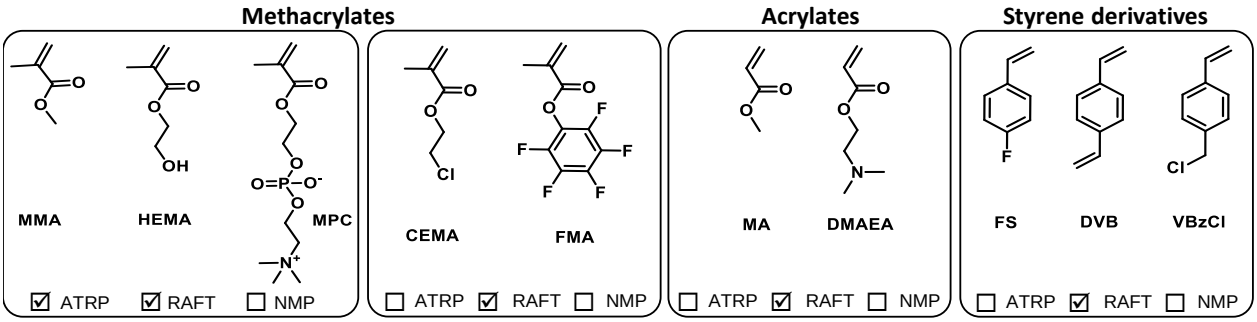

Figure 2.5. Representative vinylic monomers polymerized *via* combination of ROP and RDRP techniques employing dual initiators or end functionalization strategies.

Copolymerization of PLA based macromonomers with small molecules provides access to graft copolymers.[36] The amount of the macromonomer in the feed determines the degree of grafting (DG), whereas the side chain length of the graft copolymer is easily pre-adjusted by the degree of polymerization (DP) of the macromonomer used. Comb polymers with PLA side chains are accessible when the macromonomers are copolymerized without addition of a small monomer. Common synthetic approaches include the chain extension to synthesize block copolymers with a palm-tree like structure,[41] as well as the copolymerization with other macromonomers types to obtain heterografted comb polymers.[40] The main advantage of this method is the possibility to purify and characterize the resulting PLA based macromonomer prior to (co)polymerization, which is of great importance to ensure a high DF.

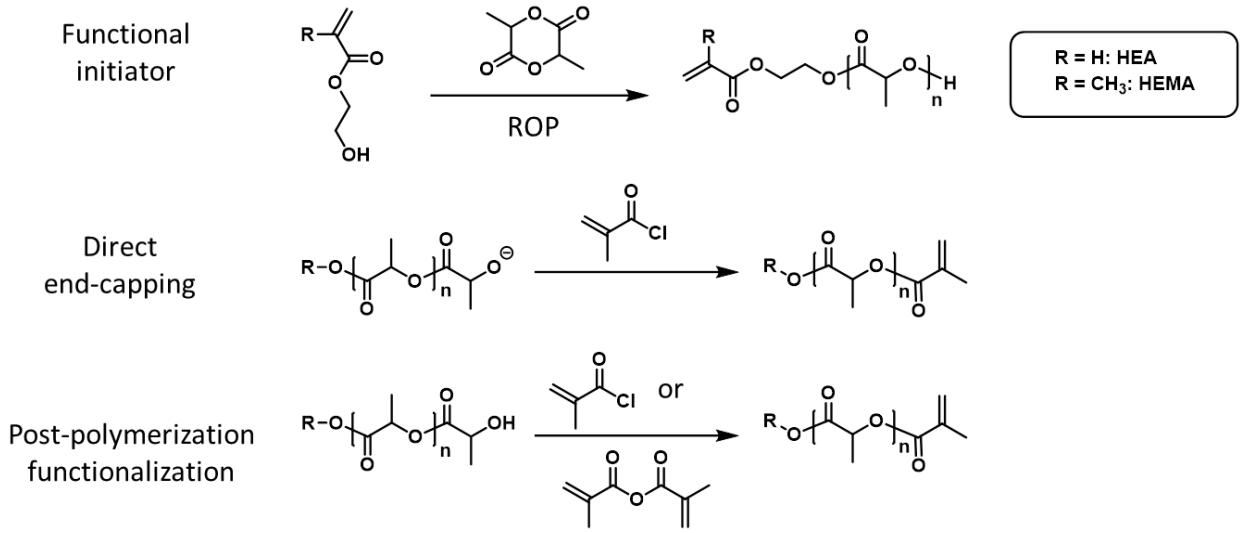

Scheme 2.1. Schematic representation of the general approaches for the preparation of PLA macromonomers *via* ROP of lactide initiated with a hydroxyl functional monomer or direct end capping and post-polymerization modification.

Polymer backbones comprising pendant hydroxyl groups can be utilized as initiators for the ROP of lactide in a grafting-from approach. For this purpose, a hydroxyl-functional monomer is polymerized *via* the RAFT technique first. Subsequently, the PLA side chains are grafted from the hydroxyl functionalities *via* ROP in the second step (**Figure 2.6**).[42-45] This approach enables the pre-adjustment of the DP of the polymer backbone, the DG of the final comb or graft copolymer as well as the distribution of the PLA side chains. Although, the most commonly used hydroxyl-functional monomers are HEA and HEMA,[42] other pendant groups such as epoxide[43] or ketal[44] moieties liberate two hydroxyl functionalities, which enables the synthesis of extremely dense comb polymers.

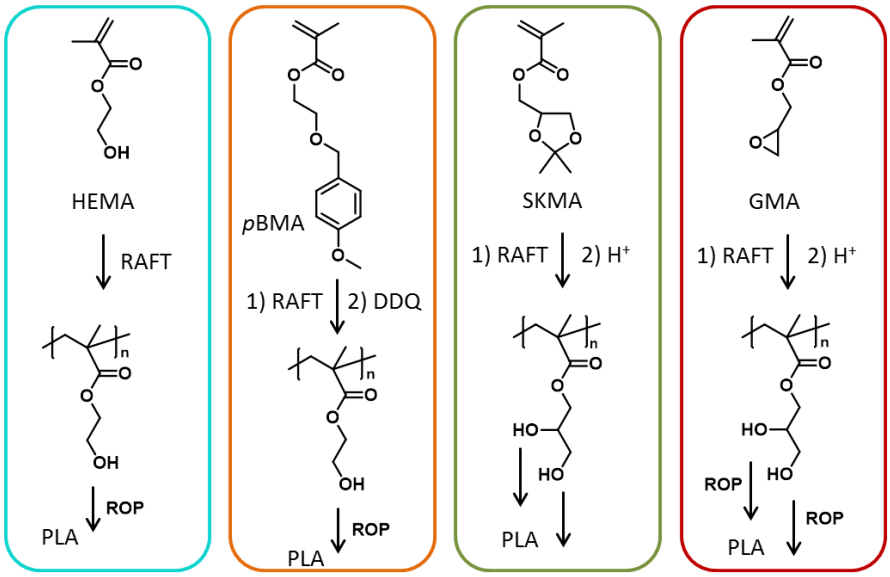

Figure 2.6. Schematic representation of the grafting approaches from hydroxy-functional polymer backbones; 2-(*p*-methoxybenzyloxy)ethyl methacrylate (*p*BMA), 2,3-dichloro-5,6-dicyanobenzoquinone (DDQ), solketal methacrylate (SKMA), glycidyl methacrylate (GMA).

A wide range of macromolecular architectures is accessible by the combination of ROP of lactide with RDRP techniques. Thereby, introduction of many functional groups to the PLA based copolymers is possible that would not be tolerated during the ROP process. The advantage of functional group tolerance is in particular of great importance for the ROP first approach. This fact also holds true for the end functionalization of PLA by post-polymerization methods. The preparation of block and comb type copolymers of PLA by the combination ROP and RAFT will be discussed polymerization in detail in **Chapters 5** and **6**, respectively.

3. End-functionalized polylactides

Parts of this chapter have been published **P2**) Julia Kötteritzsch, Stefan Bode, Ilknur Yildirim, Christine Weber, Martin D. Hager, Ulrich S. Schubert, Reversible oligomerization of 3-aryl-2-cyanothioacrylamides *via* [2_s + 4_s] cycloaddition to substituted 3,4-dihydro-*2H*-thiopyrans, *Des. Monomers Polym.* **2015**, *18*, 627–640. **P3**) Ilknur Yildirim, Sarah Crotty, Claas H. Loh, Grit Festag, Christine Weber, Pier-Francesco Caponi, Michael Gottschaldt, Matthias Westerhausen, Ulrich S. Schubert, End-functionalized polylactides using a calcium-based precatalyst: Synthesis and insights by mass spectrometry, *J. Polym. Sci., Part A: Polym. Chem.* **2016**, *54*, 437–448.

The ring opening polymerization (ROP) of lactide in the presence of functional initiators enables the synthesis of end-functionalized polylactides (PLAs) in a facile approach.[46, 47] However, the choice of the catalyst/co-initiator system for the ROP represents the crucial step in order to introduce the end functionality in an efficient manner and to control the polymerization process. Although there are some issues regarding the toxicity of $Sn(Oct)_2$, it is the most widely used catalyst for the ROP of lactide due to its high activity and ability to produce high molar mass PLA both in bulk and in solution.[5] In this chapter $Sn(Oct)_2$ will be employed to prepare an exemplary end-functional PLA for a reversible dimerization application where a potential toxicity of the catalyst used for the ROP is not crucial. However, the utilized catalyst/co-initiator system is important in particular for the further biological applications of the synthesized polymers. Therefore, *in situ* calcium alkoxide formation will be covered by utilizing a calcium based precursor complex ($Ca[N(SiMe_3)_2]_2(THF)_2$) with respect to the possibility to covalently attach a wide range of therapeutic molecules, targeting moieties, fluorescent probes or reactive groups to the PLA. The in-depth characterization of the obtained end-functional PLAs by mass spectrometry will be discussed as well to gain insights into the ROP mechanism.

2-Cyano-3-(3-((11-hydroxyundecyl)oxy)phenyl)prop-2-enethioamide was used as initiator for the $Sn(Oct)_2$ catalyzed ROP of L-lactide in order to prepare an thioamide end-functional PLA which can undergo reversible dimerization *via* hetero Diels-Alder reaction (**Scheme 3.1**).

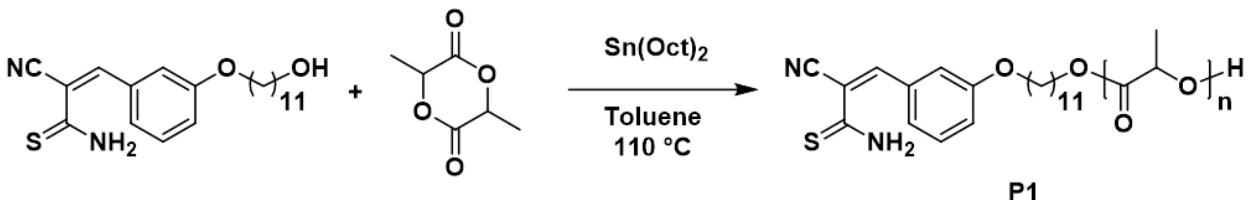

Scheme 3.1. Schematic representation of the synthesis of thioamide functional PLA by using $Sn(Oct)_2$ and 2-cyano-3-(3-((11-hydroxyundecyl)oxy)phenyl)prop-2-enethioamide.

The ROP of L-lactide was performed in toluene with a monomer concentration of 1.0 M at 110 °C ($[L\text{-lactide}]_0/[R\text{-OH}]_0$ = 15). Both matrix-assisted laser desorption/ionization (MALDI) and electrospray ionization (ESI) time-of-flight (ToF) mass spectra of **P1** (**Figure 3.1**) revealed a single distribution with a m/z difference of 144 Da between two neighboring peaks, which corresponds to the mass of one lactide monomer. This distribution can be assigned to sodiated PLA chains with the desired thioamide α-end and hydroxyl ω-end groups. The excellent agreement of calculated and measured isotopic patterns is shown in **Figure 3.1**. Although the utilized alcohol functional initiator also bears a thioamide functionality, which would interfere with the ROP mechanism, the thioamide functional PLA could be prepared successfully by careful adjustment of the polymerization conditions. The resulting end-functional PLA revealed reversible dimerization *via* hetero Diels-Alder reaction, which was proved by detailed size exclusion chromatography (SEC) investigations.

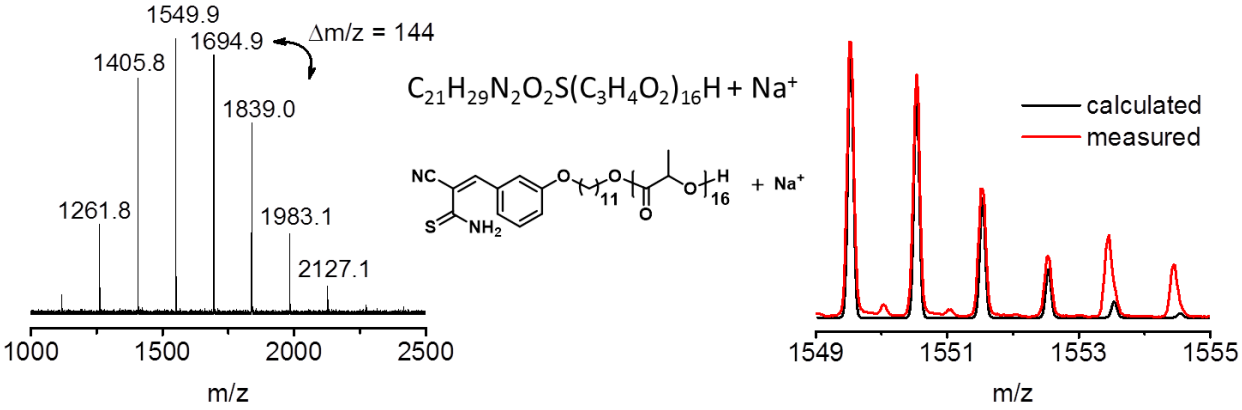

Figure 3.1. Left: MALDI-ToF mass spectrum (NaCl, DCTB) of **P1**. **Right:** Overlay of the calculated and measured isotopic patterns obtained from ESI-ToF-MS analysis.

In order to eliminate the contamination of the synthesized PLAs by the presence of any residual toxic catalysts, a calcium based complex was used for the ROP of L-lactide for the rest of the studies. The ROP of L-lactide was performed by employing $Ca[N(SiMe_3)_2]_2(THF)_2$ as the precursor complex for the *in situ* calcium alkoxide formation in THF at room temperature under nitrogen atmosphere (**Scheme 3.2**). In order to facilitate an accurate structural determination of the introduced PLA α-end groups, the ratio of [monomer] to [initiator] was set to 15 for all polymerizations ($[L\text{-lactide}]_0/[R\text{-OH}]_0/[Ca]_0$ = 15/1/0.5).

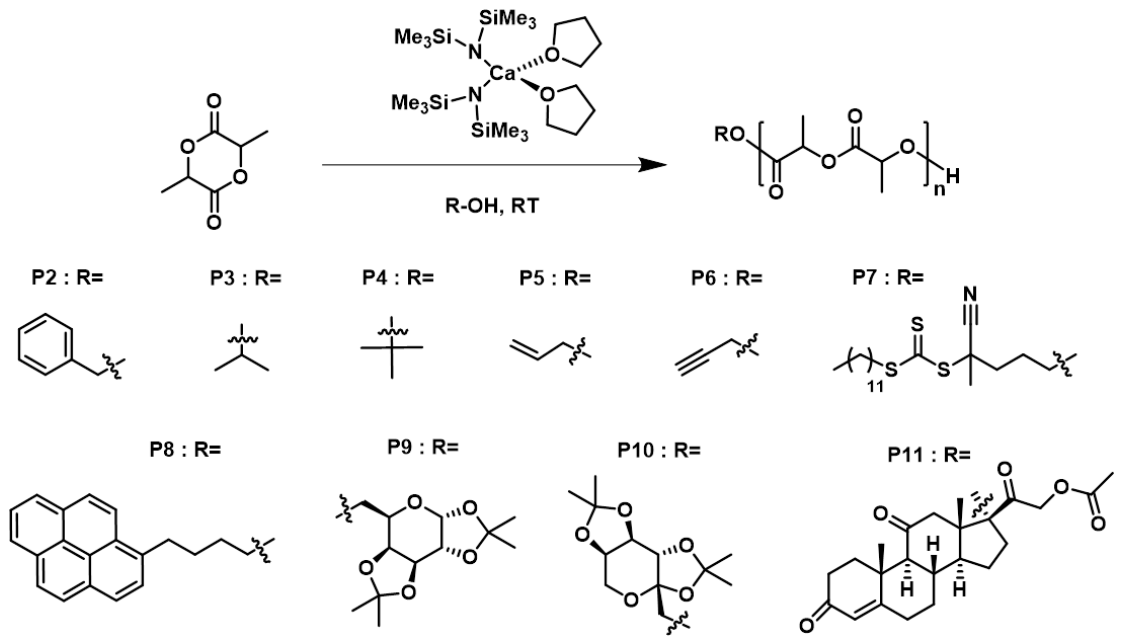

Scheme 3.2. Schematic representation of the synthesis of end-functional PLAs by using various alcohols and $Ca[N(SiMe_3)_2]_2(THF)_2$.

In order to exploit the versatility of the calcium alkoxide formation in the presence of primary and secondary alcohols, the ROP of L-lactide was carried out in the presence of benzyl alcohol (**P2**) and 2-propanol (**P3**). Although it is not common to utilize tertiary alcohols as ROP initiators, 2-methyl-2-propanol was utilized as a model tertiary alcohol as well (**P4**). After 10 minutes the monomer conversions were almost quantitative for **P2** and **P3**, whereas relatively lower (85%) for **P4** (**Table 3.1**). After purification, monomodal SEC traces with low dispersities ($Đ \leq 1.22$) were obtained for each polymer. The ^{1}H NMR spectra of the isolated polymers clearly revealed the covalent attachment of each alcohol. The molar masses calculated based on the integration of specific signals of the initiating groups and the methine protons of lactide ($M_{n,\,NMR}$) were very close to the theoretical values ($M_{n,\,theo.}$), suggesting a high initiation efficiency and the absence of chain transfer reactions during the polymerization process. **Table 3.1** summarizes the ROP conditions and characterization results of the obtained functional PLAs by means of SEC, ^{1}H NMR spectroscopy and mass spectrometry.

Table 3.1. Selected characterization results of the end-functionalized PLAs **P2** to **P11**.[a]

Entry	Initiator	Conv.[b] [%]	$M_{n,theo}$[c] [g mol^{-1}]	$M_{n,NMR}$[d] [g mol^{-1}]	$M_{n,SEC}$[e] [g mol^{-1}]	$Đ_{SEC}$[e]	$M_{n,MALDI}$[f] [g mol^{-1}]	$Đ_{MALDI}$[f]	$M_{n,ESI}$[g] [g mol^{-1}]	$Đ_{ESI}$[g]
P2	Benzyl alcohol	100	2,270	2,100	1,750	1.17	2,100			
P3	2-Propanol	95	2,110	2,000	1,950	1.22	1,900			
P4	2-Methyl-2-propanol	85	1,900	2,900	3,000	1.22			3,000	1.17
P5	Allyl alcohol	100	2,220	1,950	1,600	1.23	1,900	1.17		
P6	Propargyl alcohol	100	2,220	2,200	2,800	1.24			2,800	1.08
P7	CDP	100	2,550	2,700	2,300	1.18	2,400	1.07		
P8	1-Pyrenebutanol	100	2,440	2,600	2,800	1.25			3,000	1.08
P9	DIP-Gal	100	2,420	2,200	2,200	1.15	2,100	1.12		
P10	DIP-Fru	100	2,420	2,300	2,400	1.20	2,600	1.12		
P11	Cortisone-21-acetate	60	1,540	1,600	1,900	1.23			1,700	1.16

[a][L-lactide]$_0$/[R-OH]$_0$/[Ca]$_0$ = 15/1/0.5, [L-lactide]$_0$ = 1 M in THF, t_{pol} = 10 min, T = 25 °C; 4-cyano-4-[dodecylsulfanylthiocarbonyl)sulfanyl]pentanol (CDP), 1,2:3,4-Di-*O*-isopropylidene-α-D-galactopyranose (DIP-Gal), 2,3:4,5-Di-*O*-isopropylidene-β-D-fructopyranose (DIP-Fru). [b]Conversion values determined by ^{1}H NMR spectroscopy from the polymerization mixtures. [c]Number average molar mass (M_n) calculated according to $M_{n,theo}$ = [L-lactide]$_0$/[R-OH]$_0$ · conv. · 144.13 g mol^{-1} + $M_{(R-OH)}$. [d]Calculated from suitable signal integrals in the ^{1}H NMR spectra of the purified polymers. [e]Dispersity ($Đ$) determined by SEC (THF, RI detection, PLA calibration). [f]Determined by MALDI-ToF-MS analysis. [g]Determined by ESI-Q-ToF-MS analysis.

The end group fidelity of the PLAs was further confirmed by mass spectrometry (**Figure 3.2**). For the analysis of **P2** and **P3** MALDI-ToF technique was used**,** whereas ESI-ToF was utilized as an alternative technique for **P4**. The resulting spectra**,** revealed a single distribution of peaks spaced by Δm/z = 72, which corresponds to one lactic acid repeating unit **(Figure 3.2)**. The peak masses can be assigned to respective alcohol initiated PLA chains with ω-hydroxyl end groups, which are ionized with a silver (**P2** and **P3**) or sodium (**P4**) cation. Two minor distributions were also evident from the mass spectra of **P4**, which could not be assigned to initiation by water or to any cyclic products. **Figure 3.2** depicts the excellent agreement of the calculated and measured isotopic patterns for **P3** and **P4**.

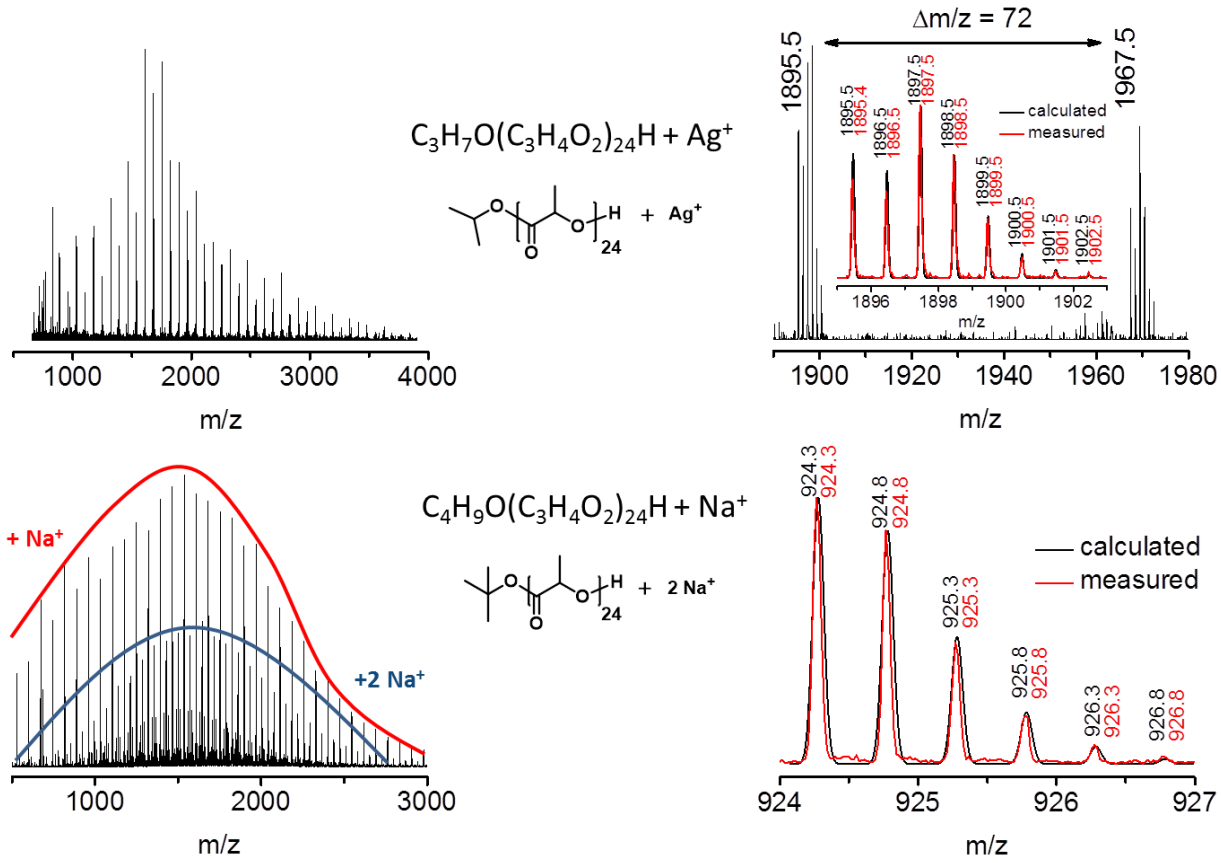

Figure 3.2. Top: Full and zoomed-in view of the MALDI-ToF mass spectrum of **P3** together with overlay of the calculated and experimental patterns. **Bottom:** ESI-ToF mass spectrum of **P4** together with overlay of the calculated and measured isotopic patterns.

The use of primary alcohol bearing initiators enabled the synthesis of PLAs in a more efficient manner. Therefore, we utilized several primary alcohols to introduce different functionalities to PLA which could be useful either for biomedical applications or for further functionalization. In order to obtain PLAs with unsaturated end functionality that can be further functionalized *via* azide-alkyne or thiol-ene click reactions allyl alcohol (**P5**) and propargyl alcohol (**P6**) were used as initiating alcohols.[48] Additionally, CDP, a hydroxyl functionalized trithiocarbonate chain transfer agent (CTA), was utilized as an initiator, yielding a PLA based a macro-CTA (**P7**). The covalent attachment of allyl alcohol, propargyl alcohol and CDP was ensured by ^{1}H NMR analysis of the isolated PLAs (**Figure 3.3**). SEC analysis revealed monomodal mass distributions with relatively low dispersities for both polymers (**Table 3.1**). The end-functionality of **P5-P7** was further confirmed by mass spectrometry. The mass spectra revealed a single distribution with a repeating unit of m/z = 72 which can be assign to the expected PLA chains with allyl, propargyl, and CDP as the initiating groups, respectively. The CDP end-functional PLA was further utilized for the synthesis of block copolymers, which is described in **Chapter 5** in detail.

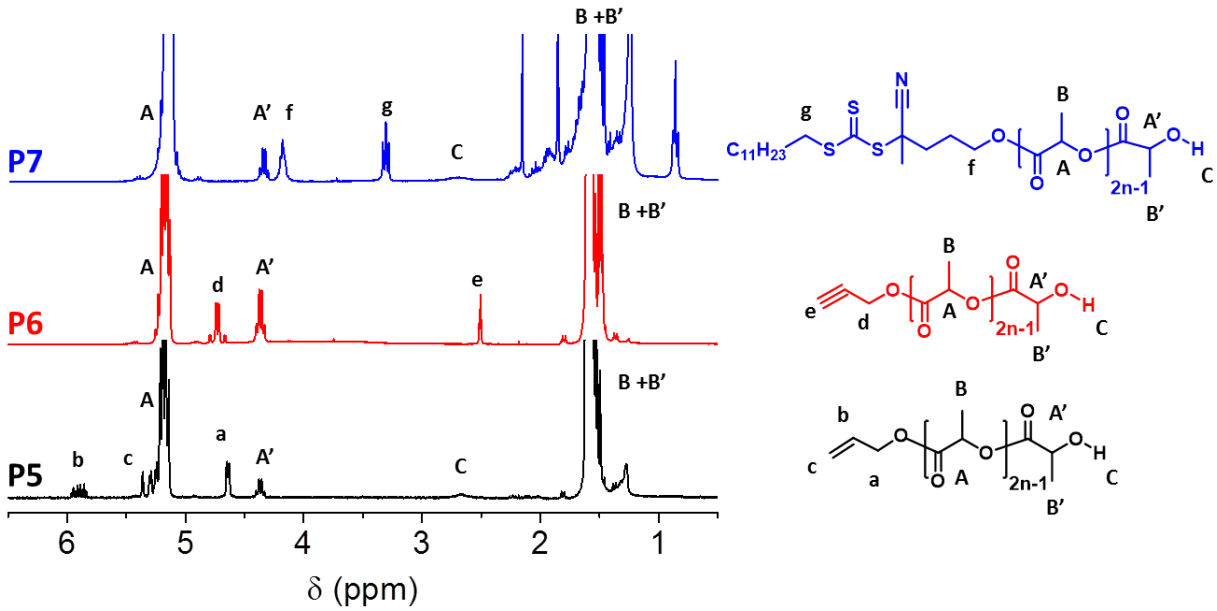

Figure 3.3. Overlay of ^{1}H NMR spectra of **P5** to **P7** and structural assignment of the observed peaks.

Since PLA is commonly utilized in the biomedical field, functionalization with a fluorescent label is very useful for cellular uptake studies.[49] For this purpose, 1-pyrenebutanol was employed as initiator for the ROP of L-lactide. ^{1}H NMR analysis of the isolated PLA (**P8**) confirmed the covalently attachment of 1-pyrenebutanol. The use of fluorescent pyrene functional PLA for cellular uptake studies of PLA based comb polymers is described in **Chapter 6**.

Saccharide polymer conjugates are of high interest for site specific targeted drug delivery and for cell recognition studies.[50] In order to prevent multiple initiations from one sugar molecule isopropylidene protected galactose (DIP-Gal) and fructose (DIP-Fru) were employed as ROP initiators. The end-group fidelity of the isolated PLAs was confirmed by ^{1}H NMR spectroscopy and mass spectrometry analysis. The experimental isotopic pattern obtained by MALDI-ToF-MS analysis corresponds exactly to the theoretical values for the expected isotopes, demonstrating the successful end-functionalization of PLA with the protected saccharides (**Figure 3.4**).

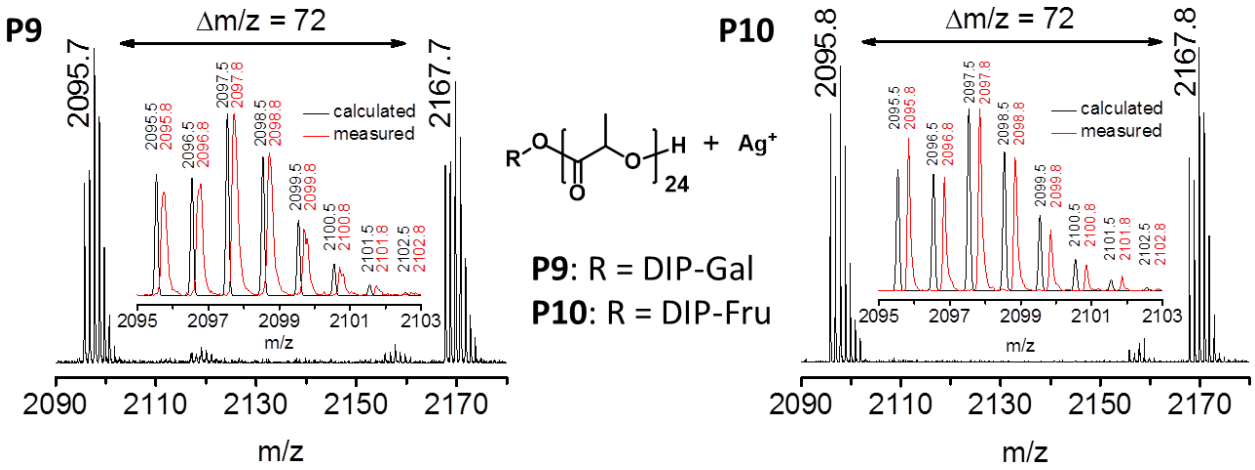

Figure 3.4. MALDI-ToF mass spectrum of **P9** and **P10** together with overlay of the calculated and measured isotopic patterns.

Cortisone-21-acetate is a topical corticosteroid and is used in the treatment of inflammatory diseases.[51] PLA-cortisone conjugate could be advantageous for targeted drug delivery to the site of inflammation. When compared to the other alcohols described above, the use of cortisone-21-acetate as an initiator resulted in lower monomer conversion (80%). However, the covalent attachment of cortisone to the PLA was evidenced by ^{1}H NMR spectroscopy and ESI-ToF-MS analysis. The singly charged region of the ESI-ToF mass spectrum of **P11** (**Figure 3.5**) reveals the presence of two main distributions with Δm/z = 144. Both distributions correspond to the masses expected for the PLA chains which bear cortisone-21-acetate at the α-end group either with an even (distribution **B** in **Figure 3.5**) or uneven (distribution **A** in **Figure 3.5**) number of lactic acid repeating units.

Since the mass of one lactide monomer corresponds to 144 Da, upon addition of one lactide monomer to the growing PLA chain, one would expect a Δm/z = 144 in the mass spectra. However, all the mass spectra discussed above revealed a distribution of peaks spaced by regular intervals of 72 Da except when cortisone-21-acetate is used as initiator. The easiest explanation for the occurrence of Δm/z = 72 in the mass spectra would be an in-source fragmentation taking place during the measurements. For this reason, during MALDI-ToF-MS analysis several measurement conditions were tested by utilizing different salts during sample preparation. The tested salts induced fragmentation of the PLA except AgTFA, while the Δm/z remained 72.

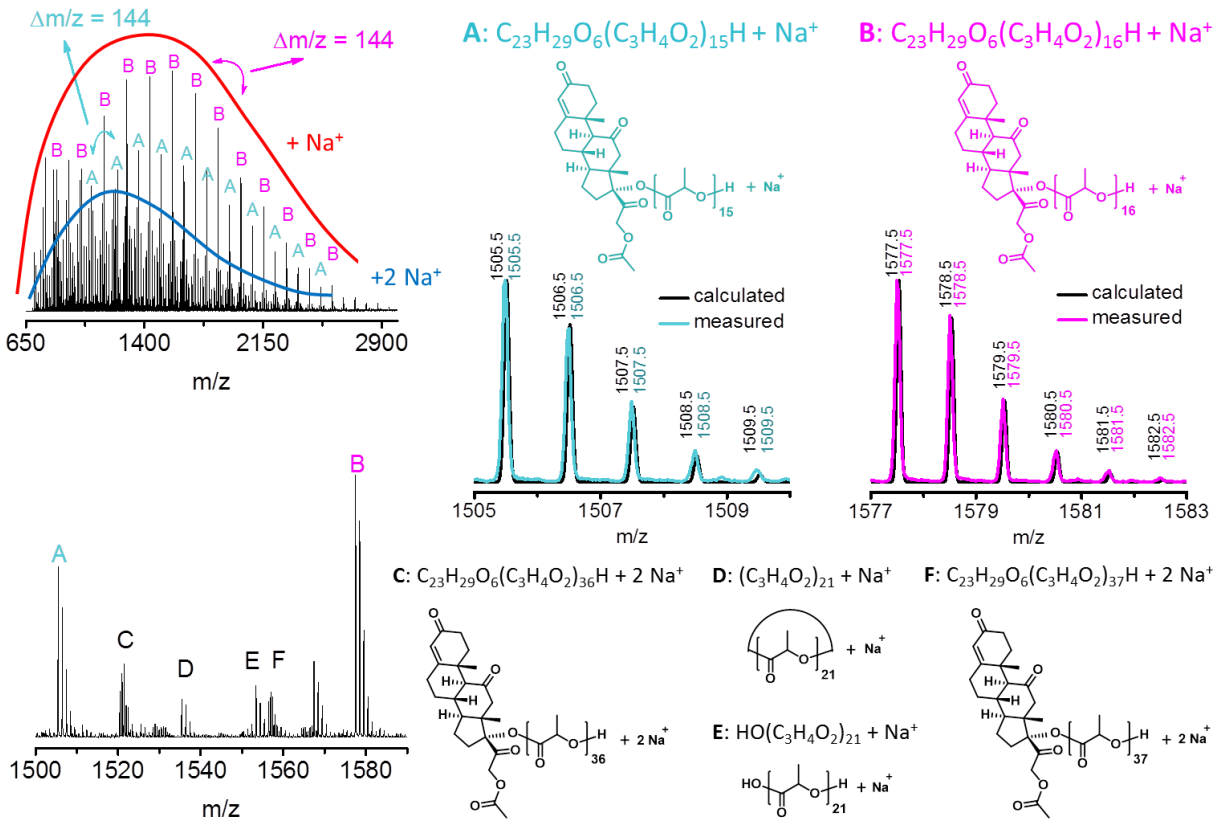

Figure 3.5. ESI-ToF mass spectra and overlay of calculated and measured isotopic patterns for the structural assignment of the observed peaks of **P11**.

The most common explanation in literature for the observed Δm/z of 72 in the mass spectra of PLA is the occurrence of transesterification reactions, where usually the relative abundance of the PLA chains with odd number of repeating units is lower than the ones which possess even number of repeating units.[52-55] An intramolecular chain transfer also results in formation of cyclic PLA and PLA chains with lower degree of polymerization (DP).[5] However, cyclic species were not observed in any of the discussed mass spectra except for **P11**. The end groups of the intermolecular transesterification products do not differ from those of the initial PLA chains. Therefore, analysis by mass spectrometry alone is not sufficient enough to judge the presence of intermolecular transesterification products.

One would expect transesterification especially towards the end of the polymerization resulting in significantly increased dispersity at high monomer conversion.[56] For this reason, kinetic studies were performed employing benzyl alcohol, DIP-Gal and DIP-Fru as initiators (**Figure 3.6**). SEC analysis revealed that the molar mass was increasing in a linear fashion with increasing monomer conversion, whereas *Đ* remained constant or even slightly decreased. Due to

temperature increase at the early stages of the polymerization a fast propagation was observed, then the polymerization rate decreased significantly (**Figure 3.6**).

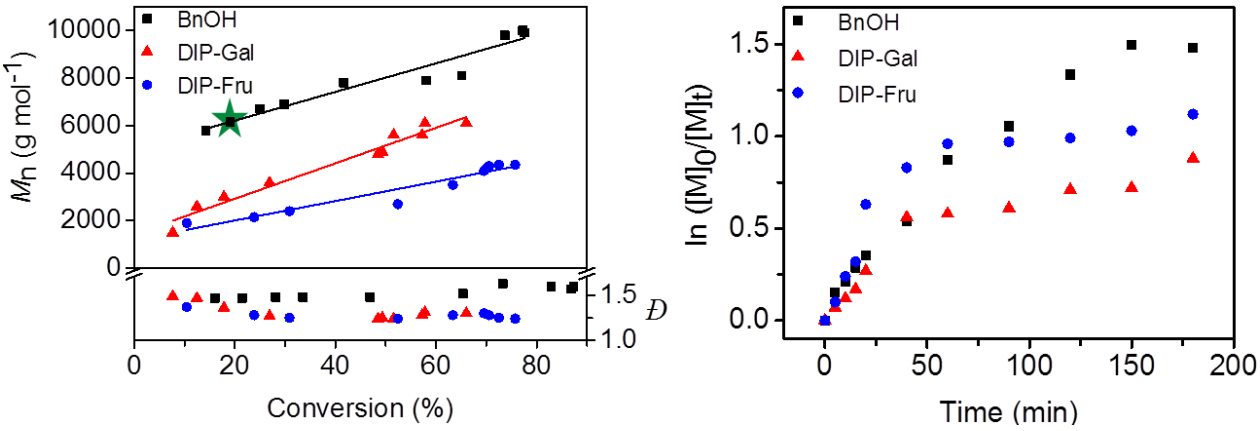

Figure 3.6. Kinetic studies performed at room temperature in THF with a total monomer concentration of 1 mol L^{-1}. $[M]_0/[R\text{-}OH]_0/[Ca]_0$ = 100/1/0.5. **Left:** Dependence of $M_{n,SEC}$ and $Đ$ of the obtained PLA on L-lactide conversion. ★ indicates the sample analyzed by MALDI-ToF-MS in comparison with **P2. Right:** Semilogarithmic kinetic plots.

Figure 3.7 shows a MALDI-ToF mass spectrum obtained from the sample taken at a very early stage of the polymerization (t = 10 min) in the presence of benzyl alcohol at 18% monomer conversion in direct comparison with the spectrum of **P2** (quantitative conversion). If the Δm/z of 72 in the mass spectra was caused by an intramolecular chain transfer reaction the relative abundance of the peaks associated with an odd number of repeating units should increase with monomer conversion.[57] However, both spectra almost match each other, revealing a single distribution with Δm/z = 72 that can be assigned to alcohol initiated and hydroxyl terminated PLA chains.

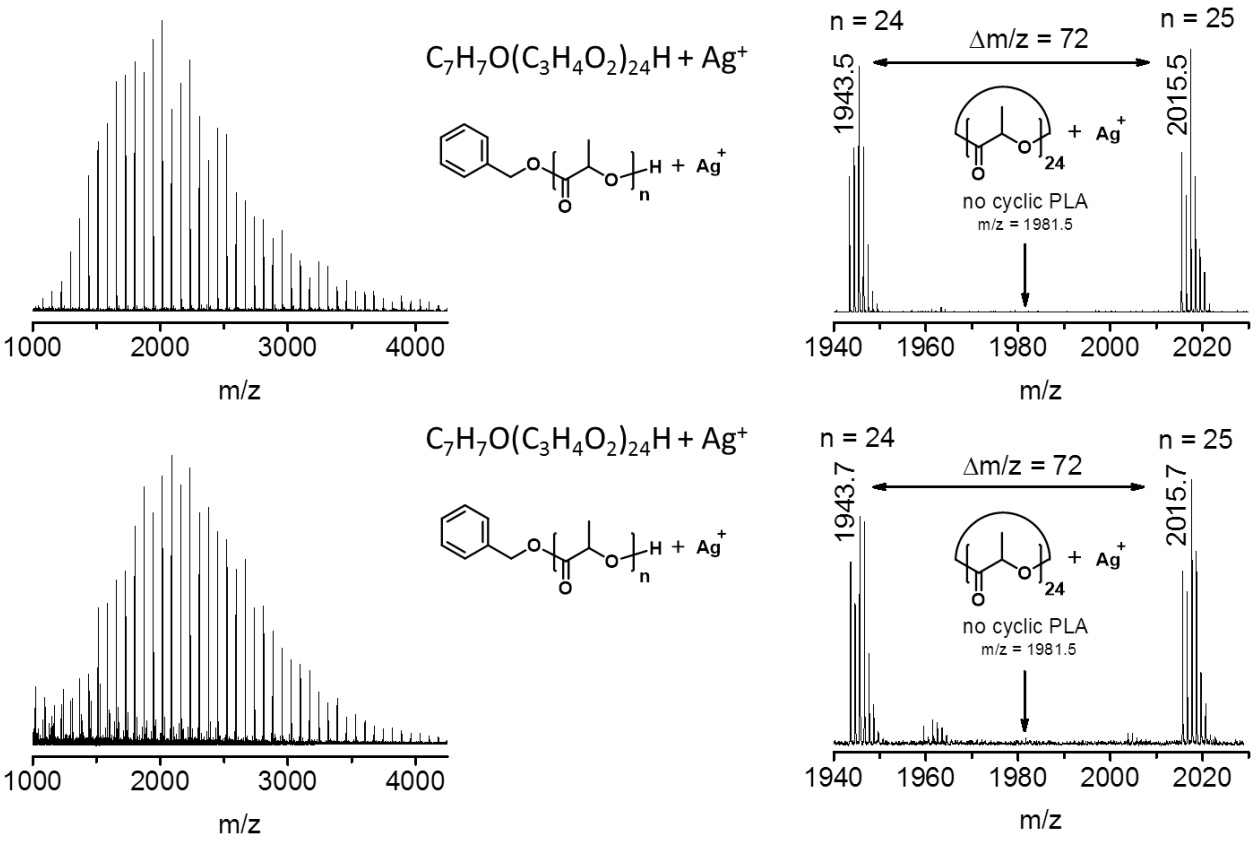

Figure 3.7. Full and zoomed-in view MALDI-ToF mass spectra (AgTFA, DCTB) of benzyl alcohol initiated PLAs. **Top:** The mass spectrum of **P2** with quantitative conversion. **Bottom:** The mass spectra of the sample taken from polymerization mixture during kinetic study at 10 min with 18% monomer conversion.

An alternative explanation for the odd number of repeating units could be the possible coordination of more than one alkoxide to one calcium atom during the ROP in the presence of $Ca[N(SiMe_3)_2]_2(THF)_2$.[58] However, the exact structure and the number of THF ligands of the calcium complex during polymerization are not known yet. A proposed mechanism is shown in **Scheme 3.3.** After opening of the lactide monomer, the newly formed alkoxide species remains coordinated on the calcium. However, further nucleophilic attack to the carbonyl oxygen of the already opened lactide monomer is possible *via* formation of a 5-membered ring. This would indeed result in a "splitting" of the lactic acid dimer yielding a homoleptic $Ca(O\text{-}CH(Me)\text{-}COOR)_2$. If this intramolecular ester cleavage proceeded throughout the entire polymerization, PLA chains would form with both even and odd numbers of repeating units in an equal ratio, independent from the monomer conversion.

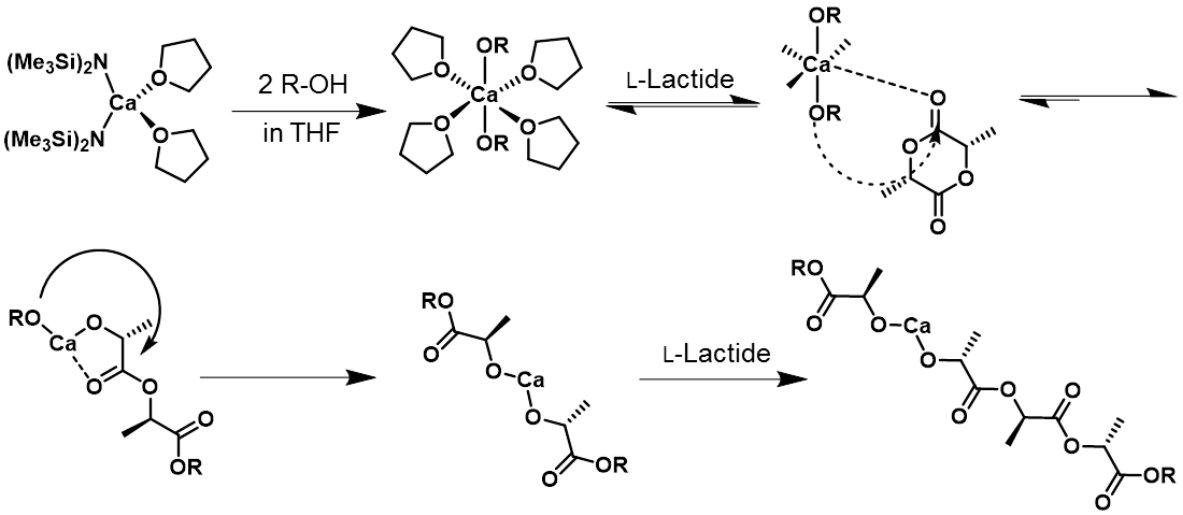

Scheme 3.3. Schematic representation of the ring opening of lactide by $Ca(OR)_2$ and subsequent intramolecular ester cleavage by the second alcoholate anion yielding a homoleptic complex that would lead to an uneven number of repeating units in the PLA chain.

In summary, the ROP of lactide in the presence of both $Sn(Oct)_2$ and $Ca[N(SiMe_3)_2]_2(THF)_2$ gave access to well-defined end-functional PLAs. In particular the utilized calcium based precatalyst enabled the functionalization of PLA with a range of primary, secondary and tertiary alcohols. The mass spectrometry techniques not only allowed the in-depth characterization of the end-functional PLAs, but also provided fundamental information regarding the ROP mechanism. The following chapter will concentrate on the exploitation of the very potent *in situ* calcium alkoxide formation for the possibility to obtain PLA-conjugates in the presence of (sensitive) biologically active alcohol initiators.

4. Bioactive compounds as ROP initiators

Parts of this chapter will be published **P4**) Ilknur Yildirim, Turgay Yildirim, Diana Kalden, Grit Festag, Nicole Fritz, Christine Weber, Stephanie Schubert, Matthias Westerhausen, Ulrich S. Schubert, Retinol initiated poly(lactide)s: Stability upon polymerization and nanoparticle preparation, *Polym. Chem.* **2017**, *8*, 4378–4387. Adrian T. Press, Anja Traeger, Ilknur Yildirim, Christine Weber, Michael Bauer, Ulrich S. Schubert (manuscript in preparation, first results).

The term "retinoid" refers to metabolites and biosynthetic analogues (precursors) of Vitamin A.[59] These include retinol (the main form of Vitamin A), retinal and retinoic acid. Retinoids have vital involvement in many biological processes, including the visual cycle[60] and during cell proliferation/differentiation.[61, 62] They are used as potential chemopreventive/ chemotherapeutic agents (Vesanoid®, Targretin®) and for the treatment of a number of dermatological disorders (Roaccutane®, Soriatane®).[59, 63] However, retinoids suffer from low aqueous solubility and chemical instability especially in the presence of light and oxygen,[64] which results in partial or total loss of bioactivity.[65, 66] The possible degradation products include epoxides, bis-epoxides, endoperoxides, dioxetanes, furans as well as compounds resulting from the cleavage of the conjugated polyene chain such as varying aldehydes.[67, 68] As a consequence, they represent appealing candidates for polymer conjugation to enhance their bioavailability and chemical stability.[69, 70] The utilization of bioactive molecules as initiators for the ring opening polymerization (ROP) of lactide is a common technique which represents an efficient way to obtain quantitatively functionalized polylactide (PLA) as a rate controlling matrix and to overcome the drawbacks of drug loaded polymeric nanocarriers.[71]

Since the *in situ* calcium alkoxide formation presented in **Chapter 3** provided an effective and highly versatile platform for the preparation of PLAs under mild conditions in the presence of various alcohol initiators, all-*trans*-retinol was applied as an initiator (**Scheme 4.1**). Based on our previous studies utilizing the precursor $Ca[N(SiMe_3)_2]_2(THF)_2$, all polymerizations were performed in THF at room temperature ($[retinol]_0/[Ca]_0 = 1/0.5$). Due to the instability of retinol, the polymerizations were conducted under dim illumination.

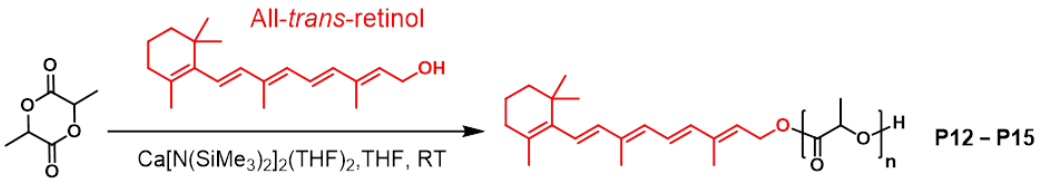

Scheme 4.1. Schematic representation of the ROP of L-lactide using $Ca[N(SiMe_3)_2]_2(THF)_2$ as precatalyst and all-*trans*-retinol as initiator by *in situ* calcium-alkoxide formation.

A kinetic study of the ROP of L-lactide was performed in the presence of retinol in order to understand if retinol can act as an efficient co-initiator ($[L\text{-lactide}]_0/[retinol]_0/[Ca]_0$ = 100/1/0.5, $[L\text{-lactide}]_0$ = 1 M). **Figure 4.1** depicts the semilogarithmic kinetic plot, which clearly reveals that an induction period is not observed. The first kinetic sample obtained after 1 minute already revealed a conversion of ≈ 55%, which is fairly high compared to a total conversion of ≈ 85% obtained after 25 minutes. Monomodal mass distributions were obtained from SEC analysis of the kinetic samples throughout the whole polymerization process. The overlapping SEC traces recorded with RI and UV (λ = 340 nm) detection indicate the covalent attachment of the retinol moiety and the (partial) preservation of the conjugated retinoid structure as well. The molar mass increased in a linear fashion with increasing monomer conversion. Moreover, during the course of the kinetic study, dispersity slightly decreased ($1.23 \leq Đ \leq 1.42$), indicating that the molar mass of the PLA can be well controlled with the utilized initiator/catalyst system.

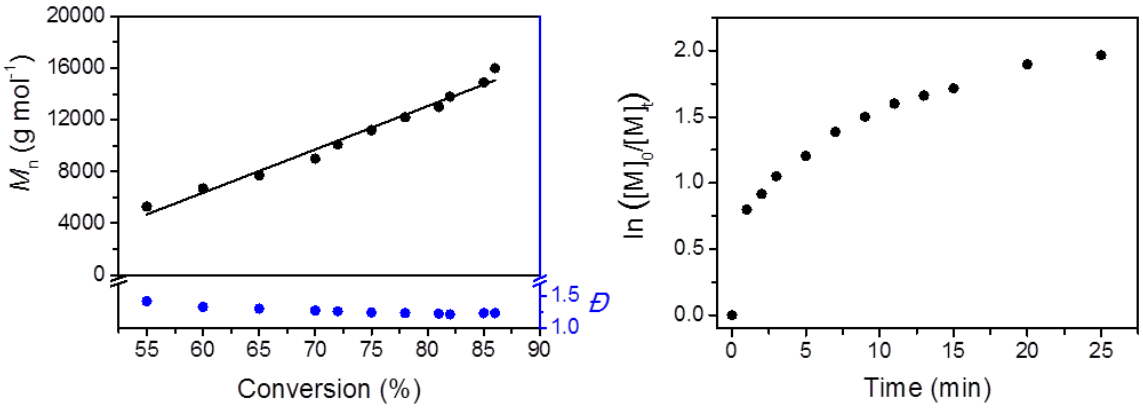

Figure 4.1. Kinetic study of retinol initiated ROP of L-lactide performed at room temperature in THF with a total monomer concentration of 1 mol L^{-1}. $[L\text{-lactide}]_0/[retinol]_0/[Ca]_0$ = 100/1/0.5. **Left:** Dependence of $M_{n,SEC}$ and $Đ$ of the obtained PLA on the conversion of L-lactide. **Right:** Semilogarithmic kinetic plot.

An oligomeric PLA (DP = 13) was synthesized (**P12**) in order to facilitate an accurate structural determination of the PLA α-end groups. The covalent attachment of retinol was evidenced by ^1H NMR analysis of the isolated **P12**. The molar mass ($M_{n,\ NMR}$) calculated by comparing the

characteristic conjugated double bond signals with methine protons of PLA is very close to the theoretical value ($M_{n,\,theo}$) which hints towards a high initiation efficiency and the preservation of the retinyl moiety. Since the UV/vis absorption spectrum of **P12** exactly overlaps with the spectrum of all-*trans*-retinol, it can be assumed that no isomerization or aggregation of the retinyl moiety took place. The SEC traces obtained with RI and UV/vis detection overlap as well, verifying the covalent attachment of the retinol and hinting towards the absence of chain transfer reactions during the ROP (**Figure 4.2**).

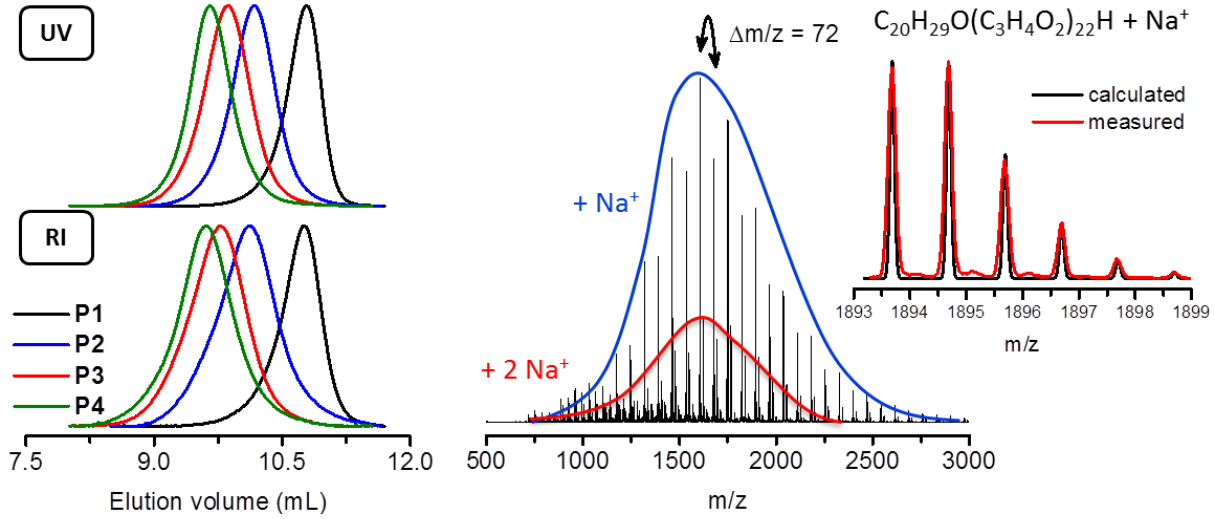

Figure 4.2. Left: Overlay of the normalized SEC traces (THF) of isolated PLAs with RI and UV (λ = 340 nm) detection. **Right:** ESI-ToF mass spectrum with an overlay of calculated and measured isotopic patterns for the structural assignment of the observed peaks for **P12**.

The matrix-assisted laser desorption/ionization time-of-flight (MALDI-ToF) mass spectrum of **P12** revealed a single distribution of peaks spaced by Δm/z = 72 and the obtained molar mass ($M_{n,\,MALDI}$) was in a good agreement with the molar masses obtained *via* NMR and SEC analysis (**Table 4.1**). However, the retinyl end group cleavage was evident from the mass spectrum which could have occurred due to the pulse laser irradiation during the measurement (at 337 nm). For this reason, electrospray ionization (ESI) ToF-MS analysis was utilized as an alternative technique for further studies since it did not induce fragmentation of the retinyl moiety. **Figure 4.2** depicts the ESI-ToF mass spectrum of **P12**, which clearly shows the presence of a single distribution of peaks with a m/z difference of 72 between two neighboring peaks. The main peak series can be assigned to sodiated PLA chains which bear α- retinol and ω- hydroxyl end groups, which is also evident from the excellent agreement of the calculated and measured isotopic patterns.

ESI MS/MS analysis of **P12** enables to assure the absence of isobaric species without a retinyl moiety conjugated to the PLA. For this reason, the selected precursor ion (m/z = 1893.7, $C_{20}H_{29}O(C_3H_4O_2)_{22}H + Na^+$) was fragmented by applying different collision energy values ranging from 50 to 160 eV. The MS/MS spectrum recorded at 50 eV reveals the precursor ion together with a fragment ion at m/z = 1625.5 corresponding to the loss of the retinyl unit (268 u) due to α-end group cleavage (**Figure 4.3**). An additional fragmentation series was observed when the applied collision energy was increased to 120 eV, which should arise through Mc-Lafferty-like rearrangements involving the migration of the hydrogen atom from a pendant methyl group to the oxygen atom of the carbonyl group of the ester moiety (**Figure 4.3**, turquoise species).[72, 73]

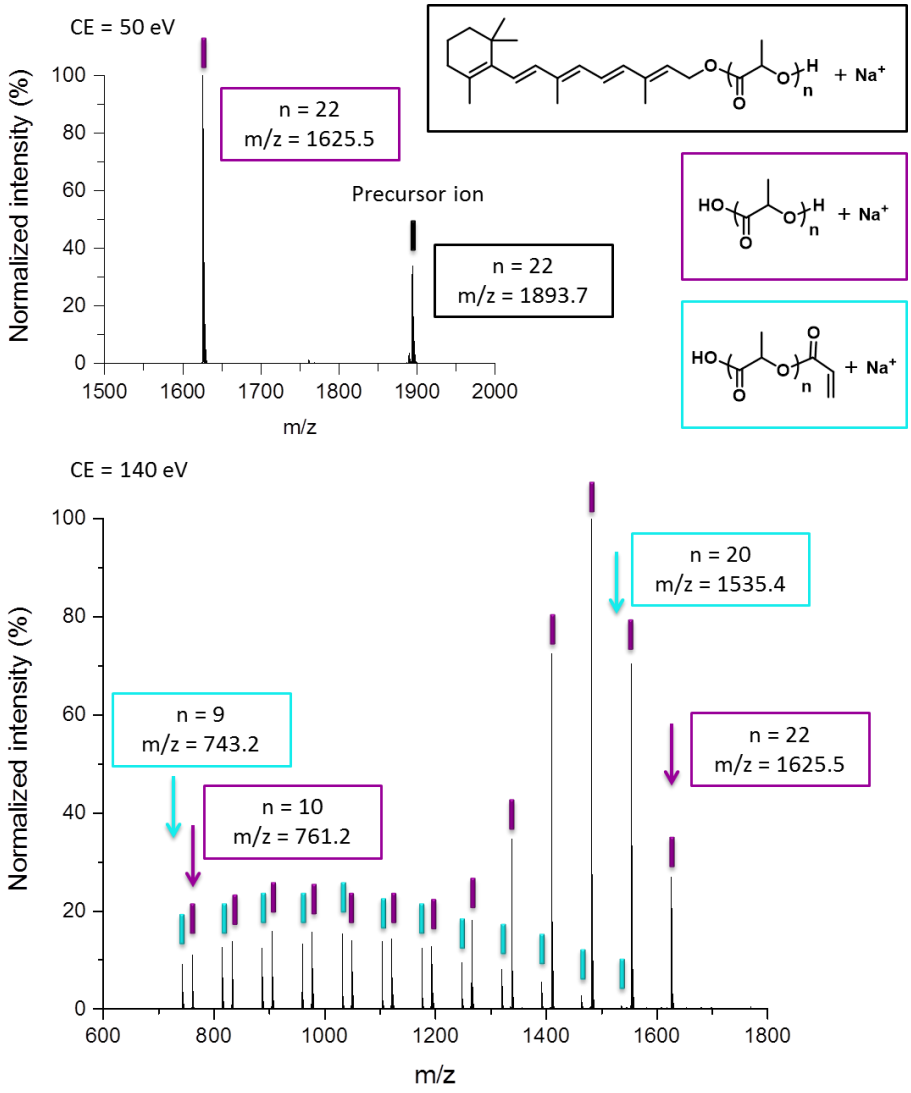

Figure 4.3. ESI-ToF MS/MS spectra of **P12** recorded at different collision energy values together with the structural assignment of the observed peaks. **Top:** The spectrum recorded at 50 eV. **Bottom:** The spectrum recorded at 140 eV.

Retinol initiated PLAs with higher molar masses (**P13** to **P15**) were prepared after confirming the covalent attachment of all-*trans*-retinol and the preservation of its structure by an in-depth characterization of **P12**. SEC and ^{1}H NMR analysis of the isolated polymers revealed that end-functionalization is still efficient and the molar mass can be controlled by the polymerization method employed. **Table 4.1** summarizes the characterization results of the obtained PLA-retinol conjugates (**P12** to **P15**).

Table 4.1. Selected characterization data of the polymers **P12** to **P15**.[a]

Entry	[L-lactide]$_0$/[retinol]$_0$/[Ca]$_0$	$M_{n,theo}$[b] [g mol^{-1}]	$M_{n,NMR}$[c] [g mol^{-1}]	$M_{n,SEC}$[d] [g mol^{-1}]	$Đ_{SEC}$[d]	$M_{n,MALDI}$[e] [g mol^{-1}]	$Đ_{MALDI}$[e]	Method[f]	Z-ave.[g] [d, nm]	PDI[g]
P12	13/1/0.5	2,160	2,000	1,800	1.15	2,200	1.10	AW	105 ± 2	0.21 ± 0.01
								WA	174 ± 1	0.03 ± 0.01
P13	30/1/0.5	4,600	4,500	3,700	1.24	3,600	1.11	AW	100 ± 1	0.17 ± 0.05
								WA	249 ± 8	0.21 ± 0.05
P14	40/1/0.5	6,050	6,100	5,900	1.25	4,400	1.09	AW	133 ± 4	0.29 ± 0.02
								WA	217 ± 6	0.28 ± 0.05
P15	60/1/0.5	8,900	7,900	7,000	1.28	4,700	1.10	AW	115 ± 3	0.24 ± 0.02
								WA	237 ± 9	0.22 ± 0.03

[a][L-lactide]$_0$ = 1 M in THF, T = 25 °C, conversion values determined by ^{1}H NMR spectroscopy from the polymerization mixtures and found to be quantitative. [b]Number average molar mass (M_n) calculated according to $M_{n,theo}$ = [L-lactide]$_0$/[retinol]$_0$·conv.·144.13 g mol^{-1} + M(retinol). [c]Calculated from suitable signal integrals in the ^{1}H NMR spectra of the purified polymers. [d]Dispersity index ($Đ$) determined by SEC (THF, RI detection, PLA calibration). [e]Determined by MALDI-ToF-MS analysis. [f]AW, dropping acetone to water; WA, dropping water to acetone. [g]Average values of three DLS measurements.

The nanoprecipitation method was utilized to prepare nanoparticles from the synthesized PLA-retinol conjugates, yielding nanoparticles with monomodal size distributions with relatively low polydispersity (PDI) values. A minor amount of aggregate formation was observed only for **P12**, which could be eliminated by filtration. **Figure 4.4** depicts a SEM image obtained from **P12** which clearly shows uniform spherical nanoparticles with size values in agreement with the DLS data. Furthermore, there was no evidence of crystal formation which would occur in the presence of unbound retinol.[70] According to DLS measurements, which were performed over the course of three months, the colloidal stability of the nanoparticles in aqueous suspension was very good, making the nanoparticles suitable for further investigations on the stability of the PLA-retinol conjugates.

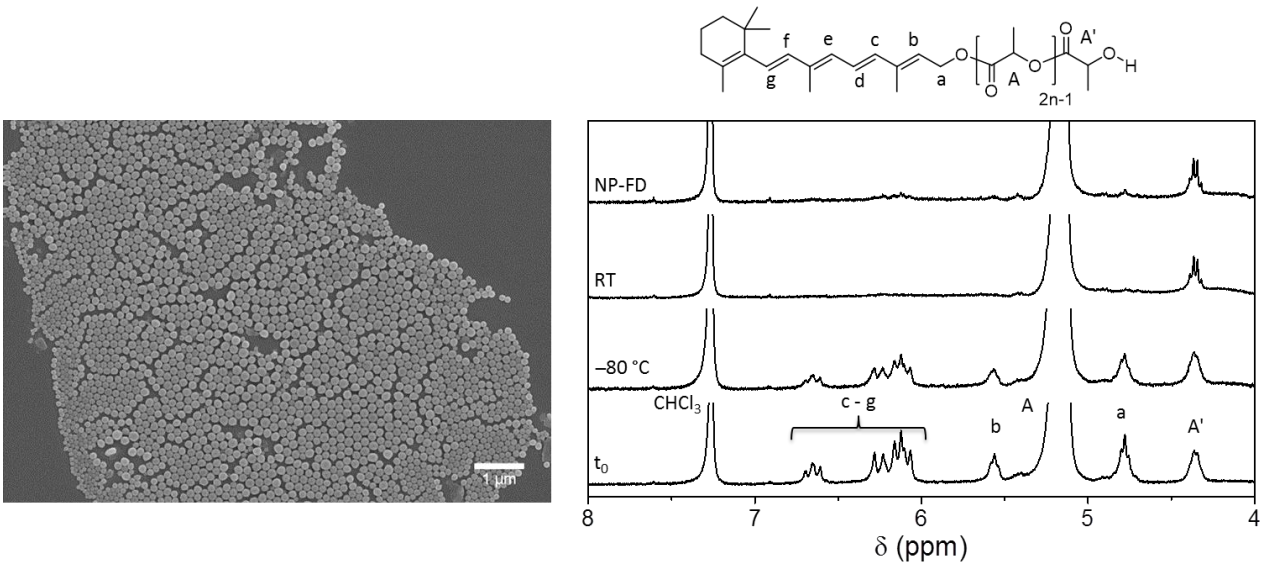

Figure 4.4. Left: SEM image of the nanoparticles obtained from **P15** with the WA method. **Right:** Overlay of the ^{1}H NMR spectra of **P12** (t_0 and different storage conditions for 15 days; RT and –80 °C), and the corresponding freeze-dried NP after storage at room temperature for 15 days.

Storage stability studies were performed in order to investigate if the PLA could shield the retinyl moiety and prevent its degradation. Therefore, **P12** and its nanoparticle suspension were kept at ambient conditions and analyzed periodically by NMR, SEC, UV/vis spectroscopy as well as ESI-MS. A sample stored in the dark at –80 °C served as control. The **P12** nanoparticle suspension was freeze-dried after 15 days to enable a more straightforward analysis of the final sample. As evident from the overlay of the final ^{1}H NMR spectra recorded after 15 days, the conjugated structure of retinol is almost completely preserved when **P12** is stored at –80 °C. However, upon storage of **P12** (bulk and nanoparticulate form) at room temperature all peaks originating from the conjugated double bonds (peaks "b" to "g") vanished revealing that the retinol moieties are (almost) completely degraded.

The decrease of the according peak integrals of retinyl moiety during course of storage stability study is shown in **Figure 4.5**. In accordance with the decrease in absorbance at 340 nm as monitored by UV/vis spectroscopy, it can be clearly seen that the major fraction of the retinoid is affected already after three days of storage. However, a slightly increased stability at ambient conditions can be suggested when the aqueous suspension is compared to bulk **P12**.

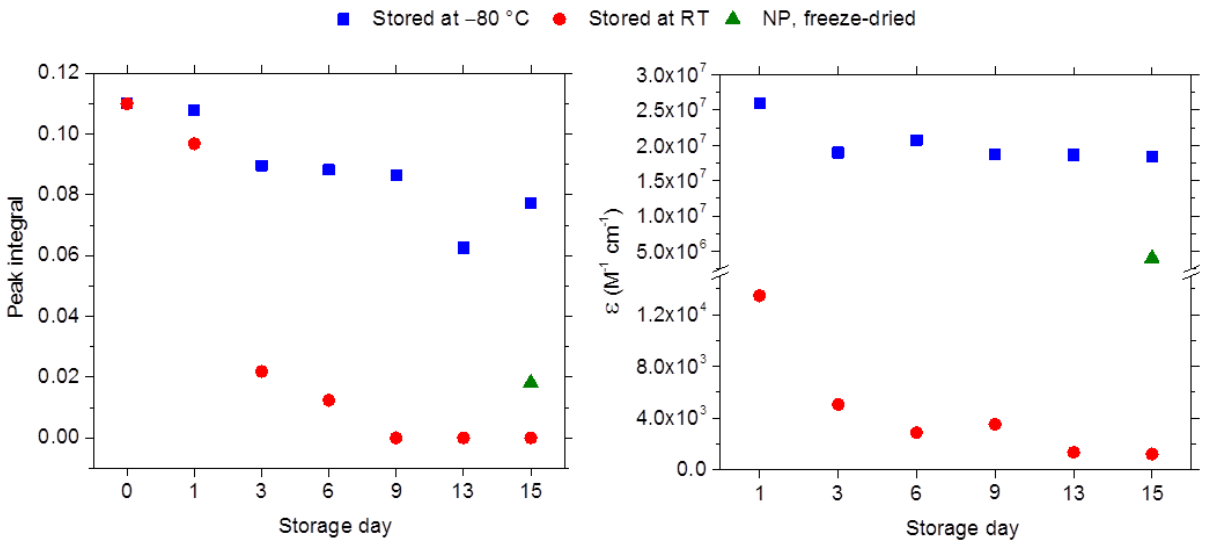

Figure 4.5. Left: Change in peak integrals assigned to retinyl moieties at 5.9 to 6.4 ppm in the ^{1}H NMR spectra. **Right:** Molar extinction coefficients at 340 nm measured by UV/vis absorption spectroscopy over 15 days.

Due to practical reasons only the freeze-dried nanoparticle suspension obtained from **P12** was investigated by UV/vis absorption spectroscopy. Nevertheless, SEC analysis of nanoparticle suspension with UV detection filled the missing absorption data, since the SEC measurements could be performed directly from the aqueous suspension by mixing with the SEC eluent THF (NP suspension/THF = 5/95 (v/v)). Supporting the results discussed before, the degradation of the retinoid structure seemed to be slightly decelerated in nanoparticle suspension when compared to bulk **P12** stored at the same conditions. The UV absorbance at 340 nm was significantly decreased for most of the samples. While none of the SEC traces recorded with UV detection revealed any broadening upon storage, conversely the RI detection indicated that coupling reactions took place between PLA chains without an intact all-*trans*-retinyl moiety. It can be clearly seen from **Figure 4.6** that molar mass and dispersity increase upon elongated storage as the occurrence of coupled PLA chains became more pronounced. In line with the previous results, storage at –80 °C significantly suppressed the side reactions, albeit not entirely.

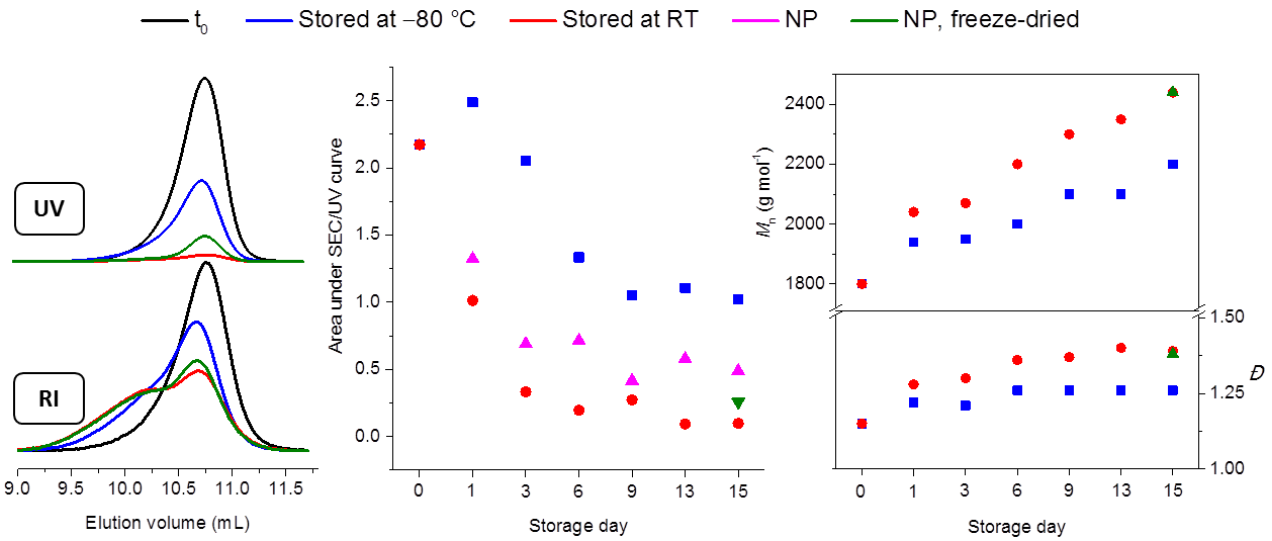

Figure 4.6. Left: Overlay of SEC elugrams of **P12** before and after 15 days storage recorded with RI and UV (λ = 340 nm) detection. **Middle:** Change in area under the SEC trace during the storage studies recorded with UV detection. **Right:** Evolution of M_n and $Đ$ during the storage studies as determined by RI detection.

ESI-ToF-MS analysis was performed periodically during the 15 day storage period in order to gain insight to the degradation products formed (**Figure 4.7**). It could be clearly seen from the mass spectra obtained during and subsequent to storage at –80 °C, that the conjugated structure of the α-end group was mostly preserved. However, upon storage at room temperature, the mass spectra of **P12** (both bulk and nanoparticle suspension) revealed additional m/z series. Complete cleavage of the retinyl moiety was evident from the mass spectra recorded after 15 days of storage (species "g" in **Figure 4.7**). According to degradation products of retinoids described in literature,[67, 68] a number of reasonable assignments were made including isobaric (*e.g.*, species "b" and "h") as well as isomeric structures. While some of the assigned structures could be formed due to fragmentation of the polyene chain following secondary reactions (*e.g.*, "d-f"), some are based on oxidation without cleavage of bonds between two carbon atoms (*e.g.*, epoxides, diols endoperoxides).

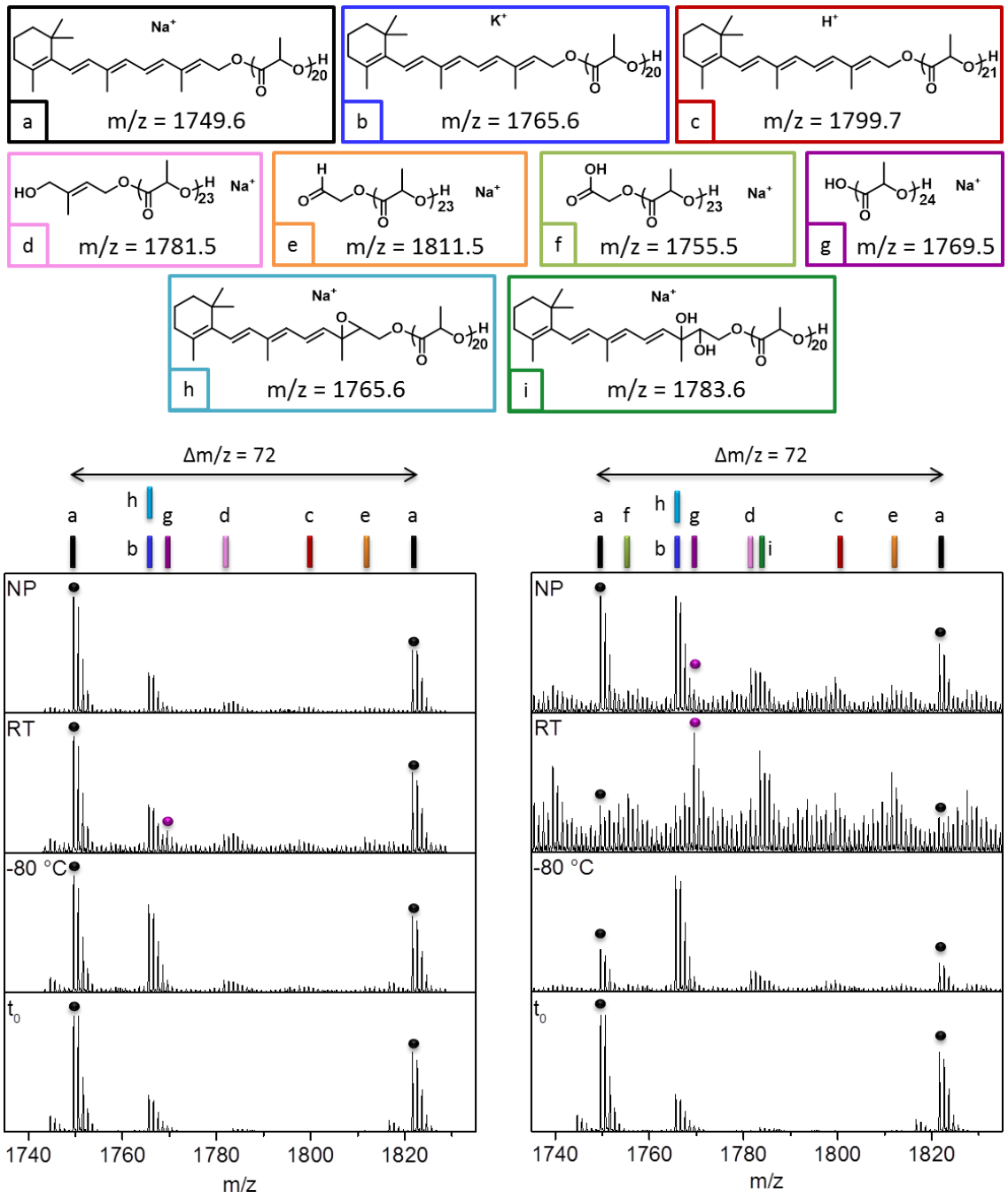

Figure 4.7. Overlay of the ESI-ToF mass spectra of **P12** (t_0 and different storage conditions; RT and –80 °C), and the corresponding NP together with the structural assignment of the observed peaks. **Left:** Mass spectra obtained after storage for 1 day. **Right:** Mass spectra obtained after storage for 15 days. The black and purple dots are added for clarity to indicate the presence of species "a" and "g".

Although the presence of isomeric and isobaric species makes the identification of the end groups difficult, the chromophore of the α-end group is affected in each during storage of **P12**. It is known that the autoxidation of retinoids occur through a radical mechanism including the

addition of oxygen to a double bond and, hence, affecting the chromophore.[74] The coupling products observed by SEC analysis with RI detection can be explained by termination reactions by recombination of two radical retinoid species. Alternatively, the opening of an epoxide functionality (compare e.g. structure "h") by nucleophilic attack of either a hydroxyl ω-end group of another polymer chain (head-tail coupling), or of a hydroxyl functionality formed during the degradation process of the retinyl moiety (head-head coupling) could explain the formation of coupling products.

Based on these promising results, another bioactive molecule, cholesterol was used as a ROP initiator (**Scheme 4.2**). Cholesterol is a lipid steroid and is a major component of eukaryotic cell membranes. It has a primary role in modulating the structural and dynamic properties of the cell membranes.[75]

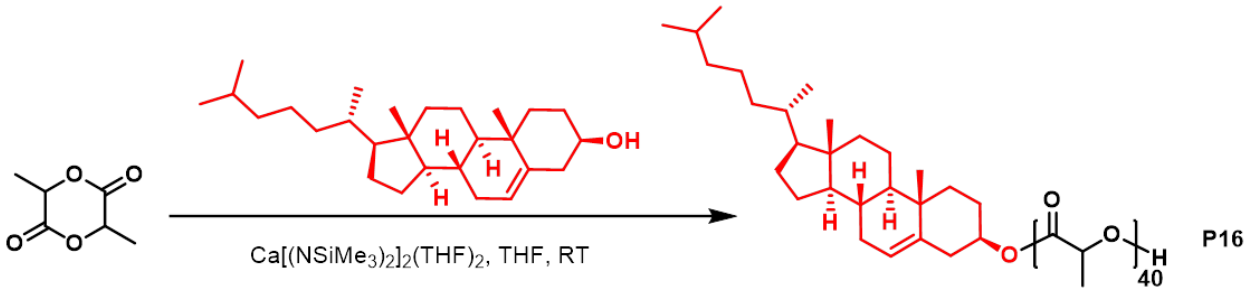

Scheme 4.2. Schematic representation of the ROP of L-lactide using $Ca[N(SiMe_3)_2]_2(THF)_2$ as precatalyst and cholesterol as initiator by *in situ* calcium-alkoxide formation.

Figure 4.8 depicts the ESI-ToF mass spectrum of **P16**, revealing a peak distribution spaced by m/z = 72. The calculated and experimental isotopic patterns obtained from ESI and MALDI-ToF MS measurements are in a good agreement which correspond to sodiated PLA chains with cholesterol initiating and hydroxyl terminating end groups. SEC analysis revealed that the resulting PLA-cholesterol conjugate has narrow dispersity ($Đ$ = 1.23). The molar mass calculated based on specific signals of cholesterol moiety and the methine protons of lactide ($M_{n,\ MNR}$) is very close to the theoretical value suggesting a high initiation efficiency.

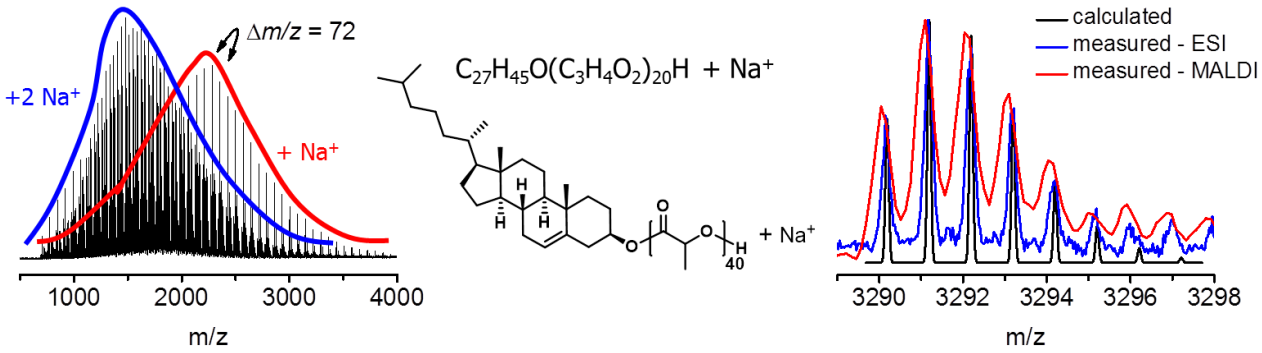

Figure 4.8 Left: ESI-ToF mass spectrum of **P16**. **Right:** Overlay of calculated and measured isotopic patterns obtained from ESI and MALDI-ToF-MS (DCTB, NaI) measurements.

In summary, the utilized catalyst/co-initiator system for ROP of L-lactide enabled the synthesis of well-defined PLA-retinol conjugates. Stable polymeric nanoparticles were obtained by nanoprecipitation method in the size range between 100 to 250 nm. Storage stability study revealed that PLA-retinol conjugate (**P12**) has an excellent stability when stored at low temperatures. However, the retinoid moiety almost completely degraded upon storage under ambient conditions in bulk, while the PLA itself remained intact. This outcome was slightly reduced when the PLA-retinol conjugates were kept in form of an aqueous nanoparticle suspension. The herein presented strategy can be expanded for bioconjugation of other sensitive hydroxyl-functional compounds to the PLA. Besides, retinol conjugates of other polyesters can be prepared that can be obtained *via* ROP of cyclic lactones. One possible application of such retinol-polyester conjugates could be targeting hepatic stellate cells which store fat and, thus, readily take up vitamin A. The utilized approach is further employed for the synthesis of PLA-cholesterol conjugates. The resulting PLA-cholesterol conjugate will be further utilized for microparticle formulation for lung-specific transportation of cholesterol to improve lung function during pneumococcal disease.

5. One-pot block copolymer preparation *via* macro-CTA approach

Parts of this chapter have been/will be published **P3**) Ilknur Yildirim, Sarah Crotty, Claas H. Loh, Grit Festag, Christine Weber, Pier-Francesco Caponi, Michael Gottschaldt, Matthias Westerhausen, Ulrich S. Schubert, End-functionalized polylactides using a calcium-based precatalyst: Synthesis and insights by mass spectrometry, *J. Polym. Sci., Part A: Polym. Chem.* **2016**, *54*, 437–448. **P5**) Ilknur Yildirim, Pelin Sungur, Anna C. Crecelius-Vitz, Turgay Yildirim, Diana Kalden, Stephanie Hoeppener, Matthias Westerhausen, Christine Weber, Ulrich S. Schubert, One-pot synthesis of PLA-*b*-PHEA *via* sequential ROP and RAFT polymerizations, *Polym. Chem.* **2017**, DOI: 10.1039/C7PY01176H.

The concept of using a heterofunctional initiator to perform orthogonal polymerization processes of dissimilar monomers enables preparation of block copolymers in a one-pot approach that cannot be obtained by one polymerization technique alone.[17, 18] Thereby intermediate transformation and purification steps are eliminated making this facile approach of particular importance for block copolymer synthesis.[76] One-pot synthesis of (amphiphilic) block copolymers of polylactide (PLA) has been reported by combining the ring opening polymerization (ROP) of lactide with reversible-deactivation radical polymerization (RDRP) of several monomer classes.[77, 78] However, the direct incorporation of a hydroxyl functional monomer (without the use of a hydroxyl protection group) is very scarce since the hydroxyl moiety of the monomer would also serve as an initiating site for the ROP of lactide.[24]

A one-pot synthesis approach was developed to obtain block copolymers of lactide and HEA, which is also a biocompatible monomer.[79] For this purpose, the ROP of L-lactide is combined with the reversible addition-fragmentation chain transfer (RAFT) polymerization of HEA in a sequential manner under mild reaction conditions enabling the preparation of block copolymers in a controlled fashion without the need of protection groups, intermediate purification steps (**Scheme 6.1**). The synthesis of a PLA based macro-CTA (**P7**) by ROP of L-lactide using the hydroxyl functional trithiocarbonate CDP is described in **Chapter 3** was, therefore, extended.

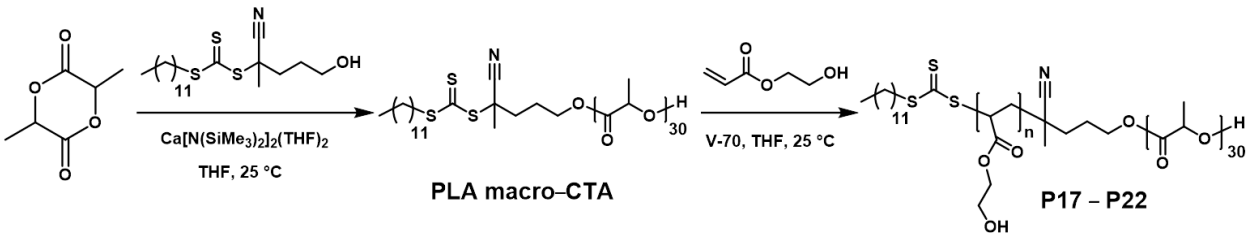

Scheme 5.1. Schematic representation of the synthesis of PLA-*b*-PHEA copolymers by combination of ROP and RAFT in a sequential one-pot approach.

For a successful chain extension *via* RAFT polymerization high end group fidelity of the macro-CTA is essential to minimize the formation of a homopolymer. Therefore the PLA macro-CTA (**P7**) was characterized by tandem MS by utilizing collision-induced dissociation (on the parent ion $C_{19}H_{34}NOS_3(C_3H_4O_2)_{22}H + Ag^+$). The MS/MS spectrum of **P7** reveals two m/z regions (**Figure 5.1**). Based on the fragmentation pathways reported in literature, four ion series could be assigned in the m/z region below 1500.[72, 80] While PLA chains with intact α-end groups were the minor abundant species (ion series "A" and "C"), complete α-end group cleavage was predominant leading to α,ω-hydroxyl end groups (ion series "B"). Additional fragmentation at the ω-end groups through Mc-Lafferty-like rearrangements formed the most abundant ion series with an acrylate ω-end group (ion series "D").[72, 73]Conversely, fragmentations only arising from the ω-chain end could be assigned in the m/z region above 1,500 in the tandem mass spectrum. The fragment series "H" may arise from a radical induced dissociation of the (CO)O-C bond of the ester group followed by further hydrogen addition,[81] whereas the fragment ion series "G" would result from cleavage of a C-C bond cleavage between the carbonyl carbon and the carbon in α-position. In addition, both fragmentation products were found with a direct positive charge as well (ion series "E" and "F").

RAFT polymerization kinetics of HEA using CDP as CTA was investigated before the synthesis of block copolymers with using the macro-CTA. The RAFT polymerization was performed at room temperature in order to avoid possible transesterification reactions as soon as the PLA macro-CTA would be used. For this purpose, V-70 was used as the radical initiator which provides controlled RAFT polymerization at room temperature.[82] Kinetic study of RAFT polymerization of HEA in the presence of CDP was conducted in THF at room temperature (**Figure 5.2)**. However, an induction period (14 hours) was observed for the RAFT polymerization of HEA. The linear first-order consumption of monomer up to 22 hours of polymerization (≈ 62% conversion, **Figure 5.2**) suggests that V-70 provides constant radical concentration for more than two times of its half-live. **Figure 5.2** depicts a linear increase of molar mass as the monomer conversion increases. SEC analysis of the kinetic samples revealed monomodal distributions with narrow dispersities ($1.08 < Đ < 1.18$).

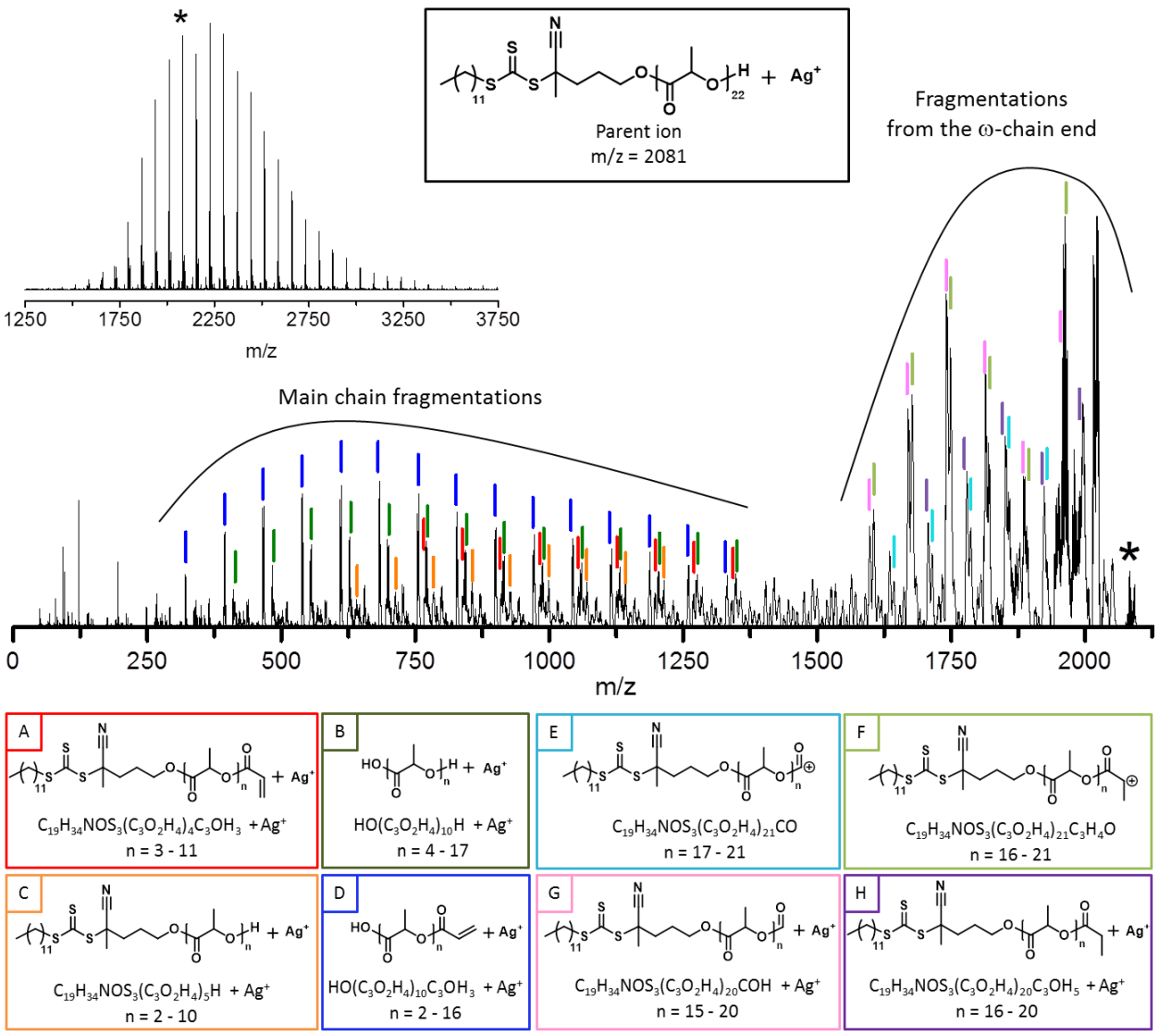

Figure 5.1 MALDI ToF MS/MS spectrum of the selected precursor ion at m/z 2081 together with the structural assignment of the observed peaks.

Prior to block copolymer synthesis, two different PHEA homopolymers were successfully prepared at room temperature (**Table 5.1**). SEC analysis of the homopolymers revealed monomodal mass distributions with narrow dispersities. However, the M_n of the homolpolymers was overestimated due to the utilized PMMA calibration. The $M_{n,\,NMR}$, which is calculated based on comparing the peak integrals of the trithiocarbonate end group with methylene protons of the PHEA is very close to the $M_{n,\,theo}$ for **PHEA-1**, whereas significantly deviates for **PHEA-2**, due to the low intensity of the trithiocarbonate end group signal.

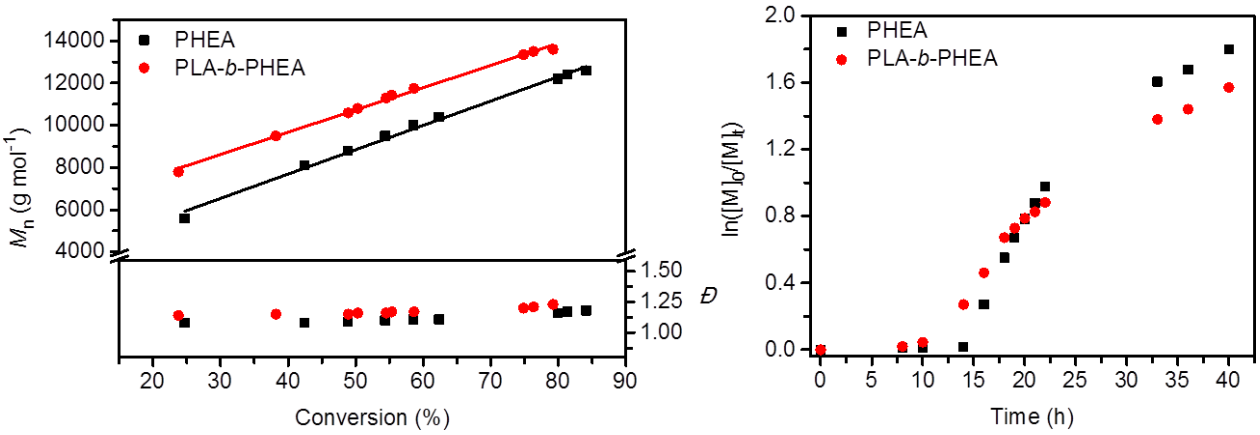

Figure 5.2 Kinetic studies of the RAFT polymerization of HEA by using CDP and the PLA macro-CTA (one-pot approach) at room temperature in THF ($[HEA]_0$ = 1 mol L^{-1}, $[HEA]_0/[CDP]_0/[V\text{-}70]_0$ = 40/1/0.25). **Left:** Dependence of $M_{n,SEC}$ and $Đ$ (SEC in DMAc, PMMA calibration) on HEA conversion. **Right:** Semilogarithmic kinetic plots.

The isolated macro CTA (**P7**) was utilized for the RAFT polymerization of HEA in order to investigate the possibility to prepare block copolymers entirely at room temperature in THF ($[HEA]_0/[macro\text{-}CTA]_0/[V\text{-}70]_0$ = 20/1/0.25, $[HEA]_0$ = 1 mol L^{-1}). 87% monomer conversion was reached after an overnight reaction. SEC and ^1H NMR analyses revealed successful chain extension with PHEA. Therefore, a one-pot synthesis procedure was developed that would eliminate the intermediate purification step. In order to compare the kinetics of the RAFT polymerization of HEA in the presence of CDP and the PLA macro-CTA, a kinetic study was performed by following the one-pot approach. For this reason, firstly the ROP of L-lactide was performed in a glove box as described in **Chapter 3** ([L-lactide]/[CDP]/[Ca] =15/1/0.5, [L-lactide] = 1 mol L^{-1}). After quantitative monomer conversion was reached (10 minutes, see **Chapter 3**), the vial was taken out of the glove box and a mixture of HEA and V-70 was added at –20°C ($[macro\text{-}CTA]_0/[CDP]_0/[V\text{-}70]_0$ = 40/1/0.25, $[HEA]_0$ = 1 mol L^{-1} in THF). Subsequently, the RAFT polymerization was performed.

When equimolar amount of the PLA macro-CTA was used (one pot approach, without purification), the kinetics of the RAFT polymerization of HEA was slightly altered (**Figure 5.2**). First of all, the induction period is shorter in the presence of the PLA macro-CTA (≈ 10 hours), which should arise from a change in the microenvironment of the trithiocarbonate moiety due to steric and/or polarity aspects.[83] Besides, the apparent polymerization rate is slightly higher at low conversions, which is in accordance with literature where PLA[84] and PCL[83] based macro-CTAs are utilized for RAFT polymerization. Indicating that the molar mass is well controlled in

the presence of the PLA macro-CTA, the molar mass increased in a linear fashion with respect to the total monomer conversion together with the low dispersities ($1.14 < Đ < 1.23$, **Figure 5.2**).

Six different block copolymers were prepared (**P17** to **P22**) with uniform PLA block (DP = 15) under similar conditions by altering the feed ratios of $[\text{macro-CTA}]_0/[\text{HEA}]_0$ (**Table 5.1**). SEC analysis of the final samples (t_f) from polymerization mixtures revealed a clear shift towards lower elution volumes (**Figure 5.3**), confirming the chain extension of the PLA macro-CTA with HEA. The isolated block copolymers have narrow dispersity ($1.15 \leq Đ \leq 1.25$). However, as a result of the PMMA calibration used, SEC analysis overestimated the molar mass values similar to PHEA homopolymers (**Table 5.1**).

Table 5.1. Characterization results of the PHEA homopolymers and the block copolymers **P17** to **P22** prepared *via* one-pot approach.

Entry	Initiator (I) or CTA	M/I or M/CTA	Conv.[a] (NMR)	$M_{n,theo}$[b] [g mol^{-1}]	$M_{n,NMR}$[c] [g mol^{-1}]	$M_{n,SEC}$[d] [g mol^{-1}]	$Đ_{SEC}$[d]	Composition (theo.)[b]	Composition (NMR)[c]
PHEA-1	CDP	15	93	2,000	2,250	7,100	1.05	$P(HEA)_{14}$	$P(HEA)_{16}$
PHEA-2	CDP	100	65	8,000	14,450	22,100	1.24	$P(HEA)_{65}$	$P(HEA)_{121}$
P17	PLA-CTA	20	82	4,450	4,500	10,300	1.13	PLA_{15}-*b*-$P(HEA)_{16}$	PLA_{15}-*b*-$P(HEA)_{17}$
P18	PLA-CTA	40	60	5,300	5,450	12,100	1.15	PLA_{15}-*b*-$P(HEA)_{24}$	PLA_{15}-*b*-$P(HEA)_{25}$
P19	PLA-CTA	40	70	5,800	6,500	15,300	1.21	PLA_{15}-*b*-$P(HEA)_{28}$	PLA_{15}-*b*-$P(HEA)_{34}$
P20	PLA-CTA	50	70	6,600	8,250	16,100	1.24	PLA_{15}-*b*-$P(HEA)_{35}$	PLA_{15}-*b*-$P(HEA)_{49}$
P21	PLA-CTA	60	85	8,500	10,700	22,700	1.23	PLA_{15}-*b*-$P(HEA)_{51}$	PLA_{15}-*b*-$P(HEA)_{70}$
P22	PLA-CTA	100	83	12,200	19,850	27,500	1.28	PLA_{15}-*b*-$P(HEA)_{83}$	PLA_{15}-*b*-$P(HEA)_{149}$

[a]Conversion values determined by ^{1}H NMR spectroscopy from the polymerization mixtures (t_0 and t_f). [b]Calculated from feed and conversion. [c]Calculated from suitable signal integrals in the ^{1}H NMR spectra of the purified polymers. [d]Determined by SEC (DMAc, RI detection, PMMA calibration).

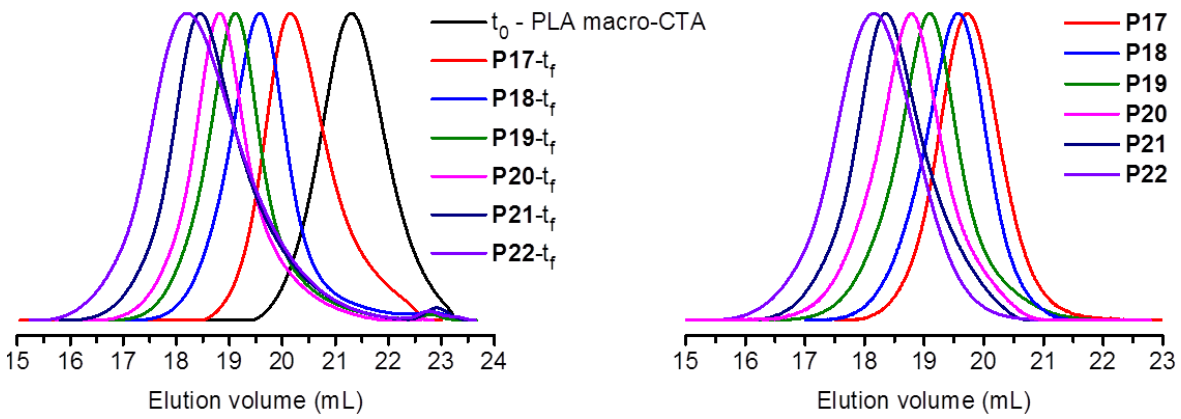

Figure 5.3. Overlay of the normalized SEC traces of the PLA macro-CTA and the block copolymers **P17** to **P22** obtained *via* one-pot approach. **Left:** The SEC traces recorded from t_0 and t_f reaction mixtures. **Right:** The SEC traces recorded from the isolated block copolymers after purification.

Figure 5.4 depicts an overlay of the ^{1}H NMR spectra of the PLA macro-CTA (**P7**), **PHEA-1**, and **P17** in DMSO-d_6. The ^{1}H NMR spectrum of **P17** clearly reveals all characteristic signals of both PLA and PHEA blocks *i.e.* methine protons of the PLA (peak f), methylene and hydroxyl protons of PHEA (peaks a-c) as the polyacrylate backbone signals (peaks d and e). It is also evident from the overlay of the ^{1}H NMR spectra of **P18** to **P22** that the intensity of the peaks arising from the PHEA block increases gradually from **P18** to **P22**.

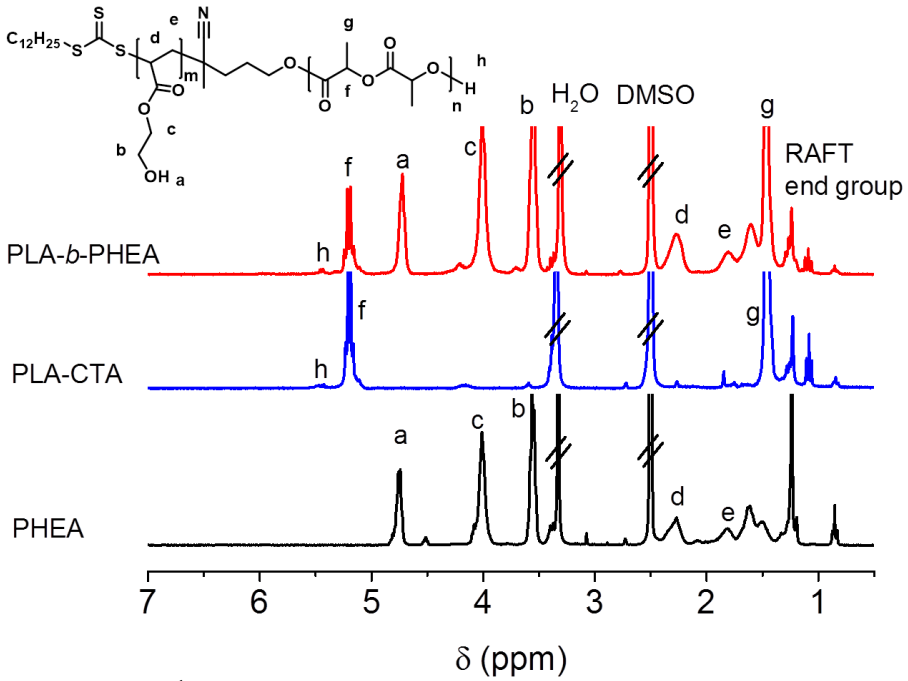

Figure 5.4 Overlay of the ^{1}H NMR spectra (DMSO-d_6, 300 MHz) of **PHEA-1**, the PLA macro-CTA (**P7**) and **P17** prepared *via* one-pot approach together with the assignment of the observed peaks.

The molar masses ($M_{n,\ NMR}$) of the block copolymers were calculated by comparing the resonance intensities of the methylene protons of PHEA (peak c) and methine protons of PLA (peak f) since the degree of polymerization (DP) of the PLA block is known (**Figure 5.4**). For the block copolymers which possess rather short PHEA blocks (**P17** to **P19**), the $M_{n,\ NMR}$ values are very close to the $M_{n,\ theo}$ values (**Table 5.1**). However, for the block copolymers with relatively high PHEA content (**P20** to **P22**) the calculated $M_{n,\ NMR}$ values gave higher values than expected from [M]/[CTA] and conversion ($M_{n,theo}$). This outcome could arise from better solubility of PHEA segments in DMSO than the hydrophobic PLA segments and, thus, resulting in enhanced mobility of the PHEA blocks. Therefore, the overestimation of the DP of the PHEA blocks *via* ^{1}H NMR analysis would be caused by the resulting difference in relaxation behavior of each block. Indeed, DLS measurements of **P22** in DMSO revealed the presence of aggregated structures.

Thermo-gravimetrical analysis (TGA) analysis of **P17** to **P22** clearly verified the block copolymer structure (**Figure 5.5**). The PLA macro-CTA features a sharp mass profile and decomposes between 200 and 320 °C, whereas **PHEA-1** decomposes over a broader temperature range with an onset of mass loss around 260 °C. The thermal decomposition of **P17** is a two-step process, which can be clearly seen in the first derivative curve of the TGA thermogram. The first degradation step corresponds to the PLA block, and the second one arises from the degradation of the PHEA block. All block copolymers (**P17** to **P22**) feature this two-step degradation profile.

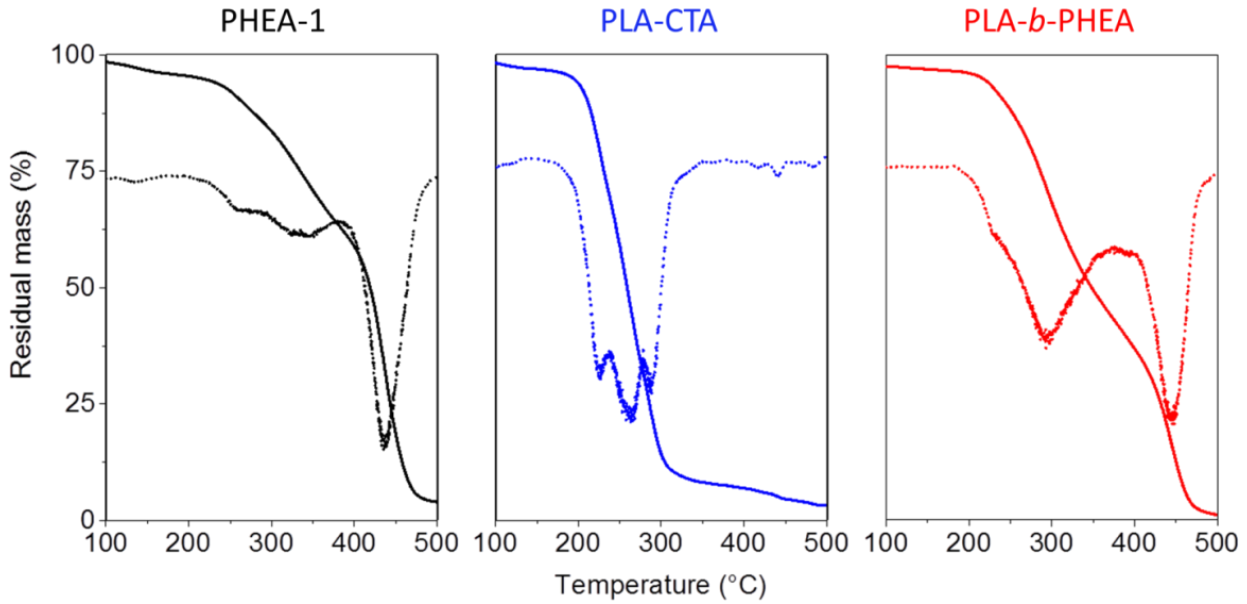

Figure 5.5. TGA thermograms of **PHEA-1**, the PLA macro-CTA (**P7**), and **P17** (20 to 600 °C, 10.0 °C min^{-1}). The dotted lines represent the first derivative of the measured traces.

The block copolymers **P17** to **P22** were analyzed by differential scanning calorimetry (DSC), in order to investigate a possible phase segregation between the PLA and PHEA blocks in bulk (**Figure 5.6**). The amorphous **PHEA-1** and **PHEA-2** revealed T_gs at −1°C and of 5 °C, respectively. The semi-crystalline PLA macro-CTA has a T_g at 38 °C and a melting temperature T_m at 139 °C, which is only visible in the first heating run. **P17**, which has nearly equal PLA and PHEA block ratios, has two distinct T_gs at 11 °C and at 30 °C, respectively. Although this indicates a microphase separation between both blocks in bulk, the shifted T_g values of the two phases in comparison to the homopolymers suggest a partial mixing between the two blocks.[85]

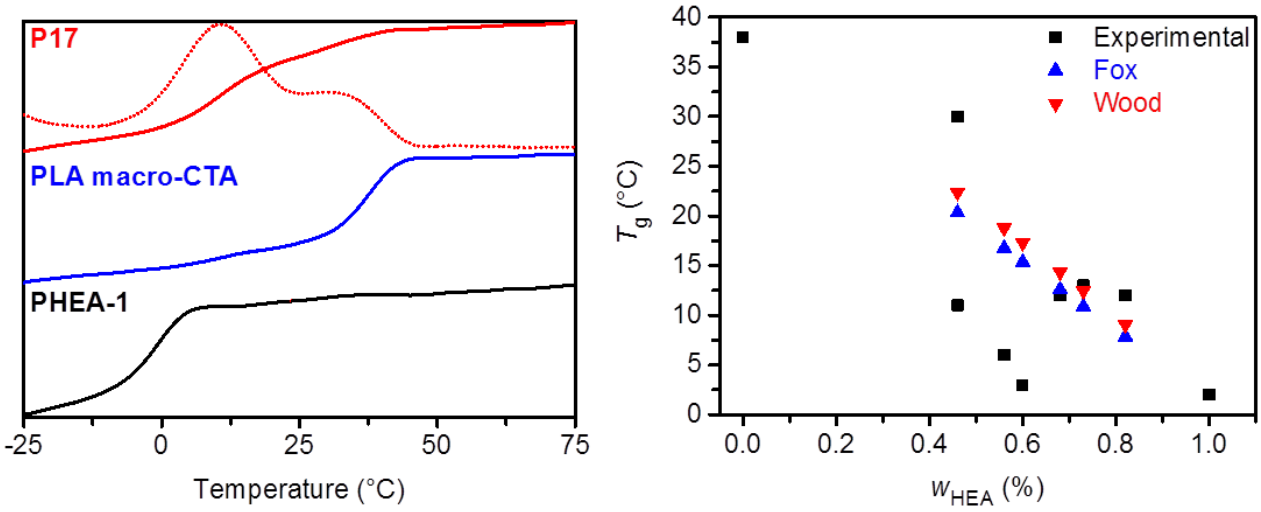

Figure 5.6. Left: Overlay of DSC thermograms of isolated the PLA macro-CTA (**P7**), **PHEA-1** and **P17** (heating rate 10 K min^{-1}, 3rd heating run). The dotted line represents the first derivative of the thermogram for **P17**. **Right:** Dependence of the T_g values of the block copolymers **P17**-**P22** on the weight fraction of HEA. $T_{g,\,Fox}$ values are calculated according to $1/T_g = M_1/T_{g1} + M_2/T_{g2}$, where M_1 and M_2 are the weight fractions of **HEA** and **LA**, respectively. $T_{g,\,Wood}$ values are calculated according to $T_g = (M_1\Delta C_{p1}T_{g1} + M_2\Delta C_{p2}T_{g2})/(M_1\Delta C_{p1} + M_2\Delta C_{p2})$.

As an indication of the increased homogeneity of the system, the block copolymers **P18** to **P22** with increased weight fraction of PHEA revealed a single T_g, which is between the T_g values of the two homopolymers. In order to verify this assumption, the Fox and Wood equations were used which represent common methods to estimate the T_g values of miscible copolymer systems (**Figure 5.6**).[85] For the block copolymers with high PHEA weight fractions (**P20** to **P22**) a reasonable agreement is evident with the experimental T_g values. However, the experimental T_g values of **P18** and **P19** are significantly lower than the calculated ones via Fox and Wood equations, which suggests that the PLA and PHEA segments are not fully miscible in at least in

these two block copolymers. Indeed, a melting peak is observed for **P18** in the first heating run, which confirms the presence of PLA domains in the sample.

To investigate the self-assembly behavior of the block copolymers **P17** to **P22** in water, aqueous suspensions were prepared by dropping THF polymer solutions into water. Dynamic light scattering (DLS) and cryo-transmission electron microscopy (cryo-TEM) analyses of the most hydrophobic block copolymers **P17** and **P18** revealed rather undefined aggregated with unclear substructures in water with diameters ranging from 100 to 200 nm (**Figure 5.8**). As the length of the PHEA block increases (**P19**), less dense nanostructures were found *i.e.* aggregation of several spherical micelles together with aggregates of thin small sheets (**Figure 5.7**).

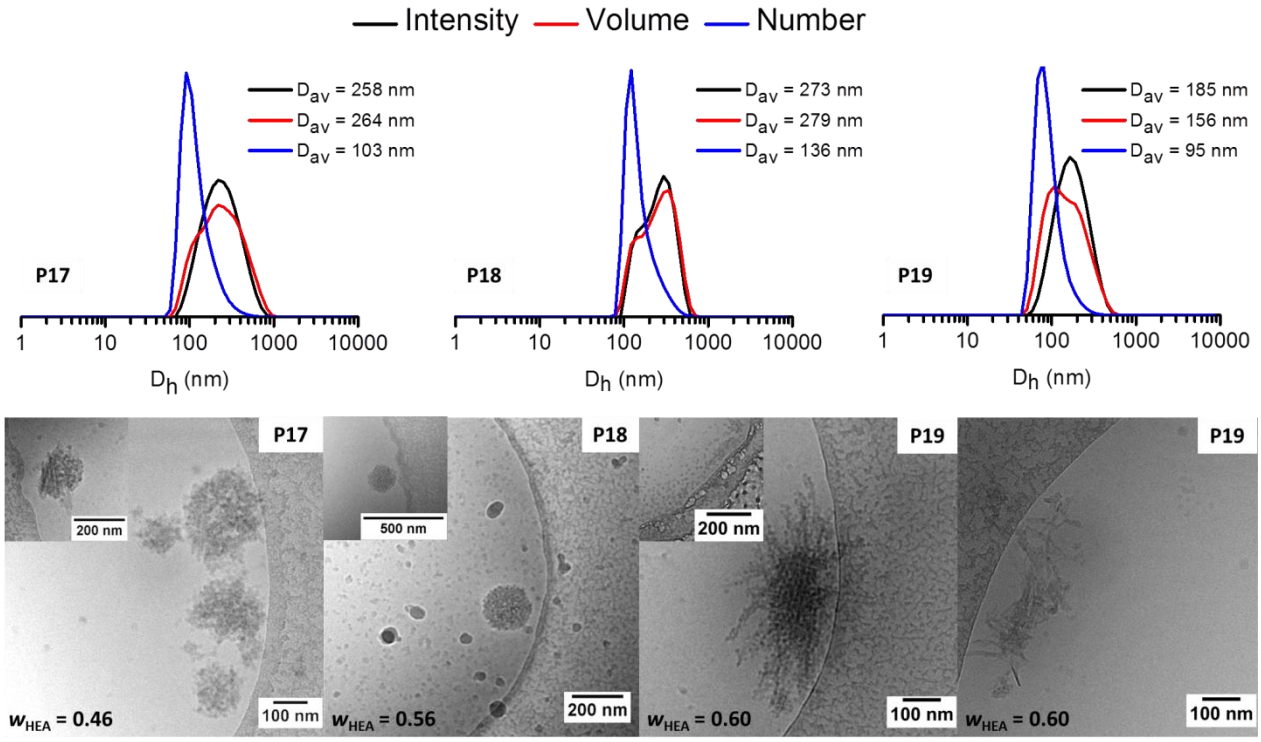

Figure 5.7. DLS size distributions and representative cryo-TEM images of the suspensions obtained from **P17**, **P18** and **P19** in water (c = 1 mg mL^{-1}). The insets show enlarged view of the suspensions at higher concentration (c = 2 mg mL^{-1}).

Self-assembly of **P20** and **P21** in aqueous media resulted in formation of homogeneously distributed and densely packed spherical micelles with diameters between 13 to 20 nm (**Figure 5.8**). Additionally, cryo-TEM analysis revealed the occasional formation of worm-like micelles, which explains the bimodal intensity weighted size distributions from DLS analysis. In case of **P22**, in addition to spherical micelles, some vesicles were visualized (20 to 40 nm) by cryo-

TEM. This outcome could be explained by rather larger dispersity of **P22** ($Đ$ = 1.28), that would include a minor amount of block copolymer chains with relatively short PHEA blocks.

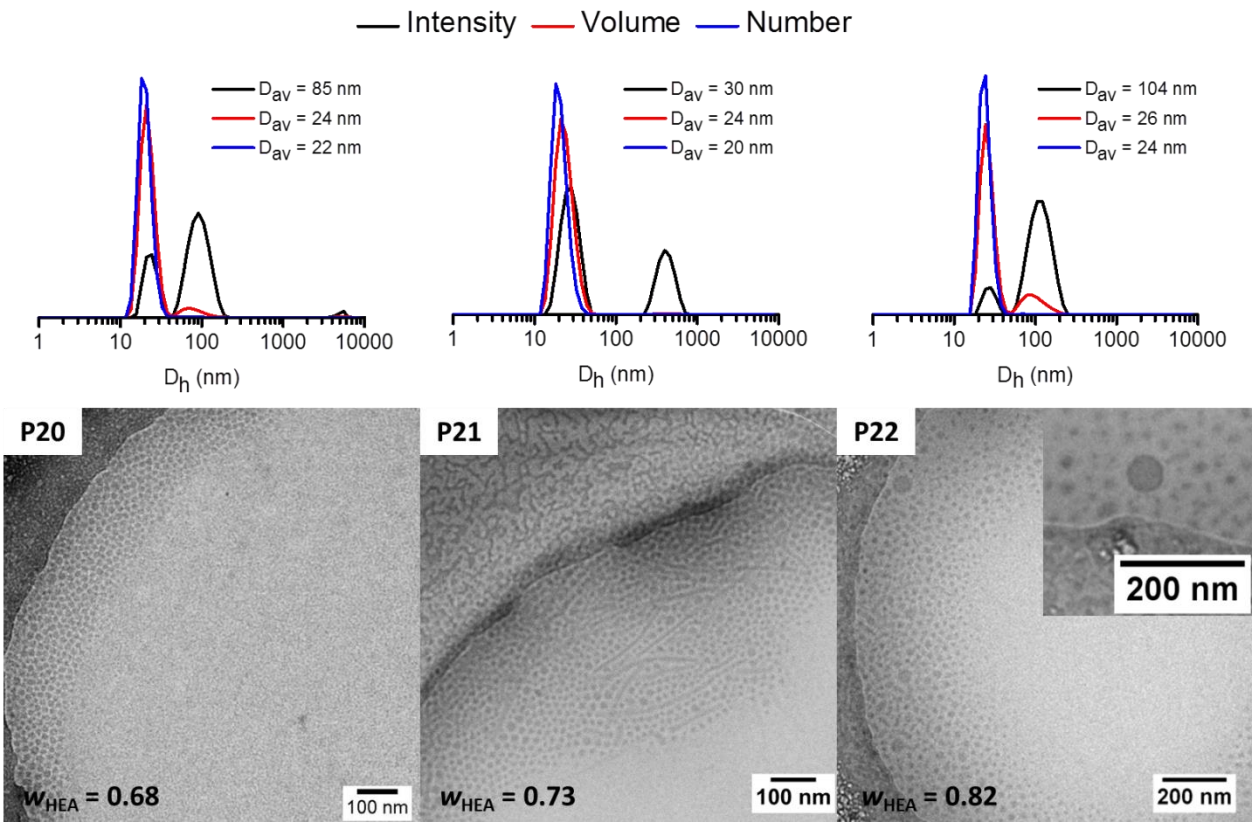

Figure 5.8. DLS size distributions and representative cryo-TEM images of the suspensions obtained from **P20** (c = 2 mg mL^{-1}), **P21** (c = 5 mg mL^{-1}) and **P22** (c = 5 mg mL^{-1}). The inset shows an enlarged view of a vesicle.

As described in **Chapter 2**, block copolymers comprising PLA as well as functional groups can be prepared using protection group chemistry, or intermediate purification steps. However, the existing scientific approaches have not been investigated with respect to the properties of the "new material" synthesized. In contrast, the developed one-pot strategy enabled the synthesis PLA-*b*-PHEA copolymers at room temperature without employing any intermediate purification steps, protection group chemistry, solvent switch or removal of residual catalyst. The developed one-pot approach is applicable to a broad range of compositions, which is demonstrated by the fact that the PLA-*b*-PHEA block copolymers revealed the expected properties both in bulk and solution. This one-pot approach could be further exploited for the chain extension of the PLA macro-CTA with other hydroxyl functional monomers since the main advantage of this system is the omission of protection chemistry. Besides, the primary hydroxyl functionalities enable further functionalization or crosslinking in a straightforward approach.

6. Comb-shaped polymers with PLA side chains *via* macromonomer approach

Parts of this chapter have been published **P6**) Ilknur Yildirim, Tanja Bus, Martin Sahn, Turgay Yildirim, Diana Kalden, Stephanie Hoeppener, Anja Traeger, Matthias Westerhausen, Christine Weber, Ulrich S. Schubert, Fluorescent amphiphilic heterografted comb polymers comprising biocompatible PLA and PEtOx side chains *Polym. Chem.* **2016**, *7*, 6064–6074.

The synthesis of functional copolymers with complex architectures designed for specialized applications has come into focus lately.[86] Besides using bifunctional macroinitiators to prepare linear block copolymers comprising polylactide (PLA) (compare **Chapter 5**), copolymers with more sophisticated topologies *i.e*. comb-shaped copolymers can be prepared *via* the macromonomer method.[36, 87] The macromonomer method relies on the attachment of a functional end group to PLA, which can be polymerized by a subsequent reversible-deactivation radical polymerization (RDRP) method. The macromonomer method also serves as a facile approach to prepare heterografted comb polymers by copolymerization of two macromonomer types, thus, representing a flexible way to combine the properties of distinct polymer classes by an appropriate selection of polymer backbone and side chains, respectively.[88, 89] Ethyl and methyl substituted poly(2-oxazoline)s (POx) feature hydrophilicity and exhibit similar properties as poly(ethylene glycol) (PEG) in biological systems, *i.e.* "stealth effect".[90] In addition, they can be polymerized by a living cationic ring opening polymerization (CROP) mechanism, thus, can be obtained with well-defined end groups. In order to prepare heterografted comb polymers comprising hydrophilic and hydrophobic side chains, macromonomers with methacrylate end groups based on PLA and poly(2-ethyl-2-oxazoline) (PEtOx) were prepared and polymerized *via* reversible addition-fragmentation chain transfer (RAFT) polymerization in a controlled fashion.

The versatile nature of the *in situ* calcium alkoxide formation does not only allow the synthesis of α-end functional PLAs, but also enables the direct ω-end functionalization of the resulting anionic PLA species using an electrophile in one pot. To enable tracking of the final polymers within the cell without need of encapsulation of an additional dye[91] 1-pyrenebutanol was selected as a ROP initiator (compare **P8** in **Chapter 3**). Two different α,ω- end functional PLA macromonomers with a degree of polymerization (DP) of 10 and 15, respectively were synthesized by using 1-pyrenebutanol as initiating alcohol and methacryloyl chloride as end-capping agent (**Scheme 6.1**). The ROP of L-lactide was performed in THF at room temperature

under nitrogen atmosphere and driven to quantitative conversion prior to end-capping with a 10-fold excess of methacryloyl chloride.

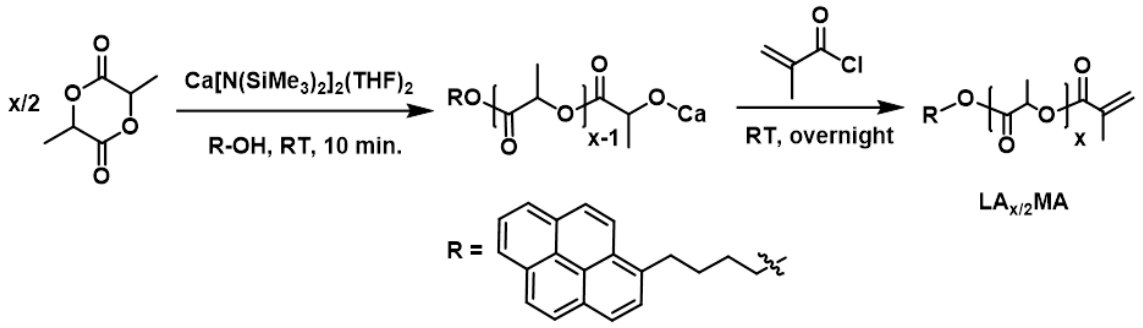

Scheme 6.1. Schematic representation of the synthesis of the PLA macromonomer *via* ROP of L-lactide and *in situ* end capping with methacryloyl chloride.

Size exclusion chromatography (SEC) analysis with UV detection at 340 nm confirmed the covalent attachment of 1-pyrenebutanol. Furthermore, both macromonomers revealed narrow molar mass distributions indicating that the quenching of the polymerization with methacryloyl chloride did not induce chain coupling or autopolymerization reaction. The isolated PLA macromonomers were quantitatively functionalized according to ^{1}H NMR analysis (**Figure 6.1**) as the calculated molar masses ($M_{n,NMR}$) are in a good agreement with the theoretical values and the ones obtained from SEC analysis with PLA calibration (**Table 6.1**).

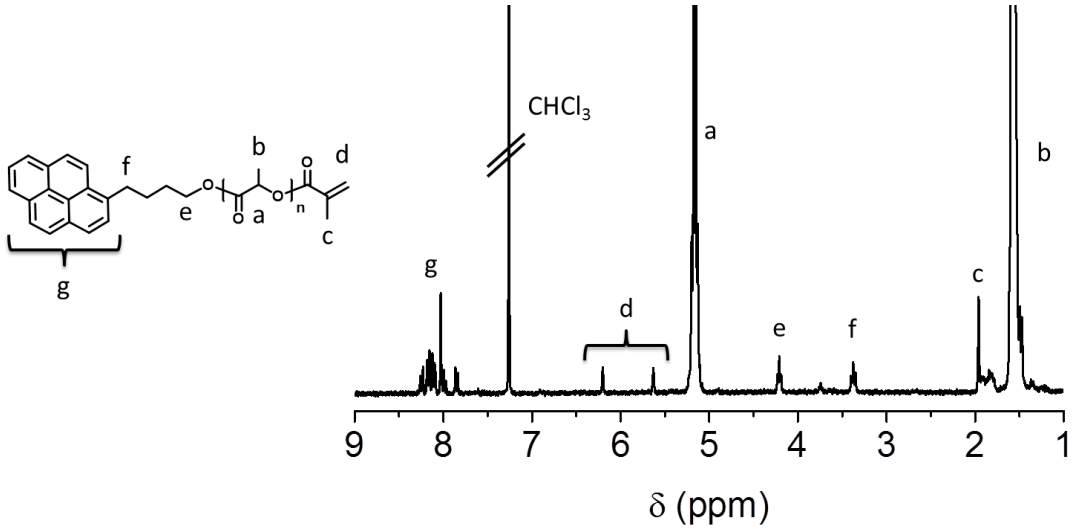

Figure 6.1. ^{1}H NMR spectrum (300 MHz, $CDCl_3$) of the PLA macromonomer $LA_{10}MA$ and structural assignment of the observed peaks.

Both matrix-assisted laser desorption/ionization (MALDI) and electrospray ionization (ESI) mass spectrometry measurements revealed a single distribution of peaks with a distance of m/z =

72 between two neighboring peaks (**Figure 6.2**). The experimental isotopic patterns overlap with the calculated pattern for the PLA chains bearing α- pyrene butanol and ω- methacrylate end functionality, which are ionized with a sodium cation.

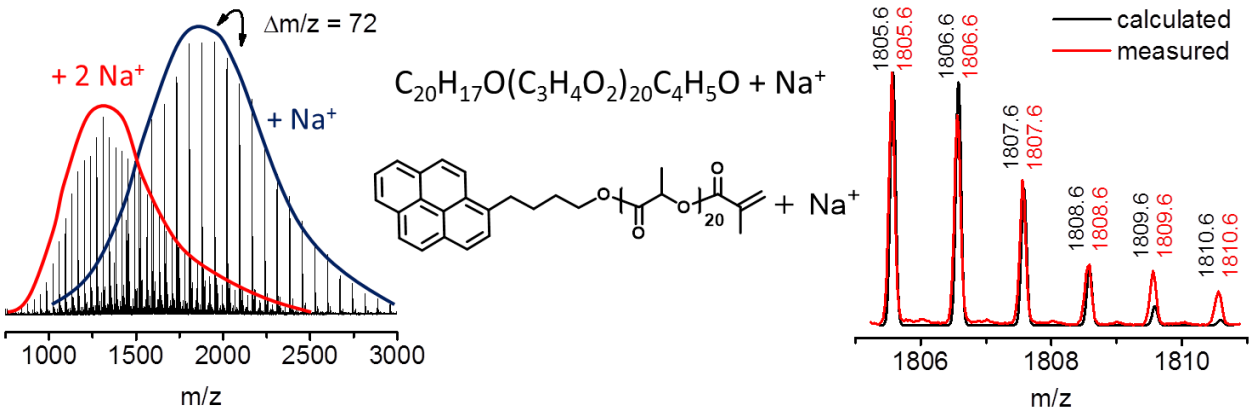

Figure 6.2. Left: ESI-ToF mass spectrum of $LA_{15}MA$. **Right:** Overlay of the isotopic patterns.

The PEtOx macromonomer ($EtOx_5MA$) was prepared by cationic ROP of EtOx using MeTos as initiator and subsequent end-capping with methacrylic acid using triethyl amine as a base. The isolated $EtOx_5MA$ was quantitatively functionalized according to ^{1}H NMR analysis.

Table 6.1. Characterization data of the PLA and POx based macromonomers.

Entry	M/I	Conv.[a] [%]	DP[b]	DF[b] [%]	$M_{n,theo}$[c] [g mol^{-1}]	$M_{n,NMR}$[b] [g mol^{-1}]	$M_{n,SEC}$[d] [g mol^{-1}]	$Đ_{SEC}$[d]	$M_{n,MALDI}$[e] [g mol^{-1}]	$Đ_{MALDI}$[e]
$LA_{10}MA$	10	100	10	90	1,800	1,800	1,500	1.32	2,000	1.13
$LA_{15}MA$	15	100	15	93	2,500	2,500	2,300	1.24	2,200	1.09
$EtOx_5MA$	5	100	5	96	596	600	500*	1.17*		

[a]Determined by ^{1}H NMR spectroscopy from the polymerization mixtures. [b]Obtained from ^{1}H NMR spectra of the purified macromonomers. [c]Calculated from M/I and conversion. [d]Determined by SEC (THF, PLA calibration or *$CHCl_3$, PMMA calibration). [e]Determined by MALDI (HABA, NaCl) measurements.

The macromonomers were copolymerized *via* RAFT polymerization in THF at 70 °C using AIBN as initiator and CPDB as chain transfer agent (CTA) (**Scheme 6.2**). In order to obtain heterografted comb polymers with varying hydrophilicity, the overall [monomer] to [CTA] ratio was kept constant at 60 but the feed ratio of the $EtOx_5MA$ and $LA_{10}MA$ macromonomer was changed. The comb polymers were isolated by successive precipitation in methanol and

preparative SEC using a BioBeads SX-1 column. **Table 6.2** summarizes the polymerization conditions and the characterization results of the isolated comb polymers **P23** to **P27**.

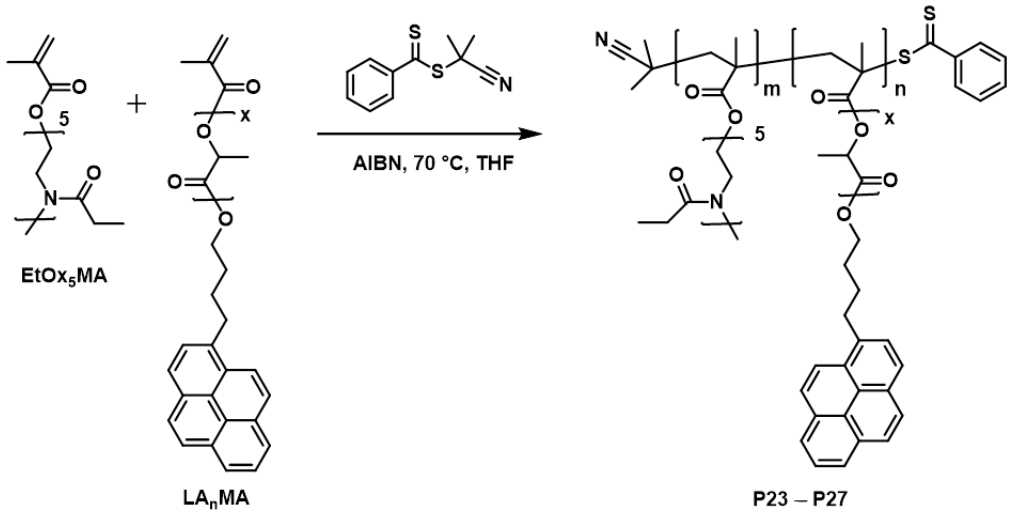

Scheme 6.2. Schematic representation of the synthesis of heterografted comb polymers.

Table 6.2. Selected characterization results of the comb polymers **P23** to **P27**.

Entry	LA_nMA	$EtOx_5MA$/ LA_nMA/ CTA/AIBN	$[EtOx_5MA]$/ [LAnMA] (feed)	Conv.[a] [%] $EtOx_5MA$:LA_nMA	$M_{n,theo}$[b] [g mol^{-1}]	$M_{n,SEC}$[c] [g mol^{-1}]	$Đ_{SEC}$[c]	$[EtOx_5MA]$/ $[LA_nMA]$ (NMR)[d]	EtOx/LA (NMR)[e]
P23	$LA_{15}MA$	42/18/1/0.25	71/29	32:25	19,300	27,500	1,17	70/30	45/55
P24	$LA_{10}MA$	42/18/1/0.25	71/29	90:85	50,000	28,200	1.37	65/35	50/50
P25	$LA_{10}MA$	50/10/1/0.25	83/17	75:73	35,600	29,000	1.25	80/20	65/35
P26	$LA_{10}MA$	53/7/1/0.25	88/12	95:90	41,000	26,300	1.25	85/15	70/30
P27	$LA_{10}MA$	54/6/1/0.25	90/10	85:85	36,800	19,500	1.23	90/10	80/20

[a]Conversion values determined by ^{1}H NMR spectroscopy from the polymerization mixtures. [b]Calculated from feed and conversion. [c]Determined by SEC ($CHCl_3$, RI detection, PMMA calibration). [d]Macromonomer molar ratio calculated from suitable signal integrals in the ^{1}H NMR spectra of the purified polymers. [e]Molar ratio of EtOx and LA repeating units calculated from suitable signal integrals in the ^{1}H NMR spectra of the purified polymers.

Figure 6.3 shows an overlay of the SEC traces obtained from the isolated comb polymers and the corresponding macromonomers. The monomodal SEC traces obtained both with RI detection and UV detection at 340 nm confirm the absence of residual macromonomer as well as the covalent attachment of the pyrene moiety. All comb polymers elute at similar retention times, but earlier than the corresponding macromonomers due to increased hydrodynamic volume.

However, SEC underestimated the molar masses of the comb polymers due to a significant difference in the hydrodynamic volume of the comb polymers and the linear standard polymers used for the calibration.

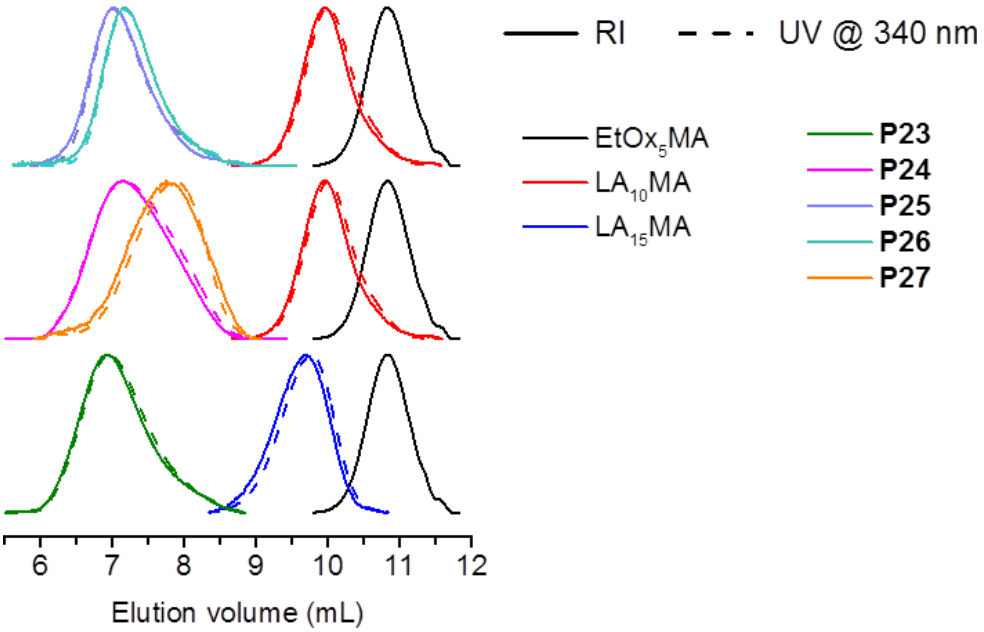

Figure 6.3. Normalized SEC traces ($CHCl_3$) of the macromonomers and comb polymers **P23** to **P27**.

^{1}H NMR spectroscopy analysis of the isolated comb polymers clearly revealed signals arising from both PLA and PEtOx macromonomers (**Figure 6.4**). A higher DP of the PLA macromonomer did not prevent the successful incorporation during the RAFT polymerization as is evident from the excellent agreement of the ratio of the two side chain types in the copolymers ([$EtOx_5MA$]/[LA_nMA]) with the feed ratio. The increased PEtOx content throughout the polymer series **P23** to **P27** is apparent from the overlay of the ^{1}H NMR spectra of the isolated comb polymers. The ^{1}H NMR spectra are normalized according to the peak maxima of the methine protons of the PLA side chains and clearly indicate that the intensity of the respective signals assigned to PEtOx side chain increases from **P23** to **P27**. During the preparation of copolymer library the ratio of the distinct side chain types was not widely varied. However, the copolymer composition still covers a broader range when the ratio of the EtOx and lactide repeating units is taken into account (EtOx/LA) due to the increased DP of the PLA based side chains (DP = 10 and 15) compared with the DP of the PEtOx-based side chains (DP = 5) (**Table 6.2**).

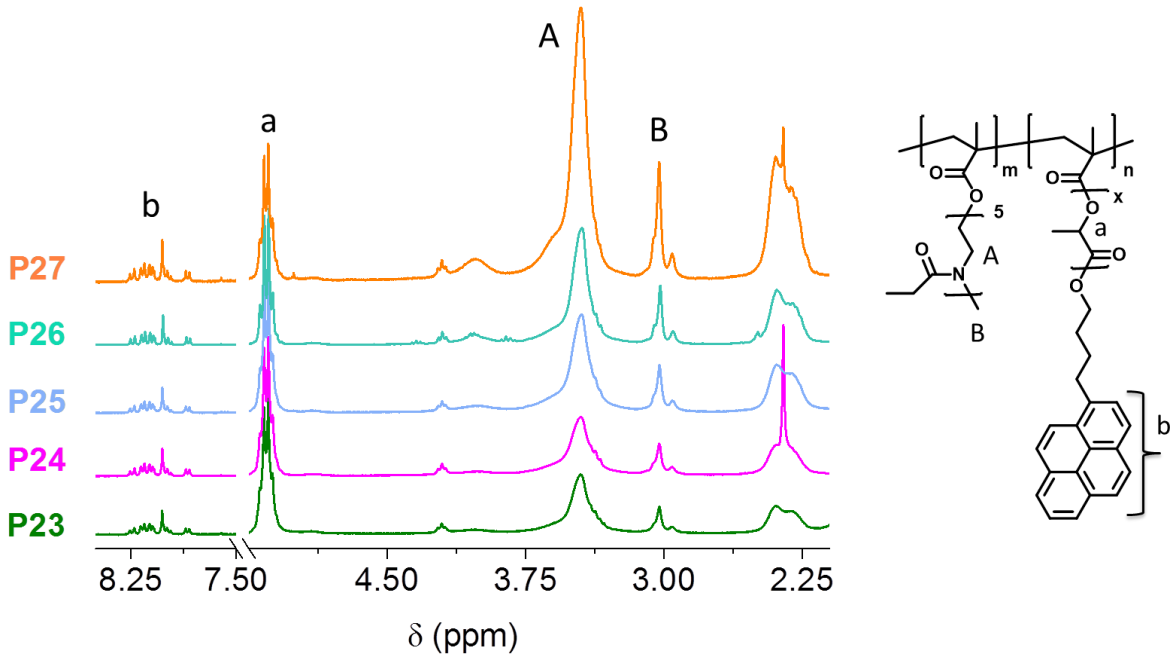

Figure 6.4. Overlay of the ^{1}H NMR spectra (300 MHz, $CDCl_3$) of comb polymers **P23** to **P27**.

The self-assembly behavior of the amphiphilic heterografted comb polymers was investigated by means of dynamic light scattering (DLS) and cryo-transmission electron microscopy (cryo-TEM) analysis in water, which represents a good solvent for PEtOx but non-solvent for the PLA based side chains. **Figure 6.5** shows the overlay of intensity, volume, and number weighted size distributions obtained from the DLS of the comb polymers **P23** to **P27**, together with the representative cryo-TEM micrographs. Only in the case of the most hydrophilic copolymer **P27**, DLS exhibited a bimodal size distribution. Cryo-TEM analysis of **P27** revealed the coexistence of smaller (*ca*. 10 nm) and larger (*ca.* 40 to 50 nm) spherical aggregates, which supports the DLS data. Since the weight fraction of the hydrophilic EtOx is too high (w_{EtOx} = 0.75) in **P27**, the EtOx side chains are probably capable of shielding the hydrophobic PLA segments even without the formation of defined copolymer assemblies. In case of **P25** and **P26** with a lower EtOx weight fraction ($w_{EtOx} \approx 0.6$), cryo-TEM analysis revealed formation of spherical micelles with more homogeneous size distribution. For **P26**, the visualized spherical micelles have a diameter around 10 nm, which roughly corresponds to the double length of a PLA macromonomer with a DP of 10 in the all-*trans* conformation. In accordance with the hydrodynamic diameters obtained from DLS measurements, larger spherical micelles (≈ 30 nm) were visualized from the assemblies of **P25**, as a result of a slight increase in the weight fraction of the hydrophobic PLA content.

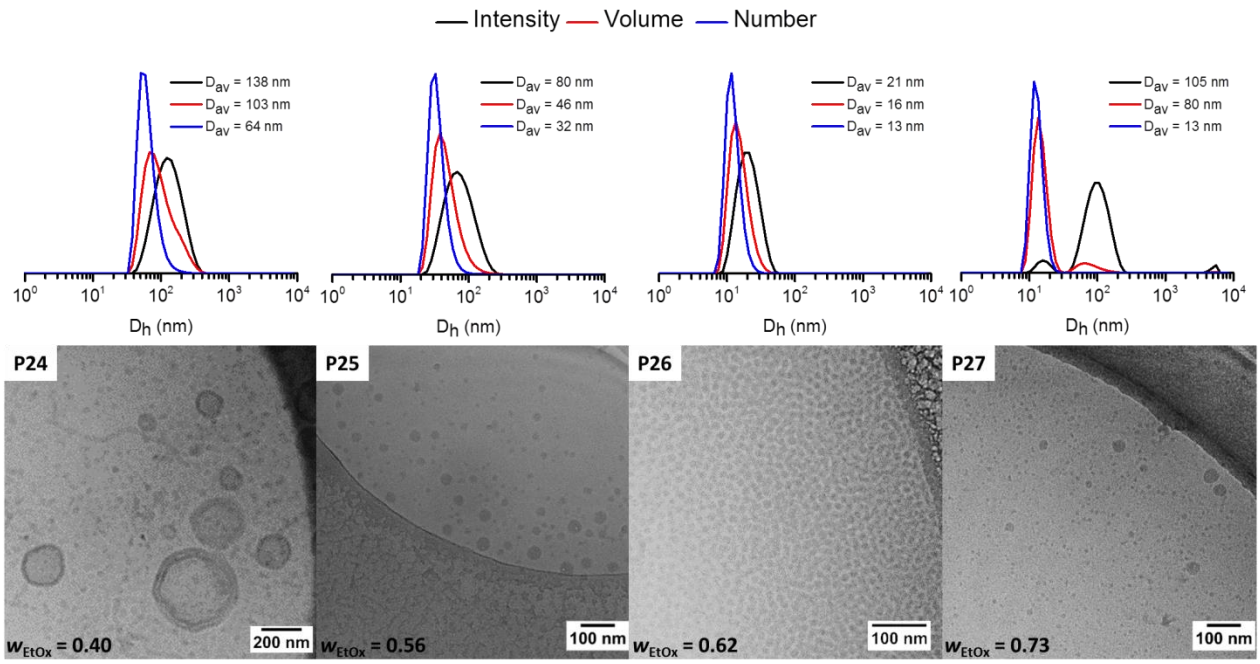

Figure 6.5. DLS size distributions and cryo-TEM images of the suspensions obtained from **P23** to **P27** in water (c = 5 mg mL^{-1}).

Further decrease of the EtOx content resulted in formation of a mixture of self-assembled structures from comb polymers **P24** and **P23**. Spherical micelles, worm like micelles, and large vesicles were visualized by cryo-TEM analysis of **P24**, which is in accordance with the increased hydrodynamic diameters and high polydispersity index (PDI = 0.27) obtained from DLS measurements. The diameter of the spherical and worm-like micelles (17 and 14 nm, respectively) corresponds well with the length of the PLA side chains of the comb polymer, as does the bilayer thickness of the vesicles (13 nm). **P23** and **P24** have similar compositions in terms of mole fraction of EtOx/LA. However **P23** bears longer PLA side chains due to the higher DP of the PLA macromonomer used for the synthesis ($LA_{15}MA$). Thus, it has a lower EtOx content (w_{EtOx} = 0.36). Accordingly, the visualized spherical micelles display slightly larger diameters (≈ 19 nm), and the membrane thickness of the vesicular structures is slightly increased (21 nm), which is in agreement with the length of the respective PLA side chain (≈ 11 nm) (**Figure 6.6A**). Apart from micelles and vesicles, more complex morphologies were also visualized, such as segmented (**B**), distorted (**C**) and lamellar vesicles (**D**) which could be attributable to a hampered phase ordering as a result of restricted side chain mobility (**Figure 6.6**).

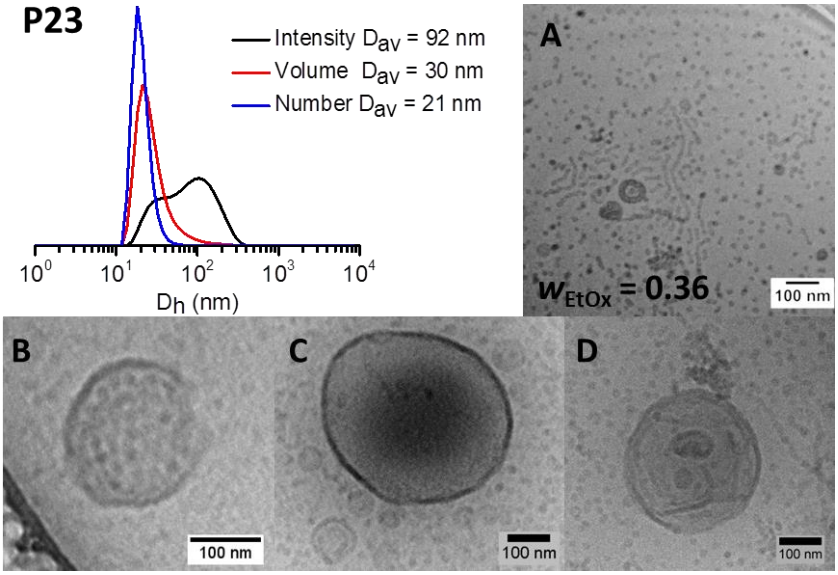

Figure 6.6. DLS size distributions and cryo-TEM images of the suspensions formed by **P23** in water (c = 5 mg mL^{-1}).

It is known that heterografted comb polymers comprising PLA and PEO can form self-assembled structures in the form of micelles or vesicles as the length of side chains is altered in analogy to variation of block lengths of linear block copolymers.[92] Although, we did not alter the DP of the side chains during the synthesis of heterografted comb polymers, changing the fraction of each type of side chain resulted in similar observations. In fact, this outcome is not surprising if one can imagine that the only difference with linear block copolymers is the covalent junction at the comb polymer backbone (**Figure 6.7**).

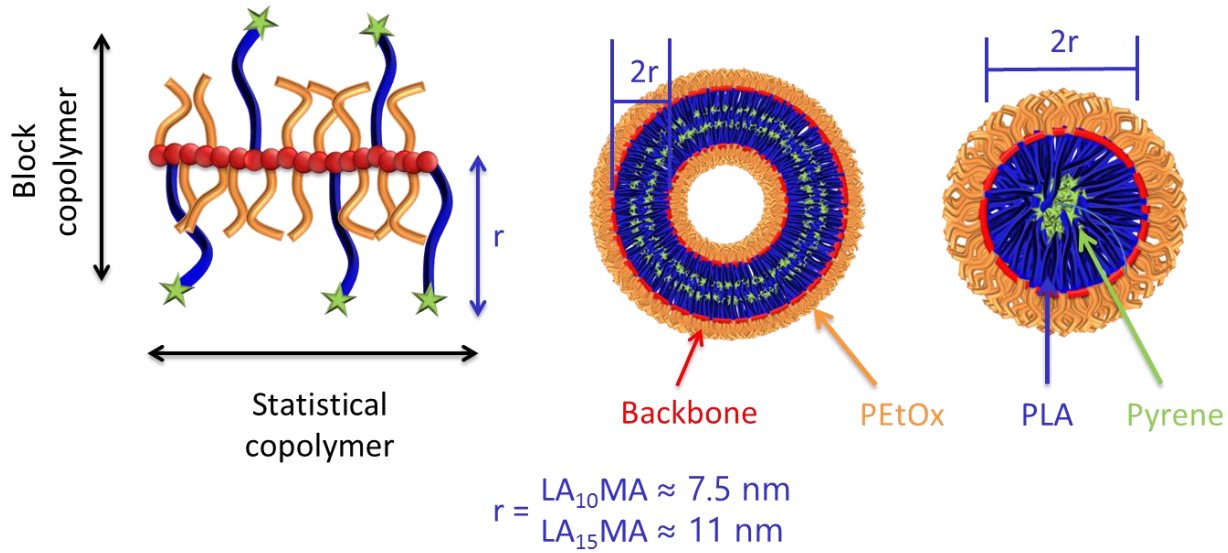

Figure 6.7. Formation of micelles from comb polymers with mixed PEtOx and PLA side chains.

Both PEtOx and PLA represent biocompatible polymers. Therefore the heterografted comb polymer comprising these side chain types was expected to be biocompatible, as well. Hence, the comb polymers showed no significant decrease in cell viability of L929 mouse fibroblast cells after 24 hours of incubation with the comb polymer suspensions **P23** to **P27** up to a concentration of 200 µg mL^{-1} **(Figure 6.8)**. Moreover, no influence of the different structural compositions of the polymers was observed.

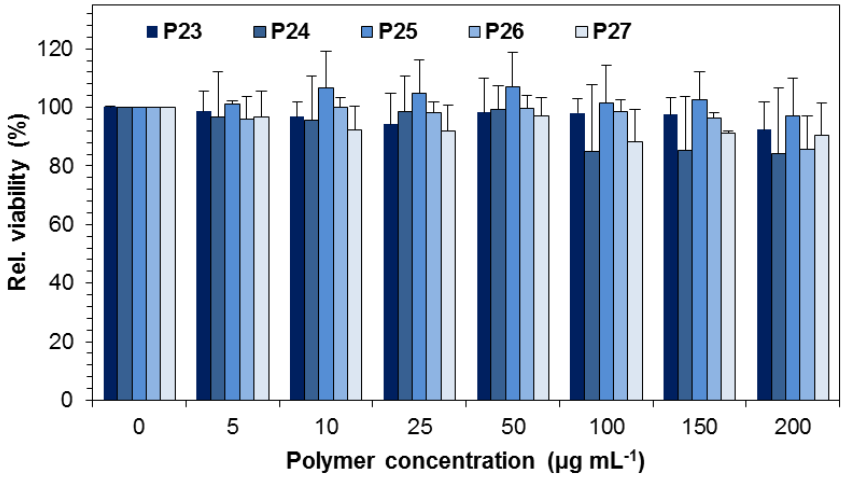

Figure 6.8. Relative viability of L929 cells after 24 hours incubation with heterografted comb polymers (**P23** to **P27**) at indicated concentrations. Values represent the mean ± S.D. (n=3).

Since the PLA side chains of the comb polymers bear a covalently attached pyrene moiety, it was possible to investigate the cellular uptake and intracellular distribution of the comb polymers without the need of encapsulation of an additional fluorophore. As a consequence, HEK cells were incubated with polymer suspensions **P23** to **P27** for four hours (**Figure 6.9**). All tested comb polymers revealed a high cellular internalization at 37 °C as evident by confocal live cell imaging. The detected pyrene signal (magenta) was equally distributed within the cytosol. However, it was just rarely co-localized within the lysosomes (green) and not detectable within the nucleus. This observation could be attributable to either a fast endosomal release or cellular uptake *via* translocation through the cell membrane.

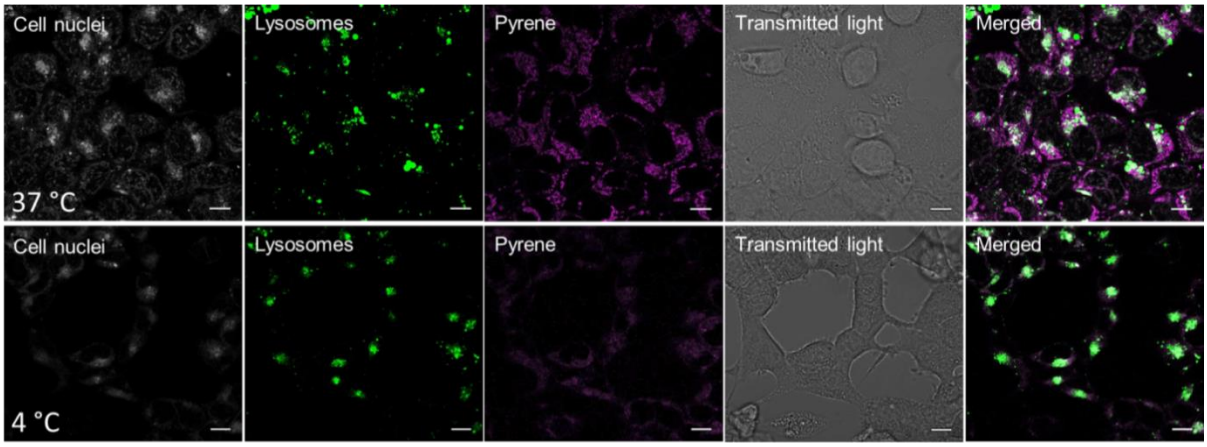

Figure 6.9. Confocal live cell imaging of HEK cells incubated with the suspension of **P23** in water (50 µg mL^{-1}) for 4 h at 37 °C (**top**) and 4 °C (**bottom**). The cell nucleus was stained with NucRed (grey) and the lysosomes/late endosomes with LysoTracker Green (green); pyrene is depicted in magenta (scale bars represent 10 µm).

It is known that uptake mechanism of nanoparticles depends on the size; particles between 20 to 500 nm are up taken in an active manner through endocytosis,[93, 94] whereas particles smaller than 20 nm may also internalize by passive diffusion through channels, protein carriers or by translocation.[95] Therefore, uptake studies of **P23** were performed again at 4 °C, to investigate if the polymers are internalized into the cells by a passive process (**Figure 6.9**). The pyrene fluorescence was decreased within the cells in comparison to the uptake at 37 °C, indicating that only a minor fraction of comb polymers is able to enter the cells by passive penetration. However, the predominant uptake mechanism for **P23** is an energy-driven process.

The facile synthesis of well-defined PLA and PEtOx based methacrylate ω-end-functional macromonomers in a one-pot procedure provides a convenient synthetic approach for fluorescent amphiphilic heterografted comb polymers which consist of oligomeric biocompatible side chains by the combination of ROP, CROP, and RAFT techniques. The self-assembly behavior of the heterografted comb polymers provided a basis for morphology change upon variation of the copolymer composition. The cellular uptake studies were performed without encapsulation of any tracker molecules thanks to the covalently attached pyrene moieties to the PLA side chains revealing that only a slight fraction is localized inside late endosomes/lysosomes. Since this observation is favorable for delivery applications, the heterografted comb polymers can be further investigated in the future for the encapsulation of a hydrophobic drug into the self-assembled structures.

7. Summary

Polylactide (PLA) is a bio-mass derived biodegradable and biocompatible polyester and, thus a key material to a number of applications in material science, drug-delivery and biotechnology. However, some features of unmodified PLA such as hydrophobicity and lacking of reactive side chain functionality limit the use of this unique material for certain applications. For this purpose, introduction of functional/reactive end groups to PLA is of great importance in order to pave the way for designing functional materials based on PLA. Several catalyst/co-initiator systems have been developed for the ring opening polymerization (ROP) of lactide to date, whereas the exploitation of the utilized systems to their full potential in terms of polymer chemistry is very scarce. The objective of the presented thesis was to develop facile synthetic approaches for end-functional PLAs and to combine ring opening polymerization (ROP) and reversible addition-fragmentation chain transfer (RAFT) polymerization for the synthesis of PLA based amphiphilic copolymers with different architectures such linear block and comb type copolymers (**Figure 7.1**).

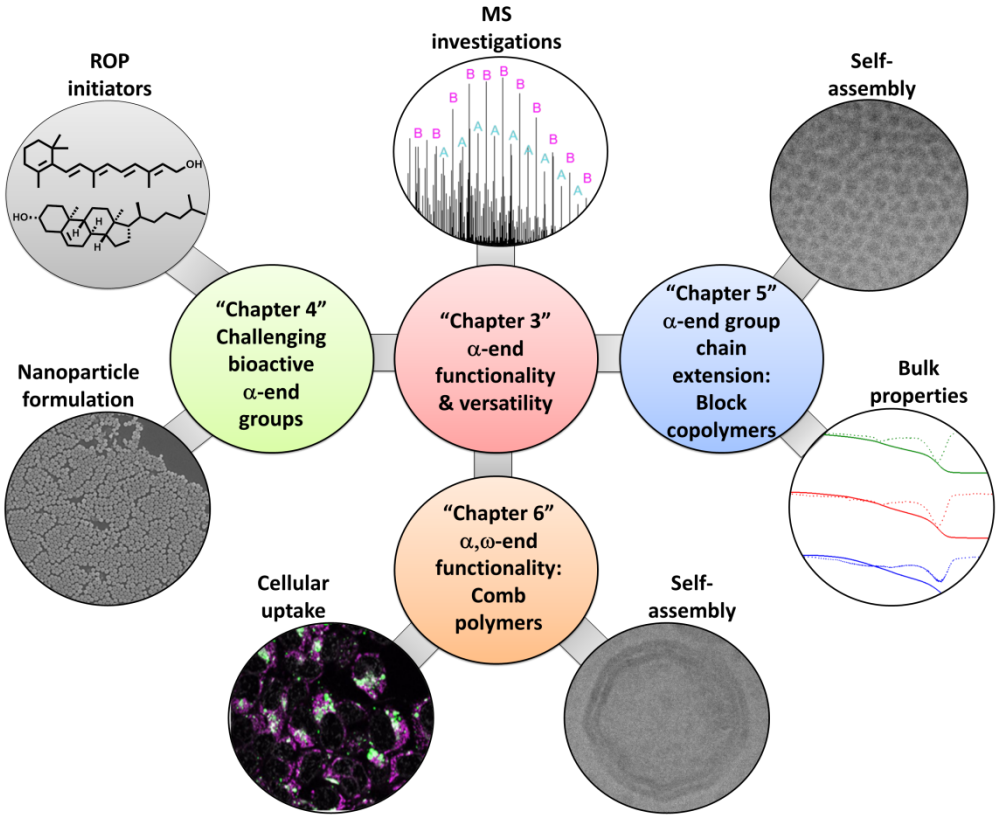

Figure 7.1. Overview of the synthesis strategies discussed in this thesis and schematic representation of the link between end functional PLAs with functional materials based on PLA homo- and copolymers.

End-functional PLAs were accessible *via* the ROP of L-lactide in the presence of $Sn(Oct)_2$ and $Ca[N(SiMe_3)_2]_2(THF)_2$. In particular, the calcium based precatalyst $Ca[N(SiMe_3)_2]_2(THF)_2$ enabled the ROP of L-lactide *via in situ* calcium alkoxide formation in the presence of numerous primary, secondary and tertiary alcohols including protected sugars, a drug molecule, a fluorescent label, and a chain transfer agent (CTA). The PLAs were well-defined both in terms of molar mass distribution and end-group fidelity. Mass spectrometry (MS) techniques such as electrospray ionization (ESI) and matrix-assisted laser desorption/ionization (MALDI) time-of-flight MS allowed in-depth characterization of the end-functional PLAs and shed light on the ROP mechanism in the presence of $Ca[N(SiMe_3)_2]_2(THF)_2$. The PLAs synthesized in the presence of $Ca[N(SiMe_3)_2]_2(THF)_2$ were composed of lactic acid repeating units instead of lactide dimers, which may arise through an intramolecular rearrangement at the active catalytic center during the ROP. Having demonstrated the excellent performance of the calcium based precatalyst $Ca[N(SiMe_3)_2]_2(THF)_2$, further focus was laid upon its exploitation in terms of the preparation of functional materials.

Moving towards potential applicable materials, the non-toxic catalyst system was further applied to obtain PLA-conjugates in the presence of (sensitive) biologically active initiators. PLA-retinol conjugates were successfully prepared by utilizing retinol as ROP initiator. Stable nanoparticles were prepared from PLA-retinol conjugates in the size range between 100 to 250 nm. Storage stability investigations showed that the PLA-retinol conjugate had an excellent stability when stored at low temperatures and in the dark. However, upon storage under ambient conditions in bulk, the retinoid moiety almost completely degraded while the PLA itself remained intact. The degradation of the retinyl moiety was slightly reduced in case of the storage of the corresponding nanoparticle suspension in the dark at room temperature. Aiming towards the preparation of polymeric microparticles which can specifically deliver cholesterol to lungs in order to reduce cell lysis resulting from bacterial toxins, cholesterol was used as an initiator for the ROP of lactide, yielding a well-defined PLA-cholesterol conjugate. First results using microparticles made from the PLA-cholesterol conjugate indeed indicated their potency in reducing cytotoxicity arising from pneumolysin in HepG2 cells.

Benefiting from the high end group fidelity of the CTA functional PLA, which was verified by tandem MS investigations, a linear block copolymer library comprising fixed PLA chain length but varying poly(2-hydroxyethyl acrylate) (PHEA) unit length was prepared. The ROP of L-lactide was combined with RAFT polymerization of 2-hydroxyethyl acrylate (HEA) by chain

extension of the PLA macro-CTA with HEA in a one-pot approach at room temperature. The described strategy is facile and does not require performing any intermediate purification step or the use of protection group chemistry. In addition, the utilized one-pot approach gave access to materials with bulk and solution properties as expected for block copolymers composed of immiscible blocks. The PLA-*b*-PHEA block copolymers featured phase segregation in bulk when the block lengths of both units are similar. The expected nanostructures *i.e.* worm like and spherical micelles were formed by self-assembly of the amphiphilic PLA-*b*-PHEA block copolymers in aqueous media.

Based on the use of 1-pyrene butanol as initiator for the ROP of lactide yielding a PLA based fluorescent probe, α,ω-end functional PLA macromonomers were prepared in a one-pot approach by utilizing methacryloyl chloride as end-capping agent *via* the direct ω-end functionalization of the resulting anionic PLA species. The copolymerization of the hydrophobic PLA based macromonomers with a hydrophilic poly(2-oxazoline) (POx) based macromonomer *via* RAFT polymerization enabled the synthesis of amphiphilic heterografted comb polymers consisting of oligomeric biocompatible side chains. The hydrophilicity of the heterografted comb polymers was varied by keeping the length of backbone constant but by changing the feed ratio of the both macromonomer types. Aqueous self-assembly of the heterografted comb polymers revealed morphology change from spherical micelles to vesicles when the feed ratio of the macromonomers altered in analogy to variation of the block lengths in linear diblock copolymers. The comb polymers were found to be non-toxic to L929 cells up to a concentration of 200 μg mL^{-1}. Cellular uptake studies were performed without encapsulation of any tracker molecules with HEK-293 cells revealed localization of the comb polymers in the cytosol after four hours.

In summary, this thesis presented the synthesis of end-functional PLAs by utilizing metal-alkoxide formation mainly in the presence of $Ca[N(SiMe_3)_2]_2(THF)_2$. The effective and mild precatalyst yielded functional PLAs with high end group fidelity which enabled the combination of mechanistically distinct ROP and RAFT polymerization techniques. This was exploited for the preparation of block and comb type copolymers with (meth)acrylate based biocompatible comonomers. Preliminary biological studies of the functional PLA (co)polymers revealed promising results, which encourages further biological applications in addition to the already begun study of the PLA-cholesterol conjugates with regard to pneumonia. For example, the PLA-retinol conjugates could be further developed so that a targeted transport of active

substances into hepatic stellate cells is made possible. In addition, the potent of the precatalyst urges its exploitation for the ROP of other cyclic lactones, either for homopolymerization or for the copolymerization with lactide. Future research will focus on the detailed elucidation of the proposed ROP mechanism in the presence of $Ca[N(SiMe_3)_2]_2(THF)_2$.

8. Zusammenfassung

Polylactid (PLA) ist ein biologisch abbaubarer und biokompatibler Polyester und damit ein wichtiges Material für eine Reihe von Anwendungen in der Materialwissenschaft, der Arzneimittelformulierung und der Biotechnologie. Allerdings beschränken einige Merkmale von unmodifiziertem PLA wie Hydrophobie und fehlende reaktive Seitenkettenfunktionalität die Verwendung dieses einzigartigen Materials für bestimmte Anwendungen. Zu diesem Zweck ist die Einführung von funktionellen/reaktiven Endgruppen am PLA von großer Bedeutung, um den Weg für die gezielte Entwicklung von funktionellen Materialien auf der Basis von PLA zu ebnen. Mehrere Katalysator-/Co-Initiatorsysteme wurden für die bisherige Ringöffnungspolymerisation (ROP) von Lactid entwickelt, während das Potenzial der bekannten Systeme bezüglich der Polymerchemie bei Weitem nicht ausgeschöpft wurde. Ziel der vorliegenden Arbeit war es, einfache synthetische Ansätze mittels Ringöffnungspolymerisation (ROP) für endfunktionelle PLAs zu entwickeln und diese gezielt zur Entwicklung von Copolymeren mit außergewöhnlichen Architekturen zu nutzen (**Abbildung 8.1**).

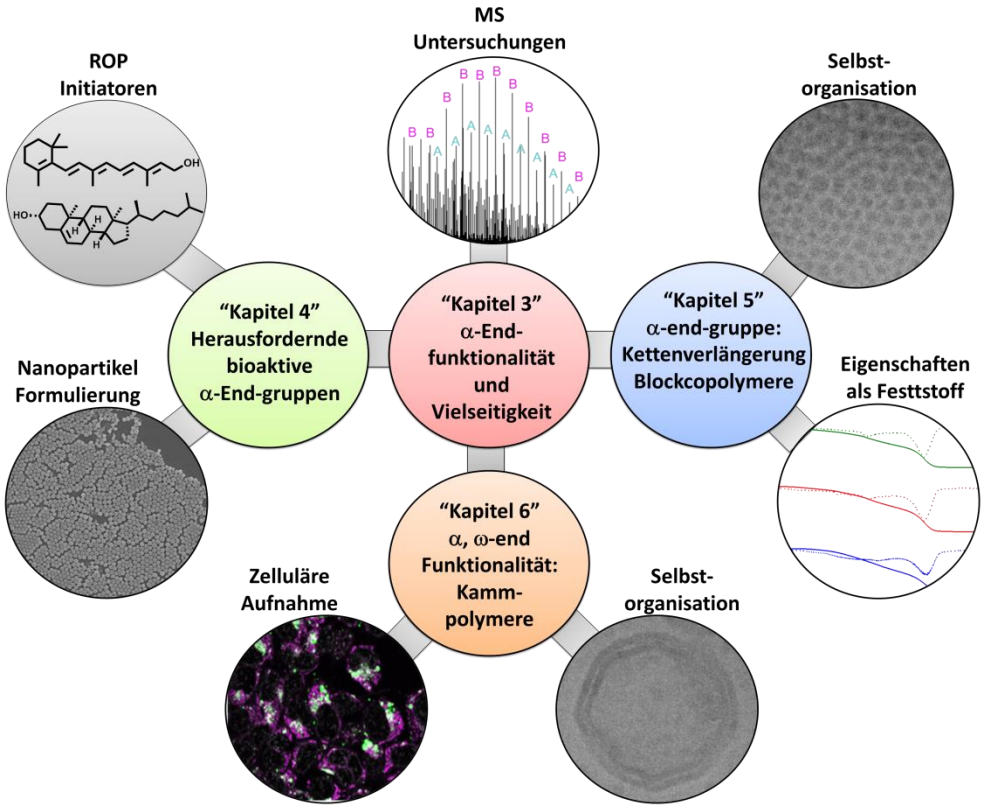

Abbildung 8.1. Übersicht über die in dieser Arbeit diskutierten Synthesestrategien und schematische Darstellung der Verknüpfung zwischen endfunktionellen PLAs mit funktionellen Materialien auf Basis von PLA-Homo- und -Copolymeren.

End-funktionelle PLAs waren über die ROP von L-Lactid in Gegenwart von $Sn(Oct)_2$ und $Ca[N(SiMe_3)_2]_2(THF)_2$ zugänglich. Insbesondere ermöglichte der Calcium-basierte Präkatalysator die ROP von L-Lactid über eine *in situ*-Calciumalkoxidbildung in Gegenwart zahlreicher primärer, sekundärer und tertiärer Alkohole, einschließlich geschützter Zucker, eines pharmazeutischen Wirkstoffs, Pyrene-1-Butanol (Py) als Fluoreszlabel und einem Kettenübertragungsagens (CTA). Die PLAs waren sowohl hinsichtlich der Molmassenverteilung als auch der Endgruppe gut definiert. Massenspektrometrie (MS)-Techniken wie Elektrospray-Ionisations (ESI) und Matrix-unterstützte Laser-Desorptions-/Ionisations-Flugzeit (MALDI-ToF) MS ermöglichten es, Einblick in den ROP-Mechanismus in Gegenwart von $Ca[N(SiMe_3)_2]_2(THF)_2$ erhalten. Die in entsprechenden PLAs bestanden aus Milchsäure-Wiederholungseinheiten anstelle deren Dimeren, was durch eine intramolekulare Umlagerung am aktiven katalytischen Zentrum während der ROP begründet werden kann. Nach der ausgezeichneten Leistung des Calcium-basierten Präkatalysators $Ca[N(SiMe_3)_2]_2(THF)_2$ wurde der weitere Schwerpunkt auf die Ausschöpfung dessen Potenzials hinsichtlich der Herstellung von funktionellen Materialien gelegt.

Hierfür wurde das nicht-toxische Katalysatorsystem zunächst weiter eingesetzt, um PLA-Konjugate in Gegenwart von (empfindlichen) biologisch aktiven Initiatoren zu erhalten. Zur zielgerichteten Verabreichung von Wirkstoffen in Leber-Sternzellen wurden PLA-Retinol-Konjugate erfolgreich unter Verwendung von Retinol als ROP-Initiator hergestellt, aus denen stabile Nanopartikel in wässriger Suspension erhalten werden könnten. Stabilitätsuntersuchungen während der Lagerung erwiesen eine ausgezeichnete Stabilität der Konjugate bei niedrigen Temperaturen im Dunkeln. Bei der Lagerung unter Normalbedingungen als Feststoff wurde die Retinoidfunktionalität jedoch nahezu vollständig degradiert, während das PLA selbst intakt blieb, was im Falle der Nanopartikel-Suspension leicht reduziert werden konnte. Cholesterin als Initiator für die ROP von Lactid ergab ein wohldefiniertes PLA-Cholesterin-Konjugat, angedacht zur Behandlung von Pneumonie. In der Tat weisen erste Ergebnisse darauf hin, dass die Zytotoxizität von Pneumolysin, eines typischen Toxins, unter Verwendung von entsprechenden Mikropartikeln in HepG2-Zellen reduziert werden kann.

Das CTA-funktionale PLA wurde zur Herstellung einer Bibliothek von PLA-*b*-PHEA Blockcopolymeren genutzt. Hierfür würde zunächst die Endgruppenfunktionalität des PLA-Makro-CTA im Detail mittels Tandem-MS-Untersuchungen verifiziert. Dieses wurde anschließend zur RAFT-Polymerisation von 2-Hydroxyethylacrylat (HEA) eingesetzt, wobei der

Polymerisationsgrad des PHEA variiert, aber der des PLA konstant gehalten wurde. Die dazu entwickelte Ein-Topf-Strategie ist bei Raumtemperatur einfach durchführbar, erfordert weder eine Zwischenreinigungsstufe noch die Anwendung von Schutzgruppen und liefert Zugang zu einer Reihe von Blockcopolymeren, die aus nicht miteinander mischbaren Blöcken bestehen. Die mit diesem neuen Ansatz erhaltenen Materialien wiesen in der Tat die erwarteten Eigenschaften auf: Eine Phasenseparation im bulk, sowie die Ausbildung entsprechender Nanostrukturen durch Selbstorganisation der amphiphilen PLA-*b*-PHEA-Blockcopolymere in wässrigen Medien.

Die Tatsache, dass durch Initiierung der ROP von Lactid mittels Py, Fluoreszenz-markierte „PLA-Bausteine“ erhalten werden können, wurde zur Entwicklung von Kammpolymeren, die sowohl PLA- als auch Seitenketten tragen, die biologische „stealth“- Eigenschaften aufweisen. Hierzu wurden α, ω-end-funktionelle PLA-Makromonomere hergestellt, und zwar durch direkte ω-Endfunktionalisierung der anionischen PLA-Spezies unter Verwendung von Methacrylsäurechlorid. Die anschließende RAFT Copolymerisation der hydrophoben PLA-basierten Makromonomere mit einem hydrophilen Poly(2-oxazolin) (POx)-basierten Makromonomer ergab eine Reihe von biokompatiblen amphiphilen Kammpolymeren, deren Hydrophilie durch das Verhältnis beider Makromonomere gesteuert werden konnte. Durch die kovalente Verknüpfung der hydrophilen und hydrophoben Seitenketten wurde das Selbstorganisationsverhalten der Kammpolymere in wässrigen Medien erschwert, was teils zu außergewöhnlichen Nanostrukturen führte, sich teils aber auch auf etablierte Modelle für lineare Blockcopolymere zurückführen lässt. Aufgrund der anfangs erfolgten kovalenten Anbindung von Py konnten Untersuchungen zur zellulären Aufnahme der in HEK-293-Zellen ohne Verkapselung von Tracker-Molekülen mit durchgeführt werden. Es zeigte sich eine aktive Aufnahme, wobei die Kammpolymere nach vier Stunden gleichmäßig im Cytosol verteilt waren, was für deren weiterführende Verwendung als Wirkstofftransporter vorteilhaft ist.

Zusammenfassend stellte diese Arbeit die Synthese von endfunktionellen PLAs unter mittels Metall-Alkoxid-Bildung vor allem in Gegenwart von $Ca[N(SiMe_3)_2]_2(THF)_2$ vor. Der wirksame und milde Präkatalysator lieferte funktionelle PLAs mit hoher Endgruppentreue, die die Kombination von mechanistisch unterschiedlichen ROP- und RAFT-Polymerisationstechniken ermöglichten. Dies wurde für die Herstellung von Block- und Kamm-Copolymeren mit (meth)acrylatbasierten biokompatiblen Comonomeren ausgenutzt. Vorläufige biologische Untersuchungen der funktionellen PLA (Co)Polymere zeigten vielversprechende Ergebnisse, die neben der bereits begonnenen Untersuchung der PLA-Cholesterin-Konjugate im Hinblick auf

Pneumonie weitere biologische Anwendungen sinnvoll erscheinen lassen. Beispielsweise könnten die PLA-Retinol-Konjugate weiter entwickelt werden, so dass ein zielgerichteter Wirkstofftransport in hepatische Sternzellen ermöglicht wird. Darüber hinaus sollte die Effektivität des Präkatalysators für die ROP anderer cyclischer Lactone ausgenutzt werden, entweder zur Homopolymerisation oder zur Copolymerisation mit Lactid. Zukünftige Studien sollten sich in diesem Zuge auf die detaillierte Aufklärung des vorgeschlagenen ROP-Mechanismus in Gegenwart von $Ca[N(SiMe_3)_2]_2(THF)_2$ stützen.

References

[1] C. M. Thomas, J.-F. Lutz, *Angew. Chem. Int. Ed.* **2011**, *50*, 9244-9246.

[2] A. J. R. Lasprilla, G. A. R. Martinez, B. H. Lunelli, A. L. Jardini, R. M. Filho, *Biotechnol. Adv.* **2012**, *30*, 321-328.

[3] K. Madhavan Nampoothiri, N. R. Nair, R. P. John, *Bioresour. Technol.* **2010**, *101*, 8493-8501.

[4] J.-M. Raquez, Y. Habibi, M. Murariu, P. Dubois, *Prog. Polym. Sci.* **2013**, *38*, 1504-1542.

[5] O. Dechy-Cabaret, B. Martin-Vaca, D. Bourissou, *Chem. Rev.* **2004**, *104*, 6147-6176.

[6] B.-T. Ko, C.-C. Lin, *J. Am. Chem. Soc.* **2001**, *123*, 7973-7977.

[7] A. Loefgren, A. C. Albertsson, P. Dubois, R. Jerome, P. Teyssie, *Macromolecules* **1994**, *27*, 5556-5562.

[8] M. H. Chisholm, J. C. Huffman, K. Phomphrai, *J. Chem. Soc. Dalton. Trans.* **2001**, 222-224.

[9] Z. Zhong, S. Schneiderbauer, P. J. Dijkstra, M. Westerhausen, J. Feijen, *J. Polym. Environ.* **2001**, *9*, 31-38.

[10] K. Nie, L. Fang, Y. Yao, Y. Zhang, Q. Shen, Y. Wang, *Inorg. Chem.* **2012**, *51*, 11133-11143.

[11] R. M. Rasal, A. V. Janorkar, D. E. Hirt, *Prog. Polym. Sci.* **2010**, *35*, 338-356.

[12] G. Mittal, D. K. Sahana, V. Bhardwaj, M. N. V. Ravi Kumar, *J. Control. Release* **2007**, *119*, 77-85.

[13] S. Zhou, X. Liao, X. Li, X. Deng, H. Li, *J. Control. Release* **2003**, *86*, 195-205.

[14] D. A. Shipp, *Polym. Rev.* **2011**, *51*, 99-103.

[15] A. P. Dove, *Chem. Commun.* **2008**, 6446-6470.

[16] J. K. Oh, *Soft Matter* **2011**, *7*, 5096-5108.

[17] R. D. Puts, D. Y. Sogah, *Macromolecules* **1997**, *30*, 7050-7055.

[18] M. W. Weimer, O. A. Scherman, D. Y. Sogah, *Macromolecules* **1998**, *31*, 8425-8428.

[19] K. V. Bernaerts, F. E. Du Prez, *Prog. Polym. Sci.* **2006**, *31*, 671-722.

[20] L. Tao, B. Luan, C.-y. Pan, *Polymer* **2003**, *44*, 1013-1020.

[21] R. C. Pratt, B. G. G. Lohmeijer, D. A. Long, P. N. P. Lundberg, A. P. Dove, H. Li, C. G. Wade, R. M. Waymouth, J. L. Hedrick, *Macromolecules* **2006**, *39*, 7863-7871.

[22] N. R. Ko, K. Yao, C. Tang, J. K. Oh, *J. Polym. Sci., Part A: Polym. Chem.* **2013**, *51*, 3071-3080.

[23] C. Ye, G. Zhao, M. Zhang, J. Du, Y. Zhao, *Macromolecules* **2012**, *45*, 7429-7439.

[24] F. F. Wolf, N. Friedemann, H. Frey, *Macromolecules* **2009**, *42*, 5622-5628.

[25] H. U. Kang, Y. C. Yu, S. J. Shin, J. H. Youk, *J. Polym. Sci., Part A: Polym. Chem.* **2013**, *51*, 774-779.

[26] G. Moad, E. Rizzardo, S. H. Thang, *Acc. Chem. Res.* **2008**, *41*, 1133-1142.

[27] A. O. Saeed, S. Dey, S. M. Howdle, K. J. Thurecht, C. Alexander, *J. Mater. Chem.* **2009**, *19*, 4529-4535.

[28] L. Mespouille, F. Nederberg, J. L. Hedrick, P. Dubois, *Macromolecules* **2009**, *42*, 6319-6321.

[29] M. Isik, H. Sardon, M. Saenz, D. Mecerreyes, *RSC Advances* **2014**, *4*, 53407-53410.

[30] L. Sun, N. Petzetakis, A. Pitto-Barry, T. L. Schiller, N. Kirby, D. J. Keddie, B. J. Boyd, R. K. O'Reilly, A. P. Dove, *Macromolecules* **2013**, *46*, 9074-9082.

[31] L. Sun, A. Pitto-Barry, N. Kirby, T. L. Schiller, A. M. Sanchez, M. A. Dyson, J. Sloan, N. R. Wilson, R. K. O'Reilly, A. P. Dove, *Nat. Commun.* **2014**, *5*, 5746.

[32] M. Barz, A. Armiñán, F. Canal, F. Wolf, K. Koynov, H. Frey, R. Zentel, M. J. Vicent, *J. Control. Release* **2012**, *163*, 63-74.

[33] A. K. Mishra, V. K. Patel, N. K. Vishwakarma, C. S. Biswas, M. Raula, A. Misra, T. K. Mandal, B. Ray, *Macromolecules* **2011**, *44*, 2465-2473.

[34] M. J. Stanford, A. P. Dove, *Macromolecules* **2009**, *42*, 141-147.

[35] J. Rzayev, M. A. Hillmyer, *Macromolecules* **2005**, *38*, 3-5.

[36] J.-F. Lutz, N. Jahed, K. Matyjaszewski, *J. Polym. Sci., Part A: Polym. Chem.* **2004**, *42*, 1939-1952.

[37] H. Shinoda, K. Matyjaszewski, *Macromolecules* **2001**, *34*, 6243-6248.

[38] J. He, X. Yang, J. Mao, F. Xu, Q. Cai, *Appl. Surf. Sci.* **2012**, *258*, 6823-6830.

[39] R. Jérôme, D. Mecerreyes, D. Tian, P. Dubois, C. J. Hawker, M. Trollsas, J. L. Hedrick, *Macromol. Symp.* **1998**, *132*, 385-403.

[40] M. Bagheri, E. Bigdeli, *J. Polym. Res.* **2013**, *20*, 84.

[41] C. Wu, A. Ying, S. Ren, *Colloid Polym. Sci.* **2013**, *291*, 827-834.

[42] H. Kakwere, S. Perrier, *J. Polym. Sci., Part A: Polym. Chem.* **2009**, *47*, 6396-6408.

[43] K. Huang, J. Rzayev, *J. Am. Chem. Soc.* **2009**, *131*, 6880-6885.

[44] R. Fenyves, M. Schmutz, I. J. Horner, F. V. Bright, J. Rzayev, *J. Am. Chem. Soc.* **2014**, *136*, 7762-7770.

[45] K. Huang, D. P. Canterbury, J. Rzayev, *Macromolecules* **2010**, *43*, 6632-6638.

[46] K. Bernard, P. Degée, P. Dubois, *Polym. Int.* **2003**, *52*, 406-411.

[47] A. J. Cross, M. G. Davidson, D. Garcia-Vivo, T. D. James, *RSC Advances* **2012**, *2*, 5954-5956.

[48] K. Kempe, A. Krieg, C. R. Becer, U. S. Schubert, *Chem. Soc. Rev.* **2012**, *41*, 176-191.

[49] M. Beija, M.-T. Charreyre, J. M. G. Martinho, *Prog. Polym. Sci.* **2011**, *36*, 568-602.

[50] K.-H. Park, W. J. Sung, S. Kim, D. H. Kim, T. Akaike, H.-M. Chung, *J. Biosci. Bioeng.* **2005**, *99*, 285-289.

[51] S. Ogawa, S. Takano, H. Fujimori, T. Itoh, S. Kaita, T. Iida, Y. Wakatsuki, *React. Funct. Polym.* **2010**, *70*, 563-571.

[52] M. R. ten Breteler, J. Feijen, P. J. Dijkstra, F. Signori, *React. Funct. Polym.* **2013**, *73*, 30-38.

[53] H.-L. Chen, S. Dutta, P.-Y. Huang, C.-C. Lin, *Organometallics* **2012**, *31*, 2016-2025.

[54] A. Otero, J. Fernández-Baeza, L. F. Sánchez-Barba, J. Tejeda, M. Honrado, A. Garcés, A. Lara-Sánchez, A. M. Rodríguez, *Organometallics* **2012**, *31*, 4191-4202.

[55] V. Katiyar, H. Nanavati, *Polym. Chem.* **2010**, *1*, 1491-1500.

[56] J. Baran, A. Duda, A. Kowalski, R. Szymanski, S. Penczek, *Macromol. Symp.* **1997**, *123*, 93-101.

[57] G. Montaudo, M. S. Montaudo, C. Puglisi, F. Samperi, N. Spassky, A. LeBorgne, M. Wisniewski, *Macromolecules* **1996**, *29*, 6461-6465.

[58] Z. Zhong, P. J. Dijkstra, C. Birg, M. Westerhausen, J. Feijen, *Macromolecules* **2001**, *34*, 3863-3868.

[59] R. Álvarez, B. Vaz, H. Gronemeyer, Á. R. de Lera, *Chem. Rev.* **2014**, *114*, 1-125.

[60] P. D. Kiser, M. Golczak, K. Palczewski, *Chem. Rev.* **2014**, *114*, 194-232.

[61] S. A. Papadimitriou, M. P. Robin, D. Ceric, R. K. O'Reilly, S. Marino, M. Resmini, *Nanoscale* **2016**, *8*, 17340-17349.

[62] K. M. Park, H. C. Kang, J. K. Cho, I.-J. Chung, S.-H. Cho, Y. H. Bae, K. Na, *Biomaterials* **2009**, *30*, 2642-2652.

[63] W. Bollag, E. E. Holdener, *Ann. Oncol.* **1992**, *3*, 513-526.

[64] J. S. Lee, Y. S. Nam, B. Y. Kang, S. H. Han, I. S. Chang, *J. Appl. Polym. Sci.* **2004**, *92*, 517-522.

[65] N. G. Eskandar, S. Simovic, C. A. Prestidge, *Int. J. Pharm.* **2009**, *376*, 186-194.

[66] P. P. Fu, Q. Xia, J. J. Yin, S.-H. Cherng, J. Yan, N. Mei, T. Chen, M. D. Boudreau, P. C. Howard, W. G. Wamer, *Photochem. Photobiol.* **2007**, *83*, 409-424.

[67] K. B. Clark, J. A. Howard, A. R. Oyler, *J. Am. Chem. Soc.* **1997**, *119*, 9560-9561.

[68] I. Washington, S. Jockusch, Y. Itagaki, N. J. Turro, K. Nakanishi, *Angew. Chem. Int. Ed.* **2005**, *44*, 7097-7100.

[69] J. Zhao, H. Schlaad, S. Weidner, M. Antonietti, *Polym. Chem.* **2012**, *3*, 1763-1768.

[70] Y. Sung Nam, K. Joong Kim, H. Seok Kang, T. Gwan Park, S.-H. Han, I.-S. Chang, *J. Appl. Polym. Sci.* **2003**, *89*, 1631-1637.

[71] R. Tong, J. Cheng, *J. Am. Chem. Soc.* **2009**, *131*, 4744-4754.

[72] J. De Winter, V. Lemaur, P. Marsal, O. Coulembier, J. Cornil, P. Dubois, P. Gerbaux, *J. Am. Soc. Mass Spectrom.* **2010**, *21*, 1159-1168.

[73] B. C. Katzenmeyer, L. R. Cool, J. P. Williams, K. Craven, J. M. Brown, C. Wesdemiotis, *Int. J. Mass Spectrom.* **2015**, *378*, 303-311.

[74] E. I. Finkelshtein, I. S. Krasnokutskaya, *J. Phys. Org.* **1996**, *9*, 411-418.

[75] F. Ercole, M. R. Whittaker, J. F. Quinn, T. P. Davis, *Biomacromolecules* **2015**, *16*, 1886-1914.

[76] D. Mecerreyes, G. Moineau, P. Dubois, R. Jérôme, J. L. Hedrick, C. J. Hawker, E. E. Malmström, M. Trollsas, *Angew. Chem. Int. Ed.* **1998**, *37*, 1274-1276.

[77] S. J. Shin, Y. C. Yu, J. D. Seo, S. J. Cho, J. H. Youk, *J. Polym. Sci., Part A: Polym. Chem.* **2014**, *52*, 1607-1613.

[78] M. Seo, C. J. Murphy, M. A. Hillmyer, *ACS Macro Letters* **2013**, *2*, 617-620.

[79] H. Kakwere, S. Perrier, *Polym. Chem.* **2011**, *2*, 270-288.

[80] J. De Winter, O. Coulembier, P. Dubois, P. Gerbaux, *Int. J. Mass Spectrom.* **2011**, *308*, 11-17.

[81] V. Scionti, C. Wesdemiotis, *J. Mass Spectrom.* **2012**, *47*, 1442-1449.

[82] A. J. Convertine, N. Ayres, C. W. Scales, A. B. Lowe, C. L. McCormick, *Biomacromolecules* **2004**, *5*, 1177-1180.

[83] H. U. Kang, Y. C. Yu, S. J. Shin, J. Kim, J. H. Youk, *Macromolecules* **2013**, *46*, 1291-1295.

[84] M. Hales, C. Barner-Kowollik, T. P. Davis, M. H. Stenzel, *Langmuir* **2004**, *20*, 10809-10817.

[85] L. H. Sperling, in *Introduction to Physical Polymer Science*, John Wiley & Sons, Inc., **2005**, pp. 687-756.

[86] L. Zhao, Z. Lin, *Soft Matter* **2011**, *7*, 10520-10535.

[87] Y. Xia, B. D. Olsen, J. A. Kornfield, R. H. Grubbs, *J. Am. Chem. Soc.* **2009**, *131*, 18525-18532.

[88] H.-i. Lee, K. Matyjaszewski, S. Yu-Su, S. S. Sheiko, *Macromolecules* **2008**, *41*, 6073-6080.

[89] C. Weber, M. Wagner, D. Baykal, S. Hoeppener, R. M. Paulus, G. Festag, E. Altuntas, F. H. Schacher, U. S. Schubert, *Macromolecules* **2013**, *46*, 5107-5116.

[90] N. Adams, U. S. Schubert, *Adv. Drug Deliv. Rev.* **2007**, *59*, 1504-1520.

[91] J. Kronek, Z. Kroneková, J. Lustoň, E. Paulovičová, L. Paulovičová, B. Mendrek, *J. Mater. Sci: Mater. Med.* **2011**, *22*, 1725-1734.

[92] H. Luo, J. L. Santos, M. Herrera-Alonso, *Chem. Commun.* **2014**, *50*, 536-538.

[93] J. Rejman, V. Oberle, I. S. Zuhorn, D. Hoekstra, *Biochem. J.* **2004**, *377*, 159-169.

[94] L. Xiao, X. Xiong, X. Sun, Y. Zhu, H. Yang, H. Chen, L. Gan, H. Xu, X. Yang, *Biomaterials* **2011**, *32*, 5148-5157.

[95] L. Treuel, X. Jiang, G. U. Nienhaus, *J. R. Soc. Interface* **2013**, *10*.

Supplementary information

Additional experimental section for **Chapter 4** containing not yet published results.

Materials

Cholesterol and L-lactide were purchased from Sigma-Aldrich. L-lactide was purified by recrystallization from dry toluene and dried under vacuum. THF was dried by refluxing over sodium/benzophenone.

Instruments

Ring opening polymerization (ROP) was carried out under nitrogen in a MBraun UNILab glove box workstation. Proton nuclear magnetic resonance (^{1}H NMR) spectra were recorded at room temperature in $CDCl_3$ using a Bruker Avance 300. Size exclusion chromatography (SEC) measurements were performed on a Shimadzu system equipped with a SCL-10A system controller, a LC-10AD pump, a RID-10A refractive index detector, SPD-10AD UV detector and SDV linear M column from PSS (Polymer Standards Service GmbH, Mainz, Germany) at 40 °C using THF as eluent at a flow rate of 1 mL min^{-1}. The system was calibrated against PLA standards (144 to 101,000 g mol^{-1}), which were purchased from PSS. The matrix-assisted laser desorption/ionization (MALDI) spectrum was measured on an Ultraflex III ToF/ToF instrument (Bruker Daltonics, Bremen, Germany). The instrument is equipped with a Nd-YAG laser and a collision cell. Measurement was performed in positive and reflector mode. The instrument was calibrated prior to each measurement with an external PMMA standard from PSS. The electrospray ionization time-of-flight (ESI-ToF) mass spectrometer was running at 4.5 kV, at a desolvation temperature of 180 °C. The mass spectrometer was operated in the positive ion mode. The ESI-ToF-MS instrument was calibrated in the m/z range from 50 to 3000 using a calibration standard (Tunemix solution) which is supplied from Agilent.

Ring opening polymerization

The ROP of L-lactide was carried out in a glove box, at room temperature under nitrogen atmosphere using THF as the solvent ($[\text{L-lactide}]_0/[\text{cholesterol}]_0/[\text{Ca}]_0$ = 15/1/0.5). $Ca[N(SiMe_3)_2]_2(THF)_2$ (61 mg, 0.12 mmol) was dissolved in 1 mL of THF. Subsequently, this solution was added under vigorous stirring to the L-lactide (0.7 g, 4.86 mmol) and cholesterol (93.9 mg, 0.24 mmol) mixture in 3.9 mL of THF. After 15 min (quant. conversion), the polymerization was quenched by adding 0.2 mL of 1 M HCl solution in methanol. PLA was isolated by precipitation in diethyl ether and subsequent drying under reduced pressure until a

constant weight was reached. $M_{n,\,theo}$ = 3,300 g mol^{-1}, $M_{n,\,NMR}$ = 3,600 g mol^{-1}, $M_{n,\,SEC}$ = 3,550 g mol^{-1}, $Đ_{SEC}$ = 1.23 (THF, RI detection, PLA calibration), $M_{n,\,MALDI}$ = 3,600 g mol^{-1}, $Đ_{MALDI}$ = 1.11.

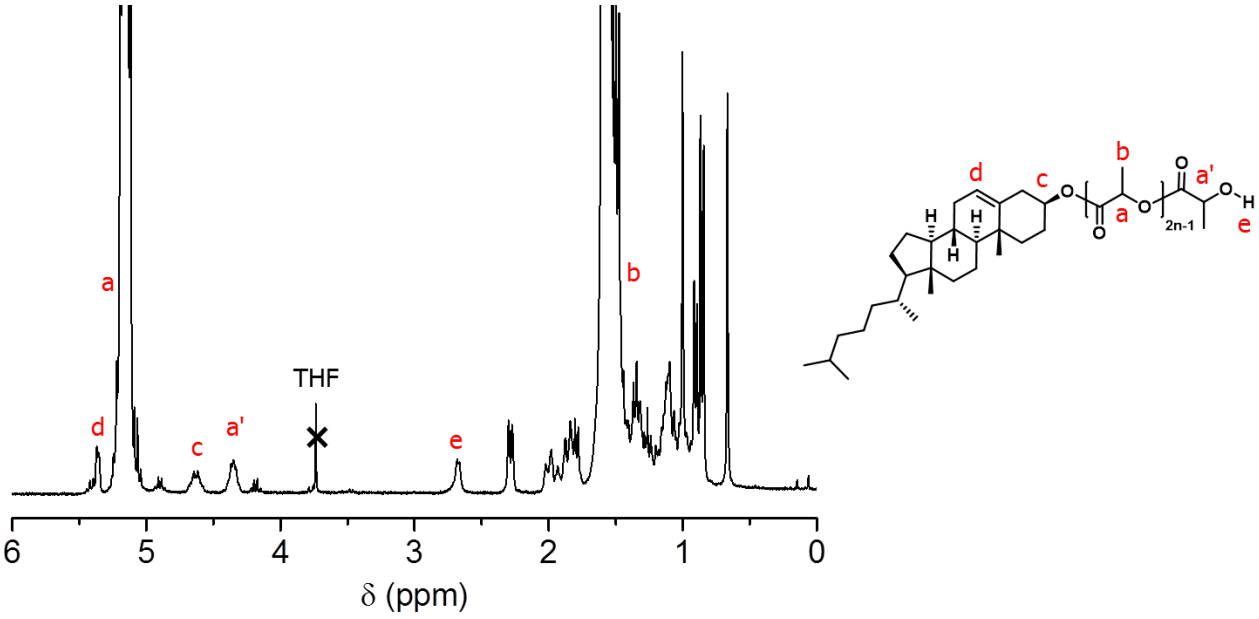

Figure S1. ^{1}H NMR spectrum (300 MHz, $CDCl_3$) of **P16** and structural assignment of the observed peaks.

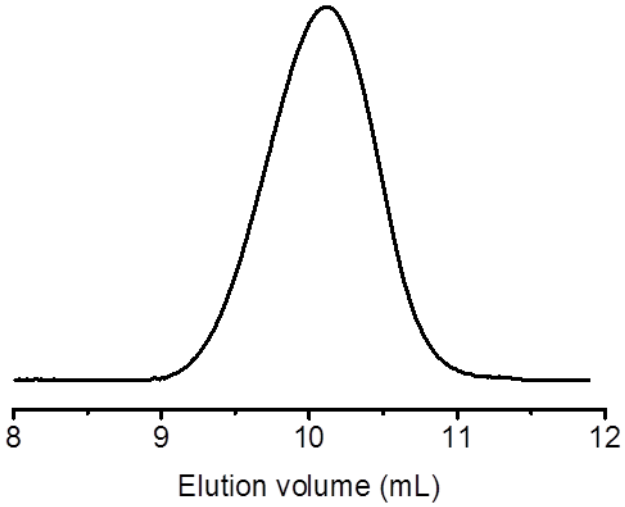

Figure S2. SEC elugram of **P16** (THF, RI detection)**.**

List of abbreviations

AIBN	2,2′-Azobis(2-methylpropionitrile)
ATRP	Atom transfer radical polymerization
CDP	4-Cyano-4-((dodecylsulfanylthiocarbonyl)sulfanyl)pentanol
CEMA	2-Chloroethyl methacrylate
CLSM	Confocal laser scanning microscopy
CPDB	2-Cyanoprop-2-yl dithiobenzoate
CROP	Cationic ring opening polymerization
cryo-TEM	Cryo-transmission electron microscopy
CTA	Chain transfer agent
$Đ$	Dispersity
DBU	1,8-Diazabicyclo[5.4.0]undec-7-ene
DDQ	2,3-Dichloro-5,6-dicyanobenzoquinone
DF	Degree of functionalization
DG	Degree of grafting
DIP-Fru	2,3:4,5-Di-*O*-isopropylidene-β-D-fructopyranose
DIP-Gal	1,2:3,4-Di-*O*-isopropylidene-α-D-galactopyranose
DLS	Dynamic light scattering
DMAEA	2-Dimethylaminoethyl acrylate
DMAP	4-(*N*,*N*-Dimethylamino)pyridine
DP	Degree of polymerization
DSC	Differential scanning calorimetry
DVB	*p*-Divinylbenzene
ESI	Electrospray ionization
FDA	Food and drug administration
FMA	Pentafluorophenyl methacrylate
FS	4-Fluorostyrene
GMA	Glycidyl methacrylate
HEA	2-Hydroxyethyl crylate
HEMA	2-Hydroxyethyl methacrylate
MA	Methyl acrylate
MALDI	Matrix-assisted laser desorption/ionization
MeTos	Methyl tosylate
MMA	Methyl methacrylate
M_n	Number average molar mass
MPC	2-(Methacryloyloxy ethyl phosphonylcholine)
MS	Mass spectrometry
NMP	Nitroxide mediated polymerization
NMR	Nuclear magnetic resonance
NP	Nanoparticle
*p*BMA	2(*p*-Methoxybenzyloxyethyl methacrylate)
PCL	Poly(ε-caprolactone)
PDI	Polydispersity index
PE	Polyethylene
PEG	Polyethylene glycol
PET	Poly(ethylene terephthalate)
PEtOx	Poly(2-ethyl-2-oxazoline)

PLA	Polylactide
PLGA	Poly(lactide-*co*-glycolide)
POx	Poly(2-oxazoline)
PP	Polypropylene
PS	Polystyrene
RAFT	Reversible addition-fragmentation chain transfer
RDRP	Reversible-deactivation radical polymerization
RI	Refractive index
ROP	Ring opening polymerization
SEC	Size exclusion chromatography
SEM	Scanning electron microscopy
SKMA	Solketal methacrylate
TBD	1,5,7-Triazabicyclo[4.4.0]dec-5-ene
T_c	Crystallization temperature
T_g	Glass transition temperature
TGA	Thermo-gravimetrical analysis
THF	Tetrahydrofuran
ToF	Time-of-flight
V-70	2,2'-Azobis(4-methoxy-2,4-dimethylvaleronitrile)
VBzCl	4-Vinylbenzyl chloride

Curriculum vitae

Ilknur Yildirim

Personal information

Date of Birth	19.08.1989
Place of Birth	Bakirkoy, Istanbul, Turkey

Education

09/2007 – 07/2011 **B.Sc. in Chemistry,** Department of Chemistry, Izmir Institute of Technology (Izmir, Turkey)
Synthesis of phenyl boronic acid derivatized benzothiazoles and their use as carbohydrate sensors (Graduation project)
Supervisor: Assoc. Prof. Dr. Ali Cagir

Summer 2010 Internship, The Council of Forensic Medicine, Department of Chemistry, Toxicology, Narcotic, Instrumental Analysis, and Foodstuff Research Laboratories (Istanbul, Turkey)

06/2011 – 06/2013 **M.Sc. in Chemistry,** Department of Chemistry, Bogazici University (Istanbul, Turkey)
Synthesis of novel pressure sensitive adhesives by emulsion polymerization
Supervisor: Assoc. Prof. Dr. Ali Ersin Acar

08/2013 - present **PhD researcher**, Institute of Organic Chemistry and Macromolecular Chemistry, Friedrich Schiller University Jena (Jena, Germany)
Functional PLA based (co)polymers *via* ROP and RAFT polymerization
Supervisor: Prof. Dr. Ulrich S. Schubert

Jena, den 25.09.2017 _____

Publication list

Peer-reviewed publications

1. Julia Kötteritzsch, Stefan Bode, **Ilknur Yildirim**, Christine Weber, Martin D. Hager, Ulrich S. Schubert, Reversible oligomerization of 3-aryl-2-cyanothioacrylamides *via* [2_s + 4_s] cycloaddition to substituted 3,4-dihydro-*2H*-thiopyrans, *Des. Monomers Polym*. **2015**, *18*, 627–640.
2. **Ilknur Yildirim**, Sarah Crotty, Claas H. Loh, Grit Festag, Christine Weber, Pier-Francesco Caponi, Michael Gottschaldt, Matthias Westerhausen, Ulrich S. Schubert, End-functionalized polylactides using a calcium-based precatalyst: Synthesis and insights by mass spectrometry, *J. Polym. Sci., Part A: Polym. Chem*. **2016**, *54*, 437–448.
3. **Ilknur Yildirim**, Tanja Bus, Martin Sahn, Turgay Yildirim, Diana Kalden, Stephanie Hoeppener, Anja Traeger, Matthias Westerhausen, Christine Weber, Ulrich S. Schubert, Fluorescent amphiphilic heterografted comb polymers comprising biocompatible PLA and PEtOx side chains, *Polym. Chem*. **2016**, *7*, 6064–6074.
4. Turgay Yildirim, **Ilknur Yildirim**, Roberto Yañez-Macias, Steffi Stumpf, Carolin Fritzsche, Stephanie Hoeppener, Carlos Guerrero-Sanchez, Stephanie Schubert, Ulrich S. Schubert, Dual pH and ultrasound responsive nanoparticles with pH triggered surface charge-conversional properties, *Polym. Chem*. **2017**, *8*, 1328–1340.
5. **Ilknur Yildirim**, Turgay Yildirim, Diana Kalden, Grit Festag, Nicole Fritz, Christine Weber, Stephanie Schubert, Matthias Westerhausen, Ulrich S. Schubert, Retinol initiated poly(lactide)s: Stability upon polymerization and nanoparticle preparation, *Polym. Chem.* **2017**, *8*, 4378–4387.

6. **Ilknur Yildirim**, Christine Weber, Ulrich S. Schubert, Old meets new: Combination of PLA and RDRP to obtain sophisticated macromolecular architectures, *Prog. Polym. Sci.* **2017**, http://dx.doi.org/10.1016/j.progpolymsci.2017.07.010.
7. Turgay Yildirim, Anja Traeger, Pelin Sungur, Stephanie Hoeppener, Carolin Kellner, **Ilknur Yildirim**, David Pretzel, Stephanie Schubert, Ulrich S. Schubert, Polymersomes with endosomal pH-induced vesicle-to-micelle morphology transition and a potential application for controlled doxorubicin delivery, *Biomacromolecules* **2017**, DOI: 10.1021/acs.biomac.7b00931.
8. **Ilknur Yildirim**, Pelin Sungur, Anna C. Crecelius-Vitz, Turgay Yildirim, Diana Kalden, Stephanie Hoeppener, Matthias Westerhausen, Christine Weber, Ulrich S. Schubert, One-pot synthesis of PLA-*b*-PHEA *via* sequential ROP and RAFT polymerizations, *Polym Chem.* **2017**, DOI: 10.1039/C7PY01176H.

Acknowledgements

I would like to thank all the people who helped me to accomplish this Ph.D. thesis and supported me over the last four years.

First of all, I would like to express my deepest gratitude to Prof. Schubert for giving me the chance to be a part of this enthusiastic and dynamic research group. It was a privilege to work in this amazing building with colleagues from all over the world. Thank you very much for being always encouraging and supportive. I am and will always be proud to be a member of this team.

Secondly, I would like to thank Prof. Westerhausen for making all these studies possible with a fruitful cooperation and guiding me with useful discussions and insightful comments whenever I needed help.

Dear Christine, without your devoted and diligent supervision this thesis would not possible. You have genuinely cared about me and my professional development. I owe you a lot! Thanks for everything you have done!

I am grateful to all the colleagues who have significantly contributed to this thesis and many publications. I want to thank Diana Kalden and Claas H. Loh for the catalyst synthesis, Sarah C. Crotty, Nicole Fritz and Dr. Anna C. Crecelius-Vitz for MS measurements, Dr. Grit Festag for SEC measurements, Dr. Julia Kötteritzsch, Dr. Stefan Zechel and Dr. Martin Hager for including me into a nice cooperation which lead to my very first publication ☺, Martin Sahn for the POx macromonomer synthesis, Tanja Bus for the cell-uptake tests and many fruitful discussions, Dr. Stephanie Hoeppener and Pelin Sungur for cryo-TEM analysis and for answering my questions with an unbelievable patience ☺, Turgay Yildirim for DLS measurements, Steffi Stumpf for SEM measurements, Prof. Westerhausen, Dr. Michael Gottschaldt, Dr. Stephanie Schubert, Dr. Anja Traeger for many helpful discussion and ideas, Dr. Pier Francesco Caponi for introducing me to ROP and supervision in my first year, Dr. Christine Weber for supervision, many ideas and discussions.

I would like to acknowledge the ‘real heroes’ of the Schubert group and the FSU Jena ☺. First of all, special thanks to Sylvia Braunsdorf, Franca Frister and Simone Burchardt for their help and support about administrative stuff, organizing every detail to make the life easier in the Schubert group, Dr. Uwe Koehn for all chemical orders and safety regulations, Sandra Koehn for keeping the labs running with consumable supplies, Dr. Grit Festag and Nicole Fritz for keeping the SEC and GC systems running and many measurements, the members of the NMR platform Dr. Peter

Bellstedt, Gabriele Sentis, Dr. Wolfgang Guenther and Friederike Pielenz for introduction to spectrometers and useful seminars, the members of the MS team Nicole Fritz, Annett Urbanek, Sarah Crotty for many many measurements, Renzo Paulus, Dr. Juergen Vitz and Alexander Meier for introduction to many instruments, IT support and help with the Glove box. Dear Renzo, I really have no explanation why the DSC was so stubborn about not working without your magic touch ☺. Dear Alex, many thanks for providing distilled THF over the years. I would probably burn down the whole building if I had to do it on my own ☺.

I want to thank my lab and office mates and the residents of the ZAF who had cheered the last four years ☺. Dear Grit, Martin, Damiano, Anne, Meike, Michi, Irina and Julien thank you for the great office and lab atmosphere. Grit and Martin, without your warm friendship and support, it would be really hard to survive in Jena! Thanks a lot for many translations, arranging doctor appointments and the most importantly showing me the real German culture ☺. I will miss our morning chats ☺. Many thanks to office 134, especially Justyna, Susi, Micha, Peng, Chris and Tobi for hosting me every lunch time ☺. Susi and Oli, thanks a lot for the IKEA trip ☺. Justyna and Tobi, thanks for the delicious Polish food. Pelin, I wish you had joined the group earlier, I will really miss you ☺.

Son olarak Turgay ve beni asla yalnız bırakmayan, desteklerini her an her saniye hissettiren aileme çok çok çok teşekkür ederim. Annecim o kadar çok geldin ki en sonunda bizden daha uzun vize almayı başardın, hala şaşkınım ☺. Ananem, canımın içi teyzem, ecoş itiraf ediyorum en çok sizi özledim. Didişmeden beş dakikadan fazla yan yana duramasak da ayrı da olmuyormuş ☺. Hatice annem, Abdullah babam, Kenan, siz olmasanız ne yapardık bilmiyorum. Gelemeseniz de resmen Türkiye'yi Jena'ya gönderdiniz. Bizimle sevindiniz, bizimle üzüldünüz. Biz de sizleri fahri doktor ilan ediyoruz ☺. Turgut abi ve Tuğçe söz, nişan ve düğün gibi aktivitelerle her yaz doktora sürecimizi şenlendirdiniz, teşekkür ederiz ☺. Jena' daki son günlerimizi sayenizde Kerem'in fotoğraflarıyla motive olarak geçiriyoruz. Esramu, candan öte arkadaşım a friend in need is a friend indeed ☺. Ve Turgay, eşim, yoldaşım, her şeyim. Belki de hayatımızın en zor dört yılını birlikte omuz omuza atlattık. Her şeye rağmen her günümüzü birbirinden güzel anılarla doldurduğun için teşekkür ederim.

Thanks to all of you

Ilknur **:)**

Declaration of authorship/Selbständigkeitserklärung

Ich erkläre, dass ich die vorliegende Arbeit selbständig und unter Verwendung der angegebenen Hilfsmittel, persönlichen Mitteilungen und Quellen angefertigt habe.

I certify that the work presented here is, to the best of my knowledge and belief, original and the result of my own investigations, except as acknowledged, and has not been submitted, either in part or whole, for a degree at this or any other university.

Jena, den 25.09.2017 _____

Publications P1-P10

Publication P1

“Old meets new: Combination of PLA and RDRP to obtain sophisticated macromolecular architectures”

Ilknur Yildirim, Christine Weber, Ulrich S. Schubert

Prog. Polym. Sci. **2017**, https://doi.org/10.1016/j.progpolymsci.2017.07.010.

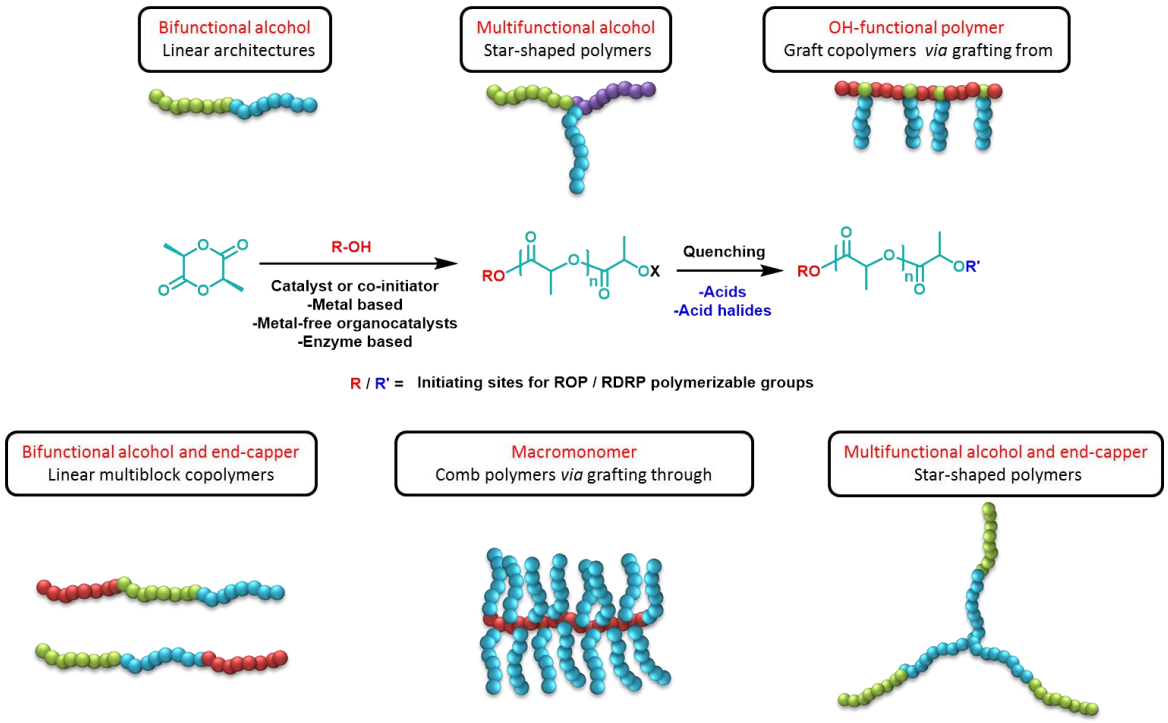

Progress in Polymer Science xxx (2017) xxx–xxx

Contents lists available at ScienceDirect

Progress in Polymer Science

journal homepage: www.elsevier.com/locate/ppolysci

Old meets new: Combination of PLA and RDRP to obtain sophisticated macromolecular architectures

Ilknur Yildirim[a,b], Christine Weber[a,b], Ulrich S. Schubert[a,b,*]

[a] Laboratory of Organic and Macromolecular Chemistry (IOMC), Friedrich Schiller University Jena, Humboldtstr. 10, 07743 Jena, Germany
[b] Jena Center for Soft Matter (JCSM), Friedrich Schiller University Jena, Philosophenweg 7, 07743 Jena, Germany

ARTICLE INFO

Article history:
Received 9 November 2016
Received in revised form 18 July 2017
Accepted 27 July 2017
Available online xxx

Keywords:
ROP
Lactide
RDRP
ATRP
RAFT
NMP

ABSTRACT

This review article highlights the research focused on the synthesis of polylactide (PLA) based copolymers by combination of reversible-deactivation radical polymerization (RDRP) techniques with ring-opening polymerization (ROP) processes. In particular atom-transfer radical polymerization (ATRP), reversible addition-fragmentation chain transfer (RAFT) polymerization, and nitroxide-mediated polymerization (NMP) will be addressed as RDRP techniques mechanistically different from ROP in the design of various sophisticated macromolecular structures. The combination of ROP with RDRP techniques has been extensively applied to prepare PLA copolymers. We discuss the synthetic methods applicable to prepare linear and star-shaped block copolymers by use of heterofunctional initiators as well as other end functionalization methods. This is complemented with the adaption of the synthetic pathways generally used for the preparation of comb and graft copolymers, *i.e.*, macromonomer, grafting-from and grafting-onto approaches, to the requirements of PLA-based building blocks.

Abbreviations: AGET, activator generated by electron transfer; AlpGP, 1,2:3,4-Di-*O*-*iso*propylidene-6-*O*-acryloyl-α-D-galactopyranose; ATRP, atom-transfer radical polymerization; BEMP, 2-*tert*-butylimino-2-diethylamino-1,3-dimethylperhydro-1,3,2-diazaphosphorine; BGMA, *cis*-1,3-benzylidene glycerol methacrylate; BIEMA, 2-bromo*iso*butyryl methacrylate; BMBIBPC, 2,2-Bis(methylene-2-bromoisobutyrate) propionyl chloride; BnA, benzyl acrylate; Bpy, bipyridine; BS, 4-(3-butenyl)styrene; CEMA, 2-chloroethyl methacrylate; CLM, 2-cholinium lactate methacrylate; CTA, chain transfer agent; CuAAC, copper catalyzed 1,3 dipolar azide alkyne cycloaddition; *Đ*, dispersity; DAEMA, dehydroabietic ethyl methacrylate; DBU, 1,8-diazabicyclo[5.4.0]undec-7-ene; DCC, *N,N′*-dicyclohexylcarbodiimide; DG, degree of grafting; DMA, *N,N*-dimethylacrylamide; DMAc, *N,N*-dimethylacetamide; DMAEA, 2-(dimethylamino)ethyl acrylate; DMAEMA, 2-(dimethylamino)ethyl methacrylate; DMAP, 4-(*N,N*-dimethylamino)pyridine; DOX, doxorubicin; DP, degree of polymerization; DTM, dithiomaleimide; DTT, dithiothreitol; DVB, *p*-divinylbenzene; EA, ethyl acrylate; $EtOx_nMA$, oligo(2-ethyl-2-oxazoline) methacrylate; FMA, pentafluorophenyl methacrylate; FRP, free radical polymerization; GAMA, D-gluconamidoethyl methacrylate; GlyMA, glycerol monomethacrylate; GMA, glycidyl methacrylate; HEA, 2-hydroxyethyl acrylate; HEMA, 2-hydroxyethyl methacrylate; HMTETA, 1,1,4,7,10,10-hexamethyltriethylenetetramine; Imes, 1,3-dimesitylimidazol-2-ylidene; MA, methyl acrylate; Me_6TREN, Tris[2-(dimethylamino)ethyl]amine; MM, macromonomer; MMA, methyl methacrylate; MPC, 2-(methacryloyloxy ethyl phosphonylcholine); MPEO, poly(ethylene oxide) methyl ether; MWCNT, multi-walled carbon nanotube; NAS, *N*-acryloxysuccinimide; NB, *p*-norbornenylethyl styrene; *n*BA, *n*-butyl acrylate; NiPAm, *N-iso*-propylacrylamide; NMP, nitroxide-mediated polymerization; NMR, nuclear magnetic resonance; NVP, *N*-vinylpyrrolidone; P(*rac*-LA), Poly(racemic lactide); P2-*t*-Bu, 1-*tert*-butyl-2,2,4,4,4-pentakis(dimethylamino)-2Λ^5,4Λ^5-catenadi-(phosphazene); PAA, poly(acrylic acid); PAGP, poly(6-*O*-acryloyl-α-D-galactopyranose); PAN, polyacrylonitrile; PBnA, poly(benzyl acrylate); PCL, poly(ε-caprolactone); PDLA, poly(D-lactide); PDLLA, poly(D,L-lactide); PDMA, poly(*N,N*-dimethylacrylamide); PDMAEA, poly(2-(dimethylamino)ethyl acrylate); PDMAEMA, poly(2-(dimethylamino)ethyl methacrylate); PDMS, poly(dimethylsiloxane); PEO, poly(ethylene oxide); PEO_nA, poly(ethylene oxide) acrylate; PEO_nMA, poly(ethylene oxide) methacrylate; PEO_nMAGlc, glucopyranoside grafted poly(ethylene oxide) methacrylate; PFMA, pentafluorophenyl methacrylate; PFS, poly(4-fluorostyrene); PGMA, poly(glycidyl methacrylate); PHEA, poly(2-hydroxyethyl acrylate); PHEMA, poly(2-hydroxyethyl methacrylate); PLA, polylactide; PLA_nMA, polylactide methacrylate; PLGA, poly(lactide-*co*-glycolide); PLLA, poly(L-lactide); PMA, poly(methyl acrylate); PMAA, poly(methacrylic acid); PMDETA, *N,N,N′,N″,N‴*-pentamethyldiethylenetriamine; PMMA, poly(methyl methacrylate); PMPC, poly(2-(methacryloyloxy ethyl phosphonylcholine)); PNiPAm, poly(*N-iso*-propylacrylamide); PNVCL, poly(*N*-vinylcaprolactam); PNVP, poly(*N*-vinylpyrrolidone); PS, polystyrene; P*t*BA, poly(*tert*-butyl acrylate); P*t*BMA, poly(*tert*-butyl methacrylate); P*t*BuS, poly(*tert*-butyl styrene); PTHPA, poly(tetrahydropyran acrylate); *rac*-LA, racemic lactide; RAFT, reversible addition-fragmentation chain transfer; RAPTA-C, dichlororuthenium(II)(p-cymene)(1,3,5-triaza-7-phosphaadamantane); RDRP, reversible-deactivation radical polymerization; ROMP, ring-opening metathesis polymerization; ROP, ring-opening polymerization; S, styrene; SEC, size exclusion chromatography; SG-1, *N-tert*-butyl-*N*-[1-diethoxyphosphoryl-2,2-dimethylpropyl] nitroxide; SiPMA, 5-(trimethylsilyl)-4-pentyn-1-ol methacrylate; SKA, solketal acrylate; SKMA, solketal methacrylate; SMA, stearyl methacrylate; $Sn(Oct)_2$, tin(II) octoate; *t*BA, *tert*-butyl acrylate; *t*BMA, *tert*-butyl methacrylate; *t*BuS, *tert*-butyl styrene; TEMPO, 2,2,6,6-tetramethyl-1-piperidinyloxyl; THF, tetrahydrofuran; TIPNO, 2,2,5-trimethyl-4-phenyl-3-azahexane-3-oxyl; VBzCl, 4-vinylbenzyl chloride.

* Corresponding author at: Laboratory of Organic and Macromolecular Chemistry (IOMC), Friedrich Schiller University Jena, Humboldtstr. 10, 07743 Jena, Germany; Jena Center for Soft Matter (JCSM), Friedrich Schiller University Jena, Philosophenweg 7, 07743 Jena, Germany .
E-mail address: ulrich.schubert@uni-jena.de (U.S. Schubert).

http://dx.doi.org/10.1016/j.progpolymsci.2017.07.010
0079-6700/

Contents

1. Introduction

Polylactide (PLA) as one of the leading polyesters is indispensable for a number of biomedical applications due to its biodegradability, biocompatibility, and excellent tissue compatibility [1–4]. Featuring mechanical properties comparable to several high performance polymers, it is also a perfect sustainable alternative to polymers derived from petrochemical resources. As apparent from its name, PLA is obtained *via* polycondensation of lactic acid. However, ring-opening polymerization (ROP) of the cyclic dimer lactide provides a better control over the polymer properties and, thus, is the far more common applied technique nowadays [5]. Controlled ROP of lactide can be achieved by several approaches, such as coordination-insertion, nucleophilic, anionic, and cationic polymerizations [4,5]. While each system has benefits and drawbacks, metal-alkoxides [6–8] and organocatalysts [9,10] are the approaches investigated most frequently, including a number of co-catalyst/initiator systems.

Unmodified PLA is a hydrophobic polymer, and the introduction of hydrophilic or functional moieties to the homopolymer is difficult to achieve by copolymerization with other cyclic esters because the ROP mechanism prohibits the presence of a range of functionalities. On the other hand, post-polymerization functionalization reactions suffer from the easily degradable ester moieties in PLA that can be affected under either acidic or alkaline reaction conditions. Apart from the utilization of the omni-present poly(ethylene oxide) (PEO) as hydrophilic building block [11], in particular modern reversible-deactivation radical polymerization (RDRP) techniques provide alternative synthetic pathways because PLA is not prone to degradation in the presence of radicals. RDRPs rely on robustness of radical chemistry yielding polymers with pre-determined molar masses, well-defined end groups, and architecture under mild experimental conditions [12]. The most common RDRP techniques include reversible addition-fragmentation chain transfer (RAFT) polymerization, atom transfer radical polymerization (ATRP), and nitroxide-mediated polymerization (NMP) processes. Due to the fact that the functional moieties required to serve as initiators or chain transfer agents (CTA) for a couple of RDRP techniques can be readily introduced as end functionalities to PLA, there is a recent revival of PLA chemistry with the purpose to create novel polymeric architectures based on this "old and boring" polymer.

A variety of catalysts and co-initiator systems are available to mediate the controlled ROP of lactide in the presence of a functional

Please cite this article in press as: Yildirim I, et al. Old meets new: Combination of PLA and RDRP to obtain sophisticated macromolecular architectures. Prog Polym Sci (2017), http://dx.doi.org/10.1016/j.progpolymsci.2017.07.010

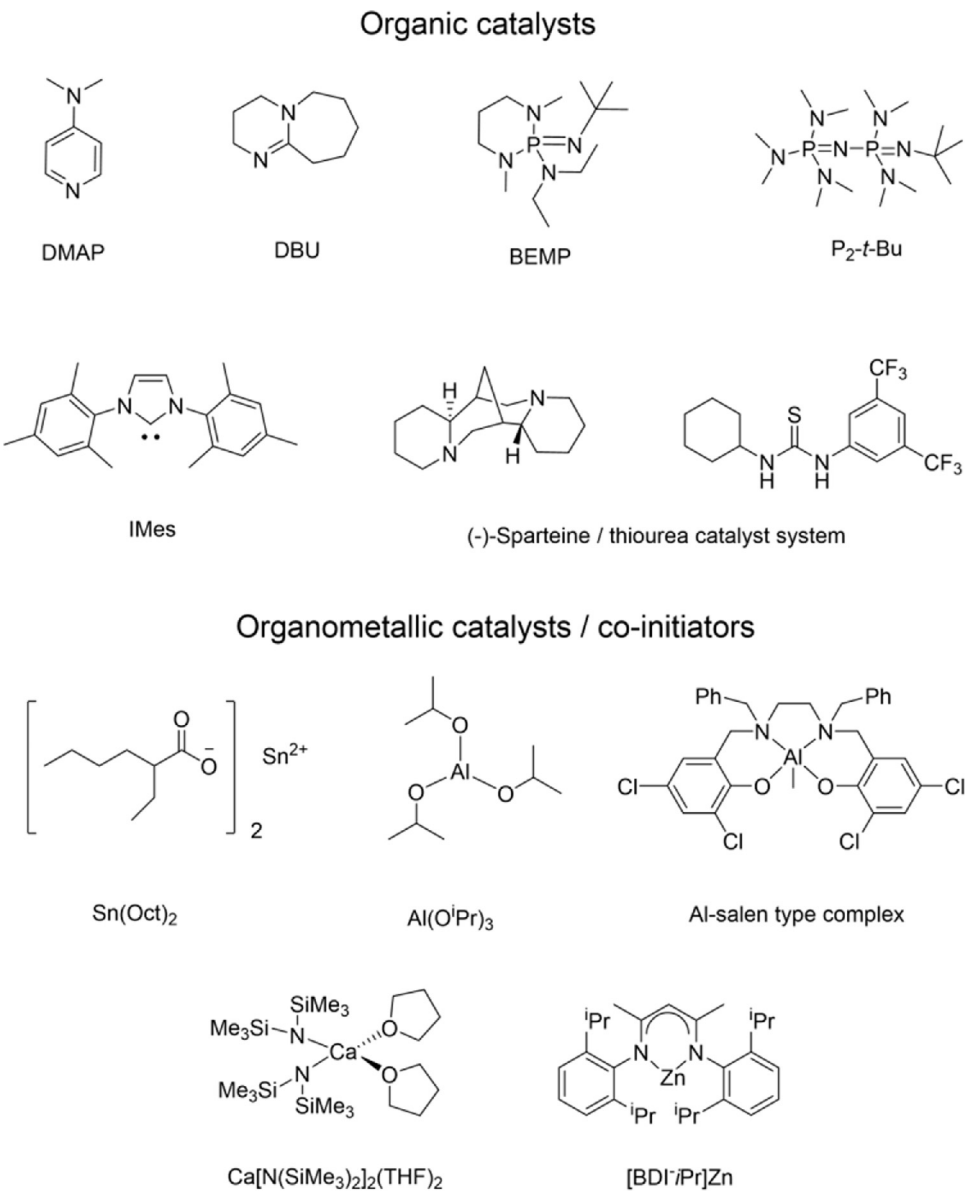

Fig. 1. Schematic representation of the catalysts/co-initiators commonly utilized for the ROP of lactide; 4-(*N*,*N*-dimethylamino)pyridine (DMAP), 1,8-diazabicyclo[5.4.0]undec-7-ene (DBU), 2-*tert*-butylimino-2-diethylamino-1,3-dimethylperhydro-1,3,2-diazaphosphorine (BEMP), 1-*tert*-butyl-2,2,4,4,4-pentakis(dimethylamino)-2Λ^5,4Λ^5-catenadi-(phosphazene) (P_2-*t*-Bu), 1,3-dimesitylimidazol-2-ylidene (IMes).

initiator, facilitating the functionalization of PLA with a RDRP initiator or with a polymerizable group (Fig. 1). The use of an alcohol with stannous octoate ($SnOct_2$) is the most commonly utilized metal-alkoxide system for the ROP of lactide. However, $SnOct_2$ requires comparably high reaction temperatures and faces increasing concerns due to the toxicity of tin compounds. Hence, alternative organometallic complexes based on more benign and biocompatible metals are used as well. Following the pioneering studies of Hedrick and Waymouth, organocatalyzed ROP of lactide is applied more often recently, which gives access to metal–free PLAs with predictable molar masses and narrow dispersities. Many of these catalyst and co-initiator systems yield quantitatively end functionalized PLA, provided a proper adjustment of the polymerization conditions. Compatible initiators and monomers, thus, facilitate the combination of ROP with several RDRP techniques and the synthesis of PLA based copolymers with a variety of architectures.

As outlined in Fig. 2, monofunctional alcohols as initiators for the ROP result in block copolymers, while multifunctional alcohols provide access to star-shaped or grafted polymer architectures. In addition, PLA with vinylic end functionalities represent macromonomers, *i.e.* building blocks required to prepare comb and graft copolymers *via* the grafting through method.

Common approaches employed for the combination of ROP of cyclic esters with RDRP for block copolymer synthesis have been addressed in the review articles by Dove [13] and Oh [14], both with a strong focus on application of the polymers in view of block copolymer self-assembly in solution and solid state. However, we will comprehensively discuss the methods outlined above aiming to scrutinize the synthetic (dis)advantages of the multi-step polymer syntheses. The various vinylic monomers applied for the syntheses discussed in this review article are summarized in Fig. 3.

2. Dual initiators and inifers

Independent from the type of radical polymerization method, dual initiators for the combination of ROP and RDRP have to bear

Please cite this article in press as: Yildirim I, et al. Old meets new: Combination of PLA and RDRP to obtain sophisticated macromolecular architectures. Prog Polym Sci (2017), http://dx.doi.org/10.1016/j.progpolymsci.2017.07.010

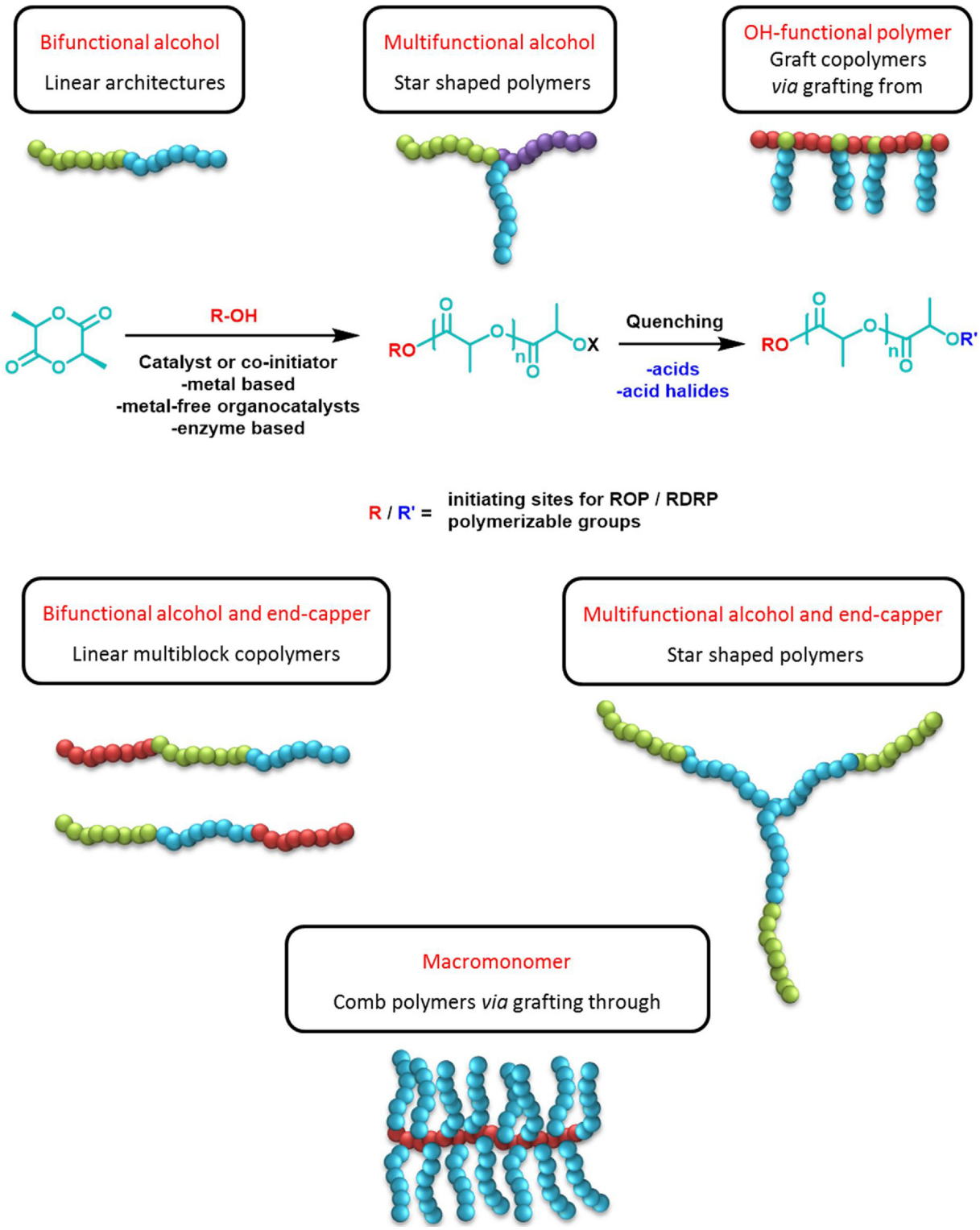

Fig. 2. Access to various copolymer architectures by exploitation of functional moieties at the α- and ω-chain ends of PLA.

a hydroxyl functionality to serve as initiator for the ROP of lactide. These initiators are often termed "heterofunctional" since they allow the combination of mechanistically distinct polymerization reactions without the need for intermediate transformation and (de)protection steps. The second functionality of the dual initiator differs according to the type of functional moiety required to provide control over the radical polymerization for each RDRP method (Fig. 4); *i.e.* alkyl halides as typical initiation sites for ATRP, or alkoxyamines for NMP. In case of the thiocarbonylthio compounds used for RAFT polymerization, the heterofunctional molecules applied for such approaches do actually not represent dual initiators since the RAFT polymerization is initiated by an external radical source (*vide infra*).

Retaining the molecular structure of the dual initiators and the final block copolymer, the synthetic pathways towards the PLA-based copolymers can vary: Which polymerization, *i.e.* ROP or

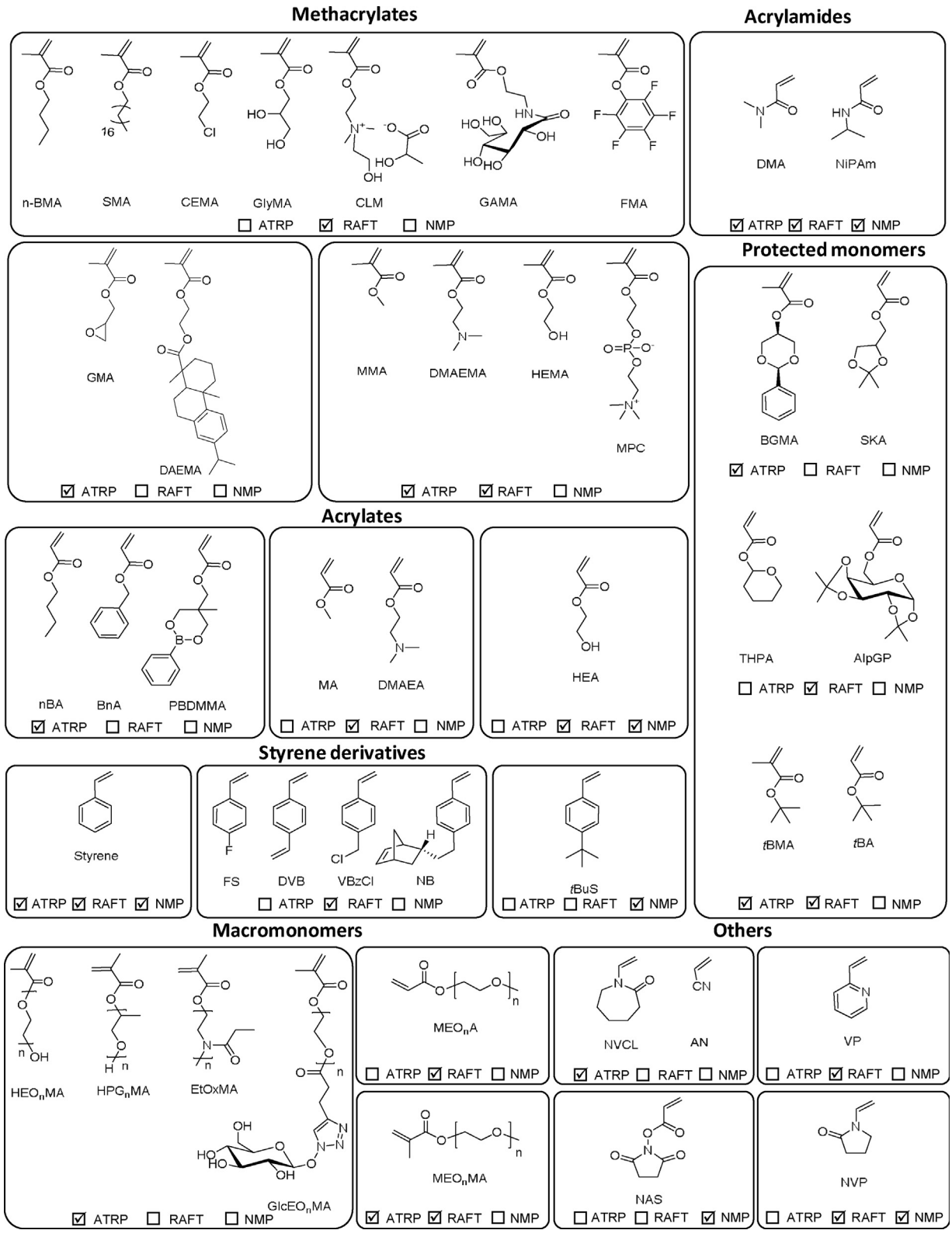

Fig. 3. Schematic representation of vinylic monomers polymerized *via* combination of ROP and RDRP techniques employing dual initiators or end functionalization strategies: *n*-Butyl methacrylate (nBMA), stearyl methacrylate (SMA), 2-chloroethyl methacrylate (CEMA), glycerol monomethacrylate (GlyMA), 2-cholinium lactate methacrylate (CLM), D-gluconamidoethyl methacrylate (GAMA), pentafluorophenyl methacrylate (FMA), glycidyl methacrylate (GMA), dehydroabietic ethyl methacrylate (DAEMA), methyl methacrylate (MMA), 2-(dimethylamino)ethyl methacrylate (DMAEMA), 2-hydroxyethyl methacrylate (HEMA), 2-methacryloyloxyethyl phosphorylcholine (MPC), *n*-butyl acrylate (nBA), benzyl acrylate (BnA), 2-phenylboronic ester-1,3-dioxane-5-methyl methylacrylate (PBDMMA), methyl acrylate (MA), 2-dimethylaminoethyl acrylate (DMAEA), 2-hydroxyethyl acrylate (HEA), 4-fluorostyrene (FS), *p*-divinylbenzene (DVB), 4-vinylbenzyl chloride (VBzCl), *p*-norbornenylethyl styrene (NB), *tert*-butyl styrene (tBuS), *N,N*-dimethylacrylamide (DMA), *N*-isopropylacrylamide (NiPAm), *cis*-1,3-benzylidene glycerol methacrylate (BGMA), solketal acrylate (SKA), tetrahydropyran acrylate (THPA), 1,2:3,4-di-*O*-isopropylidene-6-*O*-acryloyl-α-D-galactopyranose (AlpGP), *tert*-butyl methacrylate (tBMA), *tert*-butyl acrylate (tBA), poly(ethyleneoxide) methacrylate (HEO_nMA), poly(propylene glycol) methacrylate (HPG_nMA), oligo(2-ethyl-2-oxazoline) methacrylate ($EtOx_nMA$), glucose functionalized EO_nMA ($GlcEO_nMA$), poly(ethyleneoxide methyl ether) acrylate (MEO_nA), poly(ethylene oxide methyl ether) methacrylate (MEO_nMA), *N*-vinylcaprolactam (NVCL), acrylonitrile (AN), 2-vinylpyridine (VP), *N*-acryloxysuccinimide (NAS), *N*-vinylpyrrolidone (NVP).

Please cite this article in press as: Yildirim I, et al. Old meets new: Combination of PLA and RDRP to obtain sophisticated macromolecular architectures. Prog Polym Sci (2017), http://dx.doi.org/10.1016/j.progpolymsci.2017.07.010

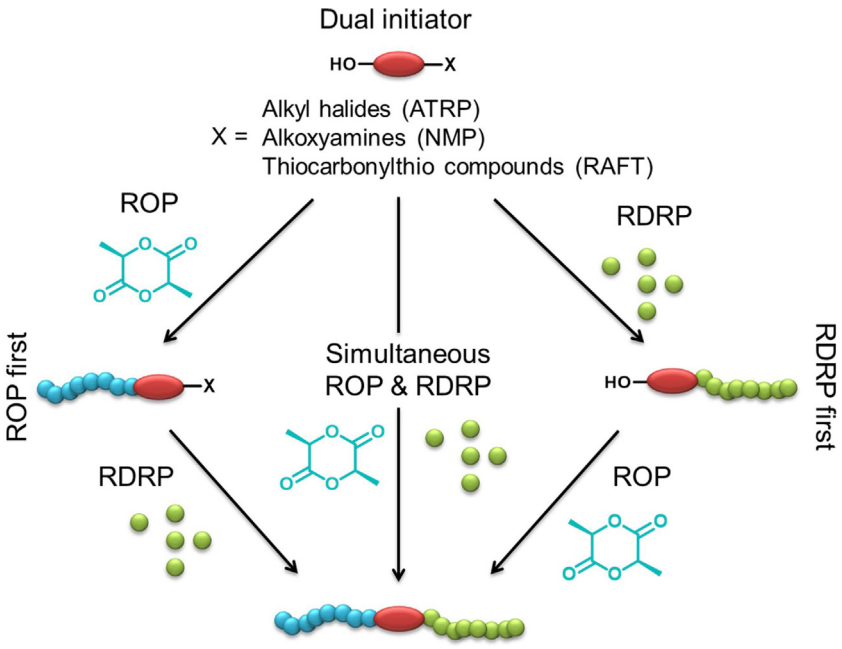

Fig. 4. Schematic representation of synthetic approaches for combination of ROP and RDRPs using dual initiators.

RDRP, is performed first, if any? In analogy to common approaches known for the synthesis of star-shaped polymers, the following section is structured according to the order the two polymerization methods are applied in. If the ROP of lactide is performed first, the "ROP first method" results in a PLA-based macroinitiator that carries the functional group to serve as initiator for a subsequent RDRP at the α-chain end. Conversely, the "RDRP first method" relies on the RDRP as the first synthetic step, yielding a macroinitiator for the subsequent ROP with terminal hydroxyl functionality. Finally, both polymerization types can be performed in one pot, and even proceed simultaneously.

2.1. Combination of ROP and ATRP using dual initiators

Being perhaps the most widely studied RDRP technique, ATRP can exhibit excellent control over the polymerization of a wide range of monomers providing tailor-made polymers with defined molar masses and end groups. The latter are introduced by the ATRP initiator used for the polymerization. Alkyl halides are required for this purpose to enable a reversible coordination of the halide to a transition metal complex. Thereby, an active radical species is formed, and the transition metal is oxidized. This reversible oxidation/reduction cycle between mostly Cu(I) and Cu(II) provides an equilibrium between active and dormant chains and, thus, lowers the concentration of active radical species. As a result of this mechanism, the halide represents the ω-end group of the final polymer, while other functional moieties, which were initially attached to the initiator, remain at the α-chain end.

Since the ATRP of vinyl monomers is compatible with hydroxyl groups, dual initiators for ATRP and ROP can represent quite simple molecules that contain an alkyl halide and a hydroxyl functionality (Fig. 5). The junction between the two blocks of a resulting block copolymer will already be determined by the choice of the dual initiator, which also facilitates the introduction of further functionalities at a defined position in the final polymer architecture.

2.1.1. Macroinitiators for the ROP of lactide prepared by the "ATRP first" method

ATRP alone tolerates several functional groups present in monomers, which represents a major advantage of any RDRP technique. Hence the heterofunctional initiators in Fig. 5 would be applicable to a much wider range of monomers than were actually used for the preparation of block copolymers with PLA. However, it has to be considered that any functional moiety present in the macroinitiator for the subsequent ROP has to be tolerated during the second polymerization as well. The limited diversity of vinylic monomers used for ATRP-first approaches is therefore caused by the sensitivity of the ROP mechanism of lactide, which interferes with many functional moieties that are well tolerated by the ATRP process. Hence, most reports are based on the ATRP of simple styrene. On the other hand, the applicability of various different dual initiators has been investigated. While the focus is mostly on an adjustment of the polymerization conditions utilized during ATRP, the research community active in this field relies on the standard ROP catalyst $Sn(Oct)_2$ (Table 1).

2.1.1.1. Simple diblock copolymers (PS-b-PLA). The typical ATRP initiation site of **5** [15] was already applied to polymerize styrene to obtain efficient macroinitiators for the ROP by Pan in 2000, who demonstrated an excellent control over both polymerization types [16]. With focus on exploitation of the self-assembly processes of the resulting PS-*b*-PLLA, also the chloride-based dual initiator **6** [17] and the secondary bromide initiator **7** [18–21] were efficiently applied using slightly modified ATRP first approaches.

The dual initiators **8** to **11** were prepared to benefit from the increased reactivity of phenolic hydroxyl functionalities in comparison to benzylic hydroxyl moieties during the synthesis of the dual initiator [22]. Although no differences were observed regarding the performance of these initiators during the ATRP of styrene, the dispersity of the final PS-*b*-PLA block copolymers was sometimes increased ($1.23 < Đ < 1.7$), in particular when L-lactide was polymerized during the ROP. Focused on totally avoiding the necessity of initiator synthesis, tribromoethanol (**1**) was also tested as dual initiator for the preparation of PS-*b*-PLA, however at the cost of rather broad molar mass distributions ($Đ = 1.55$) [23].

2.1.1.2. Triblock copolymers. When a chain extension of either the vinylic or the polyester block is performed, triblock copolymers can be obtained from the dual initiators. A chain extension of PS initiated by **5** with MMA resulted in a PS-*b*-PMMA macroinitia-

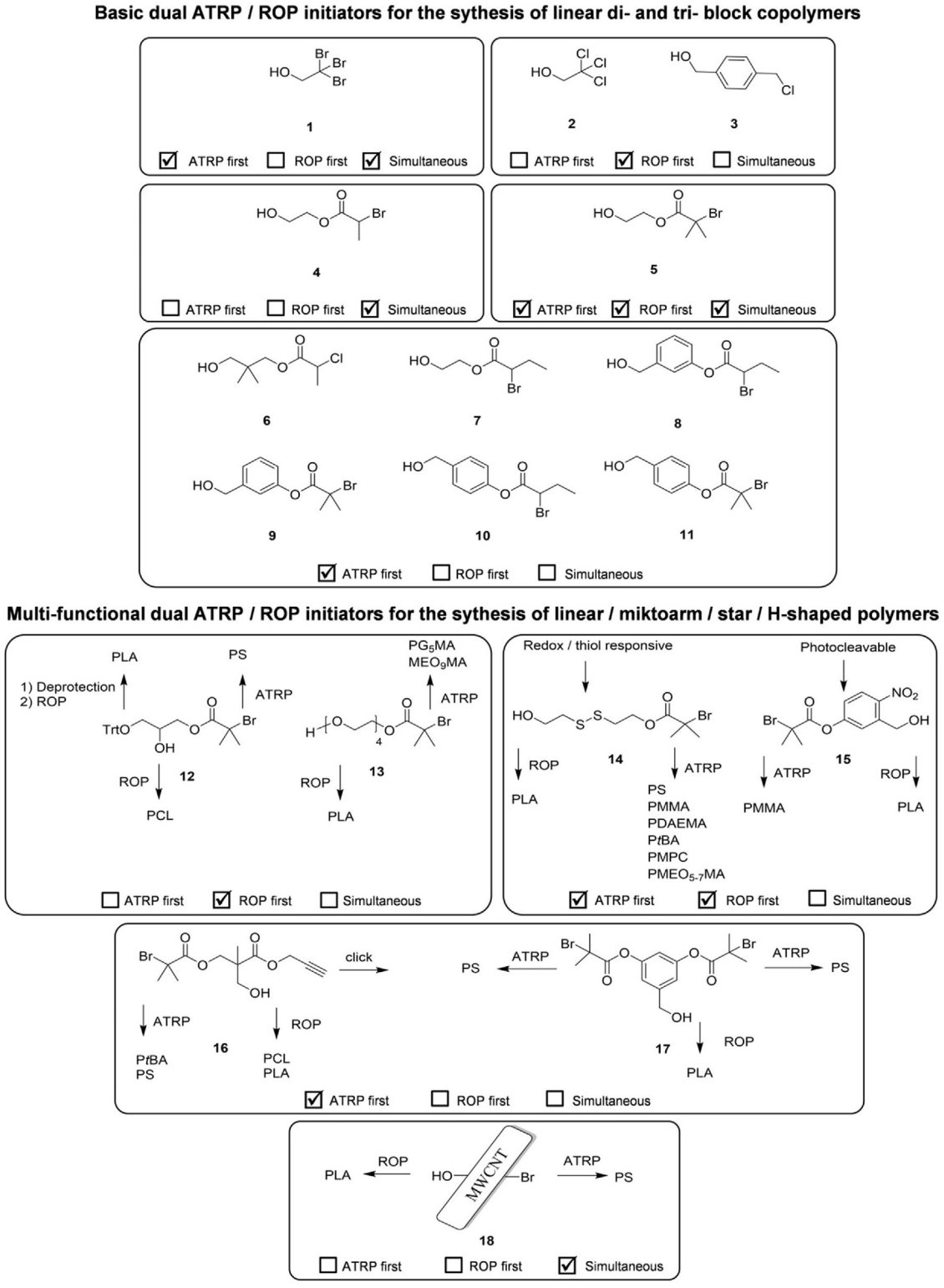

Fig. 5. Schematic representation of dual initiators employed for the combination of ATRP and ROP of lactide.

tor for the ROP, facilitating the synthesis of the triblock copolymer PS-*b*-PMMA-*b*-PLLA with a remarkably low $Đ < 1.2$ [16]. On the other hand, PLA was attached in a final chain extension to the polyester-based PCL block of P*n*BuA-*b*-PCL, which had been prepared by an ATRP first approach using the dual initiator **9** [24]. Focusing on application in drug delivery, also the synthesis of the triblock copolymer PLA-*b*-P*t*BMA-*b*-PMEO$_5$MA has been reported using the dual initiator **5** in a reaction cascade involving the ATRP of *t*BMA, the ROP of lactide, and a subsequent ATRP of MEO$_5$MA [25]. Accepting a possible degradation of the PLA-block, the P*t*BMA middle block was subsequently deprotected to yield a PMAA block, whose conformation would be sensitive to pH value changes.

2.1.1.3. Dual initiators with special design. The ATRP first approach is not limited to simple linear block copolymers but also enables

Table 1
Block copolymers prepared with a dual ROP/ATRP initiator *via* ATRP first method.

Polymer	Dual initiator	ATRP conditions	ROP conditions	$Đ$	Ref.
Diblock copolymers					
PS-*b*-PLLA	**6**	CuBr, HMTETA Bulk, 110 °C	$Sn(Oct)_2$ Toluene, 110 °C	1.17	[17]
	5	CuBr, 2,2′-bipyridine Bulk, 110 °C	$Sn(Oct)_2$ Toluene, 115 °C	1.03–1.19	[16]
	7	CuBr, PMDETA Bulk, 110 °C	$Sn(Oct)_2$ Xylene, 130 °C	1.10–1.18	[18,21]
	8	CuBr, 2,2′-bipyridine Toluene, 110 °C	$Sn(Oct)_2$ Toluene, reflux	1.4	[22]
	9	CuBr, PMDETA Toluene, 110 °C	$Sn(Oct)_2$ Toluene, reflux	1.41	[22]
	11	CuBr, 2,2′-bipyridine Toluene, 110 °C	$Sn(Oct)_2$ Toluene, reflux	1.44	[22]
PS-*b*-PDLA	**7**	CuBr, PMDETA Bulk, 110 °C	$Sn(Oct)_2$ Xylene, 130 °C	1.11–1.23	[18–21]
PS-*b*-PDLLA	**8**	CuBr, 2,2′-bipyridine Toluene, 110 °C	$Sn(Oct)_2$ Toluene, reflux	1.23	[22]
	9	CuBr, PMDETA Toluene, 110 °C	$Sn(Oct)_2$ Toluene, reflux	1.47	[22]
	10	CuBr, 2,2′-bipyridine Toluene, 110 °C	$Sn(Oct)_2$ Toluene, reflux	1.26	[22]
	1	CuBr, $CuBr_2$, HMTETA Bulk, 100 °C	$Sn(Oct)_2$ Toluene, 80 °C	1.55	[23]
Triblock copolymers					
PS-*b*-PMMA-*b*-PLLA	**5**	CuBr, 2,2′-bipyridine Bulk, 110 °C (PS block) CuBr, CuCl, 2,2′-bipyridine Toluene, 85 °C (PMMA block)	$Sn(Oct)_2$ Toluene, 115 °C	1.13–1.19	[16]
P*n*BA-*b*-PCL-*b*-PLLA	**9**	CuBr, PMDETA Toluene, 80 °C	$Sn(Oct)_2$ Toluene, reflux	n.d.[a]	[24]
PDLLA-*b*-P*t*BMA-*b*-$PMEO_5MA$	**5**	$CuBr_2$, PMDETA, $Sn(Oct)_2$ Toluene, 90 °C for *t*BuA	$Sn(Oct)_2$ Toluene, 100 °C	1.28–1.42	[25]
PDLLA-*b*-PMAA-*b*-$PMEO_5MA$ (after deprotection)		70 °C for MEO_5MA		1.32–1.36	
Copolymers from specially designed dual initiators					
PS-PDLLA-PS	**17**	CuBr, 2,2′-bipyridine Toluene, 110 °C	$Sn(Oct)_2$ Toluene, reflux	1.36–1.70	[22]
PS-*b*-PDLLA	**14**	CuBr, PMDETA Anisole/DMSO (2:1 v/v), 110 °C	$Sn(Oct)_2$ Anisole, 120 °C, μwave,	1.2–1.3	[26]

[a] Dispersity of the final triblock is not reported. Dispersity of the P*n*BA macroinitiators is reported as 1.3–1.5.

the introduction of further functional moieties and the preparation of miktoarm star-shaped polymers. However, a special design of the dual initiators is required for these purposes.

The dual initiator **14** includes a disulfide moiety at the junction point between the two initiation sites for ROP and ATRP [26]. The obtained PS-*b*-PLA was subsequently used for self-assembly in films. Subsequently, the reduction of the disulfide resulted in a cleavage of both blocks, facilitating the removal of the PLA. The resulting thiol-functional pores in the PS matrix were functionalized with gold nanoparticles and by thiol-ene reaction using allyl-functional PEO.

The dual initiator **17** enables the synthesis of two PS blocks in the first polymerization because it carries two initiation sites for the ATRP [22]. The resulting PS contains a central hydroxyl moiety, which was used for a subsequent ROP of lactide to obtain star-shaped polymers with two PS arms and one PLA arm, respectively [22].

2.1.2. Macroinitators for ATRP prepared by the "ROP first" method

When the ROP of lactide is performed as first polymerization process using the dual initiators depicted in Fig. 5, a PLA-based macroinitiator for a subsequent ATRP is obtained. Compared to the ATRP-first method, a greater variety of vinylic monomers can be applied using the ROP first approach because the risk of interference with the ROP conditions is not present anymore.

This greater variety broadens the range of possible applications of the obtained block copolymers, benefiting from functional end groups and dual initiators with further tailor-made functionalities. Also in the ROP first approach, the majority of researchers rely on the standard polymerization conditions during the ROP of lactide, while the polymerization conditions for the ATRP are mostly carefully adjusted. Table 2 provides an overview of the block copolymers obtained *via* combination of ROP and ATRP using the "ROP first" approach.

2.1.2.1. "Simple" diblock copolymers. The application of the commercial trichloroethanol (**2**) as dual initiator facilitated the synthesis of PLA-*b*-PMMA block copolymers with relatively high molar masses, albeit at the cost of high dispersities [27]. PDMAEMA features responsive properties towards pH value and temperature, making DMAEMA an interesting monomer for incorporation into a polymeric architecture comprising PLA. DMAEMA represents a typical monomer that would be problematic to polymerize *via* the ATRP first method, since the tertiary amine functionalities of a PDMAEMA block would give rise to side reactions during a subsequent ROP of lactide. On the other hand, very well-defined PLLA-*b*-PDMAEMA was obtained using **5** as dual initiator in a ROP first approach [28]. While these two methacrylate monomers are often polymerized *via* ATRP, acrylonitrile is a somewhat less common monomer nowadays. The corresponding PLLA-*b*-PAN could be

Table 2
Block copolymers prepared with a dual ROP/ATRP initiator *via* ROP first method.

Polymer	Dual initiator	ATRP conditions	ROP conditions	$Đ$	Ref.
Diblock copolymers					
PLLA-*b*-PAN	**3**	CuBr, 2,2′-bipyridine Ethylene carbonate, 70 °C	Li-alkoxide CH_2Cl_2, 0 °C	1.26	[29]
PLLA-*b*-PMMA	**2**	CuCl, PMDETA DMSO, 80 °C	$Sn(Oct)_2$ Bulk, 130 °C	1.4–1.9	[27]
PLLA-*b*-PDMAEMA	**5**	CuBr, HMTETA THF, 60 °C	$Sn(Oct)_2$ Toluene, 100 °C	1.1	[28]
PLLA-*b*-PHEO≈$_6$MA	**5**	CuBr, 2,2′-bipyridine THF, 30 °C	$Sn(Oct)_2$ Bulk, 150 °C	1.46	[30]
PDLLA-*b*-PGlcEO$_{10}$MA	**5**	CuBr, PMDETA Anisole, 60 °C	$Sn(Oct)_2$ Bulk, 130 °C	1.21	[31]
Copolymers prepared with special initiators					
PDLLA-*b*-PMMA	**14**	CuBr, PMDETA THF, 47 °C	$Sn(Oct)_2$ Toluene, 120 °C	1.22	[34]
PDLLA-*b*-PS	**14**	CuBr, PMDETA Anisole, 120 °C	$Sn(Oct)_2$ Toluene, 120 °C	1.22	[34]
PDLLA-*b*-PDAEMA	**14**	CuBr, PMDETA THF, 47 °C	$Sn(Oct)_2$ Toluene, 120 °C	1.21	[34]
PDLLA-*b*-P*t*BA	**14**	CuBr, PMDETA THF, 65 °C	$Sn(Oct)_2$ Toluene, 120 °C	1.2	[34]
PDLLA-*b*-PMEO$_{5-7}$MA	**14**	CuBr, PMDETA THF, 45 °C	$Sn(Oct)_2$ Toluene, 120 °C	1.15–1.28	[33,34]
PLGA-*b*-P(HPG$_5$MA-*co*-MEO$_9$MA)	**13**	$CuBr_2$, PMDETA, $Sn(Oct)_2$ 2-Butanone, 60 °C	$Sn(Oct)_2$ Bulk, 140 °C	1.3–1.6	[32]
PDLLA-*b*-PMPC	**14**	CuBr, 2,2′-bipyridine MeOH/DMSO, 35 °C	$Sn(Oct)_2$ Toluene, 120 °C	n.d.[a]	[35]
PDLLA-*b*-PMMA-*b*-PS	**14**	CuBr, PMDETA PMMA: THF, 47 °C, PS: Anisole, 120 °C	$Sn(Oct)_2$ Toluene, 120 °C	1.23	[34]
Miktoarm star-shaped copolymers					
PCL-PS-PLLA	**12**	CuBr, 2,2′-bipyridine THF, 110 °C	$Sn(Oct)_2$ Toluene, 110 °C	1.14–1.24	[36]

[a] Dispersity value is not reported.

obtained from the dual initiator **3**, using lithium alkoxide catalysts during the ROP [29].

2.1.2.2. Block copolymers obtained with macromonomers. Also the utilization of methacrylate macromonomers based on PEO during the ATRP step has been reported using the dual initiator **5**. The macromonomer HEO≈$_6$MA yielded amphiphilic block copolymers that carry OH-functionalities at the end groups of the side chains of the hydrophilic block and were used to coat Fe_3O_4 nanoparticles (Fig. 6A) [30]. These were subsequently functionalized with folic acid for targeted uptake by cancer cells. ATRP of the glucose-functional macromonomer GlcEO$_{10}$MA with a PLA macroinitiator resulted in well-defined amphiphilic diblock copolymers, exposing the sugar units in aqueous media [31]. This synthesis benefits greatly from the fact that the polymerization of deprotected glycomonomers is possible *via* ATRP using the ROP first method. A deprotection of the attached sugar moieties in the final block copolymer (containing degradable PLA) is not necessary.

A further enrichment of the PLA block copolymers with (short) PEO chains is possible by application of the dual initiator **13**, which was applied for the ROP copolymerization of lactide and glycolide (Fig. 6B) [32]. The subsequent ATRP was performed using a mixture of methacrylate macromonomers based on PEO and PPO to tune the lower critical solution temperature behavior of nanoparticles prepared from the obtained polymers.

2.1.2.3. Dual initiators with special design. Redox and thiol responsive block copolymers were prepared by polymerization of the macromonomer MEO$_7$MA from a PLA macroinitiator [33]. The disulfide junction present in **14** connects the PLA and the vinylic block in the block copolymer and can be cleaved, either by reduction to yield a thiol or by a thiol exchange reaction. This facilitates a cleavage of the PLA block from the PMEO$_7$MA block. The fact that the block copolymer synthesis and the cleavage of the disulfide junction can be performed with excellent control was shown by a comprehensive investigation published by Oh and co-workers [34]. Careful adjustment of the ATRP conditions was performed to match the reactivity of a wide range of vinylic monomers, so that also a triblock copolymer could be obtained. With focus on micellar drug delivery, this concept was also applied for PLA-*b*-PMPC, which additionally was end functionalized with cholesterol [35].

The heterofunctional initiator **12** provides access to miktoarm star-shaped copolymers composed of PCL, PS and PLLA (see Fig. 5) [36]. **12** contains a free hydroxyl function, a trityl-protected hydroxyl moiety and an initiation site for ATRP. The multi-step synthesis included the ROP of ε-caprolactone from the secondary alcohol, the ATRP of styrene, the deprotection of the primary alcohol under acidic conditions, and the final initiation of the PLA arm from the primary alcohol.

2.1.3. One-pot and simultaneous ROP and ATRP

The well working concept of dual ROP/ATRP initiation has driven researchers towards further investigation of the compatibility of the reagents required for both polymerization types. The feasibility of one-pot and simultaneous approaches demonstrates the robustness of the synthetic approach. However, a careful selection of the reaction conditions represents a prerequisite.

2.1.3.1. DBU as ROP catalyst. The synthesis of PMMA-*b*-PDLA using the photocleavable dual initiator **15** shows that not all catalysts are suitable always for a given one-pot approach and that predictions can be difficult to make [37]. $Sn(Oct)_2$ resulted in a well-defined PLA macroinitiator, but the instability of **15** prevented the ROP of lactide in the presence of DBU. Surprisingly, DBU proved superior

Please cite this article in press as: Yildirim I, et al. Old meets new: Combination of PLA and RDRP to obtain sophisticated macromolecular architectures. Prog Polym Sci (2017), http://dx.doi.org/10.1016/j.progpolymsci.2017.07.010

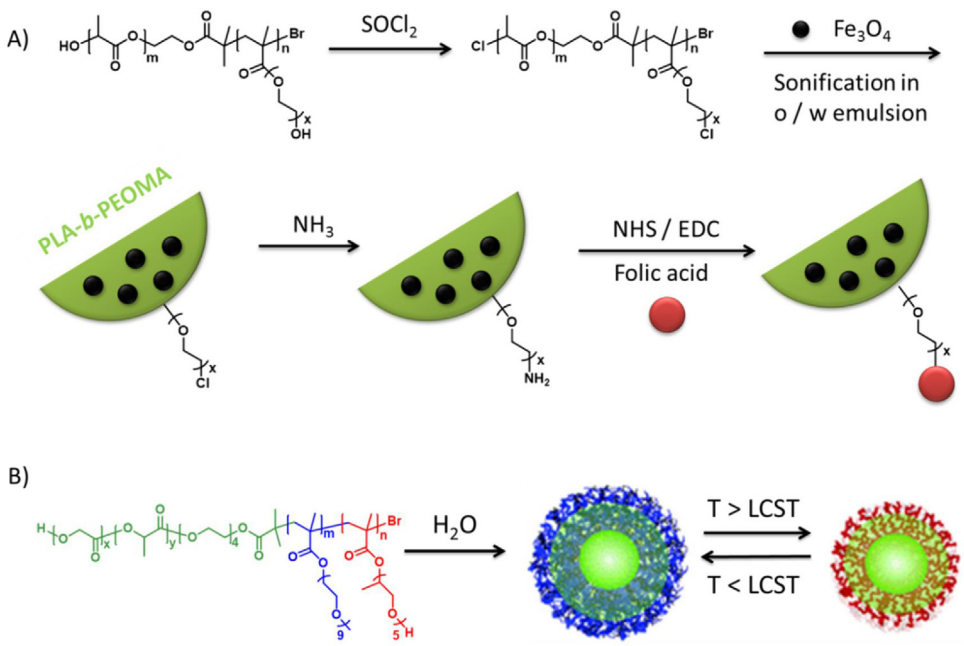

Fig. 6. Schematic representation of PLA block copolymers obtained by ATRP of EO_nMA macromonomers. (A) Folic acid functionalized PLLA-*b*-$PHEO_6MA$ nanoparticles for cancer cell targeting. Adapted from [30] with permission of John Wiley & Sons. (B) Thermo-responsive nanoparticles. Adapted from [32] with permission of The Royal Society of Chemistry.

during the ROP using the respective PMMA macroinitiator obtained by ATRP (CuBr, PMDETA).

The order of both polymerization types affected the synthesis of PLA-*b*-PBGMA block copolymers with the dual initiator **5** as well [38]. The ROP of lactide using DBU as catalyst yielded a PLA macroinitiator. However, a subsequent ATRP (CuCl, HMTETA) of BGMA proceeded with poor control producing a mixture of homo- and block copolymers. On the other hand, the ATRP first method employing the same polymerization conditions during both steps led to well-defined block copolymer structures. Also the acetal protection groups could be removed under acidic conditions without degrading the PLA block as evidenced by the rather low dispersities ($Đ \leq 1.31$), thereby liberating isoglycerol moieties on the polymethacrylate block (Scheme 1).

A direct use of DBU as both the ATRP ligand and the ROP catalyst facilitated the performance of both polymerizations in a simultaneous fashion [39]. Therefore, the monomers L-lactide and MMA, the dual initiator **1**, CuBr and DBU were heated to 85 °C in toluene. Due to the high activity of DBU for ROP at such high temperatures the ROP of lactide completed quickly, while the ATRP of MMA proceeded afterwards at a much lower polymerization rate. Unfortunately, this interesting approach led to the formation of PLA homopolymer impurities present in the PLLA-*b*-PMMA and rather broad molar mass distributions (Table 3).

2.1.3.2. $Sn(Oct)_2$ as ROP catalyst. The majority of researchers have relied on $Sn(Oct)_2$ as ROP catalyst also for one-pot and simultaneous ROP/ATRP procedures. It was noted already for a straightforward vinylic block such as PS that one-pot two-step procedures *via* "ATRP first" provided much better defined block copolymers in comparison to simultaneous polymerizations, regardless of the dual initiator employed (**4** or **5**) [40,41]. This hints towards the fact that $Sn(Oct)_2$ interferes with the ATRP mechanism. Indeed, the reduction of Cu(II) species by $Sn(Oct)_2$ has become a common approach for activator generated by electron transfer (AGET) ATRP in the meantime [42].

Frey and co-workers exploited this fact during a well-investigated one-pot two-step synthesis of PLA-*b*-PHEMA that does not require protection groups for the hydroxyl moieties of the PHEMA block (Fig. 7) [43]. The ROP of lactide was performed first using $Sn(Oct)_2$ under standard conditions. Subsequently, the required reagents for an ATRP were added, *i.e.* the monomer HEMA, CuCl, $CuCl_2$ and bipyridine. The $Sn(Oct)_2$ still present from the ROP served as reducing agent for the slight excess of copper(II) species and was thereby deactivated.

Relying on protected hydroxyl functionalities, PLLA-*b*-PSKA block copolymers were prepared as a precursor for poly(L-lactide)-*b*-poly(2,3-dihydroxypropyl acrylate) (PLLA-*b*-PDHPA) (Scheme 2) [44]. Although simultaneous one-pot ROP and ATRP were reportedly successful, a common ROP first approach provided superior control over the block lengths. An ATRP first approach remained unsuccessful. DMAEMA represents a monomer in particular challenging to combine with PLA already in an ATRP first approach due to its tertiary amine functionality [45]. Indeed, simultaneous polymerization resulted in the formation of ill-defined mixtures of block copolymers with PLA homopolymers. Presumably, the high polymerization temperatures required during simultaneous polymerization even induced a racemization of the PLLA block due to deprotonation of the lactide methine protons by the amino groups in the PDMAEMA.

Despite the difficulties encountered during the synthesis of diblock copolymers, one pot ATRP/ROP approaches were applied using dual initiators with a special design. A PLLA-*b*-P*t*BA block copolymer was prepared employing the dual initiator **16** with an alkyne functionality as building block for ABCDE type H-shaped quintopolymers bearing PLLA, PEO, PS, PCL and PAA side chains. The latter were obtained by 1,3-dipolar cycloaddition with the respective azide-functionalized star-shaped copolymer comprising PEO, PS and PCL arms followed by hydrolysis of the P*t*BA arm to yield PAA (prior to hydrolysis: $Đ = 1{,}19$, after hydrolysis: n.r.) [46]. In a one-pot two-step approach, the ATRP was first conducted at 80 °C, while the subsequent ROP proceeded upon elevation of the temperature to 110 °C. In addition, the simultaneous ROP of L-lactide and ATRP of MMA and styrene was performed successfully in bulk from multi-walled carbon nanotubes (MWCNT) functionalized with the dual initiator **18** [47]. The polymers grafted to the

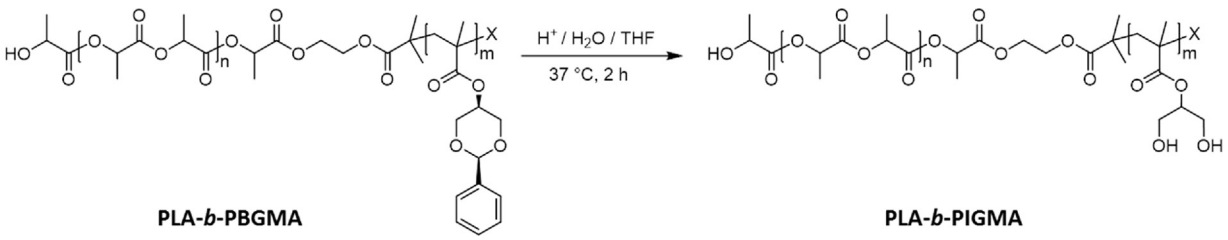

Scheme 1. Schematic representation of the preparation of poly(lactide)-*b*-poly(isoglycerol methacrylate) (PLA-*b*-PIGMA) copolymers by cleavage of the acetal protecting groups [38].

Table 3
Block copolymers prepared with a dual ROP/ATRP initiator *via*one pot approaches.

Polymer	Dual initiator	ATRP catalyst/ligand	ROP catalyst	Polym. cond.		Sequence	*Đ*	Ref.
Diblock copolymers								
PLA-*b*-PHEMA	**5**	CuCl, $CuCl_2$ bipyridine	$Sn(Oct)_2$	Toluene, 120 °C (PLA) DMSO, 80 °C (PHEMA)			1.18–1.27	[43]
PLLA-*b*-PMMA	**1**	CuBr DBU	DBU	Toluene, 85 °C		Sim.	1.40–1.75	[39]
PDLLA-*b*-PS	**4**	CuBr PMDETA	$Sn(Oct)_2$	Anisole, 110 °C		Sim.	1.52	[40]
						2 steps ATRP first	1.30–1.40	
	5					Sim.	1.5	[41]
						2 steps ATRP first	1.1–1.3	
PLLA-*b*-PDMAEMA	**5**	CuBr HMTETA	$Sn(Oct)_2$	Toluene	70 °C	Sim.	n.d.[a]	[45]
					90 °C		2.5	
					110 °C		n.d.[a]	
PLLA-*b*-PDHPA	**5**	CuCl PMDETA	$Sn(Oct)_2$	Diphenylether, 110–120 °C		Sim.	1.23–1.50[b]	[44]
		CuBr PMDETA					1.83[b]	
Copolymers from specially designed dual initiators								
PLLA-*b*-P*t*BA	**16**	CuBr PMDETA	$Sn(Oct)_2$	Toluene, 80 °C (P*t*BA) Toluene, 110 °C (PLA)		2 steps ROP first	1.13–1.19[b]	[46]
MWCNT-*g*-PLLA-PMMA	**18**	CuBr HMTETA	$Sn(Oct)_2$	Bulk, 120 °C		Sim.	n.d.[a]	[47]

[a] Dispersity value is not reported.
[b] Dispersity value is reported prior to deprotection of the corresponding protecting groups.

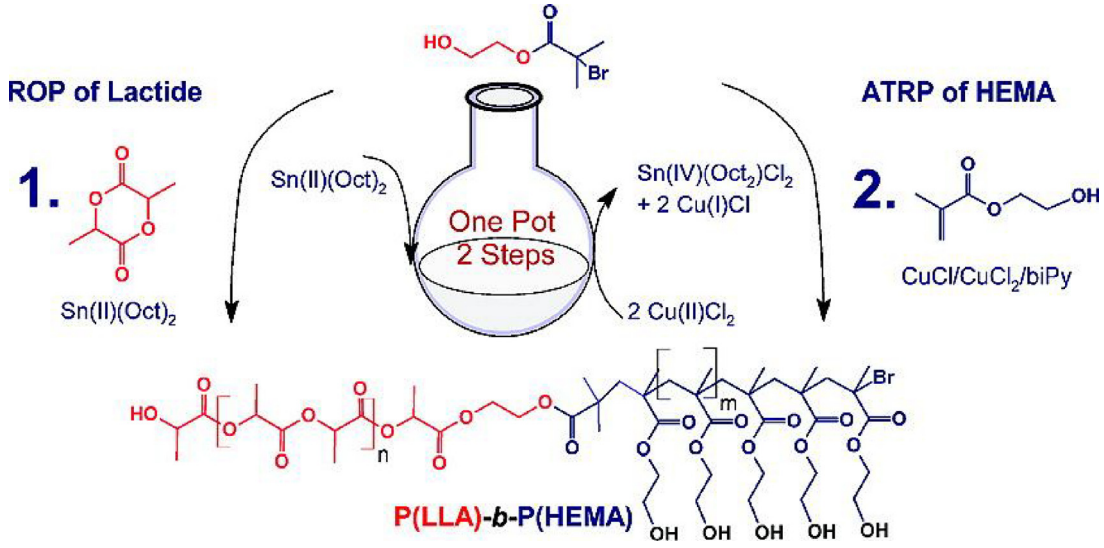

Fig. 7. Schematic representation of the synthesis of PLLA-*b*-P(HEMA) copolymers by combining ROP of L-lactide and ATRP of HEMA in a one-pot approach. Reprinted with permission from Macromolecules 2009, 42, 5622–5628 [43]. Copyright (2009) American Chemical Society.

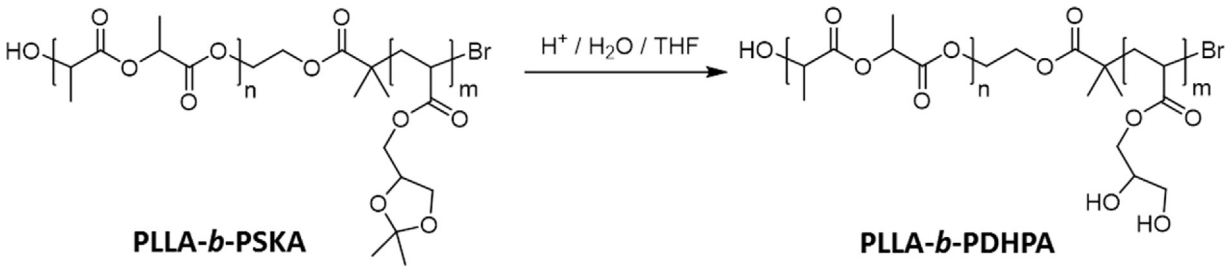

Scheme 2. Schematic representation of the synthesis of PLLA-*b*-PDHPA copolymers by deprotection of the acetal protecting groups [44].

MWCNTs revealed a similar composition as in the feed when synthesized at 100 °C (PMMA-*b*-PLLA), whereas the fraction of lactide was increased when the synthesis was conducted at 120 °C (PS-*b*-PLLA).

2.2. Combination of ROP and RAFT polymerization using inifers

RAFT polymerization represents an effective and versatile RDRP technique, which is compatible with various polar and non-polar monomers. The fact that RAFT tolerates many functional moieties would theoretically enable to prepare a multitude of functional building blocks or more advanced polymer architectures. Thus, the RAFT polymerization procedure has been one of the most extensively utilized techniques to prepare PLA based copolymers in combination with ROP. However, the ROP of lactide is not as tolerant, which restricts or complicates the synthetic opportunities.

RAFT polymerization is initiated by a common radical initiator, while an additional CTA provides control over the polymerization in terms of kinetics, end groups and molar mass [48]. Therefore, hydroxyl-functional CTAs do not represent dual initiators but would rather be named as inifers (initiator–transfer agent), since they bear a transfer agent for RAFT polymerization and an initiating function for ROP (Fig. 8) [49]. Nowadays, some OH-functional CTAs are even available commercially, which considerably lowers the synthetic effort to prepare block copolymers comprising PLA and vinylic blocks *via* the infer approach.

2.2.1. Macroinitiators for the ROP of lactide prepared by the "RAFT first" method

The RAFT-first approach relies on the use of a hydroxy-functionalized CTA for RAFT polymerization and a subsequent initiation of the ROP of lactide from the terminal hydroxyl functionality of the precursor polymer. The vinylic monomers polymerized *via* this method are summarized in Fig. 3, and Table 4 provides a general overview of the reagents used within the recent literature.

Hedrick and co-workers demonstrated the broad applicability of this synthetic approach for the preparation of block copolymers by using the infer CTA **19** [50,51]. For this purpose, a series of hydroxy-functional macro-initiators were prepared by RAFT polymerization exploiting methacrylate, acrylate, and styrenic monomer classes. Subsequently, a variety of diblock and triblock copolymers with poly D,L-lactide (PDLLA) was prepared by using the hydroxyl functional precursors as macroinitiators for a ROP of D,L-lactide in combination with a thiourea catalyst at room temperature. Copolymers with molar masses up to 50,000 g/mol and low dispersity values were obtained, showing the excellent control over ROP and RAFT polymerizations.

The synthetic approach is not limited to proof of principle studies but has been exploited for the development of micellar drug carriers composed of a biodegradable PLA-core and a thermo-responsive shell [52–54]. For this purpose, CTA **20** was employed for the RAFT copolymerization of NiPAm and DMA to subsequently perform the ROP of D,L-lactide using the standard catalyst $Sn(Oct)_2$. The fluorescent dye Oregon Green 488 was covalently attached to the block copolymer *via in situ* aminolysis of the terminal dithiobenzoate groups and Michael addition using the maleimide functional dye as acceptor [53].

Also more complicated polymeric architectures, such as H-shaped or miktoarm star polymers, can be prepared with the RAFT-first technique. This requires more complex non-commercial inifers, which have to be tailor-made. The PEO based macro CTAs **28** and **29** were developed for this purpose [55,56]. RAFT polymerization of styrene with the CTA **28** yielded the block copolymer PEO-*b*-PS with a central hydroxyl functionality [55]. The ROP of L-lactide in the presence of $Sn(Oct)_2$ in the next step resulted in the formation of ABC miktoarm star copolymers composed of PEO, PS, and PLA. With some variations in the inifer design, this methodology was adapted for the synthesis of even more complex H-shaped terpolymers of similar composition [56].

2.2.2. PLA-based macro-CTAs prepared by the "ROP first" technique

The ROP first technique represents a reasonable alternative method, in particular to facilitate the synthesis of PLA-containing copolymers with functional moieties that would not be tolerated by the ROP of lactide. Consequently, a greater variety of vinylic monomers has been utilized (Table 5). Basically, the same type of CTAs can be applied for this purpose as for the RAFT-first approach, although the research groups active in this field rather rely on trithiocarbonates. However, special care has to be taken that the functional vinylic monomers applied in the second polymerization do not induce a degradation of the PLA block that is already present. The main prerequisite during the ROP-first approach is the fact that the CTA does not undergo or induce undesired side reactions during the ROP process. Indeed, many CTAs remain intact with various catalysts that have been applied during the ROP, although the structural characterization of the macroCTAs is often disregarded in view of bio-applications of the final block copolymers. However, suitable macro CTAs based on PLA have been prepared using tin(II) [57], DBU [58,59], the thiourea/(−)-sparteine co-catalyst system [60,61], and a calcium complex [62]. These precursors are mostly applied to attach a hydrophilic second block by the subsequent RAFT polymerization, facilitating the preparation of micellar structures. Examples include $PMEO_nMA$ [57], the thermo-responsive PNiPAm [58], PDMAEA [63], and charged poly(methacrylate)s based on cholinium building units [59].

2.2.2.1. Diblock copolymers with subsequent deprotection. Despite the versatility of the RAFT polymerization itself, protection groups had to be applied to obtain poly(acrylic acid) (PAA) as a second block. For this purpose, Dove and O'Reilly prepared a library of well-defined PLLA-*b*-PTHPA diblock copolymers as precursors using the CTA **21** (Fig. 9) [60,63]. Since the tetrahydropyranyl acetal (THP) moieties could be readily hydrolyzed under mild acidic conditions or heating in a water/THF mixture, the targeted PLLA-*b*-PAA was obtained directly in a self-assembled form. The developed

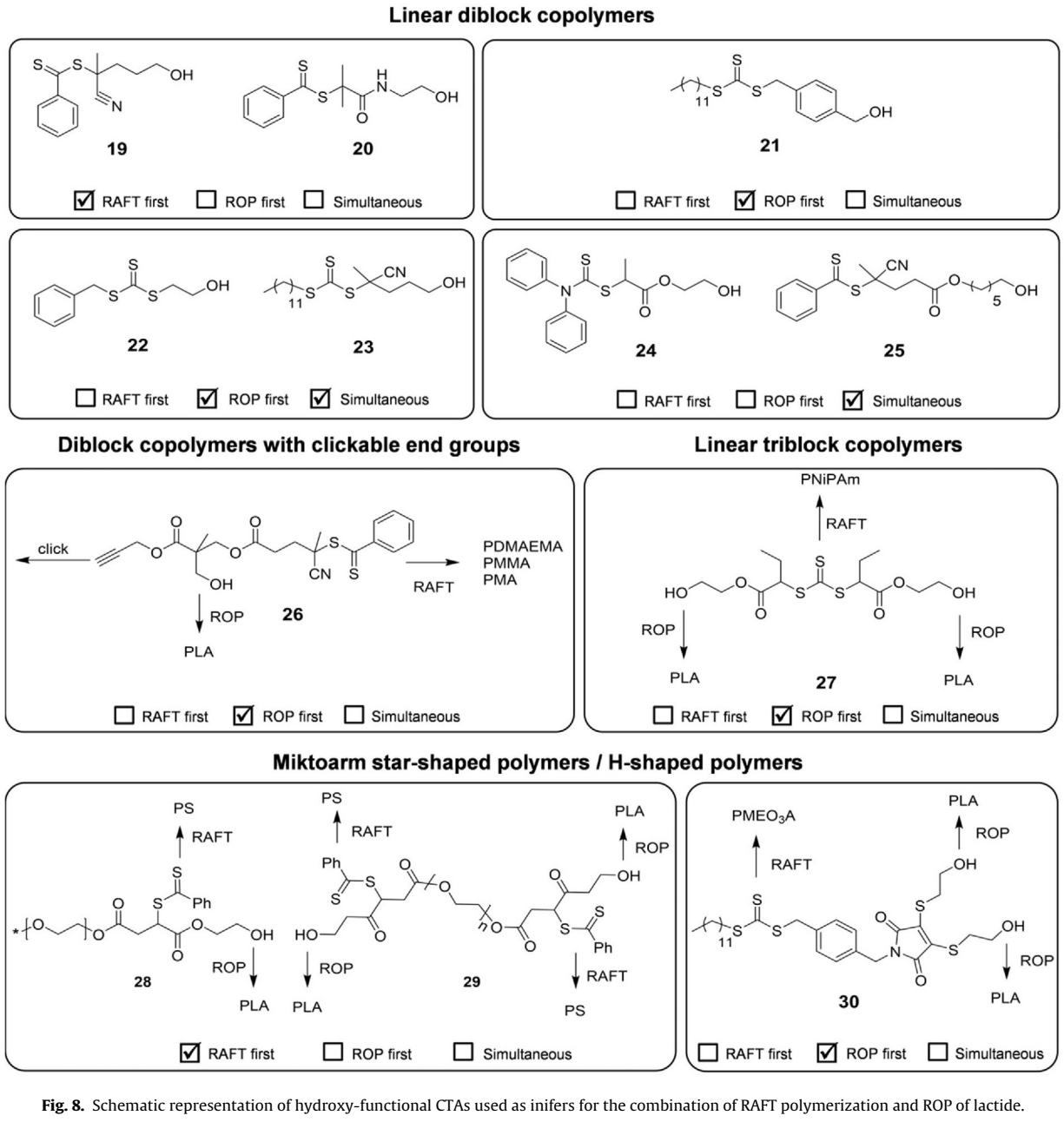

Fig. 8. Schematic representation of hydroxy-functional CTAs used as inifers for the combination of RAFT polymerization and ROP of lactide.

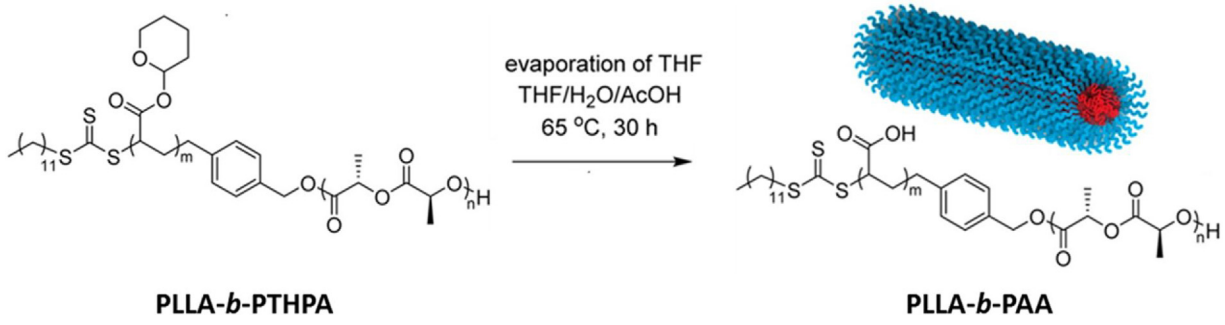

Fig. 9. Schematic representation of the crystallization driven self-assembly of PLLA-*b*-PAA during deprotection of PLLA-*b*-PTHPA. Reprinted with permission from Macromolecules 2013, 46, 9074–9082 [60]. Copyright (2013) American Chemical Society.

procedure could even be adopted for the direct preparation of stereocomplex micelles from a mixture of PLLA-*b*-PAA and PDLA-*b*-PAA copolymers in water *via* crystallization driven self-assembly [61].

2.2.2.2. Diblock copolymers subjected to further functionalization. The synthetic possibilities of the ROP-first method are by far not exhausted by the simple preparation of diblock copolymers. A range

Table 4
Block copolymers prepared with an inifer *via* RAFT first method.

Polymer	CTA	RAFT conditions	ROP catalyst/co-initiator	ROP conditions	Đ	Ref
Diblock copolymers						
PMMA-*b*-PLA	**19**	Benzene 60 °C	Phosphazene base BEMP Thiourea Thiourea/(−)-sparteine	CH_2Cl_2, 25 °C CH_2Cl_2, 25 °C	1.17 1.12 1.1	[51] [50]
PDMAEMA-*b*-PLA	**19**	EtOAc 60 °C	Thiourea	CH_2Cl_2, 25 °C	1.32	[50]
P(MMA-*co*-HEMA)-*b*-PLA	**19**	EtOAc 60 °C	Thiourea	CH_2Cl_2, 25 °C	1.21	[50]
P*t*BA-*b*-PLA	**19**	n.r.[a]	Thiourea Thiourea/(−)-sparteine	CH_2Cl_2, 25 °C	1.1 1.11	[50]
PVP-*b*-PLA	**19**	Bulk 60 °C	Thiourea Thiourea/(−)-sparteine	CH_2Cl_2, 25 °C	1.09 1.1	[51]
PMMA-*b*-PS-*b*-PLA	**19**	Bulk 60 °C	Thiourea	CH_2Cl_2, 25 °C	1.18	[51]
P(NiPAm-*co*-DMA)-*b*-PLA	**20**	1,4-dioxane 70 to 85 °C	$Sn(Oct)_2$	Xylene 110–150 °C	1.07–1.12	[52–54]
ABC mictoarm star-shaped polymer						
MPEO-PS-PLA	**28**	THF 110 °C	$Sn(Oct)_2$	Toluene 115 °C	1.05–1.14	[55]
H-shaped polymer						
[(PLLA)(PS)]PEO[(PS)(PLLA)]	**29**	THF 110 °C	$Sn(Oct)_2$	Toluene 120 °C	1.10–1.17	[56]

[a] Polymerization conditions are not reported.

Table 5
Block copolymers prepared with an inifer *via* ROP first method.

Polymer	CTA	ROP catalyst	ROP conditions	RAFT conditions	Đ	Ref.
PLA-*b*-$PMEO_nMA$ PLGA-*b*-$PMEO_nMA$	**22**	$Sn(Oct)_2$	Bulk 140 °C	THF 80 °C	1.4 1.6–1.7	[57]
PLA-*b*-PNiPAm	**22**	DBU	CH_2Cl_2 RT	DMF 70 °C	1.19	[58]
PLA-*b*-PDMAEA	**21**	Thiourea/ (−)-sparteine	CH_2Cl_2 RT	$CHCl_3$ 60 °C	1.48	[63]
PLLA-*b*-PCLM	**23**	DBU/ Benzoic acid salt	CH_2Cl_2 40 °C	Methanol/CH_2Cl_2 (5:1 v/v) 70 °C	1.25–1.32	[59]
PLLA-*b*-PAA	**21**	Thiourea/ (−)-sparteine	CH_2Cl_2 RT	$CHCl_3$ 60 °C	1.09–1.42[a]	[60,61,63]
PDLA-*b*-PAA	**21**	Thiourea/ (−)-sparteine	CH_2Cl_2 RT	$CHCl_3$ 60 °C	1.11–1.38[a]	[61,63]
PDLLA-*b*-PAA	**21**	Thiourea/ (−)-sparteine	CH_2Cl_2 RT	$CHCl_3$ 60 °C	1.31[a]	[63]
PDLLA-*b*-PNiPAm	**22**	$Sn(Oct)_2$	Bulk 140 °C	DMAc 60 °C	1.38–1.46	[65]
PDLLA-*b*-P(HEA-*co*-CEMA)	**22**	$Sn(Oct)_2$	Bulk 140 °C	DMAc 60 °C	1.34–1.38	[64]
PDLLA-*b*-PAGP	**22**	$Sn(Oct)_2$	Bulk 140 °C	α, α, α-trifluoro-toluene	1.2	[66]
PLA-*b*-PNiPAm-*b*-PLA	**27**	$Sn(Oct)_2$	Toluene 115 °C	THF 100 °C	1.19–1.30	[67]
$PMEO_3A$-*b*-$PDLLA_2$	**30**	Thiourea/ (−)-sparteine	CH_2Cl_2 RT	$CHCl_3$ 60 °C	1.22–1.42	[69,70]
PLLA-*b*-PDMAEMA PLLA-*b*-PMMA PLLA-*b*-PMA	**26**	$Sn(Oct)_2$	Toluene 90 °C	Toluene 80 °C	1.11 1.08 1.12	[71]

[a] Dispersity values are reported prior to deprotection of the corresponding protection groups.

of subsequent functionalization reactions provide access to interesting materials specially designed for numerous kinds of potential applications. Stenzel and co-workers reported the synthesis of polymeric prodrugs from PLA-*b*-P(HEA-*co*-CEMA) [64]. The ruthenium metallodrug RAPTA-C was conjugated to the hydrophilic block, utilizing the chloro moieties introduced by CEMA in a Finkelstein reaction (Scheme 3).

Also pre-assembled nanostructures (*i.e.* vesicles) made from PLA-*b*-PNiPAm can be further modified to obtain a covalently attached and crosslinked shell [65]. For this purpose, a RAFT polymerization of hexamethylene diacrylate was conducted, utilizing the trithiocarbonate moieties of the block copolymer. Similarly crosslinked shells were applied to prepare hollow nanospheres composed of poly(6-*O*-acryloyl-α-D-galactopyranose) (PAGP, Scheme 4) [66]. The isopropylidene protected precursor PLA-*b*-PAlpGP was deprotected using formic acid to yield the glycopolymer PLA-*b*-PAGP. SEC and ^{1}H NMR analysis did not indicate any noticeable degradation of the PLA. Subsequent to micellar assembly and crosslinking, the PLA core was removed by aminolysis.

2.2.2.3. Triblock copolymers and specially designed inifers. The symmetric CTA **27** with two hydroxyl functionalities provides access to symmetric triblock copolymers. The ROP step results in a

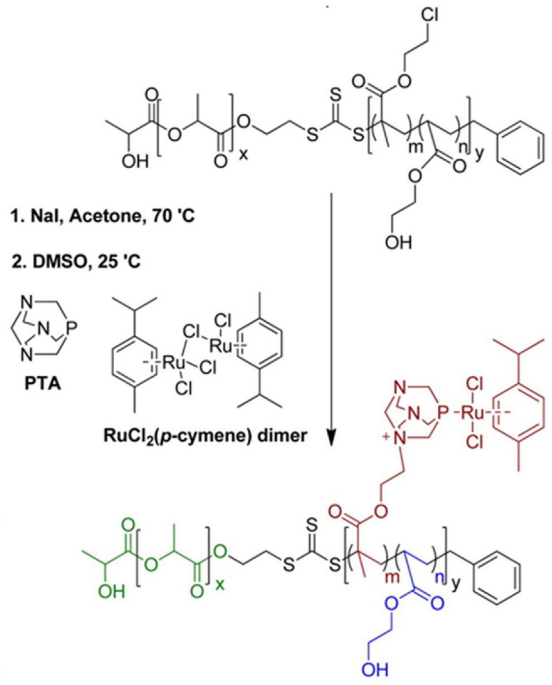

Scheme 3. Schematic representation of the functionalization of PDLLA-*b*-P(HEA-*co*-CEMA) copolymers with RAPTA-C *via* the Finkelstein reaction. Reprinted with permission from Biomacromolecules 2013, 14, 4177–4188 [64]. Copyright (2013) American Chemical Society.

PLA-macro-CTA with a central trithiocarbonate unit, which was subsequently applied for the polymerization of NiPAm to obtain micelles with a thermo responsive shell [67].

O'Reilly and Raymond prepared the dithiomaleimide (DTM) based CTA **30** [68], which features a fluorophore at the junction between the orthogonal polymerization sites. This compound was used to prepare Y-shaped amphiphilic $PMEO_3A$-*b*-PLA_2 block copolymers. The emission of fluorophore served as probe to track local changes during the self-assembly process of the polymer [69]. In addition, thiol exchange at the fluorophore led to block copolymer disassembly and a transition from micellar to vesicular morphology [70].

The alkyne functional inifer **26** was employed to obtain diblock copolymers composed of PLA and a poly(meth)acrylate block that feature an alkyne functionality at the junction of the blocks. 1,3-Dipolar cycloaddition with an azide end-functional counterpart yielded miktoarm star-shaped polymers comprising a PEO, a PCL and a PS arm [71].

2.2.3. *One-pot and simultaneous ROP and RAFT polymerization*

The combination of ROP and RAFT polymerization can be simplified by performing both reactions in cascade without intermediate purification steps [72]. The simultaneous performance of ROP and RAFT polymerization takes the one-pot approach one step further, requiring catalysts, initiators and monomers compatible to each other [72–75]. Despite these challenges, it represents a convenient and experimentally elegant way of combining two mechanistically distinct polymerization techniques (Table 6).

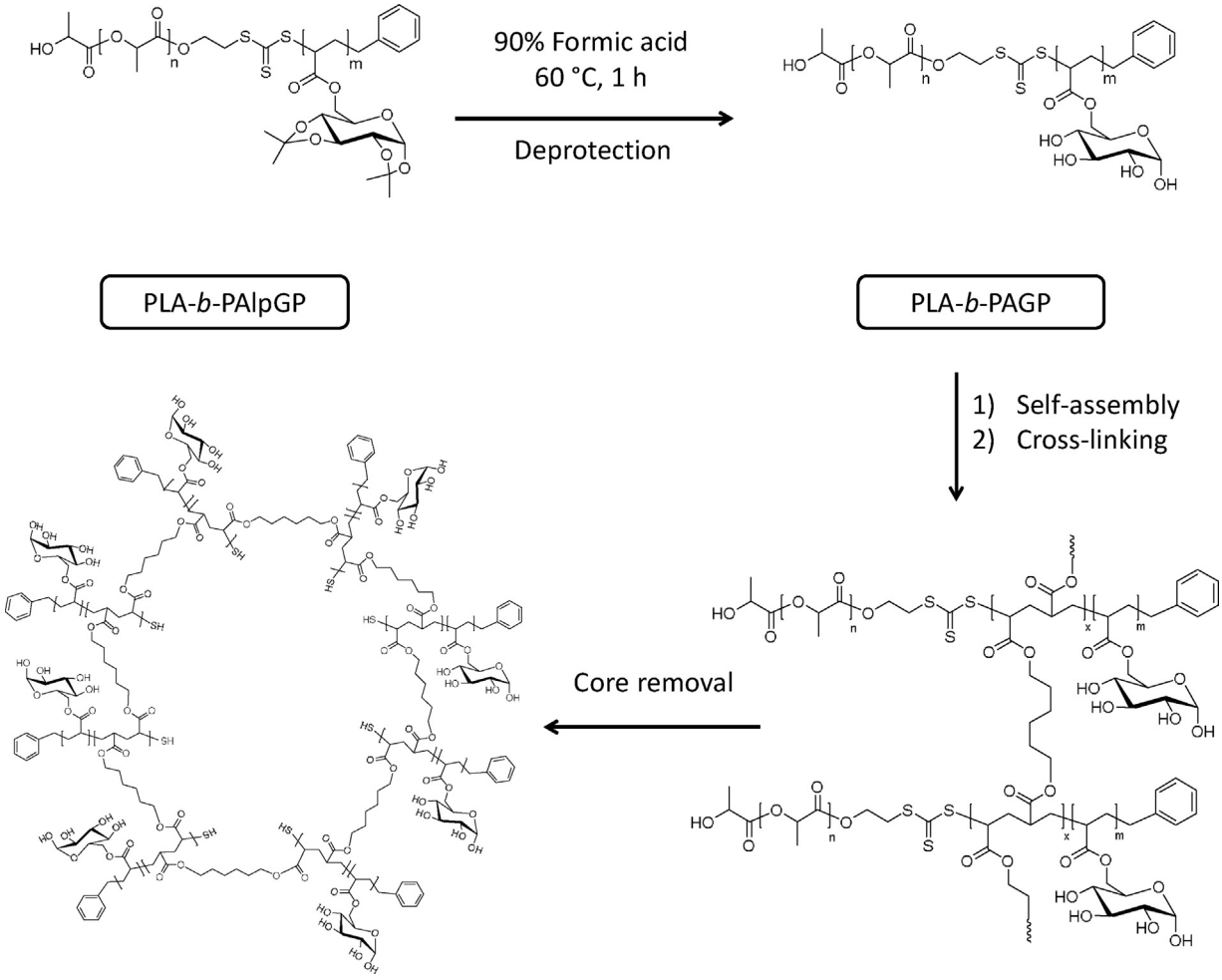

Scheme 4. Schematic representation of the synthesis of PDLLA-*b*-PAGP glycopolymers used to obtain hollow nanospheres [66].

Table 6
Block copolymers prepared with an inifer *via* one pot approaches.

Polymer	CTA	ROP catalyst	Conditions	Sequence	Đ	Ref.
PLLA-*b*-PS	**23**	DMAP	1,4-Dioxane	Simultaneous	1.06	[73]
PLLA-*b*-PMMA			60 °C		1.07	
PLLA-*b*-P*n*BMA					1.06	
PLLA-*b*-P*t*BMA					1.05	
PLLA-*b*-PSMA					1.09	
PLLA-*b*-PNiPAm					1.1	
PLLA-*b*-PNVP	**24**	DMAP	Anisole	Simultaneous	1.18–1.23	[74]
			60 °C			
PLLA-*b*-PGlyMA	**25**	DMAP	1,2-Dichloroethane	2 steps	1.27	[72]
			74 °C	ROP first		
PLLA-*b*-PDMAEMA	**25**	DMAP	1,2-Dichloroethane	2 steps	1.41	[72]
			74 °C	ROP first		
				Simultaneous	1.30–1.39	
PLLA-*b*-PMEO$_{7-8}$MA	**25**	DMAP	1,2-Dichloroethane	Simultaneous	1.32	[72]
			74 °C			
PLLA-*b*-PMPC	**25**	DMAP	1,2-Dichloroethane,	2 steps	1.35–1.43	[72]
			74 °C (ROP)	ROP first		
			Ethanol, 78 °C (RAFT)			
			1,2-dichloroethane/ethanol (1:5 v/v)			
PDLLA-*b*-P(S-*co*-DVB)	**22**	Sn(Oct)$_2$	Bulk	Simultaneous	n.d.[a]	[75]
			120 °C			

[a] Dispersity value is not reported.

Youk and co-workers explored such approaches using a variety of hydrophobic methacrylate monomers and NiPAm, DMAP as catalyst for the ROP, and the trithiocarbonate **23** [73]. However, the kinetics of the simultaneous polymerizations deviated from the respective individual polymerizations, making the final composition of the block copolymers difficult to predict in some cases. A subsequent alteration of the CTA towards the dithiocarbamate **24** made the synthetic approach compatible with NVP as additional monomer type for the RAFT polymerization [74].

Armes and Themistou applied the same strategy to synthesize diblock copolymers of PLA with various hydrophilic methacrylate monomers in one pot, using DMAP as the ROP catalyst and the CTA **25** [72]. Both polymerizations could be performed simultaneously for the RAFT of DMAEMA and MEO$_{7-8}$MA, albeit to a slight cost of dispersity compared to a one-pot/two-step approach. Also the challenging methacrylates GlyMA (hydroxyl-functional) and MPC (solubility only in protic solvents) could be polymerized in an experimentally simple one-pot/two-step synthesis. In addition, the simultaneous RAFT/ROP approach was applied to obtain *in-situ* cross-linked PLA-based block polymers by incorporation of divinylbenzene (DVB) as comonomer to a PS block [75]. Subsequent etching of the PLA domains under alkaline conditions yielded a nanoporous thermoset PS.

2.3. Combination of NMP and ROP using dual initiators

NMP is an efficient technique for the polymerization of vinylic monomers featuring advantages such as experimental as well as mechanistic simplicity, and functional group tolerance [76,77]. Yielding metal-free products, NMP relies on the use of alkoxyamine initiators that are based on stable nitroxide radicals such as TEMPO, TIPNO or SG-1 (Fig. 10). Less frequently, the respective free nitroxide is added to control a radical polymerization initiated by common radical initiators, benefiting from the commercial availability of the nitroxide radicals. Although this is currently not the case for the respective alkoxyamines, more and more tailored reagents become commercially available, which will minimize the synthetic effort for polymer chemists in the future.

NMP requires rather high temperatures (typically 110 °C or higher) to homolytically cleave the carbon-oxygen bond. It provides control over the polymerization of styrenic, acrylate and acrylamide monomers, but its applicability for the polymerization of methacrylates is limited. The monomers used to prepare block copolymers with PLA from dual initiators are depicted in Fig. 3. Mostly, the NMP first method has been employed to obtain macroinitiators for the ROP of lactide, but also ROP first and one-pot methods have been reported (Table 7).

2.3.1. SG-1 based initiators

Starting from the commercially available carboxylic acid functional alkoxyamine BlocBuilder^{TM}, Vinas *et al.* prepared the dual ROP/NMP initiator **34** in a two-step synthesis (using the *N*-Hydroxysuccinimide (NHS) activated ester and ethanolamine) [78]. In a NMP first approach, PS-*b*-PLA with a molar mass of $M_n \approx 12{,}000$ g/mol and a unimodal molar mass distribution could be obtained, despite the relatively high temperature required for the ROP of lactide using Sn(Oct)$_2$ in the second step.

2.3.2. TIPNO based initiators

The dual initiator **33** [79] was extensively applied by the Hedrick-group to synthesize various PLA-*b*-PS and PLA-*b*-PDMA block copolymers, mostly relying on NMP first approaches. The effective ROP organocatalysts developed in house, *i.e.* thiourea-amine compounds [50] and phosphazene bases [51], were applicable under mild ROP conditions. As a consequence, extremely well-defined block copolymers were obtained. The dispersity of the final block copolymers remained below 1.1, even when the ROP was driven to quantitative conversion (DP of each block up to 100). Extension of the accessible range of the block lengths of PLA-*b*-PDMA facilitated the preparation of nanostructured films with varying morphology by self-assembly approaches [80,81]. The synthetic approach was also applicable for PDMA-*b*-PLA with varying stereochemistry of the PLA block (PDLLA, PLLA, *rac*PLA, and *sb*PLA), providing access to nanostructures through the formation of stereocomplexes [82]. The polymerization of NiPAM during the NMP enabled the preparation of mixed micelles with patchy thermoresponsive coronas by stereocomplexation of the obtained PNiPAm-*b*-PLLA with PEO-*b*-PDLA [83].

2.3.3. TEMPO-based initiators

The free nitroxide 4-hydroxy-TEMPO (**31**) does not represent an actual dual initiator for ROP and NMP, since it requires an additional radical source (such as benzoyl peroxide, BPO) to initiate the polymerization. The free nitroxide provides control in terms

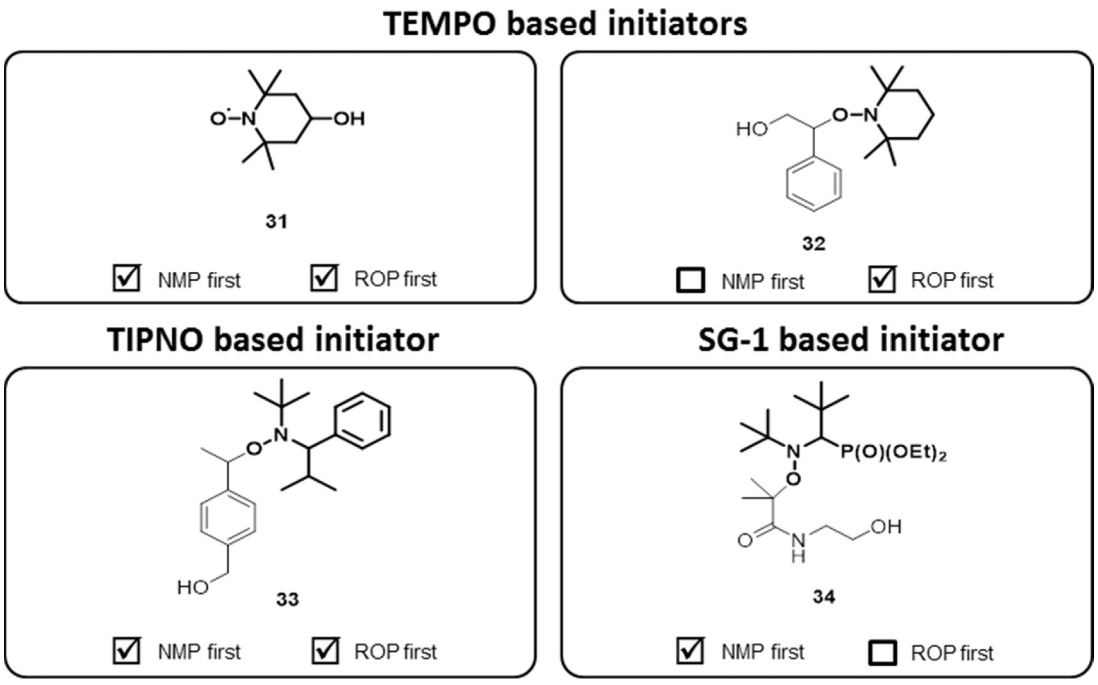

Fig. 10. Schematic representation of the dual initiators used for the combination of ROP of lactide and NMP. The respective stable nitroxide radical is indicated in bold. TEMPO: 2,2,6,6-Tetramethyl-1-piperidinyloxyl, TIPNO: 2,2,5-Trimethyl-4-phenyl-3-azahexane-3-oxyl, SG-1: *N*-*tert*-butyl-*N*-[1-diethoxyphosphoryl-2,2-dimethylpropyl] nitroxide.

Table 7
Block copolymers prepared *via* combination of ROP and NMP.

Polymer	Initiator	Method	ROP conditions	NMP conditions	$Đ$	Ref.
Diblock copolymers						
PS-*b*-PDLLA	**34**	NMP first	$Sn(Oct)_2$ Toluene, 105 °C	Bulk, 120 °C	1.11	[78]
PS-*b*-P(*rac*-LA)	**33**	NMP first	Thiourea/amine CH_2Cl_2, 25 °C	Bulk, 125 °C	1.05–1.09	[50]
		NMP first	Phosphazene base BEMP CH_2Cl_2, RT	Bulk, 125 °C	1.07	[51]
PDMA-*b*-PLLA	**33**	NMP first	Thiourea/(−)-sparteine	Bulk, 125 °C	1.08	[82]
PDMA-*b*-PDLA	**33**	NMP first	CH_2Cl_2, RT		1.16	
PDMA-*b*-P(*rac*-LA)	**33**	NMP first	Thiourea/amine CH_2Cl_2, 25 °C	Bulk, 125 °C	1.08	[50]
		NMP first	Thiourea/(−)-sparteine	Bulk, 125 °C	1.11	[80]
		NMP first	CH_2Cl_2, RT		1.05–1.12	[81]
PDMA-*sb*-PLA	**33**	ROP first	Phosphazene base P_2-*t*-Bu Toluene, −90 °C	Bulk, 125 °C	1.19	[82]
PNiPAm-*b*-PLLA	**33**	NMP first	Thiourea/(−)-sparteine CH_2Cl_2, RT	DMF, 125 °C	1.13	[83]
PS-*b*-PLLA	**31**	NMP first	Li-alkoxide CH_2Cl_2, 0 °C	Bulk, 130 °C	1.11–1.28	[84]
PDLLA-*b*-PS	**31**	ROP first	$AlEt_3$ Toluene, 80 °C	Bulk or DMF, 120–130 °C	1.28–1.80 125–165	[85]
PLLA-*b*-PS	**31** **32**	ROP first	[BDI⁻-*i*Pr]Zn, Styrene, RT	Bulk, 125 °C Bulk, 135 °C	1.8 1.6	[86]
P(*rac*-LA)-*b*-PS	**31** **32**			Bulk, 125 °C Bulk, 135 °C	1.8 1.9	
PLLA-*b*-PS	**32**	One-pot (ROP first)	[BDI⁻-*i*Pr]Zn, Styrene, 100 °C	135 °C	1.18	
Triblock copolymers						
PDLLA-*b*-PS-*b*-P*t*BuS	**31**	ROP first	$AlEt_3$ Toluene, 80 °C	DMF, 130 °C Bulk, 130 °C	1.54–1.69 1.56	[85]
PDLA-*b*-P(*t*BuS-*r*-S)-*b*-P*t*BuS	**31**	ROP first	$AlEt_3$ Toluene, 80 °C	DMF, 120 °C	1.52–1.54	

of molar mass and forms the ω-end-group of the polymer obtained after NMP. In contrast to the polymeric structures discussed above, the alkoxyamine structure connects the PLA and the vinylic block because the hydroxyl functionality of **31** is attached to the nitroxide. In an NMP first approach, **31** was applied during the NMP of styrene [84]. Subsequent to a covalent attachment of a lithium

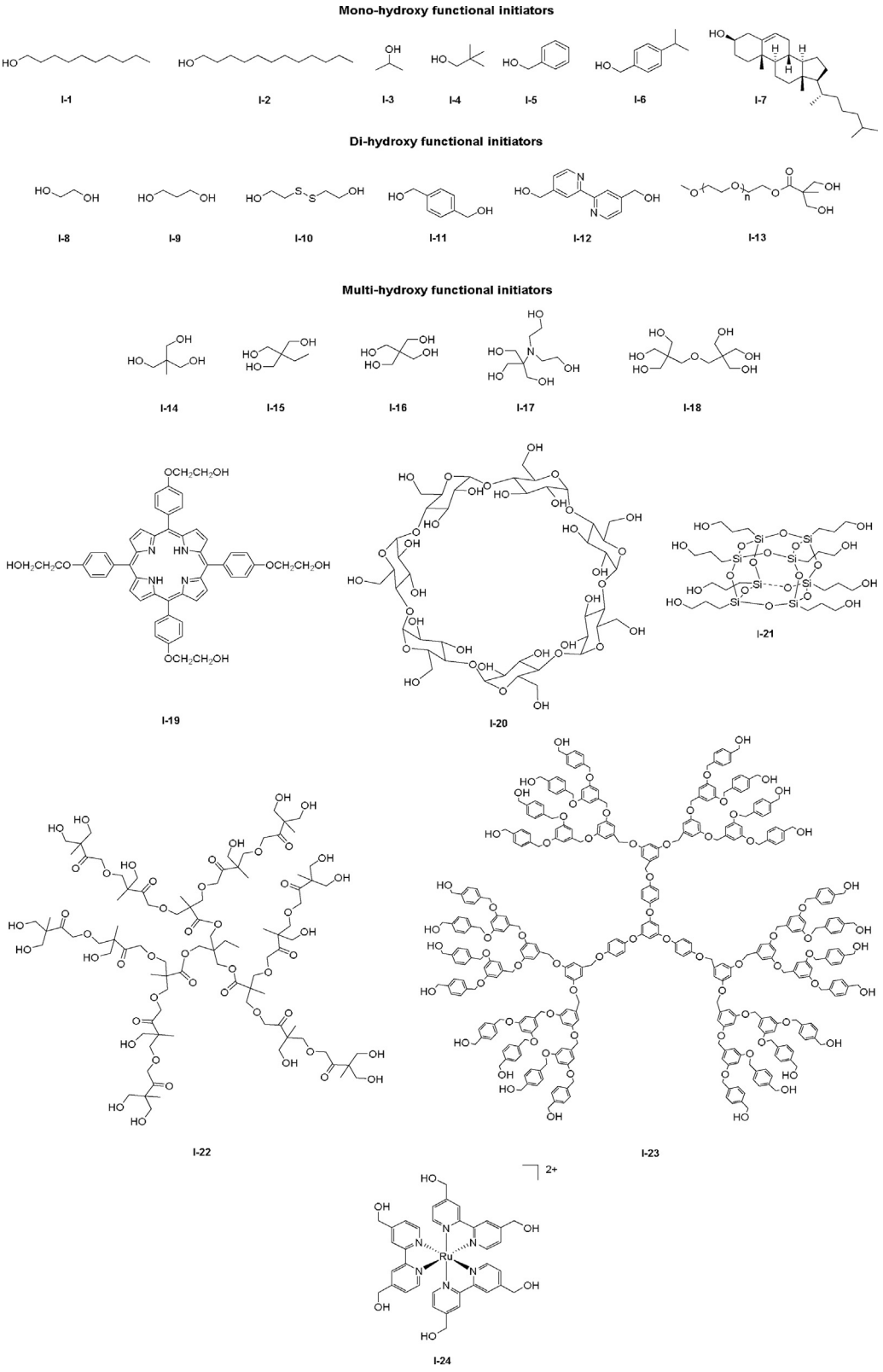

Fig. 11. Schematic representation of the mono-, di-, and multi-hydroxy functional initiators employed for the synthesis of PLA, which was further subjected to ω-end functionalization with a CTA or ATRP initiator.

alkoxide to the hydroxyl ω-end group to act as ROP catalyst, a series of high molar mass PS-*b*-PLA were prepared with excellent control. In a ROP first approach, Marić and co-workers employed **31** as initiator for the $AlEt_3$ catalyzed ROP of D,L-lactide [85]. The resulting TEMPO-functional PLA was used as a macromediator for the polymerization of styrene and *t*BuS intitiated by benzoylperoxide, yielding several di- and triblock and tapered copolymers with rather broad dispersities ($Đ > 1.3$).

31 and the corresponding alkoxyamine **32** were applied to prepare PLA-*b*-PS in a ROP first approach using the zinc complex

[BDI⁻-iPr]Zn as catalyst for the ROP by Carpentier and Sarazin [86]. *rac*-Lactide and L-lactide were polymerized directly in styrene as solvent at room temperature. Matrix-assisted laser desorption/ionization mass spectrometry (MALDI MS) confirmed the high end-group fidelity of the PLA macromediators. Although the dispersity of the PLLA remained low ($Đ \leq 1.20$), the NMP of styrene yielded quite disperse block copolymers ($Đ > 1.6$) that contained PS homopolymer. Surprisingly, a modified one-pot sequential polymerization procedure resulted in well-defined block copolymers using the alkoxyamine **32**: The ROP of L-lactide was performed in styrene at 100 °C, and an additional temperature increase towards 130 °C facilitated the NMP of styrene.

3. End functionalization of PLA

Traditionally, the ROP of lactide is quenched by a protic source to yield PLA with a hydroxyl moiety at the ω-chain end. As a consequence, further chemistry is often focused on the exploitation of this hydroxyl functionality. These post-polymerization modifications rely on the transformation of the hydroxyl group into initiating sites for RDRP techniques. However, the more elegant way is a direct quenching of the ROP with suitable electrophilic reagents that already contain the functional group to control or initiate a subsequent RDRP, *i.e.* CTAs or ATRP initiators.

The functionalization of PLA at the ω-chain end facilitates the introduction of other moieties at the α-chain end *via* the alcohol that is used as initiator for the ROP. These can either represent other functional groups to serve various purposes, or possess multiple hydroxyl functionalities, which gives straightforward access to star-shaped PLA block copolymers (Fig. 11).

3.1. ω-End functionalization of PLA with an ATRP initiator

Fundamental strategies used to functionalize PLA with an initiating moiety for ATRP at the ω-chain end have been published already more than a decade ago and are depicted in Scheme 5. Although these routes include direct end capping of living PLA chains with a suitable electrophile (*i.e.* an acyl bromide) and the direct chlorination of PLA-OH with thionyl chloride, the esterification of PLA's hydroxyl ω-end functionality clearly prevailed. In consequence, we first introduce these different synthetic pathways and subsequently focus on the variety of polymer architectures that are accessible using the ROP initiators depicted in Fig. 11. Table 8 provides an overview about the range of block polymers obtained *via* end group transformation of PLA with ATRP initiators.

3.1.1. Direct end-capping

The direct end-functionalization of anionic PLA chains with 2-bromo-2-methylpropionyl bromide (**35**) initiated by the BuLi/benzylalcohol system was reported with degrees of functionalization (DF) between 70 and 85% (^{1}H NMR) [87]. Since MPC, *i.e.* the monomer used for the subsequent ATRP, represents a zwitterion, non-functional PLA homopolymers could be readily separated by precipitation. The block copolymers comprised a low fraction of the PMPC block and self-assembled to giant vesicles and large compound micelles [88,89]. However, despite the simplicity of the synthetic procedure, the direct end-capping is rarely applied by researchers active in the field. Other ROP catalysts could potentially provide better DF for this most direct route to obtain PLA macroinitiators for ATRP *via* end-functionalization approaches.

3.1.2. Chlorination of PLA-OH with thionyl chloride

PLA's ω−terminal hydroxyl functionality can be transformed towards a chloride using thionyl chloride and pyridine in a quantitative manner (^{1}H and ^{13}C NMR) [90]. Messmann and co- workers applied the initiator/catalyst combination ethylene glycol/$SnOct_2$ to obtain chloro-end functionalized PLA *via* this method, and performed the ATRP of *t*BuA and BnA from the resulting PLA macroinitiator [91]. Although detailed characterization by means of NMR spectroscopy was performed and the dispersity of the final ABA triblock copolymers was promising ($1.11 < Đ < 1.48$), also this synthetic route remains scarcely investigated to date.

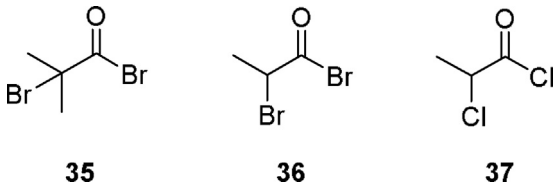

35 **36** **37**

Fig. 12. Schematic representation of the reagents used for ω-end functionalization of PLA with an ATRP initiator.

3.1.3. Esterification of PLA-OH

The esterification of PLA-OH using acid bromides and chlorides with the respective α-halo moieties (Fig. 12) in the presence of triethylamine has become a "standard" procedure to prepare PLA macroinitiators for a subsequent ATRP during the last decade (Scheme 5C). Typically, both reactants are used in slight excess with respect to PLA's hydroxyl moieties to ensure full end group conversion and to avoid undesired side reactions. Dichloromethane or THF are usually applied as solvents since the precipitation of triethylammonium bromide, which is formed as byproduct, drives the reaction to high conversions. Although structural confirmation of the macroinitiators by MS is uncommon in the field, some researchers employed detailed ^{1}H and ^{13}C NMR studies to confirm the quantitative end group fidelity. Although less frequently reported, simple SEC overlays of PLA-OH and the respective PLA macroinitiators represent a complementary information source: They could confirm that the PLA does not degrade during the end group transformation reaction. In case of a sufficient DP of the block synthesized by ATRP, a complete shift of the molar mass distribution provides the final proof of a successful end group transformation.

3.1.3.1. Linear diblock copolymers. Common monofunctional alcohols such as **I-1**, **I-2**, **I-5** or **I-6** (Fig. 11) as ROP initiators provide access to linear diblock copolymers. Due to the pH value and temperature responsiveness of PDMAEMA, DMAEMA represents the vinylic monomer most frequently polymerized with a PLA macro-initiator for ATRP. Mainly bromoisobutyryl bromide (in combination with triethylamine) (**35**) has been employed to modify the PLA end groups. Subsequent to a ROP catalyzed by $Al(O^iPr)_3$ [92] and $Sn(Oct)_2$ [93,94], the PLA macroinitiator quantitatively initiated the ATRP of DMAEMA in all cases. Similar synthetic approaches were applied to obtain PLA-*b*-PMMA [95] and PLA-*b*-PNVCL [96] after PLA end group modification with **35** [95] and **37** [96], respectively. Utilization of cholesterol (**I-7**) to initiate the ROP of L-lactide facilitated the attachment of a cholesteryl moiety at the α-chain end of PLA prior to ω-end group transformation using **35** and subsequent ATRP of GMA [97].

3.1.3.2. ABA triblock copolymers. Symmetric ABA triblock copolymers comprising a central PLA block can be prepared when the ROP of lactide is performed using a diol as initiator. Subsequent modification of the two hydroxyl end groups provides access to telechelic PLA macroinitiators for ATRP. Focused on the application of thermo-responsive micelles for drug delivery [98,99], Darcos and co-workers synthesized several series of ABA triblock copolymers from **I-11.** Careful structural characterization subsequent to the esterification of the PLA revealed that the treatment with triethylamine and **35** or **36** did not induce any degradation of the PLA [100].

Please cite this article in press as: Yildirim I, et al. Old meets new: Combination of PLA and RDRP to obtain sophisticated macromolecular architectures. Prog Polym Sci (2017), http://dx.doi.org/10.1016/j.progpolymsci.2017.07.010

Table 8
Block copolymers prepared *via* ATRP with a macro initiator for ATRP obtained by post-polymerization end functionalization of PLA.

Polymer	ROP initiator	ROP conditions	End mod.	ATRP conditions	Đ	Ref.
Linear diblock copolymers						
PDLLA-*b*-PMPC	**I-5**	*n*-BuLi Toluene RT	**35**	CuBr/bipyridine DMSO/methanol (1:1)[a]	1.47–1.52	[87]
PDLLA-*b*-PDMAEMA		$Al(O^i Pr)_3$ Toluene 75 °C	**35**	CuBr/HMTETA THF 60 °C	1.39	[92]
	I-1	$Sn(Oct)_2$ THF 110 °C	**35**	CuBr/HMTETA DMF 60 °C	1.26–1.32	[93]
PLLA-*b*-PDMAEMA		$Al(O^i Pr)_3$ Toluene 75 °C	**35**	CuBr/HMTETA THF 60 °C	1.42	[92]
	I-6	$Sn(Oct)_2$ Toluene 120 °C	**35**	CuBr/HMTETA Toluene 70 °C	1.10–1.20	[94]
PDLLA-*b*-PNVCL	**I-2**	$Sn(Oct)_2$ Bulk 130 °C	**37**	$CuCl/CuCl_2/Me_6$Cyclam 1,4-Dioxane 30 °C	1.10–1.26	[96]
PLLA-*b*-PMMA	**I-5**	$Sn(Oct)_2$ Bulk or toluene 120 °C	**35**	$CuCl_2$/PMDETA/$Sn(Oct)_2$ Toluene 90 °C	1.32–1.45	[95]
PLLA-*b*-PGMA	**I-7**	$Sn(Oct)_2$ Bulk 150 °C	**35**	CuCl/bipyridine DMF 50 °C	1.37	[97]
Triblock copolymers						
PBnA-*b*-PLLA-*b*-PBnA	**I-8**	$Sn(Oct)_2$ Toluene	**$SOCl_2$**	CuCl, PMDETA Toluene	1.11–1.35	[91]
P*t*BA-*b*-PLLA-*b*-P*t*BA		95 °C		95 °C	1.38–1.48	
PNiPAm-*b*-PLLA-*b*-PNiPAm	**I-11**	$Sn(Oct)_2$ Toluene 80 °C	**36**	CuCl, Me_6TREN DMF/water (5:1 v/v) 25 °C	1.08–1.28	[101]
P(NiPAm-*co*-DMA)-*b*-PLLA-*b*-P(NiPAm-*co*-DMA)	**I-11**	$Sn(Oct)_2$ Toluene 80 °C			1.1–1.18	[99,102]
P(MEO_5MA-*co*-MEO_2MA)-*b*-PLLA-*b*-P(MEO_2MA-*co*-MEO_5MA)	**I-11**	$Sn(Oct)_2$ Toluene 80 °C		CuCl, Me_6TREN DMF 80 °C	1.37–1.42	[98]
PMEO_{4-5}MA-*b*-PLLA-*b*-PMEO_{4-5}MA	**I-11**	$Sn(Oct)_2$ Toluene 80°	**35**	CuBr PMDETA DMSO, 90 °C THF, 60 °C	 1.50–1.61 1.20–1.30	[100]
PMEO_7MA-*b*-PDLLA-*b*-PMEO_7MA	**I-10**	$Sn(Oct)_2$ Toluene 120 °C	**35**	CuBr/PMDETA THF 47 °C	1.13	[103]
Bpy(PDLLA-*b*-P*t*BA)$_2$	**I-12**	$Sn(Oct)_2$ Bulk 130 °C	**35**	$NiBr_2(PPh_3)_2$ Toluene 90 °C	1.06–1.08	[105]
Bpy(PDLLA-*b*-PMMA)$_2$				CuBr, HMTETA Anisole 80 °C	1.21–1.26	
MPEO-(PLA-*b*-PPBDMMA)$_2$	**I-13**	$Sn(Oct)_2$ Toluene 70 °C	**36**	CuBr, PMDETA Anisole 90 °C	1.16–1.36	[107]
Star-shaped/dendritic-star block copolymers						
PDLLA-*b*-PNiPAm	**I-15**	$Sn(Oct)_2$ Xylene 135 °C	**37**	CuCl, HMTETA DMSO/*i*PrOH (1:1 v/v) 70 °C	1.01–1.06	[108]
PLLA-*b*-PMMA	**I-23**	$Sn(Oct)_2$ Bulk 120 °C	**35**	CuBr, PMDETA Bulk or anisole 80–100 °C	1.06–1.15	[109,110]
PLLA-*b*-PS					1.05–1.15	
PLLA-*b*-P*t*BA	**I-23**	$Sn(Oct)_2$ Bulk 120 °C	**35**	CuBr, PMDETA Bulk or anisole 80–100 °C	1.05–1.10	[109]
	I-24	DMAP Bulk 135 °C	**35**	$NiBr_2(PPh_3)_2$ Toluene 90 °C	1.28	[106]
PLLA-*b*-PDMAEMA	**I-22**	$Sn(Oct)_2$ Bulk 115 °C	**36**	CuBr, PMDETA THF 60 °C	1.14–1.23	[111]
β-CD-(PDLLA-*b*-PDMAEMA-*b*-P$EtOx_7$MA)	**I-20**	$Sn(Oct)_2$ Toluene 100 °C	**35**	$CuBr_2$, HMTETA, $Sn(Oct)_2$ Toluene, 70 °C (PDMAEMA block) Anisole, 60 °C (P$EtOx_7$MA block)	1.05–1.36	[112]

[a] Polymerization temperature is not reported.

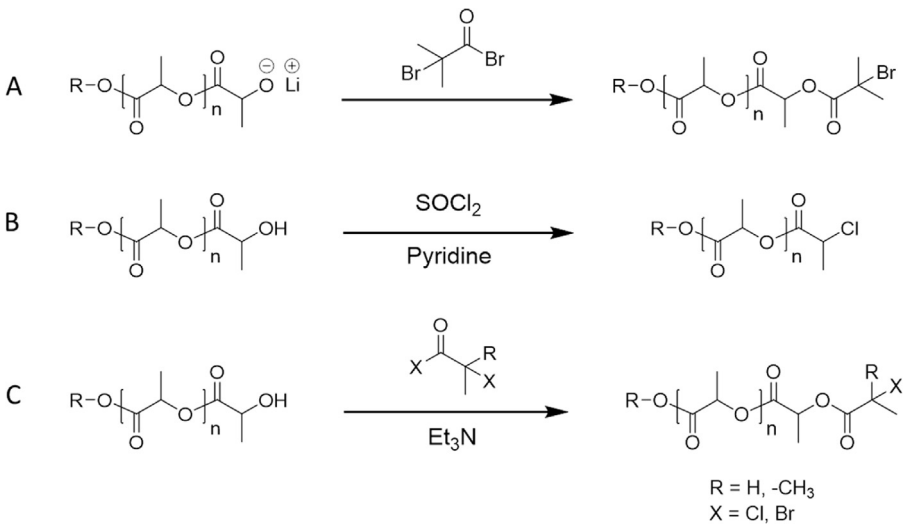

Scheme 5. Schematic representation of synthetic approaches for ω-end functionalization of PLA in order to obtain a macro ATRP initiator*via* direct end capping (A) or post polymerization modification by direct chlorination (B) and esterification (C).

Subsequent detailed investigations of the ATRP of NiPAm [101,102], DMA [102], and $MEO_{2\text{-}5}MA$ [100] demonstrated the excellent control as well as the quantitative end group conversion during the attachment of the ATRP initiating moiety (complete shift of unimodal SEC traces) [101,102].

The diol **I-10** features a disulfide moiety and represents the basis to prepare thiol responsive micelles composed of a PLA core and a $PMEO_7MA$ shell (Fig. 13) [103,104]. The disulfide moiety did not interfere during either of the synthetic steps (*i.e.* ROP of lactide, end-group modification with **35**, and ATRP of MEO_7MA), as demonstrated by the small dispersity of the triblock copolymer ($Đ = 1.13$). The micellar aggregates formed by the amphiphilic copolymers in water rearranged upon addition of dithiothreitol (DTT), which was exploited for the release of the hydrophobic anti-cancer drug Doxorubicin (DOX).

As one of the first to apply the esterification route to attach an ATRP initiating moiety on PLA's hydroxyl end groups, Fraser and coworkers initiated the ROP of lactide with the di-hydroxyl functional bipyridine (Bpy) **I-12** [105]. Subsequent to modification with **35**, the PLA was used as a macroinitiator for ATRP of *t*BA and MMA. The respective triblock macroligands were further employed for the complexation of iron, yielding metal centered block copolymer analogues. When the pre-formed $RuBpy_3$ complex **I-24** was applied as macroinitiator for the ROP, the respective metal-centered star-shaped PLA-*b*-P*t*BuA could be obtained as well, featuring slightly bimodal molar mass distributions [106].

3.1.3.3. Star-shaped copolymers. The ROP initiator **I-13** features two hydroxyl moieties at one end of a MPEO chain and was used for the synthesis of mikto-three arm star-shaped copolymers [107]. The respective hydroxyl end groups of the two PLA arms of $MEO\text{-}(PLA\text{-}OH)_2$ were converted to ATRP initiating sites by treatment with **36**. Subsequent to ATRP of the phenylborate ester functionalized methacrylate PPBDMA, micellar aggregates of the copolymers disaggregated upon glucose addition due to the phenylboronate ester moiety, making then promising materials for insulin delivery.

The use of multi-hydroxyl functional compounds as ROP initiators represents a more common route to prepare star-shaped block copolymers. Thereby, the number of hydroxyl groups determines the number of arms of the regular star-shaped block copolymer. Three-arm stars composed of PLA-*b*-PNiPAm were obtained from **I-15** [108].

When dendrimers are used as ROP initiators, star-shaped PLAs with higher number of arms are obtained. Xi and co-workers were among the first researchers to establish the esterification route using polyarylether dendrimers (**I-23**), ROP of L-lactide and end group modification with **35** [109]. The subsequent ATRP of styrene, *t*BA and MMA yielded high molar mass star-shaped polymers ($M_n \approx 250$ kg/mol; $Đ \approx 1.1$). However, the dense polymer architecture makes SEC results alone insufficient to judge the control during the final ATRP step. Although completely shifted SEC traces after ATRP and kinetic studies provided first hints about the excellent control, further investigations were performed by hydrolysis of the PLA blocks. [109,110] Star-shaped polymers with 6–24 arms composed of PLA-*b*-PS were investigated: Although the PS blocks alone revealed slightly broader molar mass distributions ($Đ < 1.32$), the molar mass of the PS corresponded well with the expected values, showing that all arms of the PLA-stars had indeed initiated an ATRP.

Focused on exploitation of the pH value sensitivity of PDMAEMA for the delivery of chlorambucil, star-shaped PLA-*b*-PDMAEMA was prepared from the polyester type dendrimer **I-22** [111]. The fact that the DP of the PDMAEMA blocks was comparably short makes it difficult to evaluate if the synthesis was as controlled as suggested by the low $Đ$ values, since these often result from the little difference in hydrodynamic volume for dense star-shaped polymers. β-Cyclodextrin (β-CD) (**I-20**) features 21 hydroxyl moieties and, thus, would theoretically enable the preparation of star-shaped block copolymers with 21 arms. However, primary and secondary hydroxyl moieties might differ in their initiation efficiency for the ROP of lactide. In addition, steric hindrance in the cyclic oligosaccharide can also play a major role. Nevertheless**, I-20** was used to attach PLA-*b*-PDMAEMA-*b*-$PEtOx_7MA$, with very low DP's of either block [112].

3.2. ω-End functionalization of PLA with a CTA

In general, two synthetic methods exist for the introduction of CTAs to the ω-chain ends of PLA (Scheme 6): The usual hydroxyl end groups that arise from the common quenching of the ROP can be coupled to suitable CTA precursors. This route relies on activated carboxylic acid derivatives, which can be either prepared separately or formed *in situ* from commercially available CTA's with carboxylic acid functionality (Fig. 14). However, the more direct route is to quench the living PLA chain ends using an acyl chloride functional CTA. The formed PLA based macromolecular CTAs (macro-CTA) can

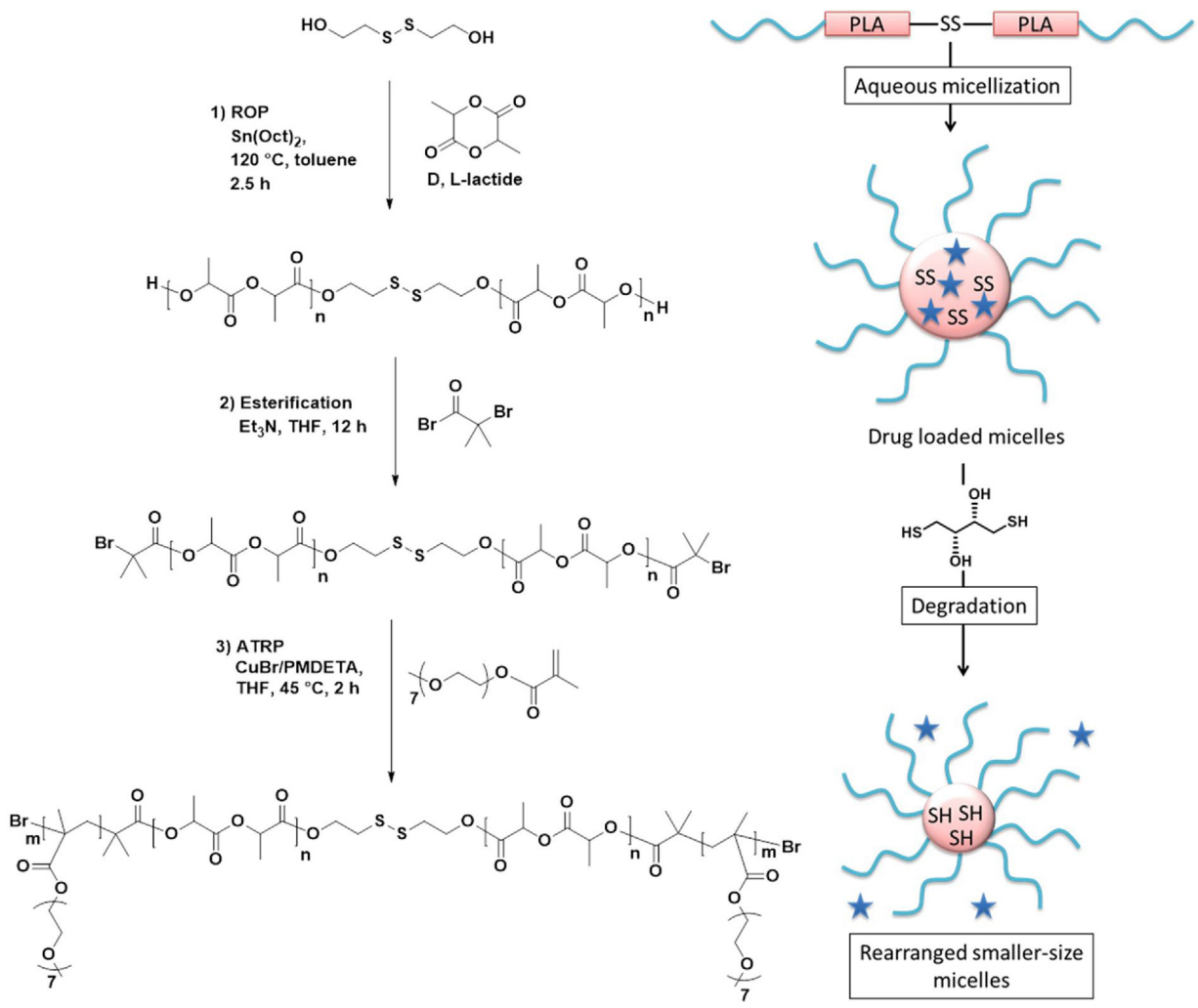

Fig. 13. Schematic representation of the synthesis of thiol-responsive triblock copolymer brushes by Cunningham et al. [103].

be utilized in the RAFT polymerization of several monomers in order to obtain block copolymers with desired properties (Table 9).

3.2.1. *Direct end capping using acyl chloride functional CTAs*

Stanford and Dove developed a method that enables the direct synthesis of α,ω- end functional PLA *via in-situ* end capping and that is applicable for various initiators as well as end capping agents [113]. Among others, the ROP of D,L-lactide mediated by aluminum salen complexes was quenched quantitatively using an excess of the acyl chloride functional trithiocarbonate CTA **40**. The subsequent RAFT polymerization of styrene yielded PLA-*b*-PS copolymers in various architectures such as linear di- and tri-block copolymers and star-shaped polymers. Careful structural investigation during all steps revealed the success of this synthetic method. However, the acyl chloride functional CTA has to be synthesized, which might explain why most researches rely on alternative synthetic routes.

3.2.2. *Esterification of PLA-OH using acyl chloride functional CTAs*

The employment of acyl chloride functional CTAs for the post-polymerization functionalization of PLA's ω-hydroxyl end groups adds another step to the synthetic pathway. This route was reported for star-shaped (ss) PLA synthesized from **I-21** with eight hydroxyl groups to obtain ss(PLA-*b*-PNiPAm) [114], or the buffer **I-17** with five hydroxyl groups to prepare ss(PCL-*b*-PLLA-*b*-PDMAEMA) [115]. Multifunctional initiators for the ROP complicate the direct determination of the DF that can be achieved by the end-functionalization method. However, detailed kinetic studies during the RAFT polymerization and structural investigation of the obtained star-shaped triblock copolymer confirmed the success of this synthetic route [115].

3.2.3. *In situ formation of acyl chloride functional CTA's*

Hillmyer and co-workers developed a straightforward method to convert the carboxylic acid functional CTA **41** to a more reactive acyl chloride *in situ* by addition of oxalyl chloride during the ω-end functionalization of PLA-OH [116]. For the preparation of nanoporous materials, the PLA is degraded selectively in ordered block copolymer bulk structures, but the matrix phase is preserved. PLA-*b*-PDMA-*b*-PS triblock copolymers were etched to enhance the hydrophilicity of the nanoscopic pores in the PS matrix [116–118]. The initial PLA-*b*-PS system [119] has since been refined by including other vinylic (co)monomers to adjust the properties of the matrix phase [120]. In particular, additional functional moieties enhanced the mechanical performance and the stability of the membranes by crosslinking. The latter was reported *via* cross-metathesis of the pendant norbornene groups in PLA-*b*-P(NB-*stat*-S) [121,122], or by urethane bond formation between the hydroxyl moieties of PLA-*b*-P(S-*stat*-HEA) and PLA-*b*-P(S-*stat*-HEMA) in the presence of a diisocyanate [123]. The use of divinyl benzene as a comonomer facilitated *in-situ* crosslinking of diblock copolymers such as PLA-*b*-P(S-*co*-DVB) [124,125]. PLA-*b*-P(VBzCl-

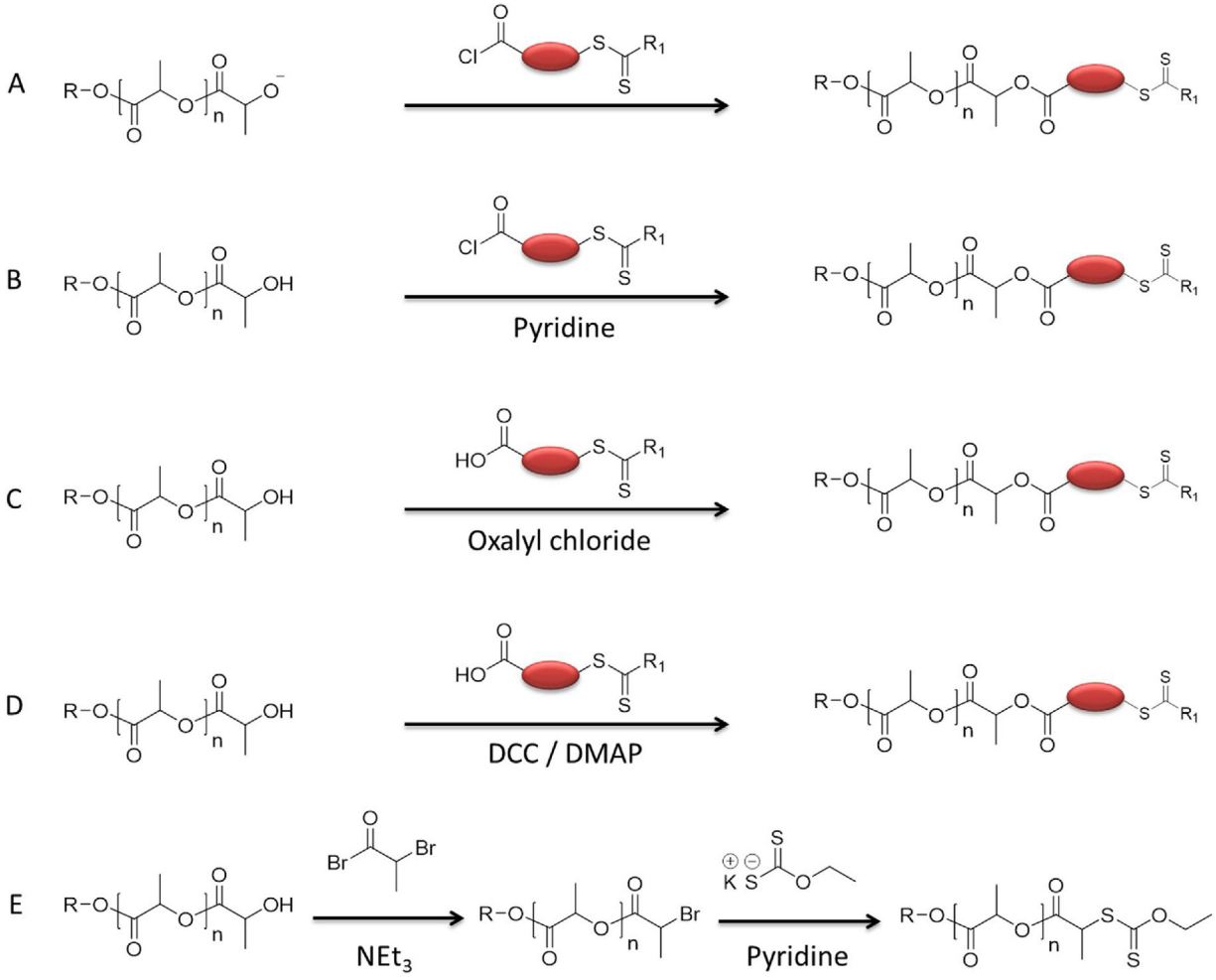

Scheme 6. Schematic representation of synthetic approaches for ω-end functionalization of PLA with a CTA: Direct end capping using acyl chloride functional CTAs (A), post polymerization modification *via*esterification of PLA-OH using acyl chloride functional CTAs (B), *in-situ* formation of acyl chloride functional CTAs (C), Steglich esterification (D), and attachment of xanthates (E). R_1 represents either the homolytic leaving group (R) or the activating/stabilizing group (Z).

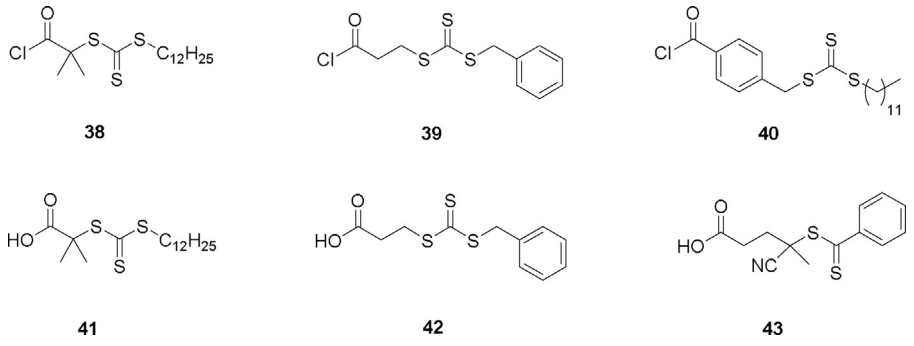

Fig. 14. Schematic representation of the CTAs employed for functionalization of PLA at the ω-end group.

co-DVB) was further crosslinked *via* Friedel-Crafts alkylation during etching of the PLA block in the presence of $FeCl_3$ [126].

3.2.4. Steglich esterification

N,*N*'-Dicyclohexylcarbodiimide (DCC) represents a reagent for *in situ* activation of carboxylic acids towards a nucleophilic addition-elimination. If DMAP is added as catalyst, the Steglich esterification and proceeds readily at room temperature, even with weak or sterically hindered nucleophiles, such as hydroxyl end groups of a polymer.

With focus on the development of PLA-based micellar drug delivery vehicles for paclitaxel [127], this method was applied using the dithiobenzoate CTA **43** by Zentel and co-workers [128]. Subsequent RAFT polymerization of FMA yielded block copolymers with a polymethacrylate block that is extremely prone to attack by nucleophiles. This was exploited by a final post-polymerization modification reaction using 2-hydroxpropyl amine and the amino-functional dye Oregon 488 cadaverine, resulting in a fluorescently labelled copolymer of *N*-(2-hydroxypropyl) methacrylamide (HPMA). Due to the high reactivity of the PFMA

Please cite this article in press as: Yildirim I, et al. Old meets new: Combination of PLA and RDRP to obtain sophisticated macromolecular architectures. Prog Polym Sci (2017), http://dx.doi.org/10.1016/j.progpolymsci.2017.07.010

Table 9
Block copolymers prepared *via*RAFT with a macro-CTA obtained by post-polymerization end functionalization of PLA.

Polymer	ROP initiator	ROP conditions	ω-end funct.[a]	CTA	RAFT conditions	Đ	Ref.
Linear block copolymers							
PLA-*b*-PS	**I-3**	Al salen complex Toluene 70 °C	**A**	**40**	Toluene 120 °C	1.26	[113]
	I-5	$AlEt_3$ Toluene 95 °C	**C**	**41**	Bulk 120 °C	1.19	[119]
PLA-*b*-PFS	**I-5**	$AlEt_3$ Toluene 90 °C	**C**	**41**	Bulk 120 °C	1.17	[120]
PLA-*b*-PNVP	**I-5**	$Sn(Oct)_2$ Bulk 150 °C	**E**		THF 80 °C	1.36–1.60	[131]
PLA-*b*-P(NB-*stat*-S)	**I-5**	$AlEt_3$ Toluene 90 °C	**C**	**41**	Toluene 70 °C Bulk 120 °C	1.4 1.17–1.20 1.17–1.37	[121] [122] [122]
PLA-*b*-P(S-*co*-HEA)	**I-5**	$AlEt_3$ Toluene 90 °C	**C**	**41**	1,4-Dioxane 60 °C	1.19–1.26 1.18–1.26	[123]
PLA-*b*-P(S-*co*-HEMA)							
PLA-*b*-PDMA-*b*-PS	**I-5**	$AlEt_3$ Toluene 90 °C	**C**	**41**	1) PDMA block DMF, 60 °C 2) PS block Bulk, 120 °C	1.12 1.12–1.24 1.14	[116] [117] [118]
Diblock copolymers obtained with post polymerization modification							
PLA-*b*-PFMA[b]	**I-4**	DBU CH_2Cl_2 RT	**D**	**43**	Dioxane 80 °C	1.3 1.31–1.45	[127] [128]
In situ cross-linked diblock copolymers							
PLA-*b*-P(S-*co*-DVB)	**I-5**	$AlEt_3$ or $Sn(Oct)_2$ Toluene 90–95 °C	**C**	**41**	Bulk 120 °C	(1^{st} step) 1.08–1.11	[124,125]
PLA-*b*-P(VBzCl-*co*-DVB)	**I-5**	$AlEt_3$ or $Sn(Oct)_2$ Toluene 95 °C	**C**	**41**	Bulk 120 °C	(1^{st} step) 1.11–1.14	[126]
Star-shaped block copolymers							
PLA-*b*-PS	**I-9** **I-14** **I-18**	Al salen complex Toluene 70 °C	**A**	**40**	Toluene 120 °C	1.33 1.22 1.18	[113]
PLA-*b*-PNiPAm	**I-21**	$Sn(Oct)_2$ Bulk 130 °C	**B**	**38**	1,4-Dioxane 65 °C	1.34–1.55	[114]
	I-19	DMAP THF 50 °C	**D**	**42**	THF 50 °C	1.29–1.32	[130]
PLA-*b*-PNVP	**I-16**	$Sn(Oct)_2$ Bulk 150 °C	**E**		THF 80 °C	1.24–1.32	[132]
PLA-*b*-PGAMA	**I-19**	DMAP THF 50 °C	**D**	**42**	1-Methyl-2-pyrrolidinone 70 °C	1.48–1.74	[129]
PCL-*b*-PLA-*b*-PDMAEMA	**I-17**	$Sn(Oct)_2$ Bulk 115 °C	**B**	**39**	1,4-Dioxane 80 °C	1.19–1.37	[115]

[a]See Scheme 6 for the corresponding end functionalization methods.
[b]Dispersity values of the PLA-*b*-PHPMA (obtained *via* aminolysis reaction of PLA-*b*-PFMA with hydroxypropylamine) are reported as 1.3 [127] and 1.31–1.45 [128].

block, an amidation of the PLA block could be avoided by careful adjustment of the reaction conditions.

I-19 and CTA **42** were applied to end-functionalize star-shaped PLA with a porphyrin core *via* Steglich esterification [129,130]. Subsequent RAFT polymerization of NiPAm [130] and the unprotected methacrylate-based glucose-based methacrylate GAMA [129] yielded the respective star-shaped block copolymers. The resulting glycopolymeric or thermo-responsive shell is favorable for application of nanoparticles in photodynamic therapy.

3.2.5. Attachment of xanthates

Pre-designed carboxylic acid functional CTA's are unnecessary for the synthesis of a PLA macro-CTA suitable for xanthate mediated polymerization by ω-end-group transformation [131]. For this purpose, a 2-step polymer analogous reaction is required, involving the esterification of hydroxyl end functional PLA with **36** (Scheme 5). The bromide moiety of the resulting macroinitiator for ATRP (see Section 3.1) is subsequently substituted by xanthate. This method was applied for linear [131] or star-shaped [132] PLA and gave access to PLA block copolymers with PNVP of both architectures.

Please cite this article in press as: Yildirim I, et al. Old meets new: Combination of PLA and RDRP to obtain sophisticated macromolecular architectures. Prog Polym Sci (2017), http://dx.doi.org/10.1016/j.progpolymsci.2017.07.010

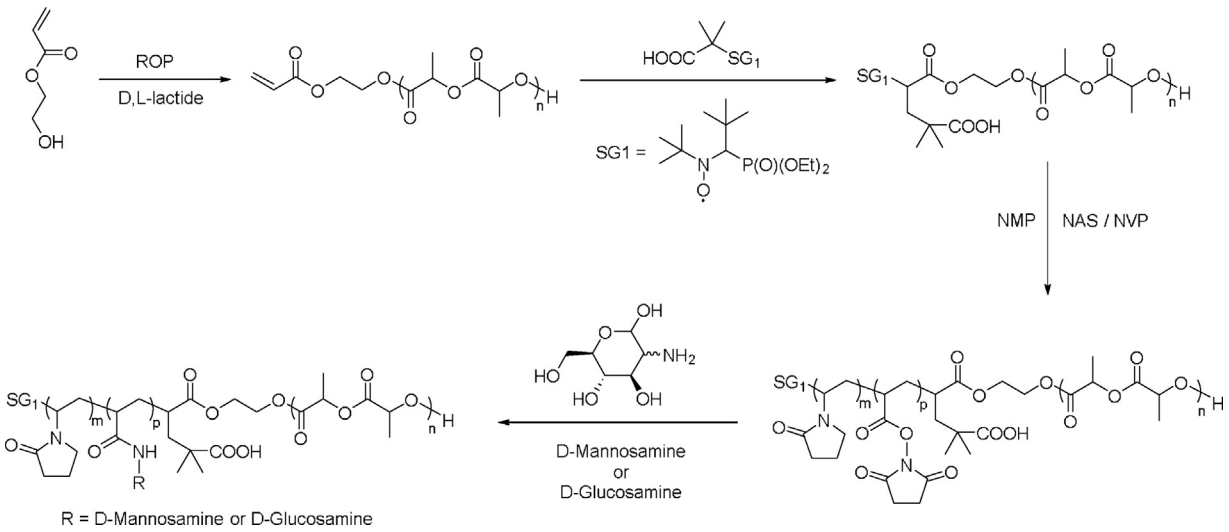

Scheme 7. Schematic representation of the synthesis of amphiphilic glycopolymers with a PLA based macro initiator for NMP [136].

3.3. Other end functionalization approaches

3.3.1. End-functionalization methods designed for block copolymers prepared by ROP and NMP

Trimaille and co-workers developed a well-investigated pathway to obtain linear PLA block copolymers by combination of ROP and NMP (Scheme 7) [133]. HEA was utilized to initiate the ROP of lactide, providing an acrylate α-end-functional PLA. Subsequent treatment with an excess of the SG-1 based alkoxyamine BlocBuilder® resulted in a macroinitiator for NMP *via* a 1,2-intermolecular radical addition (IRA). The polymerization of styrene and HEA proceeded with good control over the molar mass, albeit sometimes with $Đ > 1.5$. However, the NMP of HEMA remained uncontrolled, as common for the polymerization of methacrylates using SG-1. Focusing on biomaterials for peripheral nerve repair, the degradation properties of the PLA-*b*-PHEA copolymers were investigated in detail *in vitro* and *in vivo* [134]. Also the polymerization of NVP and *N*-acryloxysuccinimide (NAS) was successful, revealing a strong tendency towards an alternating copolymerization during the NMP [135]. Since NAS features an activated carboxylic acid functionality in form of a *N*-succinimidyl ester, these amphiphilic block copolymers were further functionalized with D-mannosamine or D-glucosamine to prepare glycopolymeric micelles [136].

3.3.2. Divergent end functionalization methods for the synthesis of branched polymers

Conversion of the end groups derived from ROP into initiating functions for ATRP and *vice versa* using multifunctional reagents allowed the introduction of branching points into the polymeric architecture (Scheme 8). Therefore, the bromide end groups derived from ATRP were substituted by diethanolamine to introduce two ROP initiating moieties. In an analogous fashion, a hydroxyl end group of PLA was esterified with BMBIBPC to provide two functional groups capable to initiate an ATRP. This facilitated the synthesis of H-shaped copolymers such as $(PLLA)_2PS(PLLA)_2$ [137] or third generation dendrimer-like copolymers based on PS and PLA [138].

3.3.3. Coupling of end-functional building blocks

The coupling of two or more end-functionalized polymers represents a flexible and modular approach to combine polymer types obtained by various polymerization methods within one polymeric architecture. Highly efficient and "click" reactions such as the copper catalyzed 1,3-dipolar azide alkyne cycloaddition (CuAAC), or the radical addition of thiols to alkenes (thiol-ene reaction) represent a major advantage as such techniques enable the use of both reactants in an, at best, equimolar ratio. In theory, this avoids the separation of residual unreacted building blocks from the targeted product. However, this can be challenging in practice, because the individual building blocks must fulfill various requirements: The absolute molar masses should be known, and the DF with the according functional end should be quantitative. Besides, the analytical confirmation of the identity and purity can represent a challenge, in particular if the hydrodynamic volumes of reactant(s) and the coupling product are rather similar, as for star-shaped polymers with varying number of arms.

The CuAAC "click" reaction was used to couple PEO-*b*-PEAEMA to a star-shaped PLLA polymerized from a dendrimer core (Fig. 15) [139]. For this purpose, a PEO macro initiator was employed for the ATRP of DEAEMA, and the bromo-end group of the resulting block copolymer was converted to an azide by nucleophilic substitution with sodium azide. The synthesis of the alkyne functional counterpart included the ROP of L-lactide from a dendrimer core comprising 16 hydroxyl functionalities, and esterification with a propargyl functional carboxylic acid *via* DCC coupling. Subsequent CuAAC of both building blocks yielded the according star-shaped terblock copolymer ($Đ \approx 1.3$).

A variety of miktoarm star polymers has been reported, benefiting from the modularity of highly efficient coupling reactions comprising end functionalized polymers (Fig. 16A). Webster and co-workers used an azide functional CTA for the RAFT polymerization of BA, PEO_nA, and NiPAm [140]. In parallel, a dihydroxy functional alkyne was used as initiator for the ROP of lactide in the presence of $Sn(Oct)_2$ (DP = 5 and 10 per arm). The coupling of both components by means of CuAAC yielded AB_2 type miktoarm star polymers ($1.10 < Đ < 1.18$). ABC type miktoarm star copolymers comprising PLA, PS, and PEO arms were prepared by combining ROP, ATRP and two complementary coupling reactions [141]. To accomplish this, a core molecule was designed, containing a hydroxyl group, a double bond, and an azide functionality (Fig. 16B). The respective counterpart for the thiol-ene addition was obtained by end group transformation of bromo- end functional PS to yield PS with a thiol end group *via* a xanthate intermediate. Subsequent to the thiol-ene reaction, the $Sn(Oct)_2$ catalyzed ROP of L-lactide was performed. Finally, alkyne-end functional PEO was attached *via* CuAAC, yielding PS-PLA-PEO miktoarm star copolymers ($Đ = 1.21$).

Please cite this article in press as: Yildirim I, et al. Old meets new: Combination of PLA and RDRP to obtain sophisticated macromolecular architectures. Prog Polym Sci (2017), http://dx.doi.org/10.1016/j.progpolymsci.2017.07.010

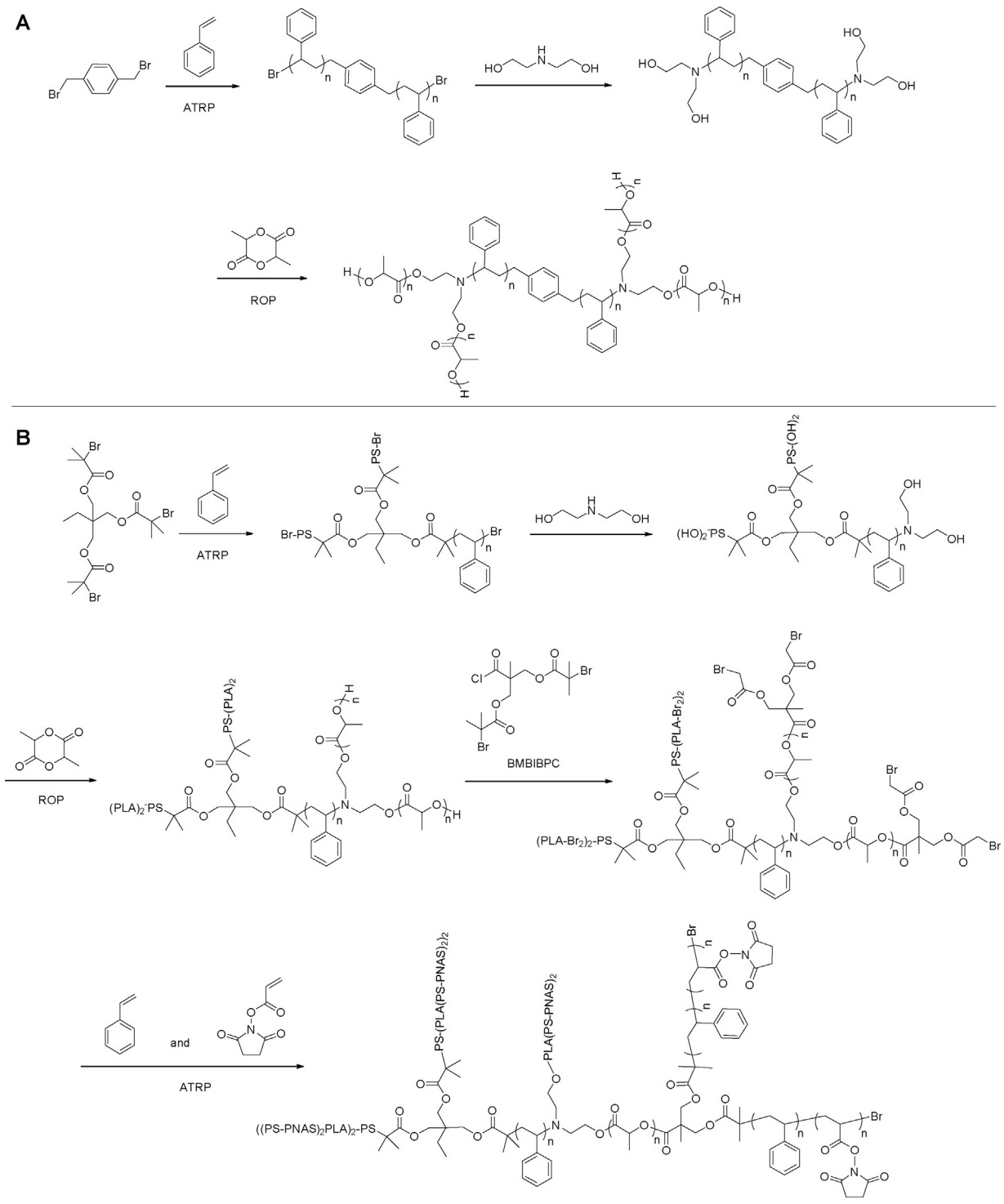

Scheme 8. Schematic representation of the synthesis of H-shaped (A) [137] and dendrimer like (B) [138] branched copolymers *via* divergent mechanism transformation approaches utilizing multifunctional initiators and end-capping strategies.

4. Comb and graft copolymers comprising PLA

Dual CTAs or initiators, and mechanism transformation approaches give access to linear and star-shaped block copolymers comprising PLA. For the synthesis of comb and graft copolymers, the appropriate synthetic strategies such as macromonomer (grafting through) method and grafting from method are adopted according to the requirements of the combination ROP/RDRP. The utmost majority of the polymeric architectures feature PLA side chains attached to a backbone synthesized by RAFT or ATRP. On the other hand, comb or graft copolymers with a PLA backbone require the synthesis of tailor-made lactide-based functional monomers, which can indeed be a challenging organic synthesis for some polymer chemists. To the best of our knowledge, grafting onto approaches have not been reported, although this method comes into play for the additional attachment of other building blocks to the polymeric architectures.

Please cite this article in press as: Yildirim I, et al. Old meets new: Combination of PLA and RDRP to obtain sophisticated macromolecular architectures. Prog Polym Sci (2017), http://dx.doi.org/10.1016/j.progpolymsci.2017.07.010

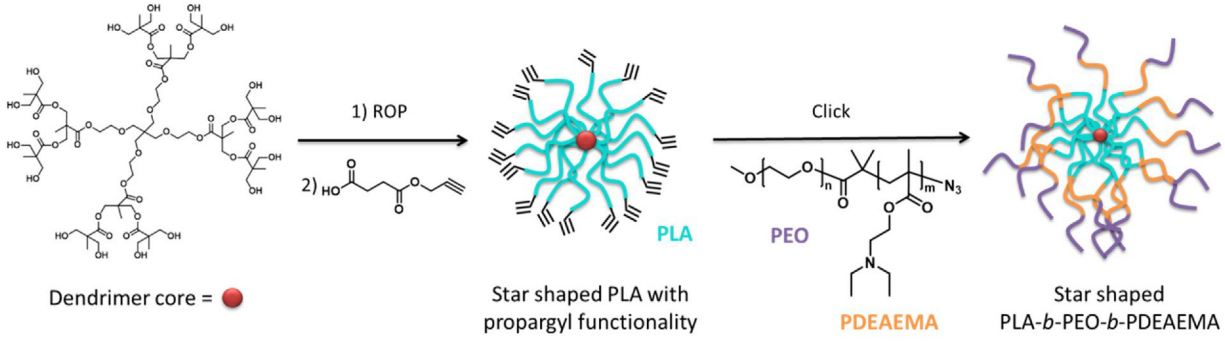

Fig. 15. Synthesis of star-shaped PLA-*b*-PEO-*b*-PDEAEMA terpolymers with a dendrimer core *via* CuAAC of end-functional building blocks.

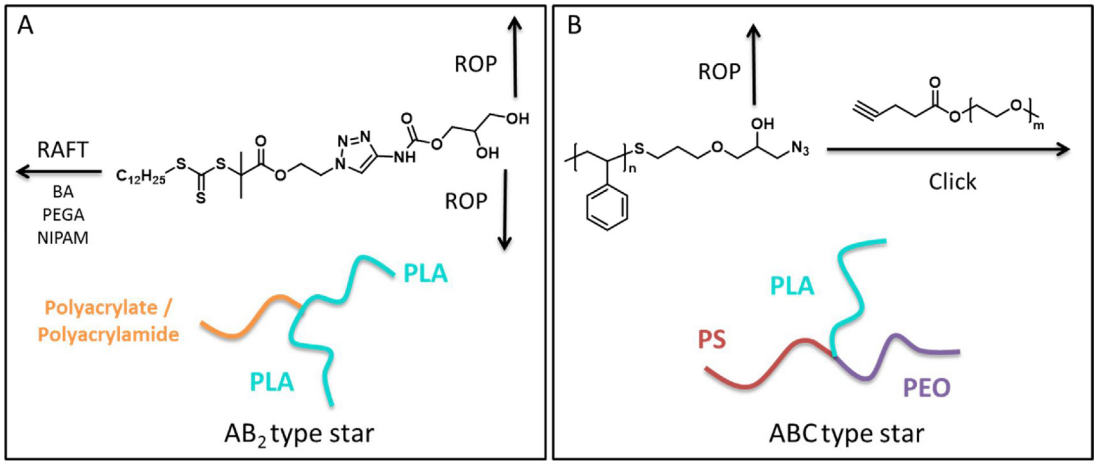

Fig. 16. Schematic representation of the approaches for the synthesis of (A) AB_2 [140] and (B) ABC [141] type star copolymers by coupling of end functional building blocks.

4.1. Macromonomer method for the synthesis of comb and graft copolymers with PLA side chains

The macromonomer method relies on the attachment of a functional end group to PLA, which can be polymerized by a subsequent RDRP method. The fact that the resulting macromonomer can be properly purified and characterized prior to (co)polymerization represents a major advantageous of this synthetic method. The robustness of the various RDRP methods is valuable if the DF of the macromonomer with the desired vinylic moiety is not quantitative, as such residues can be separated from the comb or graft copolymer together with residual macromonomers. The latter might be present after the polymerization of the backbone. Sterical hindrance during polymerization of the macromonomer can make it difficult to obtain high backbone DP's and achieve quantitative macromonomer conversion. The macromonomer method is modular. Several macromonomers can be copolymerized to obtain comb polymers with high grafting densities, or tailor-made polymer architectures comprising polymer types that would otherwise be incompatible. ATRP, NMP, as well as RAFT have been applied for the backbone polymerization. While early reports were concerned with an in-depth comparison of these RDRP techniques with free radical polymerization (FRP), the synthesis of highly functional polymer architectures designed for specialized applications has come into focus lately.

PLA macromonomers can be obtained by functionalization of PLA with a polymerizable moiety at either end (Scheme 9). If a hydroxyl-functional monomer such as HEMA [142,143] or HEA [143] is used as initiator for the ROP together with $Sn(Oct)_2$ as a catalyst [142–145], a PLA macromonomer with a methacrylate or acrylate α-end functionality can be obtained in one step (route A). Alternative ROP catalysts, *i.e.* aluminum [146,147], or titanium [148] based complexes, make an additional modification of the precursors a necessity. Alternatively, the ω- chain end of PLA can be functionalized with a functional group to be (co)polymerized *via* an RDRP technique (Route B). In analogy to section 3, this can be achieved by direct quenching of the ROP with methacryloyl chloride [149], or by post polymerization modifications of PLA with a hydroxyl end group. Complemented by triethylamine as an auxiliary base, methacrylic anhydride [150], or methacryloyl chloride [151,152], represent suitable reagents for that latter approach. Route B has been employed together with functional ROP initiators, facilitating the synthesis of α,ω- end functional macromonomers [149,152]. The respective functional initiators will subsequently form the side chain end groups of the final comb polymers (see below).

4.1.1. Graft copolymers with PLA side chains

Graft copolymers with PLA side chains are accessible when PLA macromonomers are copolymerized with small monomers. The degree of grafting (DG) can be tailored by the amount of macromonomer in the feed. The DP (n) of the PLA macromonomer LA_nMA or LA_nA pre-determines the side chain DP of the graft copolymer. The additional use of other macromonomers facilitates the incorporation of further building blocks into the polymeric architectures (Fig. 17).

In 1997, Hawker and Jerome reported the very first examples of combining NMP and ROP to synthesize graft copolymers *via* the macromonomer technique [146,151]. For this purpose two α−methacrylate terminated PDLLA macromonomers (DP = 15, 50) were prepared using an aluminum-alkoxide ROP initiating system. TEMPO-mediated copolymerization with styrene and in bulk

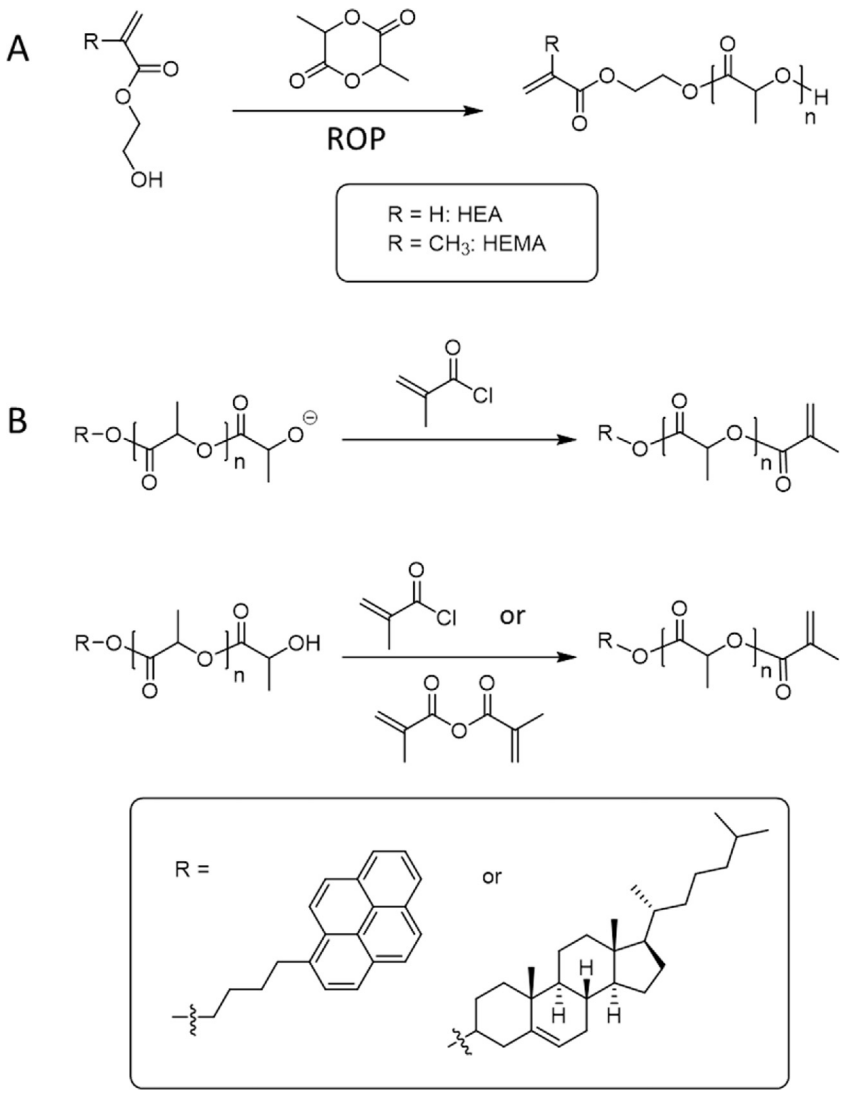

Scheme 9. Schematic representation of the general approaches for the preparation of PLA macromonomers: (A) ROP of lactide initiated with a hydroxyl functional monomer, (B) direct end capping and post-polymerization modification.

provided well-defined graft copolymers with narrow dispersities ($1.20 < Đ < 1.40$). As both macromonomers were well incorporated during the NMP, the DG (10% and 25%) corresponded to the macromonomer fraction in the feed.

Hadjichristidis and coworkers reported a full conversion of a PLA-methacrylate macromonomer in an ATR copolymerization with MMA to yield PMMA-*g*-PLLA [148]. Matyjaszewski and coworkers investigated the reactivity of several macromonomers in detail [144]. For this purpose, PLA macromonomers with a DP of 15 and an acrylate ($LA_{15}A$) or methacrylate ($LA_{15}MA$) functionality were used at a low feed fraction (3.5 mol%) during the ATR copolymerization with MMA. In contrast to FRP, the reactivity of $LA_{15}MA$ was reduced in comparison with MMA during ATRP ($1/r_{MMA} = 1.75$), affecting the distribution of the grafted chains along the PMMA backbone. This could be compensated by utilization of a mixture of both macromonomers, as $LA_{15}A$ was less reactive ($1/r_{MMA} = 0.61$).

This different reactivity of $LA_{20}MA$ and MMA was further exploited for the preparation of PMMA with grafted PLA and PDMS in tailored gradients [143]. Therefore, the third monomer $DMS_{40}MA$ was added. The ATR copolymerization provided the respective terpolymers with enriched PDMS grafts at the end of the growing backbone chain, which is due to the lowered reactivity of $DMS_{40}MA$. Replacement of MMA by BMA resulted in a random distribution of both side chain types along the backbone. Several block copolymerization experiments were performed to further control the side chain distribution along the backbone of the graft copolymers. Two-dimensional liquid chromatography was utilized to verify the molecular structure of the terpolymers.

4.1.2. Comb polymers

The homopolymerization of methacrylate-functional PLA macromonomers *via* RDRP provides access to PLA comb polymers with a polymethacrylate backbone (Fig. 18). Modified synthetic approaches include a) the grafting from surfaces to obtain dense polymer layers b) the chain extension with "small monomers", yielding a "palm tree like" block copolymers and c) the copolymerization with other macromonomers, yielding heterografted comb polymers. Due to the dense polymer structure of comb polymers, recent research efforts are directed towards a comparison of several properties with their linear analogues.

Wu and co-workers obtained a triblock copolymer (PEO-*b*-PHEMA-*g*-PLA-*b*-PNiPAm; $Đ = 1.35$) by RAFT polymerization of LA_5MA using a PEO macro-CTA and subsequent chain extension with NiPAm [145]. The resulting thermoresponsive copolymers were subsequently applied for micellar encapsulation and release of doxorubicin [142]. The functionalization of hydroxyapatite

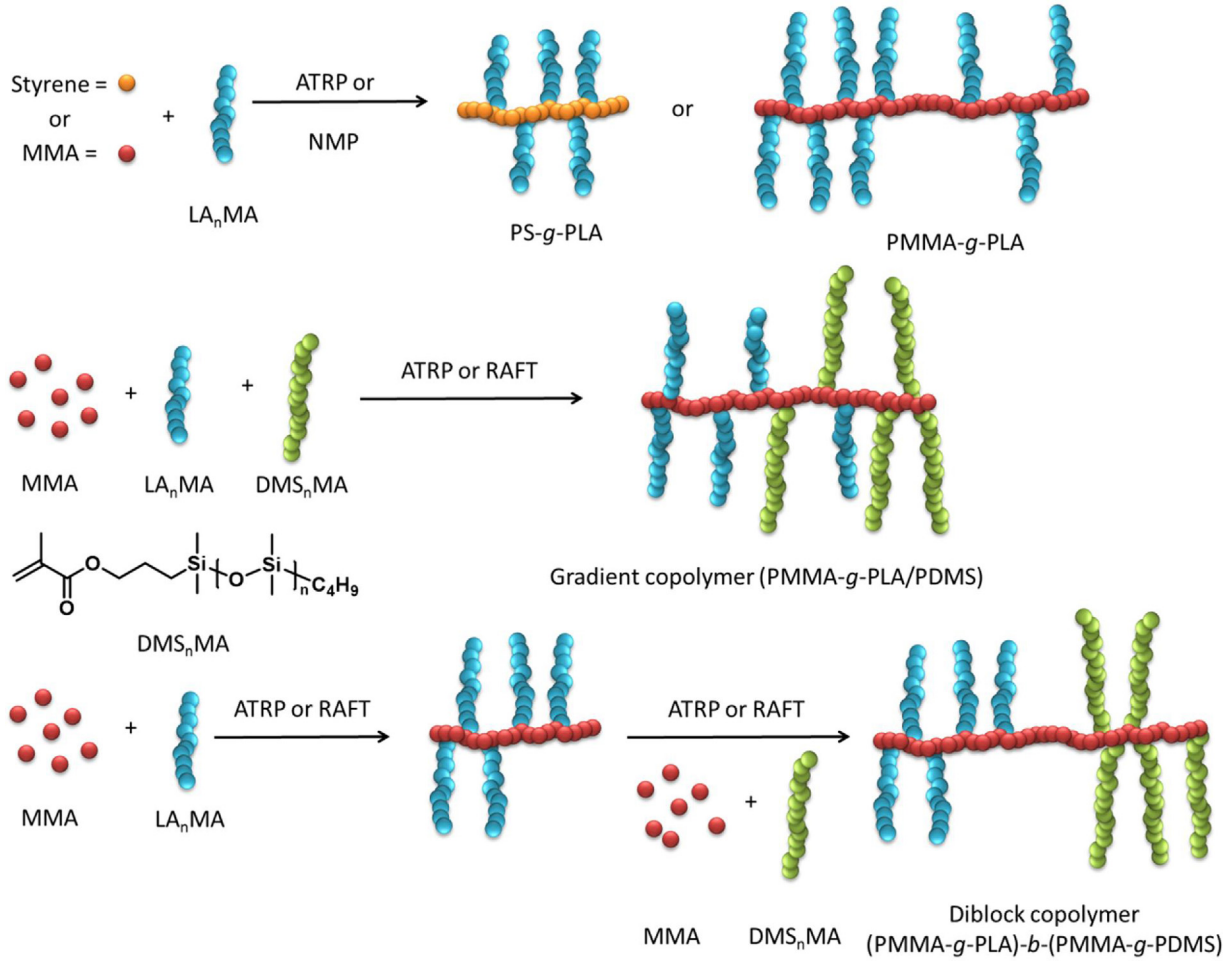

Fig. 17. Schematic representation of synthesis of graft copolymers with PLA side chains *via* the macromonomer approach.

nanoparticles with **35** as initiating moiety for a surface initiated ATRP of $LA_{20}MA$ facilitated the grafting of comb-shaped PLLA from the surface [150]. Characterization by means of IR spectroscopy and thermo-gravimetric analysis confirmed the successful synthesis of nanohybrid materials.

PLA macromonomers featuring a methacrylate ω-end functionality have also been obtained using functional initiators during the ROP. Subsequent to the radical polymerization of the comb polymer backbone, the respective α-end functionality will decorate the end groups of the comb polymer side chains (Fig. 18). Benefiting from the modularity of the macromonomer approach, these functional PLA macromonomers were copolymerized with other hydrophilic macromonomers. Hence, nanoparticles prepared from cholesterol functionalized $LA_{25}MA$ and hydrophilic $MEO_{100}MA$ were used for encapsulation and release of naproxen [152]. In a study more focused on detailed analysis of the heterografted comb polymers, $LA_{10}MA$ and $LA_{15}MA$ with a pyrene moiety were copolymerized by RAFT in varying ratios with a hydrophilic $EtOx_5MA$ macromonomer [149]. The self-assembly of the well-defined amphiphilic comb polymers with varying hydrophilic character in water was studied in detail, and the covalently attached pyrene served as fluorescence label for cellular uptake studies.

4.2. Macromonomer method for the synthesis of graft copolymers with a PLA backbone

Comb and graft copolymers with a PLA backbone are rarely reported. This might be due to the fact that any approach towards such architectures requires the synthesis of functional monomers based on lactide. For this purpose, Coulembier and coworkers prepared a bromine substituted lactide to be employed as initiator for the ATRP of MMA (Fig. 19) [153]. The resulting PMMA macromonomer comprised a lactide end group and was subsequently homopolymerized or copolymerized with L-lactide, yielding comb polymers and loosely grafted copolymers (DG = 7%) with a PLA backbone and PMMA side chains. The *N*-heterocyclic carbene ROP catalyst IMes (compare Fig. 1) produced a cyclic PLA-based backbone, resulting in "jellyfish-like" polymeric architectures ($Đ$ = 1.36–1.46). Conversely, the initiator/catalyst combination benzyl alcohol/IMes gave access to non-cyclic graft copolymers. Careful analysis by means of NMR spectroscopy and mass spectrometry confirmed these structures. The cyclic PLA-*g*-PMMA graft copolymers assembled into various cylinder-shaped topologies, as studied by atomic force microscopy (AFM).

4.3. Macromonomer method for comb polymers with a backbone synthesized by ROMP

In addition to the comb and graft copolymers comprising a backbone prepared either by ROP or a RDRP technique, Grubbs [154–156] and Cheng [157] developed norbornene functional macromonomers, facilitating a backbone formation of comb polymers by means of ROMP (Fig. 20).

The required PLA macromonomers were obtained by $Sn(Oct)_2$ catalyzed ROP initiated by a norbornenyl-functional alcohol

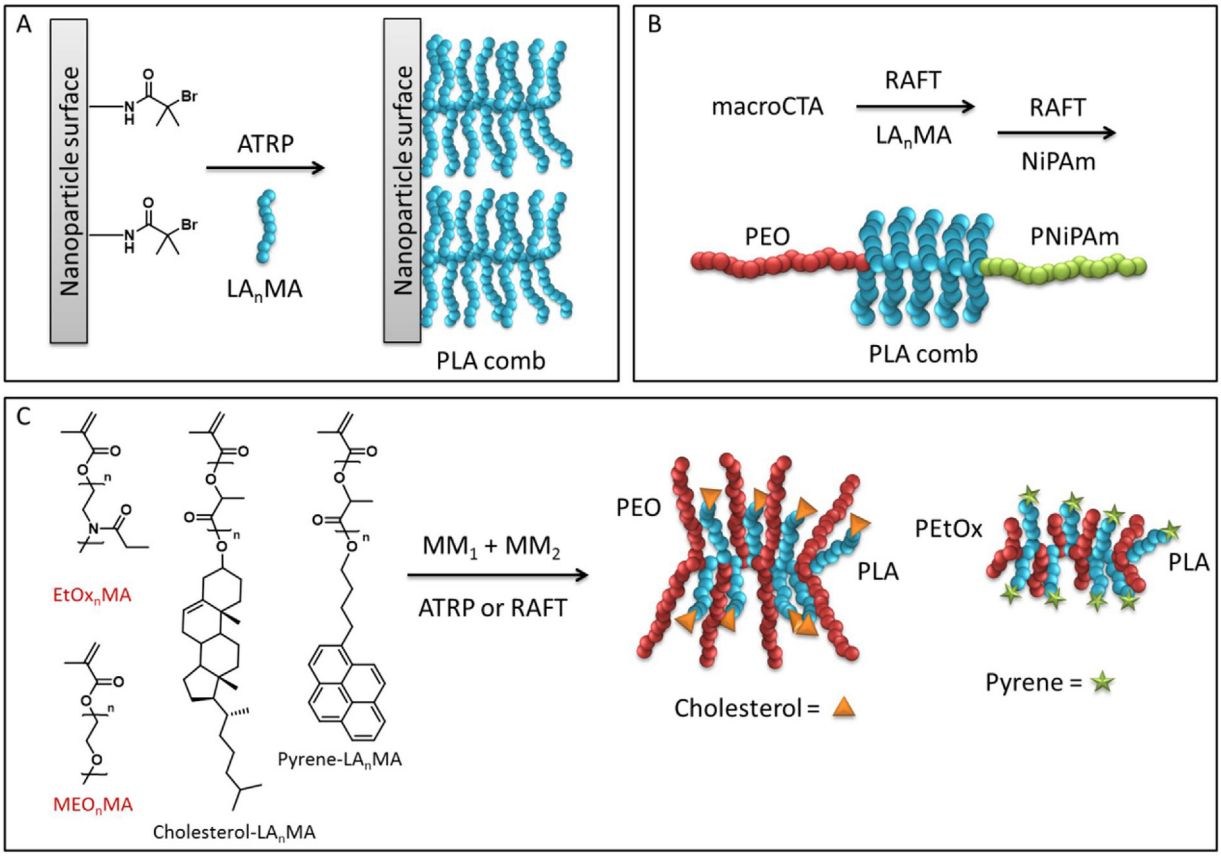

Fig. 18. Schematic representation of the synthesis of comb polymers with PLA side chains obtained *via* the macromonomer approach. (A) Surface initiated polymerization of the macromonomer. (B) Polymerization of the macromonomer utilizing a macroCTA and subsequent chain extension with NiPAm resulting in a "palm tree like" structure. (C) Copolymerization of two different macromonomers yielding heterografted comb polymers.

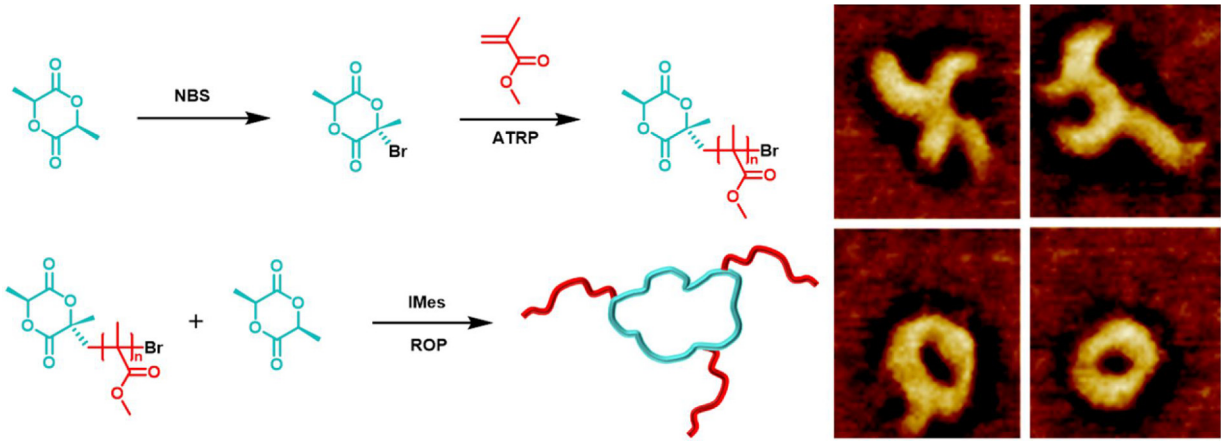

Fig. 19. Schematic representation of the synthesis of linear and cyclic PLA-*g*-PMMA *via* the macromonomer method by employing a functional lactide monomer and AFM phase images of cyclic graft copolymer. The catalyst IMes favors the formation of cyclic PLA directly during the ROP. Reprinted with permission from Macromolecules 2010, 43, 575–579 [153]. Copyright (2010) American Chemical Society.

[154–156]. Similarly, a norbornenyl functionalized ATRP initiator gave access to the corresponding PS or P*n*BA macromonomer [155]. An alternative route towards the latter included the ATRP of *n*BA, substitution of the bromide ω-end group with sodium azide, and the attachment of the norbornenyl moiety *via* CuAAC [154]. Subsequent copolymerization of the macromonomers resulted in statistical [154] or block copolymers [154–156]. Both approaches have been extensively exploited in order to prepare brush copolymers comprising PLA and P*n*BA [154] or PS [155,156] side chains with narrow dispersities (Fig. 20).

An *exo*-norbornene with a hydroxyl and a CTA functionality was applied for simultaneous ROP and RAFT, yielding a PS-*b*-PLA with a norbornenyl moiety at the junction of both blocks (Fig. 20) [157]. ROMP of this macromonomer resulted in well-defined graft copolymers with a PS and a PLA chain attached to each repeating unit ($1.15 < Đ < 1.28$) that formed Janus type structures.

Please cite this article in press as: Yildirim I, et al. Old meets new: Combination of PLA and RDRP to obtain sophisticated macromolecular architectures. Prog Polym Sci (2017), http://dx.doi.org/10.1016/j.progpolymsci.2017.07.010

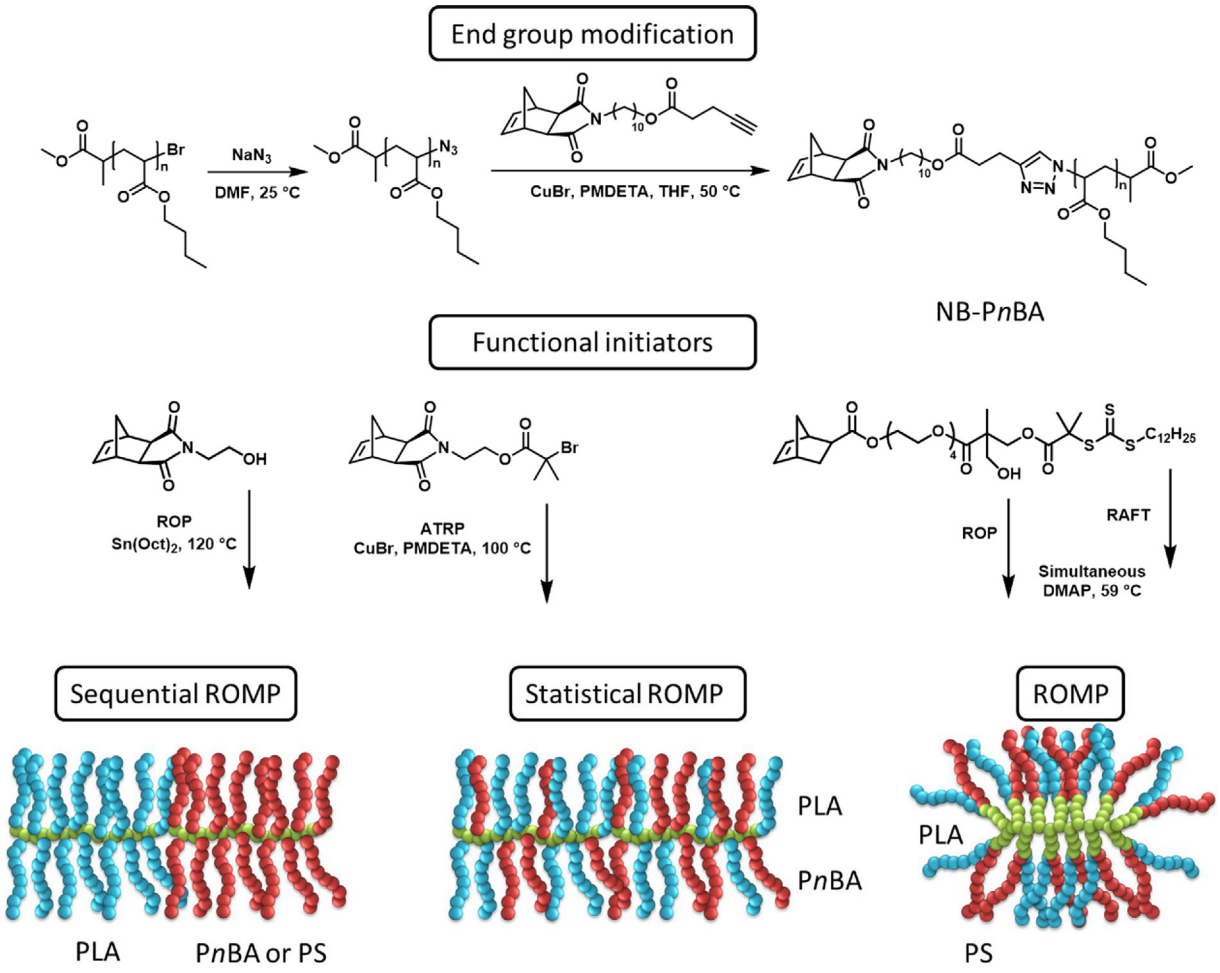

Fig. 20. Schematic representation of the synthesis of norbornene functional macromonomers and the corresponding comb polymer architectures with a polynorbornene backbone obtained *via*ROMP.

4.4. *Grafting-from method for the synthesis of comb and graft copolymers with PLA side chains*

Polymers comprising pendant hydroxyl groups can be utilized in a grafting-from approach. Thereby, the polymer backbone is polymerized first by means of an RDRP technique. The hydroxyl functionalities act as initiators for the polymerization of the PLA side chains *via* ROP in the second step (Fig. 21). In consequence, the DP of the polymer backbone, the DG of the final comb or graft copolymer as well as the distribution of the PLA side chains along the graft copolymer backbone are pre-determined already during the first synthesis step, *i.e.* the (co)polymerization of the backbone. Hydroxyl-functional monomers (such as HEMA or HEA) can be polymerized by all RDRP techniques discussed here, facilitating straightforward access to the comb or graft polymer backbone. Other pendant moieties such as epoxides or ketals liberate two hydroxyl functionalities attached at one backbone repeating unit, enabling the synthesis of extremely dense comb polymers.

4.4.1. *Comb polymers prepared by ROP from PHEMA*

The ATRP of HEMA has often been applied as first step for the synthesis of comb-shaped PLA *via* the grafting-from approach (Fig. 21). A conventional ATRP initiator and the subsequent ROP of L-lactide from the PHEMA backbone yielded comb-shaped PLLA (M_n = 80 kDa, $Đ$ = 1.68). The significantly reduced crystallinity of the material compared to its linear analogue resulted in altered thermal bulk properties [158].

A covalent attachment of comb-shaped PLA to inorganic materials is advantageous for the development of composite materials with PLA. For this purpose, the surface of cobalt-chromium implants [159] or silica nanoparticles [160] was functionalized with an ATRP initiator. Subsequent surface initiated ATRP of HEMA and ROP of lactide provided hybrid materials with high compatibility to a PLA matrix.

As the ω-chain end of a PHEMA prepared by ATRP remains active, the grafting from approach enables the attachment of a second poly(meth)acrylate-based block to the comb polymer backbone. Lactide and the vinylic monomer have been polymerized in a simultaneous ROP/ATRP from PHEMA featuring a bromide end group. [160,161] Thereby, $Sn(Oct)_2$ acted as ROP catalyst as well as reducing agent for the AGET ATRP ($CuBr_2$, Bpy) of $EO_{23}MA$. Several amphiphilic block copolymers with varying composition were prepared ($1.12 < Đ < 1.26$) and studied in detail with respect to their thermal properties in bulk. [161] The same approach was applied to functionalize silica nanoparticles with block copolymers comprising comb-shaped PLA and P*n*BuA. [160]

The hydroxyl functionalities of the PHEMA backbone can be partially esterified by treatment with 2-bromo-2-methylpropanoyl bromide (**35**), yielding pendant ATRP initiating moieties. The residual hydroxyl functionalities can simultaneously serve as ROP initiators (Fig. 22) [162]. This approach provided access to comb polymers with mixed PLA and PS side chains of varying compositions ($1.2 < Đ < 1.8$) by simultaneous ROP of L-lactide and AGET ATRP of styrene ($Sn(Oct)_2$, $CuBr_2$, PMDETA).

Please cite this article in press as: Yildirim I, et al. Old meets new: Combination of PLA and RDRP to obtain sophisticated macromolecular architectures. Prog Polym Sci (2017), http://dx.doi.org/10.1016/j.progpolymsci.2017.07.010

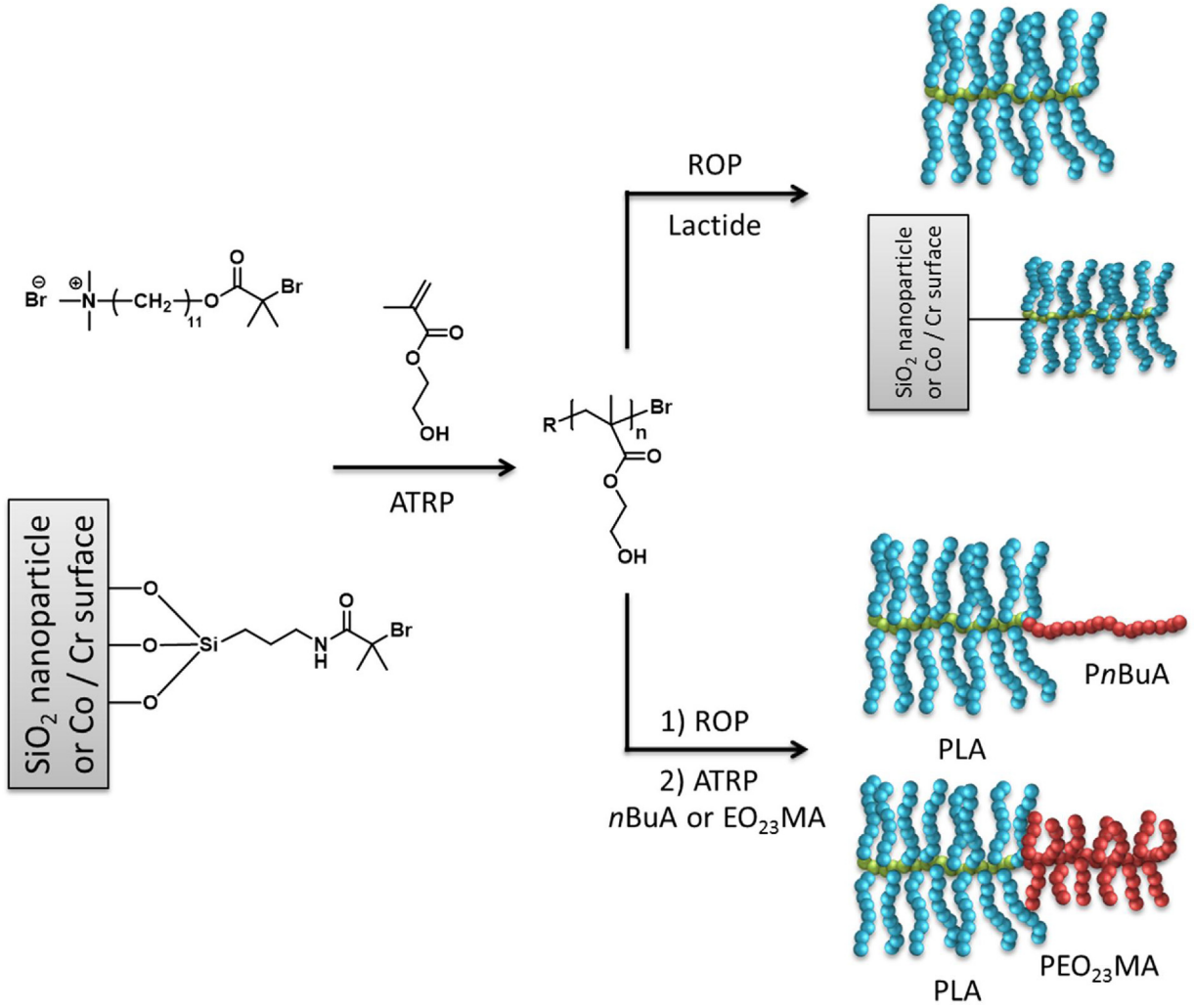

Fig. 21. Schematic representation the synthesis polymeric architectures comprising comb-shaped PLA by grafting of PLA from PHEMA.

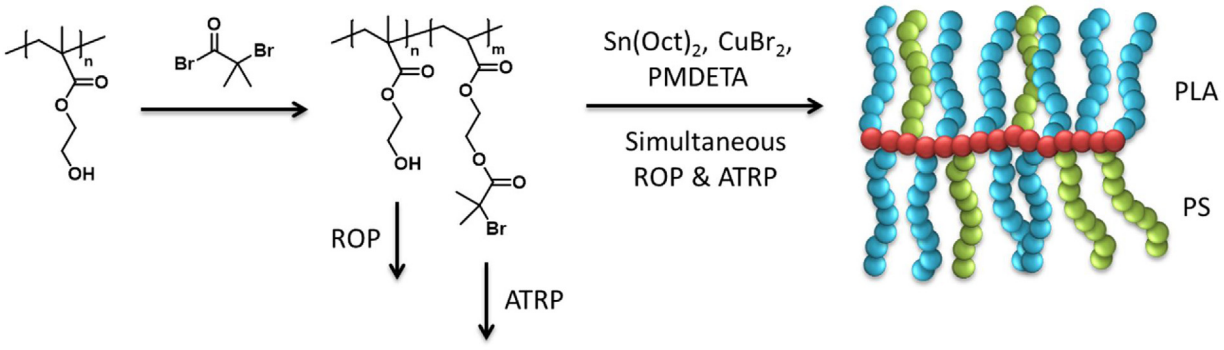

Fig. 22. Schematic representation of the synthesis of comb polymers with mixed PLA and PS side chains *via* simultaneous ROP of lactide and AGET ATRP of styrene.

4.4.2. Graft copolymers prepared by ROP from copolymers comprising HEA or HEMA

The copolymerization of HEMA or HEA with other vinylic monomers enables the preparation of graft copolymers with PLA side chains *via* grafting-from approach (Fig. 23). Thereby, the molar fraction of hydroxyl-functional monomer used in the first synthesis step determines the DG of the graft copolymer. The reactivity of both monomers during the RDRP pre-determines the side chain distribution along its backbone. During the ATR copolymerization of HEMA with MMA, preferential incorporation of HEMA was evidenced ($r_{MMA} = 1.58$, $r_{HEMA} = 4.76$), resulting in graft copolymers with enriched PLA side chains towards the α-chain end of the backbone (DG ≈ 15; $1.22 < Đ < 1.63$) [163].

Chain extension of the ω-end groups of the graft copolymer facilitates the attachment of, *e.g.*, hydrophilic building blocks. Zhang and co-workers reported the synthesis of block copolymers containing PMAA-*g*-PLA and $PMEO_9MA$ blocks to be used as carrier material for oral drug delivery [164]. The reaction cascade involved the copolymerization of HEMA with *t*BMA by activator regenerated by electron transfer (ARGET) ATRP, the ROP of D,L-lactide, a chain

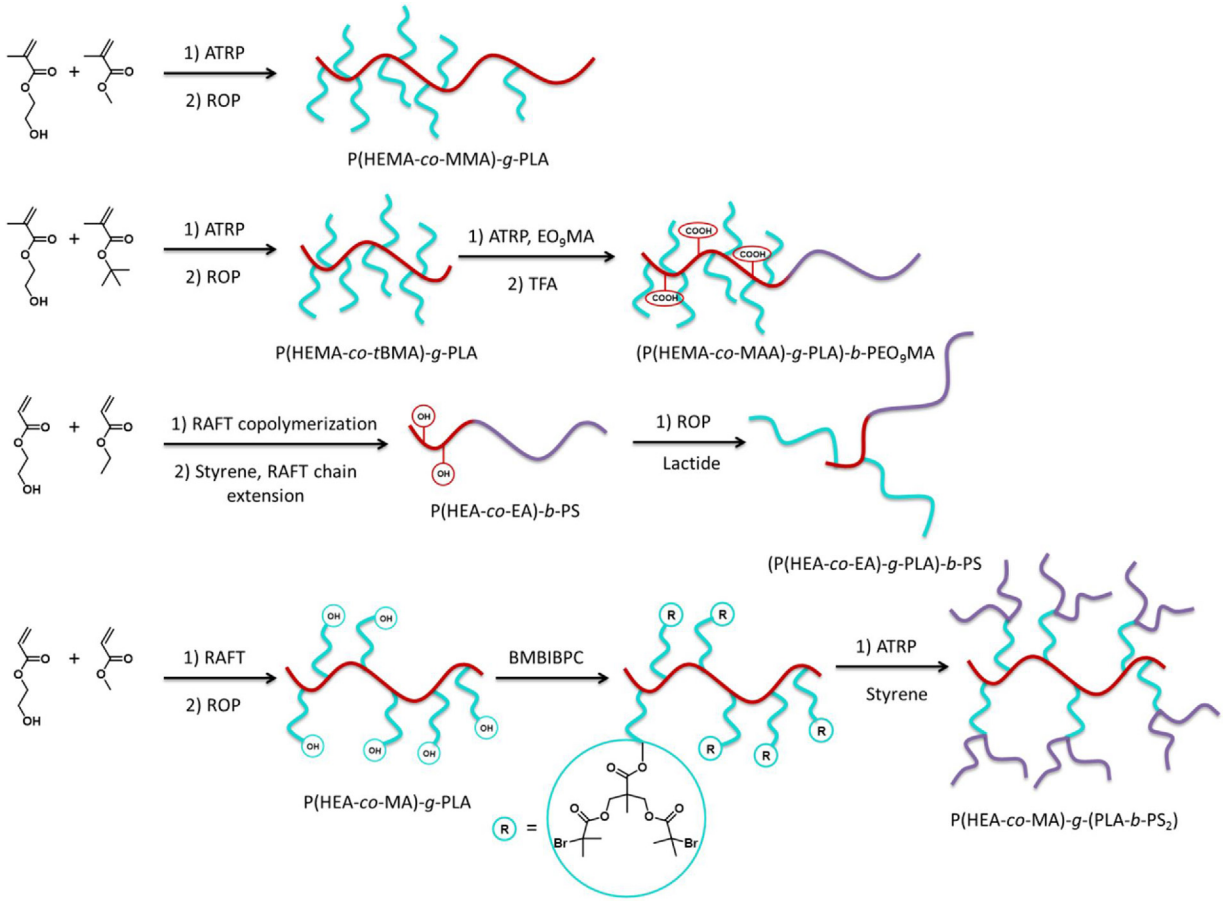

Fig. 23. Schematic representation of the synthesis of graft copolymers with PLA side chains from precursor copolymers comprising HEMA or HEA.

extension with MEO_9MA, and a final deprotection of the *tert*-butyl groups by treatment with trifluoroacetic acid ($Đ \approx 1.25$).

A graft copolymer featuring a very low backbone DP and DG along with a higher PLA side chain DP rather resembles a star-shaped polymer (Fig. 23) [165]. Perrier and co-workers prepared P(EA-*co*-HEA) co-oligomers with a DP of 10 and in average 2–4 units of HEA, subsequently serving as multifunctional initiators for the sparteine/thiourea catalyzed ROP of L-lactide. The use of multifunctional initiators comprising a PS block led to pseudo-miktoarm star-shaped copolymers with one PS arm. However, the presence of mixtures of macromolecules with the according number of PLA "arms" could not be avoided ($1.3 < Đ < 1.9$) since the DP of HEA represents an average value.

The PLA side chains of graft copolymers can act as initiators for a second block as well. For this purpose, the hydroxyl end groups of the PLA side chains of PMA-*g*-PLLA (prepared by RAFT and ROP using $Sn(Oct)_2$) and were esterified with BMBIBPC (see Section 3.3, Scheme 8), attaching two initiating sites for the ATRP of styrene at each PLLA side chain (Fig. 23). [166] The final branched copolymers revealed a non-homogeneous distribution of the AB_2 type side chains ($1.07 < Đ < 1.42$) because MA revealed higher reactivity than HEA during the initial RAFT copolymerization.

4.4.3. Poly(glycidyl methacrylate) as precursor for grafting from approaches

Glycidyl methacrylate (GMA) represents an interesting monomer for the grafting from approach since the pendant epoxide units can be opened by several nucleophiles, liberating hydroxyl functionalities along with other functional groups (Scheme 10). Simple hydrolysis of the epoxide functionality under acidic conditions yields two hydroxyl functionalities at each methacrylate repeating unit, enabling the preparation of very dense comb polymers. Azidolysis using sodium azide produces a pendant hydroxyl as well as an azide moiety, which is useful to incorporate "click" chemistry approaches [167]. Nucleophilic attack by α-bromobutyric acid results in pendant initiating sites for both ROP as well as ATRP [168].

Hydrolysis of the epoxide functionality of PGMA was extensively applied by Rzayev and co-workers to synthesize densely grafted bottlebrush copolymers (Fig. 24) [169–174]. Grafting of PLA from the resulting hydroxy-functional polymethacrylate backbone was performed *via* a ROP procedure catalyzed by DBU. Subsequently, the hydroxyl end groups of the PLA side chains were esterified with the acyl chloride functional trithiocarbonate CTA **38**, which was formed *in situ* from CTA **41** and oxalyl chloride (compare Section 3.2). Finally, several RAFT copolymerizations of different monomer types were performed, which were selected according to the desired application of the comb polymers comprising block copolymer side chains.

The vinylic block was mostly based on PS, and several functional comonomers were incorporated to serve as cross-linkers for the shell. Permanent cross-linking of butenylstyrene (BS) was reported *via* cross-metathesis using Grubbs catalyst [169–171]. Subsequently, hydrolysis of the PLA core under acidic conditions yielded hollow nanotubes [169]. The surface of the nanotubes was modified for a variety of applications. A P*t*BuA block inserted between the PLA and the PS block provided a negatively charged PAA interior subsequent to hydrolysis, making the nanotubes effec-

Please cite this article in press as: Yildirim I, et al. Old meets new: Combination of PLA and RDRP to obtain sophisticated macromolecular architectures. Prog Polym Sci (2017), http://dx.doi.org/10.1016/j.progpolymsci.2017.07.010

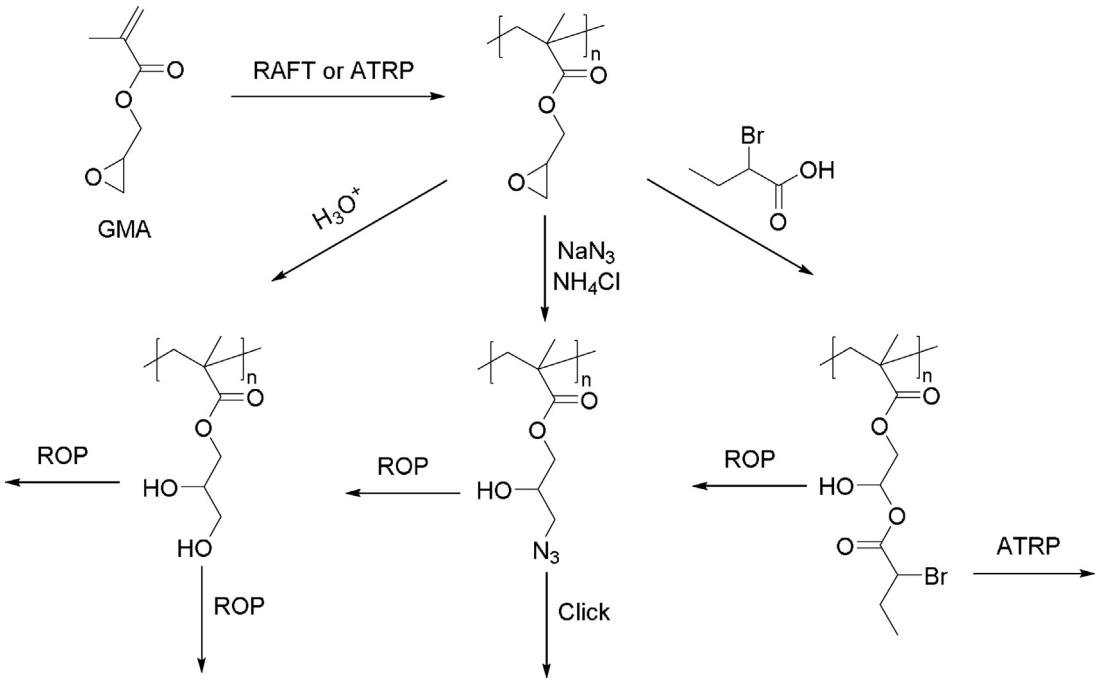

Scheme 10. Schematic representation of ring-opening strategies involving a PGMA backbone to be used for grafting-from approaches.

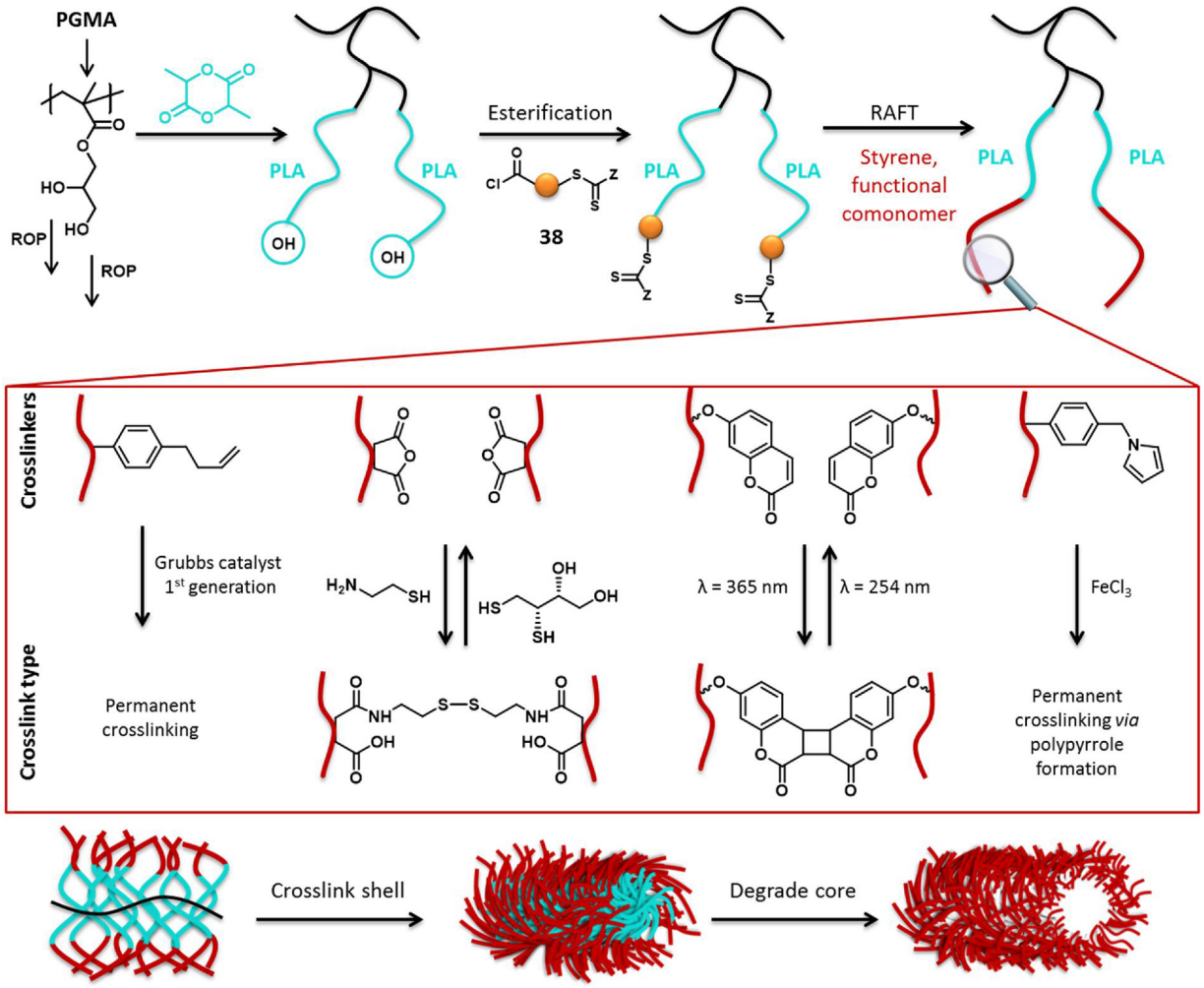

Fig. 24. Schematic representation of the synthetic pathways to multicomponent bottlebrush copolymers and fabrication of polymeric nanotubes with tailor-made functionalities followed by Rzayev and co-workers.

Please cite this article in press as: Yildirim I, et al. Old meets new: Combination of PLA and RDRP to obtain sophisticated macromolecular architectures. Prog Polym Sci (2017), http://dx.doi.org/10.1016/j.progpolymsci.2017.07.010

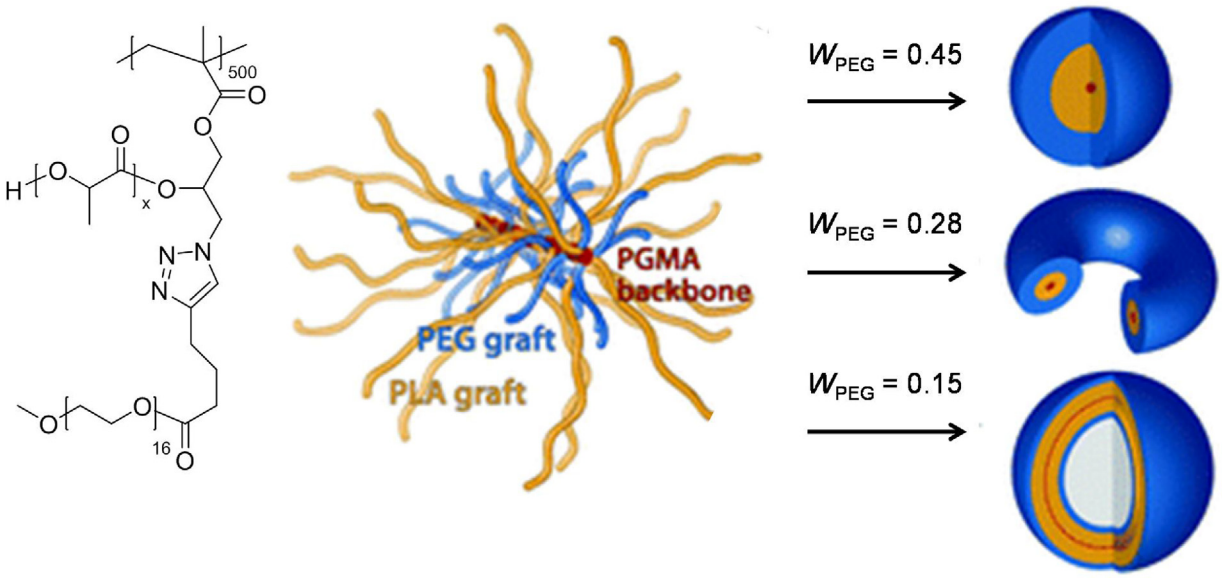

Fig. 25. Schematic representation of the self-assembly of amphiphilic brush copolymers with PLA and PEO side chains. Adapted from [167] with permission of The Royal Society of Chemistry.

tive carriers for cationic guest molecules [171]. Modification of the outside of the nanotubes was performed accordingly by chain extension of the PS-based side chains with P*t*BuA or with P(S-*alt*-maleic anhydride) [170]. Chain extension of the PGMA backbone with $PMEO_{23}MA$ resulted in nanotubes that are open on one side [169].

P(S-*alt*-maleic anhydride) served as basis for a reversible crosslinking of the nanotubes by nucleophilic addition of cysteamine [172]. The resulting mercapto moieties were used for crosslinking under oxidative conditions, and the formed disulfide bonds could be cleaved by DTT, leading to scission of the nanotubes. Pendant pyrrole moieties were crosslinked by treatment with $FeCl_3$ *via* polymerization of the pyrrole functionalities [173]. Crosslinking by means of photodimerization of a coumarin functionalized shell was also reported [174].

The opening of the epoxide with α-bromobutyric acid facilitated the attachment of a PS and a PLA side chain at one GMA repeating unit (Scheme 10). [168] The ROP of L-lactide ($Sn(Oct)_2$) and the ATRP of styrene (CuBr, Bpy) yielded asymmetric comb polymers (DP(backbone) = 65, DP(PLA) = 22–54, DP(PS) = 5–120, $1.07 < Đ < 1.24$). Hydrolysis of the PLA enabled a detailed analysis of the PS side chains, revealing that not every backbone repeating unit had indeed initiated a PS chain.

The azidolysis of PGMA's epoxide ring represents a modular approach to attach alkyne-functional side chains to the same repeating unit as a PLA side chain (Fig. 25) [167]. The DBU catalyzed ROP of D,L-lactide was initiated from the liberated hydroxyl groups, and a subsequent click reaction with alkynyl-terminated PEO yielded the final amphiphilic comb polymers ($1.63 < Đ < 1.92$). A variation of the PDLLA side chain length resulted in an altered hydrophilic/hydrophobic balance and, thus, in different self-assembled morphologies in aqueous medium.

4.4.4. Grafting of PLA from (co)polymers comprising solketal methacrylate

Solketal methacrylate (SKMA) represents an isoproylidene protected glycerol methacrylate that can be polymerized *via* RAFT. In consequence, acidic deprotection liberates two hydroxyl groups to be subsequently employed as initiators for the ROP of lactide. SKMA was intensively utilized for the synthesis of multi-component comb and graft copolymers in combination with other functional monomers by Rzayev and coworkers (Fig. 26). The various synthetic strategies comprised multiple steps, which will be shortly outlined below, structured according the type of monomer copolymerized with SKMA.

2-Bromoisobutyryl methacrylate (BIEMA) can be polymerized by RAFT and is functionalized with an initiating moiety for ATRP (Fig. 26). In consequence, sequential RAFT polymerization of SKMA and BIEMA was used to prepare a block copolymer backbone with latent ROP and ATRP initiating sites [175–179]. Successive ATRP of EO_9MA [175] or styrene [176–179], hydrolysis of the ketal moieties, and ROP of lactide resulted in well-defined brush copolymers with very high molar masses ($1100\ g/mol < M_n < 2.4 \times 10^6\ g/mol$, $1.05 < Đ < 1.29$).

Additional incorporation of the trimethylsilyl protected alkyne functional methacrylate SiPMA into the backbone enabled the addition of further side chain types to the polymeric architecture by CuAAC. (Fig. 26) [180]. The synthetic steps subsequent to RAFT polymerization of SKMA, BIEMA, and SiPMA comprised a) the grafting of PMMA from the pendant α–bromoesters by ATRP, b) the deprotection of the alkynyl moiety, c) its functionalization with an azide-functional trithiocarbonate, d) grafting of PS from the pendant trithiocarbonate *via* RAFT, e) hydrolysis of the ketal moieties, and f) DBU catalyzed grafting of PDLLA from the glycerol moieties. The triblock bottlebrush copolymer obtained with this 10-step synthesis revealed a molar mass (M_n) of 626 kg/mol and a $Đ$ of 1.35.

Orthogonally protected hydroxyl groups facilitated the grafting of two different types of PLA side chains from the same backbone (Fig. 26) [181]. For this purpose, a BAB triblock copolymer with a central PSKMA block and two outer blocks based on *p*-methoxybenzyl protected HEMA, *i.e.* P*p*BMA, was synthesized *via* RAFT utilizing a bifunctional CTA. Selective hydrolysis of PSKMA's ketal groups under acidic conditions liberated the hydroxyl moieties in the central block to graft PLA. The ω-end groups of the PLA side chains were esterified with the trithiocarbonate CTA **38** to allow further chain extension with P(S-*stat*-BS) *via* RAFT (see above). The deprotection of the *p*-methoxybenzyl protecting groups at the outer blocks by oxidative debenzylation with 2,3-dichloro-5,6-dicyanobenzoquinone (DDQ) liberated PHEMA's hydroxyl functionalities, which were used to graft a second set of PLA side chains ($Đ = 1.36$). Subsequent to crosslinking of the P(S-

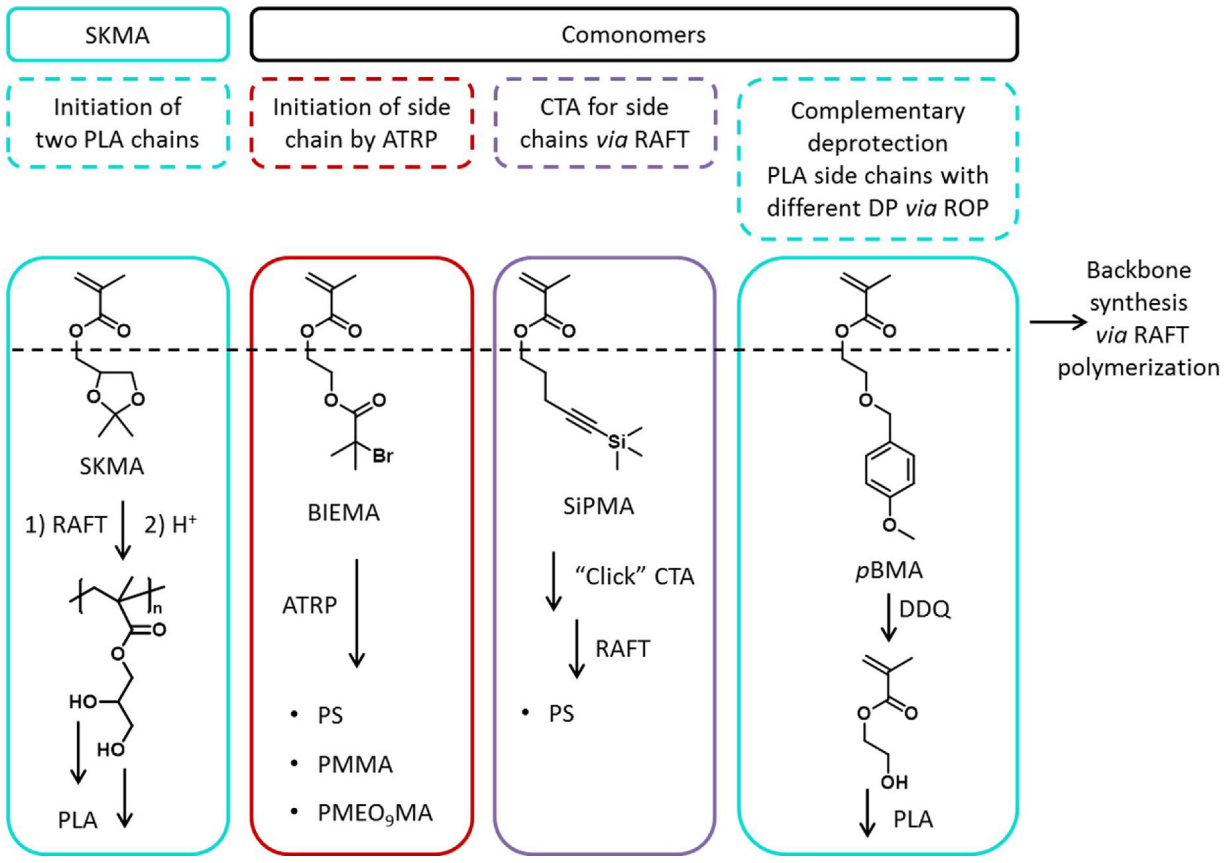

Fig. 26. Schematic representation of the synthesis of comb polymer architectures comprising PLA side chains from a PSKMA backbone and the comonomers polymerized with SKMA *via* RAFT polymerization to introduce various other side chain types to the same polymethacrylate backbone.

stat-BS) segments and hydrolysis of the PLA-based segments, this strategy gave access to open end nanotubes.

5. Conclusion

The combination of the ROP of lactide with all three RDRP techniques discussed here gives access to a wide range of macromolecular architectures. Thereby, the RDRP techniques proved valuable for the introduction of many functional groups that would not be tolerated in a ROP process for polyester syntheses, omitting the need to apply protection group chemistry. The synthetic routes applied are mostly independent from the type of RDRP technique. For all three methods, *i.e.* ATRP, RAFT and NMP, dual initiators provide access to block copolymers. The advantage of functional group tolerance comes into play in particular for ROP first approaches. This holds true as well for the post-polymerization end functionalization of PLA with the respective initiators or CTAs that are used in an RDRP as a second step. Despite the fact that this approach adds at least one synthetic step to the overall synthesis pathway, it is extremely useful for the straightforward preparation of star-shaped block polymers comprising a PLA core.

The general methods to obtain comb and graft copolymers have been mainly applied to prepare macromolecular architectures comprising PLA as side chains. The polymer backbone is formed by means of RDRP or ROMP. In addition, the polymer chemistry playground facilitated synthesis of a wide range of comb polymers with mixed or block-type side chains, representing an impressive example of the capabilities of modern synthetic polymer chemistry. RDRP techniques also facilitated grafting of PLA-based polymers from surfaces, an undertaking that could be difficult to achieve with ROP alone because of its sensitivity towards contaminations that would interfere with the ROP mechanism.

The (bio)degradability of PLA is probably the main reason for its manifold applications, certainly within the biomedical field. However, this feature can be a challenge during the synthesis of polymers comprising PLA. On the other hand, a range of reactions can be performed successfully despite the sensitivity of PLA towards hydrolytic degradation. Unfortunately, the structural analysis of products obtained during the varying synthetic steps is often disregarded in view of a potential bio-medical application of the materials. In particular when deprotection reactions of functional moieties are performed subsequent to a ROP process, characterization data are often missing. However, the deprotection is the crucial step during that degradation of the PLA can possibly occur. The use of multifunctional initiators for the ROP complicates the structural confirmation of the macromolecules obtained in any case, especially taking into account the initiation efficiency during a subsequent RDRP. Detailed kinetic studies during the RDRP and the degradation of the PLA building blocks in the final polymer can, in fact, provide a very clear picture of the macromolecular structure. Although the latter option is not always applicable, and advanced characterization techniques are more readily accessible nowadays, some researchers tend to neglect the possibilities of modern polymer characterization techniques.

Independent from the pathway selected, researchers active in the field follow protocols well established in their lab. On the other hand, recent advances in the field provide a variety of alternative reagents for ROP or RDRP. In addition, more and more functional reagents become commercially available. This will certainly trigger new ideas in the combination of both polymerization methods, omitting the need of extensive organic synthesis of tailor-made ini-

Please cite this article in press as: Yildirim I, et al. Old meets new: Combination of PLA and RDRP to obtain sophisticated macromolecular architectures. Prog Polym Sci (2017), http://dx.doi.org/10.1016/j.progpolymsci.2017.07.010

tiators or end capping agents. This will drive forward particularly research on one-pot and simultaneous polymerizations of lactide and vinylic monomers, as such experimentally simple procedures are highly appreciated in general.

Acknowledgements

This work was supported by the Carl-Zeiss-Stiftung, the Thüringer Ministerium für Wirtschaft, Wissenschaft, und Digitale Gesellschaft (TMWWDG, ProExzellenz II, NanoPolar) and the Collaborative Research Center SFB ChemBioSys (SFB 1127).

References

[1] Thomas CM, Lutz JF. Precision synthesis of biodegradable polymers. Angew Chem Int Ed 2011;50:9244–6.
[2] Raquez JM, Habibi Y, Murariu M, Dubois P. (PLA)-based nanocomposites. Prog Polym Sci 2013;38:1504–42.
[3] Lasprilla AJR, Martinez GAR, Lunelli BH, Jardini AL, Filho RM. Poly-lactic acid synthesis for application in biomedical devices — A review. Biotechnol Adv 2012;30:321–8.
[4] Albertsson AC, Varma IK. Recent developments in ring opening polymerization of lactones for biomedical applications. Biomacromolecules 2003;4:1466–86.
[5] Dechy-Cabaret O, Martin-Vaca B, Bourissou D. Controlled ring-opening polymerization of lactide and glycolide. Chem Rev 2004;104:6147–76.
[6] O'Keefe BJ, Hillmyer MA, Tolman WB. Polymerization of lactide and related cyclic esters by discrete metal complexes. J Chem Soc Dalton Trans 2001:2215–24.
[7] Chisholm MH, Gallucci J, Phomphrai K. Lactide polymerization by well-defined calcium coordination complexes: comparisons with related magnesium and zinc chemistry. Chem Commun 2003;4:8–9.
[8] Harder S. From limestone to catalysis: application of calcium compounds as homogeneous catalysts. Chem Rev 2010;110:3852–76.
[9] Kiesewetter MK, Shin EJ, Hedrick JL, Waymouth RM. Organocatalysis opportunities and challenges for polymer synthesis. Macromolecules 2010;43:2093–107.
[10] Kamber NE, Jeong W, Waymouth RM, Pratt RC, Lohmeijer BGG, Hedrick JL. Organocatalytic ring-opening polymerization. Chem Rev 2007;107:5813–40.
[11] Zhou S, Liao X, Li X, Deng X, Li H. Poly-D,L-lactide–co-poly(ethylene glycol) microspheres as potential vaccine delivery systems. J Control Release 2003;86:195–205.
[12] Shipp DA. Reversible-deactivation radical polymerizations. Polym Rev 2011;51:99–103.
[13] Dove AP. Controlled ring-opening polymerisation of cyclic esters: polymer blocks in self-assembled nanostructures. Chem Commun 2008;644:6–70.
[14] Oh JK. (PLA)-based amphiphilic block copolymers: synthesis, self-assembly, and biomedical applications. Soft Matter 2011;7:5096–108.
[15] Xu Y, Pan C, Tao L. Block and star block copolymers by mechanism transformation II. Synthesis of poly(DOP-b-St) by combination of ATRP and CROP. J Polym Sci Part A: Polym Chem 2000;38:436–43.
[16] Tao L, Luan B, Pan C. Block and star block copolymers by mechanism transformation. VIII Synthesis and characterization of triblock poly(LLA-b-St-b-MMA) by combination of ATRP and ROP. Polymer 2003;44:1013–20.
[17] Ho RM, Chen CK, Chiang YW, Ko BT, Lin CC. Tubular nanostructures from degradable core–shell cylinder microstructures in chiral diblock copolymers. Adv Mater 2006;18:2355–8.
[18] Hou X, Li Q, He Y, Jia L, Li Y, Zhu Y, et al. Visualization of spontaneous aggregates by diblock poly(styrene)-b-poly(L-lactide)/poly(D-lactide) pairs in solution with new fluorescent CdSe quantum dot labels. J Polym Sci Part B: Polym Phys 2009;47:1393–405.
[19] Hou X, Li Q, Cao A. Synthesis and microphase separation of polystyrene-b-polylactide block copolymers aimed at preparation of ordered nanoparticle/block copolymer hybrid materials. Polym Int 2014;63:1159–67.
[20] Hou X, Li Q, Cao A. Solvent annealing-induced microphase-separation of polystyrene-b-polylactide block copolymer aimed at preparation of ordered nanoparticles/block copolymer hybrid thin film. J Polym Res 2014;21:491:1–15.
[21] Hou X, Li Q, Cao A. In situ aggregates of enantiomeric poly(styrene)-block-poly(lactide) diblock copolymers via stereocomplexation in a non-selective solvent. Macromol Chem Phys 2013;214:1569–79.
[22] Likhitsup A, Parthiban A, Chai CLL. Combining atom-transfer radical polymerization and ring-opening polymerization through bifunctional initiators derived from hydroxy benzyl alcohol—Preparation and characterization of initiators, macroinitiators, and block copolymers. J Polym Sci Part A: Polym Chem 2008;46:102–16.
[23] Dirany M, Lacroix-Desmazes P, Vayer M, Erre R, Boutevin B, Sinturel C. Polystyrene-block-polylactide obtained by the combination of atom transfer radical polymerization and ring-opening polymerization with a commercial dual initiator. J Appl Polym Sci 2011;122:2944–51.
[24] Parthiban A, Likhitsup A, Choo FM, Chai CLL. Triblock copolymers composed of soft and semi-crystalline segments-synthesis and characterization of poly[(n-butyl acrylate)-block-(ε-caprolactone)-block-(L-lactide)]. Polym Chem 2010;1:333–8.
[25] Yang YQ, Lin WJ, Zhao B, Wen XF, Guo XD, Zhang LJ. Synthesis and physicochemical characterization of amphiphilic triblock copolymer brush containing pH-sensitive linkage for oral drug delivery. Langmuir 2012;28:8251–9.
[26] Le Droumaguet B, Poupart R, Grande D. Clickable thiol-functionalized nanoporous polymers: from their synthesis to further adsorption of gold nanoparticles and subsequent use as efficient catalytic supports. Polym Chem 2015;6:8105–11.
[27] Wang WW, Ren WY, Jiang L, Dan Y. Synthesis and characterization of AB-type copolymers poly(L-lactide)-block-poly(methyl methacrylate) via a convenient route combining ROP and ATRP from a dual initiator. J Appl Polym Sci 2010;118:2379–88.
[28] Mao J, Ji X, Bo S. Synthesis and pH/temperature-responsive behavior of PLLA-b-PDMAEMA block polyelectrolytes prepared via ROP and ATRP. Macromol Chem Phys 2011;212:744–52.
[29] Yu TL Huang BH, Hung WC, Lin CC, Wang TC, Ho RM. Preparation and characterization of poly(ε-caprolactone)-b-polyacrylonitrile (PCL-b-PAN) and poly(l-lactide)-b-polyacrylonitrile (PLLA-b-PAN) copolymers by aluminum and lithium alkoxides containing double-headed initiators. Polymer 2007;48:4401–11.
[30] Hu F, Neoh KG, Kang ET. Synthesis of folic acid functionalized PLLA-b-PPEGMA nanoparticles for cancer cell targeting. Macromol Rapid Commun 2009;30:609–14.
[31] Jubeli E, Moine L, Barratt G. Synthesis, characterization, and molecular recognition of sugar-functionalized nanoparticles prepared by a combination of ROP, ATRP, and click chemistry. J Polym Sci Part A: Polym Chem 2010;48:3178–87.
[32] Abulateefeh SR, Saeed AO, Aylott JW, Chan WC, Garnett MC, Saunders BR, et al. Facile synthesis of responsive nanoparticles with reversible, tunable and rapid thermal transitions from biocompatible constituents. Chem Commun 2009;606:8–70.
[33] Khorsand Sourkohi B, Cunningham A, Zhang Q, Oh JK. Biodegradable block copolymer micelles with thiol-responsive sheddable coronas. Biomacromolecules 2011;12:3819–25.
[34] Ko NR, Yao K, Tang C, Oh JK. Synthesis and thiol-responsive degradation of polylactide-based block copolymers having disulfide junctions using ATRP and ROP. J Polym Sci Part A: Polym Chem 2013;51:3071–80.
[35] Wang Y, Wang H, Liu G, Liu X, Jin Q, Ji J. Self-assembly of near-monodisperse redox-sensitive micelles from cholesterol-conjugated biomimetic copolymers. Macromol Biosci 2013;13:1084–91.
[36] Gordin C, Delaite C, Medlej H, Josien-Lefebvre D, Hariri K, Rusu M. Synthesis of ABC miktoarm star block copolymers from a new heterotrifunctional initiator by combination of ATRP and ROP. Polym Bull 2009;63:789–801.
[37] Li H, Rathi S, Sterner ES, Zhao H, Ling Hsu S, Theato P, et al. Synthesis of photocleavable poly(methyl methacrylate-block-d-lactide) via atom-transfer radical polymerization and ring-opening polymerization. J Polym Sci Part A: Polym Chem 2013;51:4309–16.
[38] Wolf FK, Hofmann AM, Frey H. Poly(isoglycerol methacrylate)-b-poly(D or L-lactide) copolymers: a novel hydrophilic methacrylate as building block for supramolecular aggregates. Macromolecules 2010;43:3314–24.
[39] Song J, Xu J, Pispas S, Zhang G. One-pot synthesis of poly(L-lactide)-b-poly(methyl methacrylate) block copolymers. RSC Adv 2015;5:38243–7.
[40] Gorzolnik B, Davidson P, Beurroies I, Denoyel R, Grande D. Novel functional mesoporous materials obtained from nanostructured diblock copolymers. Macromol Symp 2010;287:127–34.
[41] Grande D, Penelle J, Davidson P, Beurroies I, Denoyel R. Functionalized ordered nanoporous polymeric materials: from the synthesis of diblock copolymers to their nanostructuration and their selective degradation. Microporous Mesoporous Mater 2011;140:34–9.
[42] Matyjaszewski K, Tsarevsky NV. Macromolecular engineering by atom transfer radical polymerization. J Am Chem Soc 2014;136:6513–33.
[43] Wolf FF, Friedemann N, Frey H. Poly(lactide)-block-poly(HEMA) block copolymers: an orthogonal one-pot combination of ROP and ATRP, using a bifunctional initiator. Macromolecules 2009;42:5622–8.
[44] Kipping M, Krahl F, Döring A, Adler HJP, Kuckling D. Synthesis and characterization of particles consisting of a biodegradable poly(l-lactide) core and a functional hydrophilic shell. Eur Polym J 2010;46:313–23.
[45] Kryuchkov MA, Detrembleur C, Bazuin CG. Linear amphiphilic diblock copolymers of lactide and 2-dimethylaminoethyl methacrylate using bifunctional-initiator and one-pot approaches. Polymer 2014;55:2316–24.
[46] Liu H, Li S, Zhang M, Shao W, Zhao Y. Facile synthesis of ABCDE-type H-shaped quintopolymers by combination of ATRP, ROP, and click chemistry and their potential applications as drug carriers. J Polym Sci Part A: Polym Chem 2012;50:4705–16.
[47] Priftis D, Sakellariou G, Baskaran D, Mays JW, Hadjichristidis N. Polymer grafted Janus multi-walled carbon nanotubes. Soft Matter 2009;5:4272–8.
[48] Moad G, Rizzardo E, Thang SH. Toward living radical polymerization. Acc Chem Res 2008;41:1133–42.

Please cite this article in press as: Yildirim I, et al. Old meets new: Combination of PLA and RDRP to obtain sophisticated macromolecular architectures. Prog Polym Sci (2017), http://dx.doi.org/10.1016/j.progpolymsci.2017.07.010

[49] Bernaerts KV, Du Prez FE. Dual/heterofunctional initiators for the combination of mechanistically distinct polymerization techniques. Prog Polym Sci 2006;31:671–722.
[50] Pratt RC, Lohmeijer BGG, Long DA, Lundberg PNP, Dove AP, Li H, et al. Exploration, optimization, and application of supramolecular thiourea-amine catalysts for the synthesis of lactide (co)polymers. Macromolecules 2006;39:7863–71.
[51] Zhang L, Nederberg F, Pratt RC, Waymouth RM, Hedrick JL, Wade CG. Phosphazene bases: a new category of organocatalysts for the living ring-opening polymerization of cyclic esters. Macromolecules 2007;40:4154–8.
[52] Akimoto J, Nakayama M, Sakai K, Okano T. Molecular design of outermost surface functionalized thermoresponsive polymeric micelles with biodegradable cores. J Polym Sci Part A: Polym Chem 2008;46:7127–37.
[53] Akimoto J, Nakayama M, Sakai K, Okano T. Temperature-induced intracellular uptake of thermoresponsive polymeric micelles. Biomacromolecules 2009;10:1331–6.
[54] Li W, Li J, Gao J, Li B, Xia Y, Meng Y, et al. The fine-tuning of thermosensitive and degradable polymer micelles for enhancing intracellular uptake and drug release in tumors. Biomaterials 2011;32:3832–44.
[55] Shi PJ, Li YG, Pan CY. Block and star block copolymers by mechanism transformation X. Synthesis of poly(ethylene oxide) methyl ether/polystyrene/poly(L-lactide) ABC miktoarm star copolymers by combination of RAFT and ROP. Eur Polym J 2004;40:1283–90.
[56] Han DH, Pan CY. Preparation and characterization of heteroarm H-shaped terpolymers by combination of reversible addition-fragmentation transfer polymerization and ring-opening polymerization. J Polym Sci Part A: Polym Chem 2007;45:789–99.
[57] Saeed AO, Dey S, Howdle SM, Thurecht KJ, Alexander C. One-pot controlled synthesis of biodegradable and biocompatible co-polymer micelles. J Mater Chem 2009;19:4529–35.
[58] Mespouille L, Nederberg F, Hedrick JL, Dubois P. Broadening the scope of functional groups accessible in aliphatic polycarbonates by the introduction of RAFT initiating sites. Macromolecules 2009;42:6319–21.
[59] Isik M, Sardon H, Saenz M, Mecerreyes D. New amphiphilic block copolymers from lactic acid and cholinium building units. RSC Adv 2014;4:53407–10.
[60] Sun L, Petzetakis N, Pitto-Barry A, Schiller TL, Kirby N, Keddie DJ, et al. Tuning the size of cylindrical micelles from poly(L-lactide)-b-poly(acrylic acid) diblock copolymers based on crystallization-driven self-assembly. Macromolecules 2013;46:9074–82.
[61] Sun L, Pitto-Barry A, Kirby N, Schiller TL, Sanchez AM, Dyson MA, et al. Structural reorganization of cylindrical nanoparticles triggered by polylactide stereocomplexation. Nat Commun 2014;5:5746:1–9.
[62] Yildirim I, Crotty S, Loh CH, Festag G, Weber C, Caponi PF, et al. End-functionalized polylactides using a calcium-based precatalyst: synthesis and insights by mass spectrometry. J Polym Sci Part A: Polym Chem 2016;54:437–48.
[63] Petzetakis N, Dove AP, O'Reilly RK. Cylindrical micelles from the living crystallization-driven self-assembly of poly(lactide)-containing block copolymers. Chem Sci 2011;2:955–60.
[64] Blunden BM, Lu H, Stenzel MH. Enhanced delivery of the RAPTA-C macromolecular chemotherapeutic by conjugation to degradable polymeric micelles. Biomacromolecules 2013;14:4177–88.
[65] Hales M, Barner-Kowollik C, Davis TP, Stenzel MH. Shell-cross-linked vesicles synthesized from block copolymers of poly(D,L-lactide) and poly(N-isopropyl acrylamide) as thermoresponsive nanocontainers. Langmuir 2004;20:10809–17.
[66] Ting SRS, Gregory AM, Stenzel MH. Polygalactose containing nanocages: the RAFT process for the synthesis of hollow sugar balls. Biomacromolecules 2009;10:342–52.
[67] You Y, Hong C, Wang W, Lu W, Pan C. Preparation and characterization of thermally responsive and biodegradable block copolymer comprised of PNIPAAM and PLA by combination of ROP and RAFT methods. Macromolecules 2004;37:9761–7.
[68] Robin MP, Wilson P, Mabire AB, Kiviaho JK, Raymond JE, Haddleton DM, et al. Conjugation-induced fluorescent labeling of proteins and polymers using dithiomaleimides. J Am Chem Soc 2013;135:2875–8.
[69] Robin MP, Mabire AB, Damborsky JC, Thom ES, Winzer-Serhan UH, Raymond JE, et al. New functional handle for use as a self-reporting contrast and delivery agent in nanomedicine. J Am Chem Soc 2013;135:9518–24.
[70] Mabire AB, Robin MP, Willcock H, Pitto-Barry A, Kirby N, O'Reilly RK. Dual effect of thiol addition on fluorescent polymeric micelles: ON-to-OFF emissive switch and morphology transition. Chem Commun 2014;50:11492–5.
[71] Ye C, Zhao G, Zhang M, Du J, Zhao Y. Precise synthesis of ABCDE star quintopolymers by combination of controlled polymerization and azide–alkyne cycloaddition reaction. Macromolecules 2012;45:7429–39.
[72] Themistou E, Battaglia G, Armes SP. Facile synthesis of thiol-functionalized amphiphilic polylactide-methacrylic diblock copolymers. Polym Chem 2014;5:1405–17.
[73] Kang HU, Yu YC, Shin SJ, Youk JH. One-step synthesis of block copolymers using a hydroxyl-functionalized trithiocarbonate RAFT agent as a dual initiator for RAFT polymerization and ROP. J Polym Sci Part A: Polym Chem 2013;51:774–9.
[74] Shin SJ, Yu YC, Seo JD, Cho SJ, Youk JH. One-step synthesis of poly(N-vinylpyrrolidone)-b-poly(L-lactide) block copolymers using a dual initiator for RAFT polymerization and ROP. J Polym Sci Part A: Polym Chem 2014;52:1607–13.
[75] Seo M, Murphy CJ, Hillmyer MA. One-step synthesis of cross-linked block polymer precursor to a nanoporous thermoset. ACS Macro Lett 2013;2:617–20.
[76] Nicolas J, Guillaneuf Y, Lefay C, Bertin D, Gigmes D, Charleux B. Nitroxide-mediated polymerization. Prog Polym Sci 2013;38:63–235.
[77] Grubbs RB. Nitroxide-mediated radical polymerization: limitations and versatility. Polym Rev 2011;51:104–37.
[78] Vinas J, Chagneux N, Gigmes D, Trimaille T, Favier A, Bertin D. SG1-based alkoxyamine bearing a N-succinimidyl ester: a versatile tool for advanced polymer synthesis. Polymer 2008;49:3639–47.
[79] Bosman AW, Vestberg R, Heumann A, Fréchet JMJ, Hawker CJ. A modular approach toward functionalized three-dimensional macromolecules: From synthetic concepts to practical applications. J Am Chem Soc 2003;125:715–28.
[80] Choi J, Hermans TM, Lohmeijer BGG, Pratt RC, Dubois G, Frommer J, et al. Monolayered organosilicate toroids and related structures: A phase diagram for templating from block copolymers. Nano Lett 2006;6:1761–4.
[81] Hermans TM, Choi J, Lohmeijer BGG, Dubois G, Pratt RC, Kim H-C, et al. Application of solvent-directed assembly of block copolymers to the synthesis of nanostructured materials with low dielectric constants. Angew Chem Int Ed 2006;45:6648–52.
[82] Kim SH, Nederberg F, Zhang L, Wade CG, Waymouth RM, Hedrick JL. Hierarchical assembly of nanostructured organosilicate networks via stereocomplexation of block copolymers. Nano Lett 2008;8:294–301.
[83] Kim SH, Tan JPK, Nederberg F, Fukushima K, Yang YY, Waymouth RM, et al. Mixed micelle formation through stereocomplexation between enantiomeric poly(lactide) block copolymers. Macromolecules 2009;42:25–9.
[84] Ho RM, Chiang YW, Tsai CC, Lin CC, Ko BT, Huang BH. Three-dimensionally packed nanohelical phase in chiral block copolymers. J Am Chem Soc 2004;126:2704–5.
[85] Jabbar R, Graffe A, Lessard B, Marić M. Nitroxide-mediated synthesis of styrenic-based segmented and tapered block copolymers using poly(lactide)-functionalized TEMPO macromediators. J Appl Polym Sci 2008;109:3185–95.
[86] Poirier V, Duc M, Carpentier J-F, Sarazin Y. One-pot synthesis of lactide–styrene diblock copolymers via catalytic immortal ring-opening polymerization of lactide and nitroxide-mediated polymerization of styrene. ChemSusChem 2010;3:579–90.
[87] Hsiue GH, Lo CL, Cheng CH, Lin CP, Huang CK, Chen HH. Preparation and characterization of poly(2-methacryloyloxyethyl phosphorylcholine)-block-poly(D,L-lactide) polymer nanoparticles. J Polym Sci Part A: Polym Chem 2007;45:688–98.
[88] Liu G, Hu X, Chen C, Jin Q, Ji J. Self-assembly and degradation of poly[(2-methacryloyloxyethyl phosphorylcholine)-block-(D,L-lactide)] diblock copolymers: large compound micelles to vesicles. Polym Int 2011;60:578–83.
[89] Liu G, Hu X, Chen C, Ji J. Construct biomimetic giant vesicles via self-assembly of poly(2-methacryloyloxyethyl phosphorylcholine)-block-poly(D, L-lactide). J Appl Polym Sci 2010;118:3197–202.
[90] Lee SH, Kim SH, Han YK, Kim YH. Synthesis and degradation of end-group-functionalized polylactide. J Polym Sci Part A: Polym Chem 2001;39:973–85.
[91] Messman JM, Scheuer AD, Storey RF. Synthesis and characterization of A–B–A triblock copolymers derived from chloro-telechelic poly(L-lactide): combining ring-opening polymerization (ROP) and atom transfer radical polymerization (ATRP). Polymer 2005;46:3628–38.
[92] Spasova M, Mespouille L, Coulembier O, Paneva D, Manolova N, Rashkov I, et al. Amphiphilic poly(D- or L-lactide)-b-poly(N,N-dimethylamino-2-ethyl methacrylate) block copolymers: controlled synthesis, characterization, and stereocomplex formation. Biomacromolecules 2009;10:1217–23.
[93] Karanikolopoulos N, Zamurovic M, Pitsikalis M, Hadjichristidis N. Poly(DL-lactide)-b-poly(N,N-dimethylamino-2-ethyl methacrylate): synthesis, characterization, micellization behavior in aqueous solutions, and encapsulation of the hydrophobic drug dipyridamole. Biomacromolecules 2010;11:430–8.
[94] Kryuchkov MA, Detrembleur C, Jérôme R, Prud'homme RE, Bazuin CG. Synthesis and thermal properties of linear amphiphilic diblock copolymers of L-lactide and 2-dimethylaminoethyl methacrylate. Macromolecules 2011;44:5209–17.
[95] Choochottiros C, Park E, Chin I-J. Synthesis and characterization of polylactide–poly(methyl methacrylate) copolymer by combining of ROP and AGET ATRP. J Ind Eng Chem 2012;18:993–1000.
[96] Yang Y, Li J, Hu M, Chen L, Bi Y. Well-defined poly(DL-lactide)-b-poly(N-vinylcaprolactam) copolymers: synthesis, solution properties and in vitro degradation. J Polym Res 2014;21:549:1–9.
[97] Bagheri M, Motirasoul F. Synthesis, characterization, and micellization of cholesteryl-modified amphiphilic poly(L-lactide)-block-poly(glycidyl methacrylate) as a nanocarrier for hydrophobic drugs. J Polym Res 2013;20:59:1–9.
[98] Hu Y, Darcos V, Monge S, Li S. Thermo-responsive drug release from self-assembled micelles of brush-like PLA/PEG analogues block copolymers. Int J Pharm 2015;491:152–61.

Please cite this article in press as: Yildirim I, et al. Old meets new: Combination of PLA and RDRP to obtain sophisticated macromolecular architectures. Prog Polym Sci (2017), http://dx.doi.org/10.1016/j.progpolymsci.2017.07.010

[99] Hu Y, Darcos V, Monge S, Li S, Zhou Y, Su F. Thermo-responsive release of curcumin from micelles prepared by self-assembly of amphiphilic P(NIPAAm-co-DMAAm)-b-PLLA-b-P(NIPAAm-co-DMAAm) triblock copolymers. Int J Pharm 2014;476:31–40.
[100] Bakkour Y, Darcos V, Coumes F, Li S, Coudane J. Brush-like amphiphilic copolymers based on polylactide and poly(ethylene glycol): synthesis, self-assembly and evaluation as drug carrier. Polymer 2013;54:1746–54.
[101] Hu Y, Darcos V, Monge S, Li S. Synthesis and self-assembling of poly(N-isopropylacrylamide-block-poly(L-lactide)-block-poly(N-isopropylacrylamide) triblock copolymers prepared by combination of ring-opening polymerization and atom transfer radical polymerization. J Polym Sci Part A: Polym Chem 2013;51:3274–83.
[102] Hu Y, Darcos V, Monge S, Li S, Zhou Y, Su F. Tunable thermo-responsive P(NIPAAm-co-DMAAm)-b-PLLA-b-P(NIPAAm-co-DMAAm) triblock copolymer micelles as drug carriers. J Mater Chem B 2014;2:2738–48.
[103] Cunningham A, Oh JK. New design of thiol-responsive degradable polylactide-based block copolymer micelles. Macromol Rapid Commun 2013;34:163–8.
[104] Ko NR, Oh JK. Glutathione-triggered disassembly of dual disulfide located degradable nanocarriers of polylactide-based block copolymers for rapid drug release. Biomacromolecules 2014;15:3180–9.
[105] Johnson RM, Fraser CL. Iron tris(bipyridine)-centered star block copolymers: chelation of triblock macroligands generated by ROP and ATRP. Macromolecules 2004;37:2718–27.
[106] Johnson RM, Fraser CL. Metalloinitiation routes to biocompatible poly(lactic acid) and poly(acrylic acid) stars with luminescent ruthenium tris(bipyridine) cores. Biomacromolecules 2004;5:580–8.
[107] Zhao L, Zhang X, Yao Y, Yu C, Yang J. Synthesis of Y-shaped copolymers containing phenylborate ester and biodegradable poly(lactic acid) blocks and their glucose-sensitive behavior for controlled insulin release. Macromol Chem Phys 2014;215:1609–19.
[108] Xu F, Zheng SZ, Luo YL. Thermosensitive t-PLA-b-PNIPAAm tri-armed star block copolymer nanoscale micelles for camptothecin drug release. J Polym Sci Part A: Polym Chem 2013;51:4429–39.
[109] Zhao Y, Shuai X, Chen C, Xi F. Synthesis of novel dendrimer-like star block copolymers with definite numbers of arms by combination of ROP and ATRP. Chem Commun 2004;160:8–9.
[110] Zhao Y, Shuai X, Chen C, Xi F. Synthesis of star block copolymers from dendrimer initiators by combining ring-opening polymerization and atom transfer radical polymerization. Macromolecules 2004;37:8854–62.
[111] Yuan W, Yuan J, Zheng S, Hong X. Synthesis, characterization, and controllable drug release of dendritic star-block copolymer by ring-opening polymerization and atom transfer radical polymerization. Polymer 2007;48:2585–94.
[112] Yao N, Lin W, Zhang X, Gu H, Zhang L. Amphiphilic β-cyclodextrin-based star-like block copolymer unimolecular micelles for facile in situ preparation of gold nanoparticles. J Polym Sci Part A: Polym Chem 2016;54:186–96.
[113] Stanford MJ, Dove AP. One-pot synthesis of α, ω-Chain end functional, stereoregular, star-Shaped poly(lactide). Macromolecules 2009;42:141–7.
[114] Zhang W, Wang S, Li X, Yuan J, Wang S. Organic/inorganic hybrid star-shaped block copolymers of poly(L-lactide) and poly(N-isopropylacrylamide) with a polyhedral oligomeric silsesquioxane core: synthesis and self-assembly. Eur Polym J 2012;48:720–9.
[115] Li J, Ren J, Cao Y, Yuan W. Synthesis of biodegradable pentaarmed star-block copolymers via an asymmetric BIS-TRIS core by combination of ROP and RAFT: From star architectures to double responsive micelles. Polymer 2010;51:1301–10.
[116] Rzayev J, Hillmyer MA. Nanoporous polystyrene containing hydrophilic pores from an ABC triblock copolymer precursor. Macromolecules 2005;38:3–5.
[117] Rzayev J, Hillmyer MA. Nanochannel array plastics with tailored surface chemistry. J Am Chem Soc 2005;127:13373–9.
[118] Phillip WA, Rzayev J, Hillmyer MA, Cussler EL. Gas and water liquid transport through nanoporous block copolymer membranes. J Membr Sci 2006;286:144–52.
[119] Kim JC, Seo M, Hillmyer MA, Francis LF. Magnetic microrheology of block copolymer solutions. ACS Appl Mater Interfaces 2013;5:11877–83.
[120] Crossland EJW, Ludwigs S, Hillmyer MA, Steiner U. Freestanding nanowire arrays from soft-etch block copolymer templates. Soft Matter 2007;3:94–8.
[121] Chen L, Phillip WA, Cussler EL, Hillmyer MA. Robust nanoporous membranes templated by a doubly reactive block copolymer. J Am Chem Soc 2007;129:13786–7.
[122] Chen L, Hillmyer MA. Mechanically and thermally robust ordered nanoporous monoliths using norbornene-functional block polymers. Macromolecules 2009;42:4237–43.
[123] Seo M, Amendt MA, Hillmyer MA. Cross-linked nanoporous materials from reactive and multifunctional block polymers. Macromolecules 2011;44:9310–8.
[124] Seo M, Hillmyer MA. Reticulated nanoporous polymers by controlled polymerization-induced microphase separation. Science 2012;336:1422–5.
[125] Saba SA, Mousavi MPS, Bühlmann P, Hillmyer MA. Hierarchically porous polymer monoliths by combining controlled macro- and microphase separation. J Am Chem Soc 2015;137:8896–9.
[126] Seo M, Kim S, Oh J, Kim SJ, Hillmyer MA. Hierarchically porous polymers from hyper-cross-linked block polymer precursors. J Am Chem Soc 2015;137:600–3.
[127] Barz M, Armiñán A, Canal F, Wolf F, Koynov K, Frey H, et al. P(HPMA)-block-P(LA) copolymers in paclitaxel formulations: polylactide stereochemistry controls micellization, cellular uptake kinetics, intracellular localization and drug efficiency. J Control Release 2012;163:63–74.
[128] Barz M, Wolf FK, Canal F, Koynov K, Vicent MJ, Frey H, et al. Synthesis, characterization and preliminary biological evaluation of P(HPMA)-b-P(LLA) copolymers: a new type of functional biocompatible block copolymer. Macromol Rapid Commun 2010;31:1492–500.
[129] Dai XH, Wang ZM, Liu W, Dong CM, Pan JM, Yuan SS, et al. Biomimetic star-shaped porphyrin-cored poly(L-lactide)-b-glycopolymer block copolymers for targeted photodynamic therapy. Colloid Polym Sci 2014;292:2111–22.
[130] Dai XH, Jin H, Cai MH, Wang H, Zhou ZP, Pan JM, et al. Fabrication of thermosensitive, star-shaped poly(L-lactide)-block-poly(N-isopropylacrylamide) copolymers with porphyrin core for photodynamic therapy. React Funct Polym 2015;89:9–17.
[131] Ramesh K, Mishra AK, Patel VK, Vishwakarma NK, Biswas CS, Paira TK, et al. Synthesis of well-defined amphiphilic poly(D,L-lactide)-b-poly(N-vinylpyrrolidone) block copolymers using ROP and xanthate-mediated RAFT polymerization. Polymer 2012;53:5743–53.
[132] Hira SK, Ramesh K, Gupta U, Mitra K, Misra N, Ray B, et al. Methotrexate-loaded four-arm star amphiphilic block copolymer elicits CD8+ T cell response against a highly aggressive and metastatic experimental lymphoma. ACS Appl Mater Interfaces 2015;7:20021–33.
[133] Clément B, Trimaille T, Alluin O, Gigmes D, Mabrouk K, Féron F, et al. Convenient access to biocompatible block copolymers from SG1-based aliphatic polyester macro-alkoxyamines. Biomacromolecules 2009;10:1436–45.
[134] Clément B, Decherchi P, Féron F, Bertin D, Gigmes D, Trimaille T, et al. Poly(D,L-Lactide)-block-poly(2-hydroxyethyl acrylate) block copolymers as potential biomaterials for peripheral nerve repair: in vitro and in vivo degradation studies. Macromol Biosci 2011;11:1175–84.
[135] Handké N, Trimaille T, Luciani E, Rollet M, Delair T, Verrier B, et al. Elaboration of densely functionalized polylactide nanoparticles from N-acryloxysuccinimide-based block copolymers. J Polym Sci Part A: Polym Chem 2011;49:1341–50.
[136] Handké N, Lahaye V, Bertin D, Delair T, Verrier B, Gigmes D, et al. Elaboration of glycopolymer-functionalized micelles from an N-vinylpyrrolidone/lactide-based reactive copolymer platform. Macromol Biosci 2013;13:1213–20.
[137] Han DH, Pan CY. Simple route for synthesis of H-shaped copolymers. J Polym Sci Part A: Polym Chem 2006;44:2794–801.
[138] Kong LZ, Pan CY. Preparation of dendrimer-like copolymers based on polystyrene and poly(L-lactide) and formation of hollow microspheres. Polymer 2008;49:200–10.
[139] Yuan W, Zhang J, Wei J, Zhang C, Ren J. Synthesis and self-assembly of pH-responsive amphiphilic dendritic star-block terpolymer by the combination of ROP, ATRP and click chemistry. Eur Polym J 2011;47:949–58.
[140] Vora A, Singh K, Webster DC. A new approach to 3-miktoarm star polymers using a combination of reversible addition–fragmentation chain transfer (RAFT) and ring opening polymerization (ROP) via click chemistry. Polymer 2009;50:2768–74.
[141] Ozlem S, Iskin B, Yilmaz G, Kukut M, Hacaloglu J, Yagci Y. Synthesis and pyrolysis of ABC type miktoarm star copolymers with polystyrene, poly(lactic acid) and poly(ethylene glycol) arms. Eur Polym J 2012;48:1755–67.
[142] Wu C, Ying A, Ren S. Fabrication of polymeric micelles with core–shell–corona structure for applications in controlled drug release. Colloid Polym Sci 2013;291:827–34.
[143] Lutz JF, Jahed N, Matyjaszewski K. Preparation and characterization of graft terpolymers with controlled molecular structure. J Polym Sci Part A: Polym Chem 2004;42:1939–52.
[144] Shinoda H, Matyjaszewski K. Structural control of poly(methyl methacrylate)-g-poly(lactic acid) graft copolymers by atom transfer radical polymerization (ATRP). Macromolecules 2001;34:6243–8.
[145] Wu C, Ying A, Ren S. Synthesis of stimuli responsive graft triblock polymers via combination of reversible addition-fragmentation chain transfer polymerization and ring opening polymerization. Asian J Chem 2013;25:3344–8.
[146] Hawker CJ, Mecerreyes D, Elce E, Dao J, Hedrick JL, Barakat I, et al. Living free radical polymerization of macromonomers: preparation of well defined graft copolymers. Macromol Chem Phys 1997;198:155–66.
[147] Barakat I, Dubois P, Jérôme R, Teyssié P, Goethals E. Macromolecular engineering of polylactones and polylactides XV. Poly(D,L)-lactide macromonomers as precursors of biocompatible graft copolymers and bioerodible gels. J Polym Sci Part A: Polym Chem 1994;32:2099–110.
[148] Petzetakis N, Pitsikalis M, Titanium-mediated Hadjichristidis N. [CpTiCl2(OEt)] ring-opening polymerization of lactides: a novel route to well-defined polylactide-based complex macromolecular architectures. J Polym Sci Part A: Polym Chem 2010;48:1092–103.
[149] Yildirim I, Bus T, Sahn M, Yildirim T, Kalden D, Hoeppener S, et al. Fluorescent amphiphilic heterografted comb polymers comprising biocompatible PLA and PEtOx side chains. Polym Chem 2016;7:6064–74.
[150] He J, Yang X, Mao J, Xu F, Cai Q. Hydroxyapatite–poly(L-lactide) nanohybrids via surface-initiated ATRP for improving bone-like apatite-formation abilities. Appl Surf Sci 2012;258:6823–30.

Please cite this article in press as: Yildirim I, et al. Old meets new: Combination of PLA and RDRP to obtain sophisticated macromolecular architectures. Prog Polym Sci (2017), http://dx.doi.org/10.1016/j.progpolymsci.2017.07.010

[151] Jérôme R, Mecerreyes D, Tian D, Dubois P, Hawker CJ, Trollsas M, et al. Synthesis of novel polymeric materials based on aliphatic polyesters by combination of different controlled polymerization methods. Macromol Symp 1998;132:385–403.
[152] Bagheri M, Bigdeli E. Preparation of stealth micellar nanoparticles of novel biodegradable and biocompatible brush copolymers with cholesteryl-modified PLA and PEG side chains. J Polym Res 2013;20:84:1–11.
[153] Coulembier O, Moins S, De Winter J, Gerbaux P, Leclère P, Lazzaroni R, et al. From jellyfish macromolecular architectures to nanodoughnut self-assembly. Macromolecules 2010;43:575–9.
[154] Xia Y, Olsen BD, Kornfield JA, Grubbs RH. Efficient synthesis of narrowly dispersed brush copolymers and study of their assemblies: the importance of side chain arrangement. J Am Chem Soc 2009;131:18525–32.
[155] Sveinbjörnsson BR, Weitekamp RA, Miyake GM, Xia Y, Atwater HA, Grubbs RH. Rapid self-assembly of brush block copolymers to photonic crystals. Proc Natl Acad Sci U S A 2012;109:14332–6.
[156] Hong SW, Gu W, Huh J, Sveinbjornsson BR, Jeong G, Grubbs RH, et al. On the self-assembly of brush block copolymers in thin films. ACS Nano 2013;7:9684–92.
[157] Li Y, Themistou E, Zou J, Das BP, Tsianou M, Cheng C. Facile synthesis and visualization of janus double-brush copolymers. ACS Macro Lett 2012;1:52–6.
[158] Zhao C, Wu D, Huang N, Zhao H. Crystallization and thermal properties of PLLA comb polymer. J Polym Sci Part B: Polym Phys 2008;46:589–98.
[159] Bedair TM, Cho Y, Joung YK, Han DK. Biodegradable polymer brush as nanocoupled interface for improving the durability of polymer coating on metal surface. Colloids Surf B: Biointerfaces 2014;122:808–17.
[160] Zhao H, Kang X, Liu L. Comb-coil polymer brushes on the surface of silica nanoparticles. Macromolecules 2005;38:10619–22.
[161] Wu D, Zhao C, Tian J, Zhao H. Synthesis of PLLA-PEOMA comb-block-comb type molecular brushes based on AGET ATRP and ring-opening polymerization. Polym Int 2009;58:1335–40.
[162] Wu D, Yang Y, Cheng X, Liu L, Tian J, Zhao H. Mixed molecular brushes with PLLA and PS side chains prepared by AGET ATRP and ring-opening polymerization. Macromolecules 2006;39:7513–9.
[163] Ydens I, Degée P, Dubois P, Libiszowski J, Duda A, Penczek S. Combining ATRP of methacrylates and ROP of L,L-dilactide and ε-caprolactone. Macromol Chem Phys 2003;204:171–9.
[164] Yang YQ, Guo XD, Lin WJ, Zhang LJ, Zhang CY, Qian Y. Amphiphilic copolymer brush with random pH-sensitive/hydrophobic structure: synthesis and self-assembled micelles for sustained drug delivery. Soft Matter 2012;8:454–64.
[165] Kakwere H, Perrier S. Facile synthesis of star-shaped copolymers via combination of RAFT and ring opening polymerization. J Polym Sci Part A: Polym Chem 2009;47:6396–408.
[166] Luan B, Zhang BQ, Pan CY. Synthesis and characterizations of well-defined branched polymers with AB2 branches by combination of RAFT polymerization and ROP as well as ATRP. J Polym Sci Part A: Polym Chem 2006;44:549–60.
[167] Luo H, Santos JL, Herrera-Alonso M. Toroidal structures from brush amphiphiles. Chem Commun 2014;50:536–8.
[168] Shi GY, Zou P, Pan CY. Synthesis and characterization of asymmetric centipede-like copolymers with two side chains at each repeating unit via ATRP and ring-opening polymerization. J Polym Sci Part A: Polym Chem 2008;46:5580–91.
[169] Huang K, Rzayev J. Well-defined organic nanotubes from multicomponent bottlebrush copolymers. J Am Chem Soc 2009;131:6880–5.
[170] Huang K, Jacobs A, Rzayev J. De novo synthesis and cellular uptake of organic nanocapsules with tunable surface chemistry. Biomacromolecules 2011;12:2327–34.
[171] Huang K, Rzayev J. Charge and size selective molecular transport by amphiphilic organic nanotubes. J Am Chem Soc 2011;133:16726–9.
[172] Huang K, Johnson M, Rzayev J. Synthesis of degradable organic nanotubes by bottlebrush molecular templating. ACS Macro Lett 2012;1:892–5.
[173] Huang K, Canterbury DP, Rzayev J. Organosoluble polypyrrole nanotubes from core-shell bottlebrush copolymers. Chem Commun 2010;46:6326–8.
[174] Onbulak S, Rzayev J. Cylindrical nanocapsules from photo-cross-linkable core-shell bottlebrush copolymers. Polym Chem 2015;6:764–71.
[175] Fenyves R, Schmutz M, Horner IJ, Bright FV, Rzayev J. Aqueous self-assembly of giant bottlebrush block copolymer surfactants as shape-tunable building blocks. J Am Chem Soc 2014;136:7762–70.
[176] Rzayev J. Synthesis of polystyrene-polylactide bottlebrush block copolymers and their melt self-assembly into large domain nanostructures. Macromolecules 2009;42:2135–41.
[177] Zhao L, Byun M, Rzayev J, Lin Z. Polystyrene-polylactide bottlebrush block copolymer at the air/water interface. Macromolecules 2009;42:9027–33.
[178] Bolton J, Bailey TS, Rzayev J. Large pore size nanoporous materials from the self-assembly of asymmetric bottlebrush block copolymers. Nano Lett 2011;11:998–1001.
[179] Han W, Byun M, Zhao L, Rzayev J, Lin Z. Controlled evaporative self-assembly of hierarchically structured bottlebrush block copolymer with nanochannels. J Mater Chem 2011;21:14248–53.
[180] Bolton J, Rzayev J. Synthesis and melt self-assembly of PS–PMMA–PLA triblock bottlebrush copolymers. Macromolecules 2014;47:2864–74.
[181] Huang K, Canterbury DP, Rzayev J. Synthesis of segmented polylactide molecular brushes and their transformation to open-end nanotubes. Macromolecules 2010;43:6632–8.

Please cite this article in press as: Yildirim I, et al. Old meets new: Combination of PLA and RDRP to obtain sophisticated macromolecular architectures. Prog Polym Sci (2017), http://dx.doi.org/10.1016/j.progpolymsci.2017.07.010

Publication P2

"Reversible oligomerization of 3-aryl-2-cyanothioacrylamides *via* [2_s + 4_s] cycloaddition to substituted 3,4-dihydro-*2H*-thiopyrans"

Julia Kötteritzsch, Stefan Bode, Ilknur Yildirim, Christine Weber, Martin D. Hager, Ulrich S. Schubert

Des. Monomers Polym. **2015**, *18*, 627–640.

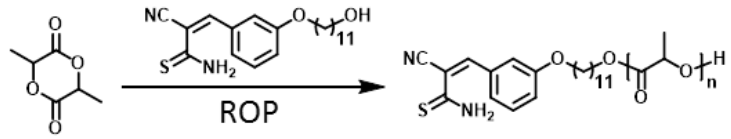

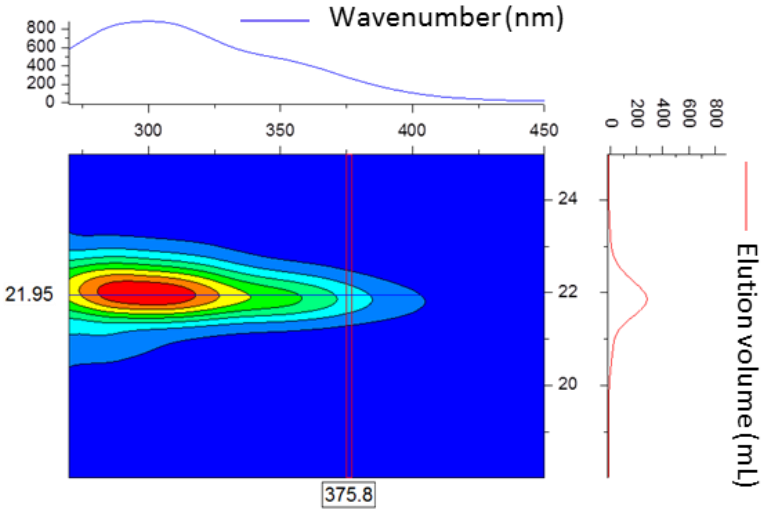

Designed Monomers and Polymers, 2015
Vol. 18, No. 7, 627–640, http://dx.doi.org/10.1080/15685551.2015.1058007

Reversible oligomerization of 3-aryl-2-cyanothioacrylamides via [2_s + 4_s] cycloaddition to substituted 3,4-dihydro-2*H*-thiopyrans

Julia Kötteritzsch[a,b], Stefan Bode[a,b], Ilknur Yildirim[a,b], Christine Weber[a,b], Martin D. Hager[a,b]* and Ulrich S. Schubert[a,b]*

[a]*Laboratory for Organic and Macromolecular Chemistry (IOMC), Friedrich Schiller University Jena, Humboldtstr. 10, Jena 07743, Germany;* [b]*Jena Center for Soft Matter (JCSM), Friedrich Schiller University Jena, Philosophenweg 7, Jena 07743, Germany*

(*Received 26 February 2015; accepted 19 May 2015*)

Novel difunctional monomers are synthesized which are able to dimerize as well as oligomerize via the hetero-Diels–Alder (HDA) mechanism. These monomers are based on 3-aryl-2-cyanothioacrylamides, which are used as functional units for the HDA reaction to form 3,4-dihydro-2*H*-thiopyrans. Different substituents of the aromatic ring are utilized to shift the equilibrium to the dimeric or oligomeric species. The HDA reaction is reversible and can be influenced by the temperature as well as the concentration. In contrast, the *N,N*-dimethylthioacrylamide analogues do not dimerize or the dimerization is not reversible. The most promising compound is furthermore investigated in detail by ^{1}H NMR spectroscopy to elucidate the dimerization kinetics. In addition, a difunctional molecule is able to oligomerize reversibly, as confirmed by means of ^{1}H NMR, size exclusion chromatography (SEC), and ESI MS measurements. A respective alcohol is employed as initiator for the ring-opening polymerization of L-lactide resulting in an end-functional polymer that undergoes reversible dimerization as confirmed by SEC measurements.

Keywords: dimers; initiator; molecular dynamics; oligomers; hetero-Diels–Alder; self-organization

1. Introduction

In recent years, the research on self-healing materials has developed rapidly due to a strong interest from both sides, fundamental research and application. To achieve intrinsic self-healing abilities of the material, in particular the Diels–Alder (DA) cycloaddition has been applied in many materials, because the original properties of the materials do not change significantly.[1–3] Due to the thermal reversibility of the retro-Diels–Alder (rDA) reaction, it is possible to obtain self-healing polymers with well-defined architectures and properties.[4,5] The DA reaction of furan and maleimide is the commonly used functional system for most reversible self-healing polymers of this type. However, the major drawback of the DA cycloaddition of maleimide and furan is the required high temperature (120 to 180 °C) of the rDA reaction, resulting in self-healing materials that can only be healed when rather drastic conditions are applied.[6,7]

In order to achieve lower rDA temperatures, hetero-Diels–Alder (HDA) systems could represent an interesting alternative for the utilization of reversible crosslinking and post-polymerization functionalization of polymers, respectively. For example, the highly electron-deficient dithioesters that are present as end-groups of polymers obtained via the reversible addition–fragmentation chain transfer polymerization using specially designed chain transfer agents have been utilized for HDA reactions by Barner-Kowollik and coworkers.[8–18] Networks based on tetrafunctional dithioesters and bifunctional cyclopentadiene showed self-healing behavior.[19]

Moreover, Lehn and coworkers investigated highly reversible and dynamic DA systems.[20–22] Various dienes and dienophiles were screened regarding their reversibility of the DA reaction. In particular, functionalized fulvenes have been utilized. These materials, bearing biologically active groups, have been converted with cyano-olefins. Both compounds react rapidly; the DA reaction is reversible in the temperature range from −10 to +50 °C. The variation of these functional units resulted in a new generation of highly dynamic polymers.[20,21] Furthermore, the DA reactions between 9,10-dimethylanthracene and cyano-functionalized dienophiles, e.g., dienes as well as tricyanoethynylethylenes, have been investigated.[22]

Another interesting reaction is the reversible HDA (i.e. dimerization) of 3-aryl-2-cyanothioacrylamides. The first systems were published by Brunskill et al. who reported the thermal dimerization of various 3-aryl-2-cyanothioacrylamides resulting in different derivatives of 3,4-dihydro-2*H*-thiopyrans.[23,24] ^{1}H NMR and IR data are reported for all 21 thioacrylamides in monomeric and/or dimeric form. Later, the authors investigated the effect of the substituents of the aryl group on the reversible

*Corresponding authors. Email: martin.hager@uni-jena.de (M.D. Hager); ulrich.schubert@uni-jena.de (U.S. Schubert)

dimerization of 3-aryl-2-cyanothioacrylamides.[24] The equilibrium constants have been determined by ^{1}H NMR spectroscopy. Furthermore, Bloxham and Dell reported the reaction of these 3-aryl-2-cyanothioacrylamides with methyl propiolate and dimethyl acetylenedicarboxylate in 1994 and observed the dimerization of selected derivates.[25]

Due to the reversible dimerization of 3-aryl-2-cyanothioacrylamides, these systems represent interesting candidates for monomers and reversible binding units, respectively. To establish self-healing polymeric or oligomeric systems, the functional moiety should meet two major requirements: a reversible HDA must take place in a 'user-friendly' temperature range, and a further functionalization must be possible to incorporate the reversible linkage into polymers.

2. Experimental procedures

2.1. Materials and instrumentation

All chemicals were purchased from Fluka, Aldrich, Acros Organics as well as Alfa Aesar and were used without further purification unless otherwise specified. The solvents were purchased from Biosolve, Aldrich as well as Acros Organics. Benzaldehyde was purified by distillation. Triethylamine was dried over $CaCl_2$. Ethanol was dried by distillation over sodium as well as toluene and THF by distillation over sodium and benzophenone; the solvents were kept under nitrogen using standard Schlenk techniques. L-lactide was purified by recrystallization from dry toluene and dried under vacuum. Sn $(Oct)_2$ was dried by distillation with toluene under reduced pressure. For preparative size exclusion chromatography (SEC), Biobeads SX-1 from BioRad were used.

1D (^{1}H, ^{13}C) nuclear magnetic resonance spectra were recorded on a Bruker AC 400 (400 MHz), Bruker AC 300 (300 MHz), and Bruker AC 250 (250 MHz) at 273, 298, 323, and 343 K. A delay time of 20–30 s was used for the calculations of the monomer to dimer ratio. Chemical shifts are reported in parts per million (ppm, δ scale) relative to the residual signal of the solvent. Coupling constants are given in Hz. The kinetic measurement at room temperature was done manually by daily measurements of the solution in the NMR tube, and the measurements at 50 and 70 °C were annealed and performed in the NMR spectrometer.

MALDI-TOF MS measurements were performed with an Ultraflex III TOF/TOF (Bruker Daltonics, Bremen, Germany) equipped with a smartbeam^{TM} laser and a collision cell. All spectra were measured in the positive reflector or linear mode. The instrument was calibrated prior to each measurement with an external PMMA standard $H(CH_2CCH_3COOCH_3)_nH + Na^+$ from Polymer Standards Services (PSS) GmbH (Mainz, Germany) in the required measurement range and *trans*-2-[3-(4-*tert*-butylphenyl)-2-methyl-2-propenylidene]-malononitrile (DCTB) (30 mg mL^{-1} in chloroform) was used as matrix. MS data were processed using the software Flex Analysis and DataExplorer 4.0 from Applied Biosystems (Foster City, CA, USA).

ESI-TOF MS measurements were performed using a micrOTOF (Bruker Daltonics) mass spectrometer, which was equipped with a syringe pump for sample injection and a standard electrospray ion source. The mass spectrometer was operating in the positive ion mode, and the data were processed with the micrOTOF control Version 3.0 and Data Analysis Version 4.0 SP2. The instrument was calibrated by a tunemix solution (*m/z* 50–3000) from Agilent.

CHN analysis was carried out on a Vario El III (Elementar) elemental analyzer.

SEC measurements were performed using an Agilent 1200 system (degasser, isocratic pump, autosampler, RI detector, DAD) as well as a Shimadzu system (degasser, isocratic pump, autosampler, RI detector) and two PSS GRAM (1000/30 Å, 10 µm particle size) columns in series (eluent: DMA with 2.1 g/L LiCl; flow rate of 1 mL/min at 40 °C) using linear PMMA and PS standards.

The melting points were measured using a Stuart™ melting point apparatus SMP3.

The flash column chromatography was carried out on a Biotage Isolera One System using Biotage SNAP Cartridges KP3Sil and a UV/vis detector.

The ring-opening polymerization (ROP) of L-lactide was performed under nitrogen in a MBraun UNILab glove box workstation.

UV/vis absorption spectra were recorded with a PerkinElmer Lambda 45 UV/vis spectrometer.

2.2. Synthesis

2,2′-(9,9-Didecyl-9*H*-fluorene-2,7-diyl)bis(1,3,2-dioxaborolane) was synthesized according to Kerszulis et al. with minor adoptions.[26] The aldehydes (**1a, 1d,** and **1e**) as well as 2-cyanoethanethioamide (**2b**) were purchased from Sigma-Aldrich and were used without further purification, besides benzaldehyde, as described above.

2.2.1. Synthesis of compounds **1b** and **1c** according to Piñol et al. [27]

*2.2.1.1. Synthesis of 4-(11-hydroxyundecyloxy)benzaldehyde (**1b**).* 4-Hydroxybenzaldehyde (2.5 g; 20.47 mmol) was dissolved in 50 mL dry dimethylformamide (DMF). Potassium carbonate (9.5 g; 68.74 mmol) and 11-bromo-1-undecanol (5.1 g; 20.30 mmol) were added, and the resulting mixture was heated for 24 h at 100 °C.

Subsequently, the DMF was evaporated and the residue was dissolved in 200 mL chloroform. The organic layer was washed with deionized water (three times 200 mL) and dried over sodium sulfate. The product was obtained by silica gel chromatography (silica, chloroform). Yield: 4.06 g (69%). ^{1}H NMR ($CDCl_3$, 300 MHz): δ = 1.30–1.85 (m, 18H), 3.63 (t, 2H, J = 6.6 Hz), 4.03 (t, 2H, J = 6.6 Hz), 6.98 (d, 2H, J = 8.7 Hz), 7.82 (d, 2H, J = 8.7 Hz), 9.87 (s, 1H) ppm. ^{13}C NMR ($CDCl_3$, 75 MHz): δ = 26.2, 26.4, 29.5, 29.7, 29.8, 29.9, 30.0, 33.2, 63.4, 68.9, 115.2, 130.2, 132.4, 164.7, 191.3 ppm.

*2.2.1.2. Synthesis of 3-(11-hydroxyundecyloxy)benzaldehyde (**1c**).* 3-Hydroxybenzaldehyde (2.0 g; 16.38 mmol) was dissolved in 50 mL dry DMF. Potassium carbonate (8.7 g; 62.95 mmol) and 11-bromo-1-undecanol (4.1 g; 16.32 mmol) were added, and the resulting mixture was heated for 24 h at 100 °C. Subsequently, the solution was filtered, the DMF was evaporated, and the residue was dissolved in 200 mL dichloromethane. The organic layer was washed with deionized water (three times 200 mL) and dried over magnesium sulfate. The product was obtained by flash column chromatography (silica, dichloromethane). Yield: 3.9 g (82%). ^{1}H NMR ($CDCl_3$, 300 MHz): δ = 1.30–1.85 (m, 18H), 3.65 (t, 2H, J = 6.0 Hz), 4.01 (t, 2H, J = 6.0 Hz), 7.1–7.2 (m, 1H), 7.3–7.5 (m, 3H), 9.97 (s, 1H) ppm. ^{13}C NMR ($CDCl_3$, 75 MHz): δ = 25.7, 26.0, 29.1, 29.3, 29.4, 29.5, 32.8, 63.0, 68.3, 112.8, 122.0 123.3, 130.0 137.8, 159.7, 192.2 ppm. $(C_{18}H_{28}O_3)$n (292.2)n: Calcd. C 73.93, H 9.65; Found C 74.27, H 9.77.

*2.2.2. Synthesis of 3,3′-(9,9-didecyl-9H-fluorene-2,7-diyl)bis(4-fluorobenzaldehyde) (**1f**)*

2,2′-(9,9-Didecyl-9*H*-fluorene-2,7-diyl)bis(1,3,2-dioxaborolane) (100 mg; 0.17 mmol), 3-bromo-4-fluorobenzaldehyde (84 mg; 0.41 mmol) and Pd(0)$(PPh_3)_4$ (6 mg; 0.01 mmol) were transferred to a microwave vial under nitrogen atmosphere. Potassium carbonate (113 mg; 0.82 mmol) and 6 drops Aliquat 366 dissolved in 3 mL H_2O and 16 mL toluene were added. The reaction mixture was stirred overnight at 120 °C. After cooling to room temperature, the mixture was washed with deionized water and dried over magnesium sulfate. The product was purified by flash column chromatography (silica, dichloromethane/*n*-hexane 1/1). Yield: 106 mg (90%). ^{1}H NMR ($CDCl_3$, 300 MHz): δ = 0.6–1.4 (m, 38H), 2.0–2.1 (m, 4H), 7.3–7.4 (m 2H), 7.55–7.65 (m, 4H), 7.8–7.95 (m, 4H), 8.05–8.15 (m, 2H) 10.07 (s, 2H) ppm. ^{13}C NMR ($CDCl_3$, 75 MHz): δ = 14.0, 22.6, 23.8, 29.2, 29.5, 29.9, 31.8, 40.2, 55.5, 117.1, 117.4, 120.2, 123.5, 127.9, 130.5, 130.6, 130.8, 132.7, 133.2, 133.3, 140.7, 151.6, 161.9, 165.3, 190.7 ppm. HR-ESI-TOF MS: $[C_{47}H_{56}F_2O_2]Na^+$ calcd.: m/z = 713.4141; found: m/z = 713.4100; error: 5.7 ppm.

*2.2.3. Synthesis of 2-cyano-N,N-dimethylethanethioamide (**2a**) according to Ransborg et al.* [28]

2-Cyano-*N,N*-dimethylacetamide (1.00 g; 8.92 mmol) was dissolved in 20 mL THF under nitrogen atmosphere. Lawesson's reagent (1.92 g; 4.73 mmol) was added, and the reaction was stirred for 20 h at room temperature. Subsequently, the solvent was removed under reduced pressure. The product was obtained by flash column chromatography (silica, dichloromethane). Yield: 0.9 g (79%). ^{1}H NMR ($CDCl_3$, 300 MHz): δ = 3.40 (s, 3H), 3.49 (s, 3H), 3.98 (s, 2H) ppm. ^{13}C NMR ($CDCl_3$, 75 MHz): δ = 33.7, 42.2, 44.5, 113.8, 187.6 ppm. $(C_5H_8N_2S)$n (128.0)n: Calcd. C 46.85, H 6.29, N 21.85, S 25.01; Found C 46.73, H 6.32, N 21.77, S 25.30.

*2.2.4. General procedure for the synthesis of compound **3a1–4** and **3b1–5** as adapted from Brunskill et al.* [23] *Aboutabl et al.* [29]*, and Bloxham et al.* [25]

A mixture of 2-cyano-*N,N*-dimethylethanethioamide (**2a**) or 2-cyanoethanethioamide (**2b**), the corresponding aldehyde (**1a-1f**) (1 or 1.1 eq.) and a base (triethylamine or piperidine) in absolute ethanol was stirred for 30 min to 3 d at 45–50 °C. After absence of precipitation, the residual solvent of the red solution was evaporated under nitrogen stream and further purified.

*2.2.5. Synthesis of 2-cyano-N,N-dimethyl-3-phenylprop-2-enethioamide (**3a1**)*

3a1 was synthesized according to the general procedure: 2-Cyano-*N,N*-dimethylethanethioamide (147 mg; 1.15 mmol), benzaldehyde (**1a**) (100 mg; 0.94 mmol), triethylamine (0.02 mL; 1.44 mmol), ethanol (2 mL); 1 h at 50 °C. The crude product was further purified by flash column chromatography (silica, dichloromethane/*n*-hexane 1/1). Yield: 95 mg (47%). ^{1}H NMR ($CDCl_3$, 300 MHz): δ = 3.18 (s, 0.5H), 3.48, 3.50, 3.53 (s, overlapping, 7H), 7.03 (s, 0.2H), 7.35–7.55 (m, 3H), 7.58 (s, 1H), 7.8–7.9 (m, 2H) ppm. $(C_{12}H_{13}N_2S)$n (216.1)n: Calcd. C 66.63, H 5.59, N 12.95, S 14.82; Found C 66.42, H 5.66, N 12.80, S 15.03.

*2.2.6. Synthesis of 2-cyano-3-(4-((11-hydroxyundecyl)oxy)phenyl)-N,N-dimethylprop-2-enethioamide (**3a2**)*

3a2 was synthesized according to the general procedure: 2-Cyano-*N,N*-dimethylethanethioamide (112 mg; 0.87 mmol), 4-(11-hydroxyundecyloxy)benzaldehyde (**1b**) (204 mg; 0.70 mmol), piperidine (85 µL; 0.84 mmol), ethanol

(4 mL); 3 d at 45 °C. The crude product was further purified by flash column chromatography (silica, dichloromethane/ethyl acetate 99/1). Yield: 209 mg (75%). ^{1}H NMR ($CDCl_3$, 300 MHz): δ = 1.1–1.9 (m, 18H), 3.20 (s, 1H), 3.46, 3.50, 3.51 (s, overlapping, 5H), 3.63 (t, 2H, J = 6.0 Hz), 3.9–4.1 (m, 2H), 6.87 (d, 0.5H, J = 9 Hz), 6.94 (d, 2H, J = 9 Hz), 7.34 (d, 0.5H, J = 9 Hz), 7.83 (s, 1H), 7.87 (d, 1.5H, J = 9 Hz) ppm. $(C_{23}H_{34}N_2O_2S)$n (402.2)n: Calcd. C 68.62, H 8.51, N 6.96, S 7.96; Found C 68.68, H 8.58, N 6.88, S 7.81.

2.2.7. Synthesis of 2-cyano-3-(3-((11-hydroxyundecyl) oxy)phenyl)-N,N-dimethylprop-2-enethioamide (3a3)

3a3 was synthesized according to the general procedure: 2-Cyano-*N,N*-dimethylethanethioamide (55 mg; 0.43 mmol), 3-(11-hydroxyundecyloxy)benzaldehyde (**1c**) (101 mg; 0.34 mmol), piperidine (41 µL; 0.41 mmol), ethanol (2 mL); 3 h at 45 °C. The crude product was further purified by flash column chromatography (silica, dichloromethane/ethyl acetate 99/1). Yield: 114 mg (83%). ^{1}H NMR (CD_2Cl_2, 300 MHz): δ = 1.2–1.9 (m, 18H), 3.15 (s, 1H), 3.43, 3.46, 3.50 (s, overlapping, 6H), 3.59 (t, 2H, J = 6.0 Hz), 3.85–3.95 (m, 0.5H), 3.95–4.05 (t, 2H, J = 6.0 Hz), 6.9–7.1 (m, 2H), 7.2–7.5 (m, 3H) ppm. $(C_{23}H_{34}N_2O_2S)$n (402.2)n: Calcd. C 68.62, H 8.51, N 6.96, S 7.96; Found C 68.84, H 8.53, N 6.65, S 7.60.

2.2.8. Synthesis of 3-(3-bromo-4-fluorophenyl)-2-cyano-N,N-dimethylprop-2-enethioamide (3a4)

3a4 was synthesized according to the general procedure: 2-Cyano-*N,N*-dimethylethanethioamide (192 mg; 1.50 mmol), 3-bromo-4-fluorobenzaldehyde (**1d**) (252 mg; 1.24 mmol), piperidine (0.15 mL; 1.50 mmol), ethanol (5 mL); overnight at 50 °C. The crude product was further purified by flash column chromatography (silica, dichloromethane/hexane 1/1). Yield: 145 mg (37%). ^{1}H NMR ($CDCl_3$, 300 MHz): δ = 3.22 (s, 0.5 H), 3.47, 3.51, 3.53 (s, overlapping, 7H), 6.91 (s, 0.2H), 7.1–7.3 (m, 1H), 7.48 (s, 1H), 7.6–7.7 (m, 0.2H), 7.8–7.9 (m, 1H), 8.0–8.1 (m, 1H) ppm. HR-ESI-TOF MS: $[C_{12}H_{10}BrFN_2S]Na^+$ calcd.: m/z = 334.9624; found: m/z = 334.9618; error: 1.9 ppm.

2.2.9. Synthesis of 2-cyano-3-phenylprop-2-enethioamide (3b1)

3b1 was synthesized according to the general procedure: 2-Cyanoethanethioamide (100 mg; 1 mmol), benzaldehyde (**1a**) (117 mg; 1.1 mmol), triethylamine (0.1 mL; 0.72 mmol), ethanol (2 mL); 30 min at 50 °C. The product was obtained by flash column chromatography (silica, dichloromethane/ethyl acetate 99/1). Yield: 30 mg (16%). ^{1}H NMR ($(CD_3)_2CO$, 300 MHz): δ = 5.10 (s, 0.1H), 5.28 (s, 0.1H), 6.18 (s, 1H), 7.3–7.4 (m, 1H), 7.5–7.7 (m, 3H), 8.0–8.1 (m, 2H), 8.40 (s, 1H), 8.85 (s, 0.5H), 8.97 (s, 0.1) 9.35 (s, 0.5H) ppm.

2.2.10. Synthesis of 2-cyano-3-(4-hydroxyphenyl)prop-2-enethioamide (3b2)

3b2 was synthesized according to the general procedure: 2-Cyanoethanethioamide (850 mg; 8.49 mmol), 4-hydroxybenzaldehyde (**1e**) (1 g; 8.49 mmol), triethylamine (0.12 mL; 0.85 mmol), ethanol (20 mL); 30 min at 45 °C. The product was obtained by recrystallization and washing with ethyl acetate. Yield: 173 mg (10%). ^{1}H NMR ($(CD_3)_2CO$, 300 MHz): δ = 3.02 (s, 1H), 6.9–7.1 (m, 2H), 7.9–8.1 (m, 2H), 8.41 (s, 1H), 8.61 (s, 1H), 9.48 (s, 1H) ppm.

2.2.11. Synthesis of 2-cyano-3-(3-((11-hydroxyundecyl) oxy)phenyl)prop-2-enethioamide (3b3)

3b3 was synthesized according to the general procedure: 2-Cyanoethanethioamide (173 mg; 1.71 mmol), 3-(11-hydroxyundecyloxy)benzaldehyde (**1c**) (500 mg; 1.71 mmol), triethylamine (0.01 mL; 0.09 mmol), ethanol (10 mL); 45 min at 45 °C. The product was obtained by flash column chromatography (silica, dichloromethane/ethyl acetate 9/1). Yield: 294 mg (46%). ^{1}H NMR (CD_2Cl_2, 300 MHz): δ = 1.2–1.9 (m, 18H), 3.59 (t, 2H, J = 6.0 Hz), 4.02 (t, 2H, J = 6.0 Hz), 7.0–7.2 (m, 1H), 7.3–7.5 (m, 1H), 7.5–7.6 (m, 2H), 8.69 (s, 1H) ppm. HR-ESI-TOF MS: $[C_{21}H_{30}N_2S]Na^+$ calcd.: m/z = 397.1920; found: m/z = 397.1907; error: 3.3 ppm.

2.2.12. Synthesis of 3-(3-bromo-4-fluorophenyl)-2-cyanoprop-2-enethioamide (3b4)

3b4 was synthesized according to the general procedure: 2-Cyanoethanethioamide (125 mg; 1.25 mmol), 3-bromo-4-fluorobenzaldehyde (**1d**) (250 mg; 1.25 mmol), triethylamine (0.01 mL; 0.07 mmol), ethanol (5 mL); 1 h at 45 °C. The crude product was washed with boiling dichloromethane. Yield: 75 mg (21%). ^{1}H NMR ($(CD_3)_2CO$, 300 MHz, Dimer): δ = 5.10 (s, 1H), 5.36 (s, 1H), 6.37 (s, 2H), 7.2–7.4 (m, 2H), 7.5–7.6 (m, 1H), 7.7–7.8 (m, 2H), 7.9–8.0 (m, 1H), 8.35 (s, 1H), 9.24 (s, 2H) ppm. ^{1}H NMR ($(CD_3)_2CO$, 300 MHz, Monomer): 7.49 (t, 1H, J = 6.0 Hz), 8.05–8.15 (m, 1H), 8.30–8.33 (m, 1H), 8.33–8.36 (s, 1H) ppm. HR-ESI-TOF MS: $[C_{10}H_6BrFN_2S]Na^+$ calcd.: m/z = 306.9303; found: m/z = 306.9303; error: 2.7 ppm.

2.2.13. Synthesis of 3-(3-(7-(5-(-3-amino-2-cyano-3-thioxoprop-1-en-1-yl)-2-fluorophenyl)-9,9-didecyl-9H-fluoren-2-yl)-4-fluorophenyl)-2-cyanoprop-2-enethioamide (3b5)

3b5 was synthesized according to the general procedure: 2-Cyanoethanethioamide (30 mg; 0.3 mmol), 3,3′-(9,9-didecyl-9H-fluorene-2,7-diyl)bis(4-fluorobenzaldehyde) (**1f**) (100 mg; 0.15 mmol), triethylamine (2 µL, 0.01 mmol), ethanol (3 mL); 1 h at 50 °C. The crude product was further purified by flash column chromatography (silica, dichloromethane). Yield: 36 mg (29%). ^{1}H NMR (CD_2Cl_2, 300 MHz): δ = 0.6–1.3 (m, 38H), 2.0–2.2 (m, 4H), 4.91 (s, 1H, D), 5.20 (0.5H, D), 7.1–7.4 (m, 4H), 7.5–7.95 (m, 10H), 8.0–8.15 (m, 1H), 8.2–8.25 (m, 1H), 8.81 (s, 1H) ppm. HR-ESI-TOF MS: $[C_{53}H_{60}F_2N_4S_2]Na^+$ calcd.: m/z = 877.4120; found: m/z = 877.4065; error: 6.2 ppm.

2.2.14. ROP with compound 3b3 as initiator

L-Lactide (530 mg; 3.68 mmol) was transferred into a microwave vial in a glove box under nitrogen atmosphere. 2-Cyano-3-(3-((11-hydroxyundecyl)oxy)phenyl) prop-2-enethioamide (**3b3**) (86 mg; 0.23 mmol) dissolved in 3 mL dry toluene and $Sn(Oct)_2$ (50 mg; 0.12 mmol) dissolved in 0.5 mL dry toluene were added to the microwave vial under vigorous stirring. Then, the microwave vial was capped and taken out of the glove box. The reaction mixture was heated at 110 °C in a preheated oil bath for 15 min. The reaction was quenched by addition of 200 µL 1 M HCl solution in methanol. The polymer was purified by precipitation in ice-cold *n*-hexane and preparative SEC (Biobeads® S-X1, dichloromethane). Yield: 284 mg (46%). Parts of the polymer sample were analyzed by SEC and MALDI-TOF MS to determine the molar mass and molar mass distribution ($M_{n,MALDI\text{-}TOF\ MS}$ = 1660 g/mol; M_w/M_n = 1.03). ^{1}H NMR (CD_2Cl_2, 300 MHz): 1.2–1.9 (60H), 3.9–4.0 (1.5H), 4.0–4.2 (1.5H), 4.4–4.4 (1H), 5.0–5.3 ppm (14.5H), 6.7–7.7 (4H), 8.68 (0.2H) ppm.

3. Results and discussion

3.1. Synthesis and characterization of the monofunctional compounds 3a1–4 and 3b1–4

To achieve a highly reversible polymeric structure or end-capped polymer, the first step was to identify suitable compounds, which should be incorporated into a polymeric self-healing material as second step. For this initial screening, eight different compounds **3a1**–**4** and **3b1**–**4** were synthesized to investigate the ability to reversibly dimerize via the (retro-)HDA cycloaddition. The synthesis route toward these designed monofunctional compounds with the subsequent dimerization reaction is depicted in Scheme 1. The first reaction step represents a Knoevenagel condensation of an arylic aldehyde (**1**) and 2-cyanoethanethioamide (**2a** or **2b**) under basic conditions. This synthetic approach provides access to a series of 3-aryl-2-cyanothioacrylamides with varied substituents on the aromatic ring as well as on the thioamide moieties by combination of different educts. An overview of the, thus, obtained products is provided in Table 1. For this purpose, five different aldehydes (**1**) as well as two different 2-cyanoethanethioamides (**2a** and **b**) were utilized. Thus, the influence of the substituents could be monitored. Compounds **1b** and **1c** were synthesized via etherification of *p*- and *m*-hydroxybenzaldehyde according to Piñol et al. [27] and compound **2a** via thionation of the corresponding aldehyde according to Ransborg et al. [28] The other educts are commercially available. The resulting 3-aryl-2-cyanothioacrylamides (**3a** and **3b**) are potentially able to dimerize via HDA reaction to form 5,6-dihydro-2*H*-thiopyrans (**4a** and **4b**).

The synthesis and characterization of the 3-aryl-2-cyanothioacrylamides with different substituents and their reversible behavior was also investigated by Brunskill

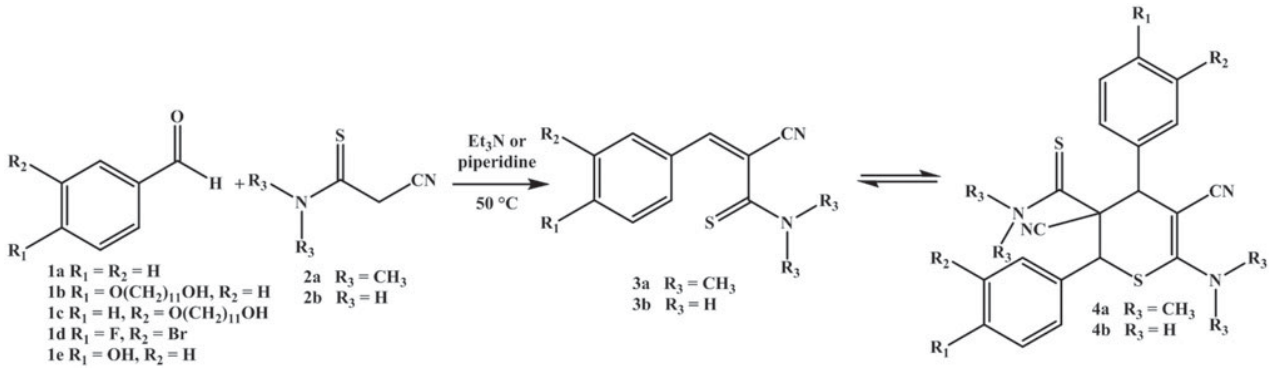

Scheme 1. Schematic representation of the synthesis of the 3-aryl-2-cyanothioacryl-*N*,*N*-dimethylamides (**3a**) and 3-aryl-2-cyanothioacrylamides (**3b**) as well as the dimerization via HDA reaction.

Table 1. Overview of the synthesized monofunctional compounds **3a1**–**4** and **3b1**–**4** and their dimerization behavior.

Compound	R_1	R_2	R_3	Dimerization	Reversibility
3a1	H	H	CH_3	yes	no
3a2	$O(CH_2)_{11}OH$	H	CH_3	yes	no
3a3	H	$O(CH_2)_{11}OH$	CH_3	yes	no
3a4	F	Br	CH_3	yes	no
3b1	H	H	H	yes	yes
3b2	OH	H	H	n.d.	n.d.
3b3	H	$O(CH_2)_{11}OH$	H	yes	yes
3b4	F	Br	H	yes	yes

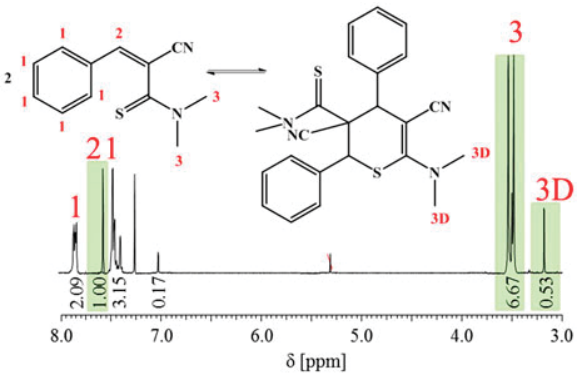

Figure 1. ^{1}H NMR spectrum of **3a1** and the dimeric species in $CDCl_3$.

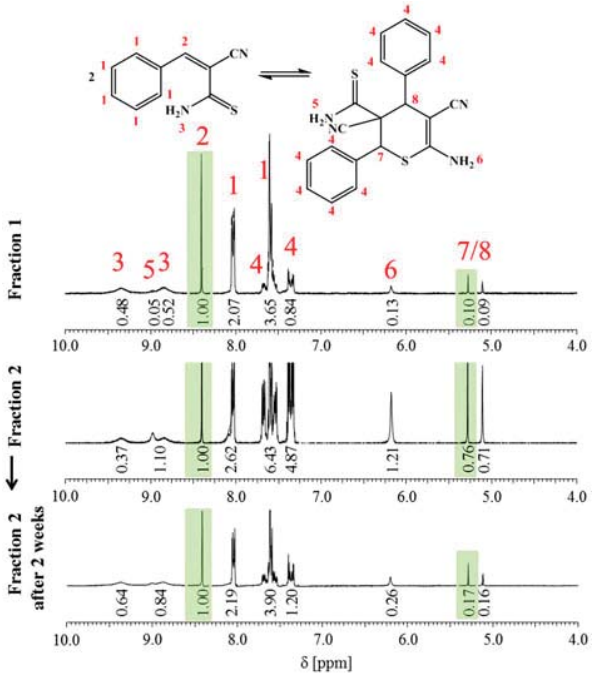

Figure 2. ^{1}H NMR spectra of fraction 1, fraction 2, and fraction 2 after two weeks in solution of **3b1** in $(CD_3)_2CO$.

et al. before.[23,24] The thioamide group is a very reactive group, which is favorable with respect to the HDA reaction, but a drawback for the incorporation into a polymeric system, which requires subsequent reaction steps. To overcome the latter restriction, the more stable compounds (**3a1**–**3a4**) with the *N,N*-dimethyl thioamide group were synthesized. **3a1** was synthesized as a model compound to gain insight into the HDA reaction of this less reactive group. **3a1** was obtained with a yield of 47% with triethylamine as base. The characterization via ^{1}H NMR spectroscopy (Figure 1) clearly indicates the fact that dimeric species are also formed with the *N,N*-dimethyl thioamide group. The monomer to dimer ratio of 5.8 to 1 is easily accessible from the integrals of suitable peaks derived from the monomeric (peaks 2 and 3 in Figure 1) and the dimeric (peak 3D in Figure 1) species.

3a2 was synthesized to introduce a linker into the system that would be broadly applicable for a number of subsequent reactions, e.g., for post-polymerization modifications. Also here, the ^{1}H NMR spectrum shows clearly a monomer to dimer ratio of 2.3 to 1 (Figure S1). Despite these very promising results, it was not possible to trigger any reversible back reaction to the monomeric species, neither by increasing the temperature up to 70 °C nor by addition of a base such as pyridine or piperidine. An explanation could be the formation of a thermodynamically stable dimeric form due to stereoisomeric rearrangements, which do not dissociate back to the monomeric form. Also for the compounds **3a3** and **3a4** with another linker position and a *p*-fluoro substitution, which should decrease the electron density within the system, no significant reversibility of the HDA reaction could be achieved. Thus, the dimethyl thioamides seem not to be suitable for the development of self-healing materials in general due to the missing reversibility of the HDA reaction.

As a consequence, the more labile 3-aryl-2-cyanothioacrylamides without substituents on the amide nitro-

gen atom were in the focus of further studies. In order to investigate the dimerization and reversibility of the cycloaddition of an already established and working system by studies using ^{1}H NMR spectroscopy, **3b1** was synthesized as a model compound as described by Brunskill et al. [23,24] Figure 2 displays the ^{1}H NMR spectra of two fractions that were isolated via column chromatography directly after the synthesis. The integration of characteristic peaks in the spectra that are originating from monomer (Peak 2 in Figure 2) and dimer (Peaks 7 and 8 in Figure 2) immediately provides access to the relative amounts of both species that are present. The first fraction revealed a monomer to dimer ratio of 10 to 1. In contrast, the second fraction showed a monomer to dimer ratio of 1.4 to 1. Upon storage of the second fraction at room temperature for two weeks, the amount of dimer is significantly increased ([M]:[D] = 6.4 to 1). Even when the sample is stored at 0 °C for 2 d, the reversibility via HDA reaction can be observed ([M]:[D] = 4.3 to 1). This shows that the ratio could easily be tuned by slight changes of the temperature.

However, to incorporate this very promising HDA system into a polymeric self-healing material, functional moieties that enable a coupling to, e.g., monomers have to be present. Thus, the hydroxyl-functional **3b2** was synthesized. This compound was also synthesized by Aboutabl et al. before.[29] Unfortunately, **3b2** could not be functionalized further via esterification due to the high reactivity of the thioamide group. To overcome this drawback and to enable a preparation of functional polymers containing the cyanothioamide moiety, **3b3** with a long linker and a hydroxyl group was synthesized using triethylamine as base with a yield of 46%. The ^{1}H NMR spectrum showed a monomer to dimer ratio of 24 to 1 directly after synthesis and purification. After storage at 0 °C overnight, the ratio decreased to 4.9 to 1, which clearly indicates the reversibility of the HDA reaction. The application of **3b3** as initiator for the ROP of L-lactide will be discussed below.

The synthesis of **3b4** was achieved with triethylamine as base. It was selected due to the best dimerization behavior of the substances with the *p*-fluoro substitution studied by Brunskilll et al. [23,24] After purification only the dimeric species could be isolated, as determined by ^{1}H NMR spectroscopy. In contrast, the ESI-TOF MS spectrum (Figure 3) showed the presence of the monomeric as well as dimeric species, but also tetrameric and hexameric species could be assigned, as confirmed by the comparison with the corresponding calculated and measured isotopic patterns (Figures 3 and S2). A possible reason might be the formation of aggregates of dimers that are not separated from each other during the ESI-TOF MS measurement.[30,31] This assumption is supported by the fact that no peaks arising from tri- or pentamers could be observed. Since the *m*-bromo substitution represents an excellent opportunity to incorporate the 3-aryl-2-cyanothioacrylamide moiety into a polymeric network by cross-coupling reactions, detailed kinetic studies of the dissociation and dimerization of this most promising compound are described in the following.

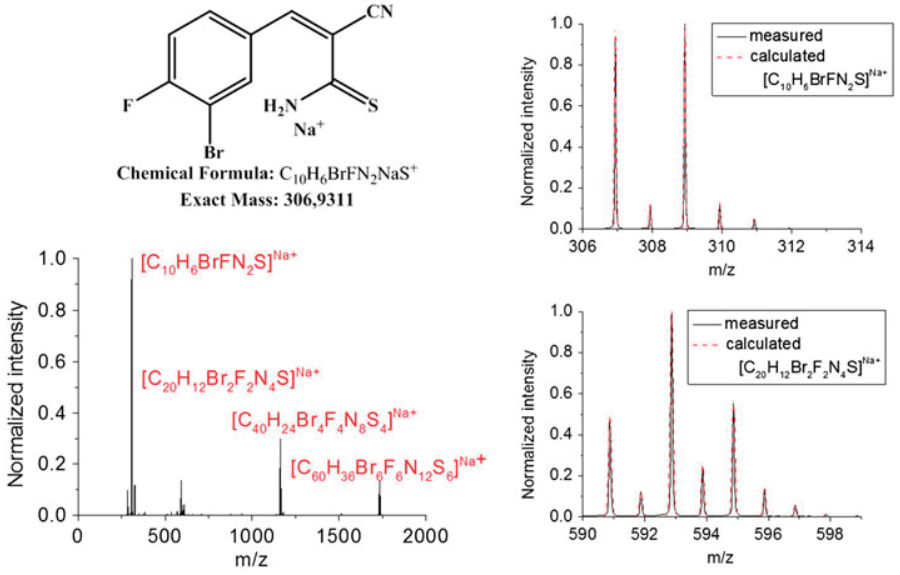

Figure 3. ESI-TOF mass spectrum of **3b4** with peak assignment and exemplary overlays of the measured and calculated isotopic patterns (monomeric and dimeric species).

3.2. Equilibration studies of 3b4 at different temperatures

For future applications of the functional moiety as key structure in a self-healing polymer, preliminary knowledge about the equilibrium is highly advantageous. For this purpose, detailed kinetic studies were performed via ^{1}H NMR spectroscopy. The retro-HDA reaction was studied at three different temperatures (room temperature, 50, and 70 °C). The equilibration of the corresponding HDA reaction was investigated using a sample that had been thermally pretreated at 70 °C (Figure 4).

For the studies of the retro-HDA reaction at room temperature and at 50 °C, acetone was used as solvent, but the studies that required a thermal pretreatment at 70 °C were performed in DMSO due to the higher boiling point. At first, the kinetic study of the equilibration of compound **3b4** at 25 °C in acetone was studied (Figure 4, left). Two selected ^{1}H NMR spectra are depicted in Figure S3. The ratio of the two species was determined by the utilization of the signals at 5.36 ppm (monomer) and the signals of the aromatic protons at 8.09–9.14 ppm (dimer). At the beginning, only the dimeric species were present; and after 16 days, a ratio of monomer to dimer of around 3 to 1 was detected. The equilibrium was reached after 8 days. A fast increase of the monomer content within the first 8 days was observed. Afterward, only slight changes could be monitored, which are most likely caused by fluctuations due to temperature differences. Furthermore, the influence of the temperature was studied. For this purpose, a kinetic study at 50 °C in acetone was performed, which is depicted in Figure 4 (right). Two selected ^{1}H NMR spectra are shown in Figure S4. Also here, the complete dimeric species was utilized as starting point. Already after 15 min, the monomer to dimer ratio was shifted to 4 to 1. The equilibrium was reached after around 5 h at a monomer to dimer ratio of 15 to 1. In order to further increase the temperature, the solvent was changed to DMSO, which has a higher boiling point. At a temperature of 70 °C, the equilibrium was completely shifted to the monomeric species after 30 min (Figure S5), thereby providing an excellent opportunity to study the equilibration of the corresponding HDA reaction at room temperature. The kinetics of the HDA reaction (Figure 4, left) showed that the equilibrium was reached after 3 days at room temperature; a monomer to dimer ratio of around 3 to 1 was determined. This shows that the solvent does not influence the composition of the mixture in equilibrium at room temperature and that the HDA reaction is indeed completely reversible.

The fact that the equilibrium is shifted more toward the side of the monomeric species with increasing temperature is typical for DA cycloaddition reactions. Hence, a potential network with crosslinks that are based on the **3b4** functionality would be completely opened already at 70 °C, while the complete reversibility of this particular HDA reaction should provide the possibility to reform the network. Therefore, the incorporation of **3b4** into a polymeric system represented the next important step.

3.3. Synthesis and characterization of 3b5 and the oligomeric species

To incorporate this very promising moiety with a thioamide group and the *p*-fluoro substitution into a polymer, the difunctional compound **3b5** was synthesized. Since **3b5** contains two cyanothioacrylamide functionalities, it should represent an AA-type monomer that can undergo a reversible polyaddition via 'dimerization'. Therefore, the fluorene diboronic ester was converted to compound **1f** via Suzuki cross-coupling with the corresponding *p*-fluoro aldehyde with a yield of 90%. The following Knoevenagel reaction toward the difunctional thioacrylamide (**3b5**) was achieved with a yield of 29% (Scheme 2).

The oligomerization of **3b5** already proceeds during the purification of the product. Consequently, analytical techniques that are typical for polymer characterization were applied. **3b5** was further fractionated on a preparative size exclusion Biobeads® S-X1 column.

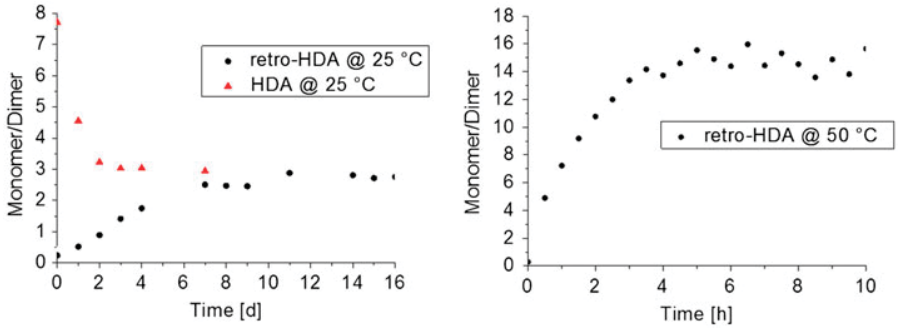

Figure 4. Equilibration study of **3b4**. Data for the rHDA reaction obtained from $(CD_3)_2CO$ solutions at 25 °C, data for the HDA reaction at 25 °C obtained after annealing at 70 °C in DMSO-d6 (left) and rHDA reaction at 50 °C in $(CD_3)_2CO$ (right).

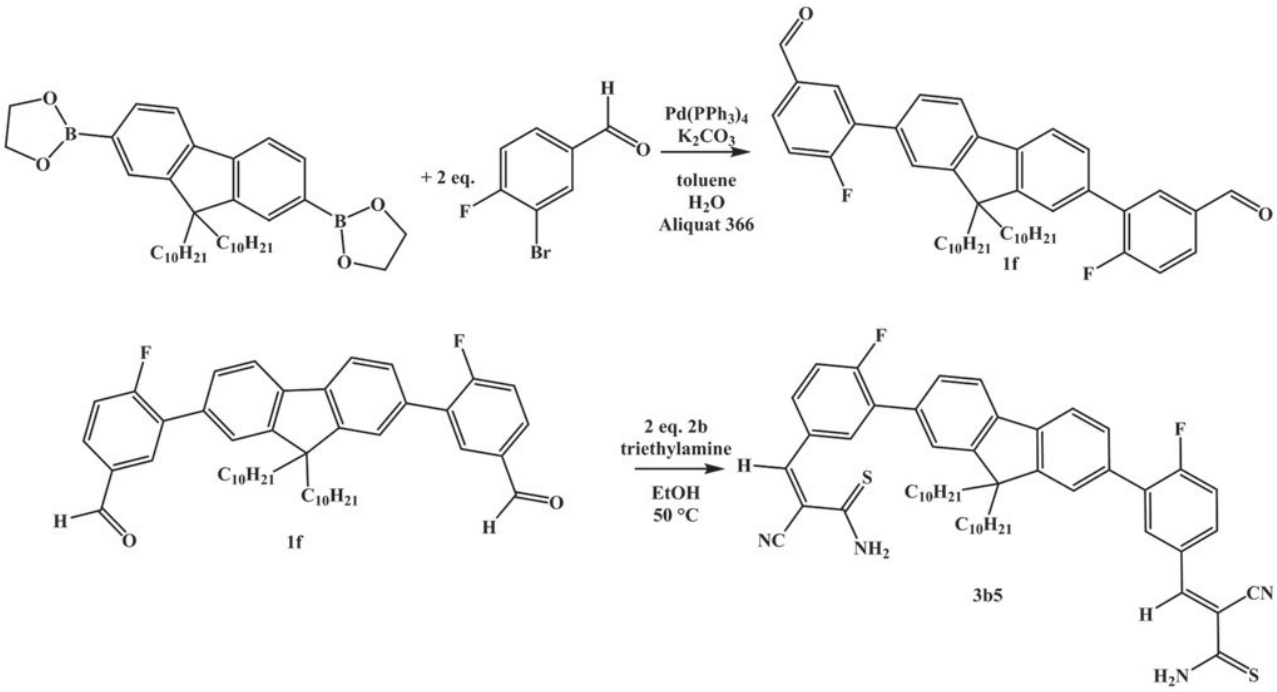

Scheme 2. Schematic representation of the synthesis of compound **1f** via suzuki cross-coupling and subsequent Knoevenagel reaction to yield **3b5**.

Accordingly, the fractions revealed different M_n values directly after fractionation, as determined by SEC. However, when all fractions were subsequently kept in solution for 5 days, repeated SEC measurements revealed the same molar mass in all fractions. The molar mass of the oligomers tends toward an equilibrium value of 1850 g/mol, which indicates the reversibility of the HDA reaction. Furthermore, we observed that the molar mass could be influenced by the evaporation of the solvent (i.e., the concentration of the monomer). Therefore, different methods were tested (Figure S6) among whose slow evaporation at room temperature was the most effective method in order to increase the molar mass. We also investigated the molar masses of **3b5** after dissolving and evaporating multiple times (Figure 5). Also in this case, the M_n value could be increased after several concentration steps. This shows that the dimerization or rather the oligomerization is faster than the retro-HDA reaction toward lower molar mass species.

In a further study (Figure 6), the dependency of the molar mass on the concentration in solution was tested. The initial concentration of **3b5** barely influenced the reaction time toward lower molar mass species. Nevertheless, after 4 days in solution, the amount of the larger molar species is only slightly higher at higher concentration. Therefore, the higher molar mass species could only be reached by slow evaporation of the solution.

To further investigate the degree of polymerization (DP) of the higher molar mass species in detail, simultaneous SEC and ^{1}H NMR measurement of the same species were performed. Figure 5 displays the ^{1}H NMR spectrum of **3b5**. As can be seen from the schematic representation of the structure of the oligomer, its end-groups will be based on unreacted cyanothioacrylamide moieties making it possible to calculate the average DP. A suitable ^{1}H NMR signal results from the vinylic proton of these end-groups (peak 1 in Figure 7). In combination with the signal derived from the methylene protons of the fluorene moieties, a DP of 3.4 (peak 4 in Figure 7) could be estimated.

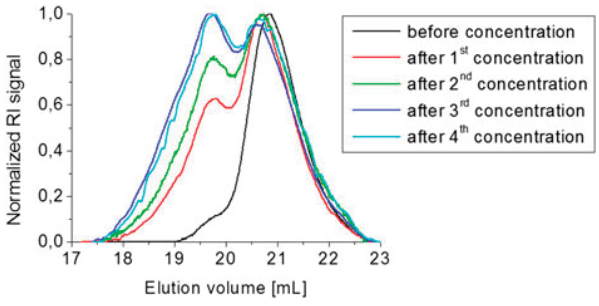

Figure 5. SEC traces of compound **3b5** after multiple concentration steps in CH_2Cl_2.

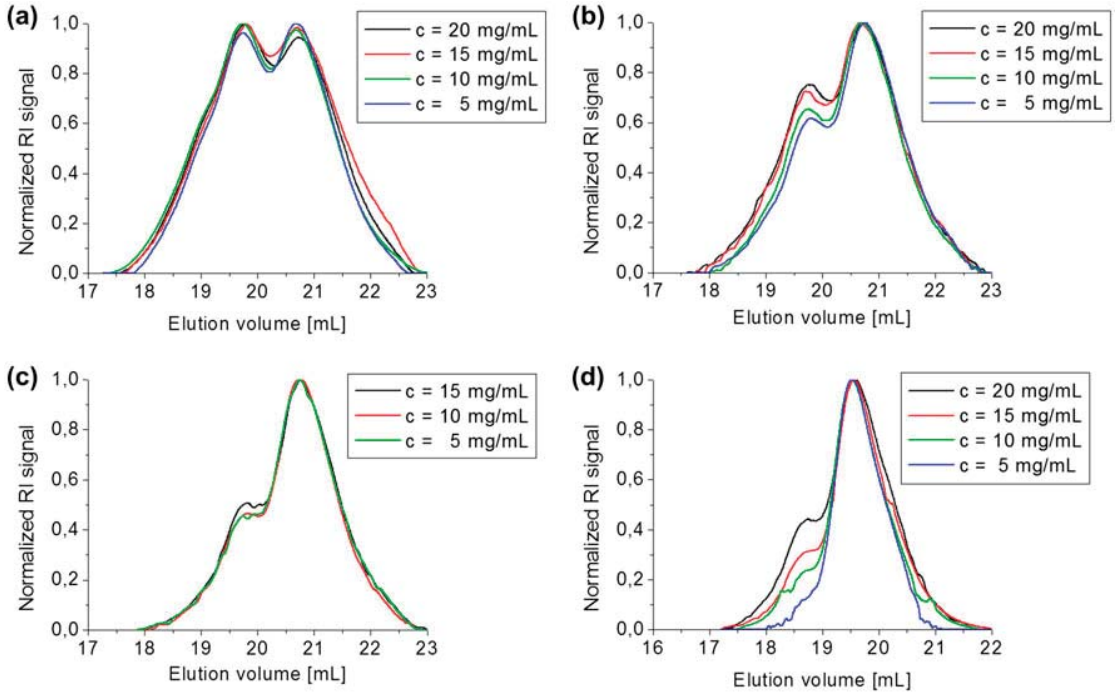

Figure 6. Study of the equilibrium of compound **3b5** at different concentrations in CH_2Cl_2, (a) directly after dissolving, (b) after 1 d in solution, (c) after 2 d in solution and (d) after 4 d in solution.

Due to the rather high molar mass of each repeating unit (M = 854 g/mol), the different oligomers could be somewhat resolved by SEC (Figure 8) with the dimer being the most abundant species after dissolving the polymer. Upon storage of **3b5** for several days in solution, the DP of the oligomers decreases even further, as confirmed by SEC and ^{1}H NMR measurements. The DP of the oligomers tends toward an equilibrium value 2.

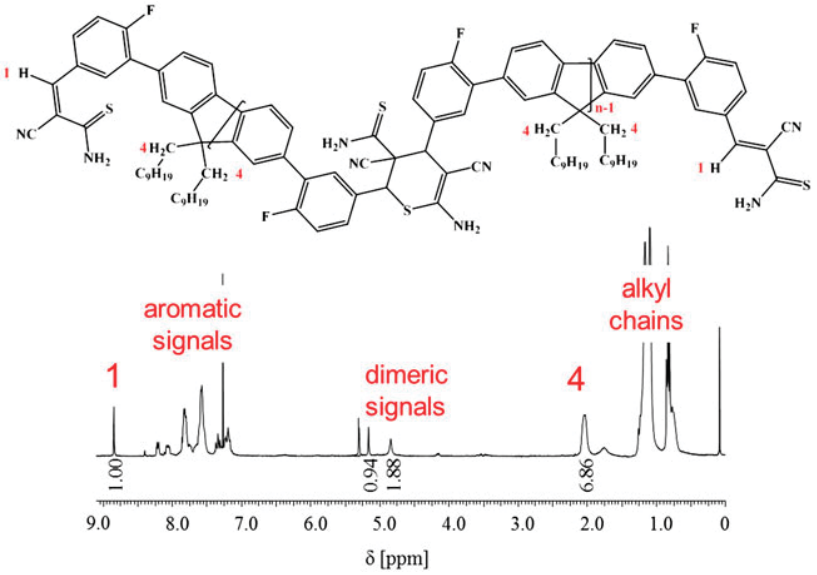

Figure 7. ^{1}H NMR spectrum of **3b5** in $CDCl_3$. For clarity, only the protons and the corresponding peaks that were used for the calculation of the average DP are labelled.

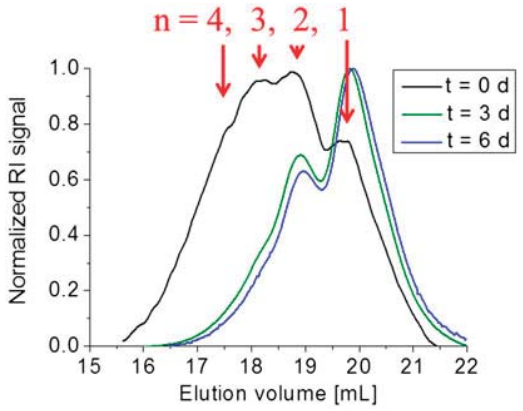

Figure 8. SEC traces of **3b5** after 0, 3, and 6 d in solution (c = 30 mg/mL).

Additional SEC measurements with a diode array detector (DAD) were performed. The corresponding refractive index detector (RID) signal is plotted as reference in the 3D contour plot obtained from the SEC-DAD in the Figures 9 and S7. The intense absorption at ca. 330 nm corresponds to the conjugated oligomer (fluorene flanked by two phenyl moieties). Additionally, the absorption at higher wavelength is caused by the thioacrylamide moiety. Consequently, this absorption is more pronounced for the monomer and dimer, respectively, than for the higher oligomers (only the end-group).

To investigate, if the reversibility of the HDA reaction could be exploited for an application as self-healing material, investigations in bulk are required. In order to obtain preliminary information about an appropriate temperature range, melting point measurements were performed, revealing a T_m around 100 °C. Indeed, the SEC curves of the thermally untreated material show a higher molar mass in comparison with samples that were heated to 100 °C (Figure S8). This demonstrated that the retro-HDA reaction (which results in lower molar masses of the oligomers) indeed takes place in bulk as well.

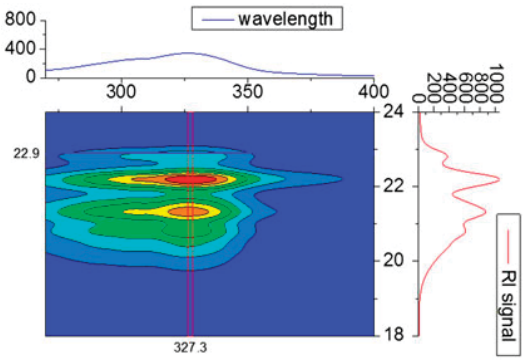

Figure 9. 3D contour plot from the SEC measurement of **3b5** with DAD. The corresponding RID signal is plotted on the right-hand side for comparison.

We also studied the effect of different Lewis acids onto the oligomeric system **3b5** due to the positive influence in other HDA reactions.[32–35] Therefore BF_3 etherate as well as $ZnCl_2$ were utilized as Lewis acids with a amount of 0.5 eq per functional unit thioamide. Addition of BF_3 resulted immediately in a brown precipitation and further degradation. $ZnCl_2$ induced a degradation of the monomer and reduced the amount of the dimeric species in the solution, as is evidenced by SEC measurement (Figure S9).

To conclude, only oligomeric species could be obtained in solution using the bis functional monomer **3b5** alone. However, due to the highly reversible oligomerization, it was possible to increase the DP by multiple concentration steps. To increase the molar masses of the cyanothioacrylamide-based oligomers while maintaining the high reversibility, the respective functional moiety was therefore combined with a polymer chain that would not be prone to undergo dissociation.

3.4. *End-functionalization of polylactide*

To introduce the thioamide functionality as end-group to a polymer, the hydroxyl-functional **3b3** was applied as an initiator for the ROP of L-lactide. The resulting polymer could potentially dimerize reversibly.

The ROP was performed under standard conditions using tin(II) bis-(2-ethylhexanoate) as catalyst (Scheme 3) with an [M]/[I] of 15 to obtain a short PLA (**P1**) that would enable a straightforward end-group determination.[36] Despite the unsubstituted thioamide functionality, which could possibly prove problematic during the ROP synthesis of a polyester, PLA with the desired end-group could be obtained. Subsequent to purification, polymer **P1** was characterized via SEC, ^{1}H NMR, MALDI, and ESI-TOF MS measurements (Table 2). The MALDI-TOF mass spectrum of **P1** (Figure 10) revealed a single distribution with a *m/z* difference of 144 between two neighboring peaks, which corresponds to the mass of one lactide monomer. This distribution can be assigned to PLA chains with the monomeric form of the HDA end-group, which are ionized by a sodium cation, as can be seen from the overlay of the measured and theoretical pattern. The high end-group fidelity is also confirmed by the ^{1}H NMR spectrum of **P1** (in Figure S10) that clearly shows the characteristic peaks resulting from the four aromatic protons of the initiator between 6.8 and 7.6 ppm. The molar mass of 1680 g/mol, which was estimated using the integrals of these signals and the methine proton signal of the PLA at 5.2 ppm, is in very good agreement to the M_n value from MALDI-TOF MS. Interestingly, a closer inspection of the ^{1}H NMR signal at 8.7 ppm corresponding to the vinyl group proton, already indicates the existence of PLA chains that are coupled via the HDA linkage.

Table 2. Characterization data of the end-functional PLA (**P1**).

$M_{n,SEC}$[a] (g/mol)	PDI_{SEC}	$M_{n,NMR}$ (g/mol)	$M_{n,MALDI}$ (g/mol)	PDI_{MALDI}
2890	1.21	1680	1660	1.03

[a]PMMA as calibration, after purification.

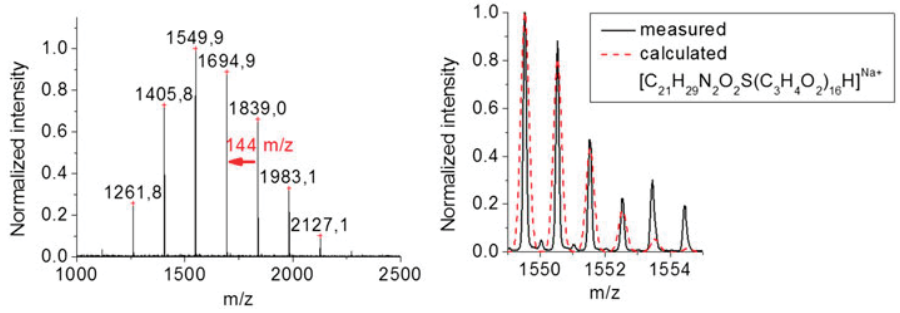

Figure 10. Characterization of **P1** via mass spectrometry. Full MALDI-TOF mass spectrum (left) and overlay of calculated and measured isotopic patterns from ESI-TOF MS analysis (right).

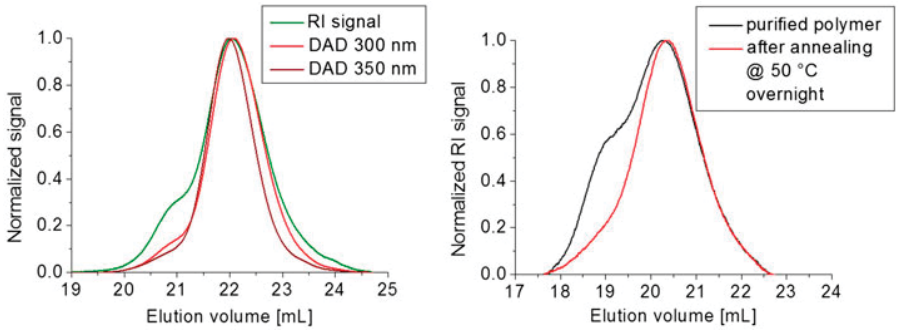

Figure 11. SEC measurement of **P1** with RID and DAD (at 300 and 350 nm, the complete contour plot including other is depicted in the supporting information) (left) and SEC traces of **P1** before and after annealing at 50 °C (right).

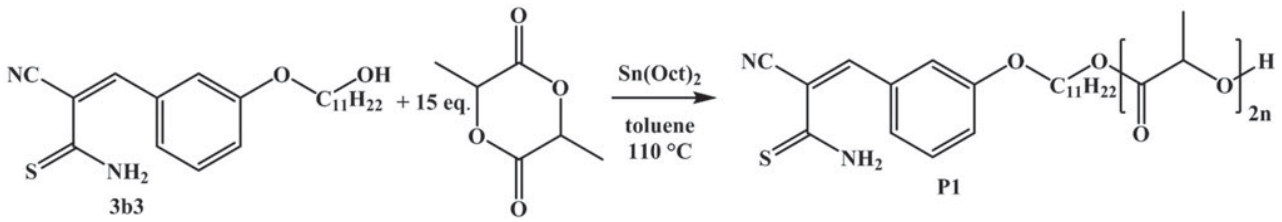

Scheme 3. Schematic representation of the ROP of L-lactide using **3b3** as initiator.

Since a HDA reaction between two end-functional PLA chains directly results in polymer chains with higher molar masses, the SEC trace of **P1** (Figure 11, left) reveals a strong shoulder at lower elution volume, which is in agreement with the considerations based on the ^{1}H NMR spectrum. Due to the UV/vis absorption of the initiator **3b3** until wavelengths λ around 450 nm (Figure S11, left) additional SEC measurements with a DAD (Figure S11, right) were performed. The fact that the polymer can be detected at higher λ once more

confirms the covalent attachment of the functional end-group. However, the shoulder arising from HDA-coupled chains is detected with the RID, but can only be seen with the DAD at lower wavelengths. This clearly indicates that the shoulder at higher molar mass corresponds to the dimer. Since the HDA reaction changes the chromophore (compare Scheme 1), the UV/Vis absorption properties will strongly be influenced as well.

With respect to a further exploitation of the polymer, the reversibility of the HDA reaction is of major importance and can simply be investigated by SEC in case of **P1**. As depicted in Figure 11 (right), the high molar mass shoulder, which is present in the purified polymer and originates from the HDA-coupled PLA chains, is not present anymore when **P1** is annealed at 50 °C overnight. This demonstrates that the reversibility of the dimerization caused by the used initiator **3b3** is retained when the functional moiety is incorporated in the PLA.

4. Conclusion

Different 3-aryl-2-cyano-*N,N*-dimethylthioacrylamides (**3a1**–**4**) and 3-aryl-2-cyanothioacrylamides (**3b1**–**5**) could be synthesized via Knoevenagel reaction. All compounds were characterized via ^{1}H NMR spectroscopy and ESI-TOF MS. The compounds **3a1**–**4** showed the presence of a dimeric species – the product of the HDA reaction. However, none of these systems was reversible. In contrast, the HDA reaction of **3b1**–**5** indicated a highly reversible behavior triggered by temperature or concentration. The most promising compound was the *p*-fluoro-substituted 3-aryl-2-cyanothioacrylamide (**3b4**), which was consequently selected for kinetic studies of the equilibration. Moreover, this compound was further converted via Suzuki cross-coupling and Knoevenagel reaction to a difunctional species (**3b5**). The oligomerization and dissociation, which were investigated by SEC measurements as well as ^{1}H NMR spectroscopy, were highly reversible. The molar mass could be adjusted by concentration of the monomer; therefore, the DP could be increased by multiple concentration steps. Nevertheless, the DP was less dependent on the concentration of the solution. Furthermore, **3b3** could be used as initiator for the ROP of L-lactide. The resulting end-functional polyester revealed reversible dimerization. Overall, the dimerization of the 3-aryl-2-cyanothioacrylamides was highly reversible under the investigated conditions (temperature, solvents, concentration,…). On the one hand, this high reversibility is promising for an application in self-healing materials, but on the other hand, the high extent might result in materials with insufficient mechanical properties due to a low cross-link density. The corresponding investigations will be in the focus of our future research.

Supplementary material

The supplementary material for this paper is available online at http://dx.doi.10.1080/15685551.2015.1058007.

Acknowledgements

Stefan Bode is grateful to the Fond der Chemische Industrie (VCI) for a generous PhD fellowship. Christine Weber acknowledges the Carl Zeiss foundation. Furthermore, Sarah Crotty and Dr. Wolfgang Günther are gratefully acknowledged.

Disclosure statement

No potential conflict of interest was reported by the authors.

Funding

This work was supported by the Deutsche Forschungsgemeinschaft within the framework of SPP 1568 [grant number SCHU 1229/13-1].

References

[1] Goussé C, Gandini A, Hodge P. Application of the Diels−Alder reaction to polymers bearing furan moieties. 2. Diels−Alder and retro-Diels−Alder reactions involving furan rings in some styrene copolymers. Macromolecules. 1998;31:314–321.
[2] Murphy EB, Bolanos E, Schaffner-Hamann C, Wudl F, Nutt SR, Auad ML. Synthesis and characterization of a single-component thermally remendable polymer network: Staudinger and Stille revisited. Macromolecules. 2008;41:5203–5209.
[3] Peterson AM, Jensen RE, Palmese GR. Room-temperature healing of a thermosetting polymer using the Diels−Alder reaction. ACS Appl. Mater. Interfaces. 2010;2:1141–1149.
[4] Bergman SD, Wudl F. Mendable polymers. J. Mater. Chem. 2007;18:41–62.
[5] Hager MD, Greil P, Leyens C, van der Zwaag S, Schubert US. Self-healing materials. Adv. Mater. 2010;22:5424–5430.
[6] Chen X, Dam MA, Ono K, et al. A thermally re-mendable cross-linked polymeric material. Science. 2002;295:1698–1702.
[7] Chen X, Wudl F, Mal AK, Shen H, Nutt SR. New thermally remendable highly cross-linked polymeric materials. Macromolecules. 2003;36:1802–1807.
[8] Sinnwell S, Inglis AJ, Davis TP, Stenzel MH, Barner-Kowollik C. An atom-efficient conjugation approach to well-defined block copolymers using RAFT chemistry and hetero Diels-Alder cycloaddition. Chem. Commun. 2008;2052–2054.
[9] Inglis AJ, Nebhani L, Altintas O, Schmidt FG, Barner-Kowollik C. Rapid bonding/debonding on demand: reversibly cross-linked functional polymers via Diels−Alder chemistry. Macromolecules. 2010;43:5515–5520.
[10] Paulöhrl T, Inglis AJ, Barner-Kowollik C. Reversible Diels-Alder chemistry as a modular polymeric color switch. Adv. Mater. 2010;22:2788–2791.
[11] Espinosa E, Glassner M, Boisson C, Barner-Kowollik C, D'Agosto F. Synthesis of cyclopentadienyl capped polyethylene and subsequent block copolymer formation via hetero Diels-Alder (HDA) Chemistry. Macromol. Rapid Commun. 2011;32:1447–1453.

[12] Brandt J, Guimard NK, Barner-Kowollik C, Schmidt FG, Lederer A. Temperature-dependent size exclusion chromatography for the *in situ* investigation of dynamic bonding/debonding reactions. Anal. Bioanal. Chem. 2013;405:8981–8993.
[13] Guimard NK, Ho J, Brandt J, et al. Harnessing entropy to direct the bonding/debonding of polymer systems based on reversible chemistry. Chem. Sci. 2013;4:2752–2759.
[14] Oehlenschlaeger KK, Guimard NK, Brandt J, et al. Fast and catalyst-free hetero-Diels–Alder chemistry for on demand cyclable bonding/debonding materials. Polym. Chem. 2013;4:4348–4355.
[15] Pahnke K, Brandt JGryn'ova G, et al. Entropy driven chain effects on ligation chemistry. Chem. Sci. 2015;6: 1061–1074.
[16] Inglis AJ, Sinnwell S, Stenzel MH, Barner-Kowollik C. Ultrafast click conjugation of macromolecular building blocks at ambient temperature. Angew. Chem. Int. Ed. Engl. 2009;48:2411–2414.
[17] Inglis AJ, Stenzel MH, Barner-Kowollik C. Ultra-fast RAFT-HDA click conjugation: an efficient route to high molecular weight block copolymers. Macromol. Rapid Commun. 2009;30:1792–1798.
[18] Langer M, Brandt J, Lederer A, Goldmann AS, Schacher FH, Barner-Kowollik C. Amphiphilic block copolymers featuring a reversible hetero Diels-Alder linkage. Polym. Chem. 2014;5:5330–5338.
[19] Oehlenschlaeger KK, Mueller JO, Brandt J, et al. Adaptable hetero Diels–Alder networks for fast self-healing under mild conditions. Adv. Mater. 2014;26:3561–3566.
[20] Boul PJ, Reutenauer P, Lehn J. Reversible Diels−Alder reactions for the generation of dynamic combinatorial libraries. Org. Lett. 2005;7:15–18.
[21] Reutenauer P, Buhler E, Boul PJ, Candau SJ, Lehn J. Room temperature dynamic polymers based on Diels-Alder chemistry. Chem. Eur. J. 2009;15:1893–1900.
[22] Reutenauer P, Boul PJ, Lehn J. Dynamic Diels-Alder reactions of 9,10-dimethylanthracene: reversible adduct formation, dynamic exchange processes and thermal fluorescence modulation. Eur. J. Org. Chem. 2009;2009:1691–1697.
[23] Brunskill JSA, De A, Ewing DF. Dimerisation of 3-aryl-2-cyanothioacrylamides. A [2_s+ 4_s] cyclo-addition to give substituted 3,4-dihydro-2H-thiopyrans. J. Chem. Soc., Perkin Trans. 1. 1978:629–633.
[24] Brunskill JSA, De A, Ewing DF. Substituent effects on a reversible cycloaddition reaction. J. Chem. Soc., Perkin Trans. 2. 1980:4.
[25] Bloxham J, Dell CP. Reaction of 3-aryl-2-cyanothioacrylamides with electron-deficient alkynes: synthesis of 4-aryl-4H-thiopyrans. J. Chem. Soc., Perkin Trans. 1. 1994:989–993.
[26] Kerszulis JA, Amb CM, Dyer AL, Reynolds JR. Follow the yellow brick road: structural optimization of vibrant yellow-to-transmissive electrochromic conjugated polymers. Macromolecules. 2014;47:5462–5469.
[27] Piñol R, Lub J, García MP, et al. Synthesis, properties, and polymerization of new liquid crystalline monomers for highly ordered guest−host systems. Chem. Mater. 2008;20:6076–6086.
[28] Ransborg LK, Albrecht Ł, Weise CF, Bak JR, Jørgensen KA. Optically active thiophenes via an organocatalytic one-pot methodology. Org. Lett. 2012;14:724–727.
[29] Aboutabl MA, Abdel Aziz MA, Magd El Din AA, Elwy HA, Fahmy HM. Electrochemical reduction of some 3-aryl-2-cyanothioacrylamide derivatives at the DME. Monatsh. Chem. 1991;122:765–770.
[30] Di Marco VB, Bombi GG. Electrospray mass spectrometry (ESI-MS) in the study of metal-ligand solution equilibria. Mass. Spectrom. Rev. 2006;25:347–379.
[31] Schug K, McNair HM. Adduct formation in electrospray ionization mass spectrometry. J. Chromatogr. A. 2003;985:531–539.
[32] Motoki S, Saito T, Karakasa T, et al. Lewis acid-promoted hetero Diels-Alder reaction of α, β-unsaturated thioketones. J. Chem. Soc., Perkin Trans. 1. 1992:2943–2948.
[33] Saito T, Fujii H, Hayashibe S, Matsushita T, Kato H, Kobayashi K. Uncatalysed (thermal) and Lewis acid-promoted asymmetric hetero-Diels–Alder reaction of 1-thiabuta-1,3-dienes (thiochalcones) with di-(–)-menthyl fumarate. Configuration determination by x-ray crystallographic analysis of (2s,3r,4r)-(+)-2,3-bis[(–)-menthoxycarbonyl]-4,6-diphenyl-3,4-dihydro-2h-thiopyran and conversion of cycloadducts into optically pure diols. J. Chem. Soc., Perkin Trans. 1. 1996:1897–1903.
[34] Bastin R, Albadri H, Gaumont A, Gulea M. Pyridinedithioesters as heterodienophiles: application to the synthesis of Aprikalim. Org. Lett. 2006;8:1033–1036.
[35] Zhou J, Guimard NK, Inglis AJ, et al. Thermally reversible Diels–Alder-based polymerization: an experimental and theoretical assessment. Polym. Chem. 2012;3:628–639.
[36] Kryuchkov MA, Detrembleur C, Jérôme R, Prud'homme RE, Bazuin CG. Synthesis and thermal properties of linear amphiphilic diblock copolymers of L-lactide and 2-dimethylaminoethyl methacrylate. Macromolecules. 2011;44:5209–5217.

Supporting information

Reversible oligomerization of 3-aryl-2-cyanothioacrylamides *via* [2_s + 4_s] cycloaddition to substituted 3,4-dihydro-2*H*-thiopyrans

Julia Kötteritzsch, Stefan Bode, Ilknur Yildirim, Christine Weber, Martin D. Hager*, Ulrich S. Schubert*

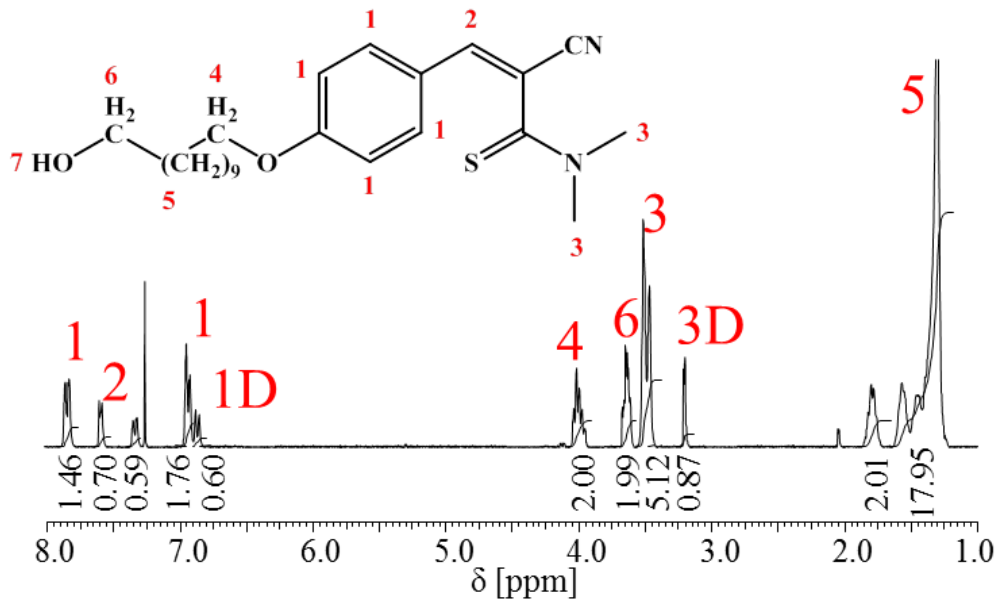

Figure S1. ^{1}H NMR spectrum of **3a2** and the dimeric species in $CDCl_3$.

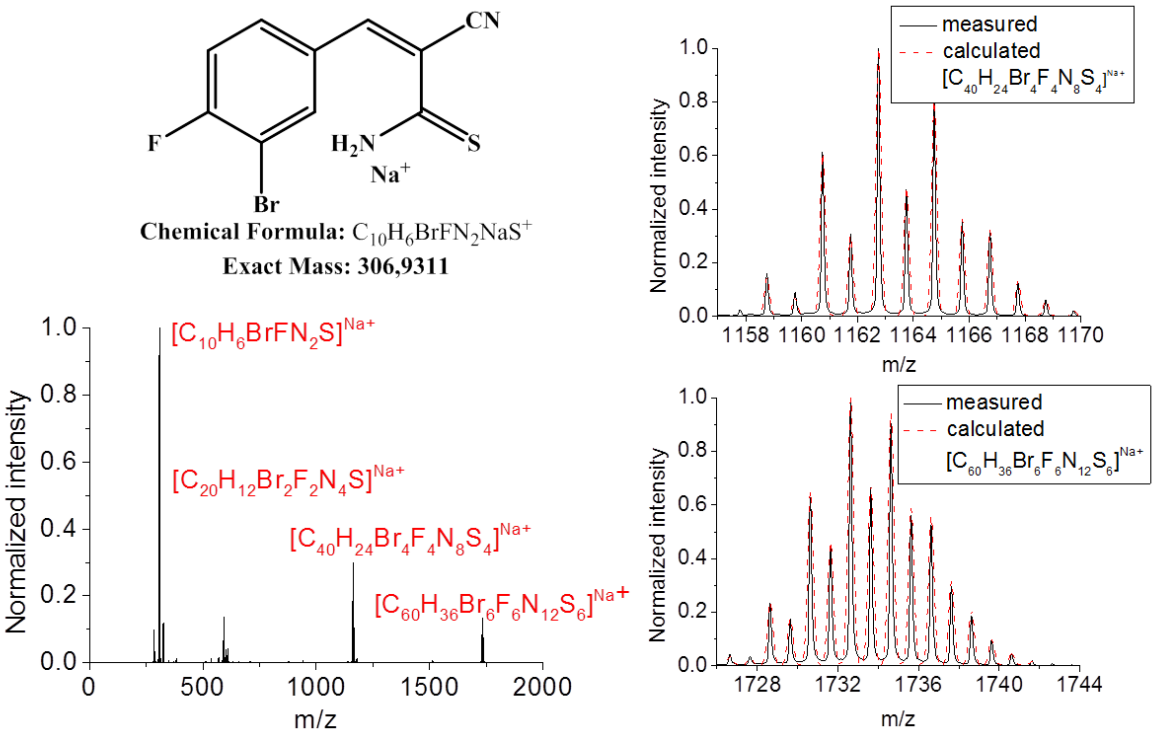

Figure S2. ESI-TOF mass spectrum of **3b4** with peak assignment and exemplary overlays of the measured and calculated isotopic patterns (tetrameric and hexameric species).

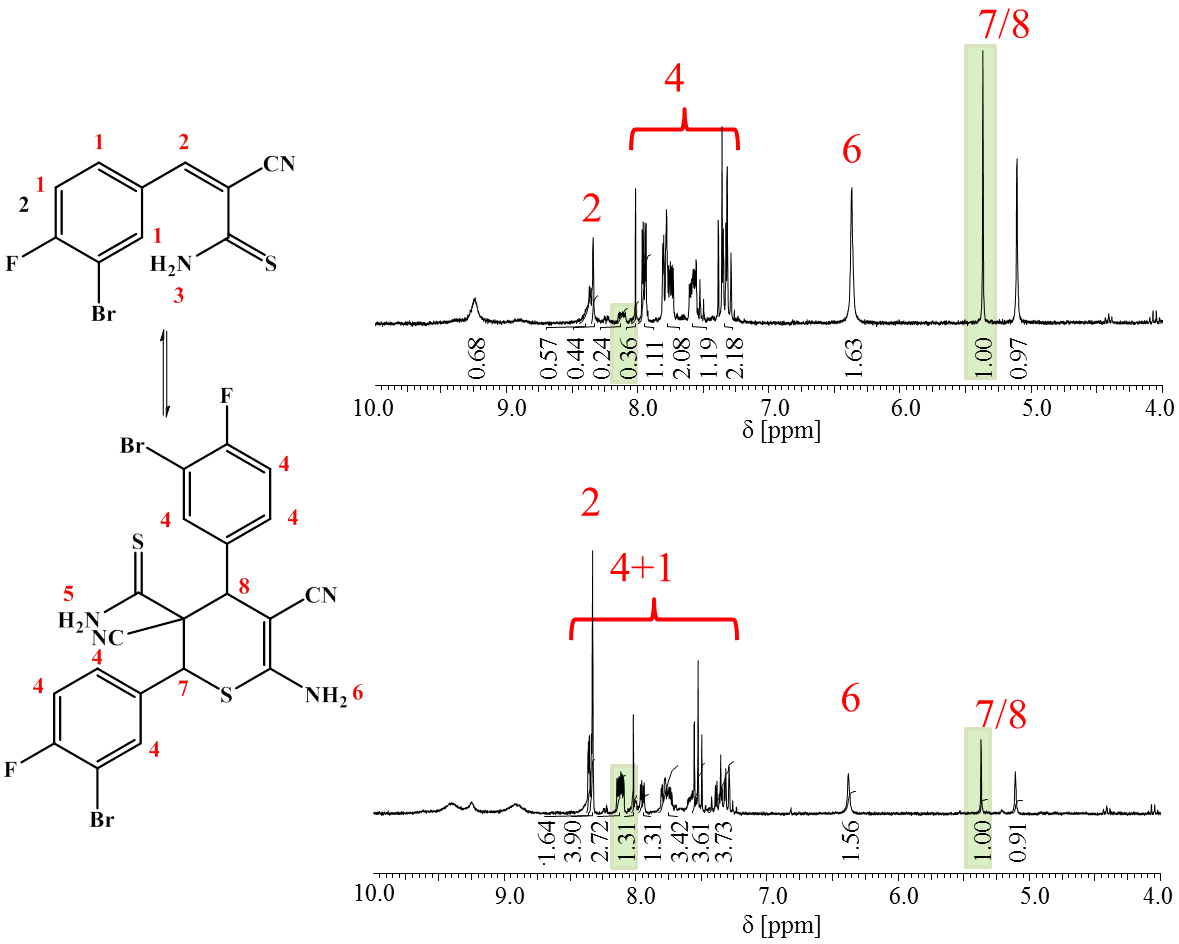

Figure S3. Kinetic study of the equilibrium of **3b4** at 25 °C in $(CD_3)_2CO$ after dissolving and after 16 d in solution.

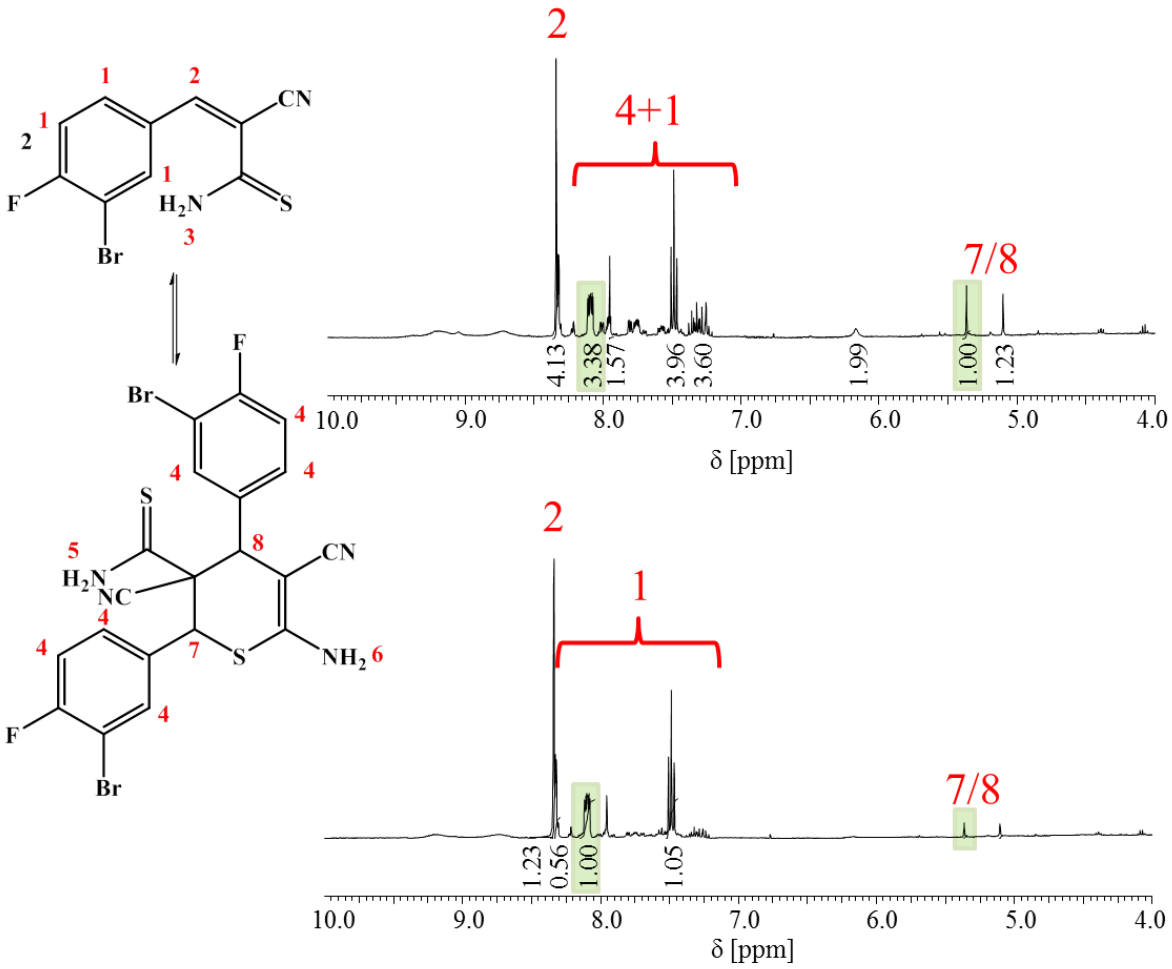

Figure S4. Kinetic study of the equilibrium of compound **3b4** at 50 °C in $(CD_3)_2CO$ after 15 min and after 16 h in solution.

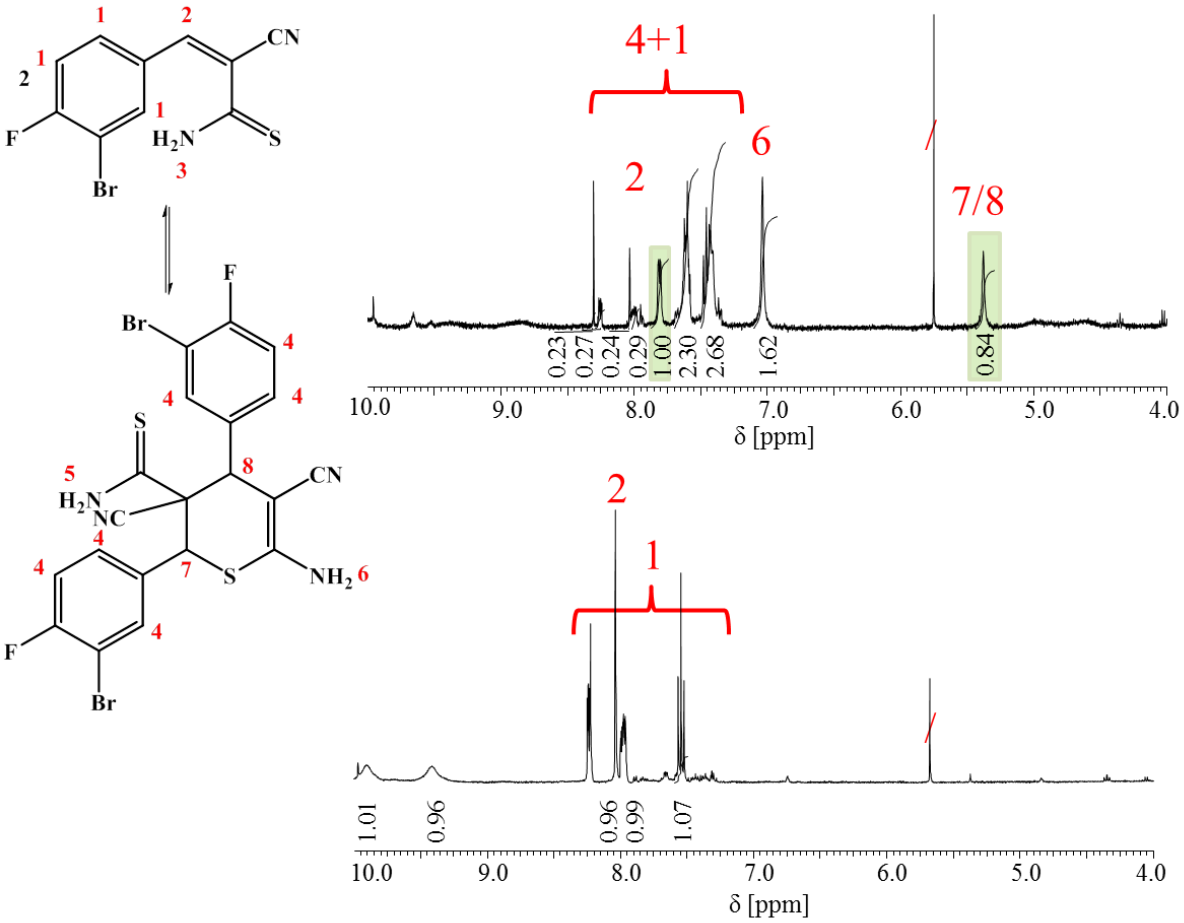

Figure S5. Kinetic study of the equilibrium of compound **3b4** at 70 °C in DMSO after dissolving and after 30 min in solution.

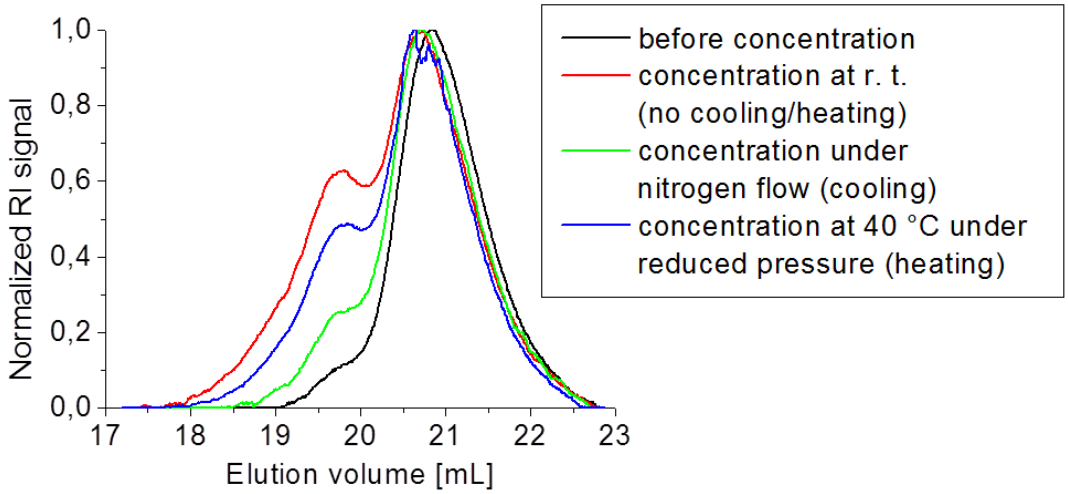

Figure S6. Concentration study of **3b5** in CH_2Cl_2.

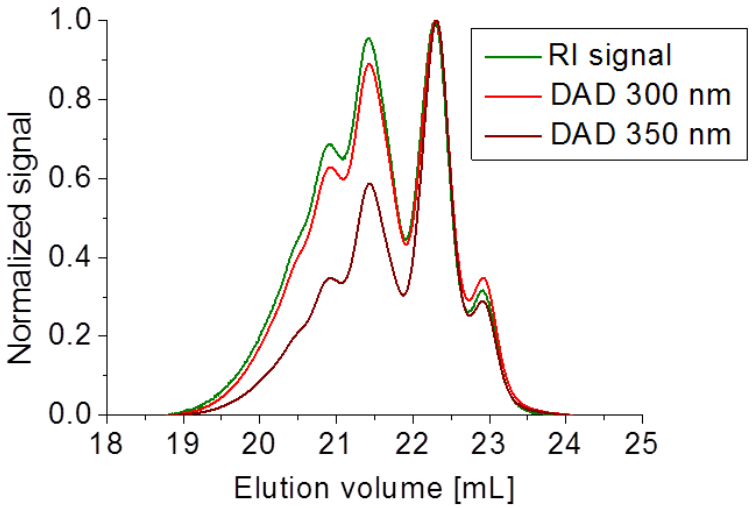

Figure S7. 2D spectrum of **3b5** with RID and DAD (at 300 and 350 nm).

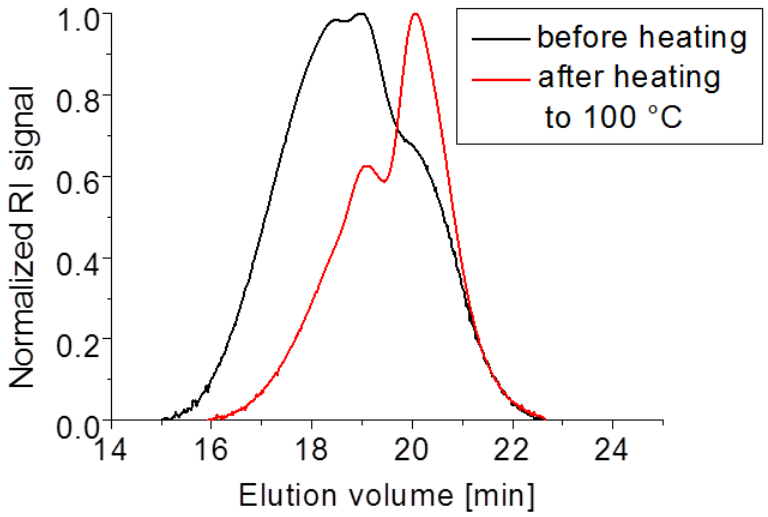

Figure S8. SEC traces of **3b5** before and after heating to 100 °C.

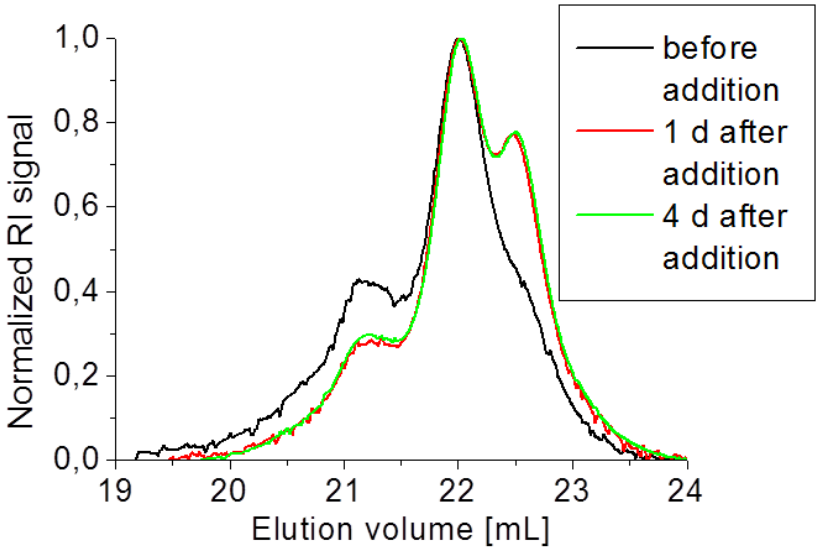

Figure S9**.** SEC traces of **3b5** before and after addition of 0.5 eq. $ZnCl_2$ per functional unit thioamide (c = 20 mg/mL).

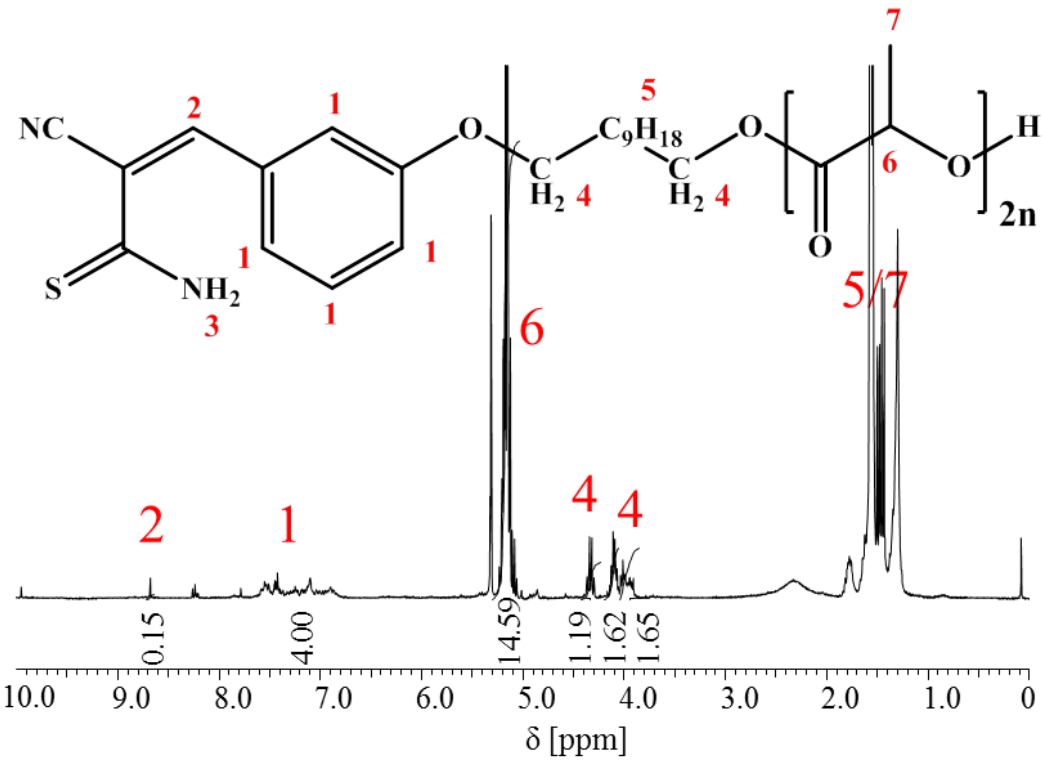

Figure S10. ^{1}H NMR spectrum of polymer **P1** in CD_2Cl_2.

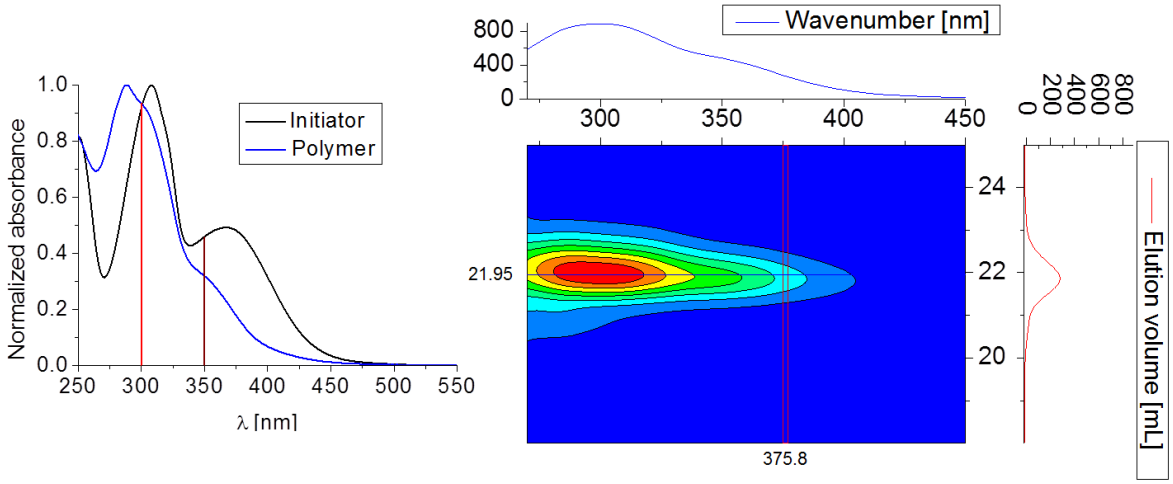

Figure S11. UV/Vis spectra of initiator **3b3** and polymer **P1** (left) and 3D plot of SEC measurement of **P1** with DAD (right).

Publication P3

“End-functionalized polylactides using a calcium-based precatalyst: Synthesis and insights by mass spectrometry”

Ilknur Yildirim, Sarah Crotty, Claas H. Loh, Grit Festag, Christine Weber, Pier-Francesco Caponi, Michael Gottschaldt, Matthias Westerhausen, Ulrich S. Schubert

J. Polym. Sci., Part A: Polym. Chem. **2016**, *54*, 437–448.

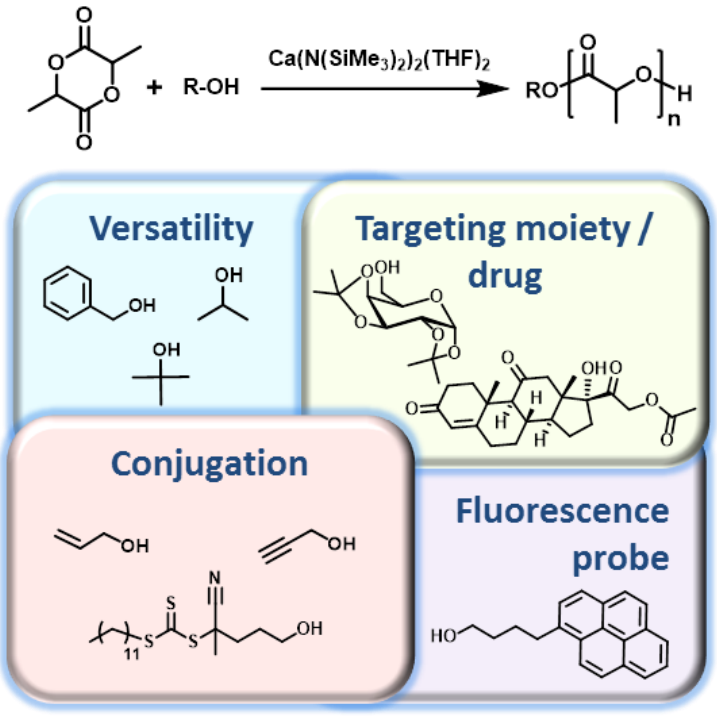

End-Functionalized Polylactides Using a Calcium-Based Precatalyst: Synthesis and Insights by Mass Spectrometry

Ilknur Yildirim,[1,2] Sarah Crotty,[1,2] Claas H. Loh,[3] Grit Festag,[1,2] Christine Weber,[1,2] Pier-Francesco Caponi,[1,2] Michael Gottschaldt,[1,2] Matthias Westerhausen,[3] Ulrich S. Schubert[1,2]

[1]Laboratory of Organic and Macromolecular Chemistry (IOMC), Friedrich Schiller University Jena, Humboldtstr. 10, 07743 Jena, Germany
[2]Jena Center for Soft Matter (JCSM), Friedrich Schiller University Jena, Philosophenweg 7, 07743 Jena, Germany
[3]Institute of Inorganic and Analytical Chemistry (IAAC), Friedrich Schiller University Jena, Humboldtstr. 8, 07743 Jena, Germany
Correspondence to: U. S. Schubert (E-mail: ulrich.schubert@uni-jena.de)

Received 1 June 2015; accepted 11 July 2015; published online 21 August 2015
DOI: 10.1002/pola.27795

ABSTRACT: A simple and convenient method for the synthesis of end functionalized polylactides (PLAs) under mild conditions by ring opening polymerization (ROP) in the absence of potentially toxic catalysts is described. Various alcohols were used as initiators in combination with $Ca[N(SiMe_3)_2]_2(THF)_2$ as the precatalyst in THF at room temperature. Tailored end functionalities were obtained in a controlled fashion. Matrix-assisted laser desorption/ionization time-of-flight mass spectrometry (MALDI-ToF-MS) and electrospray ionization quadrupole time of flight mass spectrometry (ESI-Q-ToF-MS) analysis were performed to investigate the end groups. The results confirmed that the end group fidelity was maintained in the isolated PLAs. © 2015 Wiley Periodicals, Inc. J. Polym. Sci., Part A: Polym. Chem. **2016**, *54*, 437–448

KEYWORDS: end-functional polymers; MALDI; mass spectrometry; polyesters; ring-opening polymerization

INTRODUCTION Polyesters are one of the most widely established biodegradable materials.[1] Amongst the leading polyesters, polylactide (PLA) represents a biocompatible, nontoxic, and biorenewable polymer.[2,3] Due to economic and inexpensive production procedures and attractive mechanical properties, PLA offers diverse and potent fields of application.[3] PLA is degraded by simple hydrolysis of the ester bonds. Its hydrolytic products can be transformed into nontoxic sub-products, which can be eliminated through normal cellular activity.[4] For these reasons PLA has found extensive applications in numerous fields particularly in biomedical and pharmaceutical areas,[5] such as the production of resorbable sutures, bioabsorbable implants for bone fixation, scaffolds for tissue engineering and carriers for controlled drug release systems.[6] Ring opening polymerization (ROP) of lactide initiated by stannous octoate (tin(II)−2-ethylhexanoate) is the most common strategy to produce PLA,[7,8] since stannous octoate is highly active towards the ROP of lactide and able to produce high molar mass PLA in bulk or in solution. Due to increasing concerns associated with the toxicity of tin compounds, its low control over the polymerization process with respect to tacticity and targeted molar masses, different catalyst/initiator systems for ROP of lactide have been investigated during the last decades.[8] Organocatalyzed ROP of lactide has been studied extensively by Waymouth and Hedrick resulting in metal–free polymers with predictable molar masses and narrow polydispersities.[9–11] An alternative approach involves enzyme-based catalytic systems, for example, lipases aimed at producing PLA in the absence of toxic catalytic residues.[12,13]

In parallel, new efficient initiators based on metal alkoxide systems such as aluminum alkoxides,[14] lanthanide alkoxides,[15] yttrium alkoxides,[16] and calcium alkoxides[17] are under investigation. All these catalysts are very promising in order to achieve precise control over the stereochemistry of PLA upon using a racemic mixture of monomers.[18] However, to the best of our knowledge, none of these systems have been investigated with respect to the possibility to covalently attach a wide range of therapeutic molecules, targeting moieties, fluorescent probes or reactive groups to the PLA, directly in the polymerization process. To this end, calcium-based systems are the most benign ones on account of being nontoxic, biocompatible, easily available, and suitable for biomedical purposes.[19–21] Hence several calcium-based systems

Additional Supporting Information may be found in the online version of this article.

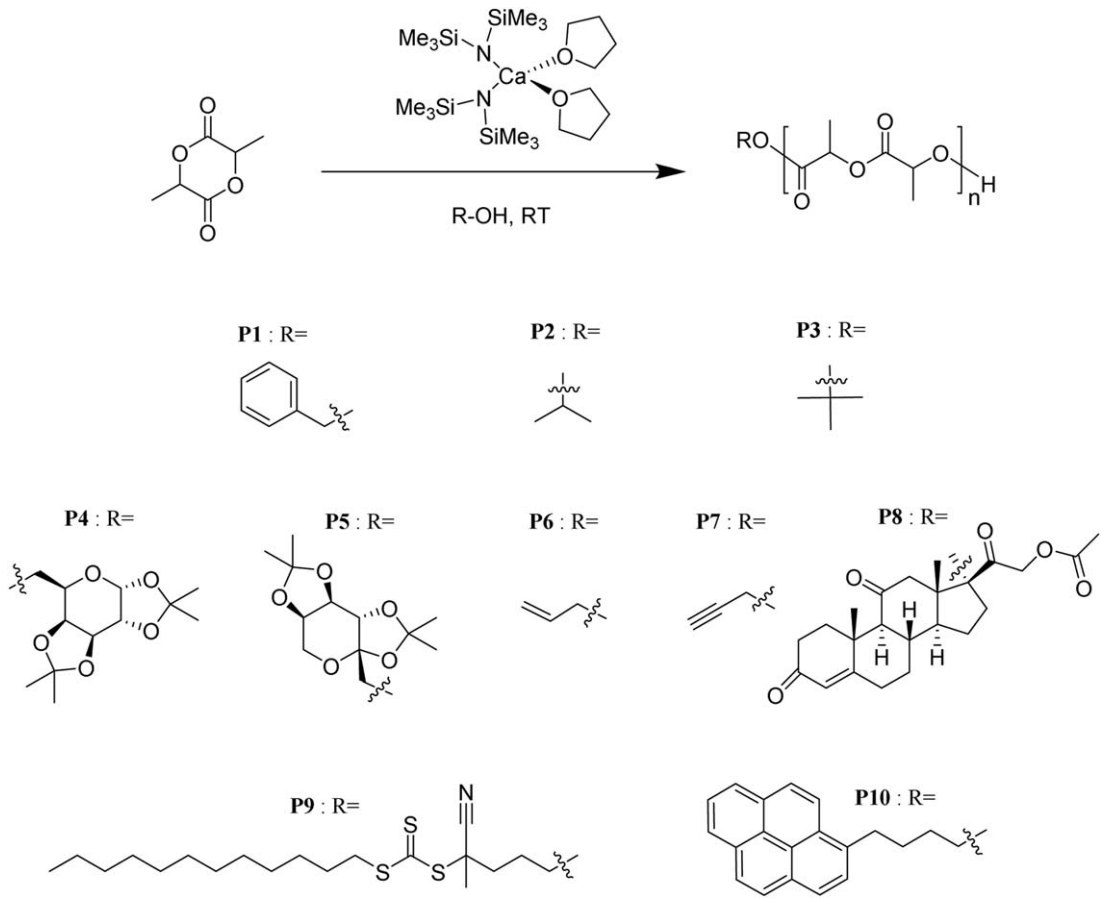

SCHEME 1 Schematic representation of the ROP of L-lactide using $Ca[N(SiMe_3)_2]_2(THF)_2$ as precatalyst and various alcohols (R-OH) as initiator precursors.

with high catalytic activity have been reported.[22–24] Calcium alkoxides can be formed *in situ* from suitable precursor complexes such as $Ca[N(SiMe_3)_2]_2(THF)_2$ and an alcohol. It could be previously demonstrated that such systems can be effective catalysts for the polymerization of both L-lactide and ε-caprolactone.[17,25] Herein, we report the synthesis of a series of end-functionalized PLA *via* ROP of L-lactide by the application of functional initiators, along with a detailed analysis by mass spectrometry. Compounds possessing primary, secondary and tertiary hydroxyl groups were used to elucidate the polymerization mechanism and to assess the reliability of the system toward the end group functionalization with a number of alcohols such as protected galactose and fructose, allyl alcohol, propargyl alcohol, a hydroxyl functionalized chain transfer agent (CTA) and 1-pyrenebutanol (Scheme 1). This synthetic technique enables the direct introduction of a series of different functional moieties (such as bioactive molecules or labels) to the PLA without the need to perform postpolymerization modifications. Nevertheless, several of the introduced functionalities are applicable to perform subsequent coupling reactions with further building blocks by application of highly efficient and mild methods, such as thiol-ene or 1,3-dipolar cycloadditions,[26,27] thereby providing a PLA counterpart for many beneficial functional moieties that are accessible nowadays. In addition, modern polymer chemistry currently benefits from the possibilities to switch from one polymerization technique to another, making it possible to combine advantageous properties of two different polymer types. As an example, we demonstrate the direct functionalization of PLA with a CTA, which enables the subsequent development of PLA block copolymers with a wide range of (meth)acrylate-based block segments by application of the reversible addition-fragmentation chain transfer (RAFT) polymerization technique.

EXPERIMENTAL

Materials

L-lactide (98%) was purchased from Sigma-Aldrich and purified by recrystallization from dry toluene and dried under vacuum. Bis(tetrahydrofuran)calcium bis[bis(trimethylsilyl)amide] ($Ca[N(SiMe_3)_2]_2(THF)_2$) was synthesized according to a previously reported procedure.[28] Benzyl alcohol (99.8%; water content $<0.003\%$), 2-propanol (99.5%; water content $<0.005\%$), 2-methyl-2-propanol ($\geq 99.5\%$; water content $<0.005\%$), 1,2:3,4-Di-O-isopropylidene-α-D-galactopyranose (DIP-Gal, 97%), allyl alcohol ($\geq 99\%$), propargyl alcohol (99%), cortisone-21-acetate ($\geq 99\%$), 1-pyrenebutanol (99%), and 4-cyano-4-[dodecylsulfanylthiocarbonyl)sulfanyl] pentanol (CDP) were purchased from Sigma-Aldrich and

used without further purification. 2,3:4,5-Di-O-isopropylidene-β-D-fructopyranose (DIP-Fru) was purchased from Carbosynth and was used as received. Tetrahydrofuran (THF) was dried by refluxing over sodium/benzophenone. All other chemicals were purchased from standard suppliers and used without further purification. All glassware was dried at 110 °C for 24 h prior to use for polymerization studies.

Instruments

All polymerizations were carried out under nitrogen in a MBraun UNILab glove box workstation. Proton nuclear magnetic resonance (^{1}H NMR) spectra were recorded at room temperature in $CDCl_3$ on a Bruker Avance 300 MHz using the residual solvent resonance as an internal standard. The chemical shifts are given in ppm relative to TMS. Size exclusion chromatography (SEC) measurements were performed on a Shimadzu system equipped with a SCL-10A system controller, a LC-10AD pump, a RID-10A refractive index detector, SPD-10AD UV detector and SDV linear M column from PSS (Polymer Standards Service GmbH, Mainz, Germany) at 40 °C using THF as eluent at a flow rate of 1 mL min^{-1}. The system was calibrated against PLA standards (144 to 101,000 g mol^{-1}), which were purchased from PSS. For the measurements of the matrix-assisted laser desorption/ionization (MALDI) spectra, an Ultraflex III ToF/ToF instrument (Bruker Daltonics, Bremen, Germany) was used. The instrument is equipped with a Nd-YAG laser and a collision cell. All spectra were measured in positive and reflector mode. The instrument was calibrated prior to each measurement with an external PMMA standard from PSS. For the MALDI-ToF-MS sample preparation, separate solutions of polymer (10 mg mL^{-1} in chloroform), *trans*−2-[3-(4-*tert*-butylphenyl)−2-methyl-2-propenylidene] (DCTB) (30 mg mL^{-1} in chloroform), and doping of sodium chloride (NaCl), lithium chloride (LiCl), silver trifluoroacetate (AgTFA) (100 mg mL^{-1} in acetone) were prepared and mixed following the dried droplet spotting technique. 1 μL of the mixture was spotted onto the target plate. For the ESI-Q-ToF-MS measurements, samples were analyzed by using a microToF Q-II (Bruker Daltonics) mass spectrometer equipped with an automatic syringe pump from KD Scientific for sample injection. The ESI-Q-ToF mass spectrometer was running at 4.5 kV, at a desolvation temperature of 180 °C. The mass spectrometer was operated in the positive ion mode. Nitrogen was used as the nebulizer and drying gas. All fractions were injected using a constant flow rate (3 μL min^{-1}) of sample solution. The ESI-Q-ToF-MS instrument was calibrated in the *m/z* range from 50 to 3000 using a calibration standard (Tunemix solution) which is supplied from Agilent. All data were processed *via* Bruker Data Analysis software version 4.0. UV-vis absorption measurements were performed on an Analytik Jena SPECORD 250 spectrometer (Analytik Jena, Jena, Germany).

Ring-Opening Polymerization

All polymerizations were carried out in a glove box, at room temperature under nitrogen atmosphere (<1 ppm H_2O, <1 ppm O_2), using THF as the solvent. In a typical polymerization, $Ca[N(SiMe_3)_2]_2(THF)_2$ (0.115 mmol) was dissolved in 1 mL of THF. Subsequently, this solution was added under vigorous stirring to the L-lactide (0.5 g, 3.47 mmol) and benzyl alcohol (0.23 mmol) mixture in 2.5 mL of THF ($[L\text{-lactide}]_0/[BnOH]_0/[Ca]_0 = 15/1/0.5$). After 10 min, the polymerization was quenched by adding 0.2 mL of 1 M HCl solution in methanol. PLA was isolated by precipitation in methanol and subsequent drying under reduced pressure until a constant weight was reached (yield: 0.3 g, 60%). ^{1}H NMR (300 MHz, $CDCl_3$): δ/ppm = 1.57 (d, —C(O)CH(C**H**$_3$)O—), 2.73 (broad, —C(O)C**H**(CH$_3$)(OH), 4.35 (q, —C(O)C**H**(CH$_3$)OH), 5.15 (q, —C(O)C**H**(CH$_3$)O—), 5.21 (s, C$_6$H$_5$(C**H**$_2$)OC(O) —), 7.33 (m, C$_6$**H**$_5$(CH$_2$)O C(O) —). M_n = 2100 g mol^{-1} (calculated based on the relative intensities of the signals at $\delta = 5.15$ and $\delta = 7.33$ ppm). SEC (THF, RI detection, PLA calibration): $M_{n,}$ = 1750 g mol^{-1}; $Đ$ = 1.17. MALDI-ToF-MS: M_n = 2100 g mol^{-1}; $Đ$ = 1.07.

Polymerization Kinetics

Kinetic studies of the ROP of L-lactide were performed in a glove box with nitrogen atmosphere (< 1 ppm H_2O, < 1 ppm O_2), at room temperature with THF as solvent ($[L\text{-lactide}]_0/[R\text{-OH}]_0/[Ca]_0 = 100/1/0.5$, $[L\text{-lactide}]_0 = 1$ M). In an exemplary kinetic study, $Ca[N(SiMe_3)_2]_2(THF)_2$ (0.035 mmol) was dissolved in 1.0 mL of THF, then added under vigorous stirring to the L-lactide (1 g, 6.9 mmol) and benzyl alcohol (0.069 mmol) solution in 6.0 mL of THF. The polymerization was monitored by sampling at defined time intervals, followed by ^{1}H NMR ($CDCl_3$, 300 MHz) and SEC analysis to determine the monomer conversion and the evolution of the molar mass, respectively. The conversion was determined by integrating the methine region of PLA (q, $\delta = 5.10$ ppm) versus that of the L-lactide (q, $\delta = 5.02$ ppm).

RESULTS AND DISCUSSION

Synthesis of PLA Using Primary, Secondary, and Tertiary Alcohols

Based on previous studies using $Ca[N(SiMe_3)_2]_2(THF)_2$ as catalyst for the ROP of L-lactide,[17] all polymerizations were performed in THF with a monomer concentration of 1.0 M. To facilitate an accurate determination of the PLA α-end groups that are introduced directly by the application of the functional alcohols, the ratio of [monomer] to [initiator] was set to 15 for all polymerizations ($[L\text{-lactide}]_0/[R\text{-OH}]_0/[Ca]_0 = 15/1/0.5$). To exploit the versatility of the calcium alkoxide system, a wide range of alcohols was utilized, comprising primary, secondary as well as tertiary hydroxyl moieties (Scheme 1). Table 1 summarizes the characterization results of the obtained polymers by means of SEC, ^{1}H NMR spectroscopy and mass spectrometry.

The ROP of L-lactide was carried out in the presence of benzyl alcohol (**P1**) and 2-propanol (**P2**) as model primary and secondary alcohols. The monomer conversions were almost quantitative after 10 min for both polymerizations, while monomodal SEC traces with low polydispersity values ($\leq$ 1.22) were obtained for each polymer (Fig. 1). The covalent attachment of each alcohol was confirmed by the ^{1}H NMR spectra of the purified polymers (Supporting Information

TABLE 1 Selected characterization data of polymers **P1** to **P10**[a]

Entry	Initiator	conv.[b] (%)	$M_{n,theo}$[c] (g mol^{-1})	$M_{n,NMR}$[d] (g mol^{-1})	$M_{n,SEC}$[e] (g mol^{-1})	$Đ_{SEC}$[e]	$M_{n,MALDI}$[f] (g mol^{-1})	$Đ_{MALDI}$[f]	$M_{n,ESI}$[g] (g mol^{-1})	$Đ_{ESI}$[g]
P1	Benzyl alcohol	100	2,270	2,100	1,750	1.17	2,100			
P2	2-Propanol	95	2,110	2,000	1,950	1.22	1,900			
P3	2-Methyl-2-propanol	85	1,900	2,900	3,000	1.22			3,000	1.17
P4	DIP-Gal	100	2,420	2,200	2,200	1.15	2,100	1.12		
P5	DIP-Fru	100	2,420	2,300	2,400	1.20	2,600	1.12		
P6	Allyl alcohol	100	2,220	1,950	1,600	1.23	1,900	1.17		
P7	Propargyl alcohol	100	2,220	2,200	2,800	1.24			2,800	1.08
P8	Cortisone-21-acetate	60	1,540	1,600	1,900	1.23			1,700	1.16
P9	CDP	100	2,550	2,700	2,300	1.18	2,400	1.07		
P10	1-Pyrenebutanol	100	2,440	2,600	2,800	1.25			3,000	1.08

[a] $[\text{L-lactide}]_0/[\text{R-OH}]_0/[\text{Ca}]_0 = 15/1/0.5$, $[\text{L-lactide}]_0 = 1$ M in THF, $t_{pol} = 10$ min, T = 25 °C.
[b] Conversion values determined by ^{1}H NMR spectroscopy from the polymerization mixtures.
[c] Number average molar mass (M_n) calculated according to $M_{n,theo} = [\text{L-lactide}]_0/[\text{R-OH}]_0 \cdot \text{conv.} \cdot 144.13 \text{ g mol}^{-1} + M_{(R\text{-}OH)}$.
[d] Calculated from suitable signal integrals in the ^{1}H NMR spectra of the purified polymers.
[e] Polydispersity index ($Đ$) determined by SEC (THF, RI detection, PLA calibration).
[f] Determined by MALDI-ToF-MS analysis.
[g] Determined by ESI-Q-ToF-MS analysis.

Figs. S1 and S2) that clearly showed peaks that can be assigned to the according α-end groups (aromatic proton signals at 7.33 ppm for **P1** and methine protons of 2-propanol end at 5.04 ppm for **P2**) next to the typical signals derived from PLA (5.15 ppm and 1.57 ppm). The molar masses of the calculated PLA was performed on the basis of the integration of these signals, which were very close to the theoretical values, hinting towards a high initiation efficiency and the absence of chain transfer reactions during the polymerization process. The end group fidelity of the polymers was further confirmed by MALDI-ToF mass spectrometry [Figs. 9(a) and S4(a)] revealing a single distribution with a repeating unit of $m/z = 72$. The peak masses can be assigned to alcohol initiated PLA chains with ω-hydroxyl end groups, which are ionized with a silver cation. The excellent agreement of the calculated and measured isotopic patterns is demonstrated by the overlays in Figure S3(a) and Figure 2(a), respectively.

2-Methyl-2-propanol was utilized as an exemplary tertiary alcohol initiator (**P3**) yielding 85% monomer conversion in 10 min. In this case, the molar mass calculated based on ^{1}H NMR analysis (Supporting Information Fig. S5) is higher than the theoretical molar mass but in good agreement with the one obtained from SEC analysis. MALDI-ToF-MS analysis was not successful due to poor ionization of **P3** although a range of different salts and sample preparation techniques were applied. In addition, the sample preparation can cause a slight offset, which is observed in the MALDI spectra. Therefore, ESI-Q-ToF mass spectrometry was used as an alternative technique and revealed spectra where the difference between two repeating units is 72 Da, which corresponds to

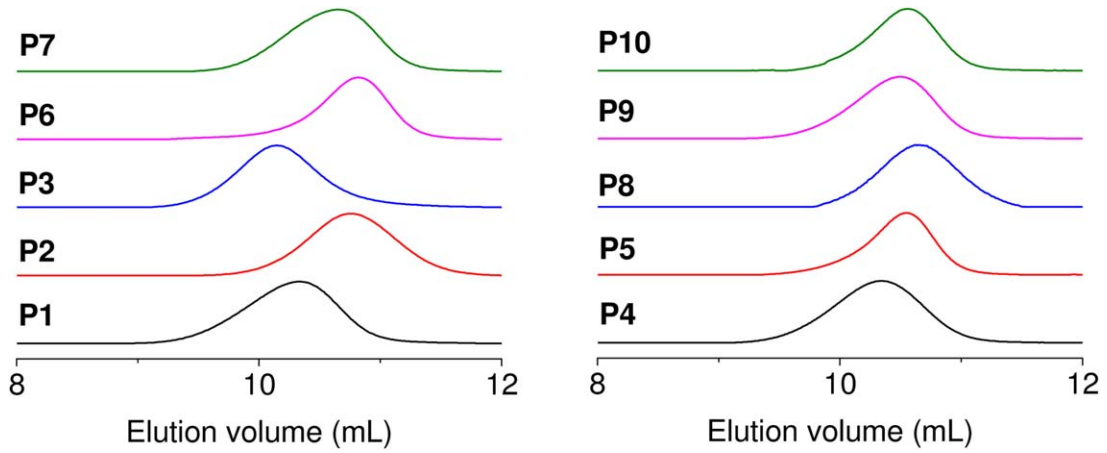

FIGURE 1 Normalized SEC traces (THF, RI detection) of the purified PLAs with different end functionalities. [Color figure can be viewed in the online issue, which is available at wileyonlinelibrary.com.]

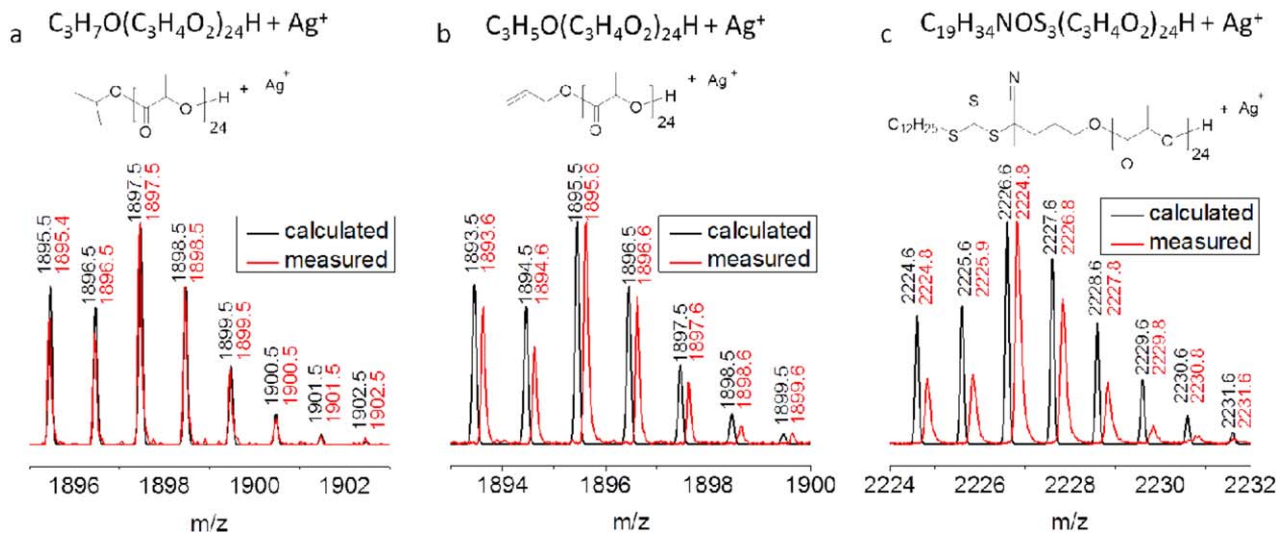

FIGURE 2 Overlay of calculated and measured isotopic patterns for the structural assignment of the observed peaks for (a) **P2**, (b) **P6**, and (c) **P9** measured by MALDI-ToF-MS. [Color figure can be viewed in the online issue, which is available at wileyonlinelibrary.com.]

2-methyl-2-propanol initiated α-end with hydroxyl terminating ω-end linear PLA chains. Besides this, two different minor distributions were also observable, which could not be assigned to initiation by water or to any cyclic products (Supporting Information Fig. S6). Although the ESI-Q-ToF mass spectrum contained additional doubly charged species, the molar mass obtained after deconvolution is in good agreement with the values from ^{1}H NMR spectra and SEC. This indicates that not all PLA chains have been initiated by the tertiary alcohol.

Synthesis of α-End Functional PLA

Considering the fact that PLA is widely applied in the biomedical field, saccharide polymer conjugates are of high interest for site specific targeted drug delivery and for cell recognition studies.[29,30] It is obvious that protected saccharides have to be used as initiators to prevent multiple initiations at one sugar molecule. Among the range of suitably protected carbohydrates, we selected to investigate *iso*-propylidene protected galactose (DIP-Gal) and fructose (DIP-Fru) as initiators for the ROP of L-lactide. The resulting polymers with the protected galactose (**P3**) and fructose (**P4**) end groups were obtained with narrow polydispersity values ($\leq$ 1.2). The introduction of these functional groups at the α-chain end of PLA was confirmed by ^{1}H NMR analysis (Fig. 3). The characteristic peaks derived from the saccharides were observed in the range of $\delta = 3.5$ to 5.5 ppm. Besides, the peak of the hydroxyl proton at the ω-chain end is clearly

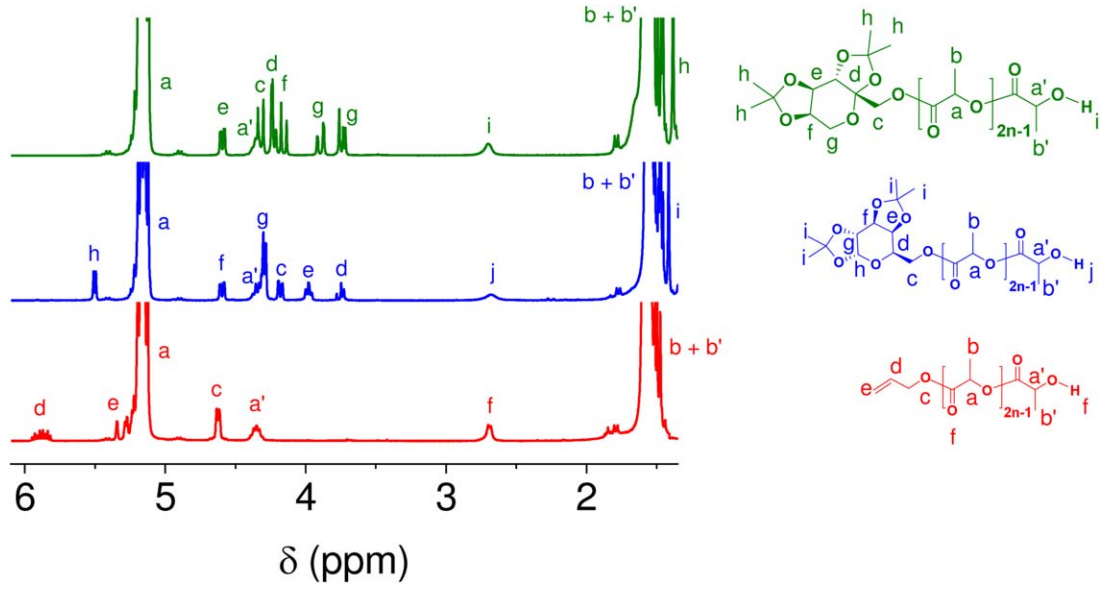

FIGURE 3 ^{1}H NMR spectra (300 MHz, $CDCl_3$) of **P4**, **P5**, and **P6** with assignment of the peaks used for M_n calculations. [Color figure can be viewed in the online issue, which is available at wileyonlinelibrary.com.]

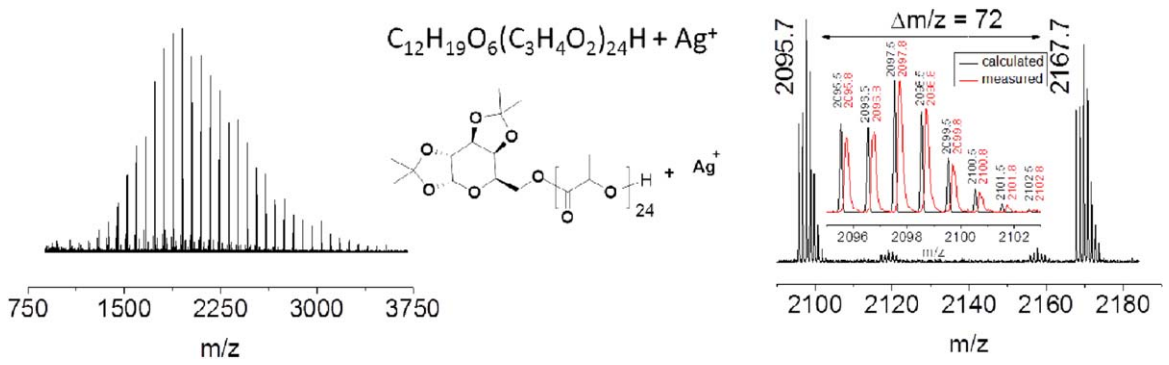

FIGURE 4 Left: MALDI-ToF mass spectrum of the **P4** (AgTFA, DCTB). Right: Zoomed-in view the MALDI-ToF mass spectrum of the DIP-Gal functionalized polymer **P4** and overlay of the calculated and measured isotopic pattern for the structural assignment of the observed peaks. [Color figure can be viewed in the online issue, which is available at wileyonlinelibrary.com.]

observed at $\delta = 2.6$ ppm. The MALDI-ToF mass spectra revealed a single series of peaks at regular intervals spaced by $m/z = 72$. The experimental isotopic pattern corresponds exactly to the theoretical values for the expected isotopes (Figs. 4 and 5), demonstrating the successful end-functionalization.

Polymers bearing unsaturated end functionality are very useful as universal building blocks for the synthesis of functional materials *via* azide-alkyne or thiol-ene click reactions.[26,27,31,32] For this reason, allyl alcohol (**P6**) and propargyl alcohol (**P7**) were used as initiators, which can be further functionalized with azide or thiol bearing molecules. The structures of PLAs containing unsaturated end groups were confirmed by ^{1}H NMR analysis. The end functionalities are clearly evidenced and quantified by the characteristic resonances of the alkene group at $\delta = 4.6$ ppm (Fig. 3) and the alkyne group at $\delta = 2.5$ ppm (Supporting Information Fig. S7), respectively. Monomodal mass distributions were obtained for both polymers (Fig. 1). MALDI-ToF MS analysis of **P6** [Supporting Information Fig. S4(b)] revealed a single distribution with a m/z difference of 72 between two neighboring peaks, which further proves that the polymers possess an alkene residue at the α-chain end and a hydroxyl residue at the ω-chain end [Fig. 2(b)]. The end group functionality of **P7** was confirmed by ESI-Q-ToF MS analysis revealing the expected PLA chains with propargyl as the initiating and hydroxyl as the terminating end groups (Fig. 6).

The catalytic performance of the precatalyst Ca[N(SiMe$_3$)$_2$]$_2$(THF)$_2$ was further confirmed by the polymerization of L-lactide using cortisone-21-acetate as initiator (**P8**), which is a topical corticosteroid used, for example, in the treatment of inflammatory diseases,[33] asthma and arthritis.[34] However, its long term use can cause severe side effects like osteoporosis and hypertension. It is known that macromolecules accumulate at sites of inflammation due to the enhanced permeability and retention (EPR) effect; they can also be used as a rate controlling matrix for biologically active compounds. An appropriate polymer conjugate could be advantageous for targeted drug delivery to the site of inflammation.[33,35,36] When cortisone-21-acetate was used as initiator, monomer conversion was 60% after 10 min, which indicates a lower initiation efficiency of cortisone-21-acetate compared to the alcohols described before. Nevertheless, the slower initiation did not prevent the achievement of a well-defined cortisone bearing PLA as demonstrated by ESI-Q-ToF-MS analysis [Fig. 7(a)] and ^{1}H NMR spectroscopy

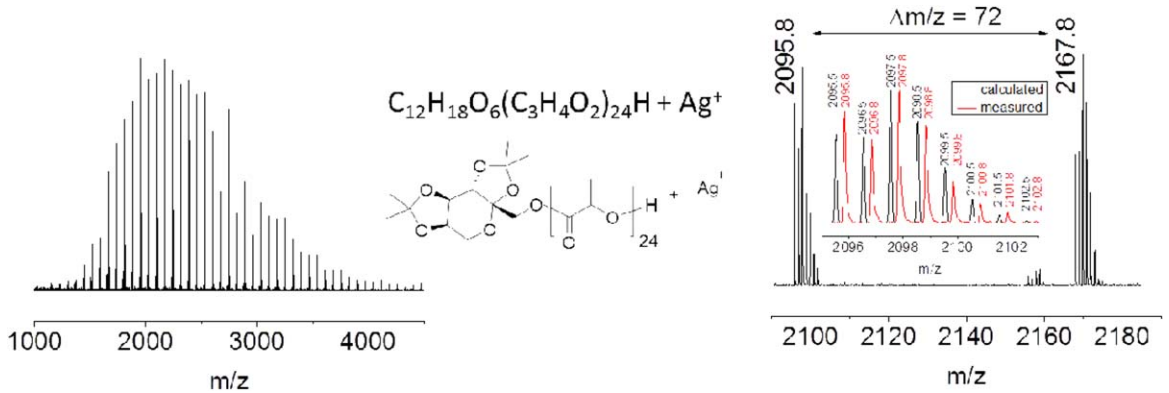

FIGURE 5 Left: MALDI-ToF mass spectrum of **P5** (AgTFA, DCTB). Right: Zoomed-in view the MALDI-ToF mass spectrum of the DIP-Fru functionalized polymer **P5** and overlay of the calculated and measured isotopic pattern for the structural assignment of the observed peaks. [Color figure can be viewed in the online issue, which is available at wileyonlinelibrary.com.]

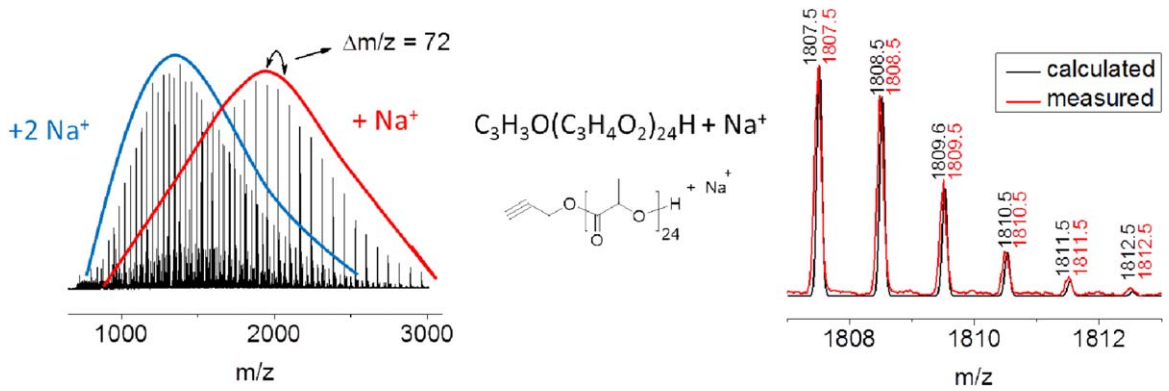

FIGURE 6 ESI-Q-ToF mass spectra and overlay of calculated and measured isotopic patterns for the structural assignment of the observed peaks **P7**. Both spectra show overlapping *m/z* series of the same PLA species that are either ionized with one ($z = 1$) or two ($z = 2$) sodium cations, respectively. [Color figure can be viewed in the online issue, which is available at wileyonlinelibrary.com.]

(Supporting Information Fig. S8). The SEC traces of **P8** were recorded both with RI and UV detection [Supporting Information Fig. S9(b)], exploiting the UV absorbance of cortisone-21-acetate at 235 nm [Supporting Information Fig. S9(a)]. Both SEC traces showed similar shapes and retention times indicating that the cortisone moiety is bound covalently to the polymer. Since the ester functionalities of the PLA alone reveal a λ_{max} at 210 nm in THF (Figure S9a), **P2**

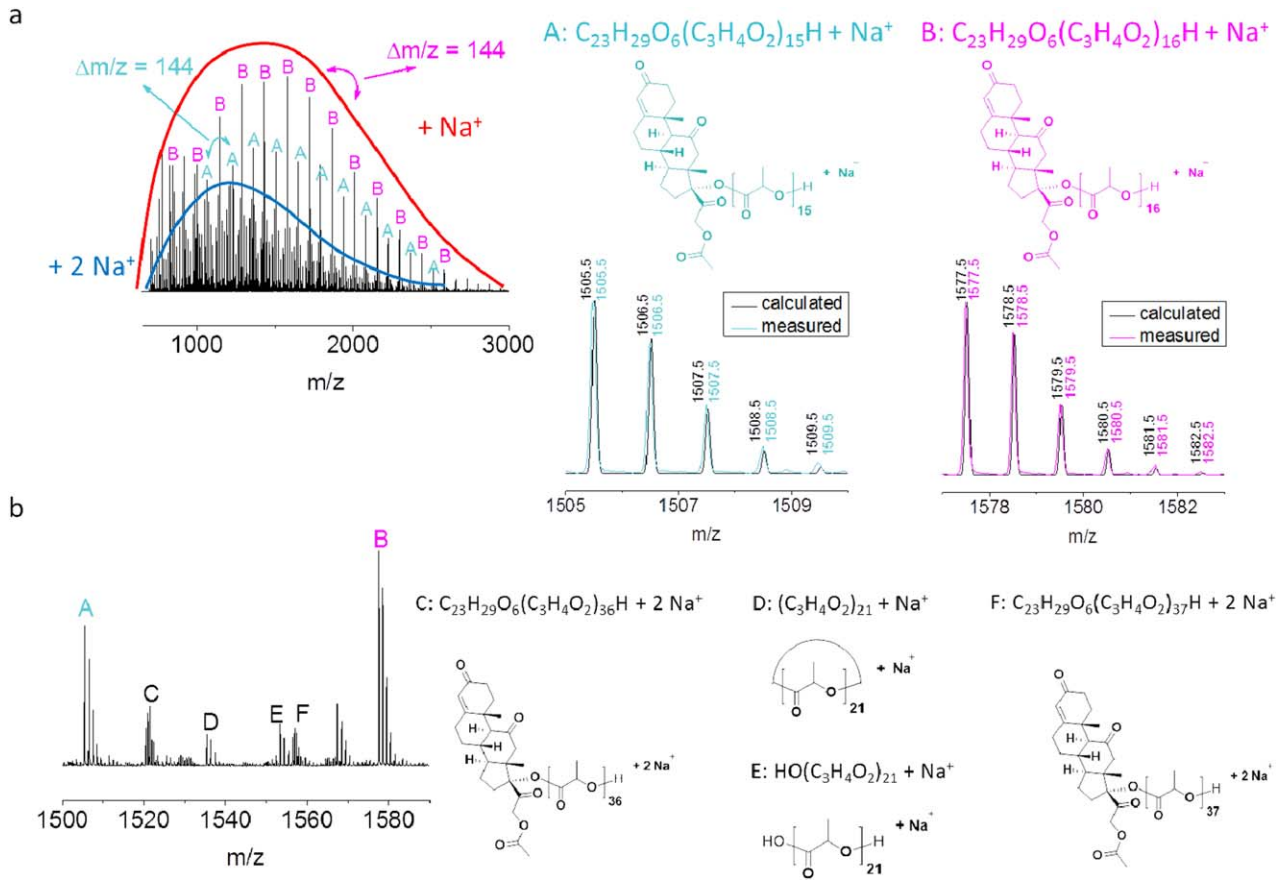

FIGURE 7 (a) ESI-Q-ToF mass spectra and overlay of calculated and measured isotopic patterns for the structural assignment of the observed peaks of **P8**. Both spectra show overlapping *m/z* series of the same PLA species that are either ionized with one ($z = 1$) or two ($z = 2$) sodium cations, respectively. (b) Zoomed-in view the ESI-Q-ToF mass spectra for the structural assignment of the minor distributions. [Color figure can be viewed in the online issue, which is available at wileyonlinelibrary.com.]

was measured with the same SEC method. A comparison of the SEC traces subsequent to normalization according to the respective RI traces shows that the UV signal is much more pronounced for **P8** than for **P2** (around 50 times, Figure S9c), thus confirming the covalent attachment of the cortisone-21-acetate.

Upon first glance, the ESI-Q-ToF mass spectrum of **P8** [Fig. 7(a)] reveals two main distributions with $\Delta m/z = 144$ in the singly charged region. However, within both distributions the peaks correspond to the masses expected for polymer chains initiated by cortisone-21-acetate (with a hydroxyl group as the ω-chain end). The main distribution corresponds to PLA chains with an even number of repeating units, whereas the second distribution corresponds to PLA chains with an odd number of repeating units.

Moreover, CDP, a hydroxyl functionalized trithiocarbonate RAFT agent, was utilized as an initiator. The resulting functional PLA represents a macro CTA, enabling the development of block copolymers of PLA with a wide range of (meth)acrylate-based monomers. A complete monomer conversion was observed in 10 min and yielded a polymer (**P9**) with monomodal mass distribution (Fig. 1) and low polydispersity (Table 1). ^{1}H NMR analysis confirmed that the hydroxyl functionalized trithiocarbonate acted as the initiator to yield PLA possessing the functional moieties (Supporting Information Fig. S10) and enabled observation of specific signals from initiator in the regions $\delta = 3.3$ and $\delta = 4.2$ ppm. The end group was confirmed by MALDI-ToF-MS analysis revealing a single distribution with peaks spaced in regular intervals of 72 Da [Fig. S4(c)] and an isotopic splitting pattern, which is in agreement with the theoretical values [Fig. 2(c)].

Finally, 1-pyrenebutanol was used as initiator to result in a polymer with a covalently attached fluorescence label, which can provide the basis for biological diagnostics, such as cellular uptake studies, optical imaging and signal amplification.[37] Almost 100% monomer conversion was achieved and a polymer (**P10**) with monomodal mass distribution (Fig. 1) was obtained within 10 min (Table 1). ^{1}H NMR analysis confirmed that the isolated PLA bears the 1-pyrenebutanol moiety (Supporting Information Fig. S11). Specific resonances of the pyrene ring were observed in the regions of $\delta = 7.80$ and $\delta = 8.30$ ppm. Supporting Information Figure S12 displays the ESI-Q-ToF mass spectrum and the mass assignments for the PLA chain, which has a 1-pyrenebutanol initiating and hydroxyl terminating end group with peak distributions spaced by $m/z = 72$.

Mass Spectrometry and Kinetic Studies

Upon comparison of all mass spectra discussed above, except when cortisone-21-acetate is used as initiator, it is remarkable that the m/z difference between two peaks of the same series is $\Delta m/z = 72$ while the mass of one lactide monomer corresponds to 144 Da. Thus, upon addition of one cyclic monomer to the growing PLA chain, one would expect a $\Delta m/z = 144$ in the mass spectra (when singly charged). Apart from a pioneering study by Montaudo et al. from 1996,[38] similar observations are mostly only briefly reported for other alkoxide complexes used as catalysts for lactide polymerization. Apparently, the metal ion does not have a large impact, since these complexes described in literature are based on actinoides,[39] alkali metals,[40] alkaline earth metals,[41] titanium,[42] zirconium,[43] and zinc.[44] The only exceptions from this trend seems to be an aluminum catalyst with a sterically demanding multidentate salen-type ligand[45,46] and a zinc catalyst[47] that was applied without addition of an alcohol as co-initiator.

To the best of our knowledge, no detailed comprehensive MS studies exist that include both the comparison of ionization conditions applying two different soft ionization techniques as well as a broad range of different alcohols as co-initiators.

The easiest explanation for the occurrence of $\Delta m/z = 72$ in the mass spectra would be an in-source fragmentation taking place during the measurements. However, this would result in PLA chains with various end groups, and fragment peaks at lower m/z values. Since ESI-Q-ToF-MS represents the "softer" ionization technique, such a fragmentation would rather be evidenced by MALDI-ToF-MS measurements. Thus, we tested several measurement conditions by the variation of the added salt during sample preparation (Supporting Information Fig. S13 for MALDI-ToF mass spectra obtained with **P9**). Indeed, LiCl and NaCl certainly do induce a fragmentation of the PLA, which is evidenced by the fragment peaks in the region below $m/z = 2000$. However, no fragment peaks could be observed when the measurements were performed using AgTFA, while the $\Delta m/z$ remained 72.

The most common explanation in literature for the observed $\Delta m/z$ of 72 is the occurrence of transesterification reactions. In most reported cases, the relative abundance of the peaks in the mass spectra that are assigned to PLA chains with an odd number of repeating units is lower compared to the peaks derived from chains with an even number of repeating units.[44,48] As depicted in Supporting Information Scheme S1, an intramolecular chain transfer results in cyclic PLA and PLA chains with a lower degree of polymerization (DP).[49,50] Since cyclic PLA chains are not evident in any of the discussed mass spectra except for **P8**, it can be concluded that the intramolecular chain transfer reaction does not cause the $\Delta m/z$ of 72. Because the end groups of the intermolecular transesterification products do not differ from those of the initial PLA chains (Supporting Information Scheme S1) analysis by mass spectrometry alone is not sufficient to judge their occurrence.

Assuming constant rate coefficients for both, chain transfer k_{tr} and propagation k_p, throughout the course of the polymerization, the transesterification should become predominant towards the end of the polymerization when the monomer concentration is already low.[50,51] High k_{tr} will, therefore, result in significantly increased polydispersities, $Đ$, at high monomer conversions.[51] Thus, kinetic studies were performed using three different alcohol precursors, namely

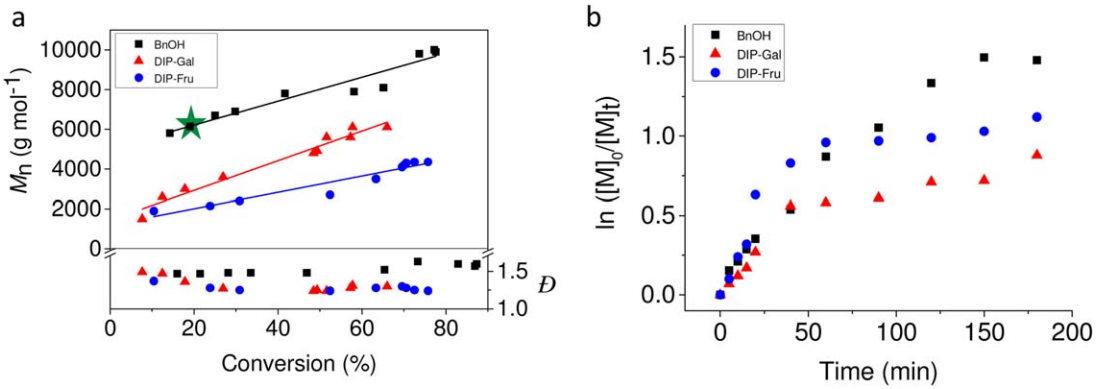

FIGURE 8 Kinetic studies initiated with benzyl alcohol, DIP-Gal and DIP-Fru at room temperature in THF with a total monomer concentration of 1 mol L^{-1}. [M]/[R-OH]/[Ca] = 100/1/0.5. (a) Dependence of $M_{n,SEC}$ and $Đ$ of the obtained PLA on L-lactide conversion. (b) Semilogarithmic kinetic plots. ★ indicates the sample analyzed by MALDI-ToF-MS in comparison with **P1**. [Color figure can be viewed in the online issue, which is available at wileyonlinelibrary.com.]

benzyl alcohol, DIP-Gal and DIP-Fru in THF at room temperature ([L-lactide]$_0$/[R-OH]$_0$/[Ca]$_0$ = 100/1/0.5, [L-lactide]$_0$ = 1 M). Aliquots were taken from the polymerization mixture at defined intervals to monitor the monomer conversion and the evolution of the molar mass during the polymerization. Monomodal SEC traces were obtained throughout the whole polymerization process. The molar mass was found to increase in a linear fashion with increasing monomer conversion for all investigated initiators, while $Đ$ remained constant or even slightly decreased [Supporting Information Fig. S14 and Fig. 8(a)]. The semilogarithmic kinetic plot for all three initiators resembles the plot that was previously reported for 2-propanol.[17] An induction period is not observed, which indicates extremely fast alcoholysis of the calcium amide. Subsequent

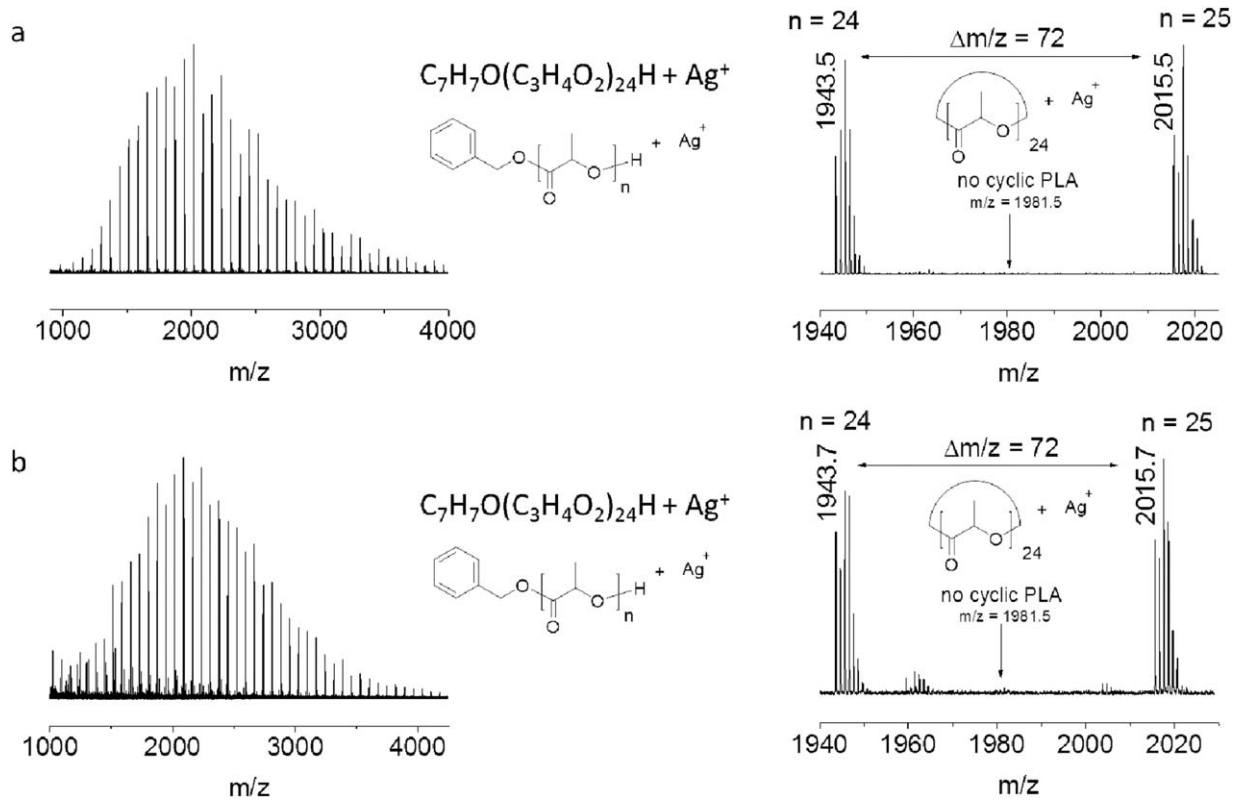

FIGURE 9 (a) Left: MALDI-ToF mass spectrum (AgTFA, DCTB) of (**P1**). Right: Zoomed-in view the MALDI-ToF mass spectrum for the structural assignment of the observed peaks. (b) Left: MALDI-ToF mass spectrum (AgTFA, DCTB) of the sample taken from polymerization mixture during kinetic study with benzyl alcohol as initiator, at 10 min with 18% monomer conversion. Right: Zoomed-in view the MALDI-ToF mass spectrum for the structural assignment of the observed peaks.

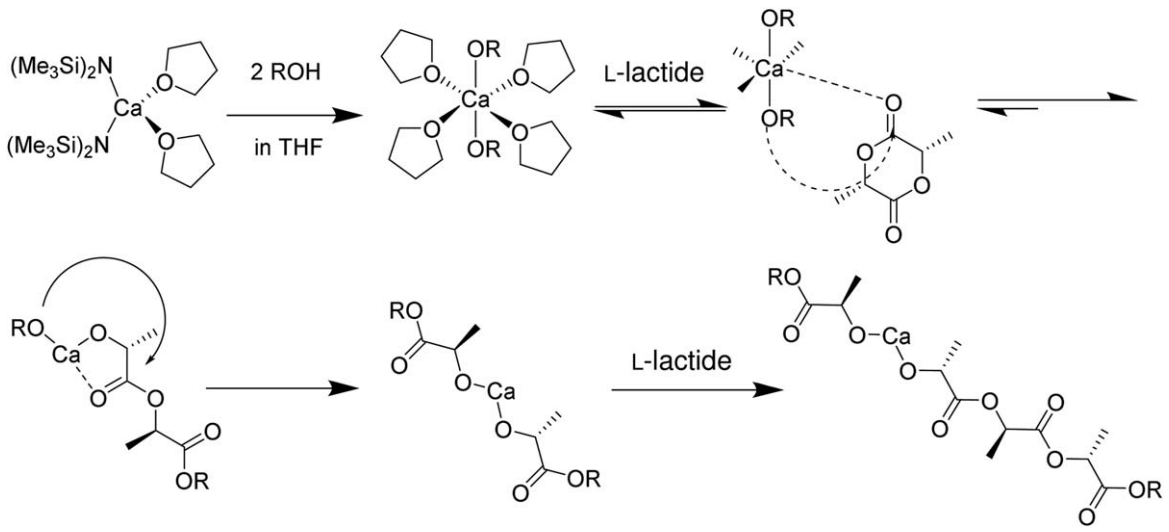

SCHEME 2 Ring-opening of lactide by $Ca(OR)_2$ and subsequent intramolecular ester cleavage by the second alcoholate anion yielding a homoleptic complex that would lead to an uneven number of repeating units in the PLA chain.

to a fast propagation at early stages as a result of an increase in temperature due to the exothermic alcoholysis of the calcium amide, the polymerization rate decreases significantly [Fig. 8(b)].

Figure 9 shows a MALDI-ToF mass spectrum obtained from a sample taken at a very early stage of the polymerization ($t = 10$ min) in direct comparison with the spectrum of **P1**. Both PLAs were initiated using benzyl alcohol and have very similar molar masses, thereby avoiding mass discrimination effects, which might influence the resulting mass spectra. The analytes differ only in the monomer conversion, which was quantitative for **P1** and 18% for the kinetic sample. If the $\Delta m/z$ of 72 in the mass spectra was caused by an intramolecular chain transfer reaction the relative abundance of the peaks associated with an odd number of repeating units should increase with monomer conversion (see above). This observation was made by Montaudo et al. for PLA synthesized with an aluminum-salen type catalyst.[38] However, the peaks resulting from PLA with an odd number of repeating units are not more prominent in the mass spectrum of **P1** than in the spectrum of the kinetic sample. In contrast, both spectra almost match each other, revealing a single distribution with $\Delta m/z = 72$ that can be assigned to alcohol initiated and hydroxyl terminated PLA chains (see Supporting Information Fig. S3).

As an alternative, the odd number of repeating units of the PLA formed by catalysis using $Ca[N(SiMe_3)_2]_2(THF)_2$ may result from the fact that more than one alkoxide is coordinated at one calcium atom.[25] However, it has to be stated that the exact structure and the number of THF ligands of the calcium complex during polymerization is not clear yet. Scheme 2 depicts a proposed mechanism that involves one calcium complex with two alkoxide ligands. Subsequent to the activation of the carbonyl oxygen of the lactide monomer one alkoxide can attack the cyclic ester, which results in an opening of the lactide monomer.[17,52] While the newly formed alkoxide species remains coordinated on the calcium, the second carbonyl oxygen of the (already opened) lactide monomer is prone to a nucleophilic attack because an activation by the same calcium ion is easily possible *via* a 5-membered ring. The subsequent formation of an ester functionality with the second coordinated alkoxide RO^- would indeed result in a "splitting" of the lactic acid dimer and yield homoleptic $Ca(O\text{-}CH(Me)\text{-}COOR)_2$. If this intramolecular ester cleavage proceeded throughout the entire polymerization, PLA chains would form with both even and odd numbers of repeating units in an equal ratio, independent from the monomer conversion.

CONCLUSIONS

In this study we have successfully synthesized end-functionalized PLAs *via* ring opening polymerization of L-lactide with heavy metal free catalysis in a mild and efficient manner using a variety of alcohols as initiator precursors. The utilized calcium-based precatalyst could be applied with primary, secondary as well as tertiary alcohols. This enabled the direct introduction of two protected sugars, which both can potentially serve as target molecules to direct a drug carrier towards the desired "site of action." As an exemplary drug molecule, cortisone-21-acetate was successfully used as initiator, demonstrating the possibility to obtain polymeric prodrugs; and the fluorescent label pyrene could be introduced in a similar fashion. Since the mechanism of the ROP prohibits the presence of many functional moieties (which are present in other bioactive molecules) during the polymerization, alkene and alkyne functionalized initiators were used. This provides the opportunity to attach such molecules by highly efficient and mild coupling methods, such as thiol-ene addition or the azide-alkyne "click" reaction, which will

be in the focus of future studies. Finally, the successful utilization of a hydroxyl-functional CTA as initiator for the ROP provides the basis to attach a second hydrophilic block to the PLA by combination with the RAFT polymerization technique.

All PLAs were well-defined in terms of molar mass distribution and end groups, as confirmed by SEC, NMR spectroscopy as well as intensive investigations by MALDI-ToF and ESI-Q-ToF MS. Although all polymer chains carried the desired end groups, the MS studies revealed the fact that the obtained PLAs are rather composed of lactic acid repeating units instead of the lactide dimers, which suggests that an intramolecular rearrangement takes place at the active catalytic center during the polymerization. Future research will concentrate on further elucidation of the proposed mechanism as well as on the exploitation of this very potent precatalyst by using other lactone-type monomers and the further functionalization of our building blocks to yield (targeted) drug delivery vehicles.

ACKNOWLEDGEMENTS

The authors wish to thank Nicole Fritz for the ESI-Q-ToF-MS measurements. We gratefully acknowledge the financial support of the Carl Zeiss Foundation, the Thuringian Ministry of Education, Science and Culture (Thüringer Ministerium für Bildung, Wissenschaft und Kultur, grants no. B515-07008 and B715-08011), the Graduate Academy of the Friedrich Schiller University Jena, and the Ernst Abbe Foundation. We also thank Bruker Daltonics for their support.

REFERENCES

1 K. E. Uhrich, S. M. Cannizzaro, R. S. Langer, K. M. Shakesheff, *Chem. Rev.* **1999**, *99*, 3181–3198.

2 C. M. Thomas, J.-F. Lutz, *Angew. Chem. Int. Ed.* **2011**, *50*, 9244–9246.

3 J.-M. Raquez, Y. Habibi, M. Murariu, P. Dubois, *Prog. Polym. Sci.* **2013**, *38*, 1504–1542.

4 A. J. R. Lasprilla, G. A. R. Martinez, B. H. Lunelli, A. L. Jardini, R. M. Filho, *Biotechnol. Adv.* **2012**, *30*, 321–328.

5 A.-C. Albertsson, I. K. Varma, *Biomacromolecules* **2003**, *4*, 1466–1486.

6 Z. Zhong, S. Schneiderbauer, P. Dijkstra, M. Westerhausen, J. Feijen, *Polym. Bull.* **2003**, *51*, 175–182.

7 A. Otero, J. Fernández-Baeza, A. Lara-Sánchez, C. Alonso-Moreno, I. Márquez-Segovia, L. F. Sánchez-Barba, A. M. Rodríguez, *Angew. Chem. Int. Ed.* **2009**, *48*, 2176–2179.

8 J. Guo, P. Haquette, J. Martin, K. Salim, C. M. Thomas, *Angew. Chem. Int. Ed.* **2013**, *52*, 13584–13587.

9 N. E. Kamber, W. Jeong, R. M. Waymouth, R. C. Pratt, B. G. G. Lohmeijer, J. L. Hedrick, *Chem. Rev.* **2007**, *107*, 5813–5840.

10 M. K. Kiesewetter, E. J. Shin, J. L. Hedrick, R. M. Waymouth, *Macromolecules* **2010**, *43*, 2093–2107.

11 E. F. Connor, G. W. Nyce, M. Myers, A. Möck, J. L. Hedrick, *J. Am. Chem. Soc.* **2002**, *124*, 914–915.

12 M. Takwa, M. W. Larsen, K. Hult, M. Martinelle, *Chem. Commun.* **2011**, *47*, 7392–7394.

13 M. Sobczak, *J. Appl. Polym. Sci.* **2012**, *125*, 3602–3609.

14 A. Loefgren, A. C. Albertsson, P. Dubois, R. Jerome, P. Teyssie, *Macromolecules* **1994**, *27*, 5556–5562.

15 K. Nie, L. Fang, Y. Yao, Y. Zhang, Q. Shen, Y. Wang, *Inorg. Chem.* **2012**, *51*, 11133–11143.

16 W. M. Stevels, M. J. K. Ankoné, P. J. Dijkstra, J. Feijen, *Macromolecules* **1996**, *29*, 6132–6138.

17 Z. Zhong, S. Schneiderbauer, P. Dijkstra, M. Westerhausen, J. Feijen, *J. Polym. Environ.* **2001**, *9*, 31–38.

18 K. Majerska, A. Duda, *J. Am. Chem. Soc.* **2004**, *126*, 1026–1027.

19 M. H. Chisholm, J. Gallucci, K. Phomphrai, *Chem. Commun.* **2003**, 48–49.

20 S. Harder, *Chem. Rev.* **2010**, *110*, 3852–3876.

21 D. J. Darensbourg, W. Choi, P. Ganguly, C. P. Richers, *Macromolecules* **2006**, *39*, 4374–4379.

22 B. Liu, T. Roisnel, J.-P. Guégan, J.-F. Carpentier, Y. Sarazin, *Chem. Eur. J.* **2012**, *18*, 6289–6301.

23 D. J. Darensbourg, W. Choi, O. Karroonnirun, N. Bhuvanesh, *Macromolecules* **2008**, *41*, 3493–3502.

24 H.-Y. Chen, H.-Y. Tang, C.-C. Lin, *Polymer* **2007**, *48*, 2257–2262.

25 Z. Zhong, P. J. Dijkstra, C. Birg, M. Westerhausen, J. Feijen, *Macromolecules* **2001**, *34*, 3863–3868.

26 C. R. Becer, R. Hoogenboom, U. S. Schubert, *Angew. Chem. Int. Ed.* **2009**, *48*, 4900–4908.

27 K. Kempe, A. Krieg, C. R. Becer, U. S. Schubert, *Chem. Soc. Rev.* **2012**, *41*, 176–191.

28 M. Westerhausen, *Inorg. Chem.* **1991**, *30*, 96–101.

29 L. W. Seymour, R. Duncan, V. Chytrý, J. Strohalm, K. Ulbrich, J. Kopeček, *J. Control. Release* **1991**, *16*, 255–262.

30 K.-H. Park, W. J. Sung, S. Kim, D. H. Kim, T. Akaike, H.-M. Chung, *J. Biosci. Bioeng.* **2005**, *99*, 285–289.

31 T. Isono, Y. Kondo, I. Otsuka, Y. Nishiyama, R. Borsali, T. Kakuchi, T. Satoh, *Macromolecules* **2013**, *46*, 8509–8518.

32 M. Bednarek, *React. Funct. Polym.* **2013**, *73*, 1130–1136.

33 D. Funk, H.-H. Schrenk, E. Frei, *J. Drug Target.* **2011**, *19*, 434–445.

34 I. E. Lundberg, C. Grundtman, E. Larsson, L. Klareskog, *Best Pract. Res. Clin. Rheumatol.* **2004**, *18*, 7–19.

35 S. Ogawa, S. Takano, H. Fujimori, T. Itoh, S. Kaita, T. Iida, Y. Wakatsuki, *React. Funct. Polym.* **2010**, *70*, 563–571.

36 B. I. Dahiyat, M. Richards, K. W. Leong, *J. Control. Release* **1995**, *33*, 13–21.

37 M. Beija, M.-T. Charreyre, J. M. G. Martinho, *Prog. Polym. Sci.* **2011**, *36*, 568–602.

38 G. Montaudo, M. S. Montaudo, C. Puglisi, F. Samperi, N. Spassky, A. LeBorgne, M. Wisniewski, *Macromolecules* **1996**, *29*, 6461–6465.

39 C. E. Hayes, Y. Sarazin, M. J. Katz, J.-F. Carpentier, D. B. Leznoff, *Organometallics* **2013**, *32*, 1183–1192.

40 L. N. Saunders, L. N. Dawe, C. M. Kozak, *J. Organomet. Chem.* **2014**, *749*, 34–40.

41 R. A. Collins, J. Unruangsri, P. Mountford, *Dalton Trans.* **2013**, *42*, 759–769.

42 L. Azor, C. Bailly, L. Brelot, M. Henry, P. Mobian, S. Dagorne, *Inorg. Chem.* **2012**, *51*, 10876–10883.

43 L. G. Alves, F. Hild, R. F. Munha, L. F. Veiros, S. Dagorne, A. M. Martins, *Dalton Trans.* **2012**, *41*, 14288–14298.

44 M. R. ten Breteler, J. Feijen, P. J. Dijkstra, F. Signori, *React. Funct. Polym*. **2013**, *73*, 30–38.

45 H.-L. Chen, S. Dutta, P.-Y. Huang, C.-C. Lin, *Organometallics* **2012**, *31*, 2016–2025.

46 M. J. Stanford, A. P. Dove, *Macromolecules* **2008**, *42*, 141–147.

47 A. Otero, J. Fernández-Baeza, L. F. Sánchez-Barba, J. Tejeda, M. Honrado, A. Garcés, A. Lara-Sánchez, A. M. Rodríguez, *Organometallics* **2012**, *31*, 4191–4202.

48 V. Katiyar, H. Nanavati, *Polym. Chem.* **2010**, *1*, 1491–1500.

49 O. Dechy-Cabaret, B. Martin-Vaca, D. Bourissou, *Chem. Rev.* **2004**, *104*, 6147–6176.

50 A. Duda, A. Kowalski, In Handbook of Ring-Opening Polymerization; P. Dubois, O. Coulembier, J.-M. Raquez, Eds.; Wiley-VCH Verlag GmbH: Weinheim, **2009**; pp 15-44.

51 J. Baran, A. Duda, A. Kowalski, R. Szymanski, S. Penczek, *Macromol. Symp*. **1997**, *123*, 93–101.

52 N. Ajellal, J.-F. Carpentier, C. Guillaume, S. M. Guillaume, M. Helou, V. Poirier, Y. Sarazin, A. Trifonov, *Dalton Trans.* **2010**, *39*, 8363–8376.

Supporting Information

End-functionalized polylactides using a calcium based pre-catalyst: Synthesis and insights by mass spectrometry

Ilknur Yildirim,[a,b] Sarah Crotty,[a,b] Claas H. Loh,[c] Grit Festag,[a,b] Christine Weber,[a,b] Pier-Francesco Caponi,[a,b] Michael Gottschaldt,[a,b] Matthias Westerhausen,[c] Ulrich S. Schubert[a,b]*

[a]Laboratory of Organic and Macromolecular Chemistry (IOMC), Friedrich Schiller University Jena, Humboldtstr. 10, 07743 Jena, Germany

[b]Jena Center for Soft Matter (JCSM), Friedrich Schiller University Jena, Philosophenweg 7, 07743 Jena, Germany

[c]Institute of Inorganic and Analytical Chemistry (IAAC), Friedrich Schiller University Jena, Humboldtstr. 8, 07743 Jena, Germany

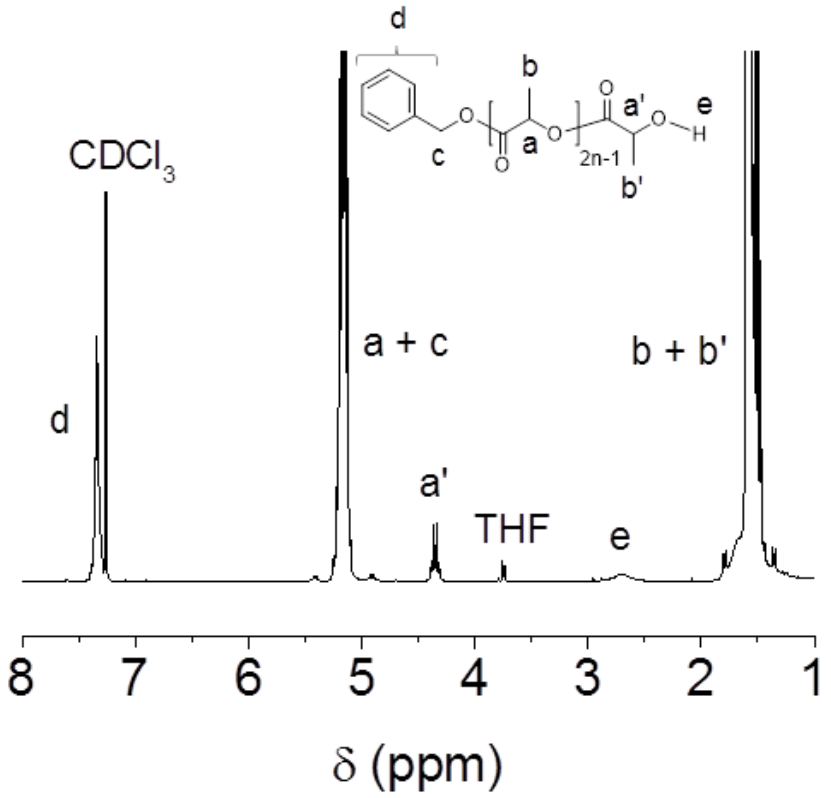

FIGURE S1. ^{1}H NMR spectrum ($CDCl_3$, 300 MHz) of **P1**.

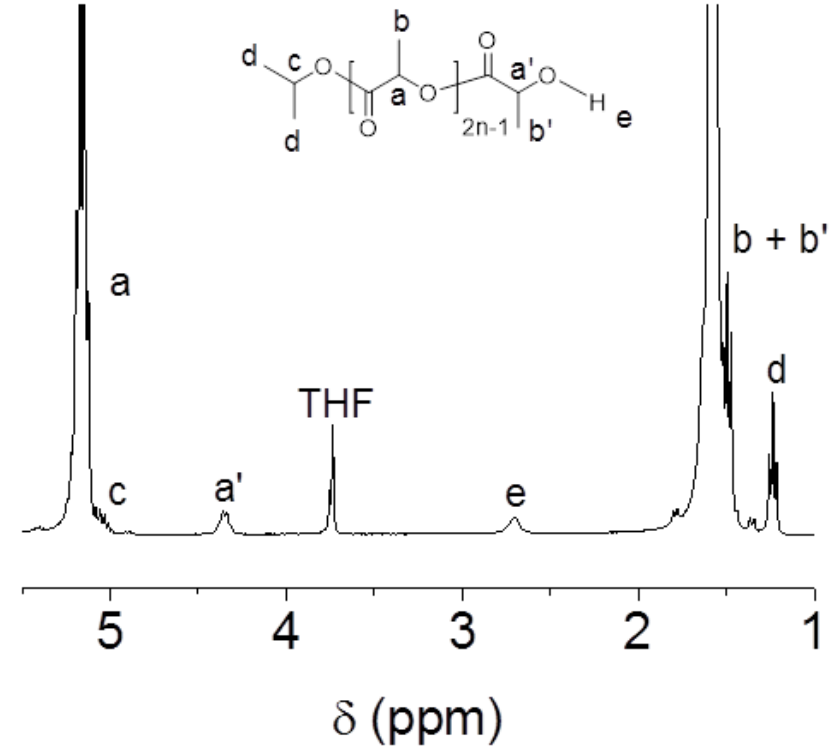

FIGURE S2. ^{1}H NMR spectrum ($CDCl_3$, 300 MHz) of **P2**.

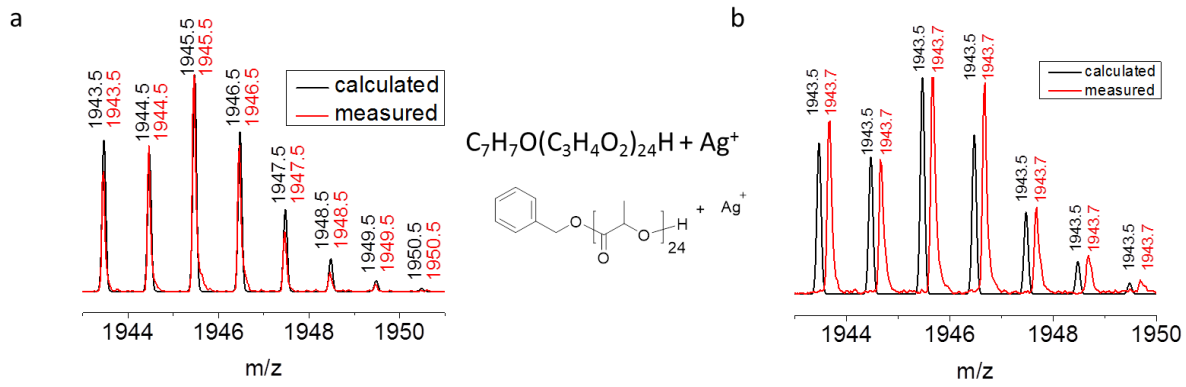

FIGURE S3. (a) Zoomed-in view the MALDI-ToF mass spectrum (AgTFA, DCTB) of (**P1**) and overlay of calculated and measured isotopic patterns for the structural assignment of the observed peaks. (b) Zoomed-in view the MALDI-ToF mass spectrum (AgTFA, DCTB) of the sample taken from polymerization mixture during kinetic study with benzyl alcohol as initiator, at 10 minutes with 18% monomer conversion and overlay of calculated and measured isotopic patterns for the structural assignment of the observed peaks.

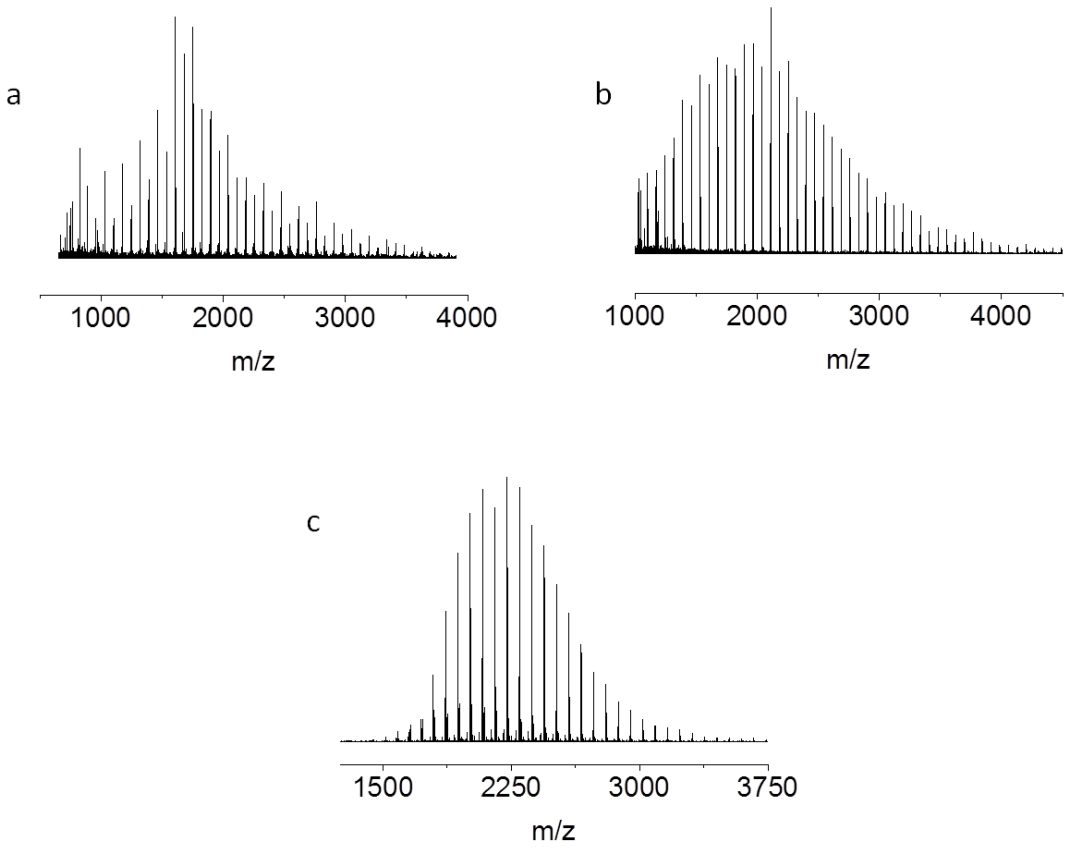

FIGURE S4. Full MALDI-ToF mass spectra (AgTFA, DCTB) of (a) **P2**, (b) **P6**, and (c) **P9**.

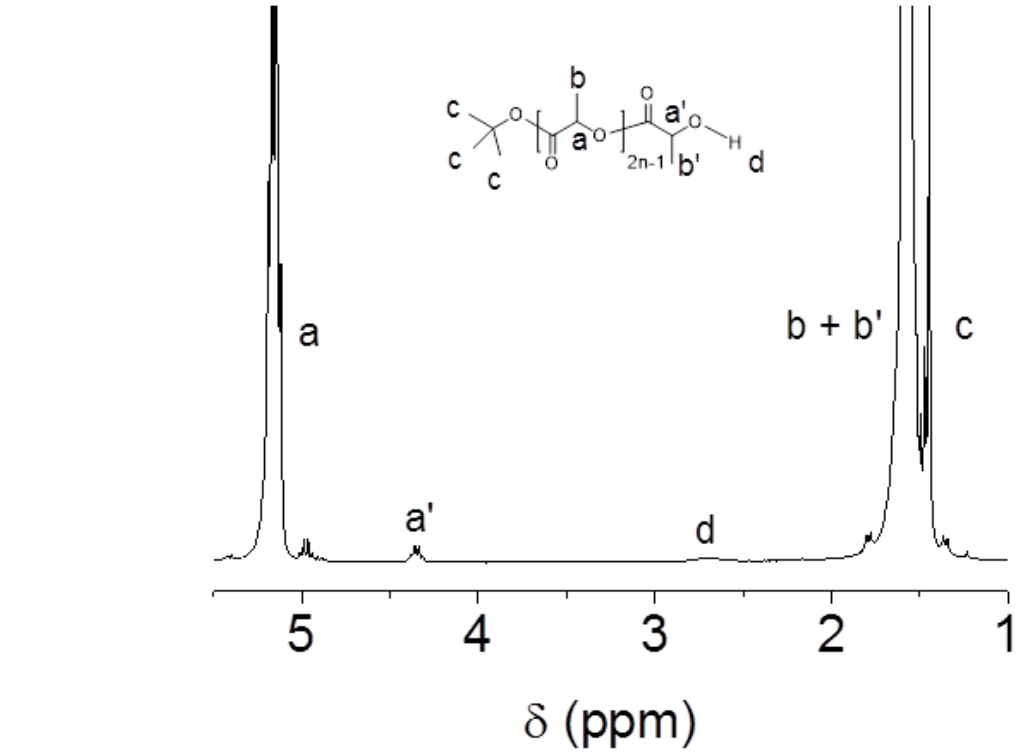

FIGURE S5. ^{1}H NMR spectrum ($CDCl_3$, 300 MHz) of **P3**.

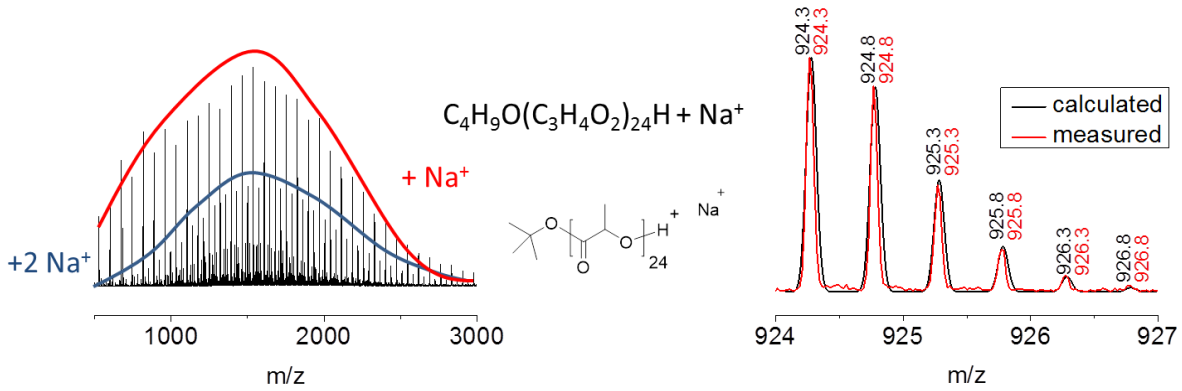

FIGURE S6. ESI-Q-ToF mass spectrum and overlay of calculated and measured isotopic patterns for the structural assignment of the observed peaks of **P3**.

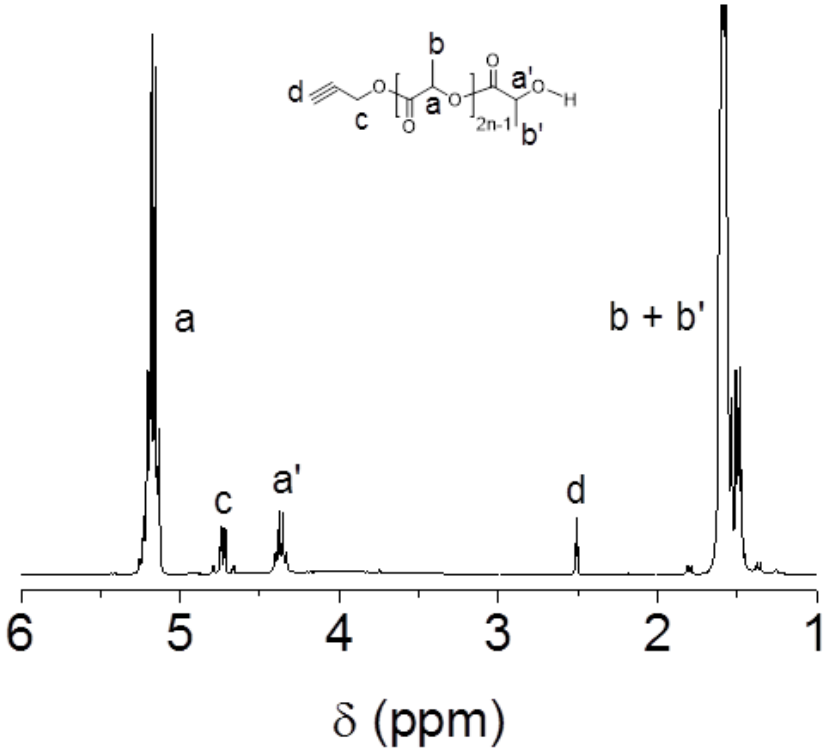

FIGURE S7. ^{1}H NMR spectrum ($CDCl_3$, 300 MHz) of **P7**.

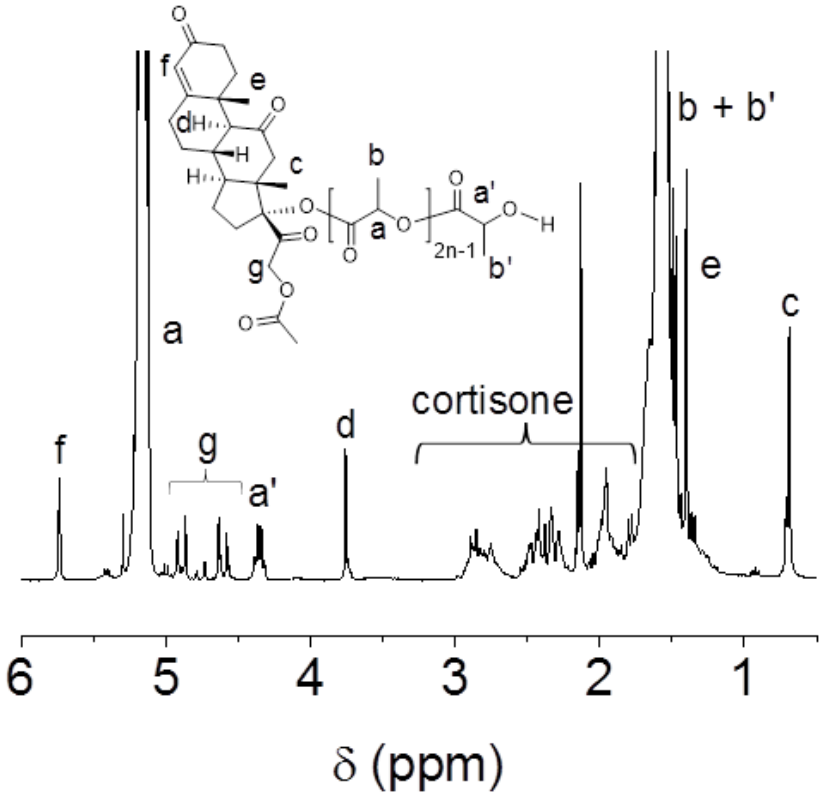

FIGURE S8. ^{1}H NMR spectrum ($CDCl_3$, 300 MHz) of **P8**.

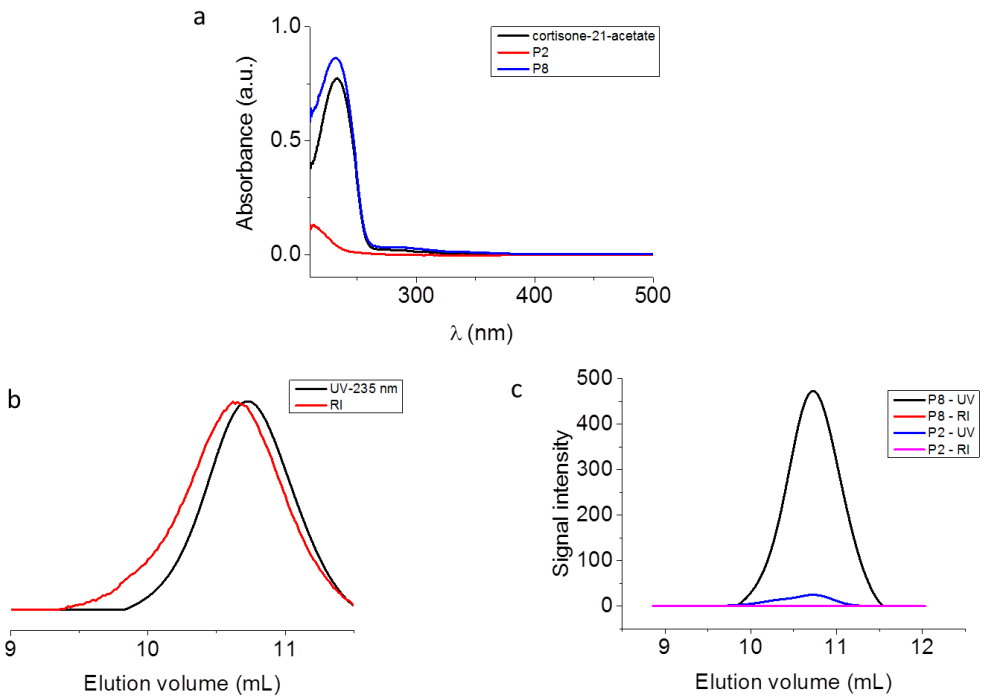

FIGURE S9. (a) Overlay of UV absorbance spectra of Cortisone-21-acetate, **P2** and **P8** dissolved in THF. (b) Normalized SEC traces (THF, RI detection) of **P8** with RI and UV detection at 235 nm. (c) Overlay of SEC traces of **P2** and **P8** with RI and UV detection at 235 nm, UV intensities of **P8** and **P2** were divided by max values of normalized refractive index intensities.

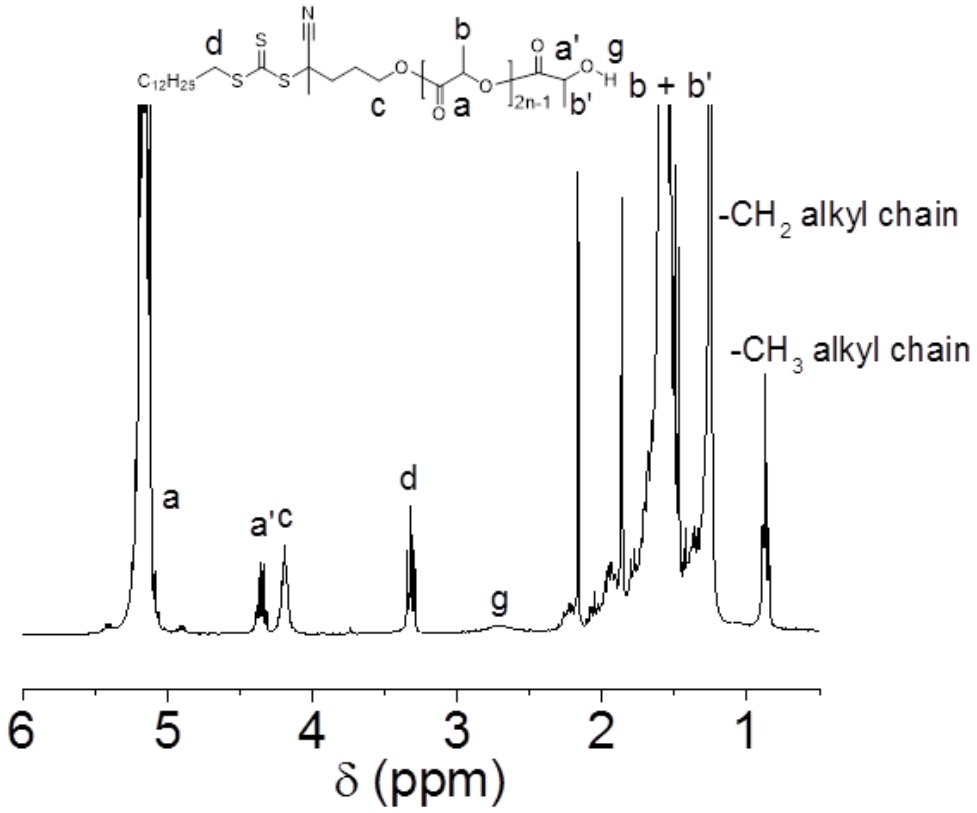

FIGURE S10. ^{1}H NMR spectrum ($CDCl_3$, 300 MHz) of **P9**.

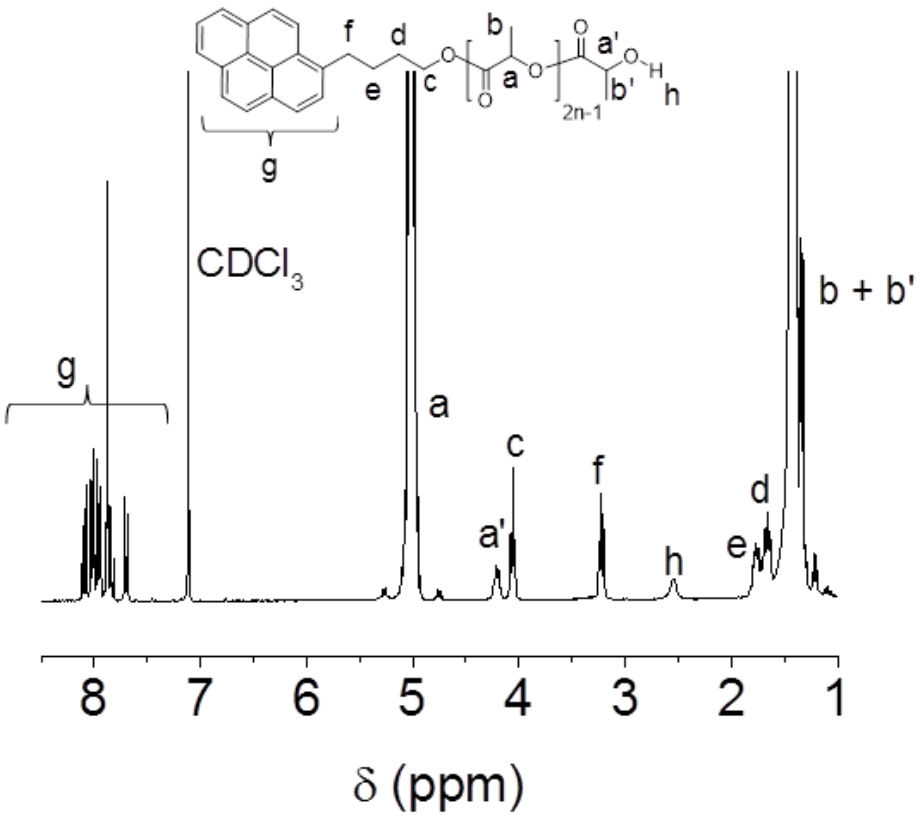

FIGURE S11. ^{1}H NMR spectrum ($CDCl_3$, 300 MHz) of **P10**.

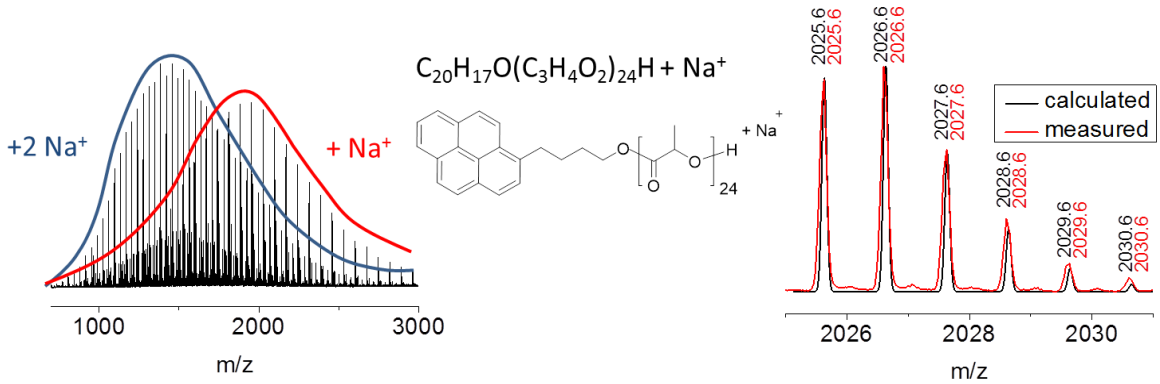

FIGURE S12. ESI-Q-ToF mass spectrum and overlay of calculated and measured isotopic patterns for the structural assignment of the observed peaks of **P10**.

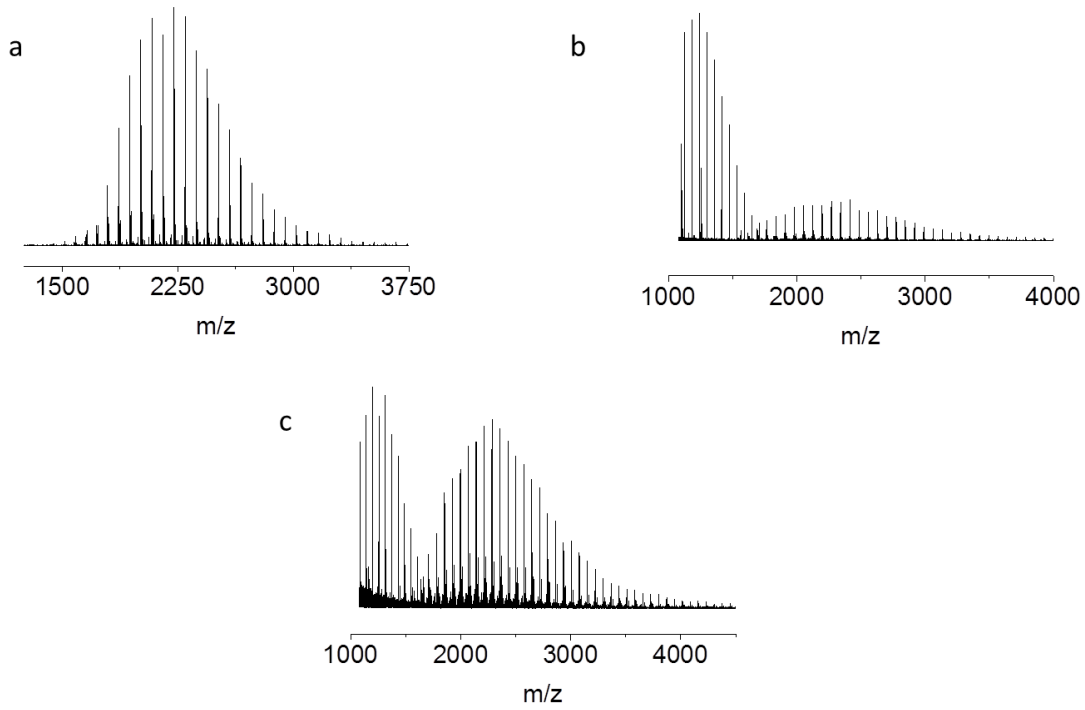

FIGURE S13. MALDI-ToF mass spectra (DCTB) of **P9** with different salts (a) AgTFA, (b) LiCl, and (c) NaCl.

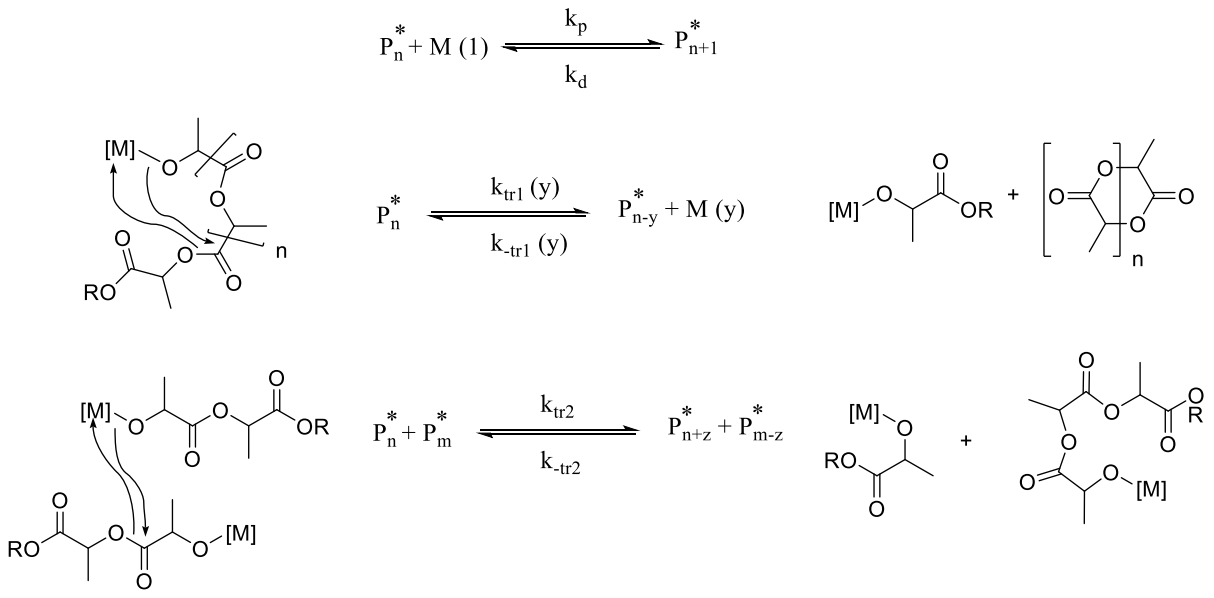

SCHEME S1 Schematic representations for the intramolecular and intermolecular chain transfer reactions and corresponding chain transfer reactions.[1, 2]

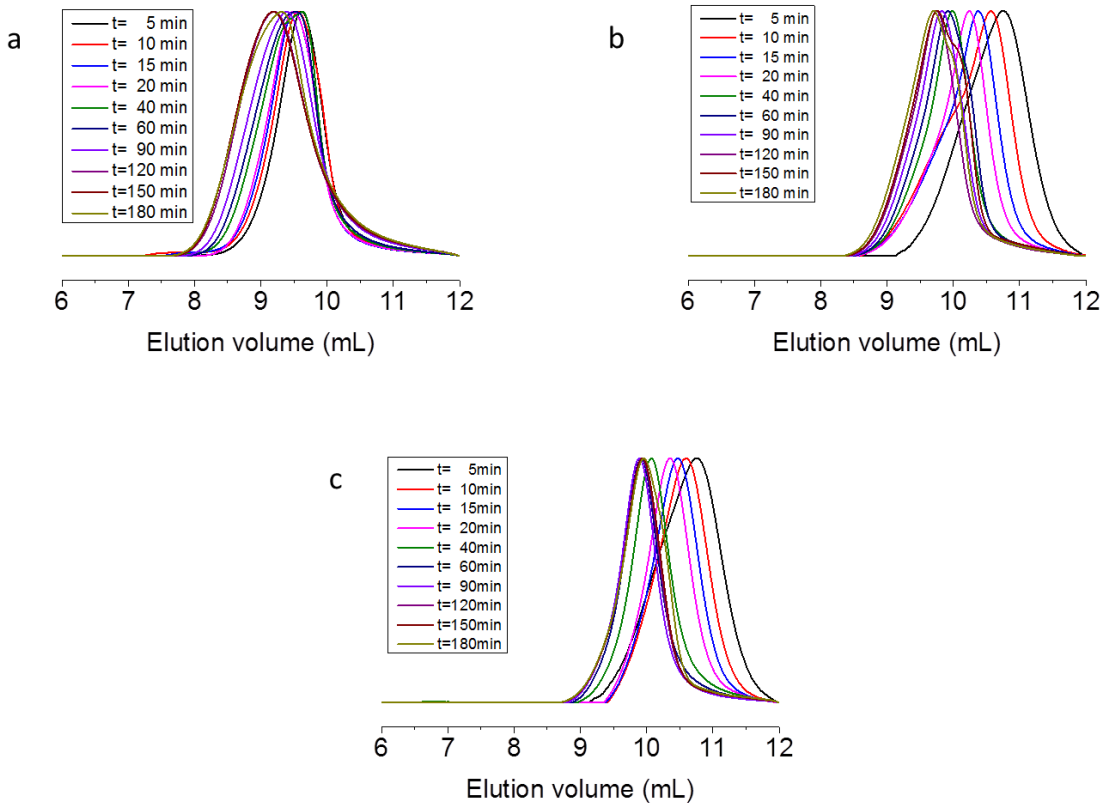

FIGURE S14. Normalized SEC traces (THF, RI detection) from kinetic studies of the polymerization of L-lactide initiated by (a) Benzyl alcohol, (b) DIP-Gal, and (c) DIP-Fru.

1. A. Duda, A. Kowalski, In Handbook of Ring-Opening Polymerization; P. Dubois, O. Coulembier, J.-M. Raquez, Eds.; Wiley-VCH Verlag GmbH: Weinheim, **2009**; pp 15-44.
2. O. Dechy-Cabaret, B. Martin-Vaca, D. Bourissou, *Chem. Rev.* **2004**, *104*, 6147-6176.

Publication P4

“Retinol initiated poly(lactide)s: Stability upon polymerization and nanoparticle preparation”

Ilknur Yildirim, Turgay Yildirim, Diana Kalden, Grit Festag, Nicole Fritz, Christine Weber, Stephanie Schubert, Matthias Westerhausen, Ulrich S. Schubert

Polym. Chem. **2017**, *8*, 4378–4387.

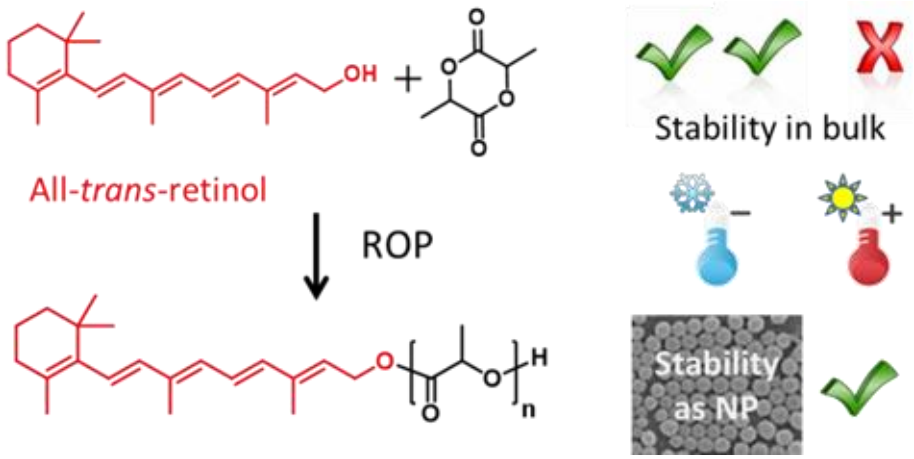

Polymer Chemistry

PAPER

View Article Online
View Journal | View Issue

Cite this: *Polym. Chem.*, 2017, **8**, 4378

Retinol initiated poly(lactide)s: stability upon polymerization and nanoparticle preparation†

Ilknur Yildirim,‡[a,b] Turgay Yildirim,‡[a,b] Diana Kalden,[c] Grit Festag,[a,b] Nicole Fritz,[a,b] Christine Weber,[a,b] Stephanie Schubert,[b,d] Matthias Westerhausen[c] and Ulrich S. Schubert*[a,b]

Received 27th May 2017,
Accepted 22nd June 2017

DOI: 10.1039/c7py00881c

rsc.li/polymers

The synthesis of retinol initiated polylactide (PLA) by ring opening polymerization (ROP) of L-lactide *via in situ* calcium alkoxide formation with all-*trans*-retinol and $Ca[N(SiMe_3)_2]_2(THF)_2$ is described. PLAs with degree of polymerization (DP) values ranging from 13 to 60 were obtained and characterized in detail by means of ^1H nuclear magnetic resonance (NMR) spectroscopy, size exclusion chromatography (SEC), UV/vis spectroscopy and (tandem) mass spectrometry techniques. Stable nanoparticles (NPs) were prepared *via* a nanoprecipitation method and characterized by DLS and SEM. The stability of retinol upon conjugation to PLA as well as the nanoparticle formulation was investigated in detail and found to be significantly affected by the storage conditions such as exposure to light, oxygen and temperature.

Introduction

The bioconjugation of polymers has been extensively studied for a wide range of controlled drug delivery, imaging and diagnostic applications over the past decades by many research groups.[1,2] Although several polymer classes have been in the focus of researchers for biomedical applications, polylactide (PLA) still represents a highly suitable candidate due to its unique properties such as biodegradability, biocompatibility, and non-toxic hydrolysis products, which can be eliminated through normal cellular activity.[3] The utilization of bioactive molecules as initiators for the ring-opening polymerization (ROP) of lactide represents an efficient approach to obtain quantitatively functionalized PLA as a release rate controlling matrix,[4] to overcome the drawbacks of drug loaded polymeric nanocarriers.[2]

The term "retinoid" is a generic name for the metabolites and biosynthetic analogues (precursors) of vitamin A, including retinol, retinal, and retinoic acid.[5] Next to their vital involvement in the visual cycle,[6] retinoids bind to specific receptors and regulate several biological processes such as cell proliferation and differentiation.[5,7,8] As a consequence, they are used as potential chemopreventive/chemotherapeutic agents (Vesanoid® and Targretin®) and for the treatment of a number of dermatological disorders (Roaccutane® and Soriatane®).[5,9,10] In spite of their benefits, retinoids are rapidly metabolized and suffer from low aqueous solubility and chemical instability.[11,12] Due to the electron-rich polyene chain, retinoids are highly unstable in the presence of light and oxygen, causing oxidative degradation and isomerization, which results in the partial or total loss of bioactivity.[10,13–15] Therefore, they represent an appealing choice as candidates for polymer conjugation to enhance their bioavailability and chemical stability.[16,17]

Although all-*trans*-retinol is the major form of vitamin A, conjugation of retinoids to polymers is mainly limited to the attachment of retinoic acid *via* coupling reactions.[17–20] While the primary hydroxyl functionality of retinol enables its use as initiating species during ROP, it has been exploited for this purpose only for the *t*-BuP_4-promoted anionic ROP of ethylene oxide to synthesize a PEO–retinol conjugate.[16] Dove and co-workers employed the bifunctional conjugated β-carotene derivative astaxanthin as a ROP initiator for functional PLA in the presence of a thiourea/amine catalyst.[21] To the best of our knowledge, a PLA–retinol conjugate has not been reported yet.

The ROP of lactide is traditionally carried out in the presence of stannous octoate, due to its high activity towards ROP. However, its toxicity, poor control over the polymerization

[a]*Laboratory of Organic and Macromolecular Chemistry (IOMC), Friedrich Schiller University Jena, Humboldtstr. 10, 07743 Jena, Germany. E-mail: ulrich.schubert@uni-jena.de*
[b]*Jena Center for Soft Matter (JCSM), Friedrich Schiller University Jena, Philosophenweg 7, 07743 Jena, Germany*
[c]*Institute of Inorganic and Analytical Chemistry (IAAC), Friedrich Schiller University Jena, Humboldtstr. 8, 07743 Jena, Germany*
[d]*Institute of Pharmacy, Department of Pharmaceutical Technology, Friedrich Schiller University Jena, Otto-Schott-Str. 41, 07745 Jena, Germany*
†Electronic supplementary information (ESI) available: Additional ^1H NMR spectra, kinetic plots, mass spectra, SEC elugrams, UV/vis spectra, and DLS data. See DOI: 10.1039/c7py00881c
‡These authors contributed equally to this work.

leading to broad dispersities and low end group fidelities[22] have given rise to the development of alternative catalysts. Besides organocatalytic and enzyme based approaches,[23,24] several metal-alkoxide based initiators have been developed to circumvent these problems.[22,25–27] Based on our previous research, *in situ* calcium alkoxide formation provides an effective and highly versatile platform for the preparation of PLAs with high end group fidelity that is applicable with numerous alcohols under mild conditions.[28,29]

In this study, we describe the ROP of L-lactide initiated by retinol *via* a facile and highly efficient approach utilizing a calcium-based precursor complex. The covalent attachment of retinol is confirmed by means of detailed spectroscopic and spectrometric analysis. In order to investigate the stability of retinol upon conjugation to PLA, storage stability studies are described using the conjugate in bulk as well as in aqueous nanoparticle suspension.

Experimental section

Materials

L-Lactide (98%) was purchased from Sigma-Aldrich and freshly recrystallized from dry toluene and dried under vacuum prior to polymerization. Bis(tetrahydrofuran)calcium bis[bis(trimethylsilyl)amide] ($Ca[N(SiMe_3)_2]_2(THF)_2$) was synthesized according to previously reported procedures that are evaluated in several reviews.[30–33] All-*trans*-retinol was purchased from Sigma-Aldrich and stored in a freezer at −80 °C. Tetrahydrofuran (THF) was dried by refluxing over sodium/benzophenone. Other chemicals were purchased from standard suppliers and were used without further purification. All glassware was dried at 110 °C for 24 hours prior to use for polymerization studies.

Instruments

All polymerizations were carried out under nitrogen in an MBraun UNILab Plus glove box workstation. Nuclear magnetic resonance (NMR) spectra were recorded at room temperature in $CDCl_3$ on a Bruker Avance 300 MHz or 400 MHz, respectively, using the residual solvent resonance as an internal standard. The chemical shifts are given in ppm relative to TMS. Size exclusion chromatography (SEC) measurements were performed on a Shimadzu system equipped with a CBM-20A system controller, an LC-10AD pump, an RID-10A refractive index detector, an SPD-10AD UV detector and an SDV linear M column from PSS (Polymer Standards Service GmbH, Mainz, Germany) at 40 °C using THF as an eluent at a flow rate of 1 mL min^{-1}. The system was calibrated against PLA standards (144 to 101 000 g mol^{-1}), which were purchased from PSS. For the measurements of the matrix-assisted laser desorption/ionization (MALDI) spectra, an Ultraflex III ToF/ToF instrument (Bruker Daltonics, Bremen, Germany) was used. The instrument is equipped with a Nd-YAG laser and a collision cell. All spectra were measured in the positive reflector mode. The instrument was calibrated prior to each measurement with an external PMMA standard from PSS. For the MALDI-ToF-MS sample preparation, separate solutions of polymer (10 mg mL^{-1} in chloroform), *trans*-2-[3-(4-*tert*-butylphenyl)-2-methyl-2-propenylidene] (DCTB) (30 mg mL^{-1} in chloroform), and doping solution of silver trifluoroacetate (AgTFA) (100 mg mL^{-1} in acetone) were prepared and mixed following the dried droplet spotting technique. 1 μL of the mixture was spotted onto the target plate. For the ESI-Q-ToF-MS measurements, samples were analyzed by using a micrOTOF-QII (Bruker Daltonics) mass spectrometer equipped with an automatic syringe pump from KD Scientific for sample injection. The ESI-Q-ToF mass spectrometer was running at 4.5 kV, at a desolvation temperature of 180 °C. The mass spectrometer was operated in the positive ion mode. Nitrogen was used as the nebulizer and drying gas. All fractions were injected using a constant flow rate (3 μL min^{-1}) of sample solution. For the CID experiments, a quadrupole was used for selection of the precursor ions, and nitrogen was used as the collision gas. The collision energy was set to certain values according to the MS/MS experiments to be carried out to identify the best collision energy value for these experiments. The ESI-Q-ToF-MS instrument was calibrated in the *m*/*z* range from 50 to 3000 using a calibration standard (Tunemix solution) which was supplied from Agilent. All data were processed *via* Bruker DataAnalysis software version 4.2. UV/vis absorption spectra were recorded on an Analytik Jena SPECORD 250 spectrometer (Analytik Jena, Jena, Germany). Dynamic light scattering (DLS) and zeta potential measurements were performed on a Zetasizer Nano ZS (Malvern Instruments, Herrenberg, Germany). After an equilibration time of 120 s, 3 × 12 runs were carried out at 25 °C (λ = 633 nm). The counts were detected at an angle of 173°. The mean particle size was approximated as the effective (*Z*-average) diameter and the width of the distribution as the polydispersity index (PDI) of the particles was obtained by the cumulants method assuming that the particles are spherical. For zeta potential measurements, 10 runs were carried out using the slow-field and fast-field reversal modes at 150 V. Each experiment was performed in triplicate at 25 °C. For scanning electron microscopy (SEM), 5 μL of the suspensions were placed on a mica surface and dried overnight at room temperature under atmospheric pressure. Afterwards, images were taken using a Gemini 1530 type LEO field emission scanning electron microscope (Carl-Zeiss AG, Germany). The samples were coated with a thin layer (4 nm) of platinum *via* sputter coating using a Bal-TEC 020 HR Sputtering Coater.

Ring-opening polymerization (ROP)

All polymerizations were carried out in a glove box, at room temperature under dim illumination and a nitrogen atmosphere (<1 ppm H_2O, <1 ppm O_2), using THF as a solvent. In a typical polymerization (**P1**), $Ca[N(SiMe_3)_2]_2(THF)_2$ (67.3 mg, 0.13 mmol) was dissolved in 1 mL of THF. Subsequently, this solution was added under vigorous stirring to the L-lactide (0.5 g, 3.47 mmol) and all-*trans*-retinol (76.4 mg, 0.27 mmol) mixture in 2.5 mL of THF ($[L\text{-lactide}]_0/[retinol]_0/[Ca]_0$ = 13/1/0.5).

After 3 minutes (10 minutes for **P2** to **P4**), the polymerization was quenched by addition of 0.1 mL of 1 M HCl solution in methanol. The conversion was determined from the ^{1}H NMR analysis of the polymerization mixture by integrating the methine proton region of PLA *versus* the one of the L-lactide. PLA was isolated by precipitation in methanol and subsequent drying under reduced pressure until a constant weight was reached. ^{1}H NMR (300 MHz, $CDCl_3$): δ/ppm = 1.02 (s, 6H, ret.), 1.55–2.0 (m, 2H ret.), 1.57–2.01(m, 2H ret.), 1.57 (d, –C(O)CH(C**H**$_3$)O–), 2.6 (d, –C(O)CH(CH$_3$)O**H**), 4.35 (q, –C(O)C**H**(CH$_3$)OH), 4.7 (m, 2H ret.), 5.15 (q, –C(O)C**H**(CH$_3$)O–), 5.21 (s, $C_6H_5(CH_2)$OC(O)–), 5.5 (m, 2H ret.), 6.0–6.7 (m, 2H ret.). M_n = 2000 g mol^{-1} (calculated based on the relative intensities of the signals at δ = 5.15 ppm and δ = 6.0 to 6.71 ppm). SEC (THF, RI detection, PLA calibration): M_n = 1800 g mol^{-1}, $Đ$ = 1.15; MALDI-ToF-MS: M_n = 2200 g mol^{-1}, $Đ$ = 1.10.

Polymerization kinetics

The kinetic study of the ROP of L-lactide was performed in a glove box under a nitrogen atmosphere at room temperature with THF as a solvent ([L-lactide]$_0$/[retinol]$_0$/[Ca]$_0$ = 100/1/0.5, [L-lactide]$_0$ = 1 M). Ca[N(SiMe$_3$)$_2$]$_2$(THF)$_2$ (17.5 mg, 0.035 mmol) was dissolved in 1 mL of THF. Then, this solution was added under vigorous stirring to a mixture of L-lactide (1 g, 6.9 mmol) and all-*trans*-retinol (19.7 mg, 0.069 mmol) in 5.94 mL of THF. The polymerization was monitored by sampling at defined time intervals, followed by ^{1}H NMR ($CDCl_3$, 300 MHz) and SEC analysis to determine the monomer conversion and the evolution of the molar mass, respectively. The conversion was determined by integrating the methine proton region of PLA (q, δ = 5.10 ppm) *versus* the one of the L-lactide (q, δ = 5.02 ppm).

Preparation of the nanoparticle suspensions

For the acetone to water (AW) method, the corresponding polymers (**P1** to **P4**) were dissolved in acetone at a concentration of 1 mg mL^{-1} and subsequently added dropwise to deionized water under continuous stirring at 500 rpm (acetone to water, AW method). For the water to acetone (WA) method, deionized water was added dropwise to the acetone polymer solution (1 mg mL^{-1}) under stirring at 500 rpm. The acetone/water (solvent/non-solvent) ratio was kept constant at 0.5 for all suspensions. Acetone was removed by stirring overnight at room temperature. The nanoparticles were characterized by DLS (performed in pure water) and SEM.

General storage conditions for stability investigations

P1 was stored under two different conditions: at room temperature under daylight and in a freezer at −80 °C. During a 15-day period, **P1** was sampled regularly for ^{1}H NMR, SEC, UV/vis, and ESI-MS analyses.

NP1 was stored at room temperature under daylight and sampled periodically for DLS, UV/vis, SEC, and ESI-MS analysis. For SEC analyses with RI and UV detection, 50 μL of nanoparticle suspension were dissolved in 950 μL of THF. For ESI-MS analyses, THF was added to the nanoparticle solution (75 : 25 vol%/vol%). Subsequently, a 100 μL aliquot was diluted with 900 μL acetonitrile.

Results and discussion

The high sensitivity of retinol makes the use of a mild and fast catalyst/co-initiator system necessary to yield high end-group fidelity and to achieve high monomer conversions in short polymerization times. Undesired side reactions to be circumvented include isomerization and degradation of retinol. Based on our previous studies using the precursor Ca[N(SiMe$_3$)$_2$]$_2$(THF)$_2$ for the *in situ* calcium alkoxide formation, we employed all-*trans*-retinol and studied the ROP of L-lactide using this co-initiator system (Scheme 1). All polymerizations were performed in THF with a monomer concentration of 1.0 M in a nitrogen filled glove box at room temperature ([retinol]$_0$/[Ca]$_0$ = 1/0.5). Due to the instability of retinol, the polymerizations were conducted under dim illumination.

In order to explore if retinol is capable of acting as an efficient co-initiator, a kinetic study of the ROP of L-lactide was performed ([L-lactide]$_0$/[retinol]$_0$/[Ca]$_0$ = 100/1/0.5, [L-lactide]$_0$ = 1 M) (Fig. S1†). Aliquots were taken from the polymerization mixture at defined time intervals and quenched with acidified methanol to monitor the monomer conversion and the evolution of the molar mass during the polymerization. The semi-logarithmic kinetic plot resembles the plot that was previously reported for 2-propanol,[34] benzyl alcohol[28] and carbohydrate based initiators.[28] An induction period is not observed, which indicates extremely fast alcoholysis of the calcium amide. Subsequent to a fast propagation at early stages the polymerization rate decreases significantly, as a result of an increase in temperature due to the exothermic alcoholysis of the calcium amide. The first kinetic sample obtained after 1 minute revealed a conversion of ≈55%, which is fairly high compared to a total conversion of ≈85% obtained after 25 minutes. Analysis of the kinetic samples by means of SEC revealed monomodal molar mass distributions throughout the whole polymerization process. The molar mass was found to increase in a linear fashion with increasing monomer conversion, while $Đ$ slightly decreased through the course of kinetic studies, which shows that the molar mass of the PLA can be well controlled using the initiator/catalyst system all-*trans*-retinol/Ca[N(SiMe$_3$)$_2$]$_2$(THF)$_2$. In addition, the SEC traces recorded with RI and UV (λ = 340 nm) detection were found to overlap. This indicated the covalent attachment of retinol to the PLA as PLA without a retinyl moiety does not absorb light at 340 nm

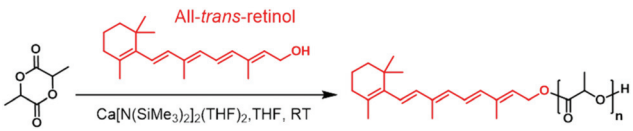

Scheme 1 Schematic representation of the ROP of L-lactide using Ca[N(SiMe$_3$)$_2$]$_2$(THF)$_2$ as a precatalyst and all-*trans*-retinol as an initiator by *in situ* calcium-alkoxide formation.

Table 1 Selected characterization data of the polymers **P1** to **P4**[a]

Entry	[L-Lactide]$_0$/[retinol]$_0$/[Ca]$_0$	$M_{n,\,theo}$[b] [g mol^{-1}]	$M_{n,\,NMR}$[c] [g mol^{-1}]	$M_{n,\,SEC}$[d] [g mol^{-1}]	$Đ_{SEC}$[d]	$M_{n,\,MALDI}$[e] [g mol^{-1}]	$Đ_{MALDI}$[e]	Method[f]	Z-ave.[g] [d, nm]	PDI[g]
P1	13/1/0.5	2160	2000	1800	1.15	2200	1.10	AW	105 ± 2	0.21 ± 0.01
								WA	174 ± 1	0.03 ± 0.01
P2	30/1/0.5	4600	4500	3700	1.24	3600	1.11	AW	100 ± 1	0.17 ± 0.05
								WA	249 ± 8	0.21 ± 0.05
P3	40/1/0.5	6050	6100	5900	1.25	4400	1.09	AW	133 ± 4	0.29 ± 0.02
								WA	217 ± 6	0.28 ± 0.05
P4	60/1/0.5	8900	7900	7000	1.28	4700	1.10	AW	115 ± 3	0.24 ± 0.02
								WA	237 ± 9	0.22 ± 0.03

[a] [L-Lactide]$_0$ = 1 M in THF, T = 25 °C, conversion values determined by ^{1}H NMR spectroscopy from the polymerization mixtures and found out to be quantitative. [b] Number average molar mass (M_n) calculated according to $M_{n,\,theo}$ = [L-lactide]$_0$/[retinol]$_0$·conv.·144.13 g mol^{-1} + $M_{(retinol)}$. [c] Calculated from suitable signal integrals in the ^{1}H NMR spectra of the purified polymers. [d] Polydispersity index ($Đ$) determined by SEC (THF, RI detection, PLA calibration). [e] Determined by MALDI-ToF-MS analysis. [f] AW, dropping acetone to water; WA, dropping water to acetone. [g] Average values of three DLS measurements.

and provided the first hint towards the (partial) preservation of the conjugated retinoid structure.

In order to facilitate an accurate structural determination of the PLA α-end groups that are introduced directly by the application of the retinol as a ROP initiator, oligomeric PLA with a degree of polymerization (DP) of 13 was synthesized (**P1**). Quantitative monomer conversion was achieved in three minutes. The ^{1}H NMR spectrum (Fig. S2†) of the purified **P1** clearly revealed peaks that can be assigned to the conjugated double bonds (signals at 5.47 to 6.75 ppm) next to the typical signals derived from methine protons of PLA (δ = 5.15 ppm). The fact that the molar mass ($M_{n,\,NMR}$) calculated from the corresponding peak integrals ("c to g" and peak "p" in Fig. S2†) is very close to the theoretical value (Table 1) hints towards a high initiation efficiency and the preservation of the retinyl moiety. This was further confirmed by the UV/vis absorption spectrum of **P1** in THF, which overlaps with the spectrum of all-*trans*-retinol (Fig. S3†). As a consequence, the absence of isomerization or aggregation of the retinyl units can be assumed.[16] Consistent with the observations during the kinetic studies, SEC measurements with both UV/vis and RI detection verified the covalent attachment of the initiator and hinted towards the absence of chain transfer reactions during the ROP (Fig. 1).

Both assumptions could be verified by characterization of **P1** by means of mass spectrometry. The matrix-assisted laser desorption/ionization time-of-flight (MALDI-ToF) mass spectrum of **P1** (Fig. S4†) revealed a single distribution of peaks spaced by $\Delta m/z$ = 72. The molar mass obtained from MALDI-ToF-MS analysis was in a good agreement with the molar masses obtained *via* NMR and SEC analyses (Table 1). However, the pulse laser irradiation during the measurement (at 337 nm) presumably resulted in a cleavage of the retinyl end group. For this purpose, electrospray ionization time-of-flight (ESI-ToF) mass spectrometry was performed for further studies, since it allowed the ionization of the retinyl functional PLA without significant fragmentation. The ESI-ToF mass spectrum of **P1** (Fig. 2) reveals a distribution of peaks spaced by $\Delta m/z$ = 72, which corresponds to one lactic acid repeating unit.

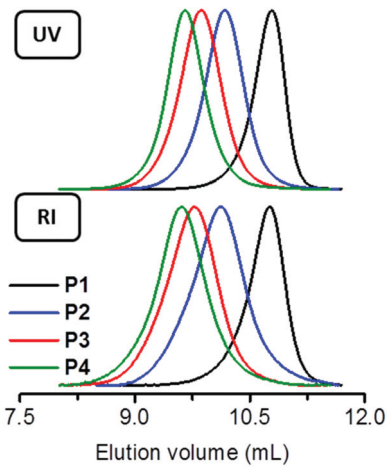

Fig. 1 Overlay of the normalized SEC traces (THF) of isolated PLAs with RI and UV (λ = 340 nm) detection.

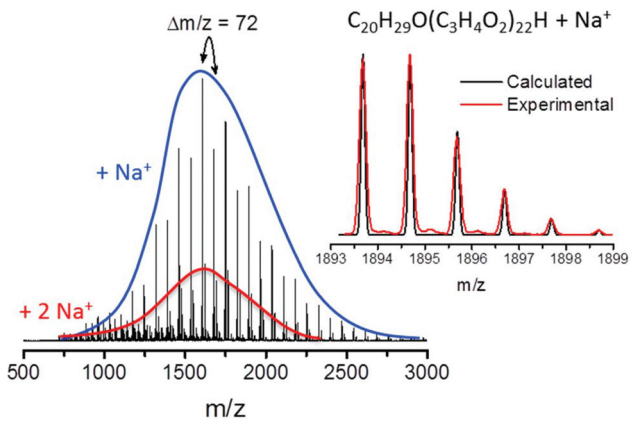

Fig. 2 ESI-ToF mass spectrum with an overlay of calculated and measured isotopic patterns for the structural assignment of the observed peaks for **P1**. Both spectra show the overlapping m/z series of the same PLA species that are either ionized with one (z = 1) or two (z = 2) sodium cations, respectively.

The main peak series can be assigned to retinol initiated PLA chains with ω-hydroxyl end groups, which are ionized with a sodium cation. The excellent agreement of the calculated and measured isotopic patterns is demonstrated in Fig. 2. A minor distribution was assigned to PLA with the same end groups ionized with a potassium cation. Neither water initiated nor cyclic PLA species were evident from the ESI spectrum. As is often observed for ESI-ToF analysis of polymers, this singly charged *m*/*z* distribution is overlaid with a second (doubly charged) *m*/*z* distribution, which results from the ionization of the same species by two sodium cations. Although a $\Delta m/z = 72$ in the mass spectra of PLA is often attributed to the presence of transesterification reactions in the literature, based on our detailed previous research on this calcium alkoxide initiator system,[28] it should be clearly stated that an intramolecular rearrangement at the active catalyst center is the reason for this observation.

In order to exclude the possibility of the presence of isobaric species without a retinyl moiety conjugated to the PLA, ESI MS/MS analysis of **P1** was performed. Therefore, the species at *m*/*z* = 1893.7 was selected as a precursor ion, corresponding to a sodiated macromolecule with 22 repeating units ($C_{20}H_{29}O(C_3H_4O_2)_{22}H + Na^+$). Fig. S5† shows the fragmentation behavior of sodiated **P1** under different collision energy values from 50 to 160 eV. The MS/MS spectrum recorded at 50 eV reveals the precursor ion together with a fragment ion at *m*/*z* = 1625.5 corresponding to the loss of the retinyl unit (268 u) due to α-end group cleavage (Fig. 3). Upon increasing the collision energy from 50 to 100 eV, **P1** gives similar fragment ions without the retinyl α-end group, thereby consecutively losing 72 u, which corresponds to one $C_3H_4O_2$ repeating unit each (Fig. 3, purple species). At a collision energy of 120 eV, an additional fragmentation series is observed, revealing higher abundance upon further increase of the collision energy. In accordance with PLA fragmentation pathways reported in the literature,[35,36] this fragment ion series should arise through Mc-Lafferty-like rearrangements that involve the migration of the hydrogen atom from a pendant methyl group to the oxygen atom of the carbonyl group of the ester moiety, which results in a 90 u loss (Fig. 3, turquoise species). Remarkably, this second fragmentation can only be observed from chains without the retinyl moiety, while no fragment ions with an intact α-end group could be assigned in any of the tandem mass spectra. This indicates that the retinyl moiety is extremely prone to cleavage under tandem MS conditions. The absence of fragment ions with less than nine $C_3H_4O_2$ repeating units in both fragmentation series might indicate the presence of an unzipping (depolymerization) pathway rather than a random main chain cleavage.

Subsequent to the assurance of the covalent attachment of all-*trans*-retinol and the preservation of its structure by an in-depth characterization of **P1**, retinol initiated PLAs with higher molar masses (**P2** to **P4**) were prepared by increasing the [L-lactide] to [retinol] ratio until 60. The monomer conversions were almost quantitative (>99%) after 10 minutes, while monomodal SEC traces with low dispersities ($D \leq 1.28$, PLA calibration) were obtained for each polymer (Fig. 1). As for **P1**, the SEC traces from UV and RI detection overlap, showing that the end-functionalization is still efficient. In addition, theoretical and experimental molar masses determined by means of ^{1}H NMR and SEC are very close to each other, indicating a good control over the molar mass of the PLA by the polymerization method employed. Only for the PLAs with the highest DP (**P3** and **P4**), MALDI-ToF-MS analysis revealed lower molar mass values compared to NMR and SEC, which is presumably due to mass discrimination effects. Table 1 summarizes the characterization results of the obtained retinol–PLA conjugates.

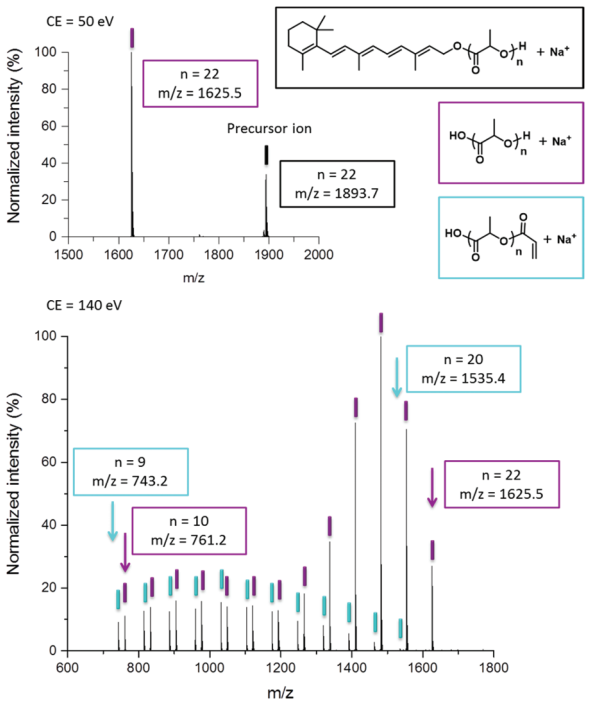

Fig. 3 ESI-Q-ToF MS/MS spectra of **P1** recorded at different collision energy values (top: 50 eV, bottom: 140 eV) together with the structural assignment of the observed peaks.

Nanoparticles were prepared from the synthesized homopolymers *via* nanoprecipitation without the addition of stabilizers or surfactants. In order to obtain a range of nanoparticles with varying size, two different dropping methods (dropping acetone polymer solution to water (AW) and dropping water to acetone polymer solution (WA)) were employed (Table 1). Smaller nanoparticles were accessible with the AW method when compared with the WA method, which is commonly observed for the nanoprecipitation technique.[37–39] Nanoparticles with monomodal size distributions with relatively low polydispersity (PDI) values could be obtained from all polymers. Only for the PLA with the lowest molar mass (**P1**), a minor amount of aggregates was formed, which could be easily removed from the nanoparticle suspension by filtration. SEM investigations of **P4** nanoparticles obtained with the WA method revealed uniform spherical shapes and sizes in agreement with the DLS data (Fig. 4). Moreover, crystal formation of

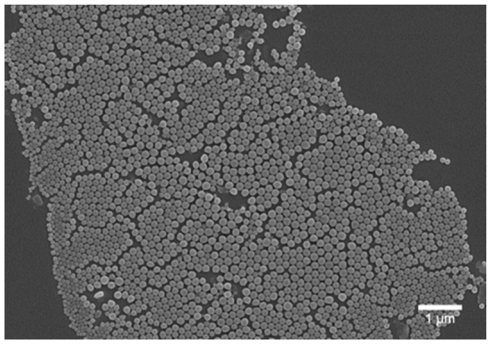

Fig. 4 SEM image of the nanoparticles obtained from **P4**.

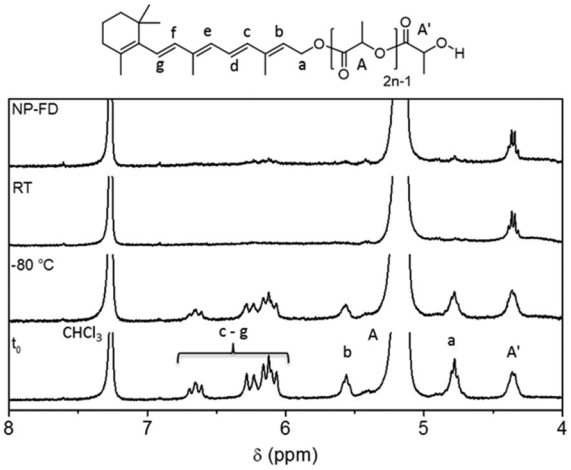

Fig. 5 Overlay of the ^{1}H NMR spectra of **P1** (t_0 and different storage conditions for 15 days; RT and −80 °C), and the corresponding freeze-dried NP after storage at room temperature for 15 days.

free retinol could not be observed, which represents a major advantage in comparison with methods that rely on simple encapsulation of unbound retinoids.[17] In line with the literature, the nanoparticles revealed negative surface charges with zeta potentials ranging from −53 to −30 mV (Table S1†).[40,41] Therefore, the colloidal stability of the nanoparticles in aqueous suspension was excellent, as demonstrated for **P1** (Fig. S6†). DLS measurements did not indicate any aggregation or degradation of the nanoparticles over the course of three months making them suitable for further in-depth structural investigations regarding the structural stability of the retinol–PLA conjugates.

Retinol is known to be stable when stored in the dark, under an inert atmosphere, and temperatures below preferably −20 °C.[42,43] However, it is prone to decomposition in the presence of light and oxygen.[10] All retinoids undergo a range of degradative reactions such as isomerization, molecular fragmentation, and chemical oxidation. The products formed by these reactions include epoxides, bis-epoxides, endoperoxides, dioxetanes, hydroxyketones and furans as well as compounds resulting from the cleavage of the conjugated polyene chain such as varying aldehydes.[44–47] As exemplarily shown by the ^{1}H NMR spectra in Fig. S7,† the conjugated structure of retinol (δ = 5.5 to 6.75 ppm) does not remain intact after storage at room temperature under daylight for 15 days. To investigate if the PLA could shield the retinyl moiety and prevent its degradation, storage stability studies were performed over a 15-day period. To enable an accurate end group analysis, **P1** was selected for this purpose due to its low molar mass. Therefore, the retinol–PLA conjugate as well as its nanoparticle suspension were kept under ambient conditions and analyzed periodically by NMR, SEC, UV/vis spectroscopy and ESI-MS. A sample stored in the dark at −80 °C served as a control. After finalization of the study, the **P1** nanoparticle suspension was lyophilized to enable a more straightforward analysis of the final sample, embracing the possible additional degradation that might occur during the procedure.

Fig. 5 depicts an overlay of the final ^{1}H NMR spectra recorded after 15 days. As can be clearly seen, the conjugated structure of retinol is almost completely preserved when **P1** is stored at −80 °C. On the other hand, all peaks originating from the conjugated double bonds (peaks "b" to "g") vanished upon storage at room temperature revealing that the retinol moieties are (almost) completely degraded for both, bulk as well as nanoparticulate **P1**. Fig. 6A depicts the decrease of peak integrals assigned to the retinyl moiety during the course of our study. As all spectra were normalized according to the peak maxima of the methine protons of the PLA (peak A in Fig. 5), this plot reflects the degradation of the retinyl moieties over time and provides a straightforward impression on the accuracy of the method applied. It is evident that the major fraction of the retinoid structure is already affected within the first three days of storage. However, these results are consistent with the decrease in absorbance at 340 nm as monitored by UV/vis spectroscopy, which is considered a more sensitive method to gain information about the preservation of the retinoid moiety (Fig. S8† and Fig. 6B). It should be noted that neither could we monitor the appearance of additional peaks in the ^{1}H NMR spectra nor was an additional band in the UV/vis spectra to be seen. Although only the final sample was investigated for the **P1** nanoparticles due to practical reasons, a slightly increased stability in aqueous suspension is suggested subsequent to the evaluation of the results obtained from both methods.

Avoiding the necessity to remove water from the nanoparticle suspension prior to analysis, SEC using UV/vis detection served as a tool to fill in the missing data throughout the course of the 15-day period (Fig. S9†). For this purpose, SEC analysis was performed directly from the aqueous suspensions by mixing with the SEC eluent THF (NP suspension/THF = 5/95 (v/v)). All bulk samples stored at RT and −80 °C were analyzed at a concentration of 1 mg mL^{-1}, which results in a 40 times lowered concentration of the nanoparticle sample. This fact was accounted for by multiplication of the area under the curve (UV/vis detection at 340 nm) obtained from the **P1** suspension throughout the interpretation of the results in Fig. 7.

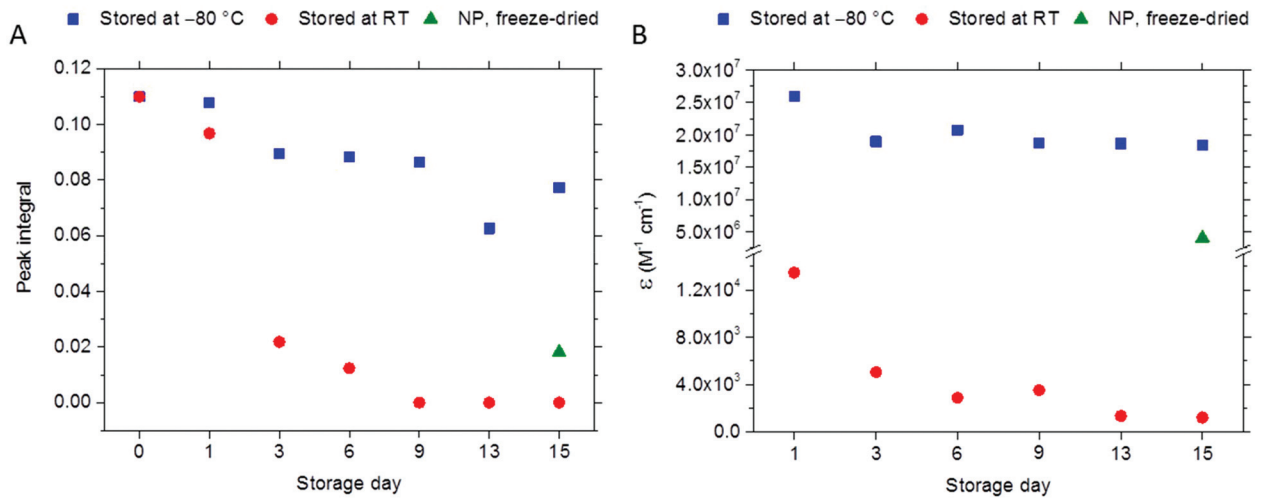

Fig. 6 Change in peak integrals assigned to retinyl moieties at 5.9 to 6.4 ppm in the ^{1}H NMR spectra (A) and molar extinction coefficients at 340 nm measured by UV/vis absorption spectroscopy (B) over 15 days.

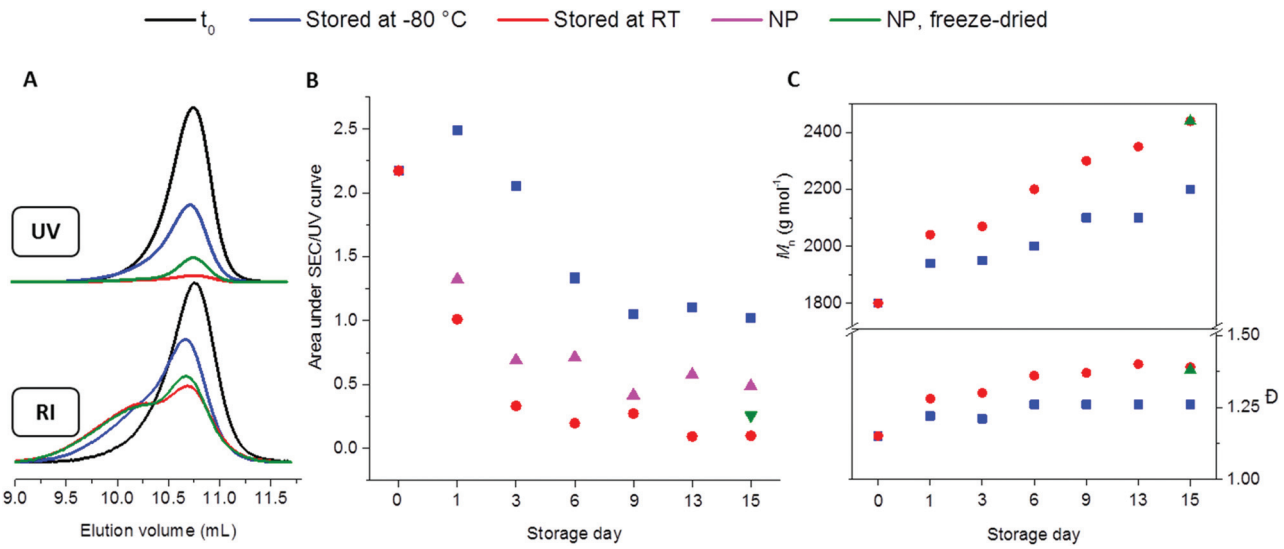

Fig. 7 Overlay of SEC elugrams of **P1** before and after 15 days storage recorded with RI and UV (λ = 340 nm) detection (A). Change in area under the SEC trace during the storage studies recorded with UV detection (B). Evolution of M_n and $Đ$ during the storage studies as determined by RI detection (C).

In line with the results discussed before, the degradation of the retinoid structure seemed to be slightly decelerated in nanoparticle suspension when compared to bulk **P1** stored under the same conditions. While for most samples, a significant decrease in the UV absorbance was noticed, none of the SEC traces recorded with UV detection revealed any broadening upon storage.

In contrast, SEC analysis using RI detection revealed a shoulder in the high molar mass region, which is indicative of coupling reactions occurring between PLA chains without an intact all-*trans*-retinyl moiety. Even in the aqueous suspensions, we could not observe any degradation of the PLA chains alone that would result in low molar mass PLA, as shown by the absence of tailing towards lower molar masses. The fact that the occurrence of coupled PLA chains became more pronounced upon elongated storage is clearly demonstrated by the increased molar mass as well as dispersity with time. Fig. 7 depicts an overlay of the elugrams obtained with RI detection after 15 days of storage (the elugram of the lyophilized NP suspensions is shown). In accordance to the other measurements described above, storage at −80 °C significantly suppressed the side reactions, albeit not entirely.

To gain structural information about the degradation products formed, ESI-ToF-MS analysis was conducted periodically during the 15 day storage period. A comparison of the ESI-Q-ToF mass spectra recorded is depicted in Fig. 8 and in

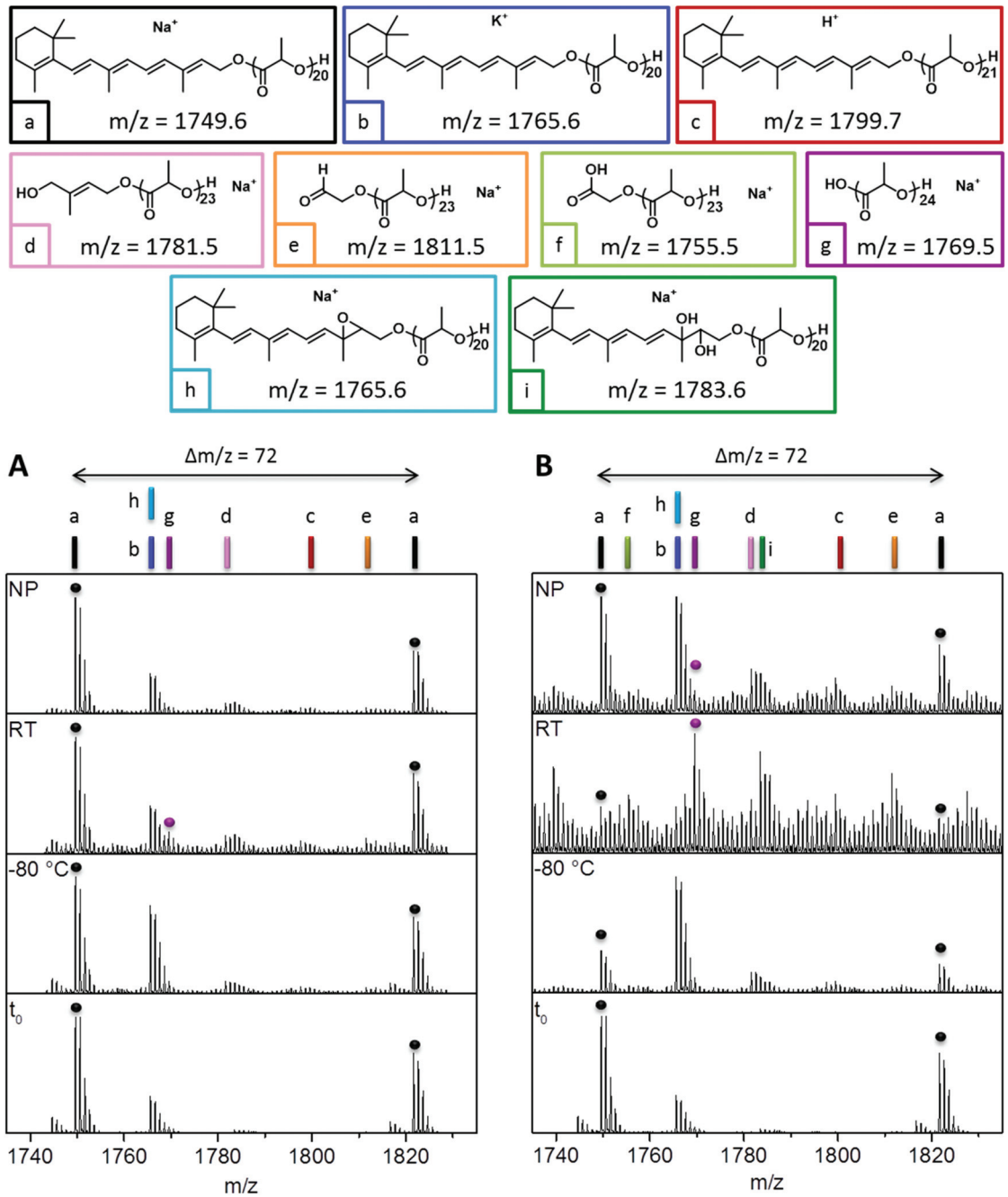

Fig. 8 Overlay of the ESI-Q-ToF mass spectra of **P1** (t_0 and different storage conditions; RT and −80 °C), and the corresponding NP recorded during storage after (A) 1 day, (B) 15 days, together with the structural assignment of the observed peaks. The black and purple dots are added for clarity to indicate the presence of species "a" and "g".

Fig. S10.† As expected, the spectra obtained during and subsequent to storage at −80 °C did not reveal major additional *m*/*z* distributions, again showing that the conjugated structure of the α-end group is mostly preserved. It should be noted that H^+ adduct ions of the preserved conjugate (Fig. 8, species "c") were also detected in the spectra of nanoparticles in addition to Na^+ and K^+ adduct ions (Fig. 8, species "a" and "b"). However, upon storage at room temperature, an additional *m*/*z* series appeared within the mass spectra for both **P1** samples, *i.e.* in bulk as well as in the nanoparticle suspension. Upon degradation of the retinoid during the course of the study, these species became more abundant. After 15 days of storage, the mass spectra clearly indicated a complete cleavage of the retinyl moiety (species "g" in Fig. 8). In particular for the bulk sample stored under ambient conditions, it could be clearly seen how this species evolved to become the most abundant one during the course of the study (Fig. S10†). However, other degradation products were apparently formed first. To assign

the according PLA α-end groups, we relied on retinol degradation products as described in the literature (see above). Indeed, a variety of reasonable assignments could be made, some of which include isobaric (*e.g.*, species "b" and "h") as well as isomeric structures. Several examples for the latter are provided in Fig. S11 and S12,† and an overlay of the mass spectrum with the calculated isotopic patterns is depicted in Fig. S13.† Some of the corresponding structures (*e.g.*, "d–f") would be formed by secondary reactions leading to a fragmentation of the polyene chain, while others are based on oxidation without cleavage of bonds between two carbon atoms (*e.g.*, epoxides, diols, endoperoxides). The MS data alone would suggest that the retinoid structure of the **P1** nanoparticles in aqueous suspension was hardly affected by storage under ambient conditions. However, it should be made clear that this statement would rely on a quantification of varying structures that can very well differ in their ability to be ionized *via* ESI. In contrast, the complementary techniques applied (SEC, UV/vis as well as ^{1}H NMR spectroscopy) are much better suited for quantification and revealed that the retinyl moiety is, in fact, prone to degradation also in nanoparticulate form of **P1**, albeit to a lesser degree in comparison with the bulk sample.

Although a variety of isomeric and isobaric structures makes it impossible to unambiguously identify the end groups being formed during the storage of **P1**, the chromophore of the α-end group is affected in each, which is in line with the decrease in UV absorbance at 340 nm during our study. The autoxidation of retinoids is known to occur through a radical mechanism.[48] The first step includes the addition of oxygen to a double bond and, hence, already affects the chromophore. Termination reactions by recombination of two radical retinoid species represent a straightforward explanation for the coupling products observed by SEC measurements with RI detection as it would lead to two PLA chains being coupled *via* their α-end groups (Fig. S14†). An alternative possibility could be the opening of an epoxide functionality (compare *e.g.* structure "h") by nucleophilic attack of either a hydroxyl ω-end group of another polymer chain (head–tail coupling), or of a hydroxyl functionality formed during the degradation process of the retinyl moiety (head–head coupling).

Conclusions

In summary, retinol-initiated PLAs were prepared by ROP *via* calcium-alkoxide formation at room temperature. Well-defined polymers were obtained with quantitative end-functionalization and low dispersities by changing the [L-lactide]/[retinol] ratio, yielding PLA–retinol conjugates with a biodegradable ester linkage. Covalent attachment of retinol to the polylactide backbone was confirmed by means of NMR spectroscopy, (tandem) mass spectrometry, and UV/vis spectroscopy. Polymeric nanoparticles were obtained by nanoprecipitation yielding stable nanoparticles in the size range between 100 and 250 nm. In-depth investigation of the stability of retinol upon conjugation to PLA revealed an excellent stability when stored at low temperatures. In contrast, storage under ambient conditions in bulk led to an almost complete degradation of the retinoid structure while the PLA itself remained intact. This effect was reduced when the PLA–retinol conjugates were kept in the form of an aqueous nanoparticle suspension. Considering the highly hydrophobic nature of the retinyl moiety, it could be speculated that it will be rarely localized on the surface of the nanoparticles in water. Thus, a shielding PLA layer could protect the retinyl functionality against oxidative processes by additional isolation from the surrounding atmosphere.[49,50] Future research will concentrate on expanding this concept for bioconjugation to other sensitive hydroxyl-functional compounds as well as to other polyesters that can be obtained *via* ROP of cyclic lactones. Such nanoparticles could be useful for targeting hepatic stellate cells as their function is fat storage and, thus, readily take up vitamin A.[20]

Acknowledgements

The authors wish to thank Steffi Stumpf for SEM investigations and Wolfgang Günther for helpful discussions. We acknowledge funding from Thuringian Ministry for Economic Affairs, Science and Digital Society (ProExcellence II, NanoPolar).

References

1 N. Larson and H. Ghandehari, *Chem. Mater.*, 2012, **24**, 840–853.
2 J. Nicolas, *Chem. Mater.*, 2016, **28**, 1591–1606.
3 A. J. R. Lasprilla, G. A. R. Martinez, B. H. Lunelli, A. L. Jardini and R. M. Filho, *Biotechnol. Adv.*, 2012, **30**, 321–328.
4 R. Tong and J. Cheng, *J. Am. Chem. Soc.*, 2009, **131**, 4744–4754.
5 R. Álvarez, B. Vaz, H. Gronemeyer and Á. R. de Lera, *Chem. Rev.*, 2014, **114**, 1–125.
6 P. D. Kiser, M. Golczak and K. Palczewski, *Chem. Rev.*, 2014, **114**, 194–232.
7 K. M. Park, H. C. Kang, J. K. Cho, I.-J. Chung, S.-H. Cho, Y. H. Bae and K. Na, *Biomaterials*, 2009, **30**, 2642–2652.
8 S. A. Papadimitriou, M. P. Robin, D. Ceric, R. K. O'Reilly, S. Marino and M. Resmini, *Nanoscale*, 2016, **8**, 17340–17349.
9 W. Bollag and E. E. Holdener, *Ann. Oncol.*, 1992, **3**, 513–526.
10 J. S. Lee, Y. S. Nam, B.-Y. Kang, S.-H. Han and I.-S. Chang, *J. Appl. Polym. Sci.*, 2004, **92**, 517–522.
11 T. Santos, R. Ferreira, J. Maia, F. Agasse, S. Xapelli, L. Cortes, J. Bragança, J. O. Malva, L. Ferreira and L. Bernardino, *ACS Nano*, 2012, **6**, 10463–10474.
12 J. Maia, T. Santos, S. Aday, F. Agasse, L. Cortes, J. O. Malva, L. Bernardino and L. Ferreira, *ACS Nano*, 2011, **5**, 97–106.

13 N. G. Eskandar, S. Simovic and C. A. Prestidge, *Int. J. Pharm.*, 2009, **376**, 186–194.
14 P. P. Fu, Q. Xia, J. J. Yin, S.-H. Cherng, J. Yan, N. Mei, T. Chen, M. D. Boudreau, P. C. Howard and W. G. Wamer, *Photochem. Photobiol.*, 2007, **83**, 409–424.
15 G. G. Gurzadyan, J. Reynisson and S. Steenken, *Phys. Chem. Chem. Phys.*, 2007, **9**, 288–298.
16 J. Zhao, H. Schlaad, S. Weidner and M. Antonietti, *Polym. Chem.*, 2012, **3**, 1763–1768.
17 Y. S. Nam, K. J. Kim, H. S. Kang, T. G. Park, S. H. Han and I. S. Chang, *J. Appl. Polym. Sci.*, 2003, **89**, 1631–1637.
18 J. Li, X. Jiang, Y. Guo, S. An, Y. Kuang, H. Ma, X. He and C. Jiang, *Bioconjugate Chem.*, 2015, **26**, 418–426.
19 R. Wang, H. Xiao, H. Song, Y. Zhang, X. Hu, Z. Xie, Y. Huang, X. Jing and Y. Li, *J. Mater. Chem.*, 2012, **22**, 25453–25462.
20 T. Yildirim, C. Matthaeus, A. T. Press, S. Schubert, M. Bauer, J. Popp and U. S. Schubert, *Macromol. Biosci.*, 2017, DOI: 10.1002/mabi.201700064.
21 H. Middleton, S. Tempelaar, D. M. Haddleton and A. P. Dove, *Polym. Chem.*, 2011, **2**, 595–600.
22 J. Guo, P. Haquette, J. Martin, K. Salim and C. M. Thomas, *Angew. Chem., Int. Ed.*, 2013, **52**, 13584–13587.
23 O. Dechy-Cabaret, B. Martin-Vaca and D. Bourissou, *Chem. Rev.*, 2004, **104**, 6147–6176.
24 N. E. Kamber, W. Jeong, R. M. Waymouth, R. C. Pratt, B. G. G. Lohmeijer and J. L. Hedrick, *Chem. Rev.*, 2007, **107**, 5813–5840.
25 B. J. O'Keefe, M. A. Hillmyer and W. B. Tolman, *J. Chem. Soc., Dalton Trans.*, 2001, 2215–2224, DOI: 10.1039/B104197P.
26 Y. Sarazin, B. Liu, T. Roisnel, L. Maron and J.-F. Carpentier, *J. Am. Chem. Soc.*, 2011, **133**, 9069–9087.
27 J.-C. Wu, B.-H. Huang, M.-L. Hsueh, S.-L. Lai and C.-C. Lin, *Polymer*, 2005, **46**, 9784–9792.
28 I. Yildirim, S. Crotty, C. H. Loh, G. Festag, C. Weber, P.-F. Caponi, M. Gottschaldt, M. Westerhausen and U. S. Schubert, *J. Polym. Sci., Part A: Polym. Chem.*, 2016, **54**, 437–448.
29 I. Yildirim, T. Bus, M. Sahn, T. Yildirim, D. Kalden, S. Hoeppener, A. Traeger, M. Westerhausen, C. Weber and U. S. Schubert, *Polym. Chem.*, 2016, **7**, 6064–6074.
30 M. Westerhausen, *Inorg. Chem.*, 1991, **30**, 96–101.
31 A. M. Johns, S. C. Chmely and T. P. Hanusa, *Inorg. Chem.*, 2009, **48**, 1380–1384.
32 M. Westerhausen, J. Langer, S. Krieck and C. Glock, *Rev. Inorg. Chem.*, 2011, **31**, 143–184.
33 A. Torvisco, A. Y. O'Brien and K. Ruhlandt-Senge, *Coord. Chem. Rev.*, 2011, **255**, 1268–1292.
34 Z. Zhong, S. Schneiderbauer, P. J. Dijkstra, M. Westerhausen and J. Feijen, *J. Polym. Environ.*, 2001, **9**, 31–38.
35 J. De Winter, V. Lemaur, P. Marsal, O. Coulembier, J. Cornil, P. Dubois and P. Gerbaux, *J. Am. Soc. Mass Spectrom.*, 2010, **21**, 1159–1168.
36 B. C. Katzenmeyer, L. R. Cool, J. P. Williams, K. Craven, J. M. Brown and C. Wesdemiotis, *Int. J. Mass Spectrom.*, 2015, **378**, 303–311.
37 T. Yildirim, A. C. Rinkenauer, C. Weber, A. Traeger, S. Schubert and U. S. Schubert, *J. Polym. Sci., Part A: Polym. Chem.*, 2015, **53**, 2711–2721.
38 T. Yildirim, A. Traeger, E. Preussger, S. Stumpf, C. Fritzsche, S. Hoeppener, S. Schubert and U. S. Schubert, *Macromolecules*, 2016, **49**, 3856–3868.
39 T. Yildirim, I. Yildirim, R. Yanez-Macias, S. Stumpf, C. Fritzsche, S. Hoeppener, C. Guerrero-Sanchez, S. Schubert and U. S. Schubert, *Polym. Chem.*, 2017, **8**, 1328–1340.
40 T. Govender, S. Stolnik, M. C. Garnett, L. Illum and S. S. Davis, *J. Controlled Release*, 1999, **57**, 171–185.
41 J. Thevenot, A.-L. Troutier, L. David, T. Delair and C. Ladavière, *Biomacromolecules*, 2007, **8**, 3651–3660.
42 A. B. Barua and H. C. Furr, *Mol. Biotechnol.*, 1998, **10**, 167–182.
43 T. E. Gundersen and R. Blomhoff, *J. Chromatogr. A*, 2001, **935**, 13–43.
44 K. B. Clark, J. A. Howard and A. R. Oyler, *J. Am. Chem. Soc.*, 1997, **119**, 9560–9561.
45 A. R. Oyler, M. G. Motto, R. E. Naldi, K. L. Facchine, P. F. Hamburg, D. J. Burinsky, R. Dunphy and M. L. Cotter, *Tetrahedron*, 1989, **45**, 7679–7694.
46 I. Washington, S. Jockusch, Y. Itagaki, N. J. Turro and K. Nakanishi, *Angew. Chem., Int. Ed.*, 2005, **44**, 7097–7100.
47 I. Washington, N. J. Turro and K. Nakanishi, *Photochem. Photobiol.*, 2006, **82**, 1394–1397.
48 E. I. Finkelshtein and I. S. Krasnokutskaya, *J. Phys. Org. Chem.*, 1996, **9**, 411–418.
49 K. Yoshida, T. Sekine, F. Matsuzaki, T. Yanaki and M. Yamaguchi, *J. Am. Oil Chem. Soc.*, 1999, **76**, 1–6.
50 P. Sauvant, M. Cansell, A. Hadj Sassi and C. Atgié, *Food Res. Int.*, 2012, **46**, 469–479.

Supporting Information

Retinol initiated poly(lactide)s: Stability upon polymerization and nanoparticle preparation

Ilknur Yildirim,[a,b]‡ *Turgay Yildirim,*[a,b]‡ *Diana Kalden,*[c] *Grit Festag,*[a,b] *Nicole Fritz,*[a,b] *Christine Weber,*[a,b] *Stephanie Schubert,*[b,d] *Matthias Westerhausen,*[c] *Ulrich S. Schubert*[a,b]*

[a] Laboratory of Organic and Macromolecular Chemistry (IOMC), Friedrich Schiller University Jena, Humboldtstr. 10, 07743 Jena, Germany

[b] Jena Center for Soft Matter (JCSM), Friedrich Schiller University Jena, Philosophenweg 7, 07743 Jena, Germany

[c] Institute of Inorganic and Analytical Chemistry (IAAC), Friedrich Schiller University Jena, Humboldtstr. 8, 07743 Jena, Germany

[d] Institute of Pharmacy, Department of Pharmaceutical Technology, Friedrich Schiller University Jena, Otto-Schott-Str. 41, 07745 Jena, Germany

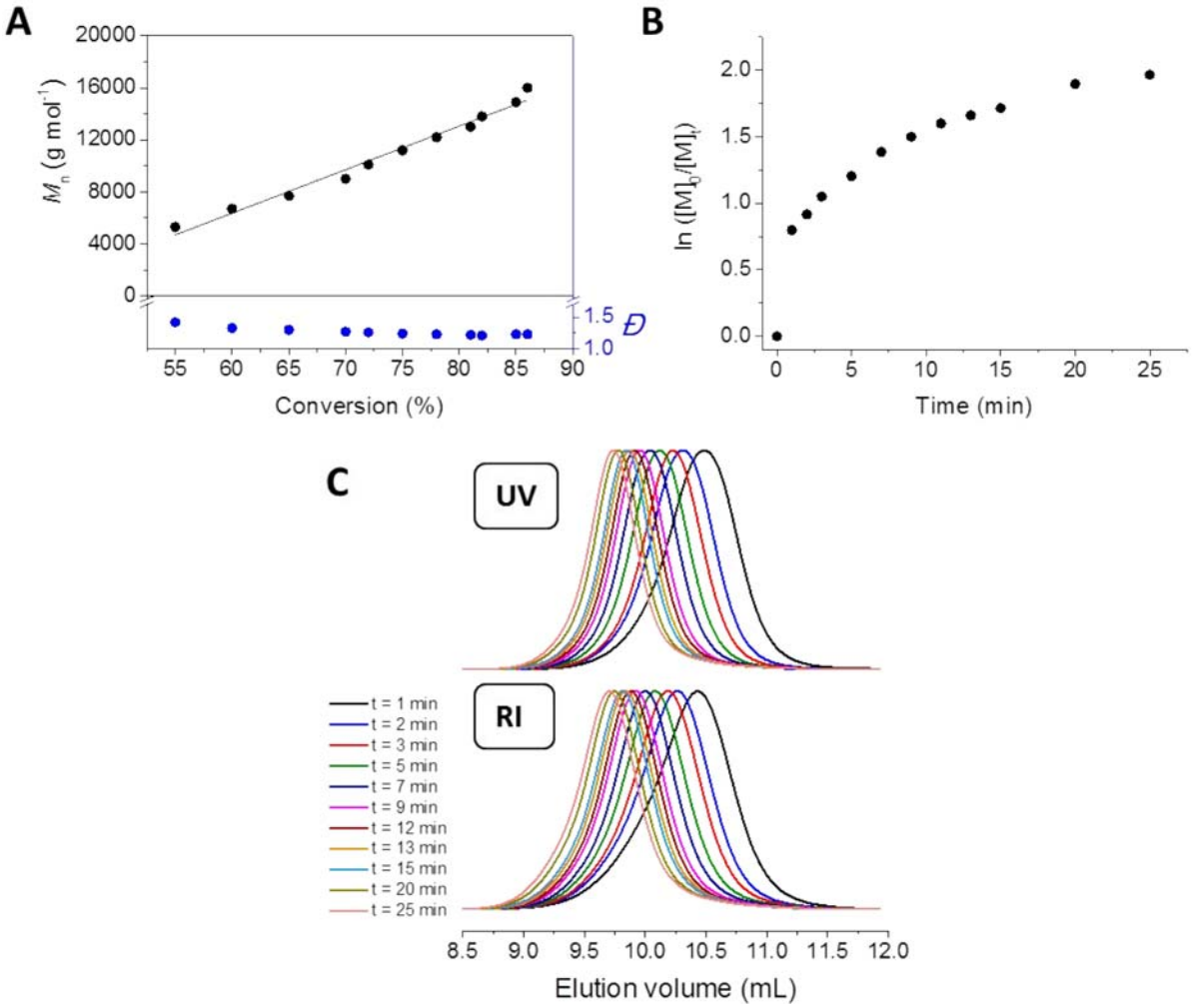

Figure S1. Kinetic study of retinol initiated ROP of L-lactide performed at room temperature in THF with a total monomer concentration of 1 mol L^{-1}. [M]/[Retinol]/[Ca]= 100/1/0.5. (**A**) Dependence of $M_{n,SEC}$ and $Đ$ of the obtained PLA on the conversion of L-lactide. (**B**) Semilogarithmic kinetic plot. (**C**) Overlay of the SEC elugrams recorded with RI and UV (λ = 340 nm) detection.

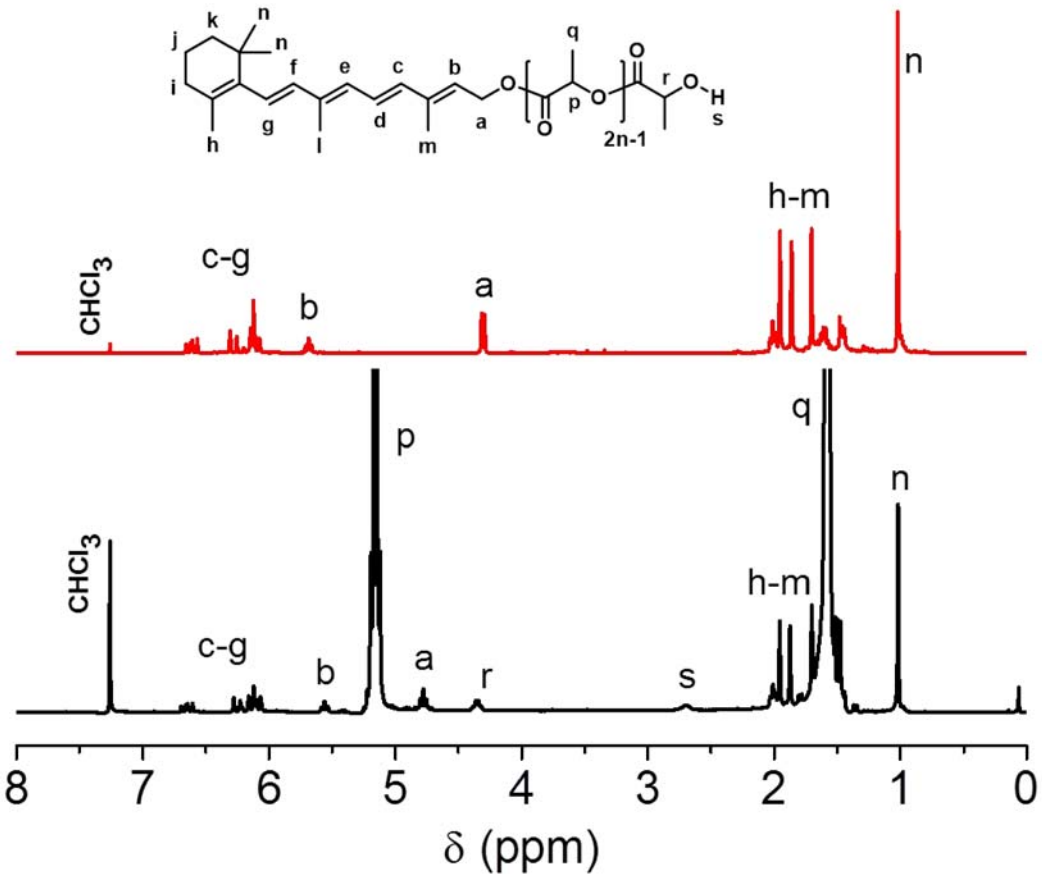

Figure S2. Overlay of ^{1}H NMR spectra (400 MHz, $CDCl_3$) of retinol and retinol initiated PLA (**P1**) together with the assignment of the observed peaks.

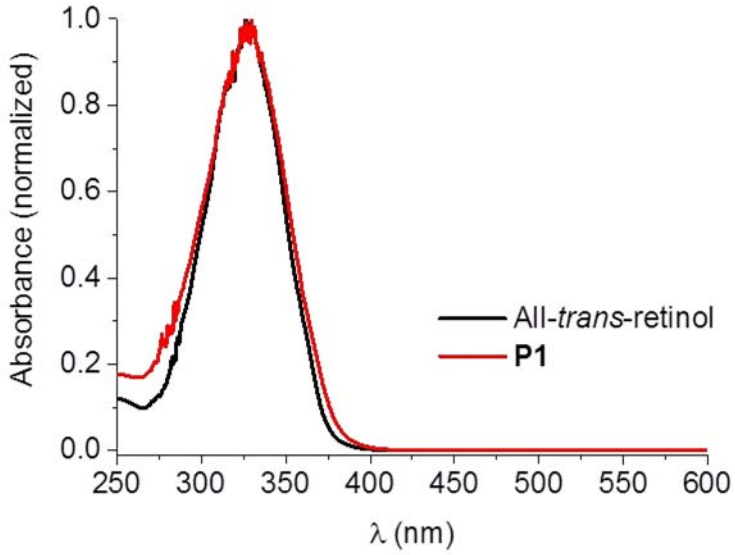

Figure S3. Overlay of UV/vis spectra of all-*trans*-retinol (c = 0.015 mg mL^{-1}) and **P1** (0.185 mg mL^{-1}) recorded in THF.

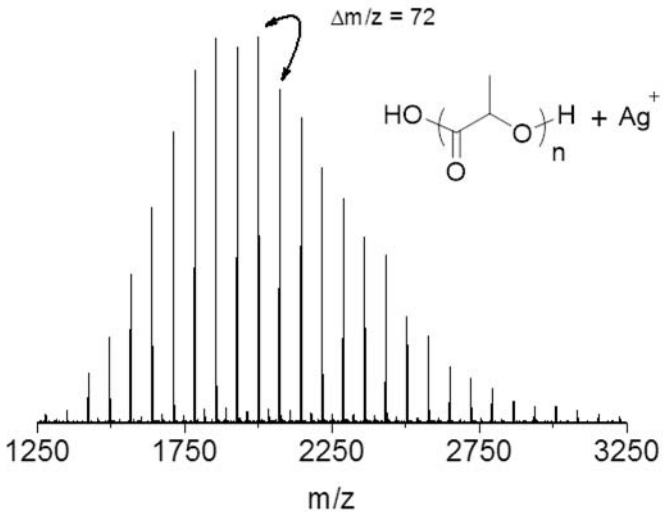

Figure S4. MALDI-ToF mass spectrum of **P1** (AgTFA, DCTB).

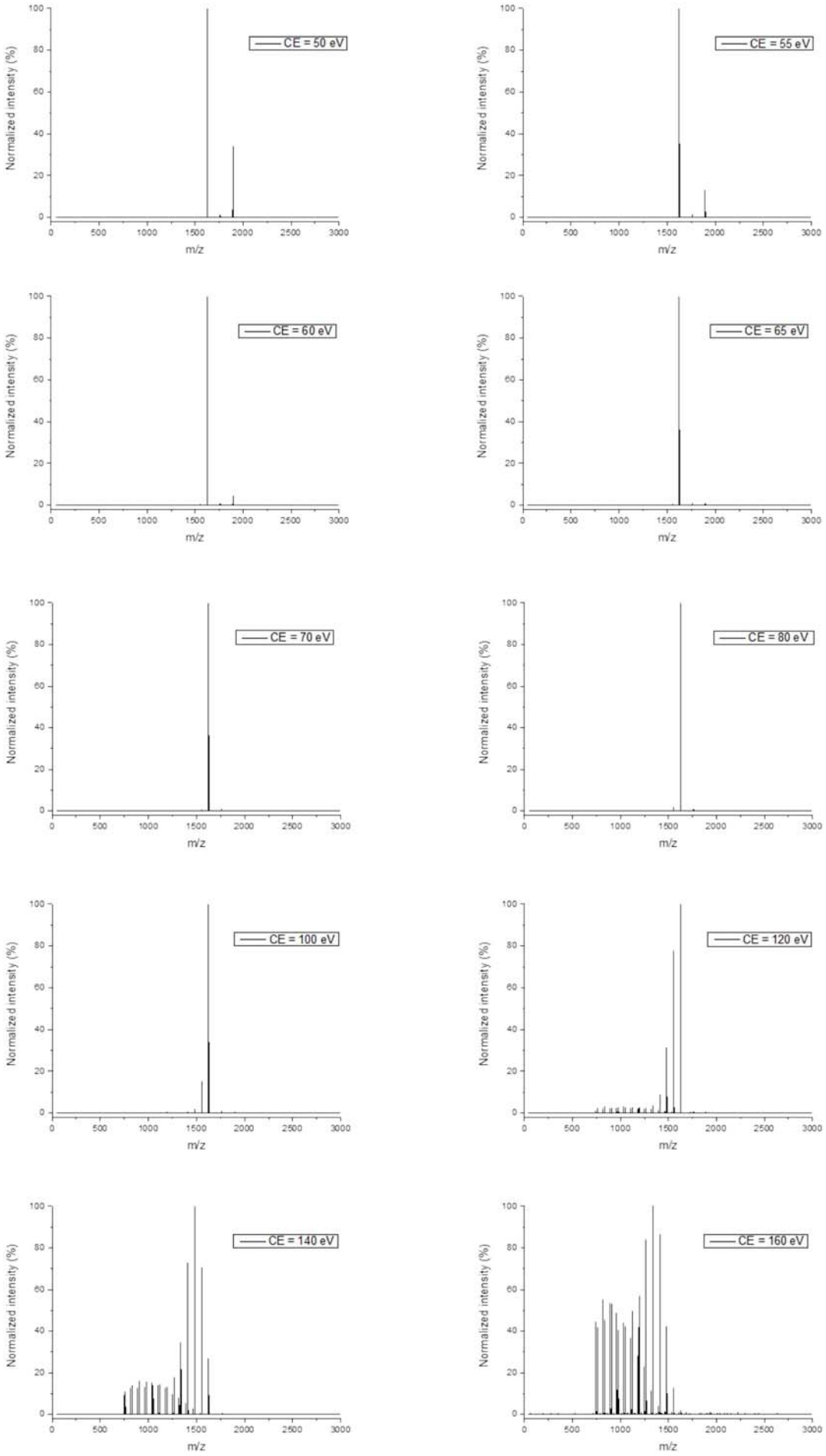

Figure S5. ESI-Q-ToF MS/MS spectra of sodiated **P1** at m/z = 1893.7 recorded at different collision energy values (50 to 160 eV).

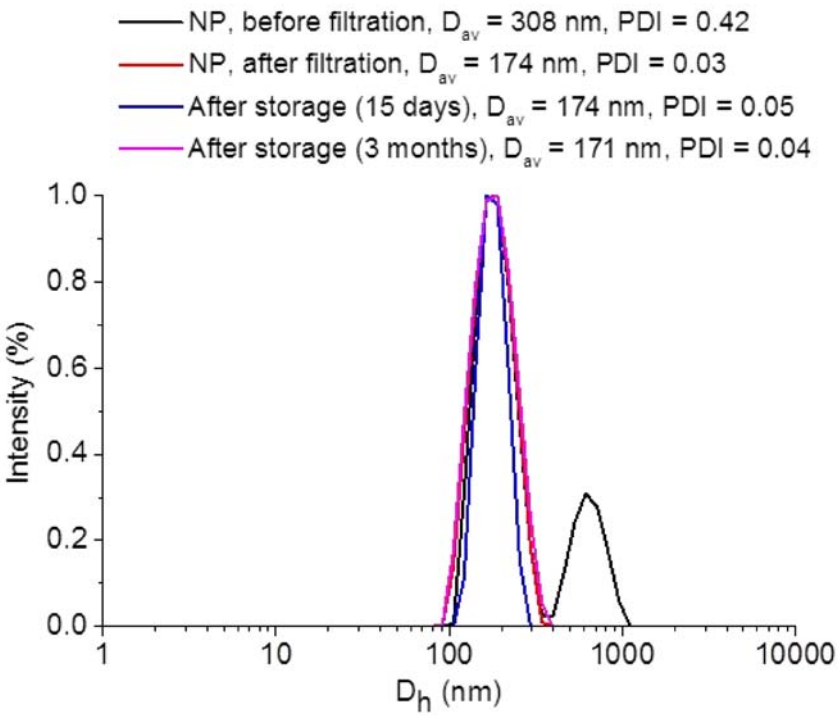

Figure S6. Normalized intensity size distributions of **P1** nanoparticles in water.

Table S1. Zeta potential values of the nanoparticles in aqueous suspension.

Entry	Method[a]	Zeta potential[b] [mV]
P1	AW	-53 ± 2
	WA	-40 ± 1
P2	AW	-52 ± 2
	WA	-49 ± 2
P3	AW	-48 ± 2
	WA	-32 ± 1
P4	AW	-30 ± 1
	WA	-50 ± 2

[a]AW, dropping acetone to water; WA, dropping water to acetone. [b]Average values of three zeta potential measurements.

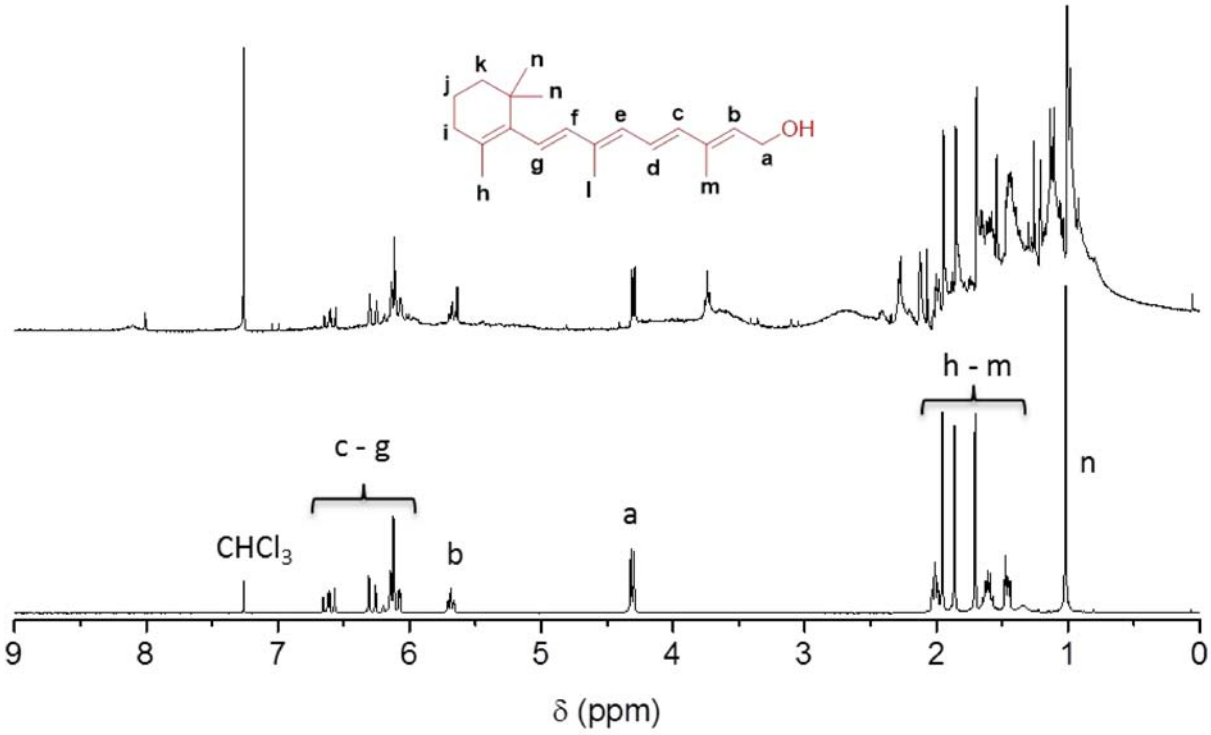

Figure S7. Overlay of ^{1}H NMR spectra of fresh retinol (bottom) and retinol after storage for 15 days at room temperature under daylight (top).

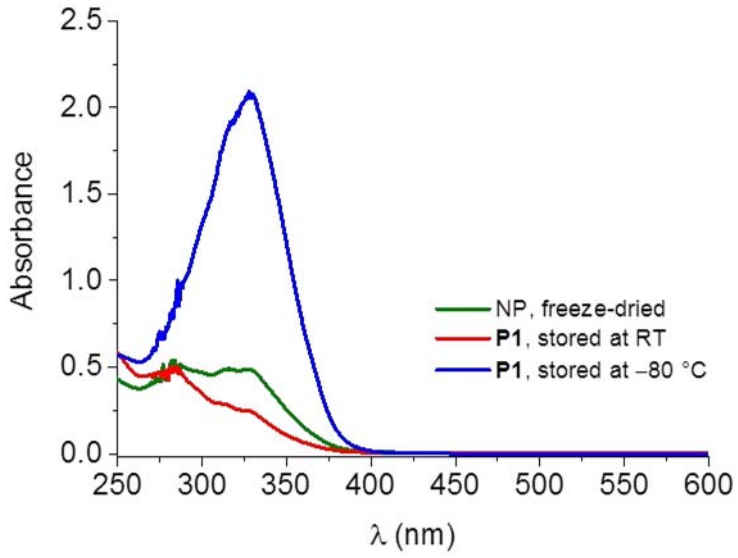

Figure S8. Overlay of UV/vis spectra of the freeze-dried NP with **P1** stored at RT and –80 °C for 15 days.

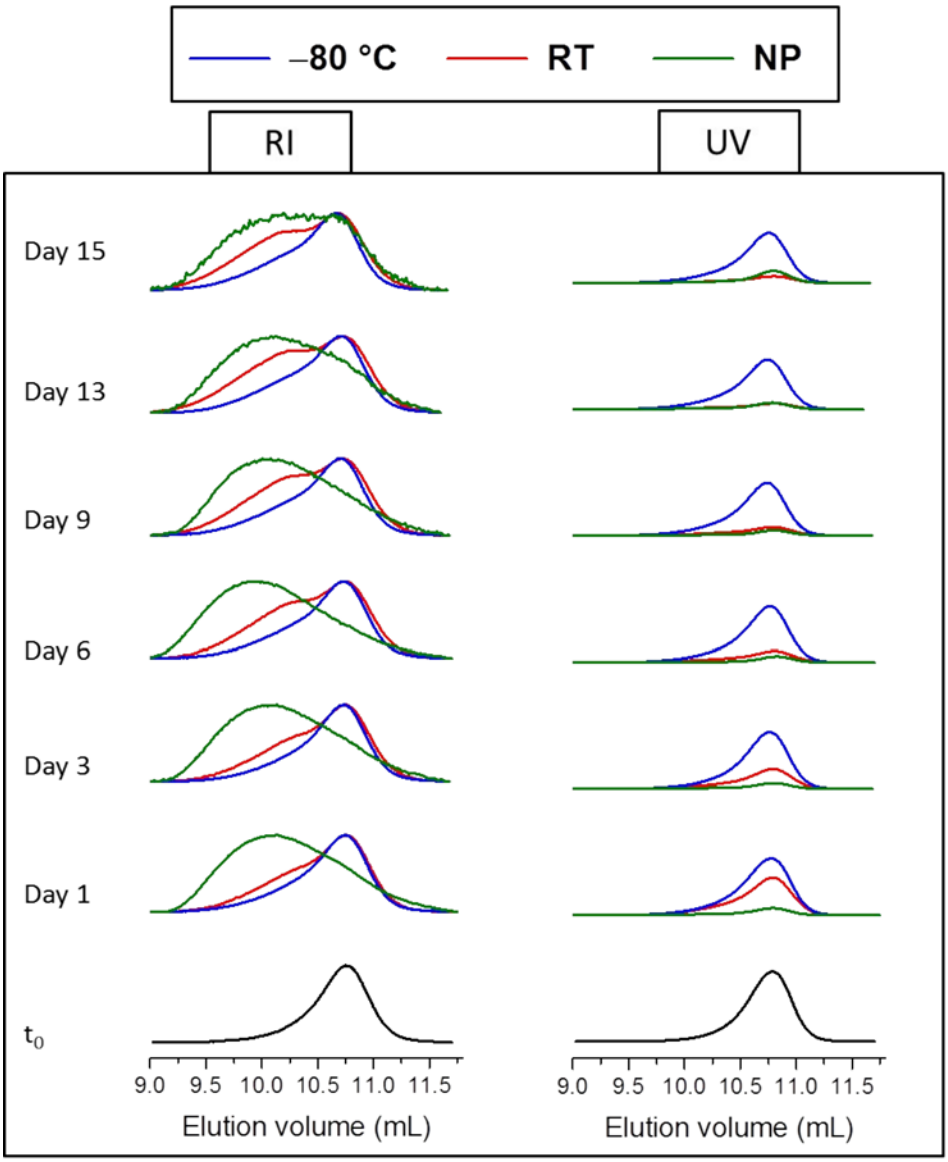

Figure S9. Overlay of normalized SEC elugrams recorded with RI and UV (λ = 340 nm) detection during stability tests of **P1** (t_0, and different storage conditions; RT and –80 °C) and the corresponding NP. SEC curves recorded with UV detection were normalized according to corresponding RI signals.

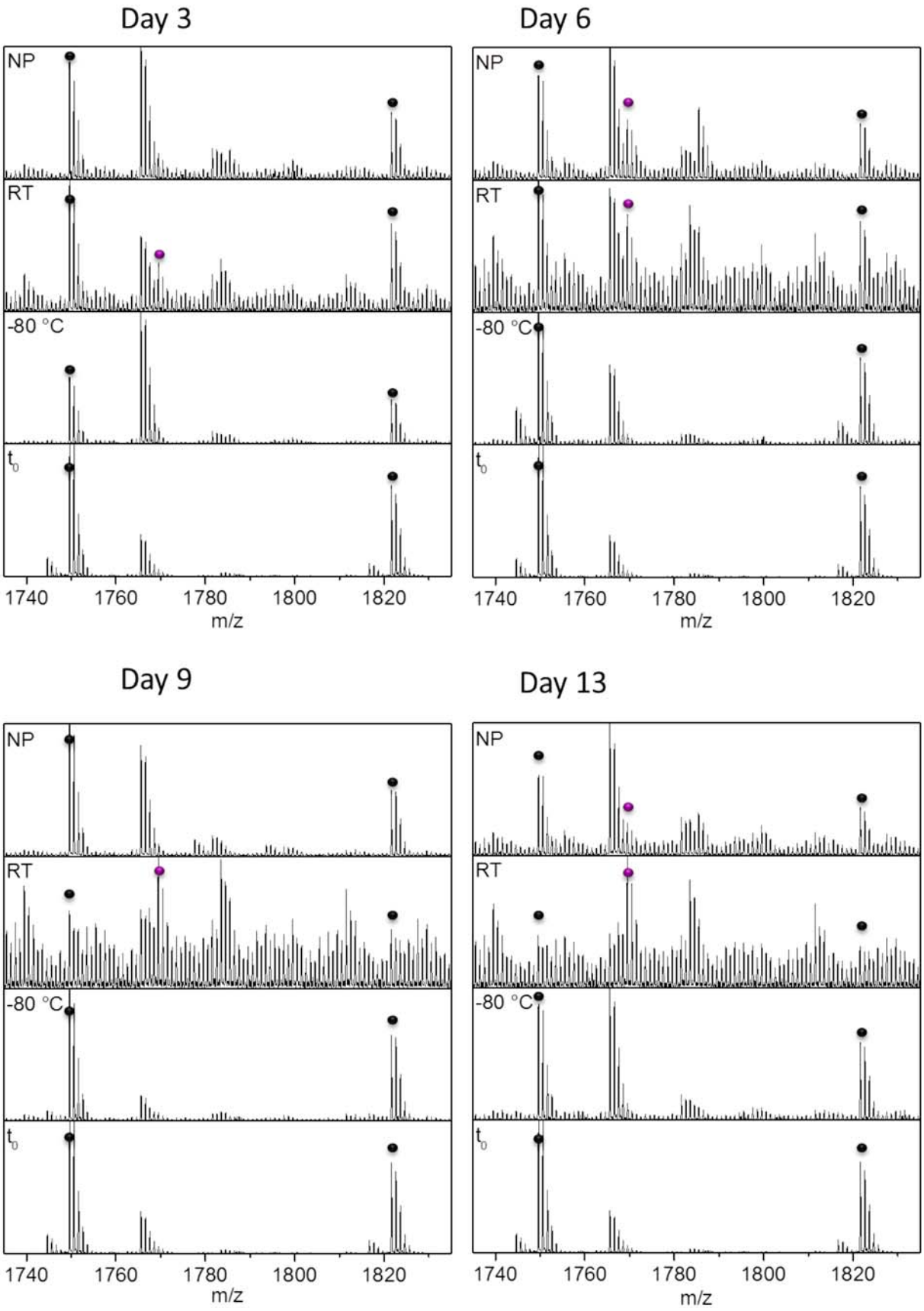

Figure S10. Overlay of ESI-Q-ToF mass spectra of **P1** (t_0 and different storage conditions; RT and -80 °C) and of the corresponding NP. The black and purple dots are added for clarity to indicate the presence of species "a" and "g" (See **Figure 8**).

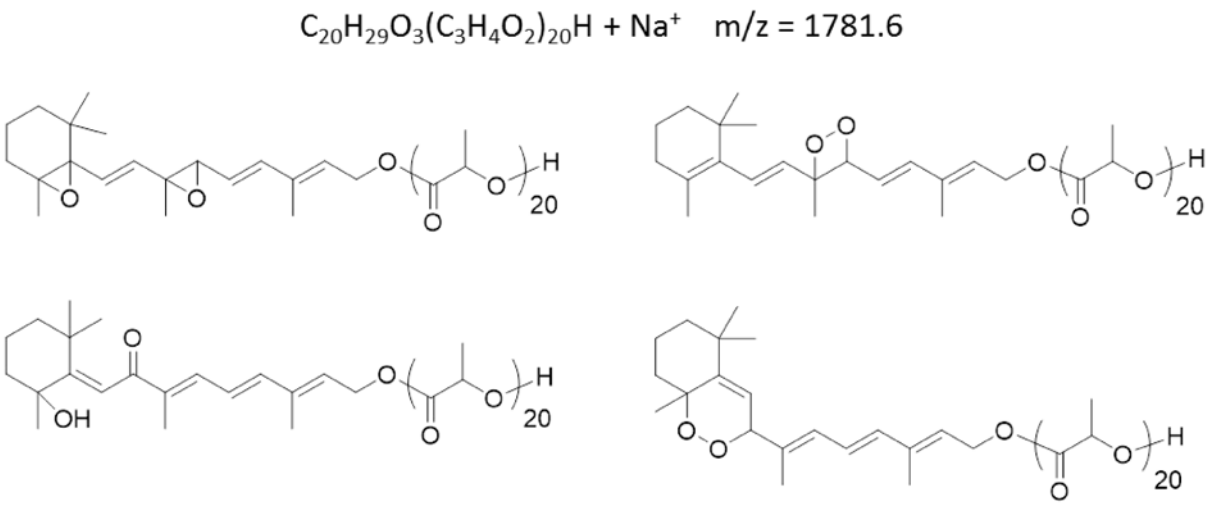

Figure S11. Examples for possible isomers of species "d" in **Figure 8**.

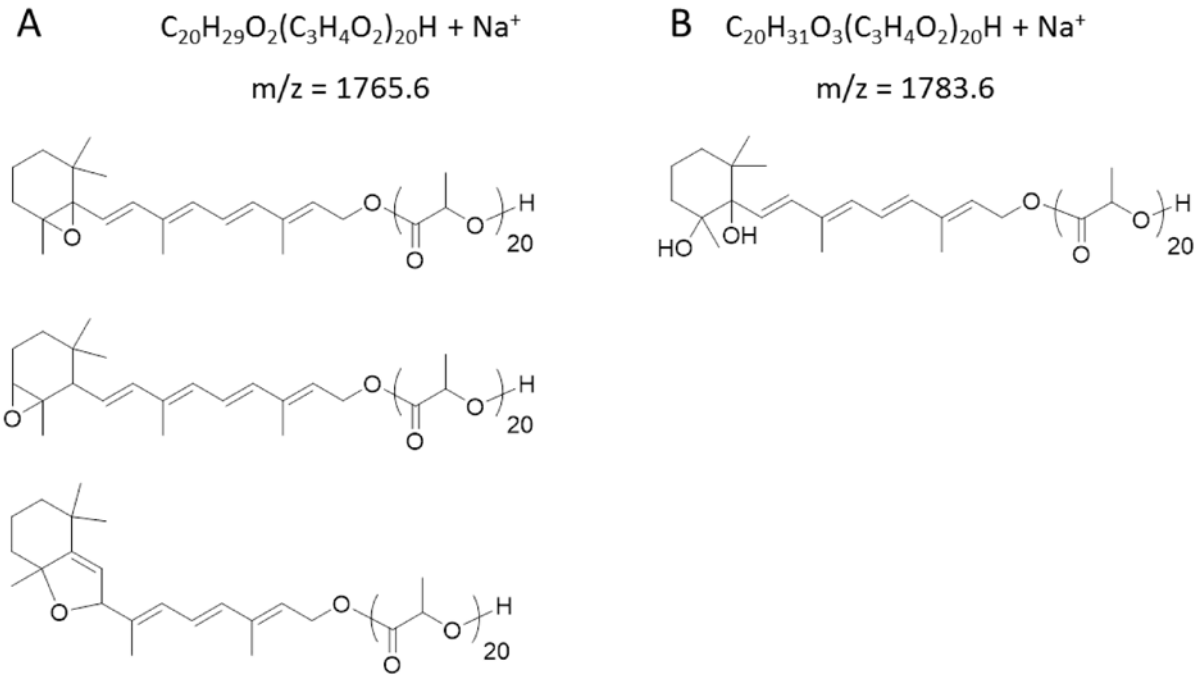

Figure S12. Examples for possible isomers of species "h" (**A**) and species "i" (**B**) in **Figure 8**.

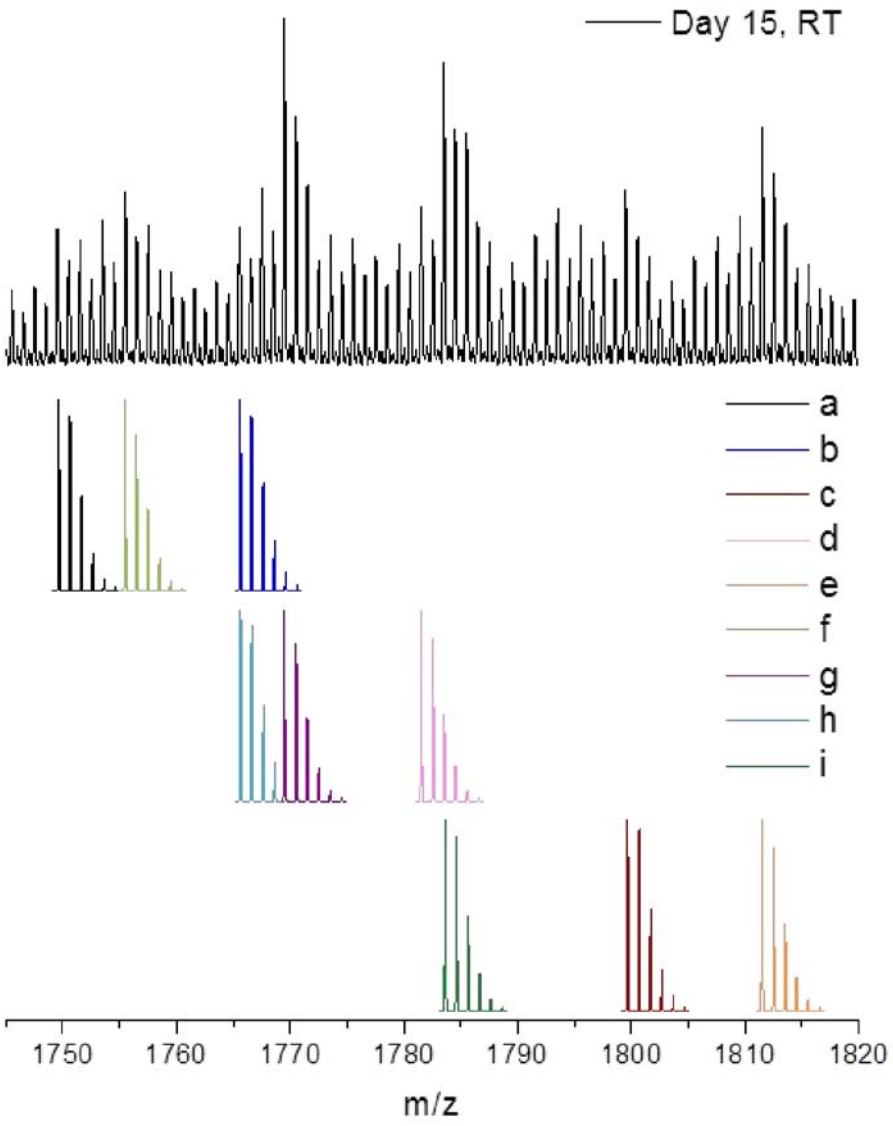

Figure S13. Overlay of the ESI-Q-ToF mass spectrum of **P1** recorded after 15 days of storage at room temperature and under daylight with the calculated isotopic patterns of likely degradation products (compare **Figure 8**).

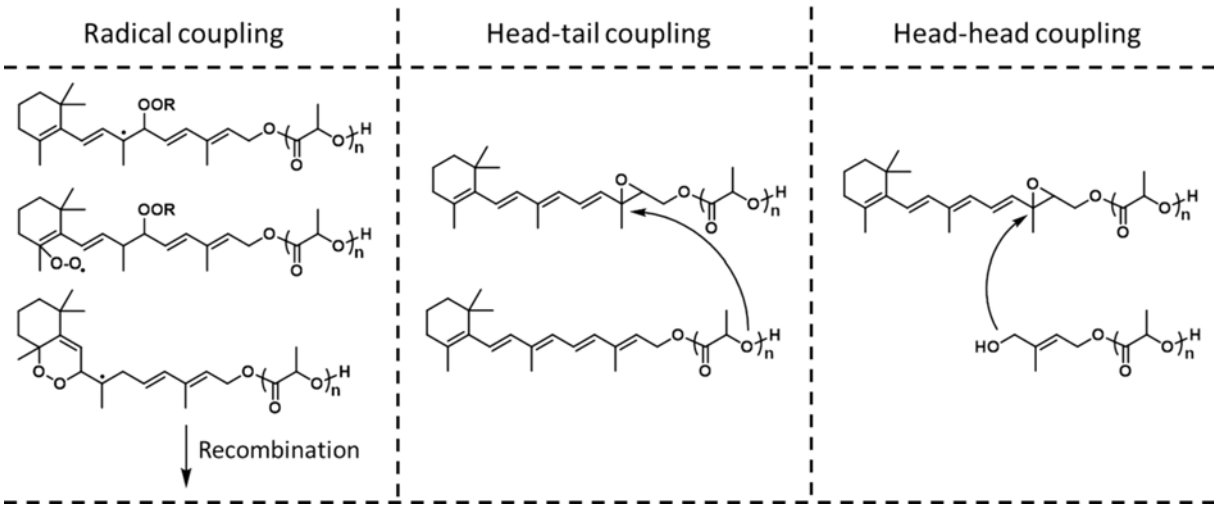

Figure S14. Examples for possible coupling pathways.

Publication P5

"One-pot synthesis of PLA-*b*-PHEA *via* sequential ROP and RAFT polymerizations"

Ilknur Yildirim, Pelin Sungur, Anna C. Crecelius-Vitz, Turgay Yildirim, Diana Kalden, Stephanie Hoeppener, Matthias Westerhausen, Christine Weber, Ulrich S. Schubert

Polym. Chem. **2017**, DOI: 10.1039/C7PY01176H.

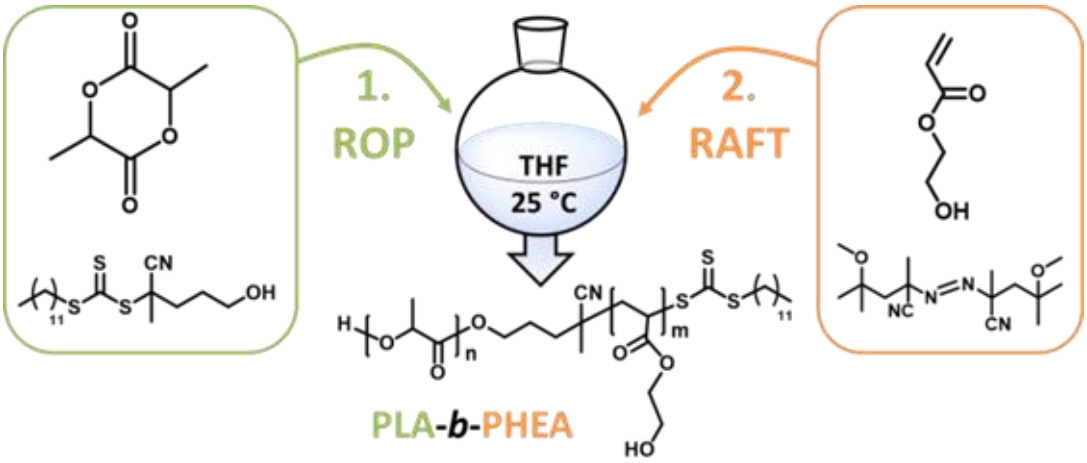

Polymer Chemistry

PAPER

View Article Online
View Journal

Cite this: DOI: 10.1039/c7py01176h

One-pot synthesis of PLA-*b*-PHEA *via* sequential ROP and RAFT polymerizations†

Ilknur Yildirim,[a,b] Pelin Sungur,[a,b] Anna C. Crecelius-Vitz,[a,b] Turgay Yildirim,[a,b] Diana Kalden,[c] Stephanie Hoeppener,[a,b] Matthias Westerhausen,[c] Christine Weber[a,b] and Ulrich S. Schubert*[a,b]

Received 15th July 2017,
Accepted 2nd September 2017

DOI: 10.1039/c7py01176h

rsc.li/polymers

A block copolymer library of polylactide (PLA) and poly(2-hydroxyethyl acrylate) (PHEA) was prepared *via* sequential ring opening polymerization (ROP) and reversible addition fragmentation chain transfer (RAFT) polymerization in a one-pot approach. The whole process was conducted at room temperature in THF without employing any protection chemistry or intermediate purification steps. The ROP of L-lactide was performed *via in situ* calcium alkoxide formation by using 4-cyano-4-[(dodecylsulfanylthiocarbonyl)sulfanyl]pentanol (CDP) and $[(THF)_2Ca\{N(SiMe_3)_2\}_2]$. The PLA based macro chain transfer agent (CTA) (M_n = 2550 g mol^{-1}, $Đ$ = 1.18) was characterized in-depth by (tandem) mass spectrometry and proved to be suitable to obtain PHEA blocks with M_n values up to 10 000 g mol^{-1} ($Đ \leq 1.28$). Thermogravimetric analysis (TGA) and differential scanning calorimetry (DSC) measurements indicated an increased miscibility between both blocks in bulk as the length of the PHEA unit increases. The amphiphilic block copolymers self-assembled into micellar structures in aqueous media, which were studied by dynamic light scattering (DLS) and cryo-transmission electron microscopy (cryo-TEM).

Introduction

Polylactide (PLA) represents a biodegradable and biocompatible polyester and has, thus, found many applications in the biomedical field for, *e.g.* implants, tissue engineering or drug delivery.[1,2] The attachment of hydrophilic blocks is useful for many of these and other applications of the material and yields amphiphilic polymers. A hydrophilic building block comprising hydroxyl functionalities provides the opportunity to further modify the material by means of post-polymerization modifications[3,4] or crosslinking.[5]

On the other hand, alcohols serve as initiators for the ring-opening polymerization (ROP) of lactide, which prohibits the presence of unprotected hydroxyl-functional building blocks during the ROP if block copolymers are targeted. This makes the application of protection group chemistry a necessity,[6,7] unless hydroxyl-functional moieties are incorporated subsequent to the ROP. Besides end-group transformation techniques,[8] reversible deactivation radical polymerization (RDRP) techniques in combination with heterofunctional initiators for ROP and RDRP have been applied for this purpose in two-pot reactions using PLA-based macroinitiators[9–12] or macro-chain transfer agents (CTA).[7,13]

Non-isolated macroinitiators and macro-CTAs have been further investigated in one-pot reactions to yield PLA-based copolymers.[14] If going smoothly, such an approach would facilitate access to block copolymers obtained by orthogonal polymerization mechanisms in an experimental fashion that is as simple as sequential monomer addition. The latter is a standard technique in block copolymer synthesis comprising only one polymerization mechanism.[15] The according block copolymers are widely investigated with respect to typical properties such as, *e.g.*, phase separation or self-assembly, and have found many applications.[16] In contrast, one-pot approaches remain challenging for the combination of ROP and RDRP, in particular regarding hydroxyl-functional monomers. As a result, typical properties of the materials are scarcely investigated.

The main reason might be the fact that all chemicals (*i.e.* initiators, catalysts, chain transfer agents, solvents) required to perform one polymerization type must not interfere with the orthogonal polymerization mechanism. A typical example is the use of the standard ROP catalyst stannous(II) octoate ($SnOct_2$) in combination with atom transfer radical polymeriz-

[a]Laboratory of Organic and Macromolecular Chemistry (IOMC), Friedrich Schiller University Jena, Humboldtstr. 10, 07743 Jena, Germany. E-mail: ulrich.schubert@uni-jena.de
[b]Jena Center for Soft Matter (JCSM), Friedrich Schiller University Jena, Philosophenweg 7, 07743 Jena, Germany
[c]Institute of Inorganic and Analytical Chemistry (IAAC), Friedrich Schiller University Jena, Humboldtstr. 8, 07743 Jena, Germany

†Electronic supplementary information (ESI) available: Additional MALDI and ^{1}H NMR spectra, SEC traces, DLS size distributions, TGA and DSC thermograms, thermal characterization data obtained *via* DSC analysis and cryo-TEM images. See DOI: 10.1039/c7py01176h

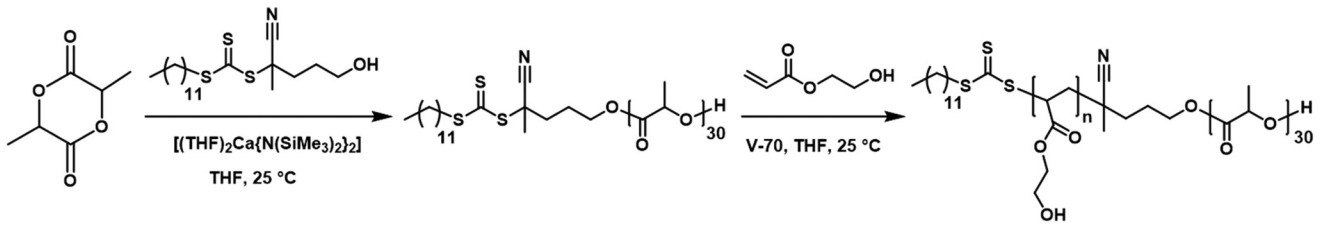

Scheme 1 Schematic representation of the synthesis of PLA-*b*-PHEA copolymers by a combination of ROP and RAFT in a sequential one-pot approach.

ation (ATRP). The tin(II) serves as reducing agent, influences the ratio of copper(I) and copper(II), and thereby interferes with the ATRP mechanism. Such effects made the kinetics of the polymerization difficult to adjust, which reportedly resulted in loss of control over the ATRP and block copolymers whose composition was difficult to predict.[17,18] Frey and co-workers exploited the reducing properties of $Sn(Oct)_2$ in an activators regenerated by electron transfer (ARGET) ATRP of 2-hydroxyethyl methacrylate (HEMA).[19] To the best of our knowledge, this carefully developed method represents the only one-pot approach that has been applied to obtain more than one (*i.e.* three) well-defined PLA block copolymers comprising a hydroxy-functional second block. However, the experimental procedure is still not as straightforward as a common chain extension *via* sequential monomer addition because it requires a solvent switch from toluene to DMSO, including freeze-drying of the polymerization mixture subsequent to the ROP.

In contrast, the organic ROP catalyst 4-dimethylaminopyridine (DMAP) is well compatible with RAFT polymerization conditions, and recent research is focused on its exploitation in simultaneous ROP and RAFT polymerization.[20–23] *Per se*, simultaneous approaches prohibit the use of hydroxyl-functionalized vinylic monomers if linear block copolymers are targeted. In consequence, we are aware of only one example (PLA_{27}-*b*-poly(glycerol monomethacrylate)$_{29}$) that is reported as a side note by Armes *et al.*[20] The fact that self-assembly of the block copolymer occurred during the one-pot two-step polymerization might have shifted the authors' attention towards other vinylic monomers that seemed more promising to investigate in depth. Further successful reagent combinations applied for the ROP of lactide remain few, although additional examples are known for the ROP of ε-caprolactone.[24–29] Despite the increasing number of excellent catalysts for the ROP of lactide, other combinations such as $Sn(Oct)_2$/RAFT,[30] DBU/ATRP,[31] or an aluminum-based complex/NMP[32] have not yet been tested for other than simply hydrophobic vinylic monomers.

Being driven by research in inorganic chemistry, the number of metal–organic ROP catalysts is vast.[33] Although many catalysts appear to be very potent, they are scarcely fully exploited from the viewpoint of synthetic polymer chemistry. Previous research conducted in our group demonstrated that *in situ* calcium alkoxide formation using $[(THF)_2Ca\{N(SiMe_3)_2\}_2]$ with numerous alcohols facilitates the synthesis of α,ω-end functional PLA with high end group fidelity at room temperature,[34–36] fulfilling one prerequisite for a successful application in a one-pot ROP/RAFT approach. In addition, the ROP can be driven to quantitative conversion without loss of the end-group fidelity, preventing the grafting of short PLA chains from hydroxyl-moieties during a subsequent RAFT polymerization. Since the catalyst is extremely sensitive to moisture, it would be easily deactivated prior to or during the addition of the reagents required for a RAFT polymerization. This would even prevent it from catalyzing transesterification reactions between the PLA and slightly nucleophilic hydroxyl-moieties of a vinylic monomer or the respective polymer.

We selected 2-hydroxyethyl acrylate (HEA) as vinylic monomer in a one-pot two-step approach because PHEA exhibits excellent water solubility even at high molar masses.[37] In addition, the biocompatibility of PHEA makes PLA-*b*-PHEA block copolymers interesting for application as biomaterials.[38]

In this contribution, we introduce a facile one-pot synthesis approach to obtain block copolymers of lactide and HEA by combining ROP and RAFT polymerizations in a sequential manner (Scheme 1). Besides being applicable at room temperature, the synthetic approach eludes protection group chemistry, intermediate purification steps or solvent switches, making it as feasible as common consecutive monomer addition. Therefore, a PLA based macro-CTA was prepared by ROP in the presence of a hydroxyl functional trithiocarbonate acting as hetero-bifunctional inifer. Subsequent to in-depth characterization by (tandem) mass spectroscopy and kinetic studies during the RAFT polymerization of HEA, a range of well-defined block copolymers was synthesized using the developed one-pot approach. Thereby, the DP of the PHEA block was altered systematically to study the self-assembly behavior of the block copolymers in water by means of dynamic light scattering (DLS) and cryo-transmission electron microscopy (cryo-TEM). In addition, the bulk properties of the block copolymers were investigated by differential scanning calorimetry (DSC) and thermogravimetric analysis (TGA).

Experimental

Materials

L-Lactide (98%) was purchased from Sigma-Aldrich and purified by recrystallization from dry toluene and dried under

vacuum prior to polymerization. Bis(tetrahydrofuran)calcium bis[bis(trimethylsilyl)amide] ([(THF)$_2$Ca{N(SiMe$_3$)$_2$}$_2$]) was synthesized according to previously reported procedures that were discussed in several reviews.[39–42] 4-Cyano-4-[(dodecylsulfanylthiocarbonyl)sulfanyl]pentanol (CDP) and HEA were purchased from Sigma-Aldrich and used without further purification. Tetrahydrofuran (THF) was dried by refluxing over sodium/benzophenone. 2,2′-Azobis(4-methoxy-2,4-dimethylvaleronitrile) (V-70) was purchased from Wako Pure Chemical Industries and stored at −20 °C. All other chemicals were purchased from standard suppliers and were used without further purification.

Instruments

The ROP of L-lactide was carried out under nitrogen atmosphere in a MBraun UNILab glove box workstation (<1 ppm H_2O, <1 ppm O_2). Nuclear magnetic resonance (NMR) spectra were recorded at room temperature in $CDCl_3$ or DMSO-d_6 on a Bruker Avance 300 MHz using the residual solvent resonance as an internal standard. The chemical shifts are given in ppm relative to TMS. Size exclusion chromatography (SEC) measurements were performed on two different setups. SEC in THF: Shimadzu system equipped with a SCL-10A system controller, a LC-10AD pump, a RID-10A refractive index detector, a SPD-10AD UV detector and a SDV linear M column from PSS at 40 °C using THF as eluent at a flow rate of 1 mL min^{-1}. The system was calibrated against PLA standards (144 to 101 000 g mol^{-1}), which were purchased from PSS. SEC in DMAc: Agilent 1200 series equipped with a G1310A pump, a G1315D DA detector, a G1362A RI detector, and PSS GRAM 30 Å/1000 Å (10 μm particle size) columns in series at 40 °C using *N*,*N*-dimethylacetamide (DMAc) with 2.1 g L^{-1} LiCl as eluent at a flow rate of 1 mL min^{-1}. The system was calibrated with PMMA standards (M_p = 505 to 981 000 g mol^{-1}). For the matrix-assisted laser desorption/ionization time-of-flight mass spectrometry (MALDI-ToF MS) measurements, an Ultraflex III ToF/ToF instrument (Bruker Daltonics, Bremen, Germany) was employed. The instrument is equipped with a 355 nm Nd-YAG laser and a collision cell. All spectra were measured in the positive reflector mode. For the MS/MS mode, argon was used as collision gas at a pressure of 2×10^{-6} mbar. The instrument was calibrated prior to each measurement with an external PMMA standard from PSS (Mainz, Germany). For the MALDI-ToF MS sample preparation, separate solutions of polymer (10 mg mL^{-1} in THF), *trans*-2-[3-(4-*tert*-butylphenyl)-2-methyl-2-propenylidene] (DCTB, 30 mg mL^{-1} in THF), and silver trifluoroacetate (AgTFA, 100 mg mL^{-1} in acetone) were prepared and mixed following the dried droplet method. 1 μL of the mixture was spotted onto a MTP 384 target plate ground steel BC (Bruker Daltonics, Bremen, Germany). Unless indicated otherwise, differential scanning calorimetry (DSC) experiments were performed on a Netzsch DSC 204 F1 Phoenix under a nitrogen atmosphere with a heating rate of 20 K min^{-1} (1st and 2nd heating runs) or 10 K min^{-1} (3rd heating run) from −50 to 170 °C. Three cycles were recorded for each sample. The glass transition temperature (T_g) values are reported for the third heating run. Thermogravimetric analyses (TGA) were performed under a nitrogen atmosphere on a Netzsch TG 209 F1 Iris from room temperature to 600 °C with a heating rate of 10 K min^{-1}.

Dynamic light scattering (DLS) was performed on a Zetasizer Nano ZS (Malvern Instruments, Herrenberg, Germany). After an equilibration time of 120 s, 3 × 12 runs were carried out at 25 °C (λ = 633 nm). The counts were detected at an angle of 173°. The size distribution of the particles was calculated applying the non-linear least square fitting method. The mean particle size was approximated as the effective (*Z*-average) diameter and the width of the distribution as the polydispersity index of the particles (PDI) obtained by the cumulants method assuming a spherical shape of the particles. For the DLS measurements in DMSO at 25 °C, the following settings were applied: viscosity η = 1.990 mPa s and refractive index n = 1.4768. Cryo-transmission electron microscopy (cryo-TEM) investigations were performed on a Tecnai G^2 20 (FEI) equipped with an Olympus Soft Imaging Solutions MegaView and a 4 × 4 k Eagle CCD camera system. Quantifoil grids (R2/2 Quantifoil, Germany) were cleaned by plasma treatment prior to use. Cryo sample preparation was conducted utilizing a FEI Vitrobot Mark IV system. 8.5 μL of the sample solution was deposited onto the grid, equilibrated shortly, and blotted for 1 s. The grids were immediately plunched into liquid ethane to obtain vitrification, and the samples were stored at liquid nitrogen temperature until transferred to the TEM utilizing a Gatan cryo transfer system.

Synthesis of the macro-CTA *via* ROP of L-lactide

The ROP of L-lactide was carried out in a glove box at room temperature under nitrogen atmosphere using THF as the solvent as described previously.[34] Briefly, [(THF)$_2$Ca{N(SiMe$_3$)$_2$}$_2$] (0.12 mmol, 58 mg) was dissolved in 1.0 mL THF. This corresponds to a molar ratio of [L-lactide]$_0$/[CDP]$_0$/[Ca]$_0$ of 15/1/0.5 and an initial monomer concentration of [L-lactide] of 1 mol L^{-1}. After 10 minutes, the polymerization was quenched by addition of acidified methanol. The conversion was determined from the ^{1}H NMR spectrum of the polymerization mixture by integrating the methine proton region of PLA *versus* that of the L-lactide. The macro-CTA was purified *via* precipitation in methanol and subsequent drying under reduced pressure until a constant weight was reached. ^{1}H NMR (300 MHz, $CDCl_3$): M_n = 2550 g mol^{-1} (calculated based on the relative intensities of the methine protons of PLA at δ = 5.16 and methylene protons of CDP at δ = 4.2 ppm). SEC (THF, RI detection, PLA calibration): M_n = 2300 g mol^{-1}, $Đ$ = 1.18. SEC (DMAc, RI detection, PMMA calibration): M_n = 4500 g mol^{-1}, $Đ$ = 1.18. MALDI-ToF-MS: M_n = 2400 g mol^{-1}, $Đ$ = 1.07. For further discussion on the characterization of the macro-CTA, the reader is referred to the literature.[34]

Kinetic study of the RAFT polymerization of HEA in the presence of CDP

The kinetic study of the RAFT polymerization of HEA was performed at room temperature with THF as solvent ([HEA]$_0$/[CDP]$_0$/[V-70]$_0$ = 40/1/0.25, [HEA]$_0$ = 1 mol L^{-1}). A microwave

Table 1 Characterization results of the macro-CTA, the PHEA homopolymers and the block copolymers **P1** to **P6** prepared *via* the one-pot approach

Polymer	Initiator (I) or CTA	M/I or M/CTA	Conv.[a] (NMR)	$M_{n,\,theo}$[b] [g mol^{-1}]	$M_{n,\,NMR}$[c] [g mol^{-1}]	$M_{n,\,SEC}$[d] [g mol^{-1}]	$Đ_{SEC}$[d]	Composition (Theo.)[b]	Composition (NMR)[c]
PLA-CTA	CDP	15	Quant.	2550	2550	2300[e]	1.18[e]	PLA_{15}	PLA_{15}
PHEA-1	CDP	15	93	2000	2250	7100	1.05	$PHEA_{14}$	$PHEA_{16}$
PHEA-2	CDP	100	65	8000	14 450	22 100	1.24	$PHEA_{65}$	$PHEA_{121}$
P1	PLA-CTA	20	82	4450	4500	10 300	1.13	PLA_{15}-*b*-$PHEA_{16}$	PLA_{15}-*b*-$PHEA_{17}$
P2	PLA-CTA	40	60	5300	5450	12 100	1.15	PLA_{15}-*b*-$PHEA_{24}$	PLA_{15}-*b*-$PHEA_{25}$
P3	PLA-CTA	40	70	5800	6500	15 300	1.21	PLA_{15}-*b*-$PHEA_{28}$	PLA_{15}-*b*-$PHEA_{34}$
P4	PLA-CTA	50	70	6600	8250	16 100	1.24	PLA_{15}-*b*-$PHEA_{35}$	PLA_{15}-*b*-$PHEA_{49}$
P5	PLA-CTA	60	85	8500	10 700	22 700	1.23	PLA_{15}-*b*-$PHEA_{51}$	PLA_{15}-*b*-$PHEA_{70}$
P6	PLA-CTA	100	83	12 200	19 850	27 500	1.28	PLA_{15}-*b*-$PHEA_{83}$	PLA_{15}-*b*-$PHEA_{149}$

[a] Conversion values determined by ^{1}H NMR spectroscopy from the polymerization mixtures (t_0 and t_f). [b] Calculated from feed and conversion. [c] Calculated from suitable signal integrals in the ^{1}H NMR spectra of the purified polymers. [d] Determined by SEC (DMAc, RI detection, PMMA calibration). [e] Determined by SEC (THF, PLA calibration).

vial containing HEA (0.537 g, 4.62 mmol), CDP (45.1 mg, 0.115 mmol), V-70 (8.91 mg, 0.029 mmol), 200 μL of anisole, and 4.62 mL of THF was placed in a cooling bath at −20 °C and gently purged with argon for 30 minutes to remove the oxygen from the reaction mixture. Afterwards, the t_0 sample was taken and the vial was immersed in an oil bath at 25 °C. The polymerization was monitored by sampling at defined time intervals with degassed syringes. Subsequently ^{1}H NMR (300 MHz, DMSO-d_6) and SEC analyses (DMAc, RI detection, PMMA calibration) were conducted to determine the monomer conversion and the evolution of the molar mass, respectively. The conversion was determined by comparing the integral values of the vinylic peaks in ^{1}H NMR spectra of the samples using anisole as an internal standard.

Synthesis of PHEA

In a representative RAFT polymerization for **PHEA-1** ([HEA]/[CDP] = 15), HEA (2.15 mmol, 0.25 g), CDP (0.14 mmol, 55.9 mg), V-70 (0.035 mmol, 10.8 mg) and 200 μL of anisole were dissolved in 2.15 mL THF in a microwave vial. Subsequently, the vial was placed in a cooling bath at −20 °C and gently purged with argon for 30 minutes. The t_0 sample was taken for the determination of the monomer conversion. Afterwards the vial was immersed in an oil bath at 25 °C and the RAFT polymerization was conducted for 36 hours. The polymerization was stopped by exposing the solution to air and the t_f sample was taken. The monomer conversion was calculated by comparing the integral values of the vinylic protons in the ^{1}H NMR spectra of the t_0 and t_f samples by using anisole as an internal standard. The **PHEA-1** was purified *via* precipitation in a mixture of ice cold hexane and diethyl ether (1 : 2 v/v) and subsequent drying under reduced pressure until a constant weight was reached. ^{1}H NMR (300 MHz, DMSO-d_6): M_n = 2250 g mol^{-1} (calculated based on the relative intensities of the methyl protons of CDP at δ = 0.85 and methylene protons of PHEA at δ = 4.0 ppm). SEC (DMAc, RI detection, PMMA calibration): M_n = 7100 g mol^{-1}, $Đ$ = 1.05. **PHEA-2** was synthesized in an analogous fashion by changing the initial monomer to CTA ratio ([HEA]/[CDP] = 100). 800 mg (6.9 mmol) HEA, 26.8 mg (0.069 mmol) CDP, 5.31 mg (0.017 mmol) V-70 and 6.9 mL THF were used, and the polymerization was conducted for 24 h. ^{1}H NMR (300 MHz, DMSO-d_6): $M_{n,\,NMR(theo.)}$ = 8000 g mol^{-1} (calculated from conversion values, see results and discussion part and Table 1). SEC (DMAc, RI detection, PMMA calibration): M_n = 22 100 g mol^{-1}, $Đ$ = 1.24.

Kinetic study of one-pot synthesis of PLA-*b*-PHEA

The ROP of L-lactide was carried out in a glove box, at room temperature under nitrogen atmosphere as described above ([L-lactide]$_0$/[CDP]$_0$/[Ca]$_0$ = 15/1/0.5, [L-lactide] = 1 mol L^{-1}) by utilizing [(THF)$_2$Ca{N(SiMe$_3$)$_2$}$_2$] (29.2 mg, 0.058 mmol), L-lactide (1.73 mmol, 0.25 g), CDP (0.116 mmol, 45.1 mg) and 1.75 mL of THF. After 10 minutes, a sample was taken from the mixture and analyzed by ^{1}H NMR spectroscopy to verify the quantitative monomer conversion. Afterwards, the vial was taken out of the glove box without quenching the polymerization. The vial was exposed to air and placed in a cooling bath at −20 °C. A mixture of HEA (0.537 g, 4.62 mmol), V-70 (8.91 mg, 0.029 mmol) and 200 μL of anisole in 2.89 mL of THF ([HEA]$_0$/[macro-CTA]$_0$/[V-70]$_0$ = 40/1/0.25, [HEA] = 1 mol L^{-1}, which was prepared prior to the ROP step and kept at −20 °C) was added to the vial containing the macro-CTA. Subsequently, the t_0 sample was taken. Afterwards, the vial was gently purged with argon for 30 minutes and then immersed in an oil bath at 25 °C. The polymerization was monitored by sampling at defined time intervals with degassed syringes. Subsequently ^{1}H NMR (300 MHz, DMSO-d_6) and SEC analyses (DMAc, RI detection, PMMA calibration) were conducted to determine the monomer conversion and the evolution of molar mass, respectively. The conversion was determined by comparing the integral values of the vinylic peaks in ^{1}H NMR spectra of the samples using anisole as an internal standard.

One-pot synthesis of PLA-*b*-PHEA

Six different block copolymers were prepared by changing the feed ratios of [HEA]$_0$/[macro-CTA]$_0$ (Table 1). In each step the

initial monomer concentration was kept as 1 mol L^{-1} in THF. In a representative one-pot sequential ROP and RAFT polymerization for **P1**, the ROP of L-lactide was carried out as described above in a glove box by utilizing $[(THF)_2Ca\{N(SiMe_3)_2\}_2]$ (29.2 mg, 0.058 mmol), L-lactide (1.73 mmol, 0.25 g), CDP (0.116 mmol, 45.1 mg) and 1.75 mL of THF ($[L\text{-lactide}]_0/[CDP]_0/[Ca]_0$ = 15/1/0.5, $[L\text{-lactide}]_0$ = 1 mol L^{-1}). After 10 minutes, a sample was taken from the mixture and analyzed by ^1H NMR spectroscopy to verify the quantitative monomer conversion. The vial was taken out of the glove box, exposed to air and placed in a cooling bath at −20 °C. A mixture of HEA (0.3 g, 2.3 mmol), V-70 (8.9 mg, 0.029 mmol), 200 μL of anisole and 580 μL of THF ($[HEA]_0/[\text{macro-CTA}]_0/[V\text{-}70]_0$ = 20/1/0.25, [HEA] = 1 mol L^{-1}) was added to the microwave vial containing the macro-CTA. Subsequently, the vial was gently purged with argon for 30 minutes. Finally, the vial was placed in an oil bath at 25 °C and the RAFT polymerization was conducted for 24 h. The monomer conversion was calculated by comparing the integral values of the vinylic protons in the ^1H NMR spectra of the t_0 and t_f samples by using anisole as an internal standard. The block copolymer was isolated by precipitation in a mixture of ice cold hexane/diethyl ether (1 : 2 v/v) (four times) and subsequent drying under reduced pressure until a constant weight was reached. The block copolymers **P2** to **P6** were synthesized in an analogous fashion by adjusting the amount of HEA and the polymerization time. Characterization data by ^1H NMR and SEC are provided in Table 1.

Synthesis of PLA-*b*-PHEA in two steps

For comparison with the one-pot approach, RAFT polymerization of HEA was performed by using the purified PLA macro-CTA in THF ($[HEA]_0/[\text{macro-CTA}]_0/[V\text{-}70]_0$ = 20/1/0.25, $[HEA]_0$ = 1 mol L^{-1}). The isolated macro-CTA (100 mg), HEA (0.78 mmol, 91 mg), V-70 (0.01 mmol, 3 mg) and 200 μL anisole were dissolved in 0.78 mL of THF. The vial was placed in a cooling bath at −20 °C and purged gently with argon for 30 minutes. Subsequently, the RAFT polymerization was conducted in an oil bath at 25 °C for 24 h. The monomer conversion was calculated by comparing the integral values of the vinylic protons in ^1H NMR spectra of the t_0 and t_f samples. Finally, the block copolymer was purified by precipitation in a mixture of ice cold hexane/diethyl ether (1 : 2 v/v) and drying under reduced pressure until constant weight was reached. ^1H NMR (DMSO-d_6): M_n = 6400 g mol^{-1}, SEC (DMAc, RI detection, PMMA calibration): 10 000 g mol^{-1}, $Đ$ = 1.20.

Sample preparation for DLS analysis

1 mg of block copolymer was dissolved in 100 μL of THF. The solution was dropped into 1 mL of deionized water in aliquots of 5 μL under vigorous stirring. The THF was evaporated by stirring the open vial for at least two days to yield aqueous suspensions with a final polymer concentration of 1 mg mL^{-1}. The other suspensions were prepared in an analogous fashion to result in a final polymer concentration of 2 or 5 mg mL^{-1}, respectively. The samples were aged for at least one week before analysis by cryo-TEM (see instruments section for further details).

Results and discussion

Synthesis and MALDI-ToF-MS characterization of the PLA macro-CTA

The PLA based macro-CTA was synthesized by ROP of L-lactide using the hydroxyl functional trithiocarbonate CDP *via in situ* calcium alkoxide formation in the presence of $[(THF)_2Ca\{N(SiMe_3)_2\}_2]$ as previously reported.[34] In order to facilitate an accurate structural determination of the PLA α-end group, oligomeric PLA with a DP of 15 was synthesized ($[L\text{-lactide}]_0/[CDP]_0/[Ca]_0$ = 15/1/0.5). Quantitative monomer conversion was achieved in 10 minutes, and SEC analysis revealed a monomodal mass distribution and a dispersity ($Đ$) of 1.18 (Fig. S1† and Table 1). The ^1H NMR spectrum (Fig. S2†) of the isolated macro-CTA confirmed the presence of the desired α-end group, and the according signals (peak a and c in Fig. S2†) were used to estimate the molar mass ($M_{n,\ NMR}$ = 2550 g mol^{-1}). The fact that $M_{n,\ NMR}$ is very close to both the theoretical value ($M_{n,\ theo}$) as well as $M_{n,\ SEC}$ already hints towards a high end group fidelity (Table 1). This was further confirmed by MALDI-ToF-MS analysis, revealing one major distribution with $\Delta m/z$ intervals of 72, which corresponds to the $C_3H_4O_2$ repeating units of PLA (Fig. S3†). According to literature, a $\Delta m/z$ interval of 72 in the mass spectra of PLA is attributed to the presence of transesterification reactions. However, based on our previous studies on this calcium alkoxide system it can be stated that an intramolecular rearrangement at the active catalyst center is the reason for this observation.[34–36] The exemplary isotopic pattern depicted in Fig. S3† can be assigned to a PLA chain composed of 22 $C_3H_4O_2$ repeating units, an α-end group derived from the CDP initiator, and a hydroxyl ω-end group, which is ionized with a silver cation. A minor distribution (only visible in the lower m/z region) is assigned to fragmentation of the CTA, which should originate from the ionization step (Fig. S4†). However, no assignments could be made that correspond to water-initiated, cyclic, or other types of PLA chains without the CTA end group.

As high end group fidelity of the macro-CTA is essential for a successful chain extension *via* RAFT polymerization, tandem MS (MS/MS) was performed on this parent ion ($C_{19}H_{34}NOS_3(C_3H_4O_2)_{22}H + Ag^+$) by utilizing collision-induced dissociation (CID). Already at a first glance, two m/z regions can be distinguished in the MS/MS spectrum (Fig. 1). In the m/z region below 1500, four ion series could be assigned according to the fragmentation pathways observed in ESI tandem MS of PLA (Fig. S5†).[43,44] Only minor abundant species assigned to PLA chains with intact α-end groups were found in this region ("A" and "C" in Fig. 1). Instead, complete α-end group cleavage was predominant, leading to α,ω-hydroxyl end group bearing PLA chains ionized with a silver cation ("B" in Fig. 1). However, the most abundant ion series in the lower m/z region resulted from an additional fragmentation at the

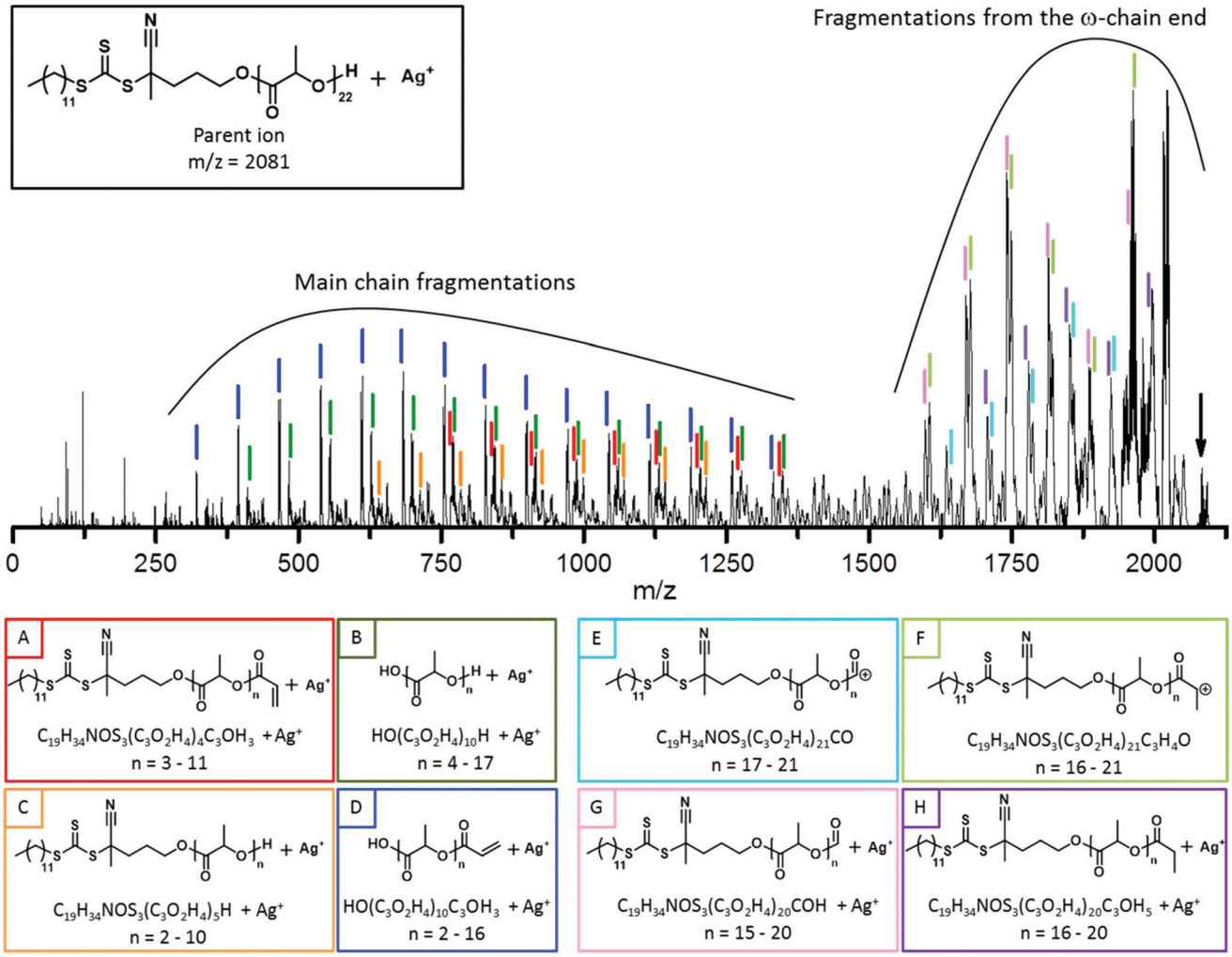

Fig. 1 MALDI ToF MS/MS spectrum of the selected precursor ion at *m/z* 2081 together with the structural assignment of the observed peaks.

ω-end group through Mc-Lafferty-like rearrangements[43,45] leading to fragment ions with an acrylate ω-end group by migration of the hydrogen atom from a pendant methyl group to the oxygen atom of the carbonyl group of the ester moiety ("D" in Fig. 1).

In contrast, the *m/z* region above 1500 in the tandem mass spectrum revealed an ion series that could be assigned solely to fragmentations originating from the ω-chain end while the α-end group was preserved (Fig. S6†). The silverated fragment series "H" was already observed by Wesdemiotis *et al.* during electron transfer dissociation (ETD) of multiply sodiated PLA species and may arise from a radical induced dissociation of the (CO)O–C bond of the ester group followed by further hydrogen addition.[46] The fragment ion series "G" could correspond to a formate ω-end group, which would result from a C–C bond cleavage between the carbonyl carbon and the carbon in α-position. In addition, both fragmentation products were found with a direct positive charge (ion series "E" and "F", Fig. 1).

Although reported for MALDI[47] or ESI[47,48] MS/MS of trithiocarbonate functional polyacrylates, fragmentation at the trithiocarbonate moiety was not observed in the MS/MS of the PLA macro-CTA.

RAFT polymerization of HEA at room temperature in the presence of CDP

Prior to the synthesis of block copolymers using the macro-CTA, we investigated the RAFT polymerization kinetics of HEA using CDP as CTA. To avoid transesterification reactions as soon as the PLA macro-CTA would be used, we aimed at performing the RAFT polymerization at room temperature. For this purpose, the radical initiator V-70 was employed (10 hours half-life at 30 °C in toluene),[49] which has already provided controlled RAFT polymerization processes at room temperature.[50,51] A kinetic study was conducted in THF at room temperature with a feed ratio of $[HEA]_0/[CDP]_0/[V\text{-}70]_0$ = 40/1/0.25 at a monomer concentration of 1 mol L^{-1}. Aliquots were taken from the polymerization mixture at defined time intervals to monitor the monomer conversion and the evolution of the molar mass during the polymerization. Fig. 2 displays the kinetic plots of the RAFT polymerization of HEA together with

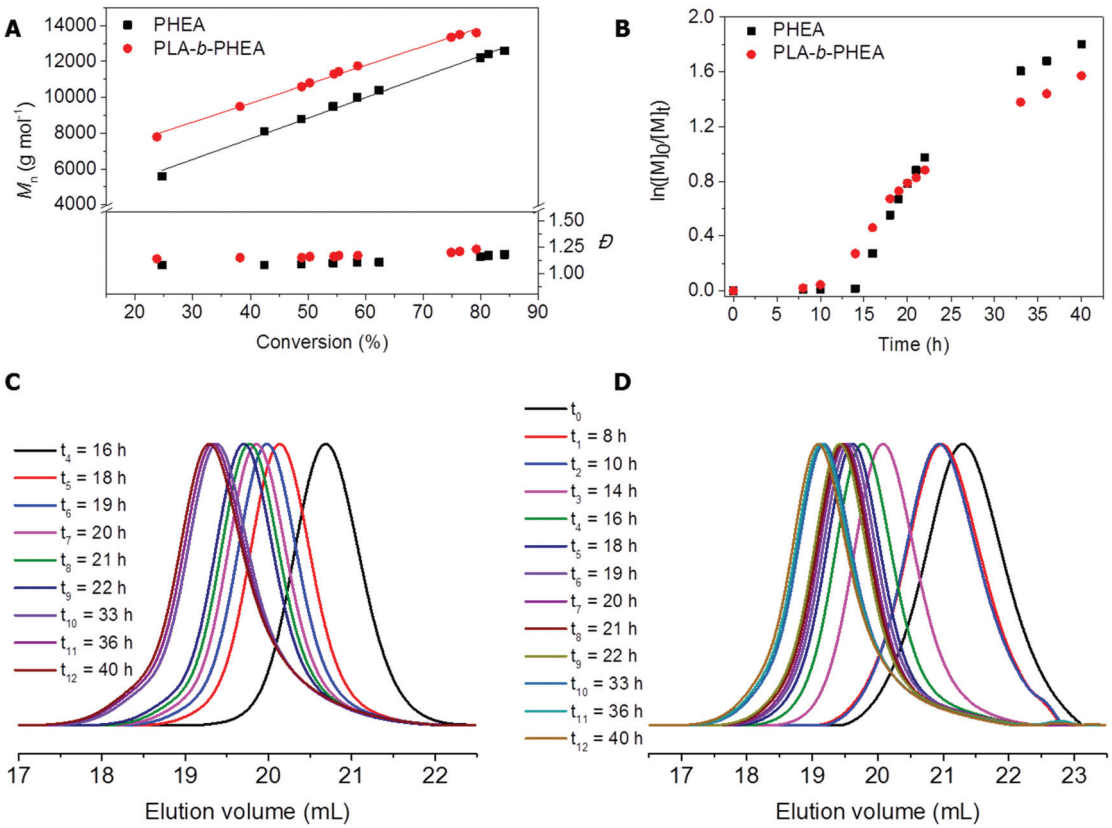

Fig. 2 Kinetic studies of the RAFT polymerization of HEA by using CDP and the PLA macro-CTA (one-pot approach) at room temperature in THF ($[HEA]_0$ = 1 mol L^{-1}, $[HEA]_0/[CDP]_0/[V\text{-}70]_0$ = 40/1/0.25). Dependence of $M_{n,SEC}$ and $Đ$ (SEC in DMAc, PMMA calibration) on the HEA conversion (A). Semilogarithmic kinetic plots (B). Normalized SEC traces (DMAc, RI detection) from kinetic studies of the polymerization of HEA in the presence of CDP (C) and in the presence of the PLA macro-CTA (D).

the overlay of the SEC traces recorded throughout the kinetic study. The RAFT polymerization of HEA proceeded after an induction period of 14 hours. An induction period is often observed in the early stages of RAFT polymerizations and can result from a low efficiency for reinitiation of the leaving group or a low fragmentation rate of the pre-equilibrium RAFT intermediate radical.[52,53] Such long induction periods are, in fact, reported for RAFT polymerizations utilizing V-70 at 30 °C, which could be reduced when the CTA/initiator ratio or the polymerization temperature is increased.[54,55] During RAFT polymerization of HEA, V-70 provides a constant radical concentration for more than two times of its half-live as evidenced by the linear first-order consumption of monomer up to 22 hours of polymerization (≈62% conversion, Fig. 2B). Towards higher conversions, a decrease in the polymerization rate was observed, which might be due to a decrease in the rate of radical generation or due to a slight oxygen contamination during the sampling. The evolution of the molar masses correlated linearly with the monomer conversion, as depicted in Fig. 2A. SEC analysis in DMAc revealed monomodal distributions with narrow dispersities ($1.08 < Đ < 1.18$, PMMA calibration), with a clear shift to lower elution volumes during the course of polymerization (Fig. 2C). Slight tailing in the low molar mass region was observed for the samples collected after 80% conversion. It is reported that the diacrylate impurities present in the commercial HEA monomer induce branching when high conversion is reached.[37] However, we did not observe any shoulder in the high molar mass region even at a monomer conversion of 84% (after 40 h), although HEA was used as received.

To gain initial experience about the molar mass range of PHEA that can be obtained *via* this method, two different homopolymers were prepared by changing the monomer to CTA ratio ($[HEA]_0/[CDP]_0$ = 15 and 100, respectively, Table 1). SEC analysis revealed a monomodal SEC trace for **PHEA-1**, and only a slight high molar mass shoulder was evident from the elugram of **PHEA-2** (Fig. S7† and Table 1). The M_n of the homopolymers was significantly overestimated due to the PMMA calibration utilized. The ^{1}H NMR spectra (Fig. 4 and Fig. S7†) of the isolated PHEAs were hence used to estimate the molar masses ($M_{n,\ NMR}$). For **PHEA-1**, the molar mass ($M_{n,\ NMR}$) calculated by comparing the peak integrals derived from the trithiocarbonate end group (δ = 0.85 ppm) and the methylene proton peaks of PHEA (peak c in Fig. 4) is very close to the theoretical molar mass (Table 1). However, as the DP of PHEA increases (**PHEA-2**), the estimation of $M_{n,\ NMR}$ becomes difficult due to the low intensity of the end group signal (Fig. S7†).

One-pot synthesis of PLA-*b*-PHEA

To evaluate the possibility to prepare PLA-*b*-PHEA block copolymers entirely at room temperature in THF, the isolated PLA macro-CTA was used for the RAFT polymerization of HEA ($[HEA]_0/[macro\text{-}CTA]_0/[V\text{-}70]_0$ = 20/1/0.25, $[HEA]_0$ = 1 mol L^{-1}). After an overnight reaction, 87% monomer conversion was reached, and analyses by means of SEC and ^{1}H NMR spectroscopy (Fig. S8†) revealed the success of the block copolymer synthesis. Hence, we further focused on the establishment and exploitation of a one-pot synthesis procedure that would omit intermediate purification steps.

A kinetic study was performed for the one-pot approach in order to compare the kinetics of the RAFT polymerization of HEA in the presence of CDP and the macro-CTA. Firstly, the ROP of L-lactide was carried out in a glove box, as described above ([L-lactide]/[CDP]/[Ca] = 15/1/0.5, [L-lactide] = 1 mol L^{-1}). After 10 minutes, quantitative monomer conversion was reached and the vial was taken out of the glove box. The calcium-based ROP catalyst was deactivated by exposing it to moisture, *i.e.* simple opening of the vial. A mixture of HEA and V-70 in THF was added at −20 °C ($[macro\text{-}CTA]_0/[CDP]_0/[V\text{-}70]_0$ = 40/1/0.25, $[HEA]_0$ = 1 mol L^{-1}). The RAFT polymerization of HEA was performed subsequently at room temperature. The kinetics of the RAFT polymerization of HEA were slightly altered when conducted in the presence of the PLA macro-CTA in comparison to using an equimolar amount of CDP (Fig. 2). The induction period (≈10 hours) was slightly shorter when the macro-CTA was employed, which might be caused by a change of the microenvironment of the trithiocarbonate moiety due to steric reasons and/or polarity aspects.[56,57] Apart from a slightly higher apparent polymerization rate at low conversions when using the macro-CTA (Fig. 2B), the semilogaritmic plot closely resembled that of the RAFT polymerization using CDP. Similar observations are reported for the RAFT polymerization of *N*-isopropylacrylamide using a PLA based macro-CTA[58] and of *N*-vinylpyrrolidone using a PCL based macro-CTA.[57] SEC analysis revealed monomodal traces throughout the course of the polymerization (Fig. 2D), and the linear increase of the molar mass with respect to the total monomer conversion together with the low dispersities ($1.14 < Đ < 1.23$, Fig. 2A) show that the molar mass can be well controlled.

Subsequently, a series of block copolymers **P1** to **P6** was prepared under similar conditions while changing the feed ratios of $[macro\text{-}CTA]_0/[HEA]_0$ from 20 to 100. The resulting block copolymers hence possess a PLA block of a uniform DP of 15, whereas the length of the PHEA unit was increased gradually to yield an amphiphilic block copolymer library with varying hydrophilicity (Table 1). SEC data of the final samples (t_f) confirmed the chain extension of the PLA macro-CTA with HEA, as is evident from the shift towards lower elution volumes (Fig. 3A). Moreover, symmetrical and monomodal traces were obtained indicating the absence of significant amounts of prematurely terminated macro-CTA, unreacted PLA, PHEA homopolymer formation, or coupling reactions. The slight tailing in the low molar mass region could be easily removed *via* precipitation (Fig. 3B). Similar to the PHEA homopolymers, the molar mass values ($M_{n,\ SEC}$) were overestimated by SEC using PMMA calibration. Yet, narrow molar mass distributions were evident ($1.13 < Đ < 1.28$) showing that the one-pot chain extension utilizing RAFT polymerization could be well-controlled with respect to the length of the PHEA block (Table 1).

An overlay of the ^{1}H NMR spectra of the PLA macro-CTA, **PHEA-1**, and **P1** as an exemplary block copolymer is shown in Fig. 4. All characteristic signals derived from both blocks, *i.e.* PLA and PHEA can be clearly distinguished in the spectrum of **P1**. This includes signals of the methine protons of the PLA (peak f), methylene and hydroxyl protons of PHEA (peaks a–c), as well as the polyacrylate backbone signals (peaks d and e), which are overlapping with the methyl proton signals of the PLA block. In the overlay of the ^{1}H NMR spectra of **P2** to **P6** (Fig. S9†), it is clearly visible that the intensity of the peaks originating from the PHEA blocks increase gradually from **P2**

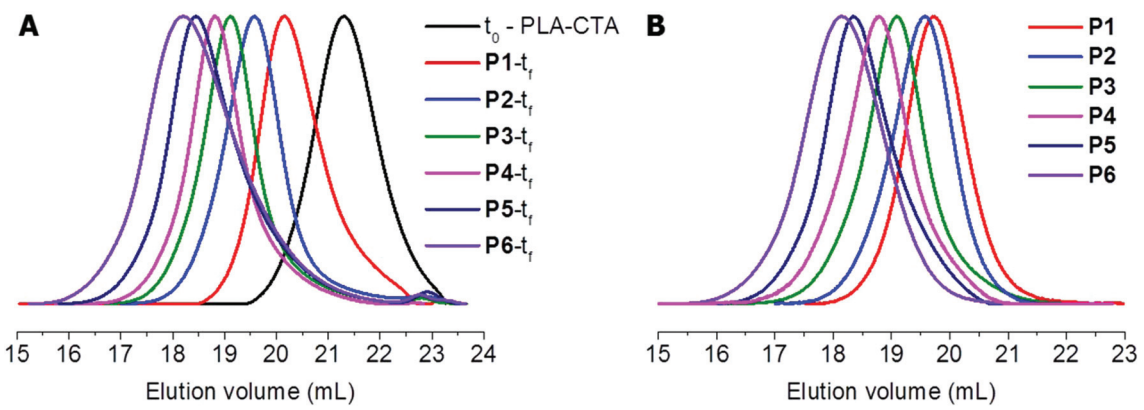

Fig. 3 Overlay of normalized SEC traces (DMAc, RI detection) of macro-CTA and block copolymers obtained *via* a one-pot approach recorded from the reaction mixtures (A), recorded from the isolated block copolymers after purification (B).

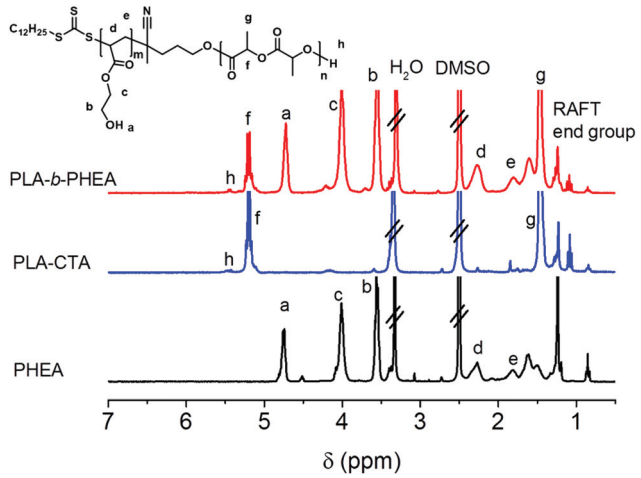

Fig. 4 Overlay of the ^{1}H NMR spectra (DMSO-d_6, 300 MHz) of **PHEA-1**, the PLA macro-CTA and **P1** prepared *via* one-pot approach together with the assignment of the observed peaks.

to **P6** after normalization according to the methine proton signal of the PLA block.

Benefiting from the known DP (or M_n) of the PLA block, the molar masses ($M_{n,\ NMR}$) of the block copolymers were calculated by comparing the signal intensities of the methine protons of PLA (peak f) and the methylene protons of PHEA (peak c) in the ^{1}H NMR spectra, thereby avoiding a calculation based on the small trithiocarbonate end group signals. The resulting $M_{n,\ NMR}$ values are in good agreement with the theoretical values ($M_{n,\ theo}$) for the block copolymers comprising rather short PHEA blocks **P1** to **P3** (Table 1). However, as the length of the PHEA block increases (**P4** to **P6**), the calculated $M_{n,\ NMR}$ values deviated and gave higher values than expected from [M]/[CTA] and conversion ($M_{n,\ theo}$). This could be explained by the fact that the polar PHEA segments are better solubilized in DMSO in comparison to the hydrophobic PLA segments, thereby resulting in an enhanced mobility of the PHEA blocks.[19,59] The resulting difference in relaxation behavior would thus be the reason for the overestimation of the DP of the PHEA blocks *via* ^{1}H NMR analysis. Less polar NMR solvents were either not capable of dissolving the block copolymers or did not reveal well resolved peaks. To affirm this assumption, a solution of the polymer with the highest PHEA content (**P6**) was investigated by DLS, indeed revealing the presence of aggregated structures (Fig. S10†). Therefore, we rely on the theoretical molar mass values ($M_{n,\ theo}$) and the respective block copolymer compositions during the discussion of the results obtained from further characterization.

Thermal properties of the block copolymers in bulk

Analysis by means of TGA clearly confirmed the block copolymer structures of **P1** to **P6**. Fig. S11† shows TGA thermograms of **PHEA-1**, the PLA macro-CTA, and **P1** as an exemplary block copolymer, which comprises similar weight percentages of both blocks. As expected for this type of polyester, the PLA macro-CTA alone decomposes between 200 and 320 °C, exhibiting a comparably sharp mass loss profile. In contrast, the homopolymer **PHEA-1** was found to decompose over a rather broad temperature range with an onset of mass loss (10%) around 260 °C that proceeds further until a maximum weight loss occurs around 430 °C. Accordingly, the thermal decomposition of **P1** represented a two-step process, which is evidenced by the appearance of two distinct peaks in the first derivative curve of the TGA thermogram, the first of which corresponds to the degradation of the PLA block and the second resulted from the degradation of the PHEA block. These two decomposition stages were observed for all block copolymers **P1** to **P6** (Fig. S12†). As the weight fraction of the PLA block decreases from **P1** to **P6**, so does the mass loss below 330 °C. However, due to the partial mass loss of the PHEA block occurring within the same temperature range, we refrained from using the TGA data to estimate the actual copolymer composition.

To explore if phase segregation between the PLA and PHEA blocks occurs in bulk, the block copolymers **P1** to **P6** were investigated by means of DSC (Table S1† and Fig. 5). In accordance with literature data,[60] the amorphous **PHEA-1** and **PHEA-2** revealed T_g values of −1 °C and of 5 °C, respectively. The PLA macro-CTA, as a semi-crystalline polymer, revealed a T_g at 38 °C and a melting temperature T_m at 139 °C, which is only visible in the first heating run (Fig. S13 and S14†). DSC analysis of the block copolymer **P1**, with nearly equal block ratios of PLA and PHEA, showed two distinct T_gs at 11 °C and at 30 °C, respectively. While this is indicative of a microphase separation between both blocks in bulk, the shifted T_g values of the two phases in comparison to the homopolymers might indicate a partial mixing between the two blocks.[61]

On the other hand, for the block copolymers **P2** to **P6** with increased weight fraction of the PHEA blocks, single glass transitions were detected between the T_g values of the two homopolymers, thereby hinting towards an increased homogeneity of the system (Fig. S15†). However, **P3** revealed a rather broad glass transition, and the small difference between the T_g values of the two homopolymers ($\Delta T_g \approx 35$ °C) could make it difficult to resolve separate second order phase transitions (Table S1†). In addition, a melting peak was evident in the thermogram of the first heating run for **P2**, hinting towards the presence of PLA domains in the aged sample. In particular the latter would not be expected for a fully miscible system. To judge, if the observed single glass transitions could conceil two T_g values, the Fox and the Wood equation were applied (Fig. 5B).

Both represent common methods to estimate the T_g values of miscible copolymer systems or polymer blends from the according parameters of both homopolymers.[61] A deviation of the experimental T_g value, therefore, indicates the presence of a system that is not completely miscible. Upon comparison of the results with the experimentally determined T_g values, a reasonable agreement was found for the block copolymers with high PHEA weight fractions (**P4–P6**). However, the experimental T_g values were significantly lowered for **P2** and **P3**. This deviation hints towards the fact that the PLA and PHEA segments are not fully miscible, in at least, these two block copolymers.

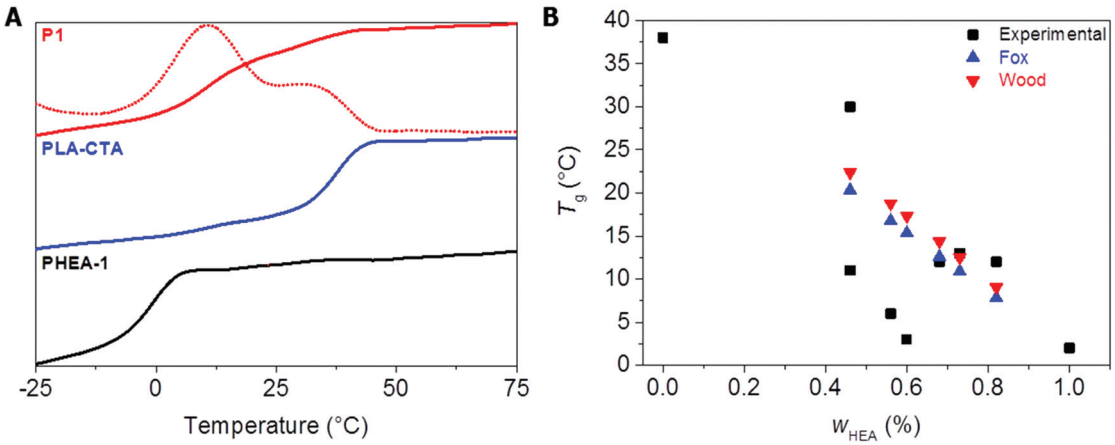

Fig. 5 (A) Overlay of DSC thermograms of isolated **PLA-CTA**, **PHEA-1** and **P1** (heating rate 10 K min^{-1}, 3rd heating run). The dotted line represents the first derivative of the thermogram for **P1**. (B) Dependence of the T_g values of the block copolymers **P1** to **P6** on the weight fraction of HEA.

In order to further assess this hypothesis, additional DSC experiments were conducted on **P2** and **P3** at varying heating and cooling rates. Two separate glass transitions could be observed for both polymers after the samples had been slowly cooled from 170 °C, supporting the idea that the two blocks are not completely miscible unless the content of PHEA is relatively high (Fig. S16†).

Self-assembly of PLA-*b*-PHEA synthesized *via* a one-pot approach in water

The self-assembly behavior of the block copolymers **P1** to **P6** was investigated in water, which represents a good solvent for the PHEA block but a non-solvent for the PLA block. A solvent exchange method from THF to water was employed, and the aqueous suspensions were aged at least for one week before cryo-TEM measurements of the block copolymers were performed.

For the most hydrophobic block copolymers **P1** and **P2**, DLS as well as cryo-TEM analysis revealed the presence of rather undefined dense aggregates with unclear substructure and diameters ranging from 100 to 200 nm (Fig. 6). The morphology of these round-shaped aggregated structures prevailed also at higher concentration, although a slightly decreased particle diameter was observed (Fig. S17†).

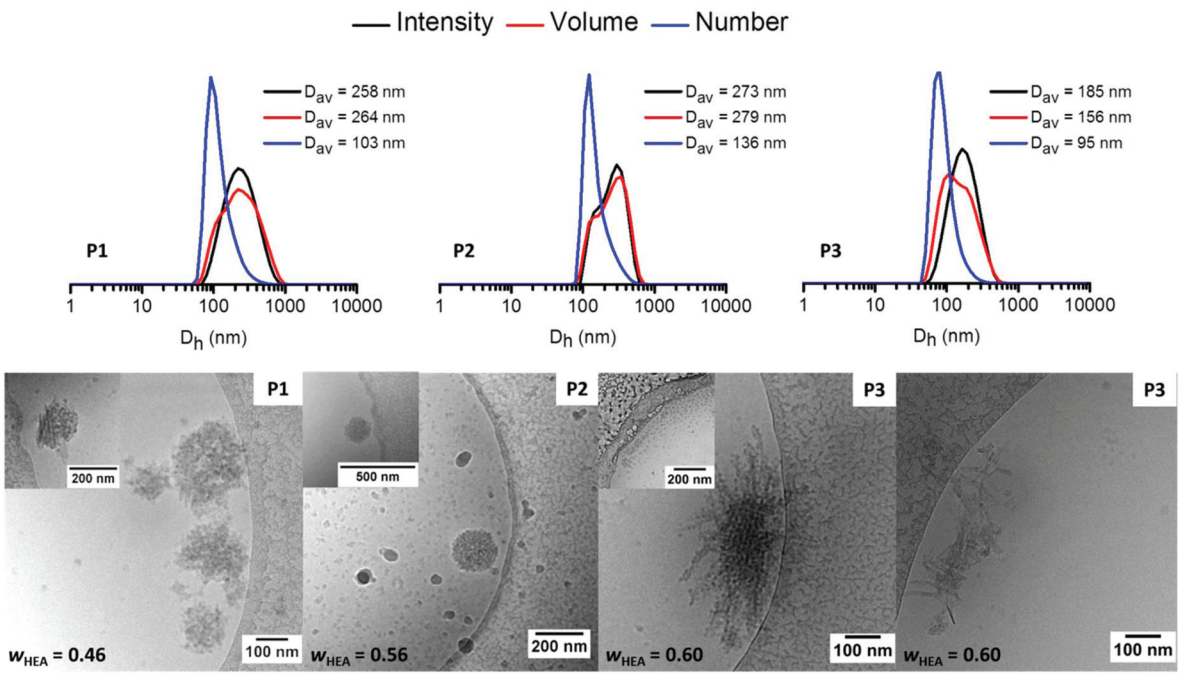

Fig. 6 DLS size distributions and representative cryo-TEM images of the suspensions obtained from **P1**, **P2** and **P3** in water (c = 1 mg mL^{-1}). The insets show an enlarged view of the suspensions at higher concentration (c = 2 mg mL^{-1}).

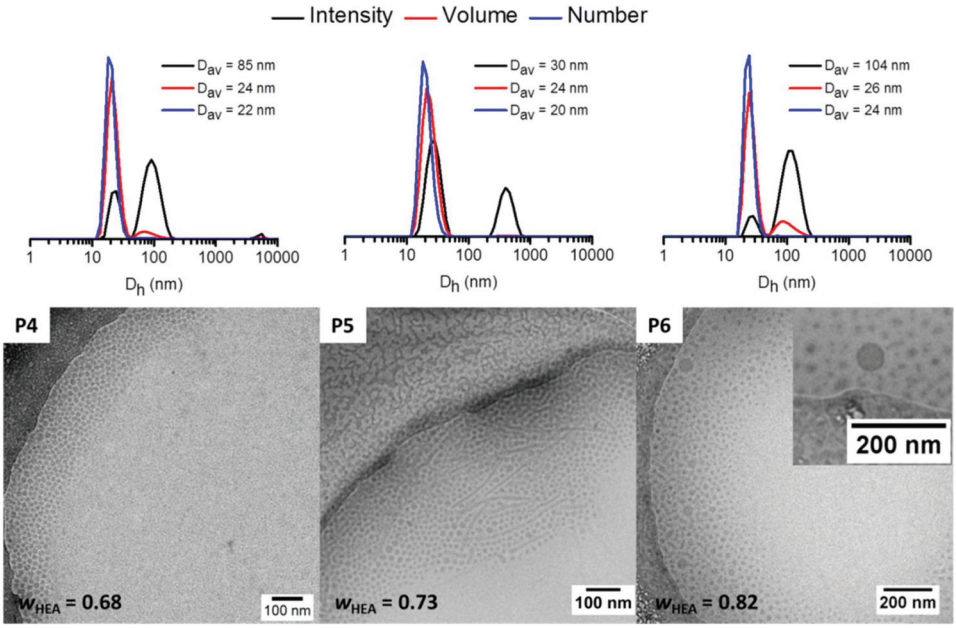

Fig. 7 DLS size distributions and representative cryo-TEM images of the suspensions obtained from **P4** (c = 2 mg mL^{-1}), **P5** (c = 5 mg mL^{-1}) and **P6** (c = 5 mg mL^{-1}). The inset shows an enlarged view of a vesicle.

First changes in the self-assembly behavior of PLA-*b*-PHEA could be seen when the weight fraction of the hydrophilic PHEA block was increased to 60% (**P3**). At a concentration of 1 mg mL^{-1}, less dense nanostructures were found that could potentially result from an aggregation of several spherical micelles (Fig. 6). Some pictures evidenced the additional presence of aggregates of thin small sheets. Since only a few aggregates were visualized the concentration was increased to 2 mg mL^{-1}. Surprisingly, DLS measurements revealed a significant decrease in hydrodynamic diameter, which was caused by the formation of spherical micelles with an average diameter of 17 nm. In good agreement with the intensity weighted size distribution from DLS, some larger aggregates were also visible in the cryo-TEM analysis (Fig. S17† and Fig. 6).

The block copolymers with further increased DP of the hydrophilic block **P4** to **P6** self-assembled to mainly spherical micelles (Fig. 7). In particular, **P4** and **P5** revealed similar features: Homogeneously distributed and densely packed spherical micelles with diameters between 13 to 20 nm were observed by cryo-TEM, while the occasional formation of worm-like micelles occured (Fig. S18†). These explain the intensity weighted size distribution observed in the DLS studies.

Self-assembly of **P6** in water resulted in the formation of spherical micelles due to the further increased PHEA content. In accordance with the bimodal intensity and volume weighted size distributions obtained from DLS measurements, some vesicles (20 to 40 nm) were visualized by cryo-TEM, however, a majority of micelles feature diameters ranging from 8 to 15 nm. This could be related to the slightly larger dispersity ($Đ$ = 1.28) of **P6** that would hence include a minor amount of block polymer chains with relatively short PHEA blocks.

Thus, the newly developed one-pot synthesis approach to obtain PLA-*b*-PHEA could be applied for a broad range of compositions ($0.46 \leq w_{HEA} \leq 0.82$), thereby enabling access to the expected range of nanostructures by self-assembly processes of these amphiphilic block copolymers in aqueous media.

Conclusions

A one-pot strategy for the synthesis of amphiphilic copolymers comprising PLA and PHEA blocks was developed. Conducted at room temperature in THF and without the need to employ any intermediate purification steps or protection group chemistry, *in situ* calcium alkoxide formation from a hydroxyl-functional CTA enabled access to a library of well-defined PLA-*b*-PHEA block copolymers. DSC analysis showed evidence for a phase separation between the two blocks in bulk for polymers with similar block lengths, and the amphiphilic block copolymers self-assembled to a variety of structures in aqueous media ranging from undefined aggregates to well-defined micellar structures for the block copolymers with large PHEA DP values.

The omission of protection chemistry during the synthesis of block copolymers composed of PLA and hydroxyl-functional polyacrylates represents the main advantage of this newly developed synthesis method. Representing a general approach similarly feasible as sequential monomer addition, the new strategy also serves as a good platform for a facile synthesis of other amphiphilic block copolymers, comprising less challenging building blocks. On the other hand, the presented materials or other hydroxy-functional block copolymers to be obtained *via* the one-pot approach could be further functiona-

lized or crosslinked easily. This straightforward method could be adapted for the combination of other controlled polymerization techniques in the one-pot preparation of polymers with various functionalities and architectures as well.

Conflicts of interest

There are no conflicts to declare.

Acknowledgements

We acknowledge funding from Thuringian Ministry for Economic Affairs, Science and Digital Society (ProExcellence II, NanoPolar). The transmission electron microscope was obtained with a grant from the European Funds for Regional Developments (EFRE) and the German Research Council (DFG).

References

1 K. Nagahama, T. Ouchi and Y. Ohya, *Adv. Funct. Mater.*, 2008, **18**, 1220–1231.
2 F. Ahmed and D. E. Discher, *J. Controlled Release*, 2004, **96**, 37–53.
3 B. Luan, B.-Q. Zhang and C.-Y. Pan, *J. Polym. Sci., Part A: Polym. Chem.*, 2006, **44**, 549–560.
4 H. Zhou, Y. Chen, C. M. Plummer, H. Huang and Y. Chen, *Polym. Chem.*, 2017, **8**, 2189–2196.
5 M. Seo, M. A. Amendt and M. A. Hillmyer, *Macromolecules*, 2011, **44**, 9310–9318.
6 F. K. Wolf, A. M. Hofmann and H. Frey, *Macromolecules*, 2010, **43**, 3314–3324.
7 S. R. S. Ting, A. M. Gregory and M. H. Stenzel, *Biomacromolecules*, 2009, **10**, 342–352.
8 M. Jesberger, L. Barner, M. H. Stenzel, E. Malmström, T. P. Davis and C. Barner-Kowollik, *J. Polym. Sci., Part A: Polym. Chem.*, 2003, **41**, 3847–3861.
9 F. Hu, K. G. Neoh and E.-T. Kang, *Macromol. Rapid Commun.*, 2009, **30**, 609–614.
10 E. Jubeli, L. Moine and G. Barratt, *J. Polym. Sci., Part A: Polym. Chem.*, 2010, **48**, 3178–3187.
11 S. R. Abulateefeh, A. O. Saeed, J. W. Aylott, W. C. Chan, M. C. Garnett, B. R. Saunders and C. Alexander, *Chem. Commun.*, 2009, 6068–6070, DOI: 10.1039/B911986H.
12 R. C. Pratt, B. G. G. Lohmeijer, D. A. Long, P. N. P. Lundberg, A. P. Dove, H. Li, C. G. Wade, R. M. Waymouth and J. L. Hedrick, *Macromolecules*, 2006, **39**, 7863–7871.
13 B. M. Blunden, H. Lu and M. H. Stenzel, *Biomacromolecules*, 2013, **14**, 4177–4188.
14 I. Yildirim, C. Weber and U. S. Schubert, *Prog. Polym. Sci.*, 2017, DOI: 10.1016/j.progpolymsci.2017.07.010.
15 G. Gody, T. Maschmeyer, P. B. Zetterlund and S. Perrier, *Nat. Commun.*, 2013, **4**, 2505.
16 Y. Mai and A. Eisenberg, *Chem. Soc. Rev.*, 2012, **41**, 5969–5985.
17 D. Grande, J. Penelle, P. Davidson, I. Beurroies and R. Denoyel, *Microporous Mesoporous Mater.*, 2011, **140**, 34–39.
18 M. A. Kryuchkov, C. Detrembleur and C. G. Bazuin, *Polymer*, 2014, **55**, 2316–2324.
19 F. F. Wolf, N. Friedemann and H. Frey, *Macromolecules*, 2009, **42**, 5622–5628.
20 E. Themistou, G. Battaglia and S. P. Armes, *Polym. Chem.*, 2014, **5**, 1405–1417.
21 H. U. Kang, Y. C. Yu, S. J. Shin and J. H. Youk, *J. Polym. Sci., Part A: Polym. Chem.*, 2013, **51**, 774–779.
22 S. J. Shin, Y. C. Yu, J. D. Seo, S. J. Cho and J. H. Youk, *J. Polym. Sci., Part A: Polym. Chem.*, 2014, **52**, 1607–1613.
23 Y. Li, E. Themistou, J. Zou, B. P. Das, M. Tsianou and C. Cheng, *ACS Macro Lett.*, 2012, **1**, 52–56.
24 D. Mecerreyes, G. Moineau, P. Dubois, R. Jérôme, J. L. Hedrick, C. J. Hawker, E. E. Malmström and M. Trollsas, *Angew. Chem., Int. Ed.*, 1998, **37**, 1274–1276.
25 C. J. Duxbury, W. Wang, M. de Geus, A. Heise and S. M. Howdle, *J. Am. Chem. Soc.*, 2005, **127**, 2384–2385.
26 N. Chagneux, T. Trimaille, M. Rollet, E. Beaudoin, P. Gérard, D. Bertin and D. Gigmes, *Macromolecules*, 2009, **42**, 9435–9442.
27 C. Fu, J. Xu, M. Kokotovic and C. Boyer, *ACS Macro Lett.*, 2016, **5**, 444–449.
28 Y. Yagci, G. Yilmaz, C. Aydogan, C. Kutahya and A. Allushi, *Polym. Chem.*, 2017, **8**, 2899–2903.
29 K. J. Thurecht, A. M. Gregory, S. Villarroya, J. Zhou, A. Heise and S. M. Howdle, *Chem. Commun.*, 2006, 4383–4385, DOI: 10.1039/B611626D.
30 M. Seo, C. J. Murphy and M. A. Hillmyer, *ACS Macro Lett.*, 2013, **2**, 617–620.
31 J. Song, J. Xu, S. Pispas and G. Zhang, *RSC Adv.*, 2015, **5**, 38243–38247.
32 V. Poirier, M. Duc, J.-F. Carpentier and Y. Sarazin, *ChemSusChem*, 2010, **3**, 579–590.
33 J.-F. Carpentier and Y. Sarazin, in *Alkaline-Earth Metal Compounds: Oddities and Applications*, ed. S. Harder, Springer Berlin Heidelberg, Berlin, Heidelberg, 2013, pp. 141–189, DOI: 10.1007/978-3-642-36270-5_5.
34 I. Yildirim, S. Crotty, C. H. Loh, G. Festag, C. Weber, P.-F. Caponi, M. Gottschaldt, M. Westerhausen and U. S. Schubert, *J. Polym. Sci., Part A: Polym. Chem.*, 2016, **54**, 437–448.
35 I. Yildirim, T. Bus, M. Sahn, T. Yildirim, D. Kalden, S. Hoeppener, A. Traeger, M. Westerhausen, C. Weber and U. S. Schubert, *Polym. Chem.*, 2016, **7**, 6064–6074.
36 I. Yildirim, T. Yildirim, D. Kalden, G. Festag, N. Fritz, C. Weber, S. Schubert, M. Westerhausen and U. S. Schubert, *Polym. Chem.*, 2017, **8**, 4378–4387.
37 H. Kakwere and S. Perrier, *Polym. Chem.*, 2011, **2**, 270–288.
38 B. Clément, P. Decherchi, F. Féron, D. Bertin, D. Gigmes, T. Trimaille and T. Marqueste, *Macromol. Biosci.*, 2011, **11**, 1175–1184.
39 M. Westerhausen, *Inorg. Chem.*, 1991, **30**, 96–101.

40 A. M. Johns, S. C. Chmely and T. P. Hanusa, *Inorg. Chem.*, 2009, **48**, 1380–1384.
41 M. Westerhausen, J. Langer, S. Krieck and C. Glock, *Rev. Inorg. Chem.*, 2011, **31**, 143–184.
42 A. Torvisco, A. Y. O'Brien and K. Ruhlandt-Senge, *Coord. Chem. Rev.*, 2011, **255**, 1268–1292.
43 J. De Winter, V. Lemaur, P. Marsal, O. Coulembier, J. Cornil, P. Dubois and P. Gerbaux, *J. Am. Soc. Mass Spectrom.*, 2010, **21**, 1159–1168.
44 J. De Winter, O. Coulembier, P. Dubois and P. Gerbaux, *Int. J. Mass Spectrom.*, 2011, **308**, 11–17.
45 B. C. Katzenmeyer, L. R. Cool, J. P. Williams, K. Craven, J. M. Brown and C. Wesdemiotis, *Int. J. Mass Spectrom.*, 2015, **378**, 303–311.
46 V. Scionti and C. Wesdemiotis, *J. Mass Spectrom.*, 2012, **47**, 1442–1449.
47 E. Altuntaş, A. Krieg, A. Baumgaertel, A. C. Crecelius and U. S. Schubert, *J. Polym. Sci., Part A: Polym. Chem.*, 2013, **51**, 1595–1605.
48 T. Gruendling, M. Kaupp, J. P. Blinco and C. Barner-Kowollik, *Macromolecules*, 2011, **44**, 166–174.
49 S. Sugihara, Y. Kawamoto and Y. Maeda, *Macromolecules*, 2016, **49**, 1563–1574.
50 C. W. Scales, A. J. Convertine and C. L. McCormick, *Biomacromolecules*, 2006, **7**, 1389–1392.
51 A. J. Convertine, N. Ayres, C. W. Scales, A. B. Lowe and C. L. McCormick, *Biomacromolecules*, 2004, **5**, 1177–1180.
52 T. S. C. Pai, C. Barner-Kowollik, T. P. Davis and M. H. Stenzel, *Polymer*, 2004, **45**, 4383–4389.
53 L. Albertin and N. R. Cameron, *Macromolecules*, 2007, **40**, 6082–6093.
54 Y. Li, J. Yang and B. C. Benicewicz, *J. Polym. Sci., Part A: Polym. Chem.*, 2007, **45**, 4300–4308.
55 Y. C. Yu, G. Li, H. U. Kang and J. H. Youk, *Colloid Polym. Sci.*, 2012, **290**, 1707–1712.
56 M. H. Stenzel, in *Handbook of RAFT Polymerization*, Wiley-VCH Verlag GmbH & Co. KGaA, 2008, pp. 315–372, DOI: 10.1002/9783527622757.ch9.
57 H. U. Kang, Y. C. Yu, S. J. Shin, J. Kim and J. H. Youk, *Macromolecules*, 2013, **46**, 1291–1295.
58 M. Hales, C. Barner-Kowollik, T. P. Davis and M. H. Stenzel, *Langmuir*, 2004, **20**, 10809–10817.
59 M. H. Stenzel and C. Barner-Kowollik, *Mater. Horiz.*, 2016, **3**, 471–477.
60 M. Semsarilar, J. Tom, V. Ladmiral and S. Perrier, *Polym. Chem.*, 2012, **3**, 3266–3275.
61 L. H. Sperling, in *Introduction to Physical Polymer Science*, John Wiley & Sons, Inc., 2005, pp. 687–756, DOI: 10.1002/0471757128.ch13.

Supporting Information

One-pot synthesis of PLA-*b*-PHEA *via* sequential ROP and RAFT polymerizations

Ilknur Yildirim,[a,b] *Pelin Sungur,*[a,b] *Anna C. Crecelius-Vitz,*[a,b] *Turgay Yildirim,*[a,b] *Diana Kalden,*[c] *Stephanie Hoeppener,*[a,b] *Matthias Westerhausen,*[c] *Christine Weber,*[a,b] *Ulrich S. Schubert*[a,b]*

[a] Laboratory of Organic and Macromolecular Chemistry (IOMC), Friedrich Schiller University Jena, Humboldtstr. 10, 07743 Jena, Germany

[b] Jena Center for Soft Matter (JCSM), Friedrich Schiller University Jena, Philosophenweg 7, 07743 Jena, Germany

[c] Institute of Inorganic and Analytical Chemistry (IAAC), Friedrich Schiller University Jena, Humboldtstr. 8, 07743 Jena, Germany

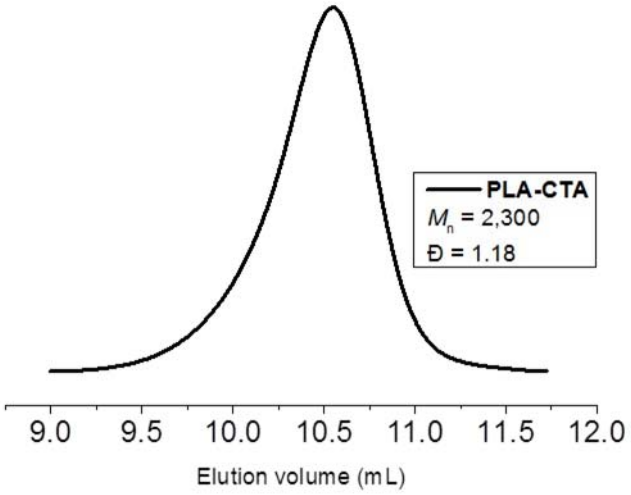

Figure S1. SEC trace of the isolated **PLA-CTA** (THF, RI detection, PLA calibration).

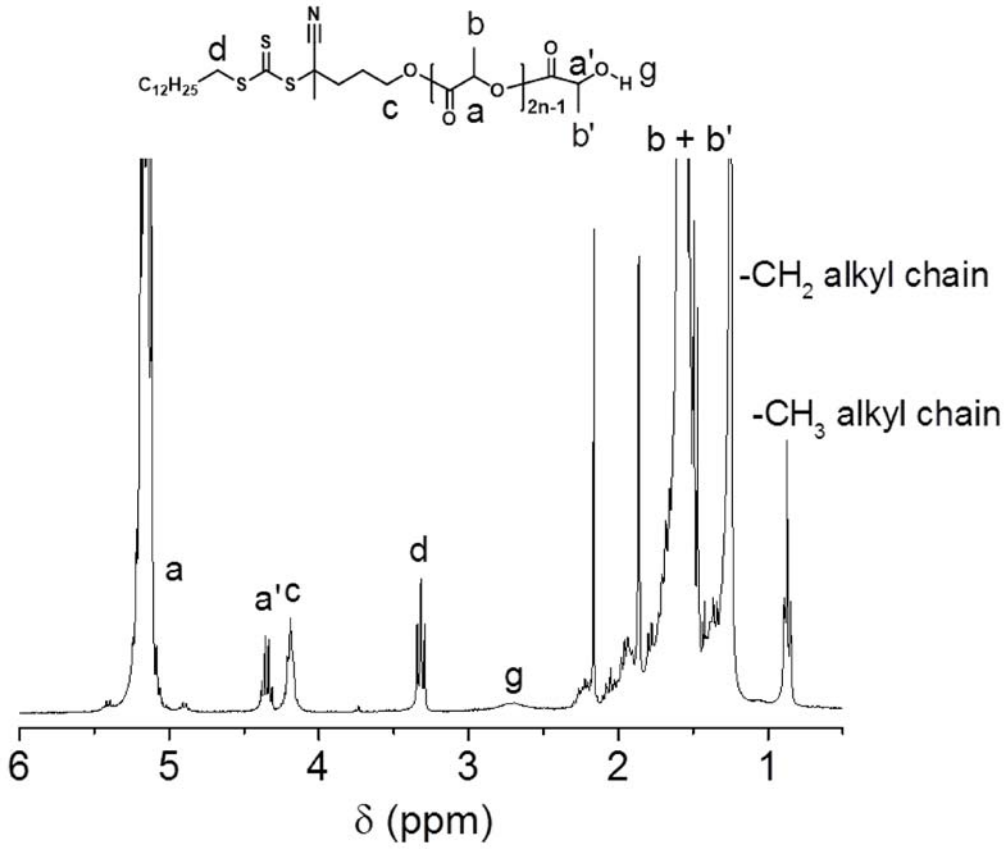

Figure S2. ^{1}H NMR spectrum ($CDCl_3$, 300 MHz) of the isolated **PLA-CTA** together with the assignment of the observed peaks.

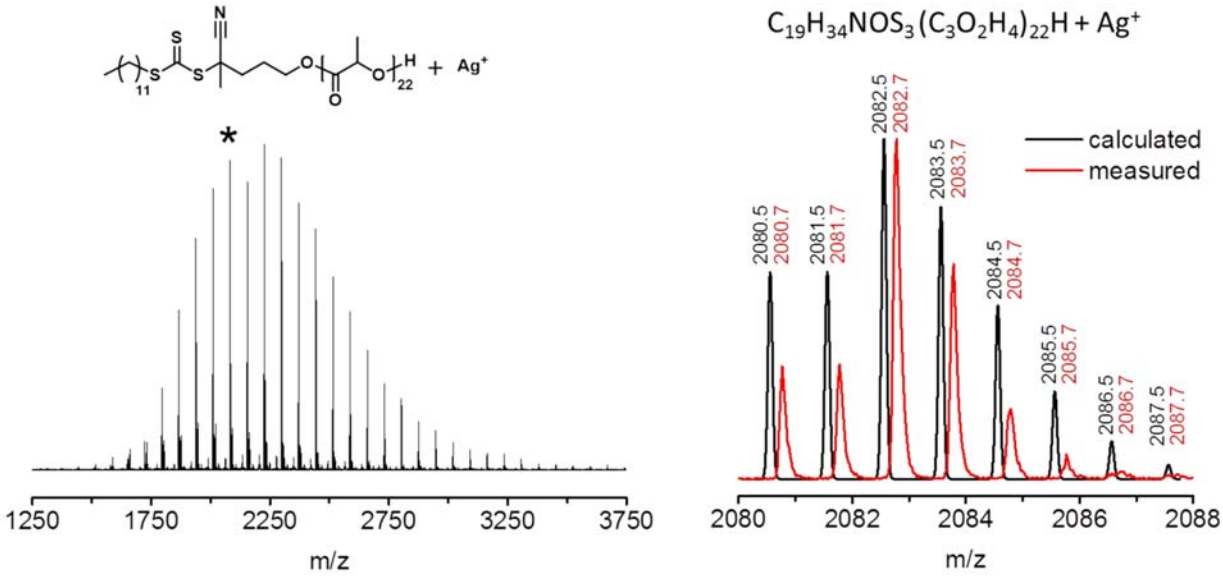

Figure S3. Left: MALDI-ToF mass spectrum of the **PLA-CTA**. **Right**: Overlay of the calculated and measured isotopic pattern for the structural assignment of the observed peaks.

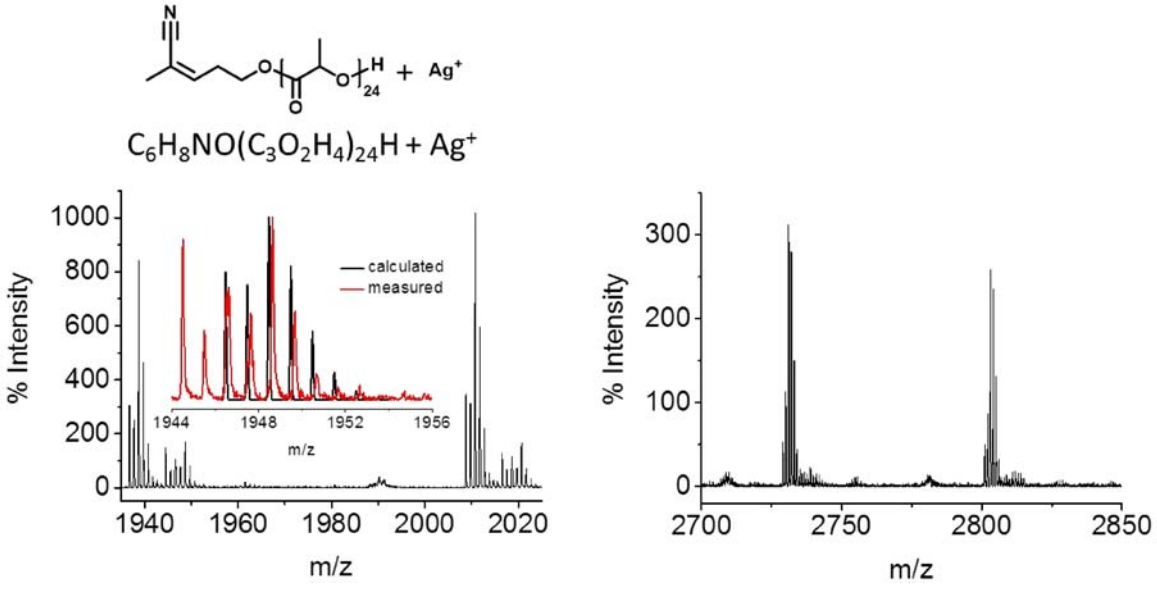

Figure S4. Left: Zoom into the lower *m/z* region of the MALDI-ToF mass spectrum of the PLA-CTA together with an overlay of the minor distribution assigned to fragmentation of the CTA. **Right:** Zoom into the higher *m/z* region of the MALDI-ToF mass spectrum of the PLA-CTA.

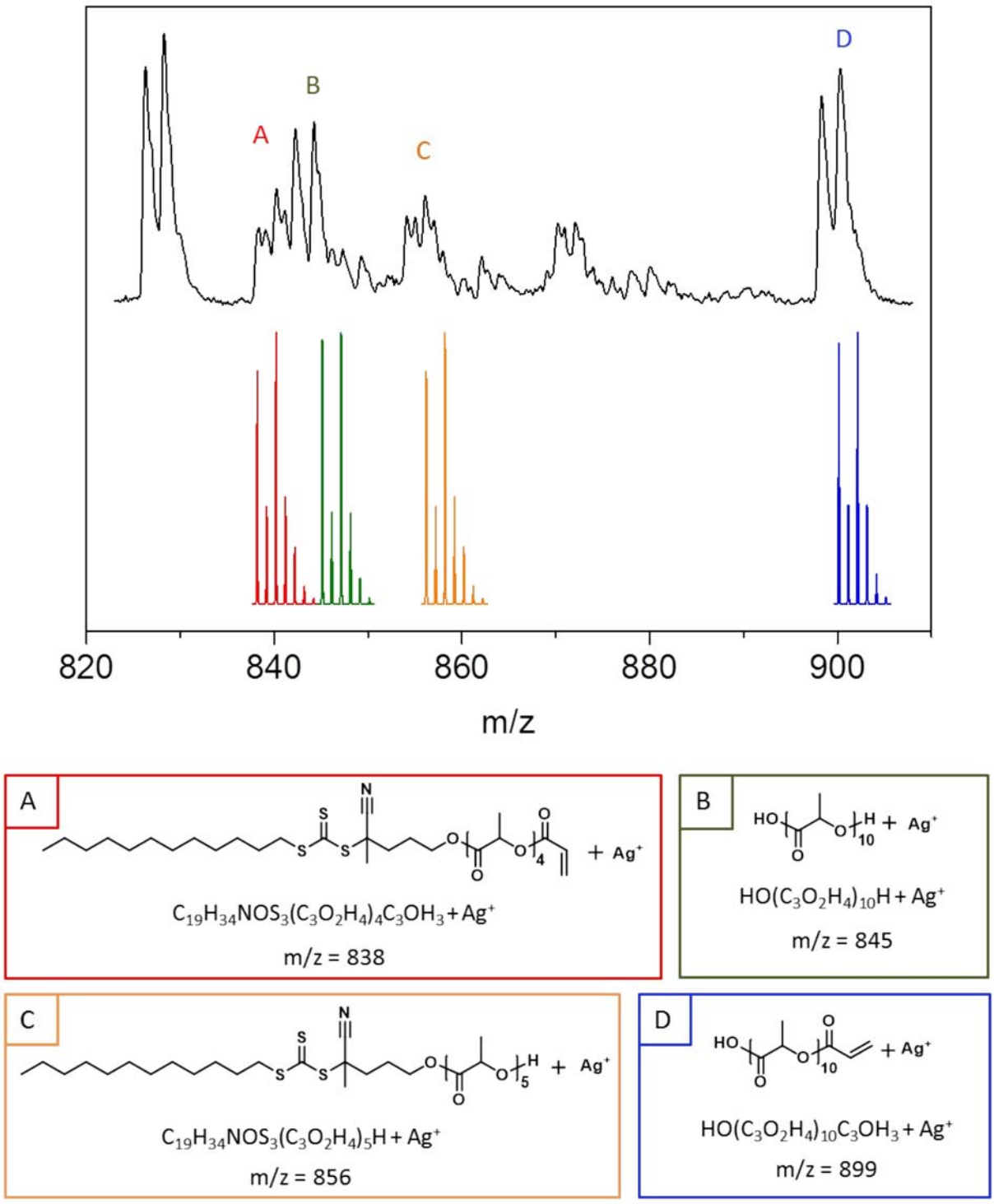

Figure S5. Zoom into the MALDI-ToF MS/MS spectrum of **PLA-CTA** (region from *m/z* 820 to *m/z* 910) together with the structural assignment of the observed peaks.

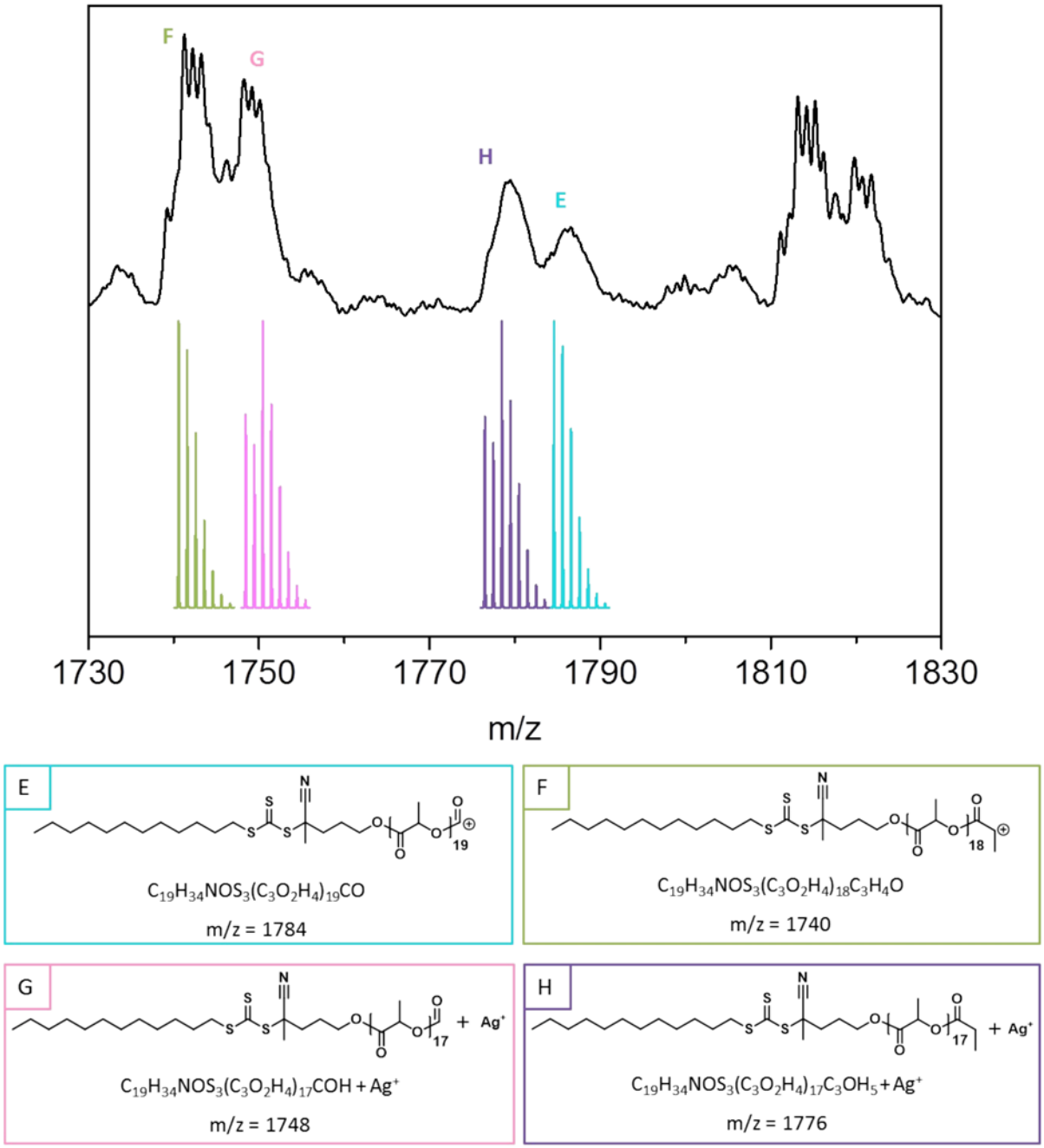

Figure S6. Zoom into the MALDI-ToF MS/MS spectrum of **PLA-CTA** (region from *m/z* 1910 to *m/z* 2040) together with the structural assignment of the observed peaks.

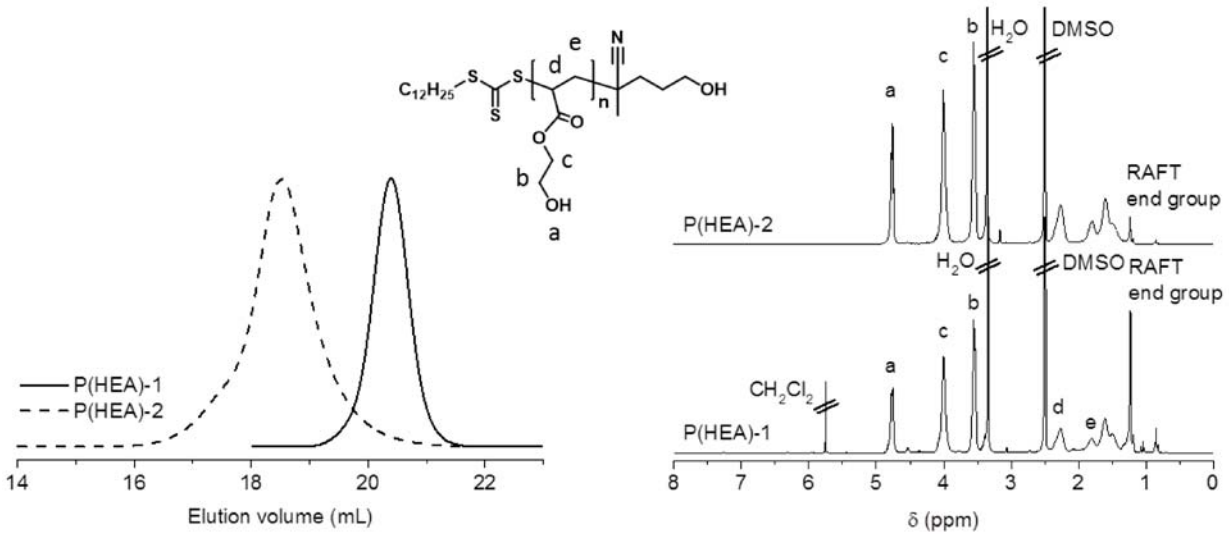

Figure S7. Analysis of the isolated **PHEA-1** and **PHEA-2**. **Left:** Overlay of the normalized SEC traces (DMAc, RI detection). **Right:** Overlay of the ^{1}H NMR spectra (DMSO-d_6, 300 MHz).

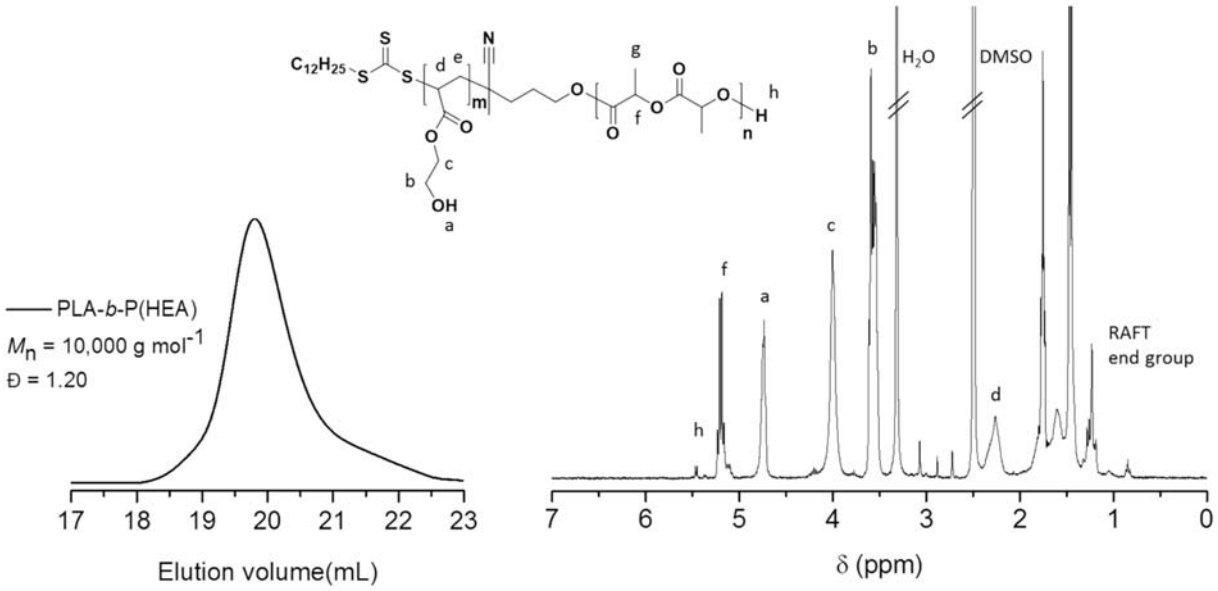

Figure S8. Analysis of the **PLA-*b*-PHEA** prepared in two steps *via* chain extension of the purified **PLA-CTA**. **Left:** SEC trace (DMAc, RI detection, PMMA calibration). **Right:** ^{1}H NMR spectrum (DMSO-d_6, 300 MHz).

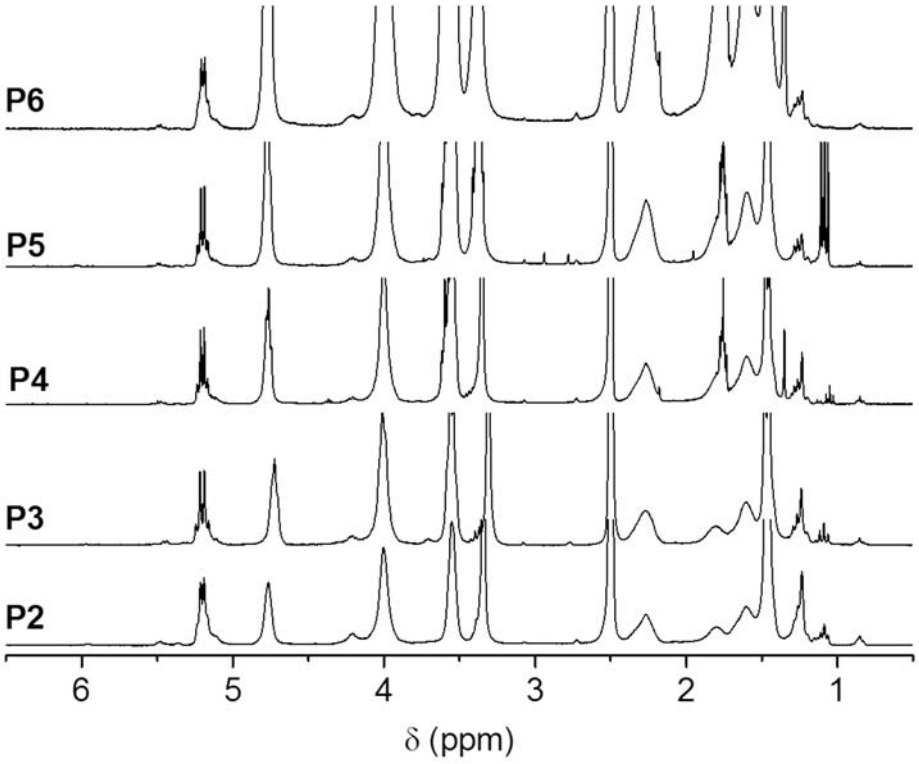

Figure S9. Overlay of the ^{1}H NMR spectra (DMSO-d_6, 300 MHz) of block copolymers **P2** to **P6** synthesized at one-pot. For clarity, the spectra were normalized according to the signal of the methine protons of PLA at δ = 5.16 ppm.

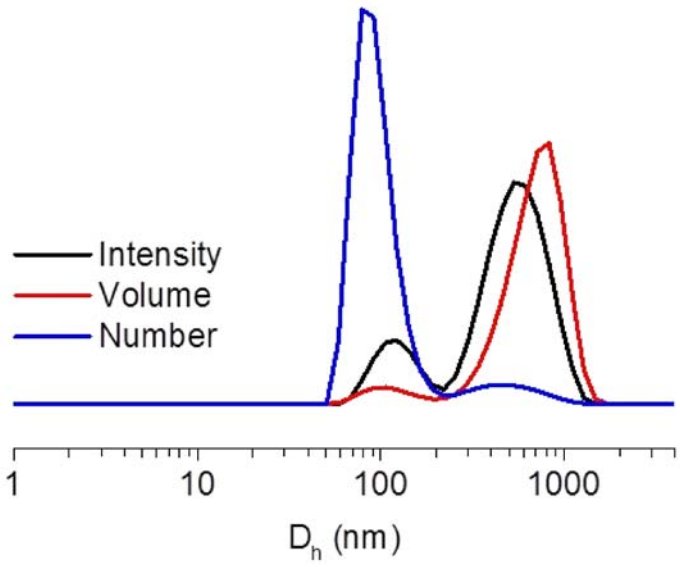

Figure S10. DLS size distribution of **P6** dissolved in DMSO.

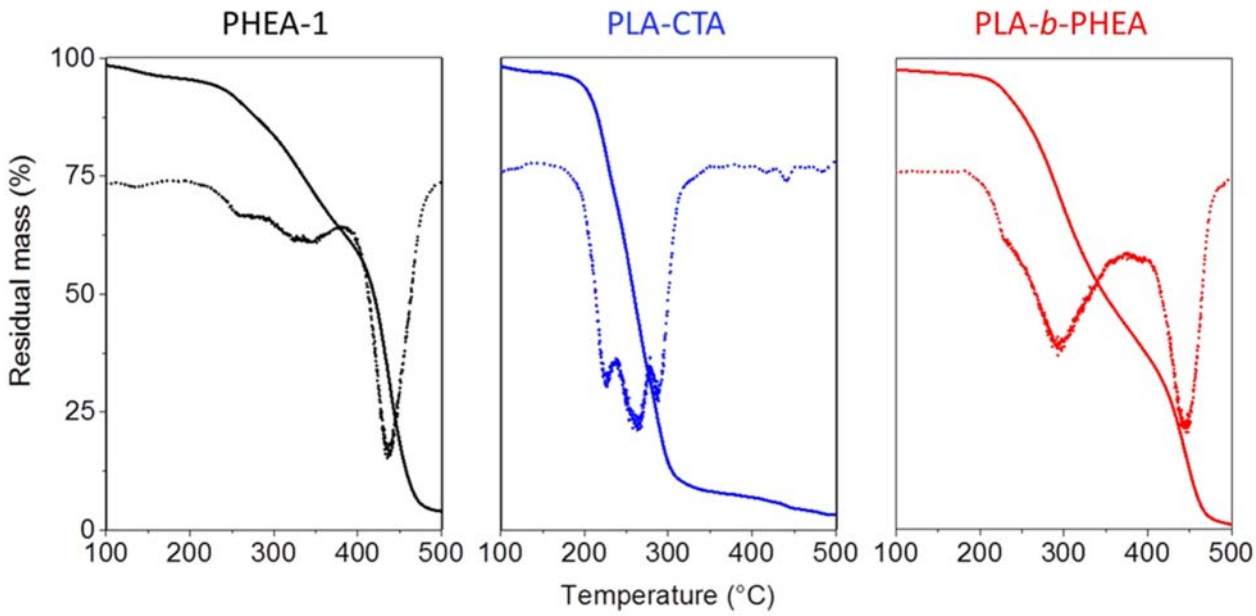

Figure S11. TGA thermograms of **PHEA-1**, the PLA macro-CTA, and **P1** (20 to 600 °C, 10.0 °C min^{-1}). The dotted lines represent the first derivative of the measured traces.

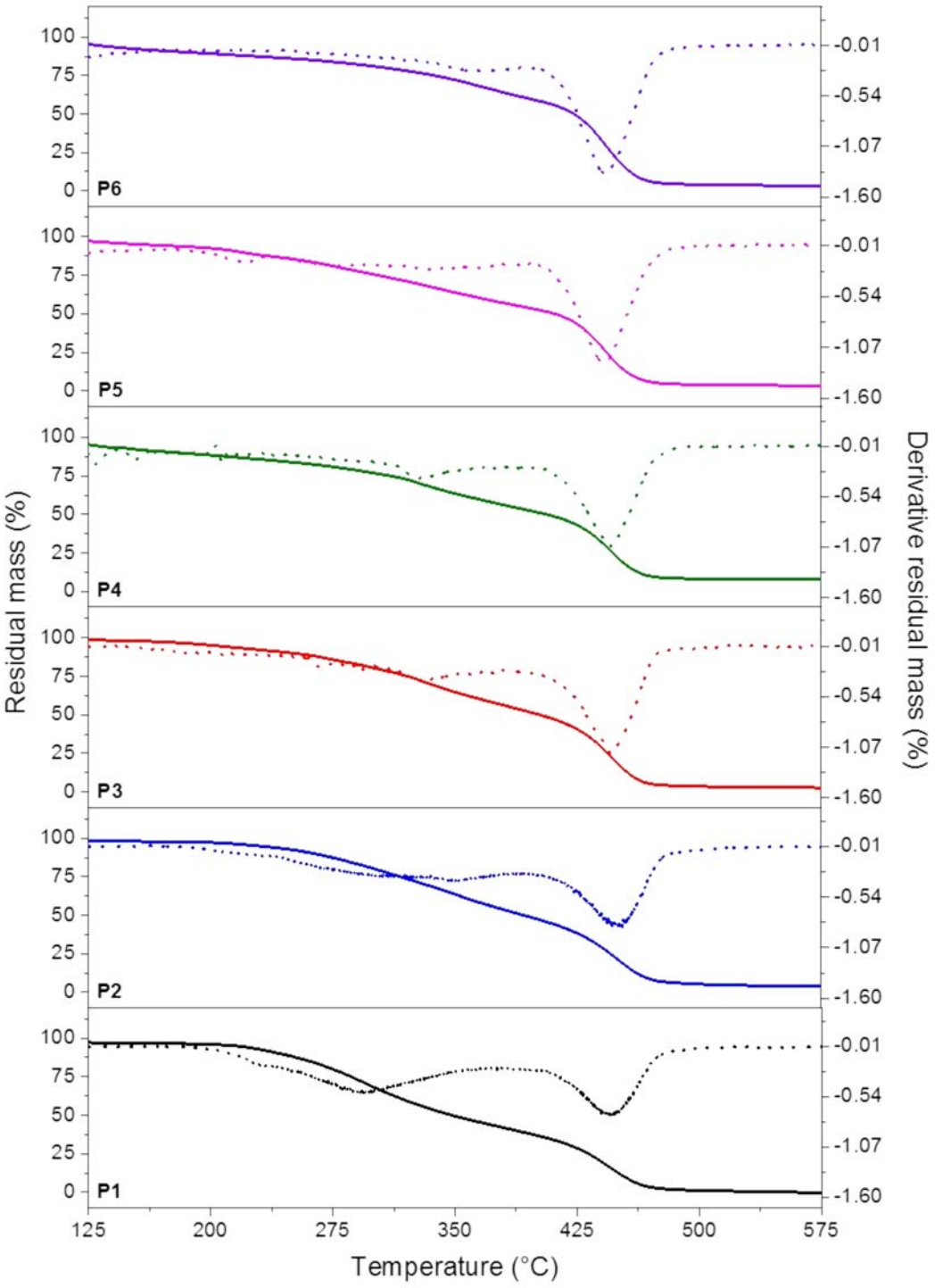

Figure S12. Overlay of the TGA thermograms of the block copolymers **P1** to **P6** synthesized in a one-pot approach (heating rate 10 K min^{-1}). The dotted lines depict the first derivative of each thermogram.

Table 1. Summary of the thermal characterization data obtained *via* DSC analysis.

	PLA-CTA	PHEA-1	PHEA-2	P1	P2	P3	P4	P5	P6
w_{HEA}*	0	100	100	0.46	0.56	0.60	0.68	0.73	0.82
$T_{g, Exp.}$ in °C[a] (inflection point)	38	–1	5	11 / 30	6	3	12	13	12
$T_{g, onset}$	32	–6	–3	4 / 28	–1	–9	5	7	4
$T_{g, mid}$	37	–1	4	10 / 33	5	2	11	12	10
$T_{g, end}$	42	4	11	17 / 39	10	13	17	17	17
Δ_{Cp} in J mol^{-1} K^{-1}	0.52	0.47	0.46	0.15 / 0.17	0.53	0.56	0.43	0.41	0.45
$T_{g, Fox}$ in °C[b]				20	17	15	13	11	8
$T_{g, Wood}$ in °C[c]				22	19	17	14	13	9

[a] Determined by DSC analysis (T_g values are reported as inflection point of the third heating trace). [b] Calculated according to $1/T_g = M_1/T_{g1} + M_2/T_{g2}$, where M_1 and M_2 are the weight fractions of ***HEA*** and ***LA***, respectively.[1, 2] [c] Calculated according to $T_g = (M_1\Delta C_{p1}T_{g1} + M_2\Delta C_{p2}T_{g2})/(M_1\Delta C_{p1} + M_2\Delta C_{p2})$.[2, 3] Averaged T_g and ΔC_p values of **PHEA** were used for the calculation of the T_g *via* Fox and Wood equations. * $\boldsymbol{M_1}$ and $\boldsymbol{M_2}$ values as estimated from feed and conversion.

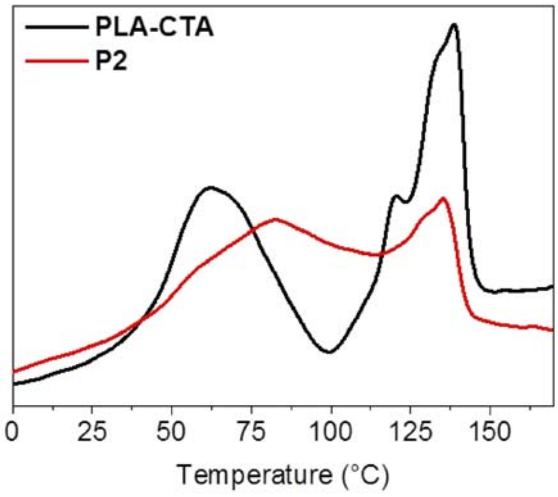

Figure S13. Overlay of the DSC thermograms of **PLA-CTA** and **P2** depicting the presence of crystallization and melting peaks (1st heating run, heating rate 20 K min^{-1}).

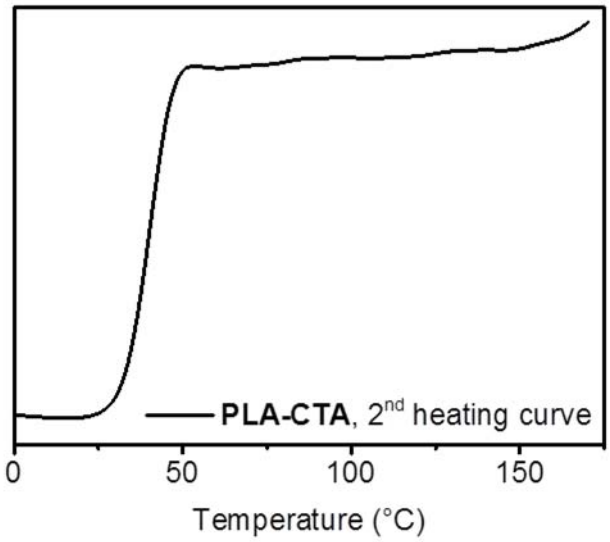

Figure S14. DSC thermogram of the **PLA-CTA** (heating rate 20 K min^{-1}) showing the absence of a melting peak in the second heating run.

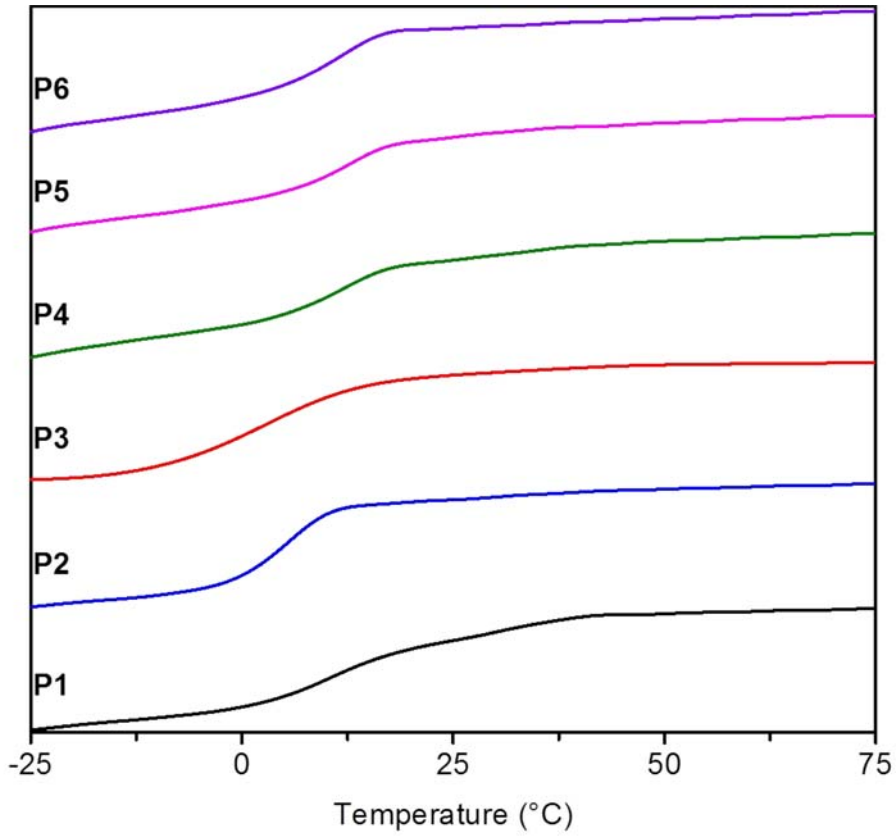

Figure S15. Overlay of the DSC thermograms of block copolymers **P1** to **P6** synthesized in a one pot approach (3rd heating run, heating rate 10 K min^{-1}). The individual thermograms are shifted vertically for clarity.

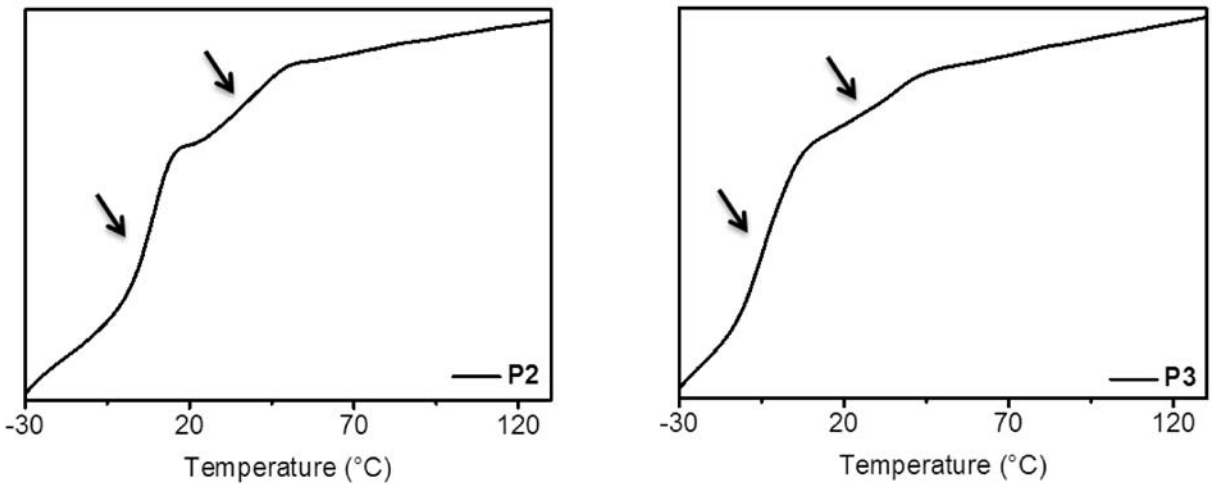

Figure S16. DSC thermograms of **P2** and **P3** obtained with a modified temperature program showing the presence of two glass transitions. The samples were heated to 170 °C and cooled to –50 °C at a rate of 5 K min^{-1}. The thermograms depict a subsequent heating run (rate 10 K min^{-1}). Increased heating rates did not improve the resolution of the two glass transitions.

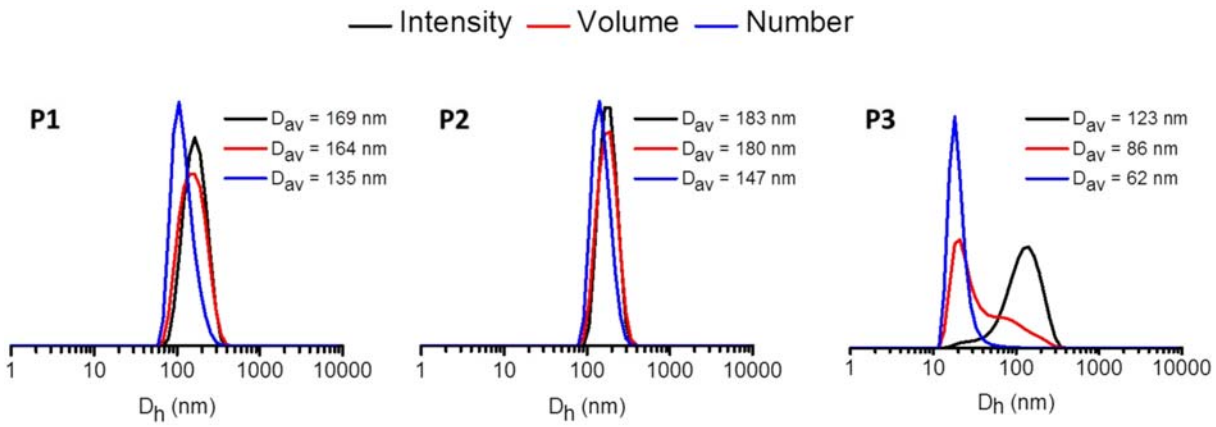

Figure S17. DLS size distributions of **P1**, **P2** and **P3** (c = 2 mg mL^{-1} in water).

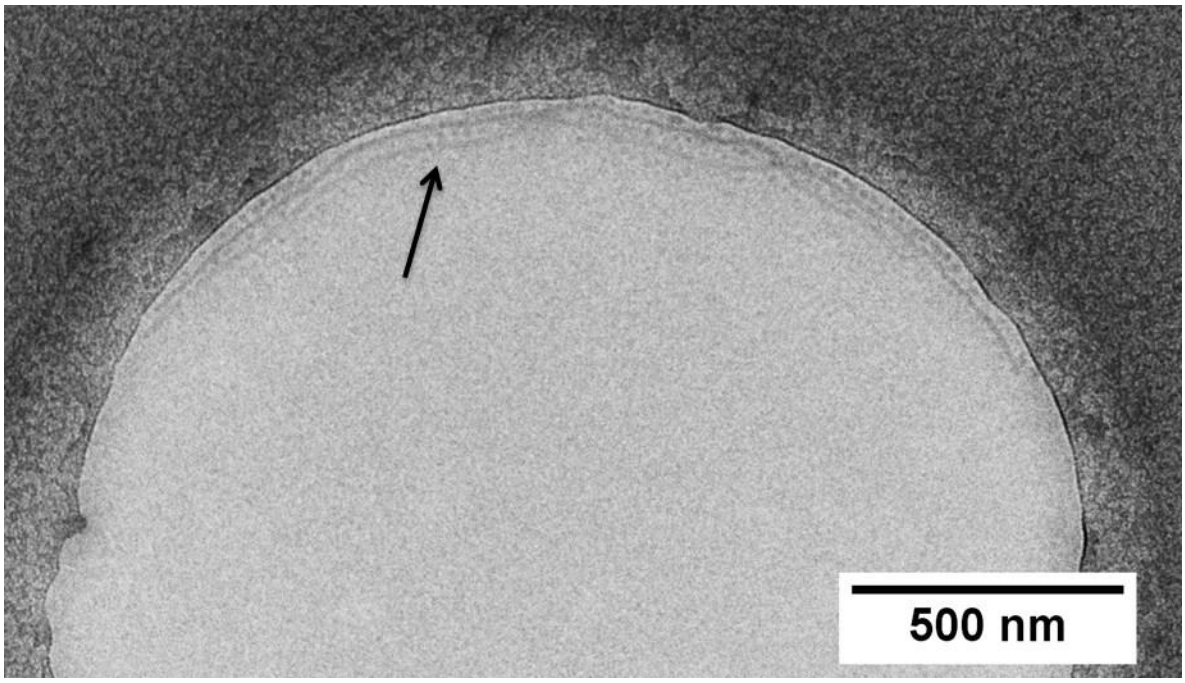

Figure S18. Additional cryo-TEM image of **P4** showing worm-like micelles occasionally found in the amorphous ice layers (c = 2 mg mL^{-1} in water).

1. T. G. Fox, *Bull. Am. Phys. Soc.,* 1956, **1**, 123.
2. P. R. Couchman, *Macromolecules,* 1978, **11**, 1156-1161.
3. L. A. Wood, *J. Polym. Sci.,* 1958, **28**, 319-330.

Publication P6

“Fluorescent amphiphilic heterografted comb polymers comprising biocompatible PLA and PEtOx side chains”

Ilknur Yildirim, Tanja Bus, Martin Sahn, Turgay Yildirim, Diana Kalden, Stephanie Hoeppener, Anja Traeger, Matthias Westerhausen, Christine Weber, Ulrich S. Schubert

Polym. Chem. **2016**, *7*, 6064–6074.

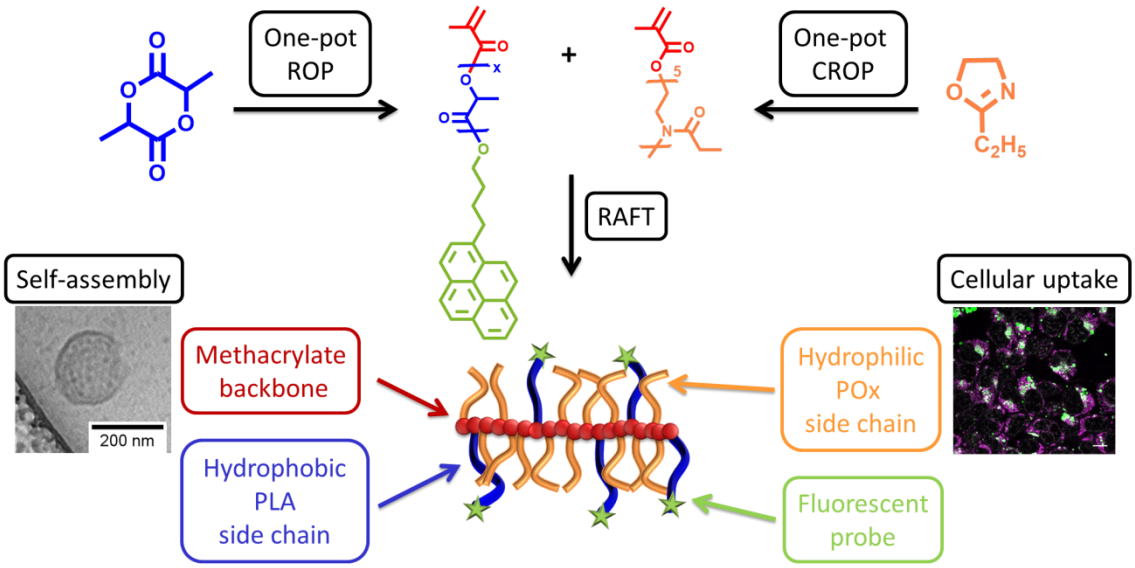

Polymer Chemistry

PAPER

View Article Online
View Journal | View Issue

Cite this: *Polym. Chem.*, 2016, **7**, 6064

Fluorescent amphiphilic heterografted comb polymers comprising biocompatible PLA and PEtOx side chains†

Ilknur Yildirim,[a,b] Tanja Bus,[a,b] Martin Sahn,[a,b] Turgay Yildirim,[a,b] Diana Kalden,[c] Stephanie Hoeppener,[a,b] Anja Traeger,[a,b] Matthias Westerhausen,[c] Christine Weber[a,b] and Ulrich S. Schubert*[a,b]

Received 29th June 2016,
Accepted 4th September 2016

DOI: 10.1039/c6py01130f

www.rsc.org/polymers

A series of amphiphilic heterografted comb polymers comprising various ratios of oligomeric polylactide (PLA) and poly(2-ethyl-2-oxazoline) (PEtOx) side chains was synthesized *via* the grafting-through method employing the reversible addition–fragmentation chain transfer copolymerization. Two well-defined PLA macromonomers were prepared *via* ring opening polymerization (ROP) of L-lactide using a calcium-based pre-catalyst, pyrenebutanol as an initiator and methacryloyl chloride as an end-capping agent. The PEtOx macromonomer was obtained from the cationic ROP of EtOx and end-capping with methacrylic acid. The amphiphilic comb polymers self-assembled in aqueous solution to form spherical and worm-like micelles, vesicles and more complex morphologies as a function of the composition, as is evident from dynamic light scattering and cryo-transmission electron microscopy studies. All polymers were found to be non-toxic to L929 cells up to a concentration of 200 μg mL^{-1}. Cellular uptake studies with HEK-293 cells by live cell confocal fluorescence microscopy revealed localization in the cytosol after 4 h and suggest an energy-driven cellular uptake mechanism.

Introduction

Certain polymer classes are often associated with distinct properties, such as biodegradability, hydrophilicity, charge or crystallinity. Although such properties can mostly be adjusted by the use of appropriate monomer types, the combination of several polymer classes that are obtained *via* completely different synthetic routes is advantageous, in particular when rather conservative application fields are in focus. As an example, the polyester polylactide (PLA) is the current gold standard as a biodegradable polymer from renewable resources to serve for encapsulation of hydrophobic guest molecules or many other applications in the bio-medical field.[1,2] PLA is obtained by the ring-opening polymerization (ROP) of lactide, however monomers which would add hydrophilic properties to a polyester are not commercially available. Hence, poly(ethylene glycol) (PEG) is often applied as a macroinitiator for the ROP due to its hydrophilic nature and stealth effect.[3]

Modern polymer chemistry offers a rich set of other hydrophilic polymers to prepare amphiphilic PLA-based macromolecules, taking into account the prerequisite that they can be obtained with well-defined end groups. This is the case for poly(2-oxazoline)s (POx)[4,5] since they can be polymerized by a living cationic ROP mechanism. POx that feature ethyl- and methyl-substituents are hydrophilic, and are candidates to replace PEG since they exhibit similar properties in biological systems: biocompatibility, protein repellency and prolonged blood circulation, *i.e.* the "stealth effect".[6]

Besides using hydroxyl end-functional macroinitiators to prepare linear block copolymers comprising PLA,[7,8] polymers with more sophisticated topologies endow further synthetic possibilities to the structural design.[9,10] Among these, comb-shaped and graft copolymers open avenues for further variations, taking into account additional factors such as main chain topology, grafting density, and the chemical composition of the backbone and the side chains. These additional factors offer the possibility to include further functionalities, but can also result in altered physicochemical properties since

[a]*Laboratory of Organic and Macromolecular Chemistry (IOMC), Friedrich Schiller University Jena, Humboldtstr. 10, 07743 Jena, Germany. E-mail: ulrich.schubert@uni-jena.de*
[b]*Jena Center for Soft Matter (JCSM), Friedrich Schiller University Jena, Philosophenweg 7, 07743 Jena, Germany*
[c]*Institute of Inorganic and Analytical Chemistry (IAAC), Friedrich Schiller University Jena, Humboldtstr. 8, 07743 Jena, Germany*

†Electronic supplementary information (ESI) available: Additional UV-vis absorption and fluorescence emission spectra, ^{1}H NMR spectra, hydrodynamic radii obtained from DLS measurements, and images from confocal microscopy. See DOI: 10.1039/c6py01130f

excluded volume interactions between grafted side chains[11,12] may lead to morphology diversification in self-assembled aggregates.[13]

A heterografted comb polymer is a special type of comb polymer[11–13] that contains two different side chain types, thus, representing a flexible means to combine the properties of distinct polymer types by an appropriate selection of polymer backbones and side chains. However, examples of heterografted comb polymers remain scarce to date, mostly due to demanding synthetic approaches as a result of the several consecutive reactions to be performed on the same polymer backbone, which is required in many synthetic approaches.[14–17] As an alternative, the copolymerization of macromonomers *via* the grafting through method comprises three independent steps: the synthesis of the two macromonomers and subsequent copolymerization.[12,13]

Aside from ring opening metathesis polymerization,[18] free radical[19–22] and controlled radical polymerization[23,24] are the most commonly utilized techniques for the polymerization of macromonomers. However, at least one macromonomer is often based on a linear polymer without substituents (such as PEG or PCL),[19–21,23] thereby decreasing the steric demand during the backbone formation. In fact, the copolymerization of PLA macromonomers with a different type of macromonomer (*i.e.* PEG,[25] poly(dimethylsiloxane)[26] and poly(*n*-butylacrylate)[18]) yielding heterografted copolymers has been rarely reported.

Herein, we present the copolymerization of a methacrylate ω-end-functional hydrophobic PLA macromonomer with a corresponding methacrylate functional macromonomer based on hydrophilic poly(2-ethyl-2-oxazoline) (PEtOx)[24,27] *via* reversible addition fragmentation chain transfer (RAFT) polymerization in order to obtain a series of amphiphilic heterografted comb polymers (Scheme 1). The hydrophilic/hydrophobic balance of the comb polymers was changed by altering the feed ratio of both macromonomers as well as the degree of polymerization (DP) of the PLA-based macromonomer to study the self-assembly behavior in water by means of dynamic light scattering (DLS) and cryo-transmission electron microscopy (cryo-TEM).

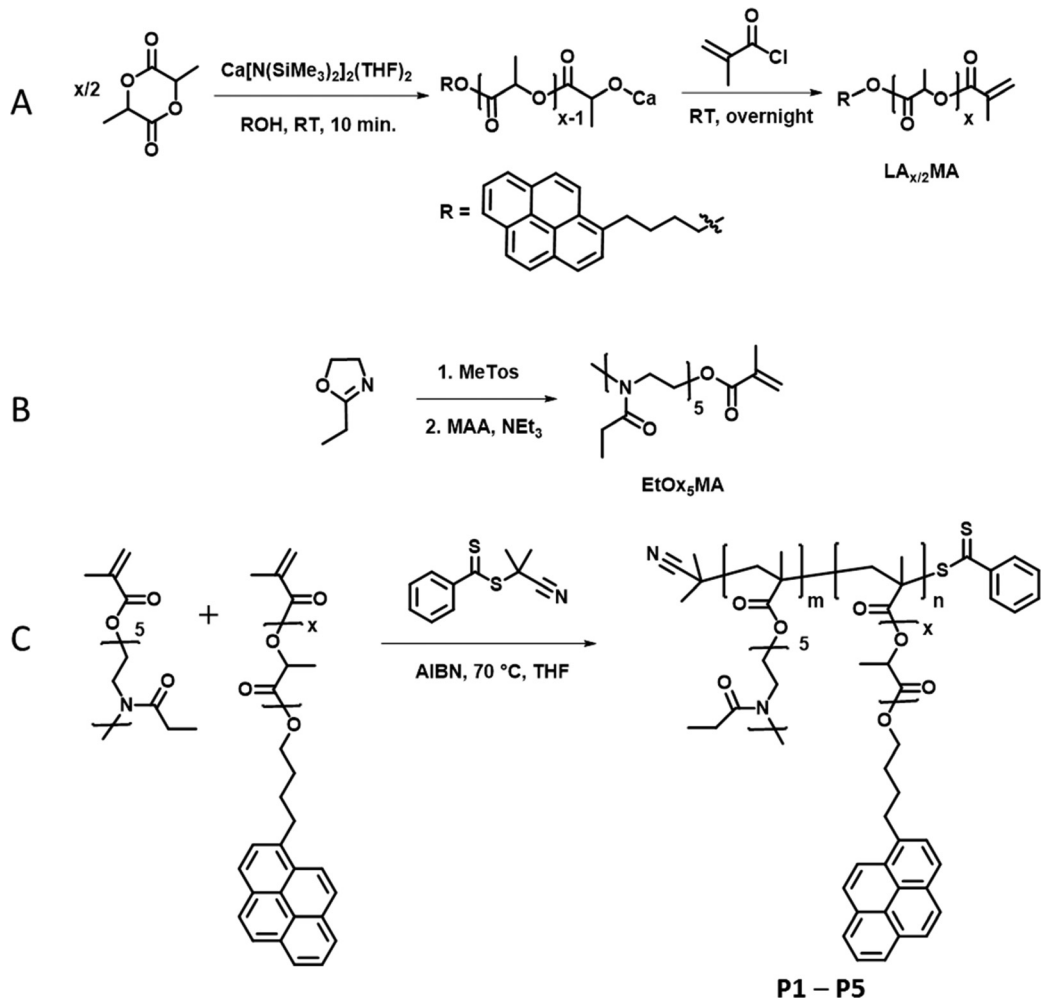

Scheme 1 Schematic representation of the synthesis of (A) the PLA macromonomer *via* ROP of L-lactide and *in situ* end capping with methacryloyl chloride, (B) the POx macromonomer *via* microwave assisted CROP of 2-ethyl-2-oxazoline, and (C) the heterografted comb polymers *via* RAFT polymerization.

Since both components represent biocompatible polymers, pyrene was attached as a fluorescent probe[28] to enable detailed studies regarding the cytotoxicity as well as the cellular uptake behavior. For this purpose, 1-pyrenebutanol was applied as an initiator during the calcium alkoxide initiated ROP of L-lactide,[29] which was converted to a macromonomer *via* end-capping with methacryloyl chloride.[30]

Experimental section

Materials

L-Lactide (98%) was purchased from Sigma-Aldrich and purified by recrystallization from dry toluene and dried under vacuum. Bis(tetrahydrofuran)calcium bis[bis(trimethylsilyl) amide] ($Ca[N(SiMe_3)_2]_2(THF)_2$) was synthesized according to previously reported procedures that are valued in several reviews.[31–34] 1-Pyrenebutanol (99%) and methacryloyl chloride (97%) were purchased from Sigma-Aldrich and used without further purification. Tetrahydrofuran (THF) was dried by refluxing over sodium/benzophenone. 2-Ethyl-2-oxazoline (99%, Acros, EtOx) was dried over barium oxide and distilled under argon prior to use. Methyl tosylate (98%, Aldrich) was distilled under reduced pressure and stored under argon. Acetonitrile (extra dry, Acros) was stored under argon. Methacrylic acid (99%, Aldrich) was used as received. Triethylamine was dried over potassium hydroxide and distilled under argon. 2,2′-Azobis(2-methylpropionitrile) (98%, Acros, AIBN) was recrystallized from methanol, and the chain transfer agent 2-cyanoprop-2-yl dithiobenzoate (CPDB) was purchased from Strem Chemicals. AlamarBlue, YOYO-1 iodide, NucRed Live 647 as well as LysoTracker Green DND-26 were obtained from Life Technologies (Thermo Fisher, Germany). Consumables for cell culture, like pipettes and cell culture plates (96 well), were obtained from Corning (USA) and Greiner Bio-one (Austria/Germany). If not stated otherwise, cell culture media and supplements (L-glutamin, antibiotics) were obtained from Biochrom (Merck Millipore, Germany). All other chemicals were purchased from standard suppliers and used without further purification. For the purification of the comb polymers a column filled with BioBeads S-X1 (exclusion limit 14 000 Da) with THF or toluene as an eluent was used.

Instruments

The ROP of L-lactide was carried out under nitrogen in an MBraun UNILab glove box workstation. The polymerization of EtOx was performed in a Biotage Initiator Sixty microwave synthesizer. Proton nuclear magnetic resonance (^1H NMR) spectra were recorded at room temperature in $CDCl_3$ on a Bruker Avance 300 MHz using the residual solvent resonance as an internal standard. The chemical shifts are given in ppm relative to tetramethylsilane (TMS). Size-exclusion chromatography (SEC) measurements were performed on two different setups. SEC in $CHCl_3$: Shimadzu system equipped with an SCL-10A system controller, an LC-10AD pump, a RID-10A refractive index detector, an SPD-10AD VP UV detector, and a PSSSDV-linear S column (5 mm particle size; Polymer Standards Service (PSS) GmbH, Mainz, Germany) at 40 °C using a chloroform, triethylamine, and 2-propanol (94 : 4 : 2) mixture as an eluent at a flow rate of 1 mL min^{-1}. The system was calibrated with PMMA standards (410 to 88 000 g mol^{-1}); SEC in THF: a Shimadzu system equipped with an SCL-10A system controller, an LC-10AD pump, an RID-10A refractive index detector, an SPD-10AD UV detector and an SDV linear M column from PSS at 40 °C using THF as an eluent at a flow rate of 1 mL min^{-1}. The system was calibrated against PLA standards (144 to 101 000 g mol^{-1}), which were purchased from PSS. For the measurements of the matrix-assisted laser desorption/ionization (MALDI) spectra, an Ultraflex III ToF/ToF instrument (Bruker Daltonics, Bremen, Germany) was used. The instrument is equipped with a Nd-YAG laser. All spectra were measured in the positive reflector mode. The instrument was calibrated prior to each measurement with an external PMMA standard from PSS. For the MALDI-ToF-MS sample preparation, separate solutions of polymer (10 mg mL^{-1} in THF), 2-(4′-hydroxybenzeneazo)benzoic acid (HABA, 30 mg mL^{-1} in THF), and doping of sodium chloride (NaCl, 100 mg mL^{-1} in acetone) were prepared and mixed following the dried droplet spotting technique. 1 μL of the mixture was spotted onto the target plate. For the ESI-Q-ToF-MS measurements, samples were analyzed by a microToF Q-II (Bruker Daltonics) mass spectrometer equipped with an automatic syringe pump from KD Scientific for sample injection. The ESI-Q-ToF mass spectrometer was operated at 4.5 kV, at a desolvation temperature of 180 °C. The mass spectrometer was operated in the positive ion mode. Nitrogen was used as the nebulizer and drying gas. The ESI-Q-ToF-MS instrument was calibrated in the m/z range from 50 to 3000 using a calibration standard (Tunemix solution) supplied from Agilent. All data were processed *via* Bruker Data Analysis software version 4.2. UV-Vis absorption measurements were performed using an Analytik Jena SPECORD 250 spectrometer (Analytik Jena, Jena, Germany). The fluorescence spectra were recorded on a Jasco FP-6500 spectrofluorometer. Dynamic light scattering was performed on a Zetasizer Nano ZS (Malvern Instruments, Herrenberg, Germany). After an equilibration time of 120 s, 3 × 12 runs were carried out at 25 °C (λ = 633 nm). The counts were detected at an angle of 173°. Each measurement was performed in triplicate. The size distribution of the particles was calculated applying the non-linear least squares fitting method. The mean particle size was approximated as the effective (Z-average) diameter and the width of the distribution as the polydispersity index (PDI) of the particles obtained by the cumulants method assuming a spherical shape of the particles. Cryo-transmission electron microscopy (cryo-TEM) investigations were performed on a Tecnai G^2 20 (FEI) equipped with an Olympus Soft Imaging Solutions MegaView and a 4 × 4k Eagle CCD camera system. Quantifoil grids (R2/2 Quantifoil, Germany) were cleaned by plasma treatment prior to use. Cryo sample preparation was conducted utilizing a FEI Vitrobot Mark IV system. 6 μL of the sample solution was de-

posited onto the grid, equilibrated shortly, and blotted for 1 s. The grids were immediately plunged into liquid ethane to obtain vitrification, and samples were stored at liquid nitrogen temperature until being transferred to the TEM utilizing a Gatan cryo transfer system.

For cytotoxicity and cellular uptake studies, a microplate reader (Tecan Infinite M200 Pro, Switzerland) and a confocal laser scanning microscope LSM880 (Carl Zeiss, Germany) were used (see below).

Synthesis

Cationic ring-opening polymerization. Oligo(2-ethyl-2-oxazoline) methacrylate ($EtOx_5MA$) was synthesized as reported previously.[27] Briefly, 1.383 g (7.44 mmol) of MeTos and 3.60 g (36.31 mmol) of EtOx were dissolved in 5.41 mL of acetonitrile and polymerized in a microwave synthesizer for 1 minute at 140 °C. 1.84 mL (21.8 mmol) of MAA and 6.04 mL (46.6 mmol) of triethyl amine were added. Subsequent to heating at 50 °C overnight, the macromonomer was dissolved in chloroform and purified by extraction with aqueous sodium bicarbonate solution and brine. The volatiles were removed under reduced pressure. $M_{n,\ NMR}$ = 600 g mol^{-1}, $M_{n,\ SEC}$ = 500 g mol^{-1}, $Đ$ = 1.17 (SEC in $CHCl_3$, PMMA calibration), DP = 5, DF = 96%.

ROP of L-lactide. The ROP of L-lactide was carried out in a glove box, at room temperature under a nitrogen atmosphere (<1 ppm H_2O, <1 ppm O_2), using THF as the solvent.

$LA_{15}MA$ 1: $Ca[N(SiMe_3)_2]_2(THF)_2$ (0.23 mmol, 116 mg) was dissolved in 1.0 mL of THF. This solution was added under vigorous stirring to a solution of L-lactide (1.0 g, 6.94 mmol) and 1-pyrene butanol (126.2 mg, 0.46 mmol) in 5.94 mL of THF in a microwave vial. This corresponds to a molar ratio of [L-lactide]/[1-pyrenebutanol]/[Ca] of 15/1/0.5 and an initial monomer concentration of $[L\text{-lactide}]_0$ of 1 mol L^{-1}. After 10 minutes, a sample was taken from the mixture and analyzed by ^{1}H NMR spectroscopy in order to determine the monomer conversion. The vial was capped, taken out of the glove box, and immersed in an ice bath. Subsequently, methacryloyl chloride (223 μL, 2.30 mmol) was added dropwise into the polymerization mixture through the septum of the vial. After 10 minutes, the ice bath was removed and the mixture was kept at room temperature for 24 hours under vigorous stirring. The excess of acid chloride was removed *via* precipitation in methanol and the purified product was dried under reduced pressure until a constant weight (yield: 0.8 g, 80%). ^{1}H NMR (300 MHz, $CDCl_3$): δ/ppm = 1.57 (d, –C(O)CH(C**H**$_3$)O–), 1.96 (s, –C(O)CH(CH$_3$)OC(C**H**$_3$)CH$_2$), 3.37 (t, $C_{16}H_9C\mathbf{H}_2C_3H_6OC(O)$–), 4.21 (t, $C_{16}H_9C_3H_6C\mathbf{H}_2OC(O)$–), 5.16 (q, –C(O)C**H**(CH$_3$)O–), 5.63 (s, –C(O)C(CH$_3$)C**H**$_2$), 6.20 (s, –C(O)C(CH$_3$)C**H**$_2$) 7.80–8.30 (m, $C_{16}\mathbf{H}_9C_4H_8OC(O)$–). The macromonomer was characterized by means of SEC (THF, RI detection, PLA calibration), MALDI-ToF-MS, and ESI-ToF-MS (see Results and discussion).

$LA_{10}MA$ 2 was obtained in an analogous fashion. 1.0 g of L-lactide (6.94 mmol), 175 mg of $Ca[N(SiMe_3)_2]_2(THF)_2$ (0.34 mmol), 190 mg of 1-pyrene butanol (0.69 mmol), 338 μL of methacryloyl chloride (3.40 mmol) and 5.94 mL of THF were used.

RAFT polymerization. Five different comb polymers were prepared by changing the ratios of the EtOx and PLA macromonomers. The $[M]_{total}$/[CPDB]/[AIBN] ratio was kept at 60/1/0.25 with an overall monomer concentration of 0.3 mol L^{-1}. In a representative RAFT copolymerization for **P1**, $LA_{15}MA$ (0.590 g, 0.19 mmol), $EtOx_5MA$ (0.562 g, 0.94 mmol), CPDB (4.2 mg, 0.019 mmol), and AIBN (0.77 mg, 0.0047 mmol) were dissolved in 3.8 mL of THF. After gently purging with argon for 30 minutes to remove the oxygen from the reaction mixture, the t_0 sample was taken for the determination of the monomer conversions. The polymerization was conducted in a pre-heated oil bath at 70 °C for 24 hours. The polymerization was stopped by cooling to room temperature and exposing the solution to air. The macromonomer conversions were calculated by comparing the integral values of the vinylic peaks in ^{1}H NMR spectra of the samples taken before and after polymerization. The comb polymers were purified by precipitation in methanol and subsequent preparative SEC on a BioBeads-SX-1 column, respectively. THF or toluene was used as the eluent based on the solubility of the comb polymers. Fractions (*ca.* 2 mL) were collected and analyzed by SEC with UV and RI detection. The desired fractions were combined and the volatiles were removed under reduced pressure.

Sample preparation for DLS and Cryo-TEM analysis

5 mg of comb polymer were dissolved in 500 μL of THF. The solution was dropped into 1 mL of deionized water in aliquots of 5 μL under vigorous stirring. THF was evaporated by stirring the open vial for at least two days to yield aqueous suspensions with a final polymer concentration of 5 mg mL^{-1}.

Determination of cytotoxicity

Cytotoxicity studies were performed with the mouse fibroblast cell line L929 (CCL-1, ATCC), as recommended by ISO10993-5. The cells were routinely cultured in Dulbecco's modified Eagle's medium supplemented with 10% fetal calf serum (FCS, Capricorn Scientific, Germany), 100 U mL^{-1} penicillin and 100 μg mL^{-1} streptomycin at 37 °C in a humidified 5% (v/v) CO_2 atmosphere. In detail, cells were seeded at 10^4 cells per well in a 96-well plate and incubated for 24 hours. No cells were seeded in the outer wells. Afterwards, the testing substances (polymers) were added to the cells at the indicated concentrations (from 5 μg mL^{-1} to 200 μg mL^{-1}) and the plates were incubated for additional 24 hours. Subsequently, the medium was replaced by a mixture of fresh culture medium and the assay reagent alamarBlue (resazurin based solution, Thermo Fisher, Germany, prepared according to manufacturer's instructions). After a further incubation of 4 hours at 37 °C in a humidified 5% (v/v) CO_2 atmosphere, the fluorescence was measured at Ex 570/Em 610 nm, with untreated cells on the same well plate serving as negative controls. The negative control was standardized as 0% of metabolism inhibition and referred to as 100% viability. Cell viability below 70% was considered indicative of cytotoxicity. Data are

expressed as mean ± standard deviation (SD) of three independent determinations.

Cellular uptake

Live cell imaging was performed using HEK-293 cells (CRL-1573, ATCC) for analyzing the cellular uptake of the comb polymers. For this purpose, HEK cells (10^5 cells per mL) were seeded in glass-bottomed, 4-chamber dishes (CELLVIEW, Greiner Bio-One, Germany) and cultured for 24 hours in RPMI 1640 medium (Lonza, Switzerland) supplemented with 10% FCS, 100 μg mL^{-1} streptomycin, 100 U mL^{-1} penicillin and 2 mM L-glutamine at 37 °C in a humidified 5% CO_2 atmosphere. One hour prior to polymer addition, the cells were rinsed with phosphate buffered saline (PBS) and the media were changed to OptiMEM (Gibco, Thermo Fisher, USA). The polymers were added to cells with a final concentration of 50 μg mL^{-1} and incubated for an additional 4 hours. Afterwards, the media were replaced with fresh culture media supplemented with LysoTracker Green DND-26 and NucRed Live 647 for lysosome and nucleus staining, respectively. The living cells were imaged with a LSM880 (Carl Zeiss, Germany) using the following excitation wavelengths/laser lines 405 nm (for pyrene), 488 nm (for lysosomes) and 633 nm (for nucleus).

Results and discussion

Macromonomer syntheses

In order to prepare heterografted comb polymers comprising hydrophilic and hydrophobic side chains, macromonomers based on PEtOx and PLA had to be prepared with methacrylate end groups. To facilitate reasonable conversions during the subsequent RAFT polymerization, the degree of polymerization (DP) of both macromonomers was kept low (DP = 5 to 15). Since several RAFT (co)polymerizations of $EtOx_5MA$ have been successfully established in our laboratories,[24,27,35] a DP of 5 was selected for the hydrophilic macromonomer. Hence, $EtOx_5MA$ was obtained by CROP of EtOx using MeTos as an initiator and subsequent end-capping with methacrylic acid using triethyl amine as a base to produce methacrylate anions *in situ*. For detailed information about the synthesis and characterization of $EtOx_5MA$, the reader is referred to the literature.[27]

So far, the catalyst $Ca[N(SiMe_3)_2]_2(THF)_2$ has proven powerful for the preparation of well-defined α-end-functional PLAs using various alcohols as initiators for the ROP of L-lactide at room temperature.[29] However, direct ω-end-functionalization of the resulting anionic PLA species has not been attempted yet. An electrophile such as methacryloyl chloride is necessary[30] to introduce a methacrylate end functionality *via* this direct end-capping route. Among the multitude of suitable alcohols that can be used as initiators for the ROP, 1-pyrenebutanol was selected for this study because of its fluorescence that makes it a suitable label for cellular uptake studies. To facilitate a similar reactivity of both macromonomer types during the subsequent RAFT copolymerization, the DP of the hydrophobic PLA macromonomers was kept low as well. Both polymerizations were driven to quantitative conversion prior to end-capping with a 10-fold excess of methacryloyl chloride. Hence, two different α,ω-end functional PLA macromonomers with a DP of 10 and 15, respectively, were prepared by ROP of L-lactide in a one-pot procedure. Table 1 summarizes the characterization results of the fluorescent PLA-based hydrophobic macromonomers $LA_{15}MA$ and $LA_{10}MA$ by means of SEC, ^1H NMR spectroscopy and mass spectrometry.

Due to the absorbance of the pyrene moieties at 340 nm, SEC analysis with UV detection provides a simple tool to confirm the covalent attachment of the initiator at the macromonomers. As is evident from the overlapping RI and UV signals in the elugrams of both macromonomers, the pyrene functionality is distributed evenly throughout the resulting PLA's, hinting at the absence of chain transfer reactions during the ROP (Fig. SI 1†). Moreover, the monomodal SEC traces and narrow molar mass distributions indicate that the quenching of the polymerization with methacryloyl chloride did not induce chain coupling or even autopolymerization of the methacrylate ω-end functionalities, neither during the course of the reaction nor during the purification.

SEC alone is incapable of providing a structural proof for a successful end-capping of the PLA chains. However, the ^1H NMR spectra of the resultant PLA macromonomers clearly reveal the presence of both pyrene and methacrylate moieties (Fig. 1). The fact that the separate integration of these signals was possible enabled the estimation of the degree of polymerization (DP) and the degree of functionalization at the ω-chain end (DF). For the former, the peak integrals corresponding to pyrene moieties (peak "g" in Fig. 1) and the methine proton of the lactide repeating units (peak "a" in Fig. 1) were used. The resulting molar masses are in good agreement with the values obtained from SEC analysis with PLA calibration as well as with the targeted molar mass for both macromonomers.

Table 1 Characterization data of the PLA macromonomers[a]

	M/I	Conv.[b] [%]	DP[c]	DF[c] [%]	$M_{n,\,theo}$[d] [g mol^{-1}]	$M_{n,\,NMR}$[c] [g mol^{-1}]	$M_{n,\,SEC}$[e] [g mol^{-1}]	$Đ_{SEC}$[e]	$M_{n,\,MALDI}$ [g mol^{-1}]	$Đ_{MALDI}$
$LA_{15}MA$	15	100	15	93	2500	2500	2300	1.24	2200	1.09
$LA_{10}MA$	10	100	10	90	1800	1800	1500	1.32	2000	1.13

[a] $[1\text{-Pyrenebutanol}]_0/[Ca]_0/[\text{methacryloyl chloride}] = 1/0.5/5$, $[\text{L-lactide}]_0 = 1$ M in THF, $t_{pol} = 10$ min, $T = 25$ °C. [b] Determined by ^1H NMR spectroscopy from the polymerization mixtures. [c] Degree of polymerization (DP) and degree of functionalization (DF) obtained from ^1H NMR spectra of the purified macromonomers. [d] Calculated from M/I and conversion. [e] Determined by SEC (THF, RI detection, PLA calibration).

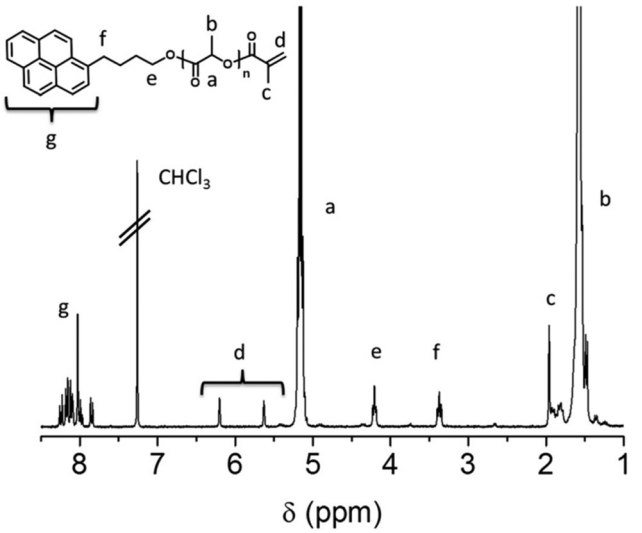

Fig. 1 ^{1}H NMR spectrum (300 MHz, $CDCl_3$) of the PLA macromonomer $LA_{15}MA$ and structural assignment of the observed peaks.

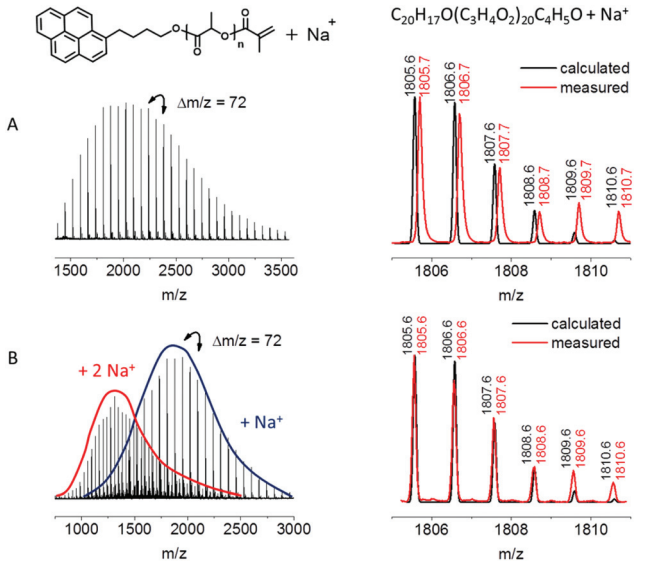

Fig. 2 Mass spectra of the PLA macromonomer $LA_{15}MA$ and the overlay of the isotopic patterns for the structural assignment of the peaks. (A) MALDI-ToF (HABA, NaCl) and (B) ESI-Q-ToF. Both spectra show an overlapping *m*/*z* series of the same PLA species that are either ionized with one (*z* = 1) or two (*z* = 2) sodium cations, respectively.

By comparison of the signals derived from both end groups, the DF was calculated. Therefore, the vinylic protons of the methacrylate moiety (peak "d") and either the pyrene signals in the aromatic region (peaks "g") or the benzylic methylene protons (peak "e") were used. The resulting DF varies between 84% and quantitative functionalization, based on the selected peak for integration due to the small intensity of the end group peaks. Hence, average values from four different integrations are reported in Table 1.

The excellent end group fidelity of the PLA macromonomers was further confirmed by mass spectrometric measurements. Fig. 2 shows the MALDI-ToF and ESI-Q-ToF MS of the PLA macromonomer $LA_{15}MA$. Both spectra reveal a single distribution of peaks at regular intervals spaced by $\Delta m/z$ = 72 between two neighboring peaks. The experimental isotopic patterns exactly overlap with the corresponding patterns calculated for the pyrene butanol α- and methacrylate ω-end functional PLA chains, which are ionized with a sodium cation. As often observed for ESI-Q-TOF analysis of polymers, this singly charged *m*/*z* distribution is overlaid with a second (doubly charged) *m*/*z* distribution, which corresponds to the same species ionized with two sodium cations. Although a $\Delta m/z$ = 72 (instead of $\Delta m/z$ = 144) in the mass spectra of PLA is often attributed to the presence of transesterification reactions in the literature,[30] it should be clearly stated that an intramolecular rearrangement at the active catalyst center is the reason for this observation in our case. This statement is based on our detailed previous research on this calcium alkoxide initiator system,[29] and sophisticated mechanistic studies are currently ongoing in our laboratories.

Grafting-through *via* RAFT copolymerization

Using both macromonomer types, *i.e.* hydrophilic $EtOx_5MA$ and hydrophobic LA_nMA, a series of heterografted comb polymers was prepared by RAFT copolymerization *via* the grafting through method. Thereby, the overall [monomer] to [CTA] ratio was kept constant at 60 using AIBN as an initiator and CPDB as a chain transfer agent in THF at 70 °C. In order to obtain comb polymers with varying hydrophilicity, the feed ratio of the $EtOx_5MA$ and $LA_{10}MA$ macromonomer was changed, however keeping a high molar fraction of the hydrophilic $EtOx_5MA$ throughout the series **P2–P5** because of the doubled DP of the hydrophobic $LA_{10}MA$. To elucidate the influence of the DP of the hydrophobic side chains, **P1** was synthesized using $LA_{15}MA$ while keeping the same feed ratio as for **P2**. As is often observed for grafting-through approaches, the macromonomer conversions were lower in this case due to the increased steric hindrance induced by the longer side chains.[27] For all comb polymers, complete removal of residual macromonomers was ensured by successive precipitation in methanol and preparative SEC using a BioBeads column. Table 2 summarizes the polymerization conditions and the characterization results of all purified comb polymers obtained by ^{1}H NMR spectroscopy and SEC analysis.

Fig. 3 shows an overlay of the SEC traces obtained from the comb polymers and the macromonomers with RI and UV detection at 340 nm. As can be clearly seen, all comb polymers elute earlier than the corresponding macromonomers due to the increased hydrodynamic volume of **P1** to **P5**. The fact that unimodal SEC traces are obtained confirms the complete removal of residual macromonomers during the purification process. The molar masses determined by SEC are similar for **P1** to **P4**, which is reasonable because the same [M]/[CTA] ratio was kept throughout the complete polymer series, and the conversions from all RAFT polymerizations were in a comparable

Table 2 Characterization results of the comb polymers **P1** to **P5**

	LA_nMA	$EtOx_5MA$/LA_nMA/CTA/AIBN	[$EtOx_5MA$]/[LA_nMA] (feed)	Conv.[a] [%]		$M_{n,theo}$[b] [g mol^{-1}]	$M_{n,SEC}$[c] [g mol^{-1}]	$Đ_{SEC}$[c]	[$EtOx_5MA$]/[LA_nMA] (NMR)[d]	EtOx/LA (NMR)[e]
				$EtOx_5MA$	LA_nMA					
P1	$LA_{15}MA$	42/18/1/0.25	71/29	32	25	20 600	27 500	1.17	70/30	45/55
P2	$LA_{10}MA$	42/18/1/0.25	71/29	90	85	50 000	28 200	1.37	65/35	50/50
P3	$LA_{10}MA$	50/10/1/0.25	83/17	75	73	35 600	29 000	1.25	80/20	65/35
P4	$LA_{10}MA$	53/7/1/0.25	88/12	95	90	41 000	26 300	1.25	85/15	70/30
P5	$LA_{10}MA$	54/6/1/0.25	90/10	85	75	36 800	19 500	1.23	90/10	80/20

[a] Conversion values determined by ^{1}H NMR spectroscopy from the polymerization mixtures. [b] Calculated from feed and conversion. [c] Determined by SEC ($CHCl_3$, RI detection, PMMA calibration). [d] Macromonomer molar ratio calculated from suitable signal integrals in the ^{1}H NMR spectra of the purified polymers. [e] Molar ratio of EtOx and LA repeating units calculated from suitable signal integrals in the ^{1}H NMR spectra of the purified polymers.

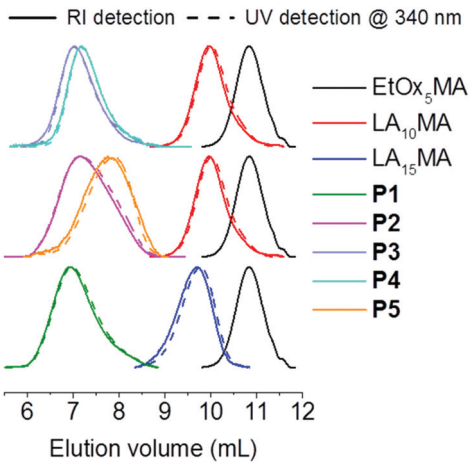

Fig. 3 Normalized SEC traces ($CHCl_3$) of the macromonomers and comb polymers **P1** to **P5**.

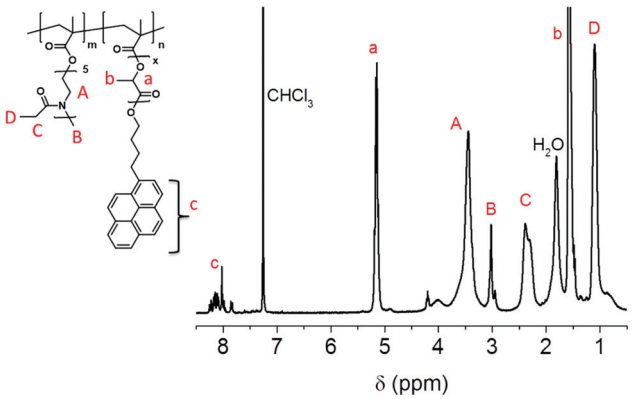

Fig. 4 ^{1}H NMR spectrum (300 MHz, $CDCl_3$) of **P3** together with the structural assignment of the observed peaks.

range (see Table 2). However, it has to be considered that SEC represents a relative method for molar mass determination and relies on the calibration with linear standard polymers, whose hydrodynamic volume strongly differs from that of comb-shaped polymers in general. Hence, SEC underestimates the molar masses of **P1** to **P5**. All comb polymers elute at similar retention times, revealing that the hydrodynamic volume of the polymeric architectures is not influenced by the side chain composition in chloroform, which represents a good solvent for both side chain types, *i.e.* PLA as well as PEtOx. In addition, the signals from UV and RI detection overlap for all polymers, confirming the incorporation of the respective PLA-based macromonomers, since $EtOx_5MA$ does not absorb at the wavelength selected for the UV detector.

Analysis of the purified comb polymers by means of ^{1}H NMR spectroscopy clearly reveals that both PLA and POx macromonomers were incorporated into the comb polymers as the signals derived from both polymer types can be clearly distinguished (Fig. 4). The signal corresponding to the methyl end groups of the PEtOx side chains (peak "B" in Fig. 4) was used to calculate the copolymer composition. Therefore, its integral was compared with the integral value of the methine proton peak of the PLA side chains (peak "a" in Fig. 4). The ratio of the two side chain types in the comb polymers is in excellent agreement with the feed ratio of both macromonomers, showing that LA_nMA was successfully incorporated during the RAFT copolymerization, despite its higher DP in comparison with $EtOx_5MA$ (compare Table 2). In addition, the aromatic protons of the pyrene unit (peak "c" in Fig. 4), which represent the end groups of the PLA side chains, are clearly visible, confirming the observations from SEC with UV detection (see above).

Fig. SI 3† depicts an overlay of the ^{1}H NMR spectra of **P1** to **P5** together with the structural assignment of the observed peaks used to estimate the copolymer composition. All spectra were normalized according to the peak maxima of the methine protons of the PLA side chains to underline the increasing PEtOx content throughout the polymer series from **P1** to **P5**. As the PEtOx content in the copolymer increases, so does the intensity of the respective signals assigned to this type of side chain. Although the ratio of the distinct side chain types was apparently not widely varied, the copolymer composition covers a broader range when the ratio of the EtOx and lactide repeating units is taken into account. This is due to the increased DP of the PLA-based side chains (DP = 10 and 15) compared with the DP of the PEtOx-based side chains (DP = 5).

Self-assembly behavior in aqueous media

To investigate the self-assembly behavior of the amphiphilic comb polymers **P1–P5** in water, aqueous suspensions were prepared by dropping THF polymer solutions into water. During the evaporation of THF, the formed structures were aged for a minimum of two days at room temperature. Subsequently, DLS and cryo-TEM measurements were performed.

Fig. 5 shows the resulting size distributions obtained from DLS of the copolymer assemblies **P2–P5**, *i.e.* the heterografted comb polymers synthesized using the macromonomers $LA_{10}MA$ and $EtOx_5MA$ along with representative cryo-TEM micrographs. Only in the case of the most hydrophilic copolymer **P5**, DLS revealed a bimodal size distribution of the self-assembled polymer structures, as is apparent by the overlay of the intensity, volume, and number weighted size distributions. Obviously, larger aggregates are visible in the intensity weighted distributions. Cryo-TEM measurements confirmed the presence of smaller (*ca.* 10 nm) and larger (*ca.* 40–50 nm) structures, which is in accordance with the DLS results. Presumably, the weight fraction of the hydrophilic EtOx is too high (w_{EtOx} = 0.73) in the case of **P5** and capable of shielding the hydrophobic PLA segments even without the formation of defined copolymer assemblies.

Monomodal size distributions were evident from DLS for the suspensions of the comb polymers **P3** and **P4** with a lower EtOx weight fraction of w_{EtOx} around 0.6. Homogeneous and densely packed spherical micelles with diameters around 15 nm were visualized by cryo-TEM analysis. This value roughly corresponds to the double length of a PLA with a DP of 10 in the all-*trans* conformation. Hence, one might assume that the micelles are formed by a spherical arrangement of several macromolecules with the PLA chains pointing towards the inside and the PEtOx side chains pointing to the outside. Already a slight increase in the weight fraction of hydrophobic PLA side chains resulted in spherical micelles with increased diameters of around 30 nm in the case of **P3**. Both observations are in accordance with the hydrodynamic diameters obtained from DLS measurements.

Further decrease of the EtOx content (**P2**, w_{EtOx} = 0.4) resulted in a mixture of self-assembled structures: spherical and worm-like micelles as well as large vesicles were found in the cryo-TEM micrographs. Accordingly the hydrodynamic diameters from DLS are increased with a rather high polydispersity index (PDI = 0.27, compare Table S1†). The diameter of the spherical and worm-like micelles (17 and 14 nm, respectively) corresponds well with the length of the PLA side chains of the comb polymer, as does the bilayer thickness of the vesicles (13 nm).

A similar variety of self-assembled structures was found by investigation of **P1** (Fig. 6), which is in good agreement with the bimodal intensity size distribution from DLS. In terms of the macromonomer mol fraction, this comb polymer has a similar composition as **P2**. However, the PLA side chains feature an increased DP of 15 since $LA_{15}MA$ was used during its synthesis, resulting in a further decreased w_{EtOx} of 0.36. In agreement with the length of the respective hydrophobic PLA side chains of the heterografted comb polymer **P1**, the micelles revealed slightly increased diameters (around 19 nm) in comparison to the structures formed by **P2**. Also the membrane thickness of the vesicular structures is slightly increased (21 nm). In addition, more complex morphologies were visualized by cryo-TEM investigations (Fig. 6b–d), which may be due to a hampered phase ordering due to the fact that hydrophilic and hydrophobic segments are covalently bound to the same comb polymer backbone. This would restrict the side chain mobility when compared with simple linear block copolymers.

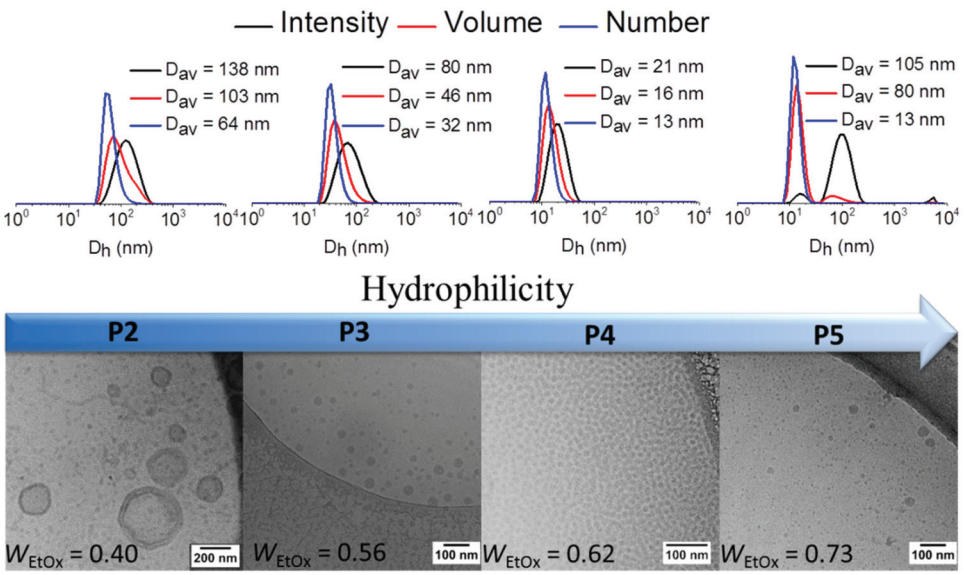

Fig. 5 DLS plots and cryo-TEM images of the suspensions obtained from **P2** to **P5** in water (c = 5 mg mL^{-1}).

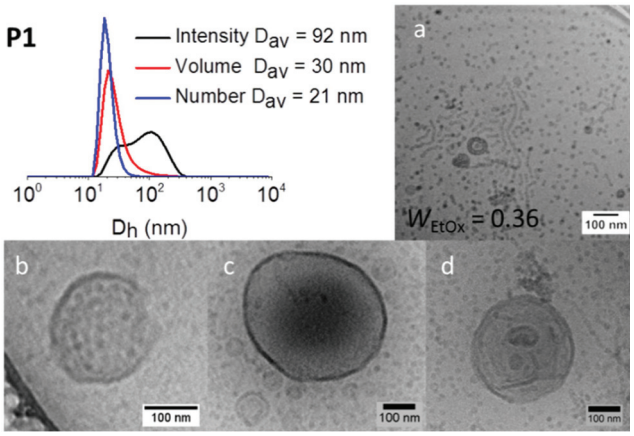

Fig. 6 DLS plots and cryo-TEM images of the suspensions formed by **P1** in water (c = 5 mg mL^{-1}; scale bars show 100 nm).

Fig. 6 shows examples of structures found for **P1**. In particular the large aggregates (up to 400 nm in diameter) featured different morphologies; however, no clearly defined structure can be elucidated in this case. Structures vary from segmented vesicles (b) (as reported by Mansfeld *et al.*[36] or Parry *et al.*[37]), distorted vesicles (c) as well as lamellar vesicles (d).

The transition from spherical micelles to vesicles has been predicted for heterografted comb polymers, and experimental confirmation has recently been provided by Luo *et al.* for heterografts with PEG and PLA side chains.[38,39] However, researchers in this field rather concentrate on an alteration of the side chain lengths of the comb polymers in analogy to variation of the block lengths in linear diblock copolymers. In fact, in these cases the only difference with linear block copolymers is the covalent junction at the comb polymer backbone (Fig. 7). We found that similar transitions are possible by keeping the DP of the side chains constant but altering the fraction of each type of side chain in the heterografted comb polymer.

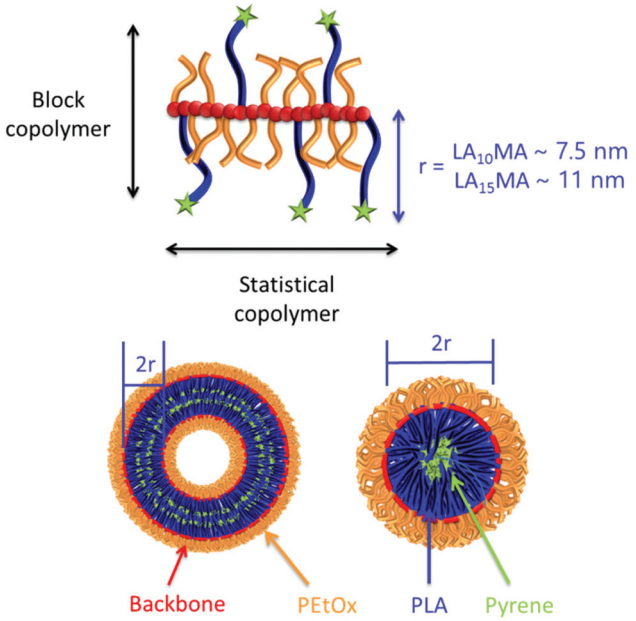

Fig. 7 Formation of spherical and worm-like micelles from comb polymers with mixed PEtOx and PLA side chains.

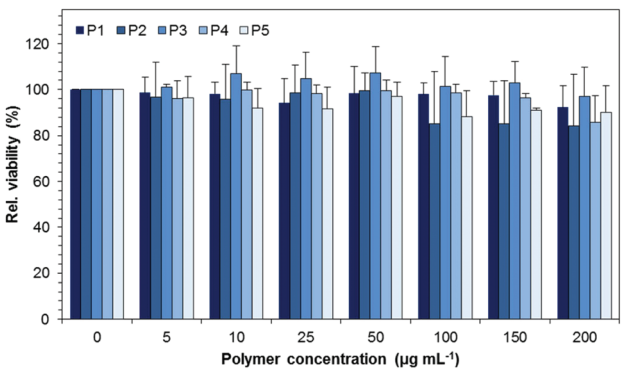

Fig. 8 Relative viability of L929 cells after 24 hours of incubation with heterografted comb polymers (**P1** to **P5**) at the indicated concentrations. Values represent the mean ± S.D. (n = 3).

Cytotoxicity and cellular uptake

As both segments of the comb polymers, *i.e.* the hydrophilic PEtOx and the hydrophobic PLA represent non-toxic polymers it was expected that the comb polymers **P1–P5** are highly biocompatible as well. Hence, an assay based on resazurin was performed to measure the metabolic activity of L929 mouse fibroblast cells after addition of polymer suspensions in water at varying concentrations. As depicted in Fig. 8, all polymers showed no significant reduction in cell viability after 24 hours at the tested conditions. Moreover, no influence of the different structural compositions of the polymers was observed. Due to the hydrophobic nature, it could be assumed that the PLA-pyrene side chains are located in the core of the self-assembled structure encompassed by the methacrylate backbone and PEtOx side chains (Fig. 7). Hence, the hydrophilic PEtOx arms, which shape the outer part of the self-assembled structures, indeed promote a high biocompatibility of the systems. A degradation of PLA combined with the release of pyrene would result in severe lethal effects, as this highly hydrophobic molecule would intercalate into cellular membranes.[40,41]

Based on these promising results, further biological investigations concerning the cellular uptake were performed. Since the pyrene at the end groups of the PLA side chains of the comb polymers enables easy detection of the polymeric structures,[42,43] it was possible to examine their intracellular distribution without the need to encapsulate any fluorescent probe. A representative UV-vis fluorescence emission spectrum is provided in Fig. S2† for **P4**. The ratio of the emission bands caused by the vibrational fine structure of pyrene corresponds very well to that of pyrene encapsulated into PLA-based nanocarriers,[44] confirming the assumption that the only potentially

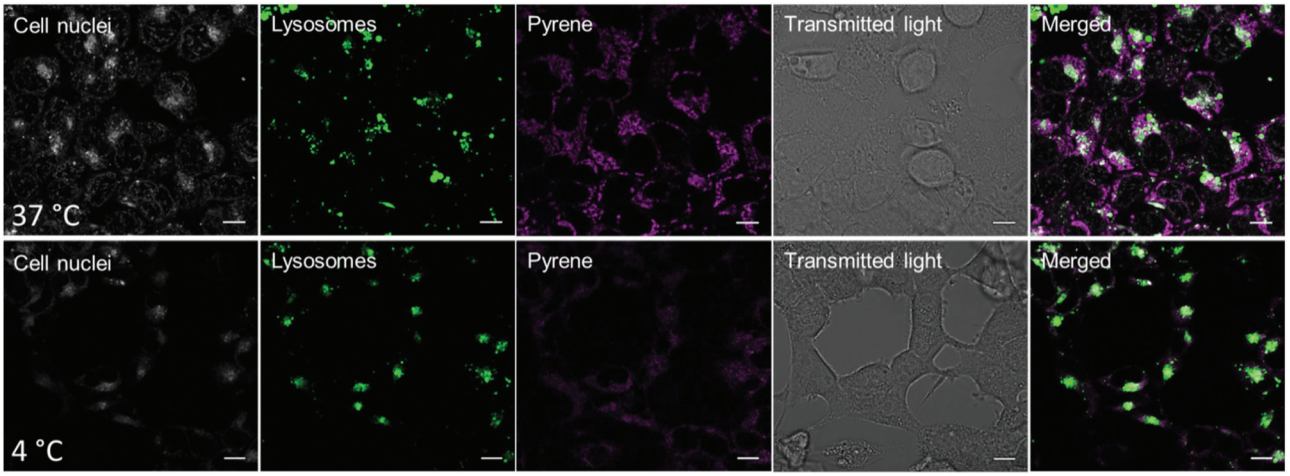

Fig. 9 Confocal live cell imaging of HEK-293 cells incubated with the suspension of **P1** in water (50 μg mL^{-1}) for 4 h at 37 °C (top) and 4 °C (bottom). The cell nucleus was stained with NucRed (grey) and the lysosomes/late endosomes with LysoTracker Green (green); pyrene is depicted in magenta (scale bars represent 10 μm).

toxic compound is not exposed to the surface of any polymeric structures formed in aqueous media. Therefore, HEK cells were incubated with **P1** to **P5** for 4 hours. Confocal live cell imaging revealed a high cellular internalization for all tested polymers at 37 °C (Fig. 9, top and Fig. SI 4 to SI 8†). The detected pyrene signal (magenta) was equally distributed within the cytosol, but was just rarely co-localized within the lysosomes (green) and not detectable within the nucleus. This could indicate either a fast endosomal release or cellular uptake *via* translocation through the cell membrane.

It is known that nanocarriers or nanoparticles possessing diameters from 20 to 500 nm enter cells in an active manner, mainly through endocytosis.[45,46] Furthermore, it is assumed that particles smaller than 20 nm may also internalize by passive diffusion[47] through channels, protein carriers or by translocation. Uptake studies of **P1** were performed at 4 °C, to investigate if the polymers are internalized into the cells by a passive process. Compared to the uptake at 37 °C, decreased pyrene fluorescence was detected within the cells. This indicates that a minor fraction of comb polymers is able to enter the cells by passive penetration. However, the predominant uptake mechanism for **P1** is an energy-driven process.

Conclusions

We present a convenient synthetic strategy for a series of fluorescent amphiphilic heterografted comb polymers comprising oligomeric biocompatible side chains *via* combination of ROP, CROP, and RAFT polymerizations. For this purpose, well-defined methacrylate ω-end-functional macromonomers based on PLA and PEtOx were prepared in separate one-pot procedures and were subsequently copolymerized *via* RAFT to obtain comb polymers with varying hydrophilicity simply by altering the feed ratio of both macromonomers. Cryo-TEM studies of the heterografted comb polymers in water revealed morphologies ranging from vesicular structures to spherical micelles. The morphology of the self-assembled structures correlated well with the hydrophilic character of the comb polymers. The fluorescent pyrene moieties attached to the PLA side chains of the comb polymers enabled performing cellular uptake studies without the need of encapsulation of any tracker molecules revealing that only a slight fraction is localized inside late endosomes/lysosomes. This is favorable for delivery applications, which will be in the focus of our future research as the PLA part of the polymer is biodegradable and a hydrophobic drug could be encapsulated into the self-assembled structures to be slowly released by degradation of the hydrophobic segments.

Acknowledgements

This project was funded by the German Federal Ministry of Education & Research (BMBF, #031A518B Vectura), the Thüringer Ministerium für Wirtschaft, Wissenschaft, und Digitale Gesellschaft (Thuringian Ministry for Economic Affairs, Science and Digital Society, ProExzellenzII, NanoPolar). AT and CW gratefully acknowledge the CarlZeiss Stiftung for funding. The LSM880 ELYRA PS.1 was further funded with a grant from the German Research Council (DFG). The transmission electron microscope was obtained with a grant from the European Funds for Regional Developments (EFRE) and the DFG. The authors wish to thank Nicole Fritz and Annett Urbanek for the mass spectrometry analysis and Carolin Fritzsche for the cytotoxicity studies.

Notes and references

1 O. Dechy-Cabaret, B. Martin-Vaca and D. Bourissou, *Chem. Rev.*, 2004, **104**, 6147–6176.

2 A. P. Gupta and V. Kumar, *Eur. Polym. J.*, 2007, **43**, 4053–4074.
3 K. Knop, R. Hoogenboom, D. Fischer and U. S. Schubert, *Angew. Chem., Int. Ed.*, 2010, **49**, 6288–6308.
4 O. Sedlacek, B. D. Monnery, S. K. Filippov, R. Hoogenboom and M. Hruby, *Macromol. Rapid Commun.*, 2012, **33**, 1648–1662.
5 R. Hoogenboom, *Angew. Chem., Int. Ed.*, 2009, **48**, 7978–7994.
6 N. Adams and U. S. Schubert, *Adv. Drug Delivery Rev.*, 2007, **59**, 1504–1520.
7 S. C. Lee, Y. Chang, J.-S. Yoon, C. Kim, I. C. Kwon, Y.-H. Kim and S. Y. Jeong, *Macromolecules*, 1999, **32**, 1847–1852.
8 C.-H. Wang and G.-H. Hsiue, *Biomacromolecules*, 2003, **4**, 1487–1490.
9 L. Zhao and Z. Lin, *Soft Matter*, 2011, **7**, 10520–10535.
10 Z. Ge and S. Liu, *Macromol. Rapid Commun.*, 2009, **30**, 1523–1532.
11 H. Shi, Y. Zhao, X. Dong, Y. Zhou and D. Wang, *Chem. Soc. Rev.*, 2013, **42**, 2075–2099.
12 S. S. Sheiko, B. S. Sumerlin and K. Matyjaszewski, *Prog. Polym. Sci.*, 2008, **33**, 759–785.
13 M. Zhang and A. H. E. Moeller, *J. Polym. Sci., Part A: Polym. Chem.*, 2005, **43**, 3461–3481.
14 H.-i. Lee, K. Matyjaszewski, S. Yu-Su and S. S. Sheiko, *Macromolecules*, 2008, **41**, 6073–6080.
15 M. Hans, H. Keul, A. Heise and M. Moeller, *Macromolecules*, 2007, **40**, 8872–8880.
16 A. Dag, H. Durmaz, E. Demir, G. Hizal and U. Tunca, *J. Polym. Sci., Part A: Polym. Chem.*, 2008, **46**, 6969–6977.
17 N. Cakir, M. Yavuzarslan, H. Durmaz, G. Hizal and U. Tunca, *J. Polym. Sci., Part A: Polym. Chem.*, 2013, **51**, 899–907.
18 Y. Xia, B. D. Olsen, J. A. Kornfield and R. H. Grubbs, *J. Am. Chem. Soc.*, 2009, **131**, 18525–18532.
19 K. Ishizu, N. Sawada, J. Satoh and A. Sogabe, *J. Mater. Sci. Lett.*, 2003, **22**, 1219–1222.
20 K. Ishizu, N. Okamoto, T. Murakami, S. Uchida and S. Nojima, *Macromol. Chem. Phys.*, 2009, **210**, 1717–1725.
21 H. Zhu, G. Deng and Y. Chen, *Polymer*, 2008, **49**, 405–411.
22 T. Stephan, S. Muth and M. Schmidt, *Macromolecules*, 2002, **35**, 9857–9860.
23 D. Neugebauer, Y. Zhang, T. Pakula and K. Matyjaszewski, *Macromolecules*, 2005, **38**, 8687–8693.
24 C. Weber, M. Wagner, D. Baykal, S. Hoeppener, R. M. Paulus, G. Festag, E. Altuntas, F. H. Schacher and U. S. Schubert, *Macromolecules*, 2013, **46**, 5107–5116.
25 M. Bagheri and E. Bigdeli, *J. Polym. Res.*, 2013, **20**, 1–11.
26 J.-F. Lutz, N. Jahed and K. Matyjaszewski, *J. Polym. Sci., Part A: Polym. Chem.*, 2004, **42**, 1939–1952.
27 C. Weber, C. R. Becer, R. Hoogenboom and U. S. Schubert, *Macromolecules*, 2009, **42**, 2965–2971.
28 J. Kronek, Z. Kroneková, J. Lustoň, E. Paulovičová, L. Paulovičová and B. Mendrek, *J. Mater. Sci.: Mater. Med.*, 2011, **22**, 1725–1734.
29 I. Yildirim, S. Crotty, C. H. Loh, G. Festag, C. Weber, P.-F. Caponi, M. Gottschaldt, M. Westerhausen and U. S. Schubert, *J. Polym. Sci., Part A: Polym. Chem.*, 2016, **54**, 437–448.
30 M. J. Stanford and A. P. Dove, *Macromolecules*, 2009, **42**, 141–147.
31 M. Westerhausen, *Inorg. Chem.*, 1991, **30**, 96–101.
32 A. M. Johns, S. C. Chmely and T. P. Hanusa, *Inorg. Chem.*, 2009, **48**, 1380–1384.
33 M. Westerhausen, J. Langer, S. Krieck and C. Glock, *Rev. Inorg. Chem.*, 2011, **31**, 143.
34 A. Torvisco, A. Y. O'Brien and K. Ruhlandt-Senge, *Coord. Chem. Rev.*, 2011, **255**, 1268–1292.
35 C. Weber, S. Rogers, A. Vollrath, S. Hoeppener, T. Rudolph, N. Fritz, R. Hoogenboom and U. S. Schubert, *J. Polym. Sci., Part A: Polym. Chem.*, 2013, **51**, 139–148.
36 U. Mansfeld, S. Hoeppener, K. Kempe, J.-M. Schumers, J.-F. Gohy and U. S. Schubert, *Soft Matter*, 2013, **9**, 5966–5974.
37 A. L. Parry, P. H. H. Bomans, S. J. Holder, N. A. J. M. Sommerdijk and S. C. G. Biagini, *Angew. Chem.*, 2008, **120**, 8991–8994.
38 H.-Y. Chang, Y.-L. Lin, Y.-J. Sheng and H.-K. Tsao, *Macromolecules*, 2012, **45**, 4778–4789.
39 H. Luo, J. L. Santos and M. Herrera-Alonso, *Chem. Commun.*, 2014, **50**, 536–538.
40 B. K. Banik and F. F. Becker, *Bioorg. Med. Chem.*, 2001, **9**, 593–605.
41 J. Sikkema, J. A. de Bont and B. Poolman, *Microbiol. Rev.*, 1995, **59**, 201–222.
42 M. Müllner, A. Schallon, A. Walther, R. Freitag and A. H. E. Müller, *Biomacromolecules*, 2010, **11**, 390–396.
43 M. Sasatsu, H. Onishi and Y. Machida, *Int. J. Pharm.*, 2008, **358**, 271–277.
44 Y. Zhang, Q. Zhang, L. Zha, W. Yang, C. Wang, X. Jiang and S. Fu, *Colloid Polym. Sci.*, 2004, **282**, 1323–1328.
45 J. Rejman, V. Oberle, I. S. Zuhorn and D. Hoekstra, *Biochem. J.*, 2004, **377**, 159–169.
46 L. Xiao, X. Xiong, X. Sun, Y. Zhu, H. Yang, H. Chen, L. Gan, H. Xu and X. Yang, *Biomaterials*, 2011, **32**, 5148–5157.
47 L. Treuel, X. Jiang and G. U. Nienhaus, *J. R. Soc., Interface*, 2013, **10**, 20120939.

Supporting Information

for

Fluorescent amphiphilic heterografted comb polymers comprising biocompatible PLA and PEtOx side chains

Ilknur Yildirim,[a,b] Tanja Bus,[a,b] Martin Sahn,[a,b] Turgay Yildirim,[a,b] Diana Kalden,[c] Stephanie Hoeppener,[a,b] Anja Traeger,[a,b] Matthias Westerhausen,[c] Christine Weber[a,b] and Ulrich S. Schubert*[a,b]

[a]Laboratory of Organic and Macromolecular Chemistry (IOMC), Friedrich Schiller University Jena, Humboldtstr. 10, 07743 Jena, Germany

[b]Jena Center for Soft Matter (JCSM), Friedrich Schiller University Jena, Philosophenweg 7, 07743 Jena, Germany

[c]Institute of Inorganic and Analytical Chemistry (IAAC), Friedrich Schiller University Jena, Humboldtstr. 8, 07743 Jena, Germany

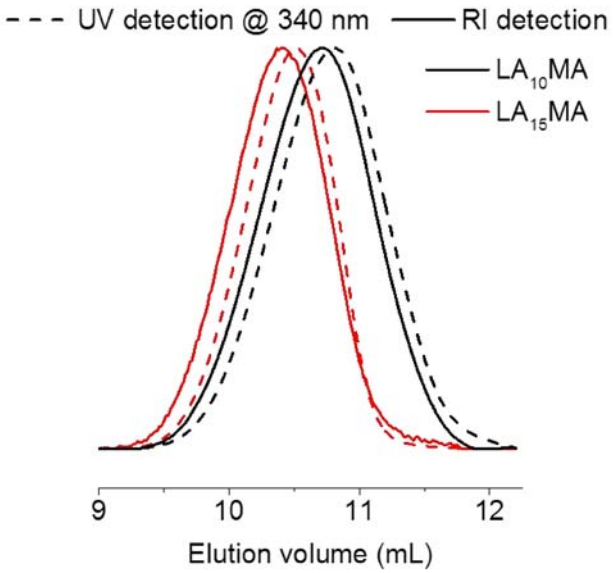

Figure S1. Normalized SEC traces (THF, PLA calibration) of the PLA macromonomers with RI and UV detection at 340 nm.

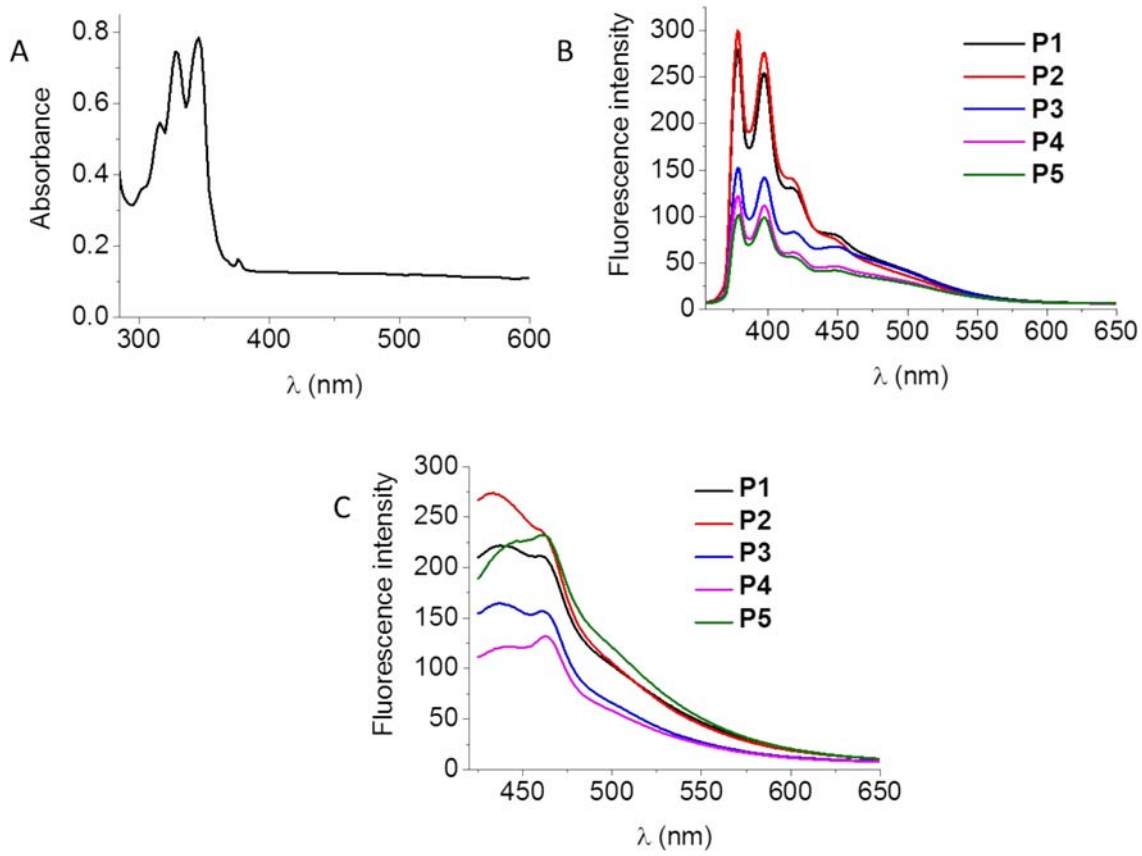

Figure S2. (A) UV-vis absorption spectrum recorded from the aqueous suspension of **P4** (c = 1 mg mL^{-1}). Overlay of fluorescence emission spectra (c = 50 µg mL^{-1}) (**B**) with the excitation wavelength set at 346 nm. (C) with the excitation wavelength set at 405 nm

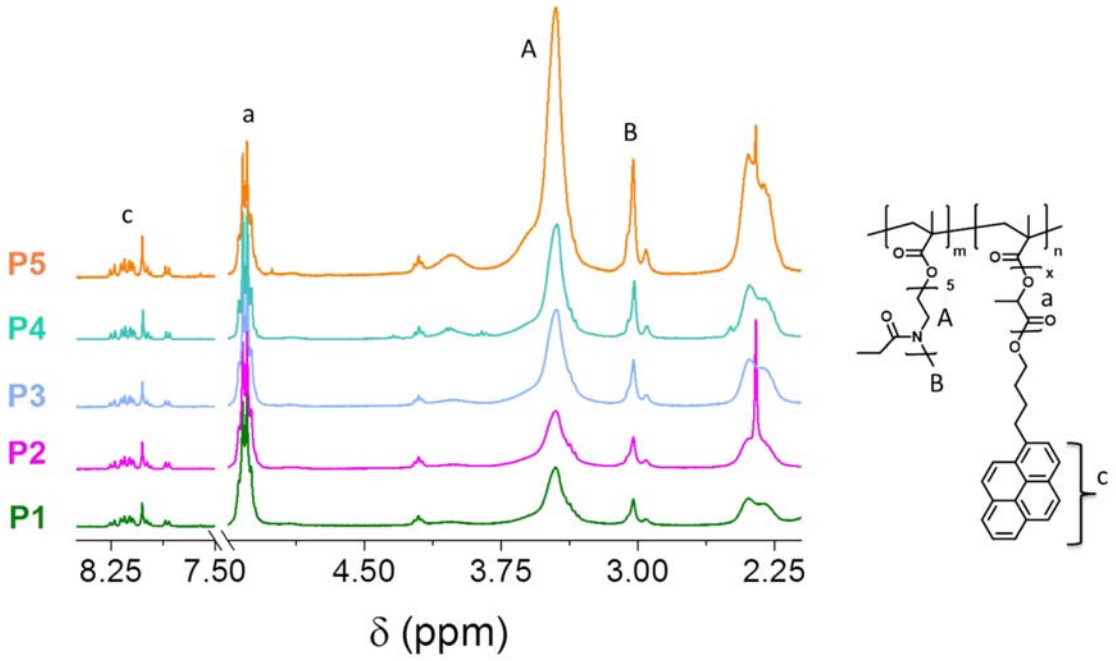

Figure S3. Overlay of the ^{1}H NMR spectra (300 MHz, $CDCl_3$) of all comb polymers **P1** to **P5**. For clarity, the spectra were normalized according to the signal of the methine protons of PLA. Only the signals used for calculation of the copolymer composition are labelled.

Table S1. Characterization results of the polymer suspension in water by means of DLS (the mean particle size was approximated as the effective (Z-average) diameter and the width of the distribution as the polydispersity index of the particles (PDI) obtained by the cumulants method).[a]

Polymer	Z-avg [d, nm]	PDI
P1	59 ± 0.7	0.349 ± 0.001
P2	103 ± 0.4	0.270 ± 0.01
P3	65 ± 0.6	0.178 ± 0.01
P4	19 ± 0.1	0.122 ± 0.002
P5	81 ± 0.3	0.309 ± 0.003

[a]c = 5 mg mL^{-1} in water.

Confocal live cell microscopy

Uptake studies I: Negative Control

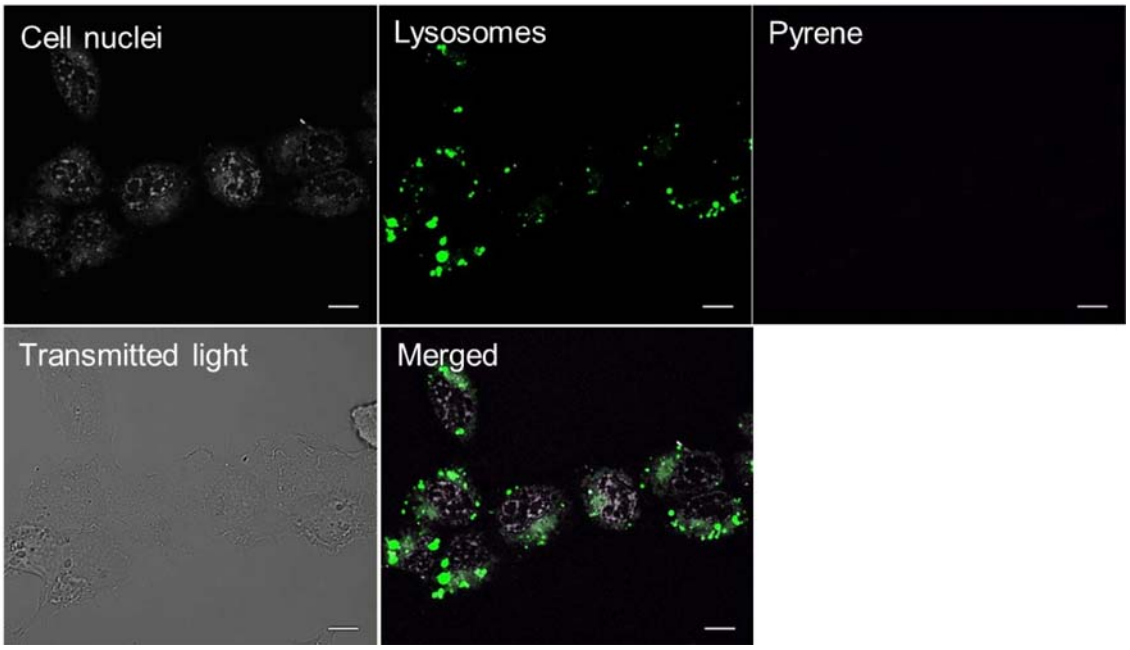

Figure S4. Confocal live cell imaging: HEK cells were cultivated for 4 h in serum-reduced media serving as negative control. The cell nucleus was stained with NucRed (grey) and the lysosomes with LysoTracker Green (green); pyrene is depicted in magenta (scale bars represent 10 μm).

Uptake studies II: **P2**

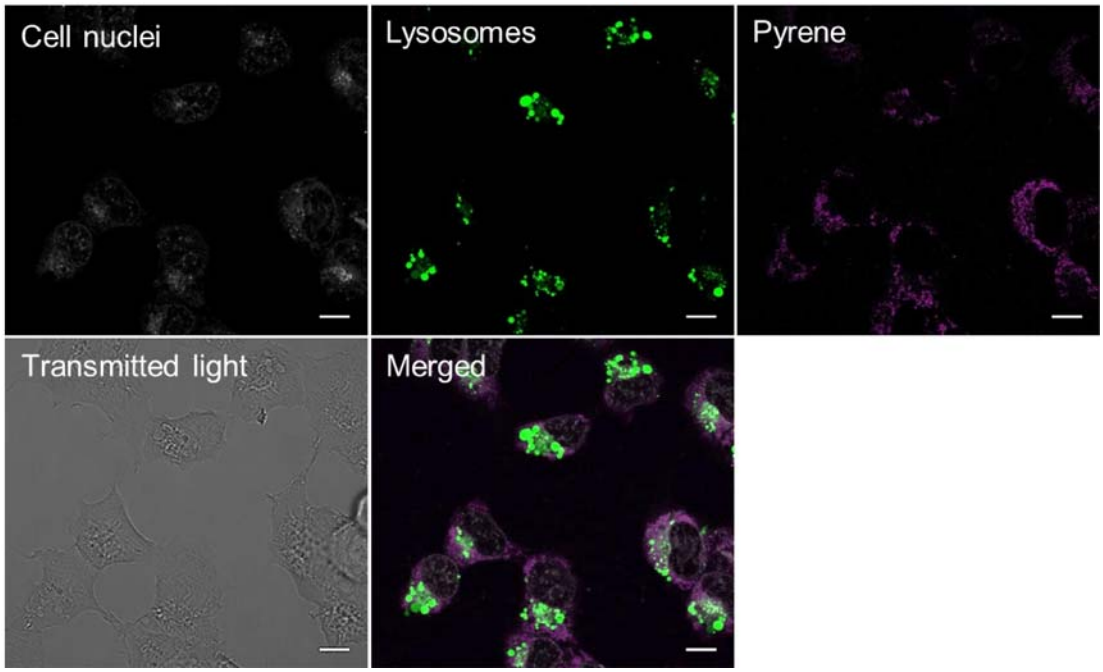

Figure S5: Confocal live cell imaging: For uptake studies, HEK cells were cultivated with **P2** for 4 h in serum-reduced media. The cell nucleus was stained with NucRed (grey) and the lysosomes with LysoTracker Green (green); pyrene is depicted in magenta (scale bars represent 10 μm).

Uptake studies III: **P3**

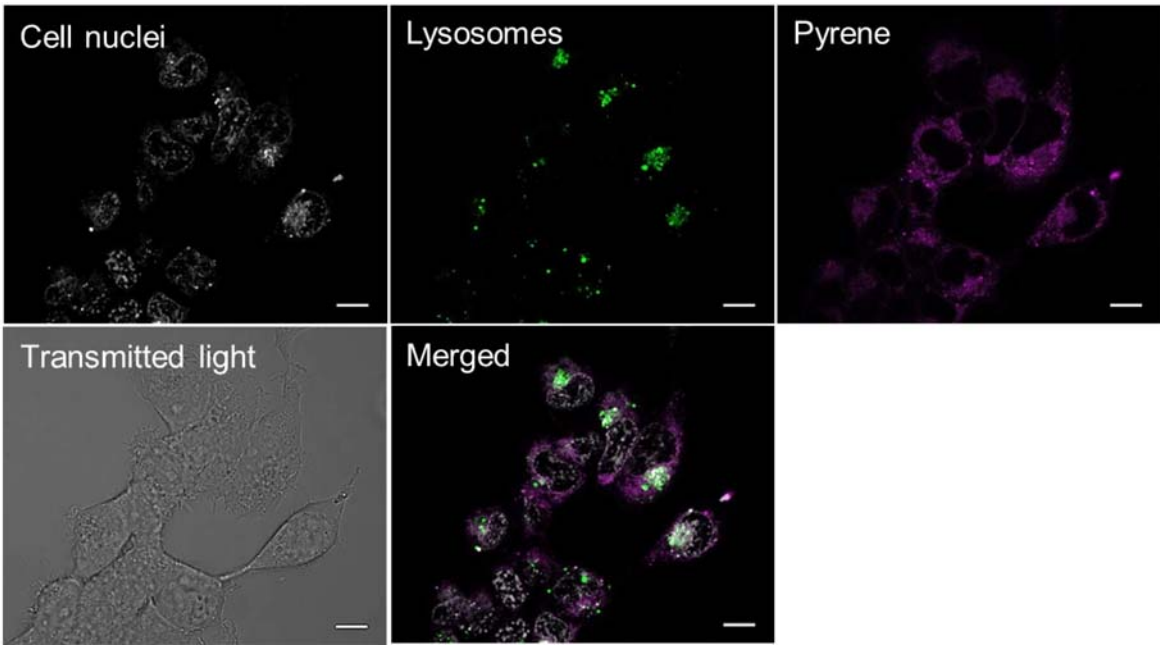

Figure S6: Confocal live cell imaging: For uptake studies, HEK cells were cultivated with **P3** for 4 h in serum-reduced media. The cell nucleus was stained with NucRed (grey) and the lysosomes with LysoTracker Green (green); pyrene is depicted in magenta (scale bars represent 10 µm).

Uptake studies IV: **P4**

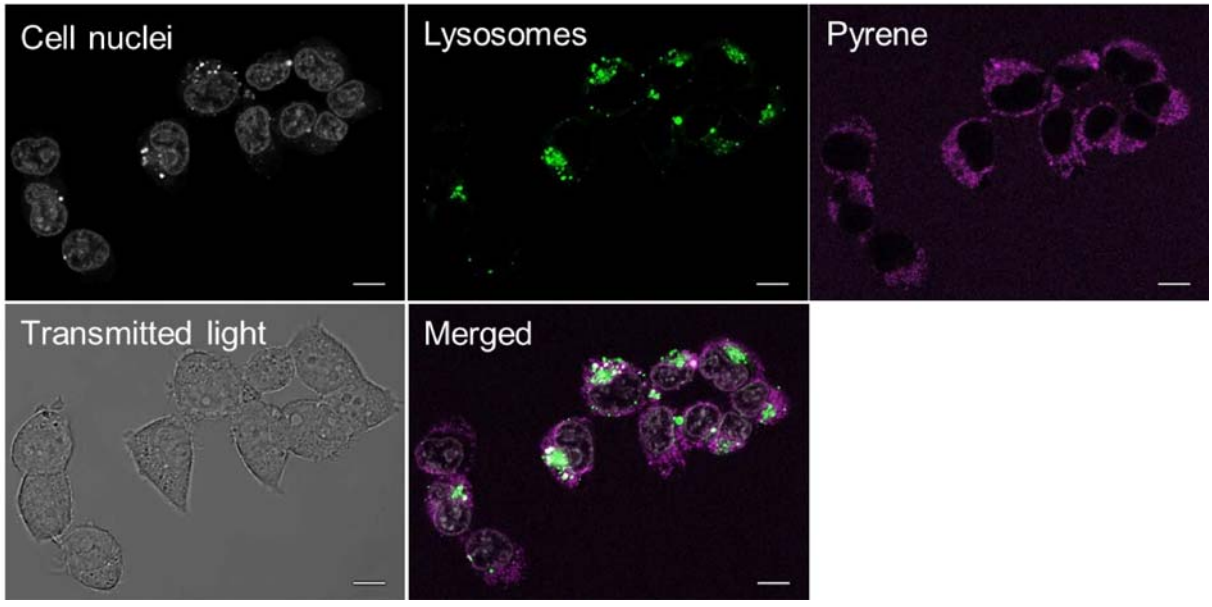

Figure S7: Confocal live cell imaging: For uptake studies, HEK cells were cultivated with **P4** for 4 h in serum-reduced media. The cell nucleus was stained with NucRed (grey) and the lysosomes with LysoTracker Green (green); pyrene is depicted in magenta (scale bars represent 10 µm).

Uptake studies V: **P5**

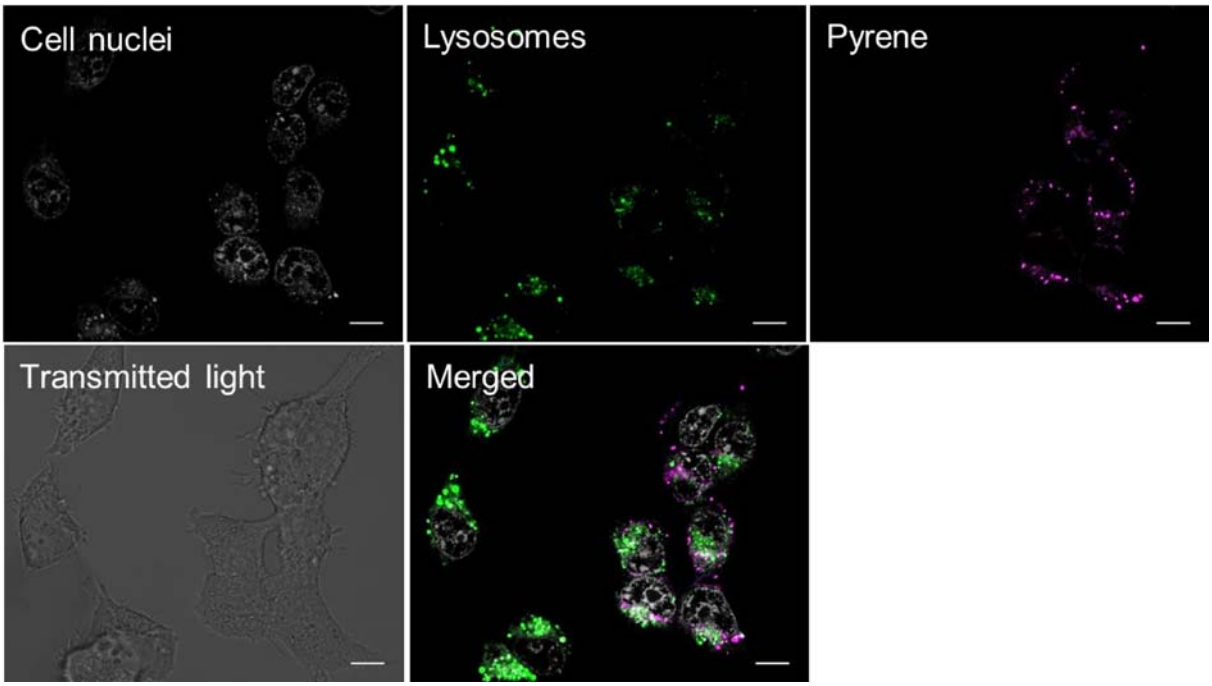

Figure S8: Confocal live cell imaging: For uptake studies, HEK cells were cultivated with **P5** for 4 h in serum-reduced media. The cell nucleus was stained with NucRed (grey) and the lysosomes with LysoTracker Green (green); pyrene is depicted in magenta (scale bars represent 10 µm).

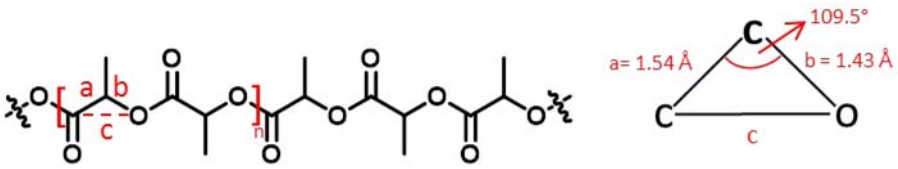

$c^2 = a^2 + b^2 - 2abcos(109.5)$

$c = 2.42\ \text{Å} = 0.242\ nm$

Length of one lactide unit = 3c

Figure S9: Estimation of the length of a fully stretched PLA side chain.